ROLE OF INTERGRANULAR CONTACTS ON MECHANISMS CAUSING LIQUEFACTION & SLOPE FAILURES IN SILTY SANDS

USGS Award Number: 01HQGR0032 & 99HQGR0021

Final Report

October 2003

S. Thevanayagam
Principal Investigator
&
T. Shenthan, and T. Kanagalingam
Research Assistants

University at Buffalo
State University of New York
Department of Civil, Struct. & Env. Eng.
212 Ketter Hall, Buffalo, NY 14260

Tel: 716-645-2114 ext:2430; Fax: 716-645-3733
theva@eng.buffalo.edu, http//www.civil.eng.buffalo.edu

Program Element: PT

Key Words: Liquefaction, silty sands

"*Research supported by the U.S. Geological Survey (USGS), Department of the Interior, under USGS award number (01HQGR0032 & 99HQGR0021). The views and conclusions contained in this document are those of the authors and should not be interpreted as necessarily representing the official policies, either expressed or implied, of the U.S. Government.*"

Abstract

Liquefaction problem has been studied worldwide for more than three decades. However, the past research addressed mainly clean or nearly clean sand, though, recent case histories indicate that the soils with significant amount of non-plastic fine particles also liquefy during earthquakes, and cause excessive settlement, lateral spreading, etc. Uncertainties prevail on the direct extrapolation of clean sand behavior for silty soils. A fundamental understanding of the behavior of silty sands and/or sandy silts under undrained loading conditions (such as during earthquakes) would pave a way to predict the degree of vulnerability of such soils to liquefaction related hazards, estimate the degree of soil improvement needed to eliminate such ill effects, and to find new and/or improved ways to achieve those improvements. This study focuses, particularly, on liquefaction potential and post-liquefaction shear strength of non-plastic silty soils from a microscopic mechanistic point of view. The ultimate goal is to improve our ability to evaluate liquefaction potential, flow-deformation potential, seismic slope stability of earth structures, dams and embankments built of natural silty sands/sandy silts and develop design strategies to mitigate earthquake damage and minimize losses.

The purpose of this report is to present data obtained from an extensive experimental program that consists of more than 150 monotonic triaxial compression and 75 cyclic triaxial tests. This experimental program was designed to study the relative effects of silt and sand particles on the overall undrained behavior of silty soils, as compared to sands. The test program included sands, gap-graded silty soils, and well-graded silty soils. New parameters that characterize contact density of a granular soil mix are presented. The complete test procedures, experimental data, and analyses are presented. The analyses focused on (a) undrained monotonic behavior of silty soils, (b) undrained cyclic behavior of silty soils, (c) undrained behavior of silty soils based on energy principles, and (d) liquefaction behavior and screening of silty soils, remediation, and other issues. The contact density parameters have been related to cyclic resistance, energy required to cause liquefaction, and large-strain monotonic undrained shear strength. The above results, and findings from this study have been published in a number of journal papers, conference proceedings, and reports. These articles are also presented and the conclusions are highlighted.

Table of Contents

	page
1.0 Introduction	1
2.0 Contact Density Indices and Intergrain Friction	3
2.1 Microstructure of Granular Mix	3
2.1.1 Grain Contact Density Indices	5
2.1.2 Equivalent Contact Density Indices	6
2.2 Energy Loss in Granular Media	7
2.3 Effective Intergrain Friction Coefficient	9
2.4 Energy – Intergrain Contact Parameter Relations	9
3.0 Experimental Study	13
3.1 Experimental Program	13
3.2 Materials	13
3.3 Apparatus	16
3.4 Test Procedure	18
3.4.1 Specimen Preparation	18
3.4.1.1 Mixing	18
3.4.1.2 Dry Pluviation Method	18
3.4.1.3 Moisture Tamping Method	20
3.4.2 Initial Saturation at the Pressure Panel	20
3.4.3 Mounting on GEOCOMP Loading Frame or GDS Apparatus	21
3.4.4 Back Pressure Saturation	22
3.4.5 Consolidation	22
3.4.6 Monotonic Shear Phase	22
3.4.7 Triaxial Cyclic Loading Phase	22
3.5 Data Acquisition	22
3.6 Data Reduction	23
3.6.1 Monotonic Compression Test	23
3.6.2 Cyclic Test	27
3.7 Experimental Errors	35
3.7.1 Device Measurement	35
3.7.2 Void Ratio Calculation	35
3.7.3 Axial Strain	35

3.7.4 Deviatoric Stress 36
3.7.5 Membrane Compliance 36
3.7.6 Rod Friction 36
4.0 Experimental Data 37
5.0 Analysis and Results 38
5.1 Undrained monotonic behavior of sand and non-plastic silty soils 38
5.1.1 Technical Articles 38
5.1.1.1 Undrained fragility of sands, silty sands, and silt 40
5.1.1.2 Intergranular state variables and stress-strain behavior of silty sands 51
5.1.2 Conclusions 38
5.2 Undrained cyclic behavior of sand and non-plastic silty soils 75
5.2.1 Technical Articles 75
5.2.1.1 Relative role of coarse and fine grains on mechanical behavior of granular mixes 77
5.2.1.2 Liquefaction and shear wave velocity characteristics of silty/gravely soils – implications for bridge foundations 88
5.2.1.3 Effect of non-plastic fines on undrained cyclic strength of silty sands 103
5.2.1.4 Contact index for liquefaction potential of silty and gravely soils 117
5.2.1.5 Liquefaction potential and undrained fragility of silty soils 124
5.2.1.6 Effects of non-plastic fines on the liquefaction resistance of sands 132
5.2.2 Conclusions 75
5.3 Undrained behavior of sand and non-plastic silty soils based on energy principles 134
5.3.1 Technical Articles 134
5.3.1.1 Intergrain friction, Contact density, and cyclic resistance of sands 135
5.3.1.2 Intergrain friction, Contact density, and cyclic resistance of silty sands 143
5.3.2 Conclusions 134
5.4 Liquefaction behavior and screening of sand and non-plastic silty soils, remediation, and other issues 149
5.4.1 Technical Articles 149
5.4.1.1 Liquefaction in Silty Soils – Screening and Remediation Issues 151
5.4.1.2 Post-liquefaction pore pressure dissipation and densification in silty soils 159

5.4.1.3 Shear wave velocity relations for silty and gravely soils 165

5.4.1.4 Intergrain contact and shear modulus of non-plastic granular mixes 171

5.4.1.5 Liquefaction in silty soils – Considerations for screening and retrofit strategies 177

5.4.2 Conclusions 149

Appendix A: Monotonic Triaxial Compression Tests Data

Appendix B: Cyclic Triaxial Tests Data

Appendix C: Notations

1.0 Introduction

This research sought to develop a fundamental understanding of the behavior of silty sands under undrained loading conditions during earthquakes. Particular focus is on liquefaction potential and post-liquefaction shear strength from a microscopic mechanistic point of view. The goal is to improve our ability to evaluate liquefaction potential, flow-deformation potential, seismic slope stability of earth structures, dams and embankments built of natural silty sands/sandy silts and develop design strategies to mitigate earthquake damage and minimize losses.

In particular the overall ultimate aim of this research is to:

(a) develop an understanding of the physical nature of inter-fine and inter-granular frictional contacts in silty sands/sandy silts at different void ratio, fines content levels, particle size ratio between coarse and fine grain and their effects on liquefaction resistance and post-liquefaction strength,

(b) develop a new unified method to characterize cyclic and post-liq. strength characteristics,

(c) re-evaluate the current methods of assessing liquefaction potential and liquefaction-related damage potential, based on this new understanding, and

(d) develop an improved method for assessment of liquefaction potential and related damage.

This research was supported by two grants (99HQGR0021 and 01HQGR0032). The primary focus of the research supported by these grants is on task (a). Specifically the work performed under these grants focused on the following sub tasks.

- Task I: Development and refinement of a physically sound conceptual and theoretical framework to understand the roles of fines in inter-granular frictional contacts at different "density levels" and different fines content levels, on the undrained behavior of silty soils, and
- Task II: Experimental evaluation of the above framework using new and other available undrained monotonic and cyclic data on gap-graded and well-graded sand-silt mix soil and refinement of the framework.

The experimental studies focused on undrained cyclic and monotonic triaxial tests on a gap-graded soil (Ottawa sand – silt mix) as well as a broadly graded soil (WG sand – silt mix). The theoretical studies focused on binary mixes of spherical particles of size D and d (size disparity ratio R_d=D/d) aimed at developing an understanding of the relative roles of coarse and fine grains on the response of the binary mix. Through semi-theoretical arguments, a set of contact density indices was developed for characterization of the undrained cyclic and monotonic strength of the binary mix. The results were promising. Further work on this study included an energy-based approach to understand, and to analyze soil liquefaction phenomena. Theoretical expression for internal energy loss has been developed, and found to agree well with the measured external energy input.

The Annual Reports (http://erp-web.er.usgs.gov/reports/annsum/vol42/pt/pt_vol42.htm and http://erp-web.er.usgs.gov/reports/annsum/vol43/pt/pt_vol43.htm) presents a summary of the work performed under these grants. This report presents the details of the experimental work, analysis, and conclusions from this research. A summary of articles resulting from this research is presented in Sec.5.0 of this report.

Section 2.0 presents a brief summary of the theoretical framework to classify the microstructure of silty soils and the associated contact densities for characterization monotonic and cyclic undrained behavior of non-plastic silty soils and the theoretical formulations developed to study the liquefaction response of such soils based on energy principles. Details of the theoretical formulations may be found in a series of technical articles presented in Sec.5.1 and 5.2, and the dissertations cited in Sec.5.0.

Section 3.0 presents the experimental work. The experimental data are presented in Appendices A and B. Further details can be found in the dissertations and theses cited in Sec.4.0

Section 5.0 presents a summary of the analysis conducted and the results and conclusions. This section consists of four subsections (a) undrained monotonic behavior of silty soils, (b) undrained cyclic behavior of silty soils, (c) undrained behavior of silty soils based on energy principles, and (d) liquefaction behavior and screening of silty soils, remediation, and other issues. The data, analysis, and conclusions for each section are presented in a series of technical articles, attached in Sec.5.0. Most of these articles have been published in a number of conferences and journals.

The insights derived from this study prompted further research on reassessing the current techniques for liquefaction potential and development of (new and modification of current) ground improvement techniques suitable for silty soils. The articles resulting from that research, sponsored by other agencies, are included in Sec.5.4.

Section 5.0 also presents a summary of the main conclusions from this study.

2.0 Contact Density Indices and Intergrain Friction

2.1 Microstructure of Granular Mix

The microstructure of a granular mix can be constituted in many different ways. Here the consideration focuses on a two-sized granular mix known as a gap graded model (Thevanayagam 1998, Thevanayagam et al. 2002). The technical articles presented in Sec.5.1 and 5.2 present the details of this work. This model classifies the granular mix into four categories depending on the particle arrangements and fines content (FC). Figures 2.1 through 2.3 show the classification in detail.

The first category (Case i) is defined when the fine grains are fully confined within the void spaces of coarser grains without supporting the coarser grain skeleton. Case i can occur only when the size disparity ratio of coarser to fine particles is greater than 6.5 and fines content is less than a threshold value (FC_{th}). Microstructure shown in case i is changed to form case ii and iii keeping the fines content same. In case ii, some of the fine particles support the coarser grain skeleton and passively participating in the internal force chain. In case iii, some fine particles act as separators between coarser grains and actively participate in the internal force chain. It can be noted that the global void ratio successively increases from case i to case iii.

Case iv-1 and iv-2 are achieved by increasing the fines content significantly ($>FC_{th}$). In these cases, fine grains may carry the contact and shear forces while the coarse grains might act as the reinforcing elements embedded within the fine grain matrix. The effect of coarse grains cannot be completely neglected until they are separated sufficiently apart. If the fines content ($FC>FC_L$) is such that the effects of coarser grains can be neglected, it is categorized as case iv-1. Otherwise the formation is case iv-2 ($FC_{th}< FC< FC_L$).

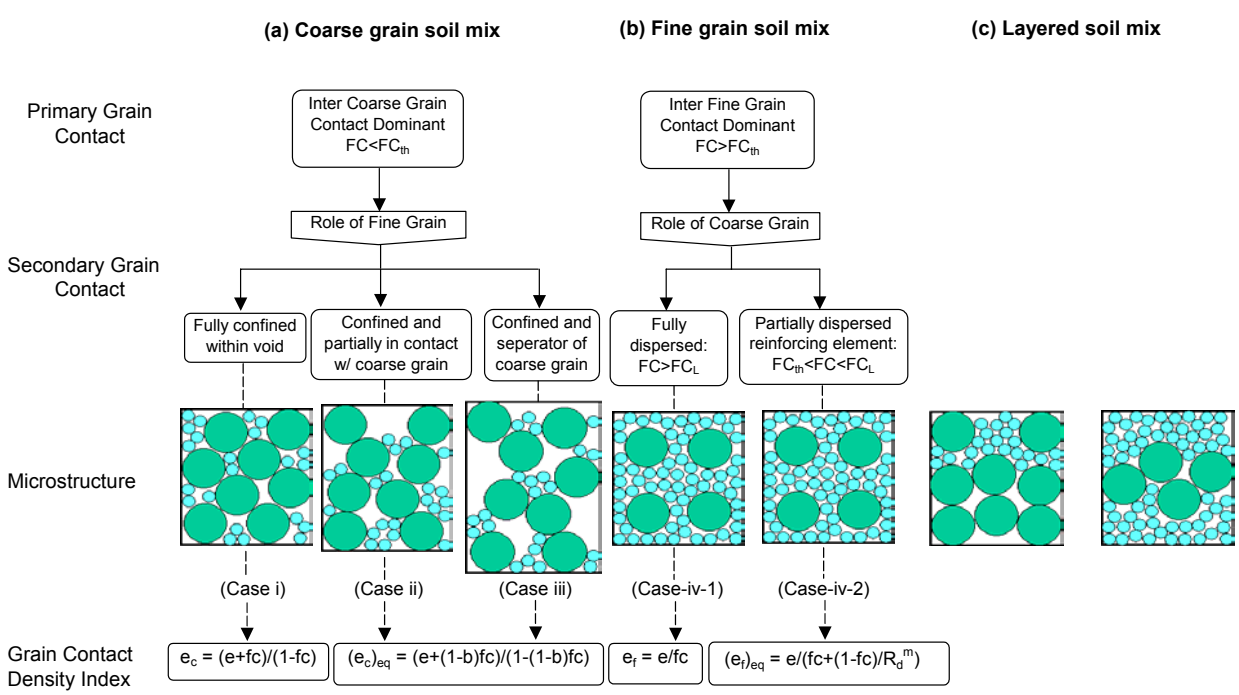

b=portion of the fine grains that contribute to the active intergrain contacts; e=global void ratio; FC=fine grains content; FC_{th}=threshhold fine grains content; FC_L=limit fines content; m: reinforcement factor; R_d=D/d=particle size disparity ratio

Fig. 2.1 Intergranular Soil Mix Classification

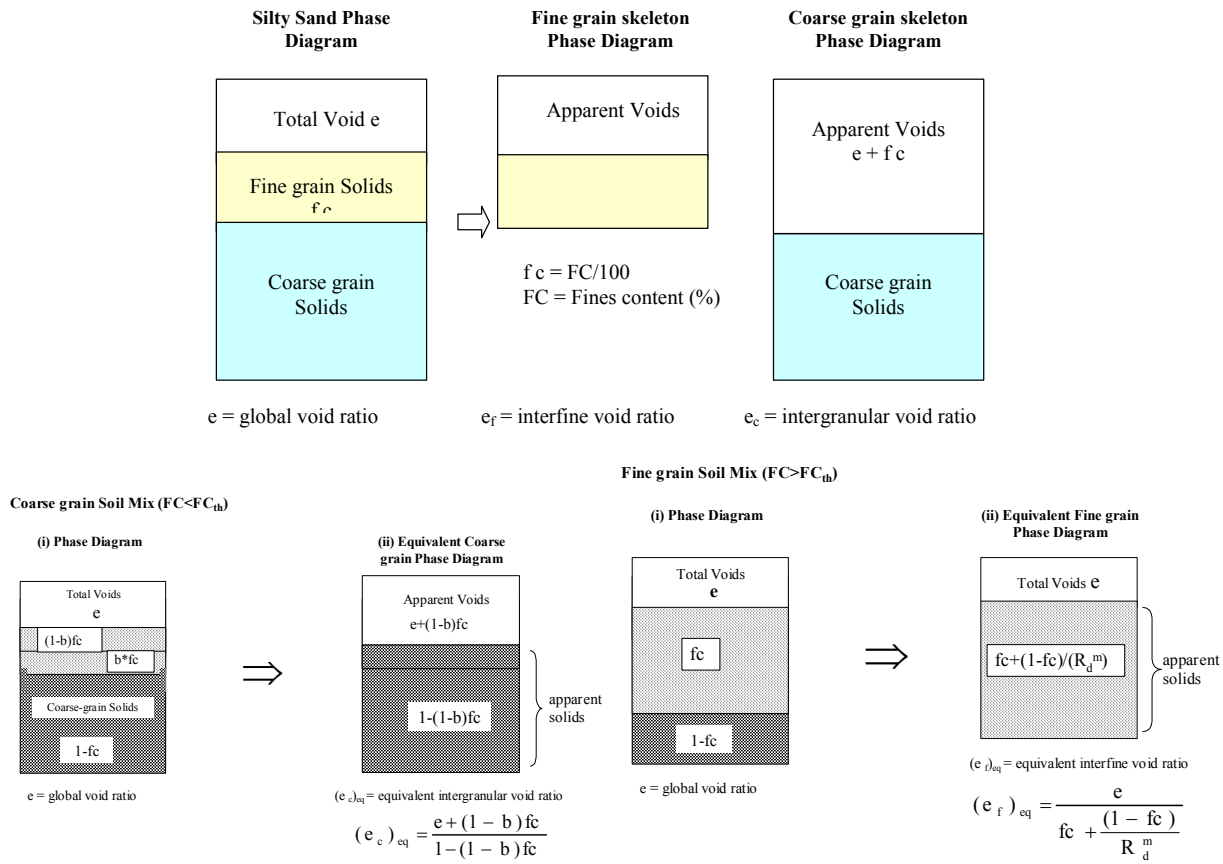

Fig. 2.2 Intergranular Phase Diagram and Contact Index Void Ratios

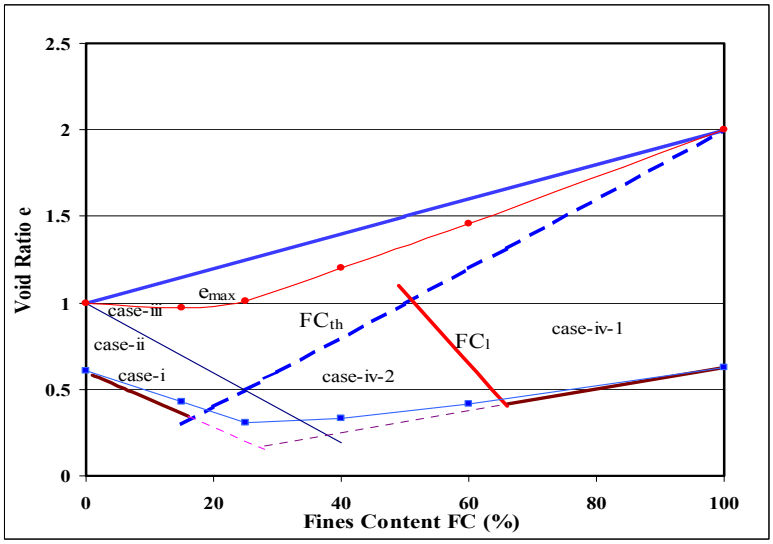

Fig. 2.3 Granular Mix Classification

Table 2.1 Granular Mix Classification (Ref. Figs. 2.1-2.3)

Case	FC	e_c	e_f	***Roles of coarser-grains and finer-grains***	Contact Index Void Ratio	Fig.
i		$e_c<e_{max,Hc}$	$e_f>e_{max,HF}$	Finer grains are inactive (or secondary) in the transfer of inter particle forces. They may largely play the role of "filler" of intergranular voids. The mechanical behavior is affected primarily by the coarser grain contacts.	$(e_c)_{eq}$	2.1(a)
ii	$FC<FC_{th}$	e_c *near* $e_{max,Hc}$		Finer grains support the coarser-grain skeleton that is otherwise unstable. They act as a load transfer vehicle between "some" of the coarse-grain particles in the soil-matrix while the remainder of the fines play the role of "filler" of voids.	$(e_c)_{eq}$	
iii		$e_c>e_{max,Hc}$		Finer grains play an active role of "separator" between a significant number of coarse-grain contacts and therefore begin to dominate the strength characteristics.	$(e_c)_{eq}$	
iv-2	$FC_{th}<FC<FC_L$		$e_f<e_{max,HF}$	The fines carry the contact and shear forces while the coarser grains may act as reinforcing elements embedded within the finer grain matrix.	$(e_f)_{eq}$	2.1(b)
iv-1	$FC_L<FC$	$e_c>>e_{max,Hc}$	$e_f<e_{max,HF}$	The fines carry the contact and shear forces while the coarser grains are fully dispersed.	e_f	

Notes: $e_{max,Hc}$, $e_{max,HF}$ = maximum void ratio of the host sand (coarser grains) and host fines (finer grains) media, respectively. They are the limiting void ratios beyond which each soil (clean coarser grained soil, pure fine grained soil) has no appreciable strength.FC_{th}=Threshold finer grains content, and FC_L = limiting finer grains content. The magnitudes of FC_{th} and FC_L depend on the size disparity ratio (R_d=D/d) of the size of the coarser (D) and finer (d) grains, shape, packing, $e_{max,Hc}$, and $e_{max,HF}$ as shown elsewhere (Thevanayagam 1998-2000). Intergranular void ratio (e_c) =[e+fc]/[1-fc], (fc=FC/100, FC=finer grain content by weight). Interfine void ratio (e_f) =e/fc, s=1+a(d/D)=1+a/R_d, where a=10 (approximately).

2.1.1 Grain Contact Density Indices

Grain contact is the fundamental principle behind the liquefaction phenomena. The contact density should represent the portion of particles, which actively participate in the internal force chains created by external loading. Relative density and global void ratio are undoubtedly accepted as contact indices for uniform sand. The effectiveness of these indices in silty soils is questionable. Intergranular void ratio (sand skeleton void ratio) has been recommended for silty soils having fines content less than a threshold fines content (FC_{th}). Intergranular void ratio (e_c) reflects only the coarser-grain contacts and neglects the effects of fines.

$$e_c = \frac{e + fc}{1 - fc} \tag{2.1}$$

where e_c= intergranular void ratio, e= global void ratio, f_c=FC/100, and FC=fines content. The interfine void ratio (e_f) is introduced as a suitable first-order contact index for fine-grain contacts neglecting the effect of coarser grains in a granular mix with higher fines content.

$$e_f = \frac{e}{fc} \tag{2.2}$$

where e_f= interfine void ratio, e= global void ratio, and f_c=FC/100.

Threshold Fines Content

As the fines content increases, the magnitude of e_c increases (Eq.2.1) indicating a decrease in coarse grain contacts and e_f decreases (Eq.2.2) indicating an increase in fine grain contacts. When the magnitude of e_f decreases below the maximum void ratio of the host- silt, the strength reversal is expected to occur. This conceptual standpoint leads to the development of an expression for FC_{th}. FC_{th} is defined as (Thevenayagam 2000):

$$FC_{th} \leq \frac{100e_c}{1+e_c+e_{\max,HF}}\% = \frac{100e}{e_{\max,HF}}\% \qquad (2.3)$$

where e = global void ratio, e_c = intergranular void ratio, $e_{\max,HF}$ = the maximum void ratio of the pure silt.

Limiting Fines Content

When FC is greater than FC_{th}, fines separate the coarser grains and significantly influence the soil behavior. Even though the coarser grains are separated at $FC>FC_{th}$, they contribute to the internal force chain and thus effectively give reinforcement effects to the soil skeleton. This effect also is expected to vanish at $FC>FC_L$ when the coarser grains are sufficiently separated by the fines. The limiting fines content FC_L is approximately given by (Thevenayagam 2000):

$$FC_L \geq 100\left[1-\frac{\pi(1+e)}{6s^3}\right]\% = 100\left[\frac{6s^3-\pi}{6s^3+\pi e_f}\right]\% \geq FC_{th}; e_f \leq e_{\max,HF} \qquad (2.4)$$

where $s=1+a/R_d$, $R_d=D/d$, D=particle diameter of coarser grain, d=particle diameter of fine grain, e_f = interfine void ratio, and a≈10.

2.1.2 Equivalent Contact Density Indices

Intergranular void ratio (e_c) has been defined assuming that there is no fine grain participation in any form to the soil structure. This concept may be true for a soil structure with very low fines content under static equilibrium. The changes in either loading or boundary conditions have much higher probability to cause particle rearrangements within the soil structure involving fine grains. e_c, which entirely neglects the effects of fines, would not represent the actual behavior of silty sands. Considering the secondary influence of the fine grains, Thevanayagam (2000) modified e_c into a new contact density index at $FC<FC_{th}$ given by:

$$(e_c)_{eq} = \frac{e+(1-b)fc}{1-(1-b)fc}; \qquad 0<b<1 \qquad (2.5)$$

where $(e_c)_{eq}$ = equivalent intergranular void ratio, b = contribution factor for fine grains, and f_c=FC/100.

Similar arguments were made in order to incorporate the reinforcement effects of coarser grains at $FC_{th}<FC<FC_L$. An approximate expression for equivalent interfine void ratio $(e_f)_{eq}$ was shown to be of the form (Thevanayagam 2000):

$$(e_f)_{eq} = \frac{e}{fc+\frac{1-fc}{R_d^m}} < e_f; \qquad 0<m<1 \qquad (2.6)$$

where R_d=D/d, D=particle diameter of coarser grain, d=particle diameter of fine grain, and m = a coefficient that depends on grain characteristics and packing.

2.2 Energy Loss in Granular Media

The technical articles presented in Sec.5.3 present the details of this work. According to thermodynamic laws, the energy dissipated into a soil system up to liquefaction should have been either transformed or used by the system. Thus, the dissipated energy E (per unit volume) up to liquefaction could be equalized as given below:

$$E = W + P - I \qquad (2.7)$$

where E = dissipated (supplied) energy, W = internal frictional energy loss, P = energy stored due to pore pressure increase, and I = energy released from internal force chains. All the energy terms are defined for a unit volume of soil. A complete quantification of each energy term is still far from grasp. It is assumed quantitatively that the weights of P and I in comparison with W are negligible.

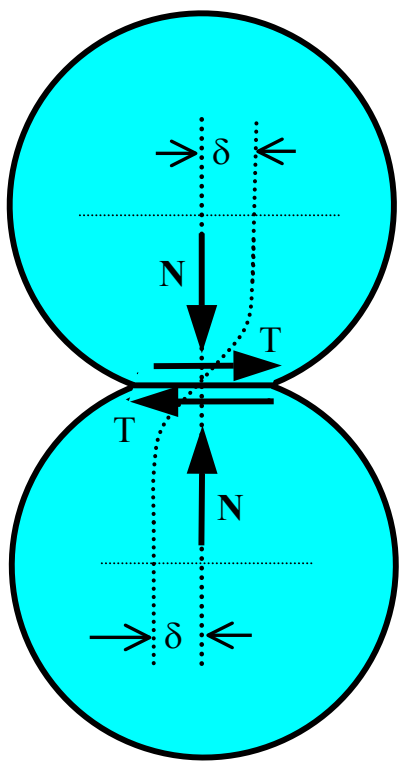

Fig. 2.4 Two Equal Size Elastic Spheres in Contact

An expression could be derived from fundamentals to quantify W for a regular array of uniform spherical particles. Fig.2.4 shows a contact between two equal size spherical particles with constant contact normal force N. For a magnitude of incremental slip Δδ along the contact plane, the incremental frictional energy loss is given by:

$$\Delta W = \frac{1}{2} \mu^* N (\Delta \delta) \qquad (2.8)$$

where ΔW = frictional energy loss per grain per contact, μ^* = effective contact friction coefficient, N = contact normal force, and Δδ = slip along contact plane.

In a regular array, the contact normal forces between all contacts are not the same, except for a few arrays subjected to isotropic confining stress (Table 2.1). Assuming that the average internal

contact normal force N_{avg} is representative enough for calculating W, Eq. 2.8 could be extended for a granular array of uniform particles. If the granular array has m_g number of grains per unit volume and n_g number of active contacts per grain, then the cumulative internal frictional energy loss W per unit volume could be shown in the form given by:

$$W = \sum [N_{avg}\mu^*(\Delta\delta)(n_g m_g)/2] \tag{2.9}$$

where μ^* = effective contact friction coefficient ($\mu^* \leq \mu$) and μ = contact friction coefficient. For small strains less than a threshold value, a magnitude of $\mu^* < \mu$ should be used to account for mobilization of friction, whereas $\mu^* = \mu$ should be used at large strains to account for full slip. Since N_{avg} is a function of mean effective confining stress σ', Eq. 2.9 could be reduced to the form given by:

$$W = 1.5\sum [\mu^*\sigma'(\Delta\gamma)] \tag{2.10}$$

where $\Delta\gamma$ = incremental shear strain amplitude and σ'= mean effective confining stress $(\sigma_1' + \sigma_2' + \sigma_3')/3$ during the incremental cyclic loading. Table 2.1 shows details of intergrain contact parameters for selected regular granular arrays. Sec.2.4 presents the detailed derivations for each regular array given in Table 2.1. Eq. 2.10 can be adjusted to a suitable form for undrained triaxial conditions as given below:

$$W = \frac{9}{8}\sum_{i=1}^{n-1} [\mu^*(\sigma_i' + \sigma_{i+1}')(\varepsilon_{i+1} - \varepsilon_i)] \tag{2.11}$$

where σ_i' = mean effective confining stress in i^{th} loading increment.

Table 2.1 Intergrain Contact Parameters for Spherical Arrays

Packing	Contact Normal, N	Contact Slips/grain, n_g	Grains/ unit vol., m_g	Void Ratio, e	Energy Loss/ Unit vol., W
SC	$D^2\sigma'$	6	$1/D^3$	0.91	$1.5\sum\mu^*\sigma'\Delta\gamma$
CT	$[D^2/3^{1/2}]\sigma'$ $[3^{1/2}D^2/2]\sigma'$	2; 6	$2/[3^{1/2}D^3]$	0.65	$1.5\sum\mu^*\sigma'\Delta\gamma$
FCC	$[D^2/8^{1/2}]\sigma'$	12	$2^{1/2}/D^3$	0.35	$1.5\sum\mu^*\sigma'\Delta\gamma$
BCC	$[D^2/3^{1/2}]\sigma'$	8	$27^{1/2}/[4D^3]$	0.47	$1.5\sum\mu^*\sigma'\Delta\gamma$

Note: SC=Simple cubic, CT=Cubical-tetrahedral, FCC=Face centered cubic, and BCC=Body centered cubic.

2.3 Effective Intergrain Friction Coefficient

If two identical solid elastic spheres are in contact under the action of contact normal force N and tangential force acting along the contact T (Fig. 2.4), assuming Hertian contact, the relative tangential displacement along the contact plane is given by (Mindlin and Deresiewicz 1953):

$$\delta = \frac{3\mu N(2-\nu)\left[1-\left(1-\mu^{*}/\mu\right)^{2/3}\right]}{16Ga} \tag{2.12}$$

where ν = Poisson's ratio of solid, G = shear modulus of solid, $a = [3(1-\nu)ND/16G]^{1/3}$ = contact radius, D = particle diameter, μ = full-slip contact friction coefficient, and μ^{*}=T/N=effective contact friction coefficient. The magnitude of slip is governed by elastic properties of solids, contact friction, and confining stress. During loading, μ^{*} increases and reaches μ at full slip.

The relative tangential slip along the contact plane δ can be related to shear strain γ and then to axial strain ε under undrained triaxial conditions by:

$$\gamma = 1.5\varepsilon = 2\delta / D \tag{2.13}$$

The mobilized friction μ^{*} may be expressed as a function of shear strain γ:

$$\mu^{*} = \mu\left[1-\left(1-\frac{16\,GDa\,\gamma}{3(2-\nu)\mu N}\right)^{3/2}\right] \tag{2.14}$$

$$\mu^{*} = \mu\left[1-\left(1-\frac{4G[3(1-\nu)/2G]^{1/3}}{3(2-\nu)\mu}\left(\frac{D^{2}}{N}\right)^{2/3}\gamma\right)^{3/2}\right] \tag{2.15}$$

where N/D^2 is proportional to σ', and is dependent on packing (Table 2.1). Hence, the mobilized friction depends on strain level, shear modulus of solid, confining stress, and packing (Table 2.1).

2.4 Energy - Intergrain Contact Parameter Relations

The expression for the internal frictional energy loss W per unit volume is derived from fundamentals assuming that the average internal contact normal force N_{avg} in a granular array is representative enough for calculating W (Eq. 2.16). The application of above expression to ideal packings of uniformly sized spheres reduced the expression to the form given in Eq. 2.17.

$$W = \sum [N_{avg}\mu^{*}(\Delta\delta)(n_g m_g)/2] \tag{2.16}$$

$$W = 1.5\sum [\mu^{*}\sigma'(\Delta\gamma)] \tag{2.17}$$

where, N_{avg} = average internal contact normal force, μ^{*} = effective contact friction coefficient ($\mu^{*} \leq \mu$), μ = contact friction coefficient, $\Delta\delta$ = slip along contact plane, m_g = number of grains per unit volume, n_g = number of active contacts per grain, $\Delta\gamma$ = incremental shear strain

amplitude, and σ' = mean effective confining stress. The intergrain contact parameters and the derivation of Eq. 2.17 are presented next in detail for selected ideal packings (a) simple cubic, (b) cubical-tetrahedral, (c) face centered cubic, and (d) body centered cubic.

(a) Simple Cubic Packing

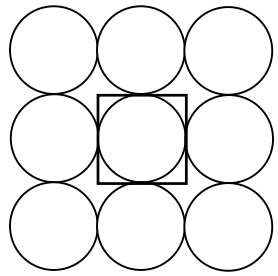

Fig. 2.5 Simple Cubic Packing

Consider a spherical particle and its spatial representative block in the above packing. In this case, the spatial representative block is a cube with dimensions D $\times$ D $\times$ D, where D is the diameter of the sphere.

$n_g = 6$

$m_g = 1/D^3$

$\Delta\delta = D\Delta\gamma/2$

Void ratio, e $= (D^3 - \Pi D^3/6)/(\Pi D^3/6)$

$= 0.91$

If the packing experiences a mean effective pressure of σ', the equilibrium of the representative block gives:

$N_{ave} = D^2\sigma'$

Substitute the above parameters in Eq. 2.16:

$W = \sum[(D^2\sigma').\ \mu^*.\ (D\Delta\gamma/2).\ 6.\ (1/D^3)/2]$

$= 1.5\sum[\mu^*\sigma'\ \Delta\gamma]$

(b) Cubical-Tetrahedral Packing

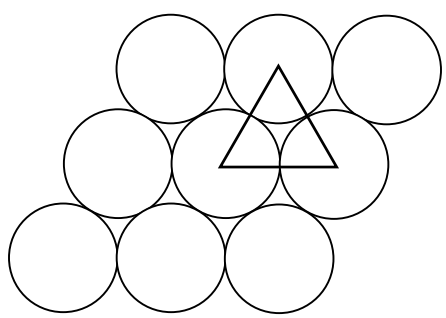

Fig. 2.6 Cubical-Tetrahedral Packing

Consider a spherical particle in the above packing.

$n_g = 8$

The spatial representative block is a cubical-tetrahedral with edge lengths D.

Volume of the representative block $= (D^3 \sin 60)/2$
Portion of the sphere within the block $= 0.5$

$$m_g = 0.5/[(D^3 \sin 60)/2]$$
$$= 2/[3^{1/2} D^3]$$

Void ratio, e $= [(D^3 \sin 60)/2 - \Pi D^3/12]/(\Pi D^3/12)$
$= 0.65$

$$\Delta\delta = D\Delta\gamma/2$$

If the packing experiences a mean effective pressure of σ', the equilibrium of the representative block gives:
Contact normal force, N_1 (perpendicular to the sheet) $= [3^{1/2} D^2/2]\sigma'$
Contact normal force, N_2 (parallel to the sheet) $= [D^2/3^{1/2}]\sigma'$
The ratio of contact normal forces N_1 and N_2 acting in each sphere is 2:6.

$$N_{ave} = [3^{3/2} D^2/8]\sigma'$$

Substitute the above parameters in Eq. 2.16:

$$W = \sum [(3^{3/2} D^2/8)\sigma'. \mu^*. (D\Delta\gamma/2). 8. [2/(3^{1/2} D^3)]/2]$$
$$= 1.5\sum[\mu^* \sigma' \Delta\gamma]$$

(c) Face Centered Cubic Packing

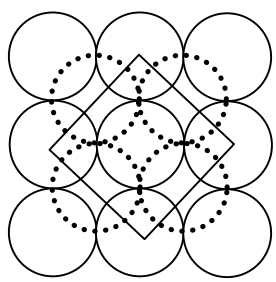

Fig. 2.7 Face Centered Cubic Packing

Consider a spherical particle in the above packing.

$$n_g = 12$$

The spatial representative block is a cube with dimensions $2^{1/2}D \times 2^{1/2}D \times 2^{1/2}D$, where D is the diameter of the sphere.
Volume of the representative block $= [2^{1/2} D]^3$
Number of spheres within the block $= 4$

$$m_g = 2^{1/2}/D^3$$

Void ratio, e $= [(2^{1/2} D)^3 - 2\Pi D^3/3)/(2\Pi D^3/3)$
$= 0.35$

$$\Delta\delta = D\Delta\gamma/2$$

If the packing experiences a mean effective pressure of σ', the equilibrium of the representative block gives:

$$N_{ave} = [D^2/8^{1/2}]\sigma'$$

Substitute the above parameters in Eq. 2.16:

$$W = \sum\{[(D^2/8^{1/2})\sigma']. \mu^*. (D\Delta\gamma/2). 12. (2^{1/2}/D^3)/2\}$$
$$= 1.5\sum[\mu^* \sigma' \Delta\gamma]$$

(d) Body Centered Cubic Packing

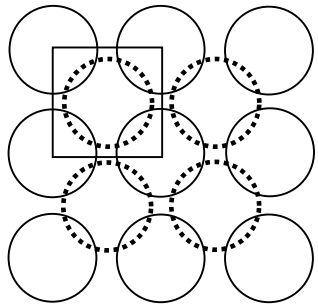

Fig. 2.8 Body Centered Cubic Packing

Consider a spherical particle in the above packing.

$n_g = 8$

The spatial representative block is a cube with dimensions $2D/3^{1/2} \times 2D/3^{1/2} \times 2D/3^{1/2}$, where D is the diameter of the sphere.

Volume of the representative block $= [2D/3^{1/2}]^3$

Number of spheres within the block $= 2$

$m_g = 27^{1/2}/[4D^3]$

Void ratio, e $=[(2D/3^{1/2})^3 - \Pi D^3/3]/(\Pi D^3/3)$

$= 0.47$

$\Delta\delta = D\Delta\gamma/2$

If the packing experiences a mean effective pressure of σ', the equilibrium of the representative block gives: $N_{ave} = [D^2/3^{1/2}]\sigma'$

Substitute the above parameters in Eq. 2.16:

$$W = \sum \{[(D^2/3^{1/2})\sigma']. \mu^*. (D\Delta\gamma/2). 8. [27^{1/2}/(4D^3)]/2\}$$

$$= 1.5\sum[\mu^*\sigma' \Delta\gamma]$$

3.0 Experimental Study

3.1 Experimental Program

More than 150 undrained monotonic, and about 75 stress controlled cyclic triaxial compression tests were conducted to study the behavior of clean sand, non plastic-silt and their mixes. Three different sands and a silt were used to prepare the granular mixes. Most of the specimens were prepared using moisture tamping method and saturated until the B-values (ratio of increase in pore pressure to increase in cell pressure = $\Delta u/\Delta\sigma_c$) were typically greater than 0.95. The saturated specimens were then isotropically consolidated to 100 kPa or 400 kPa constant effective confining pressure. Strain controlled monotonic undrained triaxial compression tests were done at a strain rate of 0.6% per minute. Stress controlled undrained cyclic loading was carried out at a frequency of 0.2 Hz or 1 Hz. During cyclic loading phase, each specimen reached an axial strain of ±8%, which was the limit of the apparatus used, with a cyclic stress ratio (CSR) of nearly 0.1, 0.2, or 0.3.

3.2 Materials

The experimental program involved undrained monotonic and cyclic triaxial tests on three sands (OS#55, FJ#80, and WG) and sand-silt mixes prepared by mixing the above sands with a non-plastic silt [Sil co sil #40 (GSF#40), US Silica Company, Illinois]. The OS#55 sand-silt mixes at silt contents of 0%, 15%, 25%, 60%, and 100% by dry weight are named OS-00, OS-15, OS-25, OS-60, and OS-100, respectively. The FJ#80 sand-silt mixes containing 0%, 25%, and 60% silt are termed FJ-00, FJ-25, and FJ-60, respectively. Similarly the WG sand-silt mixes containing 0%, 25%, and 60% are termed WG-00, WG-25, and WG-60 respectively. Table 3.1 summarizes the index properties of all the soils tested, while Figs. 3.1, 3.2, and 3.3 show the gradation curves of these soils.

Other available data on monotonic and cyclic behavior of silty sands and gravelly sands from the published literature (e.g. Figs.3.4-6) was also collected providing a large database of very broad range of gradation, grain size, shape, angularity, etc. This combined database of new and existing data is continually being updated and analyzed.

Table 3.1 Index Properties of Soils

Properties	OS#55 Sand - Silt Mixes						FJ#80 Sand - Silt Mixes			WG Sand - Silt Mixes	
	OS-00	OS-15	OS-25	OS-40	OS-60	OS-100	FJ-00	FJ-25	FJ-60	WG-00	WG-25
FC (%)	00	15	25	40	60	100	00	25	60	00	25
e_{max}	0.800	0.75	0.86	1.070	1.35	2.10	0.935	-	-	-	-
e_{min}	0.608	0.428	0.309	0.330	0.413	0.627	-	-	-	0.432	-
D_{10} (mm)	0.16	0.018	0.009	0.005	0.003	0.002	0.109	0.007	0.003	0.115	0.008
D_{30} (mm)	0.22	0.19	0.15	0.025	0.01	0.006	0.143	0.095	0.01	0.182	0.105
D_{50} (mm)	0.25	0.235	0.23	0.185	0.029	0.01	0.179	0.135	0.029	0.320	0.200
D_{60} (mm)	0.27	0.245	0.24	0.22	0.07	0.015	0.198	0.167	0.070	0.420	0.300
C_u	1.69	13.61	28.24	46.81	25.93	10.00	1.82	23.86	25.93	3.65	40.00
C_c	1.12	8.19	11.03	0.60	0.53	1.60	0.95	7.72	0.53	0.69	4.90

e_{min} = minimum void ratio (ASTM D1557), e_{max} = maximum void ratio (ASTM D4254 method C), $C_u = D_{60}/D_{10}$, and $C_c = D_{30}^2/(D_{10}D_{60})$.

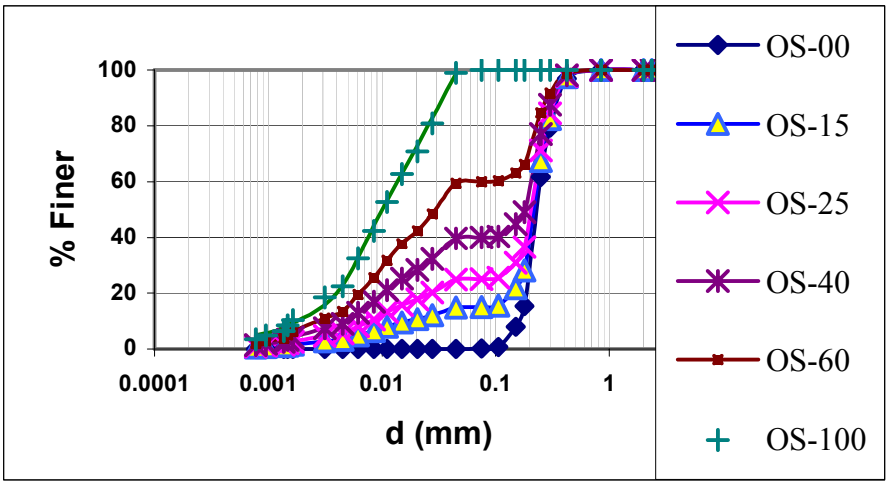

Fig. 3.1 Particle Size Distribution of OS#55 Sand - Silt Mixes

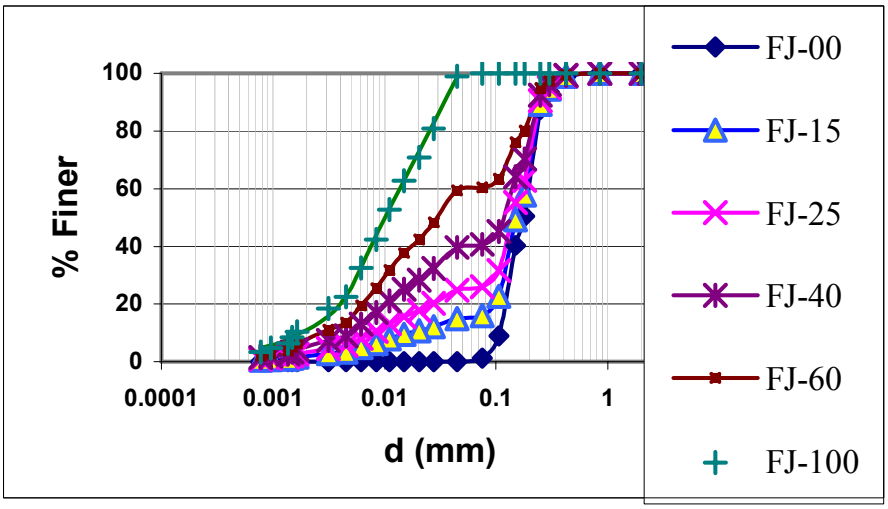

Fig. 3.2 Particle Size Distribution of FJ#80 Sand - Silt Mixes

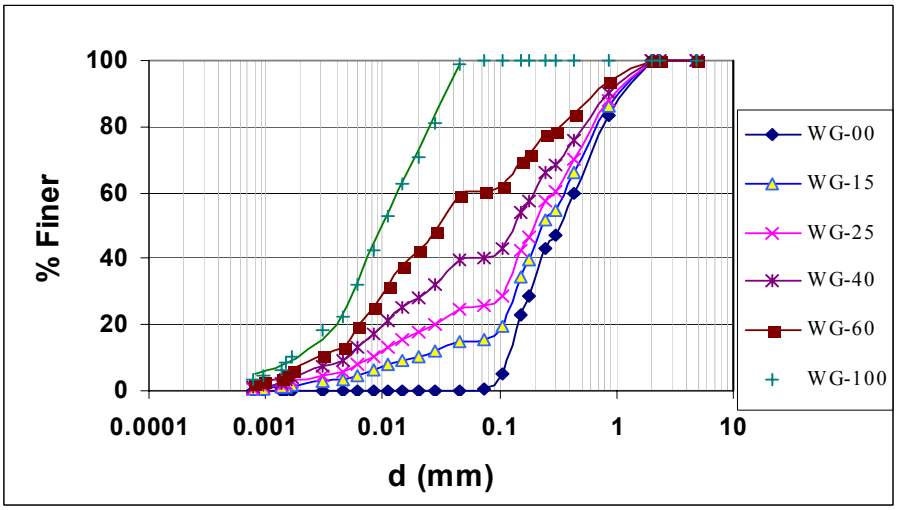

Fig. 3.3 Particle Size Distribution of WG Sand - Silt Mixes

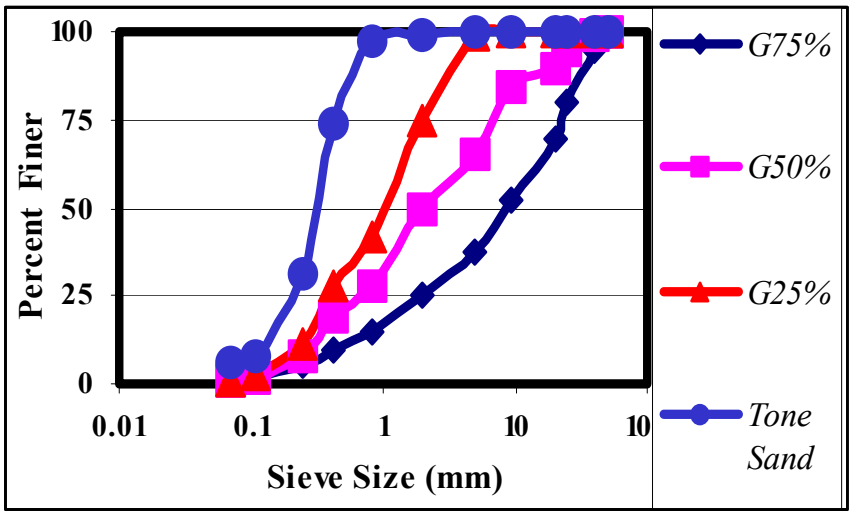

Fig. 3.4 Particle Size Distribution of Tone Sand-Gravel Mixes

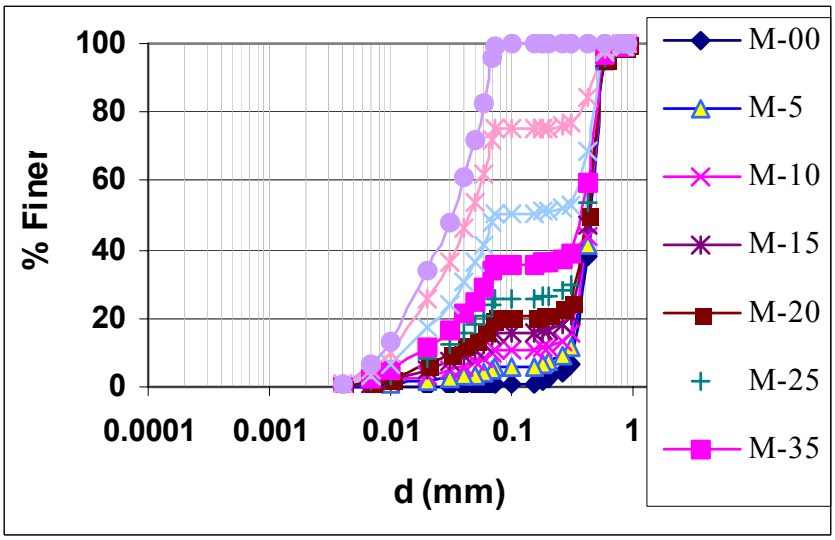

Fig. 3.5 Particle Size Distribution of Monterey Sand-Yatesville Silt Mixes

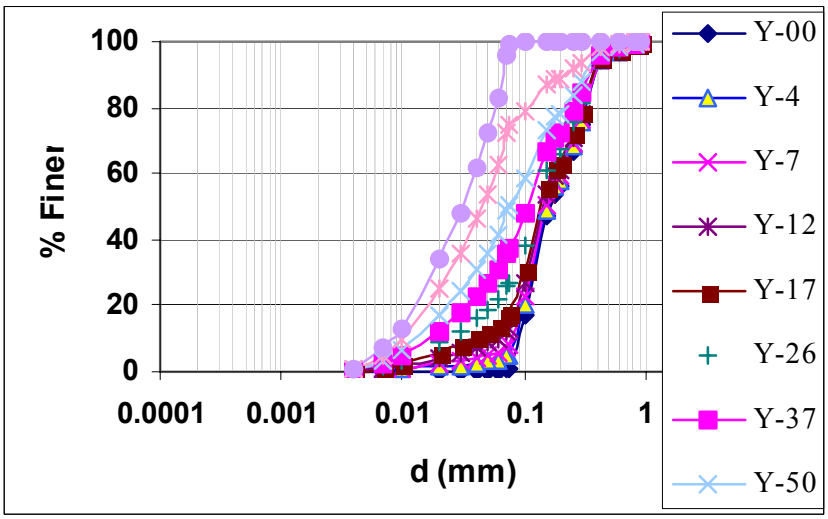

Fig. 3.6 Particle Size Distribution of Yatesville Sand-Yatesville Silt Mixes

3.3 Apparatus

The triaxial testing for this study was performed on an automated triaxial system (Model No: 01-50-KJ-2HXL-TS) designed by GEOCOMP Corp., MA (Fig. 3.7). Figure 3.8 shows a schematic diagram of the apparatus. The typical dimensions of a specimen were 74.3 mm diameter and 150-160 mm height. The system software performs a wide variety of functions including backpressure saturation, B check, isotropic consolidation, and monotonic/cyclic loading automatically. First, the manually saturated specimen is mounted on the machine and the input parameters for each step are set. Then the machine carries out the test in the predefined order. Some of the monotonic tests were conducted on another triaxial machine, GDS, which was manufactured by GDS Instruments Ltd., England. The typical dimensions of a soil specimen tested on GDS were 38 mm diameter and 80 mm height.

Fig. 3.7 GEOCOMP Triaxial Apparatus

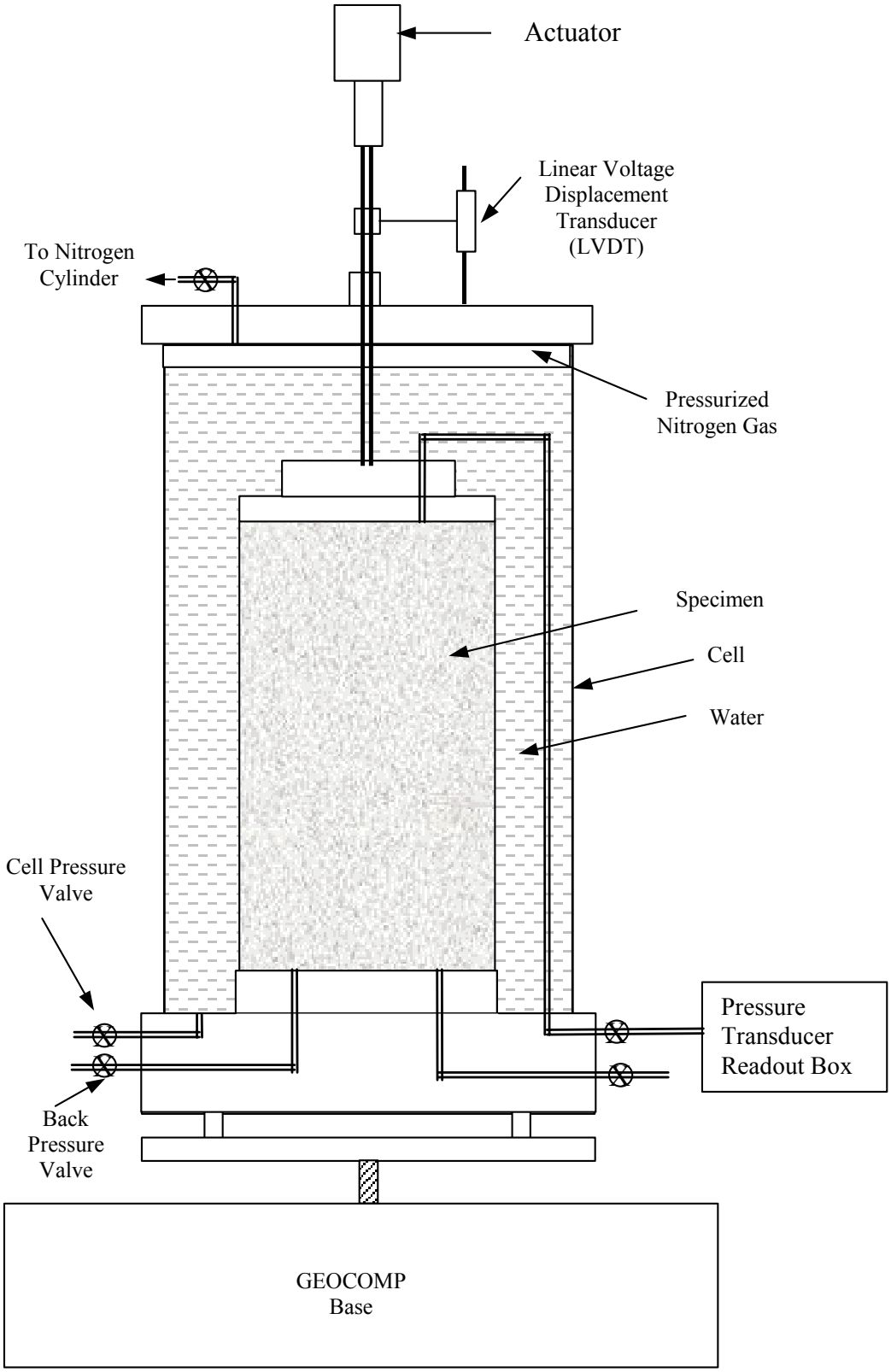

Fig. 3.8 Schematic Diagram of the GEOCOMP Triaxial Apparatus

3.4 Test Procedure

Each test consisted of the following steps:

- Specimen preparation
- Initial saturation at a pressure panel
- Mounting on GEOCOMP loading frame or GDS apparatus
- Final saturation
- Consolidation
- Monotonic shearing or cyclic loading
- Data Reduction and Interpretation

The procedures followed for each of these steps are described in the following sections.

3.4.1 Specimen Preparation

3.4.1.1 Mixing

Weights of finer grain and coarser grain materials were calculated based on the desired fines content of the mix. Both soils were put into a container, and mixed thoroughly until there was no obvious color difference and no segregation to have a uniform soil mix.

3.4.1.2 Dry Pluviation Method

Placement: Each specimen was prepared at a specific target void ratio. The weight of the dry solids required to reach this void ratio was calculated based on the prospective dimensions of the specimens [height (182mm) and inner diameter (74.3mm) of the mold (Evanston Soiltest Equipment P - 41), the height of the base of the triaxial cell (25mm), and thickness of membrane (0.25mm), Figs. 3.9 and 3.10]. In order to obtain the target void ratio, it was deemed necessary to start with a slightly higher void ratio to allow for possible densification during wetting, saturation, and consolidation (However, sometimes after consolidation the resulted void ratio could be much lower than the expected void ratio for silty sand specimens especially when a loose status was targeted). First, vacuum grease (Dow Corning, ELE Soiltest Material G – 282, Fig. 3.9) was applied along the split edges of the mold. Then the two parts of the mold were attached together firmly, which were strengthened by two aluminum C-clamps. A latex membrane (0.25 mm thick, ELE Soiltest Material T - 1287) was placed inside the mold and wrapped out around the circular edges using rubber O-rings (Figs. 3.9 and 3.10). A vacuum pressure of 10 to 15 kPa was applied to the mold to hold the membrane tightly to the inside wall of the mold. The triaxial cell and the tubes were flushed and saturated with deaired water. Then the mold was placed on the triaxial base. The targeted height of the specimen was divided into four equal ones. The dry solids then were divided into four equal weights and poured into the mold, in four equal layers, using a funnel held about 2 to 3 cm above the top surface of each layer. Each layer was compacted gently by a wooden rod (weight = 50 grams, diameter = 2 cm, Fig. 3.9) to reach its target height. The number of blows needed for the compaction of each layer varied depending on the target void ratio. No blows were needed for very loose specimens, whereas usually more than 20-30 blows were needed for dense specimens.

Fig. 3.9 Metal Mold, Wooden Rod, O-rings and Vacuum Grease

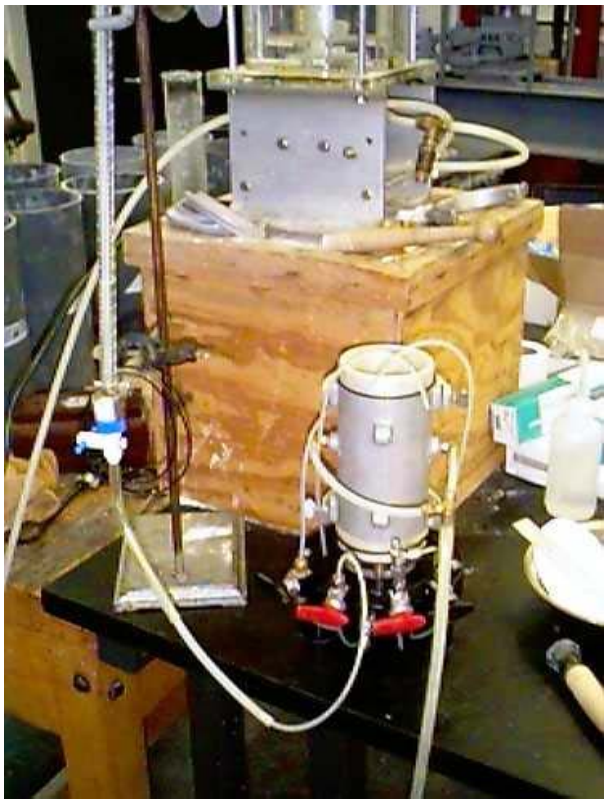

Fig. 3.10 Triaxial Cell Base, Metal Mold and Membrane

Wetting: While the soil was still inside the mold and the top of the soil still exposed to air, deaired water was introduced into the specimen from the bottom of the triaxial test cell. This was done until the top surface of the soil became very wet then recorded the total water introduced to the specimen (The water introduced into the soil was measured and recorded to the accuracy of 0.1 ml). This was accomplished using a standing pipe with the water level higher than the top surface of the specimen. Following that a wetted filter paper and a saturated porous stone were placed on the top of the specimen. And then the sample top cap was placed. Vacuum grease was fully applied around the side face of the top cap. After that the membrane was unwrapped to attach the top cap, and then fastened using rubber O-rings. The plastic tubes used to measure the pore water pressure at the top portion of the specimen during experiment were finally connected to the outlet in the top cap. A vacuum pressure of around 5 kPa was applied for a short period (1 to 2 minutes) to maintain stability of the specimen, and the volume of water extracted during this operation was also recorded. The split sampling mold was removed, and the triaxial cell was placed and sealed with the top triaxial cap. The cell was fully filled with water.

3.4.1.3 Moisture Tamping Method

Placement: The sample preparation using the moisture tamping method was similar to that using dry pluviation except the procedure for placement. A known weight of dry solids required to reach the target void ratio was weighed and mixed thoroughly (until there was no obvious color difference) with a small amount of water at water content of about 4% ~ 7%. The wet weight of the soil was measured. The specimen was prepared in 8 layers compared to 4 in the previous method. In this study this method was used for loose to medium dense soils. Also in silty sand specimen preparation, it was widely used to try to achieve from loose to very dense soil status. Further more, all the specimens for cyclic test were prepared by moisture tamping method in order to eliminate the different fabric effect caused by different specimen preparation method.

Wetting: For the specimen prepared by the moisture tamping method, external wetting was not done. After the specimen reached its target height, the filter paper, porous stone, and the top cap with vacuum greases on sidewall were placed on the top of the specimen. The membrane then was unwrapped from the mold, and the specimen was finally sealed using rubber O – rings.

3.4.2 Initial Saturation at the Pressure Panel

In order to reduce the time required for saturation of the specimen on the apparatus, the initial saturation was done using a pressure panel (Fig. 3.11). Initially a low cell pressure about 30 kPa was applied to confine the specimen. Then the specimen was percolated with carbon dioxide for 5 to 30 minutes with a pressure head difference of about 7 to 14 kPa while the cell confining pressure still at about 30 kPa (to reduce the chance of carbon dioxide finding a path between the specimen side surface and the flexible membrane wall). Carbon dioxide, which is easier to dissolve into water compared to air, helped to drive out and replace the air in the void space of the sample and made the further step of fully saturation of the sample easier. After that, deaired water was allowed to flow from the bottom of the specimen towards the top while the valve for outlet from the top of the specimen was kept open, at this stage, the left small amount of air was driven out and the

carbon dioxide melted in the introduced deaired water. The net volume of the water introduced into the specimen at this "flush out" stage was also measured and recorded accurately. Then the valve connected to the outlet of the specimen top cap was shut off. Then the cell pressure and the pore water pressure were slowly increased simultaneously by the same increments. The effective confining pressure was maintained at about 15 to 20 kPa (2 or 3 psi). Usually this was done over 24 hours period reaching a targeted pressure value. This backpressure was maintained for another 12 to 24 hours. The specimen was nearly saturated at the end of this process.

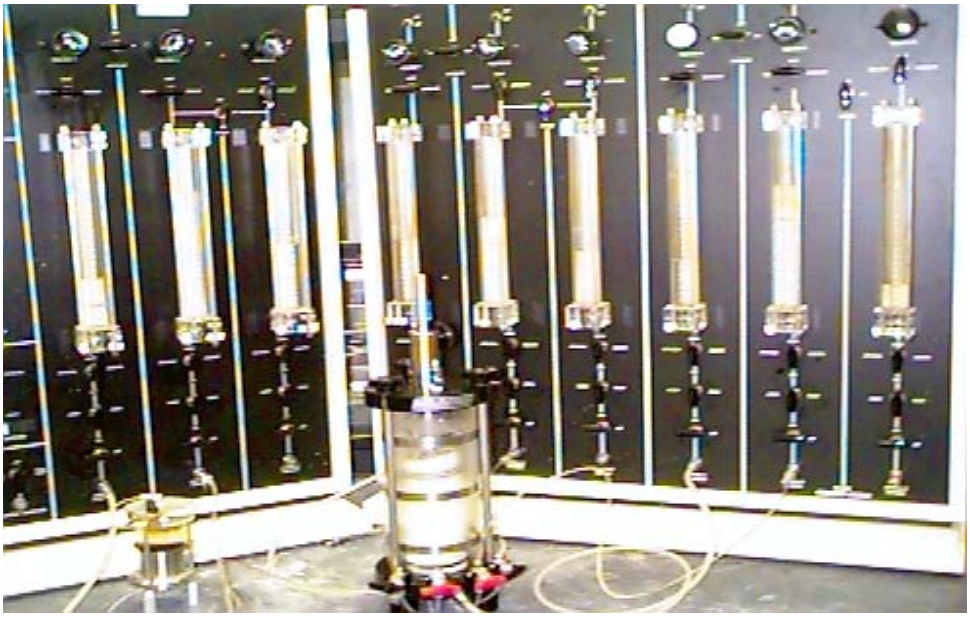

Fig. 3.11 Specimen Saturation at the Pressure Panel

3.4.3 Mounting on GEOCOMP loading frame or GDS apparatus

After the initial saturation, the specimen was mounted on the GEOCOMP triaxial test apparatus. The cell pressure that the specimen was subjected to the Pressure Panel was set as the initialization pressure in the GEOCOMP apparatus. The difference between the sample pressure and the cell pressure, the effective confining pressure, was set as 20 kPa during initialization phase. All the pressure valves to the cell and the specimen were kept closed until the initialization pressure had been reached in the GEOCOMP apparatus. After the set pressures were reached, the volume of water seen on the monitor as introduced to the specimen (which actually was due to the minor expansion of the tubes in the testing system, and need to be subtracted from the total volume of water introduced to the specimen in the final data reduction) was recorded, and then all the pressure valves that connected to the GEOCOMP triaxial system were opened. The lock for the load rod was also released after the GEOCOMP triaxial test system reached the set initialization pressures. The whole system was then let to stay at the set initialized pressure least 20 minutes to stabilize the specimen pressure status. In some cases as much as 40 minutes were needed for silty sand specimen. In case of GDS apparatus, a similar procedure was followed to initiate the test.

3.4.4 Back Pressure Saturation

After the system was stabilized in the initialization phase of the Geocomp triaxial system, the test was set to go automatically into the final saturation phase. During this phase the rate of cell and sample pressure increments were maintained at 7 kPa/min to measure the B ($=\Delta u/\Delta\sigma_c$) factor in a jump of 20 kPa until the B value exceeds 0.95. At that time the specimen can be regarded fully saturated, and then forwarded into consolidation phase. The amount of inflow water into the specimen was recorded automatically with the accuracy of 0.001 ml by the system.

3.4.5 Consolidation

The final isotropic consolidation pressure was set as 100 kPa or 400 kPa for various specimens. The cell pressure was increased in 3 increments (50, 75, 100 kPa or 100, 200, 400 kPa) while keeping the sample pressure at the same value as the final one in saturation phase. After each pressure increment a time period of 20 minutes was given to consolidate clean sand specimens. A longer time, sometimes as much as 120 minutes, was given for some dense silty sand specimens. The outflow volume of water during the consolidation was also measured and recorded automatically at an accuracy of 0.001 ml by the system.

3.4.6 Monotonic Shear Phase

After the specimen reached the targeted isotropic consolidation pressure and fully consolidated, strain controlled undrained triaxial monotonic compression test was automatically done at the strain rate of 0.6 %/min up to an axial strain level of about 20 to 25%. The readings of axial strain and pore water pressure of the specimen, the cell pressure, and the axial loading were automatically recorded by the built in system in the triaxial test apparatus.

3.4.7 Triaxial Cyclic Loading Phase

In cyclic test, once the consolidation phase had been completed, a series of manual operations were needed in order to initiate the cyclic loading on the specimen. First, the LVDT displacement sensor needed to be adjusted to its middle position in order to record the compression and extension displacement of the specimen during cyclic loading. Second, an external pressure source (compressed nitrogen) was introduced to the triaxial cell to maintain the cell pressure at the end of the consolidation while a small amount of water was extracted from the cell to make room for the loading rod which would move in and out of the triaxial cell during cyclic loading. Third, the activated power source for the cyclic loading was switched on. Finally the lower platen of the loading frame was lowered to adjust the specimen to a proper position and then the cyclic stress ratio controlled cyclic loading automatically started. The termination of the cyclic loading can be manual operation, or set by the number of cycles expected, or set by the first reach of a specific axial strain level.

3.5 Data Acquisition

The Geocomp triaxial test system consisted of a LoadTrac load frame, a FlowTrac volume and pressure control unit, sensors, and a computer for test control and data acquisition. Once a soil specimen was in place, and the test conditions selected, the system would run

the entire triaxial test from start to finish (manual manipulation was needed in the cyclic loading phase in a cyclic triaxial test). The test conditions, which controlled the LoadTrac and the FlowTrac, were set through easy-to-use menus TRIAXIAL or CYCLIC, respectively for monotonic or cyclic test.

LoadTrac utilized a high speed, precision stepper motor to apply the vertical load to the soil specimen. A dedicated PC took readings from the force transducer and displacement transducer to control the stepper motor. The system was capable of applying a constant rate of strain or stress at any displacement rates up to 0.1 inch per minute.

FlowTrac utilized two high speed, precision stepper motors with gear reducers to regulate pressure and volume to the cell and to the sample. The same microprocessor that controlled the vertical load controlled these motors as well. Each motor drove a piston in and out of a sealed cylinder. A pressure transducer on the end of the cylinder provided the feedback for the control of pressure. The number of steps of the motor was used to compute volume change. Electronic valves were used to control direction of flow and drainage conditions.

The cyclic component of vertical force was provided by an AMCS ACH4000 motion controller with a D1FH proportional directional control valve, and 2HX electro-hydraulic actuator driven by 10 gpm air-cooled hydraulic pump. The AMCS ACH4000 motion controller was programmed by the PC. The AMCS ACH4000 created the commands necessary to produce a purely sinusoidal cyclic loading, under either stress control or displacement control.

The GEOCOMP apparatus recorded (a) vertical displacement; (b) axial load; (c) triaxial cell pressure; (d) sample pore pressure; (e) volume of water introduced into or out of the cell; and (f) volume of water introduced into or out of the specimen.

Typical data and the procedure used for the calculation of axial strain, deviatoric stress, pore pressure, and the major and minor principal stresses are shown in the following chapter.

3.6 Data Reduction

3.6.1 Monotonic Compression Test

There are two kinds of output files available in Geocomp triaxial test system: the ASC file and the DMP file. The ASC file records the original machined data readings while the DMP file contains the converted actual experimental data by combining the original machined data with corresponding factors. The basic information of an experiment such as the initial information about the tested specimen is recorded in its ASC file. Various files recorded during a typical monotonic or cyclic test are shown below. Figs.4.7 – 4.10 show the results of a typical experiment.

Table 3.2 Typical GEOCOMP Data File of a Monotonic Compression Test

TEST FILE NAME	R080299			Test Date	8/02/99
Specimen Dimensions		Specimen Area		Weights	
D (mm)	73.82	Initial mm^2	4279.9428	Pis+Cap (kN)	0.0049442
H (mm)	156	Shear mm^2	4261.3451	Dry Soil (g)	1016
Loading Rod A (cm^2)	1.238			Tot. Water in (g)	277.108
Fines %	7			e_o	0.723
Ini. Water in (g)	281.7			e_c	0.852
Sample Prep. Method:	MT			e_f	N/A

Phase No.	Step No.	Time msec	Axial Load kN	Axial Disp cm	Cell Press kPa	Back Press kPa	Load Meter UNITS	Cell Vol cu-mm	Sample Vol cu-mm
1	**0**	**3**	**0**	**0.0001**	**0.78**	**0.88**	**0**	**0**	**0**
1	0	3	0.01	0.0002	10.54	5.52	0	0	0
1	0	510	0.01	0.0002	10.59	5.51	36	6	-5
1	0	1011	0.01	0.0007	10.96	5.61	76	8	-4
1	0	1517	0.01	0.0015	10.93	7.14	125	15	-6
...	...	...	...	...	...	...	...	...	...
1	**0**	**2953371**	**0.06**	**0.064**	**479.95**	**460.01**	**5143**	**2227**	**-1215**
3	**0**	**2954653**	**0.06**	**0.064**	**479.97**	**459.99**	**5143**	**2227**	**-1215**
3	0	2955160	0.06	0.0641	480.08	460.03	5143	2228	-1215
3	0	2955668	0.06	0.064	479.82	459.97	5143	2230	-1215
3	0	2956172	0.06	0.0641	480.24	459.93	5143	2229	-1215
3	0	2956677	0.06	0.0641	479.8	460.01	5143	2230	-1215
3	0	2957181	0.06	0.064	480.28	459.94	5143	2229	-1215
...	...	...	...	...	...	...	...	...	...
3	**0**	**18926878**	**0.08**	**0.07**	**639.93**	**620.4**	**5440**	**6121**	**-2469**
4	**1**	**18928188**	**0.08**	**0.07**	**639.97**	**620.02**	**5440**	**6121**	**-2469**
4	1	18928698	0.08	0.0699	639.51	619.3	5440	6127	-2469
4	1	18929199	0.08	0.07	640.86	620.59	5440	6129	-2467
...	...	...	...	...	...	...	...	...	...
4	1	20300162	0.08	0.0814	669.99	619.6	6325	9283	9
4	2	20301437	0.08	0.0813	669.88	619.88	6325	9283	9
4	2	20301942	0.08	0.0813	669.65	619.78	6325	9283	9
4	2	20302448	0.08	0.0813	670.13	620.32	6325	9286	9
...	...	...	...	...	...	...	...	...	...
4	2	21639589	0.08	0.0912	694.95	620	7067	11487	1589
4	3	21640857	0.08	0.0911	694.96	619.99	7067	11487	1589
4	3	21641363	0.08	0.0912	693.73	619.73	7067	11487	1589
4	3	21641868	0.08	0.0912	694.73	620.47	7067	11488	1588
...	...	...	...	...	...	...	...	...	...
4	**3**	**22982224**	**0.09**	**0.1002**	**719.98**	**620.02**	**7739**	**13409**	**2953**
5	**1**	**22983492**	**0.09**	**0.1001**	**719.98**	**619.99**	**7739**	**13409**	**2953**
5	1	22989568	0.18	0.1084	721.32	627.85	8450	13414	2953
5	1	22994632	0.23	0.1161	720.42	635.64	9043	13425	2953
5	1	22999784	0.26	0.1237	719.73	641.76	9647	13431	2953
5	1	23005354	0.28	0.132	720.23	647.18	10300	13431	2953
5	1	23010418	0.3	0.1399	718.58	651.3	10893	13430	2953
5	1	23015591	0.31	0.1474	719.62	654.68	11499	13437	2953
...	...	...	...	...	...	...	...	...	...
5	**1**	**25104903**	**0.12**	**3.3736**	**720.55**	**709.09**	**256276**	**9580**	**2953**

Note: Phase No.: 1-initialization, 2-consolidation A, 3-saturation, 4-consolidation B, and 5-shear.
Step Nos. in phase 4: 1-consolidation step A, 2-consolidation step B, 3-consolidation step C

Table 3.3 Monotonic Data Reduction (File: r080299.DMP)

Variable	Equation	Sample Calculation *	Comments
Net amount volume of water introduced after consolidation, V_w	$V_w = V_i - V_t - V_c$	277.1 cm^3	V_i = 281.7 cm^3 V_t = 1.64 cm^3 V_c = 2.95 cm^3
Global void ratio at the end of consolidation, e_o	$e_o = \frac{V_w G_s}{W}$	0.723	G_S = 2.65 γ_w=1g/cm^3 W = 1016.0 g
Height of the specimen after consolidation, H_o	$H_o = H-\delta_i$	155.0 mm	H=156.0mm δ_i =1.0mm
Avg. specimen area after consolidation, A_o	$\frac{W}{G_s}(1+e)\frac{1}{H_o}$	4261.4 mm^2	γ_w=1g/cm^3
Axial strain at shearing phase, ε	$\varepsilon = \frac{\delta-\delta_i}{H_o}$	0.00010	δ (Column in Table 4.4: Axial Disp.)
Area correction at shearing phase, A	$\frac{A_o}{1-\varepsilon}$	4260.4 mm^2	A_o: initial area before consolidation phase
Deviator stress, $\Delta\sigma$	$\sigma_1' - \sigma_3'$	34.02 kPa	
Excess pore pressure, Δu	$u-u_i$	15.65 kPa	
Minor principal stress, σ_3'	$\sigma_3-\Delta u$	84.78 kPa	Initial effective confining stress, σ_3 = 100 kPa
Major principal stress, σ'_1	$\sigma_3'+\Delta\sigma$	118.80 kPa	
Mean effective stress, p'	$\frac{\sigma_1'+2\sigma_3'}{3}$	96.12 kPa	
τ	$\frac{\sigma_1'-\sigma_3'}{2}=\frac{\Delta\sigma}{2}$	17.01 kPa	q = 2*τ
Friction angle, ϕ	$\sin^{-1}\left[\frac{\sigma_1'-\sigma_3'}{\sigma_1'+\sigma_3'}\right]$	22 degree	Also can be obtained by diagram

Note: *= 3th set of readings from Table 3.2 were considered for sample calculations. V_i : initial water in sample before mounting on GEOCOMP apparatus, V_t: tube expanded during final initialization in GEOCOMP apparatus, V_c: water went out of sample during consolidation phase. δ_I: height of specimen decreased after consolidation phase, δ: height decreased during shearing phase, σ_1': effective axial stress of specimen, σ_3': effective

radius stress of specimen, u: back pressure of specimen at shearing phase, u_i: back pressure of specimen at the end of consolidation phase.

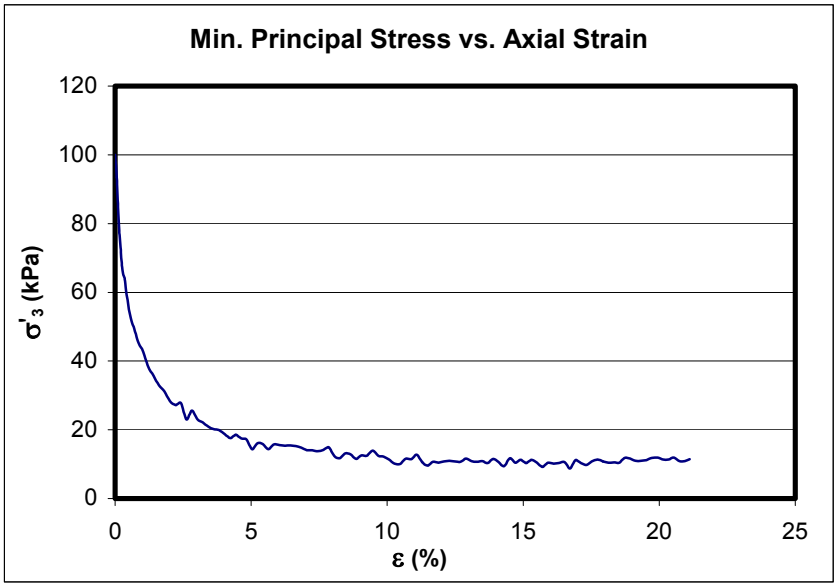

Fig. 3.12 Sample Results: Minor Principal Stress vs. Axial Strain

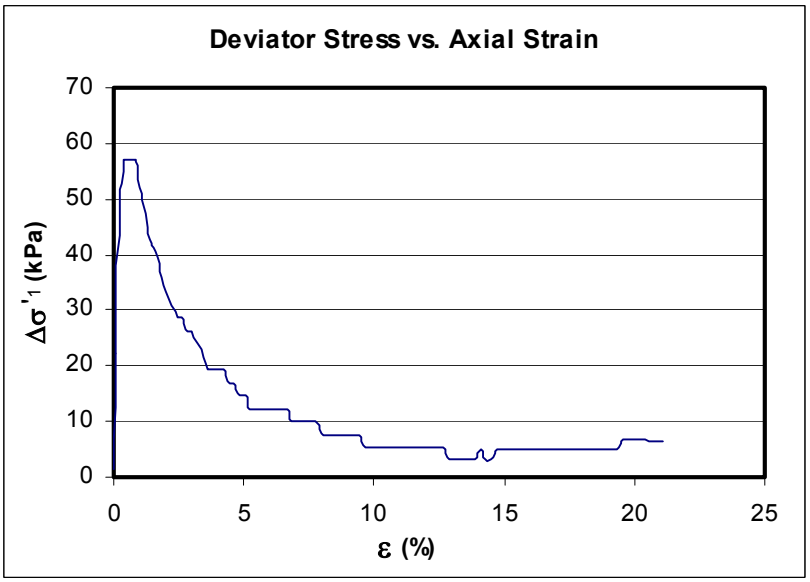

Fig. 3.13 Sample Results: Deviatoric Stress vs. Axial Strain

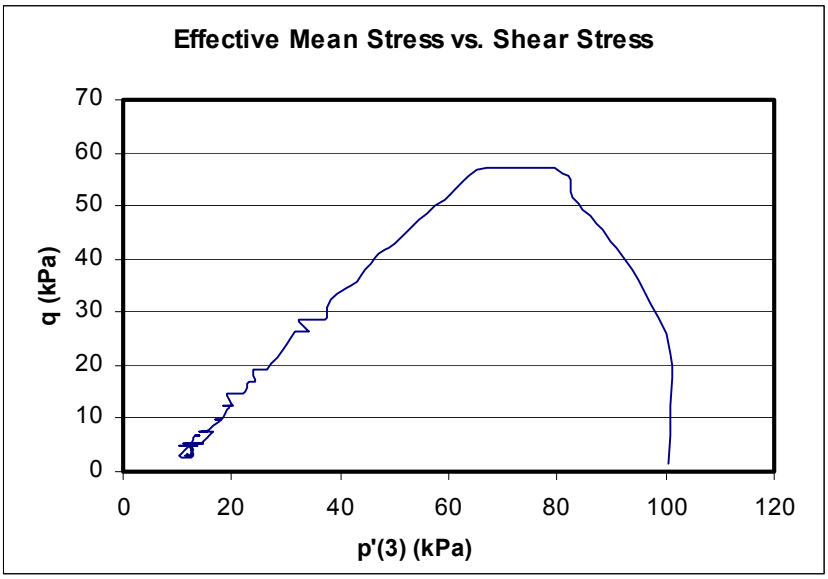

Fig. 3.14 Sample Results: Effective Mean Stress Vs. Deviatoric Strain

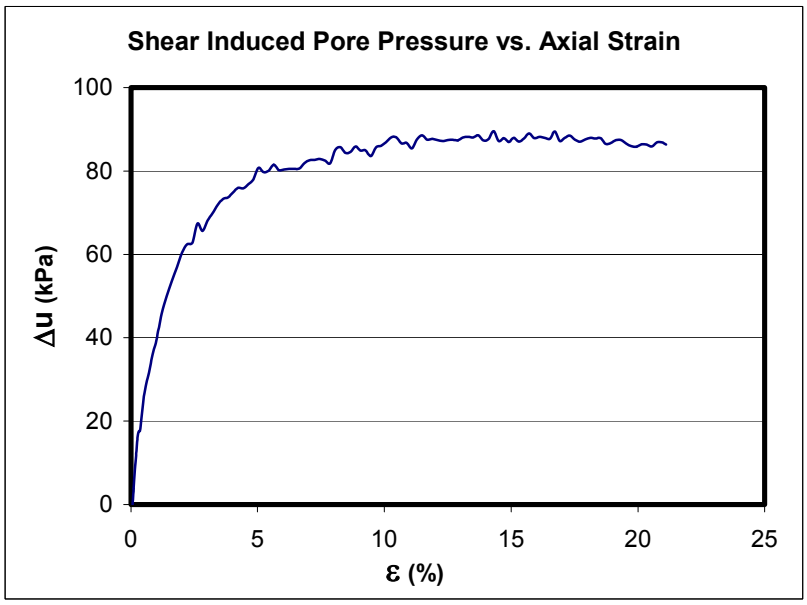

Fig. 3.15 Sample Results: Shear Induced Pore Pressure vs. Axial Strain

3.6.2 Cyclic Test

The major difference between cyclic data file and monotonic data file is that in cyclic test the time interval between two experimental data readings is much shorter (by the definition of the number of readings per cycle before test start) in cyclic loading phase, while in monotonic compression test the time interval between two experimental data readings gradually becomes larger in shearing phase. In cyclic test 25 readings are taken per cycle during cyclic loading phase. Table 3.4 shows data file a typical cyclic test. Table 3.5 is the summary information table about this cyclic test. Figs. 3.16-3.21 present the results such as

the number of cycles versus axial strain, the pore water pressure generation versus the number of cycles, etc for this cyclic test.

Table 3.4 Data Reduction (File: c120199.DMP)

Phase	Step	Time	Load	Disp	Cell	Sample	Load Mtr	Cell Pstn	Samp Pstn	Servo
No.	No.	msec	kN	cm	kPa	kPa		mm^3	mm^3	V
1	0	0	0.01	0	-1.49	2.07	0	0	0	-0.503
1	0	1003	0.01	-0.0004	-1.46	2.12	6	0	0	-0.503
…	…	…	…	…	…	…	…	…	…	…
1	0	1910894	0.04	0.006	330.17	310.3	719	265	-338	-0.503
3	0	1912061	0.04	0.0067	330.19	310.32	719	265	-338	-0.503
3	0	1913063	0.04	0.0061	330.39	310.44	758	265	-338	-0.503
…	…	…	…	…	…	…	…	…	…	…
3	0	2187425	0.04	0.0064	349.81	329.83	740	652	-365	-0.503
4	1	2188722	0.04	0.0062	350.05	329.87	740	652	-365	-0.503
4	1	2189725	0.04	0.0067	349.71	330.1	766	652	-365	-0.503
…	…	…	…	…	…	…	…	…	…	…
4	1	3342761	0.04	0.0181	379.48	329.96	1639	2717	1071	-0.503
4	2	3343899	0.04	0.0186	379.52	330.04	1639	2717	1071	-0.503
4	2	3344901	0.05	0.0182	379.48	330.22	1649	2717	1071	-0.503
…	…	…	…	…	…	…	…	…	…	…
4	2	4501456	0.05	0.0272	404.35	330.25	2328	4292	2055	-0.503
4	3	4502594	0.04	0.0275	404.39	330.26	2328	4292	2055	-0.503
4	3	4503597	0.05	0.0271	404.56	330.13	2279	4292	2055	-0.503
…	…	…	…	…	…	…	…	…	…	…
4	3	5703768	0.05	0.0356	429.48	329.77	2975	5753	2905	-0.503
5	0	6150608	0.08	0.0365	428.67	331.61	0	33665	202	-0.132
5	0	6150807	0.09	0.0363	428.8	332.36	0	33950	-40	0.168
5	0	6151006	0.13	0.038	428.71	335.25	0	34217	3	0.146
5	0	6151205	0.16	0.0392	428.88	338.08	0	34449	-21	0.159
5	0	6151404	0.19	0.0408	428.64	341.5	0	34632	-7	0.151
5	0	6151604	0.21	0.0432	428.67	344.9	0	34755	0	0.149
…	…	…	…	…	…	…	…	…	…	…
5	0	6220458	0.05	-1.2291	431.59	429.92	0	33447	196	-2.585
5	0	6220656	0.05	-1.2291	431.5	430.04	0	33731	-84	0.894
5	0	6220855	0.06	-0.1838	435.79	436.08	0	34013	-268	3.181
5	0	6221054	0.07	1.298	442.17	441.68	0	34273	-487	4.998
5	0	6221253	0.06	1.2976	439.34	439.29	0	34495	-758	4.998
5	0	6221452	0.07	1.2978	438.65	438.87	0	34666	-891	4.998

Table 3.5 Summary Information Table (Test: c120199)

Specimen ID	**OSC-6**
Date	12/1/1999
File name	c120199
Soil Type	100% F55
	0% Sil-Co-Sil # 40
Fines Content (%)	0
Sample Preparation	MT

Density Parameters		
Total void ratio (e)	0.699	*(w/100)*Gs*
Intergranular void ratio (e_c)	0.699	*(e+FC)/(1-FC)*
Interfine void ratio (e_f)	n.a.	*e/(FC)*
e_{max}	0.800	
e_{min}	0.600	
Relative density	51	*%*

Specimen Informations

Height (h)	16.00	*cm*
Diameter (d)	7.37	*cm*
Specimen dry weight	1083.20	*g*

Cross Section ($A=\pi/4*d^2$)	42.66	cm^2
Volume (V = A * h)	682.57	cm^3
Specific Gravity (G_s)	2.65	

Initialization Parameters

Cell pressure	330	*kPa*
Sample pressure	310	*kPa*
Cell volume change		*ml*
Sample volume change		*ml*
Pressure rate		*kPa/min*

Consolidation Phase

Final cell pressure	430	*kPa*
Final sample pressure	330	*kPa*
Effective isotropic stress	100	*kPa*
Final cell volume change	5.753	*ml*
Final sample volume change	2.905	*ml*
Final displacement	0.036	*cm*

Saturation Parameters

Water in (manual)	47.9	*ml*
Water in (pressure panel)	292.8	*ml*
Water in (triaxial)	-2.9	*ml*
Water out	52.1	*ml*
Total water in	285.7	*ml*
Water content (w)	26.4	*%*
Final cell pressure	450	*kPa*
Final sample pressure	430	*kPa*
Final cell volume change	4.615	*ml*
Final sample volume change	-1.816	*ml*
Final displacement	0.001	*cm*
Final B value	0.920	
Cell pressure increment	30	*kPa*

Cyclic Parameters

Cyclic stress ratio	0.2	
Cyclic period	0.083	*min*
Cyclic frequency	0.2	*Hertz*
Max axial strain	8	*%*

Number of cycles required to reach liquefaction		$\Delta u/\sigma_{vo}$
Axial strain - $\varepsilon = 1$ %	4	0.7
Axial strain - $\varepsilon = 2.5$ %	5	1
Axial strain - $\varepsilon = 5$ %	6	1

Remarks

- Negative sample volume change means water in. Positive cell volume change means water in.

- Positive displacement means compression, negative displacement extension.

Table 3.6 Interpreted Data (Test: c120199)

Cycles	Strain %	Deviator Stress	Pore Pressure	Shear induced Pore Pres.	Conf. Stress	Shear Stress	Effective mean stress	Ratio
No.	ε	$\Delta\sigma_1$ (kPa)	Δu (kPa)	$\Delta u(sh)$ (kPa)	σ'_3 (kPa)	τ (kPa)	p'(3) (kPa)	$\Delta u/\sigma'_{vo}$
0.000	0.000	0.000	0.00	0.00	100	0.000	100.000	0.000
0.040	0.006	6.912	2.65	0.35	97.35	3.456	99.654	0.003
0.080	0.004	9.216	3.27	0.20	96.73	4.608	99.802	0.002
0.120	0.015	18.429	6.25	0.11	93.75	9.215	99.893	0.001
0.159	0.023	25.338	8.91	0.46	91.09	12.669	99.536	0.005
0.199	0.033	32.245	12.57	1.82	87.43	16.123	98.178	0.018
0.239	0.048	36.846	15.94	3.66	84.06	18.423	96.342	0.037
0.279	0.054	41.449	18.38	4.56	81.62	20.725	95.436	0.046
0.319	0.058	43.750	19.75	5.17	80.25	21.875	94.833	0.052
0.359	0.056	36.843	18.27	5.99	81.73	18.422	94.011	0.060
0.398	0.050	25.331	15.64	7.20	84.36	12.666	92.804	0.072
0.438	0.048	23.029	16.61	8.93	83.39	11.514	91.066	0.089
0.478	0.049	18.423	14.96	8.82	85.04	9.211	91.181	0.088
0.518	0.036	4.606	10.53	8.99	89.47	2.303	91.005	0.090
0.557	0.029	-4.607	8.35	9.89	91.65	-2.303	90.114	0.099
0.597	0.025	-11.517	7.16	11.00	92.84	-5.759	89.001	0.110
0.637	0.021	-13.821	6.74	11.35	93.26	-6.910	88.653	0.113
0.677	0.011	-27.645	3.78	12.99	96.22	-13.822	87.005	0.130
0.717	-0.010	-34.563	3.4	14.92	96.6	-17.282	85.079	0.149
…	…	…	…	…	…	…	…	…
14.010	-7.904	0.000	98.04	98.04	1.96	0.000	1.960	0.980
14.050	-7.904	0.000	98.25	98.25	1.75	0.000	1.750	0.983
14.089	-1.371	2.336	100	99.22	0	1.168	0.779	0.992
14.129	7.890	4.244	99.22	97.81	0.78	2.122	2.195	0.978
14.169	7.888	2.122	99.66	98.95	0.34	1.061	1.047	0.990
14.209	7.889	4.244	99.93	98.52	0.07	2.122	1.485	0.985

Table 3.4 contains a typical cyclic DMP data file. The phase and step numbers here have the same meanings as they appear in the monotonic test except the last phase. While the number 5 in monotonic test represents the monotonic loading (shearing) phase, the number 5 in cyclic test indicates the cyclic loading phase.

Table 3.5 presents all the basic information for this test such as: the name of the test, the file name, the soil type tested, the fines content and the sample preparation method (MT represents Moisture Tamping method, and DP means Dry Pluviation method). All the test parameters (for example the cell pressure, sample back pressure, sample volume change, etc) at the end of each stage are presented as well. Based on the volume of water introduced into the specimen the void ratio of the specimen at the cyclic phase could be calculated.

Table 3.6 shows the test results after the interpretation of the raw data recorded in DMP file. Table 3.7 shows a set of sample calculations in order to obtain the test results in table 3.6 from Table 3.4.

Figure 3.16 displays axial strain versus the number of loading cycles for the sample test C021100a. Figure 3.17 shows the variation of deviatoric stress on the specimen versus the number of loading cycles for the same test. Figure 3.18 and 3.19 describe how the shear induced pore water pressure built up during cyclic loading. Figure 3.20 shows the specimen behavior in the diagram of deviatoric stress versus axial strain. Figure 3.21 is a p'-q diagram (effective mean stress versus deviatoric stress) of the specimen during cyclic loading phase. In a few tests, due to weakening of the specimen during this loading phase, the cyclic stress ratio could not be maintained at 0.2 (e.g. Fig. 3.17). In such cases, the traditional method using the number of cycles to reach liquefaction, and the cyclic stress ratio to describe the cyclic strength of a tested specimen might lead to some error. A more appropriate method would be based on energy approach (ref. Thevanayagam et al. 2002a,b).

Table 3.7 Cyclic Data Reduction

Variable	Equation	Sample Calculation*	Comments
Cycles N	$N = (T-T_i)*f/1000$	N=(6151006-6150408)*0.2/1000 = 0.12	the unit of time in DMP file is msec; T_i=(6150608-200)
Strain %	$\varepsilon = (D-D_i)/H_i*100$	ε = (0.0380-0.0356) *100/ (16-0.0356) =0.015%	$H_i = H_o-D_i$, at the end of consolidation
Deviator Stress, $\Delta\sigma_1$ (kPa)	$\Delta\sigma_1 = (F-F_i)/A_i * (1-\varepsilon/100)$	σ_1= (0.13-0.05) / 43.36*10000*(1-0.015/100)=18.429	F: axial loading including the weight of top cap and rod; A_i: the cross section area at the end of consolidation
Total Pore Pressure ΔU (kPa)	$\Delta u=(p_b-p_{bi}) - (p_c-p_{ci})$	ΔU=(335.25-329.77)-(428.71-429.48) =6.25	p_b: back pressure; p_c: cell pressure; $p_{(b)ci}$: back or cell pressure at the end of consolidation
Shear Induced Pore Pressure $\Delta u_{sh.}$ (kPa)	$\Delta u_{sh.}=(p_b-p_{bi}) - (p_c-p_{ci}) -\Delta\sigma_1/3$	Δu=(335.25-329.77)-(428.71-429.48)-18.429/3=0.11	p_b: back pressure; p_c: cell pressure; $p_{(b)ci}$: back or cell pressure at the end of consolidation
Effective Confining Stress σ_3' (kPa)	$\sigma_3' = \sigma_{vo}' - \Delta U$	σ_3' = 100-6.25 =93.75	σ_{vo}' can be 100 kPa or 400 kPa, depending on the initial effective confining stress
Shear Stress τ (kPa)	$\tau = 0.5*\Delta\sigma_1$	τ = 0.5*18.429 =9.215	$q = 2*\tau = \Delta\sigma_1$
effective mean stress p' (kPa)	$p' = (\Delta\sigma_1+3*\sigma_3')/3$	p' = (18.429+3*93.75)/3 = 99.893	$\Delta\sigma_1=\sigma_1-\sigma_3=(\sigma_1'+\Delta U)-(\sigma_3'-\Delta U) =\sigma_1'-\sigma_3'$
pore pressure generation ratio	$r_u = \Delta u_{sh.}/\sigma_{vo}'$	r_u = 0.11/100 =0.001	σ_{vo}' can be 100 kPa or 400 kPa, depending on the initial effective confining stress

Note: *= the 4th set of data in the sample DMP file has been used to show the above sample calculations, and the results are presented in Table 3.6.

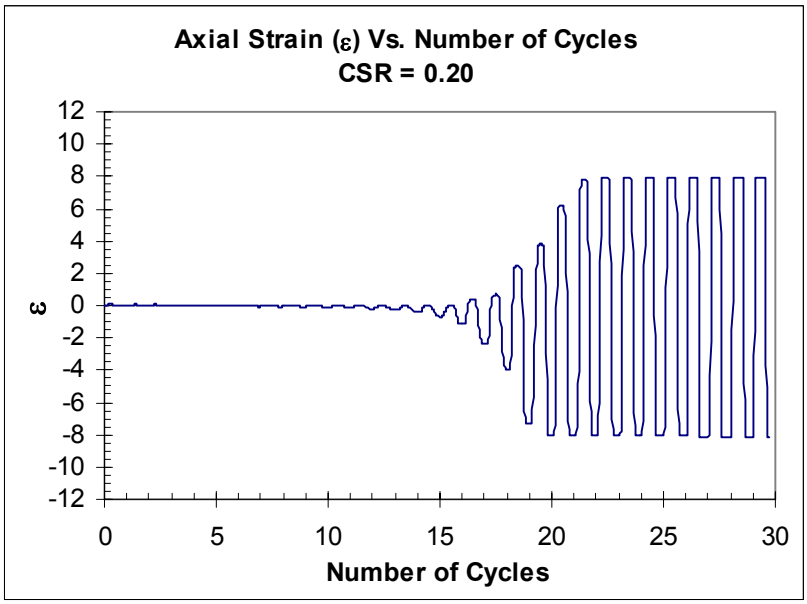

Fig. 3.16 Axial strain versus number of cycles

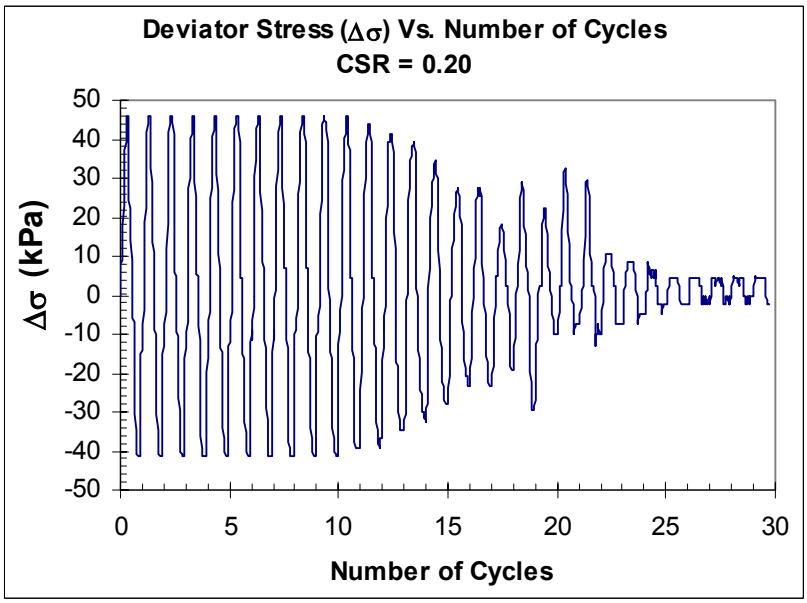

Fig. 3.17 Deviator stress versus number of cycles

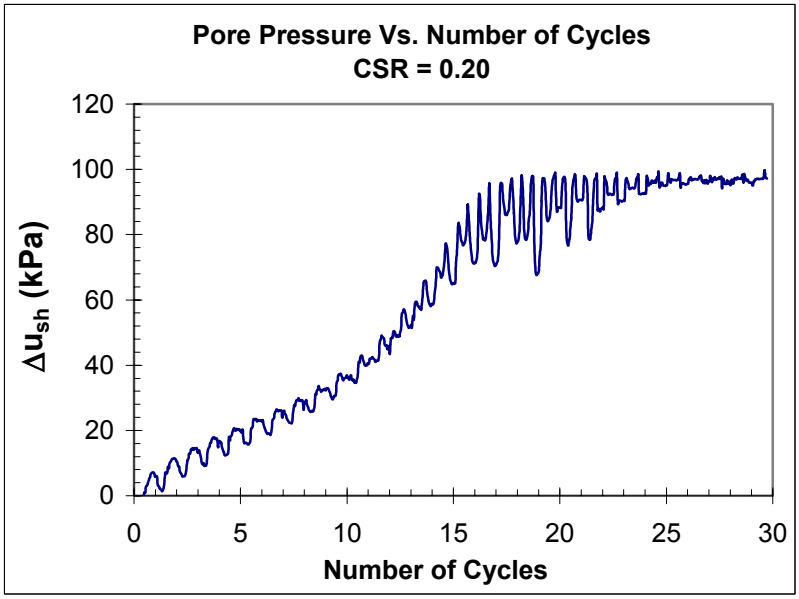

Fig. 3.18 Shear induced pore pressure versus N

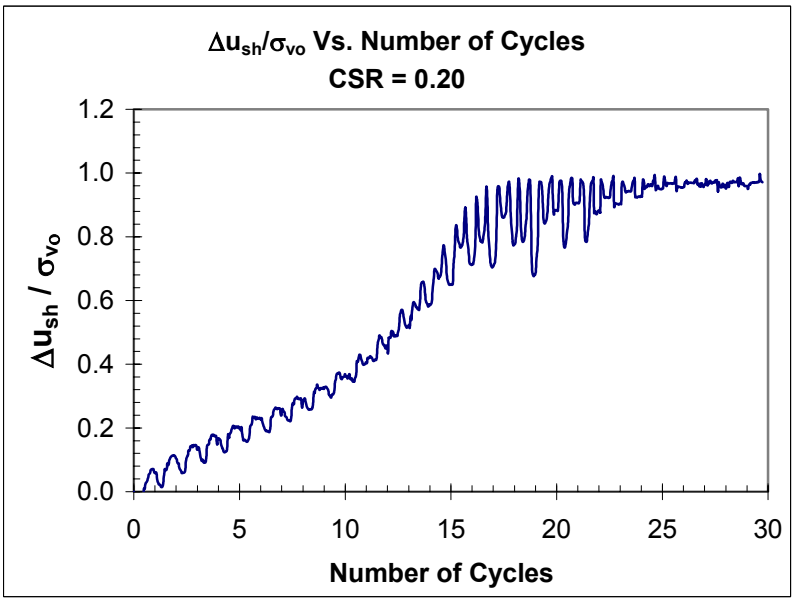

Fig. 3.19 Pore pressure ratio r_u versus N

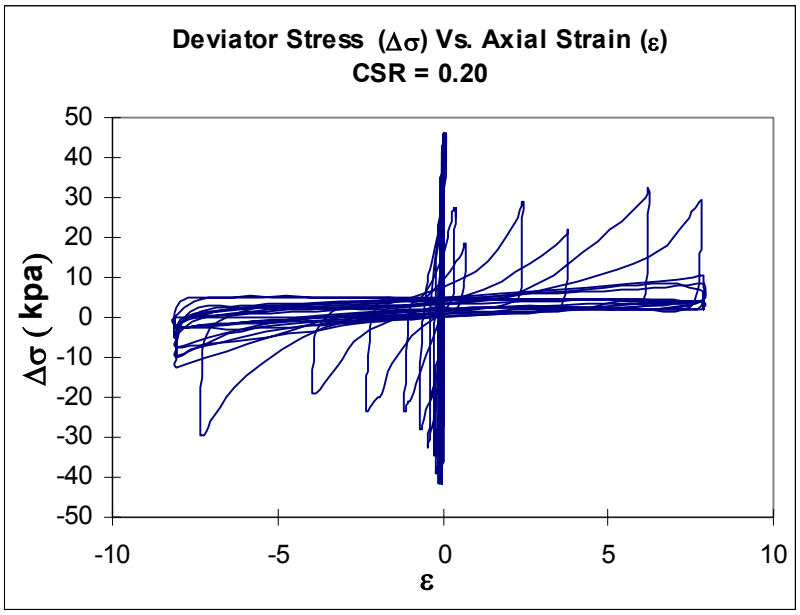

Fig. 3.20 Deviator stress versus axial strain

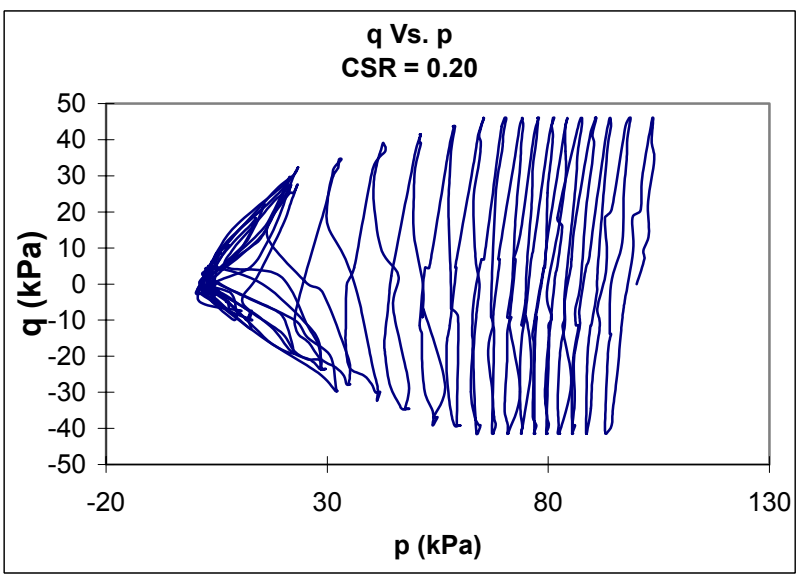

Fig. 3.21 *p' – q* diagram (effective mean stress versus deviator stress)

3.7 Experimental Errors

3.7.1 Device Measurement

Table 3.8 summarizes specifications and accuracies of devices used for measuring various parameters during monotonic and cyclic triaxial tests.

Table 3.8 Measuring Device Specifications

Measurement	Range	Device	Accuracy	Error	Units
Height	150-160	Linear scale	1	± 0.5	mm
Diameter	74.2 – 74.4	Vernier Caliper	0.02	± 0.01	mm
Weight	900-1200	Mettler PC8000 Balance	0.1	± 0.05	g
Volume	25 - 50	Graduated cylinder	0.1	± 0.05	cm^3
Displacement	40	LVDT	0.01	± 0.005	mm
Load	2.2 (500)	SSM500AJ Load Cell Calibration Factor: 0.00003856871012	0.00004	± 0.00002	kN (lbf)
Load	8.8 (2000)	SSM2000AJ Load Cell Calibration Factor: 0.00014807338135	0.00015	± 0.00008	kN (lbf)
Cell and Sample Pressure	1050 (150)	PG2000 Pressure Transducer	0.01	± 0.005	kPa (psi)

3.7.2 Void Ratio Calculation:

The error in void ratio measurement was estimated using the following expression.

$$\frac{\Delta e}{e}=\frac{\Delta V_w}{V_w}-\frac{\Delta W}{W} \qquad (3.1)$$

Errors in void ratio calculations for GEOCOMP specimens were estimated as 0.25%. Corresponding error in void ratio, typically, was 0.002.

3.7.3 Axial Strain:

The error in strain measurement was calculated using expression 3.2 for GEOCOMP.

$$\frac{\Delta \varepsilon}{\varepsilon}=\frac{\Delta \delta}{\delta}-\frac{\Delta H}{H} \qquad (3.2)$$

H = height of the specimen, and δ = measured displacement using LVDT.

3.7.4 Deviatoric Stress:

The relationship between deviatoric stress (σ_d) and the other parameters for GEOCOMP apparatus is given below:

$$\sigma_d = \frac{P(1-\varepsilon)}{A_o} \qquad (3.3)$$

where, A_o = cross sectional area of the specimen at the end of consolidation, and P = axial load. By combining Eq. 3.2 and the derivative of Eq. 3.3, the error in σ_d could be expressed as shown in Eq 3.4:

$$\frac{\Delta\sigma_d}{\sigma_d} = \frac{\Delta P}{P} - \frac{\varepsilon}{1-\varepsilon}\left(\frac{\Delta\delta}{\delta} - \frac{\Delta H}{H}\right) - 2\frac{\Delta D_0}{D_0} \qquad (3.4)$$

where, D_o = initial diameter of the specimen.

3.7.5 Membrane Compliance

Typical factors that affect membrane compliance are: 1) soil grain size and gradation; 2) effective confining stress; 3) soil grain angularity; 4) soil fabric or method of sample preparation; and 5) membrane thickness; (Nicholson et. al. 1993). Among the above, soil grain size and gradation are the most important factors. Triaxial tests on non-uniformly graded sandy soils have shown that unit membrane compliance correlates well with D_{20}. Other soil variables such as density, particle angularity, fabric or method of sample preparation, and membrane thickness or stiffness are of little or only minor influence. The empirical expression (valid for D_{20} > 0.1mm) used for normalized unit membrane penetration S ($mL/cm^2/\Delta\log\sigma'_3$) is given by: $S = 0.0019 + 0.0095\ D_{20} - 0.0000157(D_{20})^2$, where D_{20} is in mm.

For the clean sand specimens tested in this program, the maximum D_{20} was about 0.2mm. D_{20} for silty soils were even smaller. All specimens were initially saturated at about 20kPa effective stress and subsequently consolidated to 100kPa or 400 kPa . Typical effective membrane area was about 362 cm^2. The maximum volumetric change due to membrane penetration was about 1.8 mL.

Compared to the typical net volume of water introduced into a clean sand specimen (nearly 280 mL), the effect of membrane penetration was only around 0.6%, which could be neglected. For silty soils, because D_{20} values were much smaller than that of clean sand, the effect of membrane penetration was even smaller.

3.7.6 Rod Friction

In order to measure the friction between the rod and the top cap of GEOCOMP triaxial cell, a dummy monotonic test was conducted. In this test, a water-filled membrane was used instead of a soil specimen. The monotonic test procedure was followed, however, there was no consolidation phase because the cell pressure and the backpressure were set to be equal. Then shearing was carried out on the dummy (water) specimen. The data was interpreted using the same method as for soil specimens. Since water cannot resist any shear, $\Delta\sigma_1$ should have been zero provided there is no friction between the rod and the top cap. The results showed that this friction was negligible, and, most of the time, was smaller than the accuracy of the force measurement. In the case of GDS apparatus, several friction tests were done periodically, and readings were adjusted accordingly.

4.0 Experimental Data

The experimental data are presented in Appendices A and B, and in the dissertations and theses by Liang (2000, 2003), Shenthan (2001, 2003), and Kanagalingam (2003, 2004).

5.0 Analysis and Conclusions

Analysis of the experimental data and the newly developed theoretical formulations for interpretation of silty soil behavior are presented in a series of technical articles attached herein. The analyses and results are categorized into four groups.

(a) undrained monotonic behavior of sand and non-plastic silty soils
(b) undrained cyclic behavior of sand and non-plastic silty soils
(c) undrained behavior of sand and non-plastic silty soils based on energy principles
(d) liquefaction behavior and screening of sand and non-plastic silty soils, remediation, and other issues

The relevant technical articles are categorized accordingly and presented below.

5.1 Undrained monotonic behavior of sand and non-plastic silty soils

5.1.1 Technical Articles

Analyses of undrained monotonic behavior of sand and non-plastic silty soils are presented in the following technical articles.

5.1.1.1 Thevanayagam, S., Shenthan, T., Mohan, S. and Liang, J. (2002) "Undrained fragility of sands, silty sands and silt," *ASCE, J. Geotech. & Geoenv. Eng*. 128 (10): 849-859.
5.1.1.2 Thevanayagam, S., and Mohan, S. (2000) "Intergranular state variables and stress-strain behaviour of silty sands", *Geotechnique*, 50(1), London, 1-23.
5.1.1.3 Liang, J. (2000) "Monotonic undrained behavior of silt – sand mix in triaxial compression", *MS Thesis*, SUNY at Buffalo, 150p. (not included in this report)
5.1.1.4 Shenthan, T., Thevanayagam, S., and Kanagalingam, T. (2003) "Effects of confining stress on undrained monotonic behavior of silty soils," *ASCE, J. Geotech. & Geoenv. Eng*., *In preparation.* (not included in this report)

The articles 5.1.1.1 and 5.1.1.2 are presented following Sec. 5.1.2.

5.1.2 Conclusions

The main conclusions from this analysis are as follows:

- Mechanical behavior and collapse potential or fragility of silty sands and sandy silts depend on intergrain contact density. For such soils, the equivalent intergranular void ratios [$(e_c)_{eq}$ and $(e_f)_{eq}$] are found to be better contact indices to characterize their mechanical response.
- It was found that at the same global void ratio, e, and the same confining stress, collapse potential of silty sands increases with an increase in fines content (FC) up to a certain threshold value (FC_{th}) due to a reduction in intergranular contact between the coarse grains. Beyond this threshold fines content, this trend reverses as the interfine contact friction becomes significant, and the soil becomes stronger.
- In silty sands ($FC<FC_{th}$), fines may play a beneficial secondary cushioning effect or contribute to fragility, depending on the matrix structure of the soil and it's intergranular void ratio. When the fine particles fall within the voids of the coarser grain matrix, they provide a cushioning effect that reduces the fragility. However, when some of these fine particles fall in between coarser grain contacts, and partially support the coarser grain skeleton, the soil becomes more fragile.

- In sandy silts ($FC>FC_{th}$), interfine contacts control the soil's mechanical behavior, while the coarser grains act as reinforcing elements providing a beneficial secondary effect. At the same interfine void ratio, fragility of the soil decreases with an increase in coarser grain content. However, at very high fines content, this secondary effect becomes negligible, and interfine contacts alone control the soil's collapse potential.
- Similar behavior is observed in terms of state parameter (ψ). New state parameters, ψ_s and ψ_f, have been introduced, which reflect the plastic compressibility characteristics at low and high fines content, respectively.

5.1.1.1

Undrained Fragility of Clean Sands, Silty Sands, and Sandy Silts

S. Thevanayagam[1]; T. Shenthan[2]; S. Mohan[3]; and J. Liang[4]

Abstract: In this paper, intergranular (e_c) and interfine (e_f) void ratios and confining stress are used as indices to characterize the stress–strain response of gap graded granular mixes. It was found that at the same global void ratio (e) and confining stress, the collapse potential (fragility) of silty sand increases with an increase in fines content (FC) due to a reduction in intergranular contact between the coarse grains. Beyond a certain threshold fines content (FC_{th}), with further addition of fines, the interfine contact friction becomes significant. The fragility decreases and the soil becomes stronger. The value of FC_{th} depends on e and the characteristics of fines and coarse grains. At $FC<FC_{th}$, intergranular contact friction plays the primary role. It is postulated that fines either provide a beneficial secondary cushioning effect or contribute to fragility, depending on the nature of the soil's matrix structure and the magnitude of e_c. At the same e_c, the fines that fall within the intergranular voids provide a cushioning effect and slightly reduce the fragility. When fines fall between some of the coarse grains and partially support the coarse grain skeleton, the soil is very fragile. The contribution to fragility is dominant when the soil is very loose in terms of e_c. At large fines contents ($FC>FC_{th}$), fine grain friction plays a primary role and dispersed coarse grains provide a beneficial, secondary reinforcement effect. At the same e_f, the collapse potential decreases with an increase in sand content. Beyond a certain limiting fines content, the soil behavior is controlled by e_f only. An intergranular matrix diagram is presented that delineates zones of different behaviors of granular mixes as a guideline to determine the anticipated behavior of gap-graded granular mixes. New equivalent intergranular contact void ratios, $(e_c)_{eq}$ and $(e_f)_{eq}$, are introduced to characterize the behavior of such soils, at $FC<FC_{th}$ and $FC>FC_{th}$, respectively.

DOI: 10.1061/(ASCE)1090-0241(2002)128:10(849)

CE Database keywords: Sand; Stress strain curves; Soil properties; Grains.

Introduction

The engineering behavior of natural soils is dependent on mineralogy, size, shape, particle arrangement, interparticle contact, and bonding, and interactions at the particulate level. The level of participation by different types and sizes of particles within the soil matrix in the transfer of interparticle contact stresses dictates the stress–strain behavior and the resistance it can offer under different loading conditions. Traditionally, geotechnical engineering has dealt with this problem by simply broadly classifying the soil into two categories, fine-grained and coarse-grained. Furthermore, void ratio or relative density has been used as an index for mechanical response correlations. This classification has worked well for coarse-grained materials for static or slow-loading conditions as well as for fine-grained clayey soils in the case of rapid loading conditions. However its application in classifying silty sands and sandy silts under seismic conditions has faced problems.

Observations from recent earthquake case histories (e.g., Seed and Harder 1990) indicate that natural and man made fills often contain a mix of soils containing sands and a significant amount of fines, and in some cases gravel. These soils do liquefy and cause lateral spreads, in some cases defying conventional wisdom (JGS 1996). The knowledge gained from three decades of research on clean sands does not directly translate to such soils. The mechanisms leading to liquefaction and large deformation in such soils are more complex than in more uniform soils. The behavior of such granular mixes has received recent, more detailed study (Kuerbis et al. 1988; Chang 1990; Chameau and Sutterer 1994; Pitman et al. 1994; Vaid 1994; Koester 1994; Thevanayagam 1998; Zlatovic and Ishihara 1997; Yamamuro and Lade 1998; Thevanayagam 1999a,b; 2000a,b; Thevanayagam et al. 2000; Thevanayagam and Mohan 2000; Yamamuro and Covert 2001; Polito and Martin 2001). It requires a greater understanding of the soil microstructure and the contributions of soil particles of different size to its mechanical response.

This paper addresses the analysis of the undrained stress–strain behavior, shear strength, and collapse potential of granular mixes ranging from clean sands to pure silts, with due consideration for relative contributions by intergranular and interfine friction, to develop a fundamental understanding of this problem. It may be used to clarify the prevailing differences in opinion on the liquefaction and post-liquefaction strength behavior of sandy soils (Poulos 1981; Seed 1987; Seed and Harder 1990; Stark and Mesri 1992; Ishihara 1993; Baziar and Dobry 1995) and whether or not

[1]Associate Professor, Dept. of Civil, Structural and Environmental Engineering, 212 Ketter Hall, State Univ. at Buffalo (SUNY), Buffalo, NY 14260; E-mail: theva@eng.buffalo.edu

[2]Graduate student, Dept. of Civil, Structural and Environmental Engineering, 212 Ketter Hall, SUNY Buffalo, Buffalo, NY 14260.

[3]Engineer, Dept. of Transportation, Sacramento, CA 94623-0660.

[4]Graduate student, Dept. of Civil, Structural and Environmental Engineering, 212 Ketter Hall, SUNY Buffalo, Buffalo, NY 14260.

Note. Discussion open until March 1, 2003. Separate discussions must be submitted for individual papers. To extend the closing date by one month, a written request must be filed with the ASCE Managing Editor. The manuscript for this paper was submitted for review and possible publication on August 4, 1998; approved on February 19, 2002. This paper is part of the ***Journal of Geotechnical and Geoenvironmental Engineering***, Vol. 128, No. 10, October 1, 2002. ©ASCE, ISSN 1090-0241/2002/10-849–859/$8.00+$.50 per page.

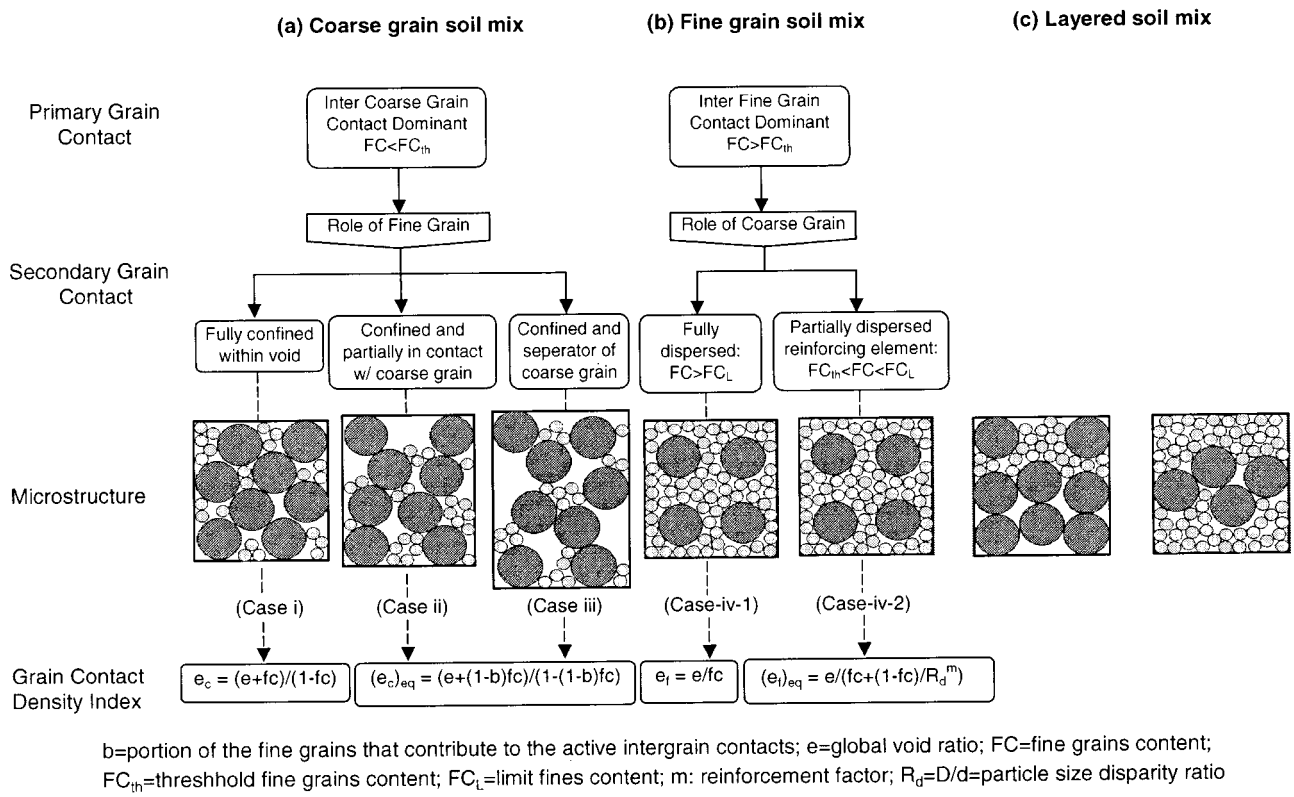

Fig. 1. Intergranular soil mix classification

fines content adversely or beneficially affects the collapse potential of silty soils.

Microstructure and Soil Behavior: Framework

Microstructure

The microstructure of a granular mix, which can be constituted in many different ways with different types of intergrain contacts, leads to different undrained shear responses. For example, consider a granular mix containing particles of sizes d and D in different proportions. Among many variations, there are three extreme limiting categories of microstructure: (a) primarily the coarse grains are in contact [cases (i)–(iii) in Fig. 1(a)], (b) primarily the fine grains are in contact with each other [case (iv) in Fig. 1(b)], or (c) a layered system [Fig. 1(c)]. Within category (a) there are three subsets: the fines are confined within the void spaces between the coarse grains with little contribution to supporting the coarse grain skeleton [case (i)]; they are partially supporting the coarse grain skeleton [case (ii)]; or they partially separate the coarse grains [case (iii)]. In category (b), the coarse grains are fully dispersed in the fine grain matrix [case (iv)]. In category (c), the coarse grain layers have no fines confined in them and vice versa. The last category is not discussed further in this paper.

Case (i) is possible only if (1) the size, d, of the fine grains is much smaller than the minimum possible pore opening size in the coarse grain skeleton, and (2) the intergranular voids are not completely filled with fines. For spherical particles, condition (1) implies that $D/d>6.5$ where D=size of coarse grains. Case (i) is expected to be rare unless the fine grain content is very low, while cases (ii) and (iii) are expected to be common. A minor difference between cases (ii) and (iii) is that in case (iii) the fine grains actively participate in the internal force chain by separating the coarse grains and supporting the coarse grain skeleton. Case (iv) is relevant at high fine grain (FC) content. At the same void ratio, a transition in microstructure from cases (i) through (iv) can occur naturally with an increase in fine grains content beyond some threshold value (FC_{th}). At $FC<FC_{th}$ [cases (i)–(iii)], the coarse grain contacts play a primary role in the soil's shear response and fines offer a secondary contribution. When $FC>FC_{th}$, the fine grain contacts begin to play a greater role as the coarse grains begin to disperse and provide a secondary reinforcement effect until they are separated sufficiently. This imposes a limiting fines content FC_L, above which the fines control the shear behavior [case (iv-2)]. There exists a transition zone between FC_{th} and FC_L before the behavior of the soil mix is entirely governed by the fine grains [case (iv-1)]. It is apparent from Fig. 1 that the global void ratio is not a suitable index by which to characterize the mechanical response of the entire spectrum of cases shown. Even at the same void ratio, differences in relative contributions of different size grains lead to different behavior at different silt contents (e.g., Koester 1994).

First-Order Indices of Active Grain Contacts and Threshold Fines Contents

A first-order solution may be to consider the various cases as a composite mix of coarse and fine grain skeletons with *apparent* intergranular and interfine void ratios, e_c and e_f (Vaid 1994; Thevanayagam 1998, respectively):

$$e_c=\frac{e+fc}{1-fc} \tag{1}$$

$$e_f = \frac{e}{fc} \tag{2}$$

The magnitudes of e_c and e_f may be considered as first-order indices of active coarse-grain and fine-grain contacts, respectively. Initially, up to a certain FC_{th}, the magnitude of e_f remains very high and the influence of fine grains remains secondary until e_f falls below a threshold value. Up to that point, the shear response of the mix is expected to weaken. Once the threshold value of e_f is reached the fine grains are expected to play a primary role. Beyond FC_{th}, the shear response is expected to strengthen with a further increase in fines content. From this conceptual standpoint, FC_{th} is expected to occur when e_f decreases below a threshold value of $e_{max,HF}$ (Thevanayagam 2000a):

$$FC_{th} \leq \frac{100 e_c}{1 + e_c + e_{max,HF}}\% = \frac{100 e}{e_{max,HF}}\% \tag{3}$$

where $e_{max,HF}$=the maximum void ratio of the pure silt above which it has no appreciable strength. The rationale is that as e_f falls below $e_{max,HF}$, the fine grains are packed closely enough so that direct fine grain-to-fine-grain friction becomes active and therefore begins to significantly contribute to the mechanical behavior of the soil mix.

At $FC > FC_{th}$, the coarse grains become spread apart and interfine contact friction begins to significantly influence soil behavior. Unless sufficiently spaced apart, the coarse grains can still (1) engage in friction with fine grains; (2) interfere with the microgeometry of the shear surface; and (3) contribute to redistribution of the normal stresses within the fine grain matrix. The zone of influence of shearing in a uniform grained soil is about 10 times the grain size (Roscoe 1970; Mooney et al. 1997). Hence, at a center-to-center spacing less than $D + 10d$, where d and D are the grain sizes of the fine and coarse grains, respectively, the coarse grains can have a reinforcement effect [case (iv-2)] in Fig. 1]. Only at $FC > FC_L$ is the soil behavior governed fully by interfine friction [case (iv-1)]. The limiting fines content FC_L is approximately given by (Thevanayagam 2000a):

$$FC_L \geq 100\left[1 - \frac{\pi(1+e)}{6s^3}\right]\% = 100\left[\frac{6s^3 - \pi}{6s^3 + \pi e_f}\right]\% \geq FC_{th}$$

$$e_f \leq e_{max,HF} \tag{4}$$

where $s = 1 + a/R_d$, $R_d = D/d$=size disparity ratio, and a=10. The FC_L value is also affected by a number of other factors not explicitly incorporated into Eq. (4), hence the inequality indicated in Eq. (4).

Equivalent Contact Density Indices

At $FC < FC_{th}$, one might entirely neglect the secondary effects of fines and use e_c as a first-order index of active grain contacts in a soil mix. However, the mechanical behavior of such a mix would be stronger than that of the host coarse grain soil at the same e_c. The relevant equivalent intergranular contact index, $(e_c)_{eq}$, has been introduced (Thevanayagam 2000a) as

$$(e_c)_{eq} = \frac{e + (1-b)fc}{1 - (1-b)fc}; \quad 0 < b < 1 \tag{5}$$

where fc=FC/100 and b denotes the portion of the fine grains that contributes to the active intergrain contacts: b=0 would mean that none of the fine grains actively participates in supporting the coarse-grain skeleton; b=1 would mean that all of the fine grains actively participate in supporting the coarse grain skeleton. The magnitude of b depends on grain size disparity ratio R_d and grain characteristics. The shear behavior of silty sand mixes in cases (i)–(iii) at $(e_c)_{eq}$ may be expected to behave similar to that of the host sand (denoted by HC) prepared at a void ratio of $e = (e_c)_{eq}$.

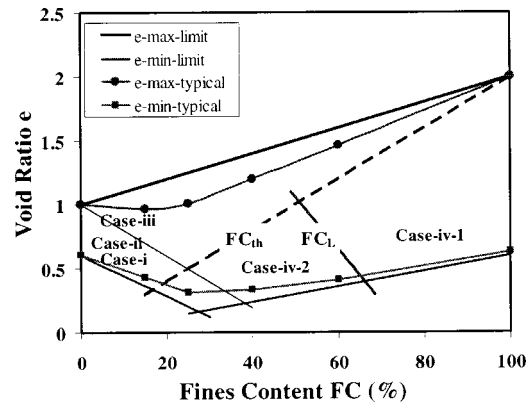

Fig. 2. Intergranular matrix diagram classification

Similarly, at $FC_{th} < FC < FC_L$, although one may use e_f as a first-order approximation for grain contact density in the soil mix, the reinforcement effect by the coarse grains must also be introduced to obtain an equivalent interfine void ratio $(e_f)_{eq}$ as the index of active contacts. For a two size particle system with large size disparity, an approximate expression for $(e_f)_{eq}$ can be derived (Thevanayagam 2000a) as

$$(e_f)_{eq} = \frac{e}{fc + \dfrac{1-fc}{R_d^m}} < e_f \tag{6}$$

where $0 < m < 1$ and m=a coefficient that depends on grain characteristics and fine grain packing. At $FC > FC_L$ the behavior is entirely governed by the fine grains. The interfine void ratio e_f *may* be considered an index of active contacts. In general, the shear behavior of a sandy silt mix in case (iv) at $(e_f)_{eq}$ may be expected to behave similar to that of the host fines prepared at a void ratio of $e = (e_f)_{eq}$.

Fig. 2 schematically shows the regions that belong to the various cases [(i)–(iv)] of microstructure, with the lines corresponding to FC_{th} and FC_L, and the theoretical boundaries for e_{max} and e_{min} and a typical trend for the measured e_{max} and e_{min} for granular mix in a void ratio versus fines content diagram.

Experimental Study

An experimental program was undertaken to investigate the relative effects of fines, intergranular and interfine void ratios, and the friction contribution of each on the undrained stress–strain behavior and collapse potential of gap-graded granular mixes. Soil mixes were prepared using a single host sand (F55, Foundry Sand, U.S. Silica Company, Ottawa, Ill.; denoted by "OS00" in Fig. 3) mixed with different amounts of nonplastic crushed silica fines (Sil co sil No. 40) at 7, 15, 25, 40, and 60% fines by dry weight. Tests were also conducted on pure sand and 100% silica fines. These soils are named OS00, OS07, OS15, OS40, OS60, and OS100, respectively. The index properties of these soils are shown in Table 1. Fig. 3 shows the grain size data for the host sand, silty sands, sandy silts, and pure crushed silica silt (passing U.S. Sieve No. 200).

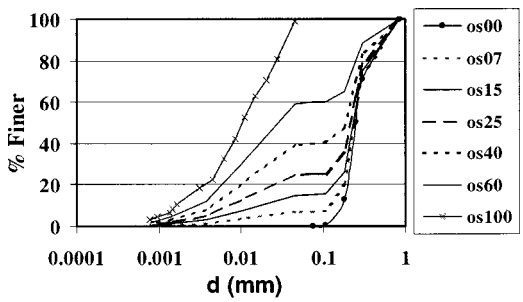

Fig. 3. Grain size distribution

Sample preparation

Cylindrical specimens were prepared by placing soils in four layers or eight layers in a triaxial mold using a dry air deposition method or moist tamping method. The mold (typically 75 mm in diameter and 175 mm in height or 38.7 mm in diameter and 112 mm in height) was filled with the soil by layers and compacted by gently tamping until reaching a specified target void ratio. The procedure was similar for each layer until the final target void ratio was reached. The target void ratios of the silty sand specimens were selected to satisfy specific constraints on global, intergranular, or interfine void ratios.

Following initial preparation, the specimens were percolated with carbon dioxide and de-aired water from the bottom of the specimen towards the top while the specimen was subjected to about 20–30 kPa effective confining pressure (σ_c'). Then the cell and pore water pressure were slowly increased simultaneously by the same increments to achieve a B value ($=\Delta u/\Delta\sigma_c$) that was typically greater than 0.95. Following this, the specimens were isotropically consolidated to a constant effective consolidation stress ($\sigma_c'=100$ kPa). The net volume of the water introduced into the specimen was measured accurately. Following consolidation the drainage valves were closed and strain controlled monotonic undrained triaxial compression tests were done at a strain rate of 0.6%/min. The pore pressure, axial load, and axial deformation were recorded using a built-in data acquisition system. The final void ratio of each specimen was calculated based on the weight of the dry solid grains in the specimen, the net volume of water introduced into the specimen during saturation, and the measured change in volume data during consolidation.

Experiments

Specific objectives of the experiments were to discern the relative effects of intergranular and interfine friction [within the context of cases (i)–(iv); Fig. 1 and Table 2] on (1) undrained stress–strain behavior; (2) ultimate shear strength; (3) collapse potential (or potential to develop positive shear induced pore pressure); and (4) the degree of further resistance to deformation following initial collapse (or following the quasi-steady state).

Constraints were placed on e (Test series A, $e=0.60\pm0.01$), e_c (series B1, B2, B3), or interfine void ratio (series B4, $e_f=0.90\pm0.02<e_{\max,HF}$). Series B1, B2, and B3 were conducted at $e_c=0.675<e_{\max,HC}$), 0.80 ± 0.01 (near $e_{\max,HC}$), and 0.86 ± 0.01 ($>e_{\max,HC}$), each representing cases (i)–(iii), respectively. The $e_{\max,HC}$ and $e_{\max,HF}$ referred to are the maximum void ratios of the host clean sand and host fines (100% silt) media, respectively. It is assumed that these are the limiting void ratios beyond which each medium has no appreciable strength. The intergranular void ratios (e_c and e_f) and the locations of these specimens on the e versus fines content diagram are shown in Fig. 4. In series A, the specimens at 25, 40, and 60% fines content could not be successfully tested at $e=0.60$ due to their excessive fragility. For pure silt the $e_{\min}$ was 0.627, and the densest silt specimen that could be successfully tested was at $e=0.77$.

In addition to the above series, several other specimens were also tested at other void ratios to study the effect of intergrain contact on the overall steady-state behavior and collapse potential of each mix, and to evaluate the usefulness of the contact void ratio indices to characterize such behavior for all mixes.

Presentation of Analysis

First, analysis is presented on the relative role of intergranular and interfine friction on the overall stress–strain behavior of the mixes by analyzing the data for Test series A. This is followed by an analysis of the relative effect of intercoarse-grain and interfine-grain contacts on steady state, collapse potential, and resistance to further deformation (following the quasi-steady state). Second, the secondary effects of confined fines and reinforcement effect of dispersed coarse grains are presented by analyzing the data at the same intergranular void ratio (for $FC<FC_{th}$) and interfine void ratio (for $FC>FC_{th}$), respectively.

Figs. 5(a and b) show a schematic of the different types of stress–strain and stress paths obtained, respectively. The steady

Table 1. Index Properties of Soil Mixes

	Soil Mix					
Property	OS00 clean sand	OS15 silty sand	OS25 silty sand	OS40 sandy silt	OS60 sandy silt	OS100 pure silt
Fines content (%)	0	15	25	40	60	100
$e_{\max}$[a]	0.8	0.75	0.86	1.07	1.35	2.1
$e_{\min}$[b]	0.608	0.428	0.309	0.33	0.413	0.627
d_{10} (mm)	0.16	0.018	0.009	0.005	0.003	0.002
d_{30} (mm)	0.22	0.19	0.15	0.025	0.01	0.006
d_{50} (mm)	0.25	0.23	0.23	0.18	0.03	0.01
d_{60} (mm)	0.27	0.25	0.24	0.22	0.07	0.015
c_u	1.7	13.6	28.2	46.8	25.9	10
c_c	1.1	8.2	11	0.6	0.53	1.6

[a]ASTM D4254 (even though this method is recommended only up to 15% fines content).

[b]Optimum moisture content using ASTM D1557.

Table 2. Experimental Program: Effect of Intergrain Contacts ($\sigma'_c = 100$ kPa)

Purpose of test	Test series	Fines (%)	Case number	Specimen number	e	e_c	e_f	ε_{max} (%)	σ'_{3f} (kPa)	Stress path	Figs.
Study of	A	0	i	00-598	0.598	0.598	n/a	7	631	D	6(a and b)
primary effect	$e=0.60$	0	i	00-604	0.604	0.604	n/a	9	635	D	
of intergrain	*=specimens	7	i and ii	07-596	0.596	0.716	8.51	20	311	D	
contact	for FC=25, 40,	15	ii	15-584	0.584	0.864	3.89	20	29	C–D	
friction at	and 60% were	15	ii	15-595	0.595	0.876	3.97	22	12	C–D	
nearly the	too weak and	25	iii	25-460*	0.460	0.947	1.84	20	10	C	6(c and d)
same global	could not be	40	iv-2	40-425*	0.425	1.375	1.06	18	17	C	
void ratio e.	prepared at	60	iv-2	60-516*	0.516	2.79	0.86	21	69	C–D	6(e and f)
	$e=0.60$	100	iv-1	100-770	0.770	N/A	0.77	21	164	D	
Study the	B1	0	i	00-665	0.665	0.665	N/A	20	555	D	10(a and b)
cushioning	$e_c=0.675\pm0.01$			00-675	0.675	0.675	N/A	21	544	D	
effect of fines		7		07-558	0.558	0.675	7.97	19	645	D	
at nearly the		15		15-423	0.423	0.674	2.82	5	599	D	
same e_c				15-426	0.426	0.678	2.84	5	596	D	
($FC<FC_{th}$)											
	B2	0		00-800	0.800	0.800	N/A	23	8	C	10(c and d)
	$e_c=0.80\pm0.01$			00-804	0.804	0.804	N/A	22	5	C	
		7	ii	07-672	0.672	0.798	9.60	21	118	C–D	
		15		15-530	0.530	0.800	3.53	21	190	D	
	B3	7		07-723	0.723	0.853	10.33	21	11	C	10(e and f)
	$e_c=0.86\pm0.01$		iii	07-735	0.735	0.866	10.50	20	5	C	
		15		15-584	0.584	0.864	3.89	20	29	C–D	
				15-595	0.595	0.876	3.97	22	12	C	
Study the	B4	40	iv-1	40-373	0.373	1.288	0.93	21	147	C-D	11
reinforcing	$e_f=0.90\pm0.02$										
effect of sand		60		60-540	0.540	2.850	0.90	19	11	C	
grains at											
nearly the same e_f		100	iv-2	100-879	0.879	N/A	0.88	19	7	C	

Note: C=contraction, CD=contraction–dilation, D=dilation (Fig.5); ε_{max}=maximum axial strain reached: some specimens were sheared only up to 5–9% axial strain, as the axial stresses reached the axial load sensor capacity; N/A=not applicable; e=postconsolidation global void ratio.

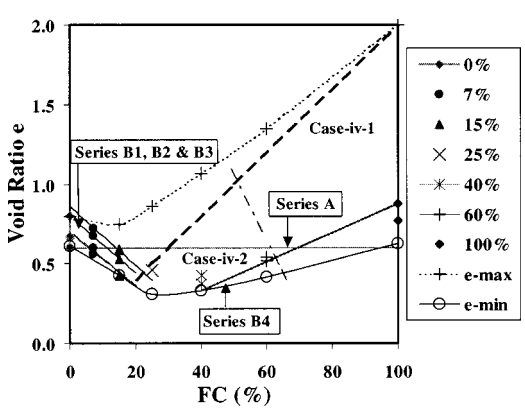

Fig. 4. Test series

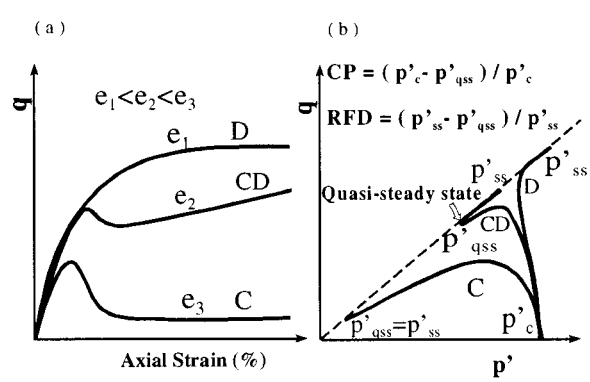

Fig. 5. Schematic stress–strain diagram

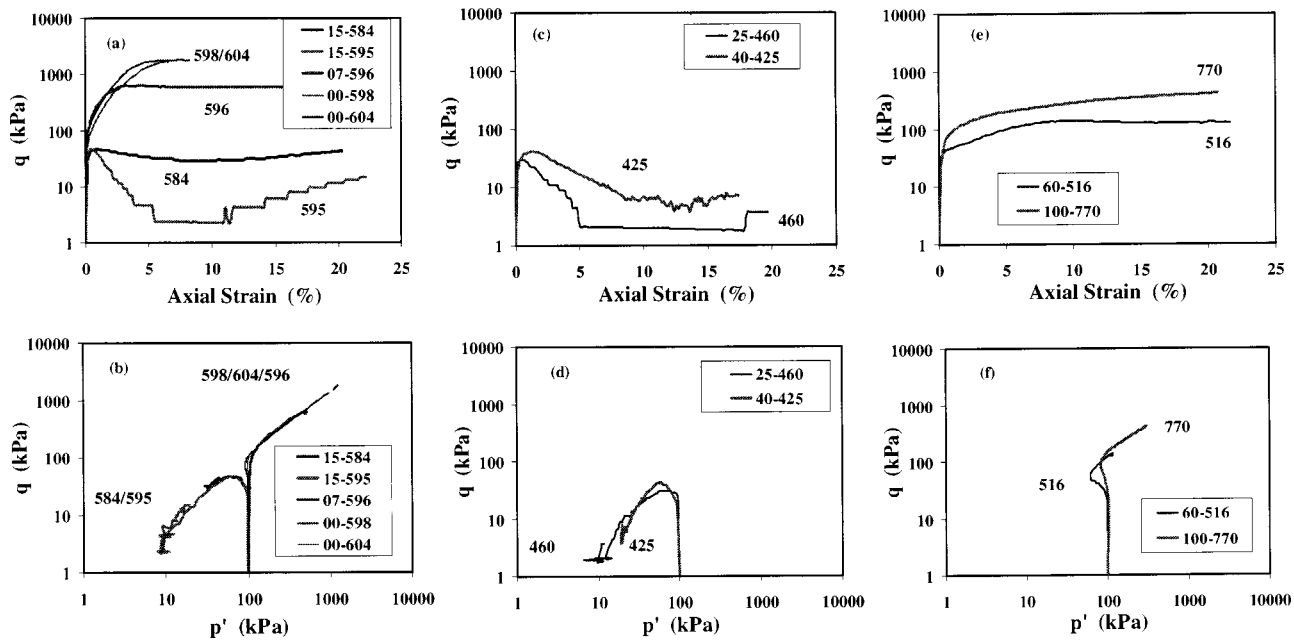

Fig. 6. Stress–strain behavior test series A

state [mean effective stress $p'_{ss}=(\sigma'_1+2\sigma'_3)/3$ at steady state] and quasi-steady state [$p'_{qss}=(\sigma'_1+2\sigma'_3)/3$ at that state] are identified, as are two index measures, namely, the collapse potential (CP) and resistance to further deformation (RFD).

The CP describes the magnitude of maximum *positive* shear induced pore pressure ratio ($=\Delta u_{sh}/\sigma'_c$) that develops during monotonic shearing. For specimens that dilate from the onset of loading, the CP is set at zero. The RFD is a measure of the degree of dilation beyond the point where the maximum positive shear induced pore water pressure develops. For specimens that show collapse behavior [C in Fig. 5(b)], the RFD is zero. For specimens that show initial collapse (quasisteady state) followed by dilation [C–D in Fig. 5(b)] the RFD is a measure of the subsequent degree of dilation beyond the quasisteady state. For soils that dilate from the onset of loading [D in Fig. 5(b)] the RFD is simply a measure of the degree of dilation.

Throughout the text and in figures and tables, specimens are labeled using a five or six digit number. The last three digits, when divided by 1,000, refer to the global void ratio, the preceding digits refer to fines content. For example, 40–425 means a specimen of 40% fines content tested at a void ratio of 0.425.

Intergrain Contact Friction Effect

Stress–Strain Behavior

Figs. 6(a and b) show the stress–strain and the effective stress path data, respectively, for Test series A at nearly the *same e* ($=0.60\pm0.01$) for fines content up to 15%. The data for FC=(25, 40) and (60, 100) are plotted in Figs. 6(c and d) and 6(e and f), respectively. The differences in stress–strain behavior shown in each figure and in those between the figures are primarily due to differences in the degree of contributions by intergranular or interfine contact friction discussed next. The secondary effects by the confined fines and dispersed coarse grains (at $FC<FC_{th}$ and $FC>FC_{th}$, respectively) are discussed later.

Intergranular Contact Friction Effect: $FC<FC_{th}$

In general, the shear strength of the specimens in Figs. 6(a and b) decreases with an increase in fines content. The dense clean sand specimen, 00-598, shows dilative behavior whereas the silty specimens, 07-596 and 15-595, at 7 and 15% fines content, respectively, are weaker than 00-598. This weakness increases with an increase in fines content. This is because both 07-596 and 15-595 are looser than 00-598 in terms of e_c. The value of e_f for 07-596 is very high, and hence interfine contact friction has only a secondary effect on its undrained behavior. Primarily the coarse grain contacts control the stress–strain behavior. Thus 07-596 is weaker than 00-598. Specimen 15-595 is much looser in terms of e_c ($=0.876>e_{max,HC}$) with e_f ($=4\gg e_{max,HF}$) that is still large. The large e_f indicates that the interfine contacts are not yet significant enough for the fine grains to fully affect the behavior of the soil. Due to the significant increase in e_c (and reduced intercoarse granular contact) 15-595 is even more fragile than 07-596 and 00-598.

With a further increase in FC, the fact that specimens at 25% fines content were too fragile and could not be prepared at the same void ratio (0.60) is indicative of the fact that the soil continues to become weaker with further increases in FC. Furthermore, Figs. 6(c and d) show that a much "denser" specimen (25-460) at $e=0.460$ that could be successfully prepared for FC =25% is still weaker than specimen 15-595. The e_f value for 25-460 is still considerably large. The e_c is 0.947 for 25-460. For this specimen, the intercoarse grain contacts still appear to provide the primary resistance with a secondary contribution being from the fine grains.

Interfine Contact Friction Effect: $FC>FC_{th}$

In this range of fines content, specimens could not be prepared at the same void ratio of 0.6 Nevertheless, the relative effects of fine and coarse grains could be studied by pair-wise comparison of the stress–strain behavior of the specimens tested at nearly the same void ratio.

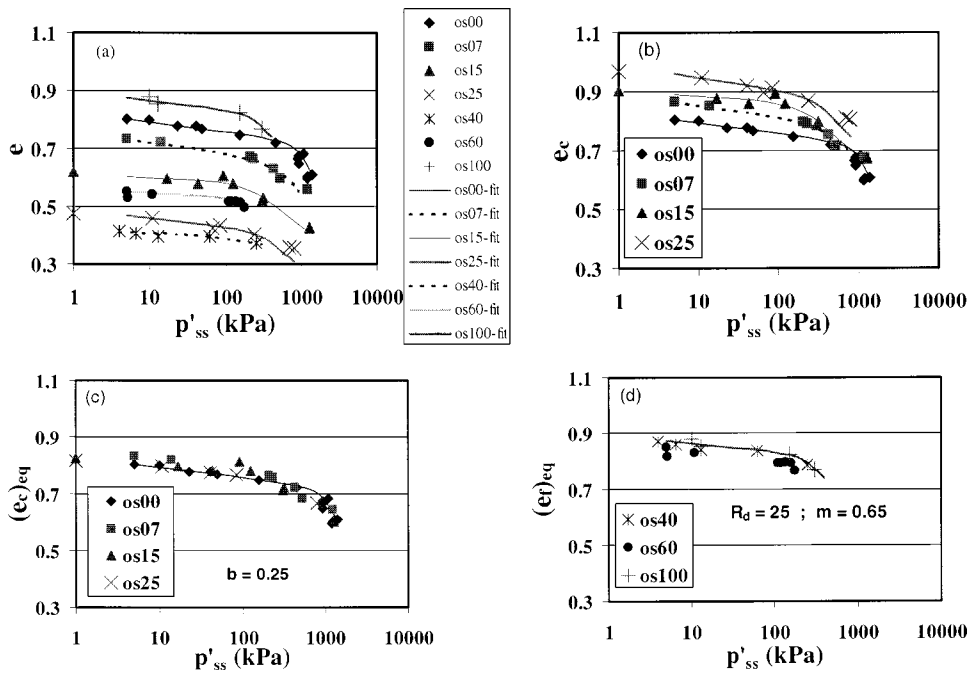

Fig. 7. Steady–state data: (a) e versus p'_{ss}; (b) e_c versus p'_{ss}; (c) $(e_c)_{eq}$ versus p'_{ss}; (d) $(e_f)_{eq}$ versus p'_{ss}

Referring to Figs. 6(c and d), with a further increase in fines to 40%, the 40-425 specimen reaches a maximum value of $e_c = 1.375$ ($>e_{max,HC}$) with a concurrent reduction in $e_f = 1.06$ ($<e_{max,HF}$). Conceptually, in terms of e_c, it should be weaker than 25-460; however, due to the much reduced e_f, 40-425 is stronger than 25-460 [Figs. 6(c and d)] and the stress–strain behavior begins to strengthen. From a conceptual standpoint this *reverse transition* is expected to occur at FC_{th} when e_f drops below $e_{max,HF}$. The rationale is that, as e_f drops below $e_{max,HF}$, the fine grains are packed close enough so that direct fine-grain-to-fine-grain friction becomes significant. Beyond $FC=FC_{th}$ the interfine contact friction begins to exert more influence on the behavior whereas the intergranular friction continues to diminish. The coarse grains become dispersed and play a secondary reinforcement role until reaching the limiting fines content FC_L with the interfine contacts primarily affecting the behavior at $FC>FC_L$. If one assumes the $e_{max,HF}$ for silt is the same as e_{max} for this soil (Table 1), FC_{th} and FC_L corresponding to $e=0.60$ are about 28 and 69%, respectively. The FC_{th} and FC_L corresponding to $e=0.45$ are about 21 and 72%, respectively.

Referring to Figs. 6(e and f), as the fines content increases further to 60%, the e_f for 60-516 decreases significantly to 0.86 whereas e_c increases to a very high value of 2.79 with the interfine contact controlling the behavior. Even though 60-516 is looser than 40-425 [Figs. 6(c and d)] in terms of e, it is much denser than 40-425 in terms of e_f. Hence, it tends to be more dilative than 40-425. The coarse grain reinforcement effect is secondary to the fine grain friction. If a comparison is made at the same e_f, however, a specimen at FC=40% would be expected to be stronger than a specimen at FC=60%, due to a greater secondary reinforcement effect. This phenomenon is analyzed later.

When 60-516 is compared to 100-770, the tendency to dilate increases with a further increase in fines, even though 60-516 is denser. This is due to the concurrent reduction in e_f in 100-770 compared to in 60-516 at $e_f=0.86$. Had these specimens been prepared at the same e_f, however, the specimen at FC=60% would have been a little stronger.

The relative primary effects of coarse and fine grains depending on $FC<FC_{th}$ and $FC>FC_{th}$, respectively, are more readily apparent in "Steady State" and "Collapse Potential and Dilation Index."

Steady State

Fig. 7a shows the steady-state data from the Test series in terms of e versus p'_{ss}. At the same global void ratio and the same initial confining stress σ'_c, the mean effective stress p'_{ss} at steady state decreases with an increase in fines content up to a certain fines content (about 25%) and decreases beyond that.

Figs. 7(b and d) show the same data plotted against e_c [or $(e_c)_{eq}$] and $(e_f)_{eq}$ for $FC<FC_{th}$ and $FC>FC_{th}$, respectively. At low fines content ($FC<FC_{th}$), p'_{ss} for all mixes correlates well with the data for pure sand [case (i)] at low values of intergranular void ratio e_c [Fig. 7(b)]. The exception is when e_c is near $e_{max,HS}$ [case (ii)] and $e_c>e_{max,HC}$ [case (iii)]. Compared with silty sands in case (iii), clean sand at such loose states is very unstable (without the support of the fine grains) and shows very low p'_{ss} compared to silty sand. Silty sand in case (ii) is somewhat stronger than the clean sand. This exception is caused by the cushioning effect provided by the fines present in the intercoarse grain voids in silty sand. When plotted against $(e_c)_{eq}$ (assuming $b=0.25$ for this soil mix) the data fall into a narrow band that surrounds the data for clean sand [Fig. 7(c)]. Such a correlation was not found for the specimens at high FC. This is indicative of the primary role of intercoarse grain contacts at $FC<FC_{th}$. Similarly, the data for $FC>FC_{th}$ are plotted against the equivalent contact index $(e_f)_{eq}$ (assuming $m=0.65$ for this soil mix); all data tend to fall into the vicinity of the data for the pure silt [Fig. 7(d)].

Collapse Potential and Dilation Index

Figs. 8(a and b) show the indices of CP and RFD versus the void ratio, respectively, for all mixes. The relative roles of intergrain

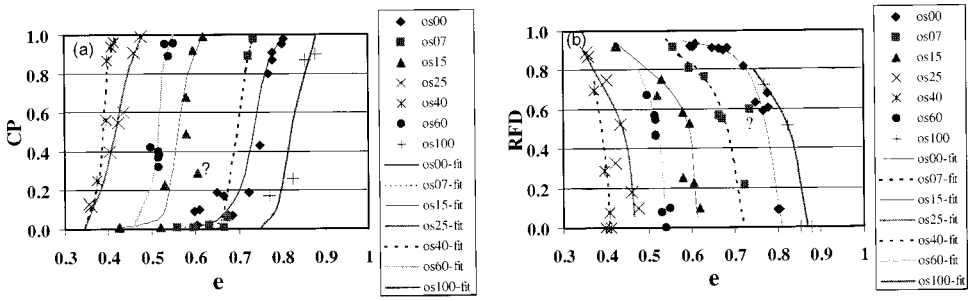

Fig. 8. Collapse potential and dilation index RFD

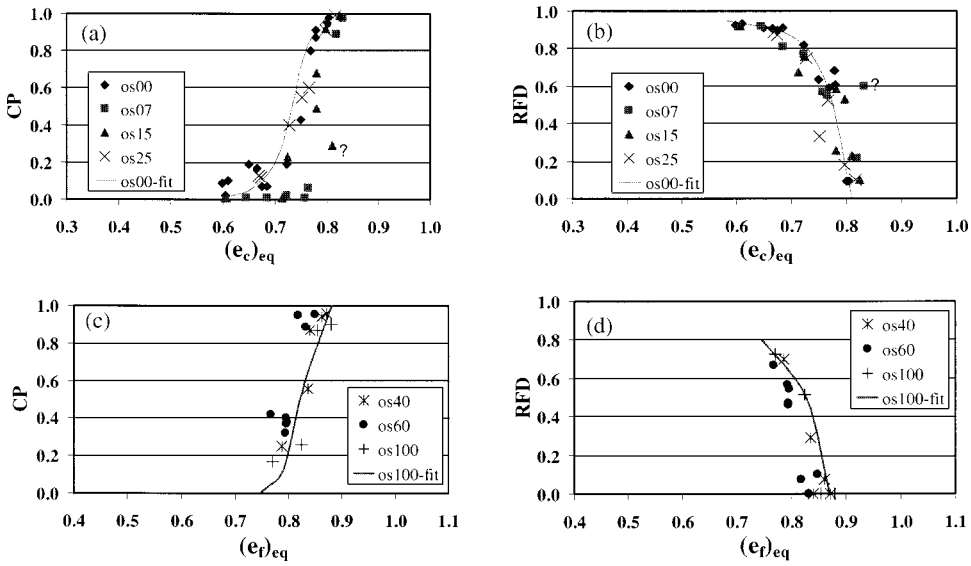

Fig. 9. CP and RFD versus $(e_c)_{eq}$ and $(e_f)_{eq}$

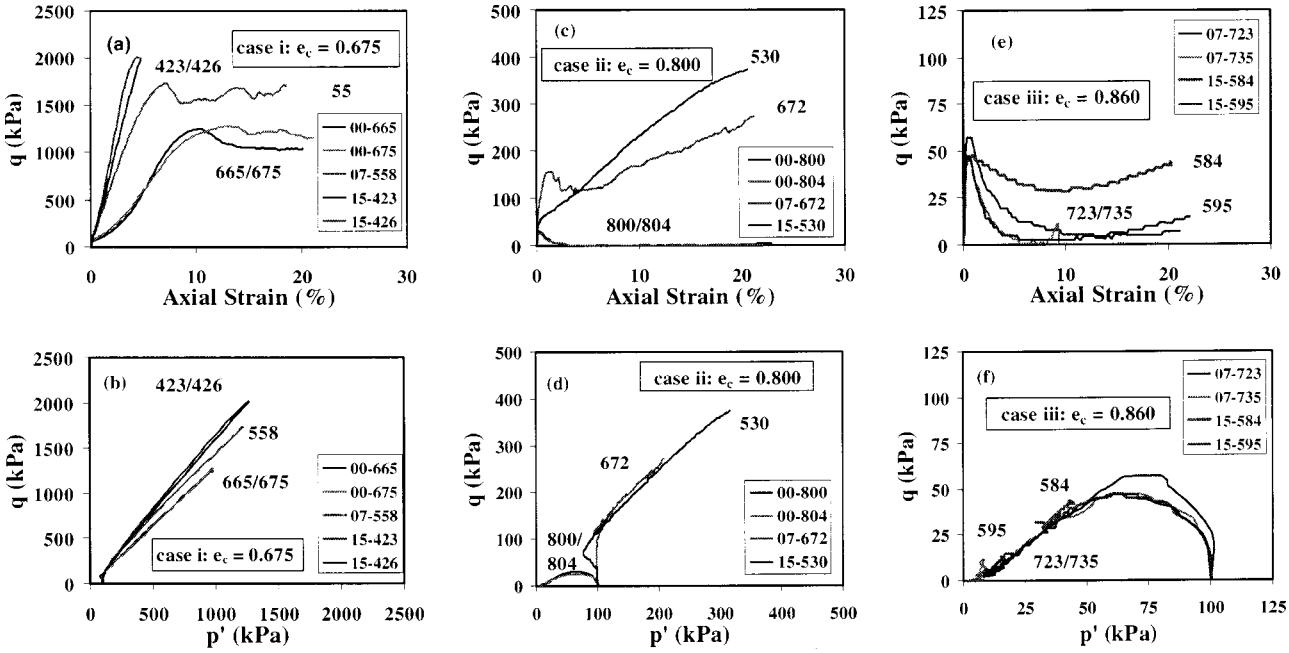

Fig. 10. Stress–strain behavior: (a and b) series B1; (c and d) series B2; and (e and f) series B3

contacts are also apparent. As observed before for steady-state and stress–strain behavior, at the same void ratio, CP increases with an increase in fines content when $FC<FC_{th}$. The trend reverses when $FC>FC_{th}$. The opposite trend is observed for the RFD for $FC<FC_{th}$ and $FC>FC_{th}$, respectively. When plotted against $(e_c)_{eq}$ and $(e_f)_{eq}$, all data fall into the vicinity of the data for the pure sand and pure silt, respectively [Figs. 9(a–d)].

Secondary Role of Fines: $FC<FC_{th}$

At low fines content, while the intergranular friction plays an important role, fine grains play a *secondary* role with regard to triggering fragility. Which grain size is dominant matters a great deal depending on whether the fines occupy the intergranular void space (providing the cushioning effect) or they begin to separate the coarse grains and lead to a metastable coarse grain skeleton ($e_c>e_{max,HC}$) that is otherwise unattainable without the aid of the fines. The former is the case when the fines occupy the intergranular voids and e_c is less than a certain threshold value [case (ii)]. The latter can be unstable if disturbed, and it occurs when the soil is like that in case (iii). This can be highlighted using test data from series B1, B2, and B3 (Fig. 10).

In Figs. 10(a and b), the specimens at nearly the same e_c ($=0.675<e_{max,HC}$) exhibit similar behavior, but the silty sands are somewhat stronger than the host sand due to the cushioning effect provided by the fines that resist the tendency to collapse. The cushioning effect of fines is more prominent in Figs. 10(c and d).

In Figs. 10(c and d), at nearly the same e_c ($=0.80\pm0.01$ near $e_{max,HC}$), the loose clean sand specimen, 00-800, is completely collapsible. In contrast, the two silty sand specimens, 07-672 and 15-530, which are equally loose in terms of e_c, are indeed dilative. While the e_c values are nearly the same, part of the intergranular void space in the silty sand specimens contains the fines compared to no fines present in 00-800. Thus, it is hypothesized that the void space into which an unstable coarse grain can fall during collapse is reduced. The host sand is in the vicinity of its loosest packing (near $e_{max,HC}$) that is inherently unstable, whereas for the silty sands, at the same e_c, the silt grains support the loose intergranular skeleton and offer more stability. Thus the collapse potential of silty sand is less than that of the host sand at the same e_c. The difference in collapse potential between two silty sands is not very high as long as the difference between the fines content is small and the voids are not full of fines ($e_f=\text{large}>e_{max,HF}$). However, with a further increase in fines (at the same e_c), interfine contact friction begins to play an active role with a further reduction in e_f ($<e_{max,HF}$); the soil moves into case (iv) (discussed later).

In Figs. 10(e and f), at the same e_c ($>e_{max,HC}$), an increase in fines tends to slightly reduce the collapse potential. The reasons for this behavior are the same as the reasons presented for case (ii). Another important observation is that, among all cases [(i)–(iii)] except for the clean sand in case (ii), the soils in case (iii) generally show fragility. The reason for the exception in case (ii) (00-800) was explained earlier. The reasons for the increase in collapse potential for case (iii) appear to be (1) the e_c is looser in case (iii) than in case (i) or (ii); and (2) a fair number of coarse grain contacts are separated by the fine grains (to reach $e_c>e_{max,HF}$. With increasing strain these contacts are dislodged into voids that are relatively large compared to the fine grain particle size. However, at the same e_c, increasing fines tend to resist collapse and offer some resistance to further deformation beyond the initial collapse in case (iii).

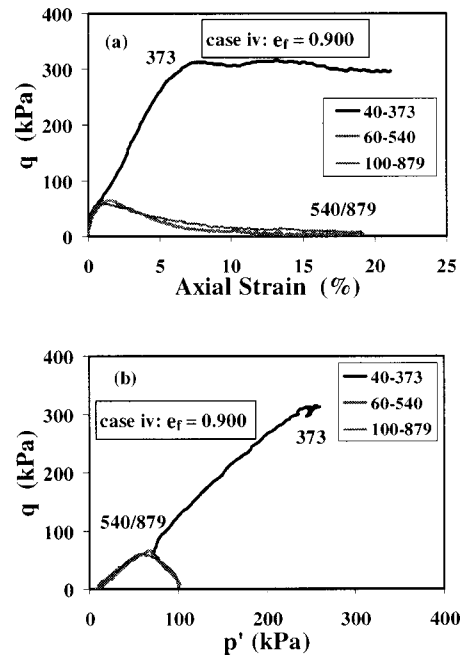

Fig. 11. Stress–strain behavior: series B4

Secondary Role of Coarse Grains: $FC>FC_{th}$

The secondary reinforcement effect by the coarse grains can be highlighted using the data from series B4. Figs. 11(a and b) show the data for specimens tested at nearly the same e_f (near 0.9). The magnitude of FC_L is about 69%, approximately, at $e_f=0.9$ for this soil. At nearly the same e_f, specimen 100-879 falls into case (iv-1), 60-540 ($e_f=0.90$, $e_c=2.85$) falls in the vicinity of the theoretical boundary for cases (iv-1) and (iv-2), and 40-373 ($e_f=0.93$, $e_c=1.29$) falls into case (iv-2). The silt specimen, 100-879, and sandy silt specimen, 60-540, show similar behavior. This is because the value of e_c for 60-540 is too large for the dispersed coarse grains to provide any significant secondary reinforcement effect. Its behavior is primarily affected by interfine contacts. Specimen 40-373 is stronger than both 100-879 and 60-540. The reason for this is the low value of e_c and the reinforcement effect by the dispersed grains.

Conclusions

Results indicate that the mechanical behavior and collapse potential of silty sands and sandy silts depend on intergrain contact density. In general, intergranular void ratios (e_c and e_f) or equivalent intergranular void ratios [$(e_c)_{eq}$ and $(e_f)_{eq}$] are found to be better contact density indices to characterize the mechanical response of granular mixes than the global void ratio.

At low fines contents [cases (i)–(iii), $FC<FC_{th}$], the intercoarse-grain friction is the dominant mechanism affecting the mechanical response of silty sands. When compared at the same $(e_c)_{eq}$, the behavior of all silty sand specimens at $FC<FC_{th}$ is similar to that of the host sand at $e=(e_c)_{eq}$.

The dominant mechanisms that affect the shear response for sandy silt [$FC>FC_{th}$, case (iv)] are interfine contact density and

friction. The strength of sandy silt is typically higher than that of pure silt at the same e_f. The collapse potential decreases with an increase in sand content at the same e_f. When compared at the same $(e_f)_{eq}$, the behavior of all sandy silt specimens is similar to that of the host silt at $e=(e_f)_{eq}$.

Silty sands and sandy silts can be deceptive in that they may have low global void ratios (or high relative density values) while having high susceptibility to undrained collapse. The intergranular matrix structure needs to be examined to predict this susceptibility. The equivalent intergranular contact void ratios $(e_c)_{eq}$ and $(e_f)_{eq}$ can be used as the primary indices to make this prediction. It is not clear what unique index would be suitable to characterize the behavior of the entire spectrum from clean sand to pure silt.

Acknowledgments

The writers appreciate the work by reviewers to improve the clarity of this paper. Financial support for this ongoing work by USGS and the National Science Foundation is gratefully acknowledged.

Notations

The following symbols are used in this paper:

b = portion of fine grains that contribute to active intergrain contacts;
CP = collapse potential index;
D = diameter of coarse grains;
d = diameter of fine grains;
e = global void ratio;
e_c, $(e_c)_{eq}$ = intergranular void ratio and equivalent intergrain contact void ratio, respectively;
e_f, $(e_f)_{eq}$ = interfine void ratio and equivalent interfine contact void ratio, respectively;
e_{max}, e_{min} = maximum and minimum void ratio of soil, respectively;
$e_{max,HC}$, $e_{min,HC}$ = maximum and minimum void ratio of host coarse grain soil (sand), respectively;
$e_{max,HF}$, $e_{min,HF}$ = maximum and minimum void ratio of host fines, respectively;
FC = fines content (%);
FC_{th}, FC_L = threshold and limiting fines content, respectively;
HC, HF = host coarse grain soil (sand) and host fines (silt), respectively;
m = reinforcement factor;
p' = mean effective stress $(\sigma'_1+2\sigma'_3)/3$;
p'_{ss}, p'_{qss} = mean effective stress at steady state and quasi-steady state, respectively;
q = deviatoric stress;
R_d = particle size disparity ratio (D/d);
RFD = index of resistance to further deformation;
s = spacing between fine grains;
u = pore pressure;
u_{sh} = shear induced pore pressure;
ε_{max} = maximum axial strain;
σ'_c = initial effective confining stress; and
σ'_1, σ'_3 = effective major and minor principal stresses, respectively.

References

Baziar, M. H., and Dobry, R. (1995). ''Residual strength and large-deformation potential of loose silty sands.'' *J. Geotech. Eng.*, 121(12), 896–906.

Chameau, J. L., and Sutterer, K. (1994). ''Influence of fines in liquefaction potential and steady state considerations.'' *Proc., 13th Int. Conf., Soil Mechanics Foundation Engineering*, New Delhi, India, A. A. Balkema, Rotterdam, The Netherlands, 5, 183–84.

Chang, N. Y. (1990). ''Influence of fines content and plasticity on earthquake-induced soil liquefaction.'' *Contract Rep. DACW3988-C-0078*, U.S. Army Waterways Experiment Station, Vicksburg, Miss.

Ishihara, K. (1993). ''Liquefaction and flow failure during earthquakes.'' *Geotechnique*, 43(3), 351–415.

Japanese Geotechnical Society (JGS). (1996). ''Geotechnical aspects of the January 17, 1995 Hyogoken–Nambu earthquake.'' *Soils Foundations, Special issue*, Japanese Soc. Geotechnical Eng.

Koester, J. P. (1994). ''The influence of fines type and content on cyclic strength.'' *Ground failures under seismic conditions, Geotech. Spec. Publ. 44*, ASCE, New York, 17–33.

Kuerbis, R., Nagussey, D., and Vaid, Y. P. (1988). ''Effect of gradation and fines content on the undrained response of sand.'' *Proc., Hyd. Fill Struc. Geotech. Spec. Publ. 21*, ASCE, New York, 330–345.

Mooney, M. A., Viggiani, G., and Finno, R. (1997). ''Undrained shear band deformation in granular media.'' *J. Eng. Mech.*, 123(6), 577–585.

Pitman, T. D., Robertson, P. K., and Sego, D. C. (1994). ''Influence of fines on the collapse of loose sands.'' *Can. Geotech. J.*, 31(5), 728–739.

Polito, C. P., and Martin, II, J. R. (2001). ''Effects of nonplastic fines on the liquefaction resistance of sands.'' *J. Geotech. Geoenviron. Eng.*, 127(5), 408–415.

Poulos, S. J. (1981). ''The steady state of deformation.'' *J. Geotech. Eng.*, 107(5), 553–562.

Roscoe, K. H. (1970). ''The influence of strains in soil mechanics.'' *Geotechnique*, 20(2), 129–170.

Seed, H. B. (1987). ''Design problems in soil liquefaction.'' *J. Geotech. Eng.*, 113(8), 827–845.

Seed, R. B., and Harder, L. F., Jr. (1990). ''SPT-based analysis of cyclic pore pressure generation and undrained residual strength.'' *Proc., Seed Memorial Symp.*, Berkeley, 2, BiTech, Ltd., Vancouver, B.C., 351–376.

Stark, T. D., and Mesri, G. (1992). ''Undrained shear strength of liquefied sands for stability analysis.'' *J. Geotech. Eng.*, 118(11), 1727–1747.

Thevanayagam, S. (1998). ''Effect of fines and confining stress on undrained shear strength of silty sands.'' *J. Geotech. Geoenviron. Eng.*, 124(6), 479–491.

Thevanayagam, S. (1999a). ''Closure to 'Effect of fines and confining stress on undrained shear strength of silty sands.' '' *J. Geotech. Geoenviron. Eng.*, 125(11), 1024–1027.

Thevanayagam, S. (1999b). ''Liquefaction and shear wave velocity characteristics of silty/gravely soils.'' *Proc., 15th U.S.–Japan Workshop on Bridge Engineering*, Public Works Research Institute, Tsukuba City, Tokyo, 133–147.

Thevanayagam, S. (2000a). ''Liquefaction potential and undrained fragility of silty sands.'' *Proc., 12th Int. Conf. Earthquake Engineering*, R. Park, ed., Auckland, New Zealand, *Paper 2383*, New Zealand Society of Earthquake Engineers, UpperHutt, New Zealand.

Thevanayagam, S. (2000b). ''Liquefaction in silty soils—Considerations for screening and retrofit strategies.'' *Proc., 2nd Int. Workshop on Mitigation of Seismic Effects on Transportation Structures*, National Center for Research on Earthquake Engineering, C. Loh and I. Buckle, eds., Taipei, Taiwan, 374–385.

Thevanayagam, S., and Mohan, S. (2000). ''Intergranular state variables and stress-strain behaviour of silty sands.'' *Geotechnique*, 50(1), 1–23.

Thevanayagam, S., Fiorillo, M., and Liang, J. (2000). ''Effect of non-plastic fines on undrained cyclic strength of silty sands.'' *Soil Dynamics Liquefaction, Geotech Spec. Publ. 107*, ASCE, Colorado, 77–91.

cVaid, Y. P. (1994). ''Liquefaction of silty soils.'' *Proc., Ground failures under seismic conditions, Geotech. Spec. Publ. 44,* ASCE, New York, 1–16.

Yamamuro, J. A., and Covert, K. M. (2001). ''Monotonic and cyclic liquefaction of very loose sands with high silt content.'' *J. Geotech. Geoenviron. Eng.,* 127(4), 314–324.

Yamamuro, J. A., and Lade, P. V. (1998). ''Steady-state concepts and static liquefaction of silty sands.'' *J. Geotech. Geoenviron. Eng.,* 124(9), 868–877.

Zlatovic, S., and Ishihara, K. (1997). ''Normalized behavior of very loose non-plastic soils: Effects of fabric.'' *Soils Found.,* 37(4), 47–56.

Thevanayagam, S. & Mohan, S. (2000). *Géotechnique* **50**, No. 1, 1–23

Intergranular state variables and stress–strain behaviour of silty sands

S. THEVANAYAGAM* and S. MOHAN†

Relative contributions by the coarser and finer grains in a silty sand to its stress–strain response are affected by the intergranular matrix structure. The nature of this contribution is illustrated using an intergranular matrix phase diagram in terms of void ratio (e), fines content (FC), and intergranular and interfine void ratios (e_s and e_f). New intergranular state parameters (ψ_s, ψ_f) and (e_s, e_f) are introduced as state variables to characterize silty sands; e_s and e_f dictate the steady-state characteristics of silty sand at low and high fines contents, respectively; ψ_s and ψ_f reflect the plastic compressibility characteristics at low and high fines contents, respectively. Using these state variables, the anticipated stress–strain–strength behaviour of silty sand in comparison to that of the host sand is presented. Similar stress-strain behaviour is expected at the same e_s and initial confining stress σ'_c, with a few exceptions.

At a constant void ratio e, e_s increases while e_f decreases with addition of fines; a silty sand passes through different states. First, at low fines content, e_s ($< e_{max,HS}$, the maximum void ratio of the host sand, case 1), and high e_f, the stress–strain behaviour is primarily governed by intergranular friction between the coarser grains. The steady-state line (SSL) is primarily dependent on e_s and is fairly independent of σ'_c; When compared at the same e_s and at the same σ'_c (or at the same ψ or ψ_s), the silty sand and the host sand show similar (not identical) stress–strain behaviour; with addition of fines, as e_s increases, the collapse potential increases and the stress–strain response becomes weaker. Second, with further addition of fines, when e_s approaches or exceeds $e_{max,HS}$, the SSL is influenced by e_s and σ'_c. When e_s is near $e_{max,HS}$ (case 2), the stress–strain curves for silty sands are similar at the same e_s and the same σ'_c (or at the same ψ or ψ_s), but different from and stronger than that of the host sand. At very loose states ($e_s > e_{max,HS}$; case 3), the stress–strain curves, normalized with respect to σ'_c, are similar at the same e_s (or at the same ψ or ψ_s). Third, with further addition of fines beyond a threshold value, e_f becomes sufficiently low (case 4); the fines impart a significant influence, while the role of intergranular (coarser-grain) friction diminishes; the silty sand is expected to behave similarly (not identical) to the host fines at the same e_f and ψ_f; at this stage, with further addition of fines, the collapse potential decreases.

Le rôle relatif des grains plus gros et des grains plus fins dans la réponse contrainte-déformation d'un sable silteux est affecté par la structure de la matrice intergranulaire. La nature de ce rôle est illustrée au moyen d'un diagramme de constitution de matrice intergranulaire en termes de taux de pores (e), teneur en fines (FC) et taux de pores intergranulaires et interfines (e_s et e_f). Nous introduisons de nouveaux paramètres d'état intergranulaire (ψ_s et ψ_f) et (e_s et e_f) comme variables d'état pour caractériser les sables silteux; e_s et e_f dictent les caractéristiques d'état stable du sable silteux pour des teneurs en fines faibles et élevées respectivement: ψ_s et ψ_f reflètent les caractéristiques de compressibilité plastique pour des teneurs en fines faibles et élevées, respectivement. En utilisant ces variables d'état, nous présentons le comportement anticipé contrainte-déformation-résistance du sable silteux par rapport à celui du sable hôte. Le comportement contrainte-déformation devrait être similaire pour le même e_s et pour une contrainte de confinement initiale σ'_c, à part quelques exceptions.

Pour un taux de pores constant e, e_s augmente alors que e_f diminue avec l'adjonction de fines; un sable silteux passe par différents états: (a) quand le contenu en fines est faible, e_s ($< e_{max\cdot HS}$, le taux de pores max. du sable hôte, Cas-i) et quand e_f est élevé, le comportement contrainte-déformation est avant tout gouverné par la friction intergranulaire entre les grains les plus gros; la ligne d'état stable (SSL) dépend avant tout de e_s et n'est pas très dépendante de σ'_c; quand on compare le sable silteux et le sable hôte aux mêmes e_s et aux mêmes σ'_c (ou aux mêmes ψ ou ψ_s), ceux-ci montrent un comportement contrainte-déformation similaire (mais pas identique); avec l'adjonction de fines, à mesure que e_s augmente, le potentiel d'affaissement augmente et la réponse contrainte-déformation devient plus faible; (b) quand on continue à ajouter des fines, quand e_s approche ou dépasse $e_{max\cdot HS}$, la SSL est influencée par e_s et σ'_c; quand e_s se rapproche de $e_{max\cdot HS}$ (Cas-ii), les courbes contrainte-déformation pour les sables silteux sont similaires pour le même e_s et identiques pour le même σ'_c (ou aux mêmes ψ ou ψ_s), mais différentes et plus fortes que celles du sable hôte; pour les états très meubles ($e_s > e_{max\cdot HS}$; Cas-iii), les courbres contrainte-déformation, normalisées par rapport à σ'_c sont similaires pour le même e_s (ou aux mêmes ψ ou ψ_s); et (c) quand on continue à ajouter des fines au-delà de la valeur seuil, e_f devient suffisamment faible (Cas-iv); les fines ont une influence significative tandis que le rôle de la friction intergranulaire (grains plus gros) diminue; le sable silteux devrait avoir un comportement similaire (mais pas identique) à celui des fines hôtes pour les mêmes e_f et ψ_f; à ce stade, avec l'adjonction de fines supplémentaires, le potentiel d'affaissement diminue.

KEYWORDS: laboratory tests; liquefaction; pore pressures; sands; silts; stress paths.

INTRODUCTION

In the past, most of the laboratory studies on undrained stress–strain behaviour of granular soils were confined to relatively clean sands. Many natural sandy soils contain a significant amount of fines (passing sieve No. 200, particle size less than 0·074 mm). Field observations of liquefaction-related failures indicate that sites with sandy soils containing fines behave differently from sites consisting of relatively clean sands (Seed *et al.*, 1983; Seed, 1987; Seed & Harder, 1990). Recognizing this, several researchers have recently begun to study the effect of fines on stress–strain behaviour, collapse potential, steady-state strength, and cyclic response of silty sands (Chang, 1990; Georgiannou *et al.*, 1990, 1991a, b; Chameau & Sutterer, 1994; Finn *et al.*, 1994; Koester, 1994; Singh, 1994; Vaid, 1994; Thevanayagam *et al.*, 1995, 1996a, b; Zlatovic & Ishihara, 1995). Efforts have also been made to develop correlations of the effect of fines on resistance to liquefaction and post-liquefaction strength based on field performance data (Seed *et*

Manuscript received 15 July 1997; revised manuscript accepted 27 July 1999. Discussion on this paper closes 31 August 2000; for further details see p. ii.
* SUNY at Buffalo.
† California Dept. of Transportation.

al., 1983; Seed, 1987; Seed & Harder, 1990; Stark & Olson, 1995). The experimental studies thus far followed a comparative approach. The behaviour of silty sands prepared at different fines contents has been compared with the behaviour of the host sand. The basis for comparison is not often clear. A rational basis is essential to extrapolate the observed differences to other silty sands at different fines contents.

Traditionally, perhaps originating from the early work on the 'e–log(p')' relation proposed by Terzaghi, void ratio e has been chosen as one of the most important state variables to characterize the behaviour of soils. This has partly influenced the work of Roscoe and co-workers (Roscoe *et al.*, 1958, 1963; Roscoe & Burland, 1968) in their choice of (p', q, e) as the state variables in critical state soil mechanics (where p' = mean effective stress, and q = deviatoric stress) and the formulation of the so-called steady-state concept (Poulos, 1981). The steady-state strength (at least for a restricted mode of failure) has been correlated with void ratio (Fig. 1(a)). Sand specimens that are at an initial state above the steady-state line (SSL) show contractive behaviour (C in Figs 1(b)–(e)). Those below the SSL show dilative behaviour (D in Figs 1(b)–(e)). If the initial state is in the vicinity of the SSL, the stress–strain behaviour is often initially contractive, followed by dilation (C–D in Figs 1(b)–(e)). Combining the effects of void ratio and confining stress on the observed stress–strain response of sands, alternative state variables have been put forward to characterize the stress–strain response of soils. They include the state parameter ψ (Fig. 1(a)) (Been & Jefferies, 1985; Jefferies & Been, 1987) and the state index (Ishihara, 1993). Relatively clean sand specimens with the same state parameters show similar stress–strain behaviour. Positive values for ψ signify contractive behaviour, whereas negative values for ψ signify dilative behaviour. Another concept that has remained dormant and has been applied only recently to study comparatively the behaviour of silty sands (Kuerbis *et al.*, 1989; Pitman *et al.*, 1994) is the concept of sand skeleton void ratio (Mitchell, 1993). All these concepts have been used in comparative studies to evaluate the shear strength and collapse potential of silty sands.

Notwithstanding their merits, application of these concepts to describe the anticipated undrained behaviour of silty sands has faced problems. Observations of stress–strain behaviour have revealed confusing behaviour. Silty sands have a smaller steady-state strength compared to clean host sands at the same void ratio (or relative density). At the same void ratio, an increase in fines content leads to a decrease in steady state strength followed by an increase in strength beyond a certain limiting fines content. This transition fines content has been observed to be in the vicinity of 20–30% by weight of total solids (Pitman *et al.*, 1994; Zlatovic & Ishihara, 1995; Thevanayagam *et al.*, 1996a, b). The stress–strain behaviour of different silty sands prepared at different fines content, when compared in terms of the state parameter ψ, did not always exhibit the expected trend of increased contractiveness with increase in ψ as observed for clean sands (Pitman *et al.*, 1994). Similarly, when compared in terms of sand skeleton void ratio, specimens of Ottawa sand prepared at four different fines contents (10%, 20%, 30% and 40% crushed silica fines), each at a progressively higher sand skeleton void ratio, showed an increased degree of dilation (Pitman *et al.*, 1994).

While there is a better understanding of the anticipated behaviour of a clean sand under undrained monotonic and cyclic loading in terms of its initial state of stress, void ratio and state parameter, there is mixed opinion in the literature on the role of fines in the stress–strain behaviour of a silty sand (e.g. Pitman *et al.*, 1994; Vaid, 1994; Zlatovic & Ishihara, 1995). The basis for determination of whether a silty sand would be contractive or dilative and what kind of stress–strain behaviour is to be expected compared with that of clean sand is less clear. What controls the behaviour of silty sands remains to be resolved. The question is one of paramount importance. Natural sands contain a significant and varying amount of fines, whereas the current knowledge is primarily based on clean sands. As was recently pointed out (Thevanayagam *et al.*, 1996a, b), many of the case histories of post-lique-faction failure (Seed & Harder, 1990) involved soils containing fines.

The present study focuses on developing a framework for understanding the matrix effects and identifying new state variables for characterizing the undrained triaxial stress–strain behaviour of (gap-graded) silty sands compared with that of the host sand and the host silt. First, the rationale for the traditional use of global void ratio (e) and state parameter (ψ) as state variables to describe the stress–strain behaviour of sands is explored. The critical state soil mechanics framework is extended to silty sands modified in terms of intergranular void ratios (e_s, e_f) and intergranular state parameters (ψ_s, ψ_f). The stress–strain behaviour of silty sand in comparison with that of the host sand and the host silt is presented. Although the experimental study is limited to triaxial compression only, the concept applies to other stress paths and modes of deformation as well.

PRESENT STUDY—FRAMEWORK

Critical state index and plastic compressibility

The soil microstructure is complex. It consists of a collection of interacting clusters ordered in some organized fashion at different scale levels, each dictated by different force fields (electrical, chemical, mechanical). The mechanisms affecting the soil response at each scale level are not necessarily the same, but they all collectively influence the macro-behaviour. The macro-behaviour can be predicted by studying and integrating the behaviour at each scale level. This concept has recently been successfully applied to study flow through clayey soils and dispersion phenomena in porous media (Thevanayagam, 1997; Thevanayagam & Nesarajah, 1998). It applies equally to the mechanical behaviour. Evidence for this can be drawn from the experiments on stress–strain behaviour of two-dimensional disc assemblies conducted by Drescher & De Josselin de Jong (1972). The system was found to behave as an assembly consisting of block-like sub-regions.

When an external force acts on a soil specimen, this force is distributed and carried internally by a hierarchy of clusters. These clusters constitute an internal force chain formed by active grain contacts that transfer the normal forces and sustain shear forces. Active sliding, rolling and interactions occur at the contact boundaries between the skeletons at each scale level. Active frictional contacts and mineral surface friction are the primary mechanisms of resistance to deformation. As the external load changes, the sub-matrices at each scale level deform. The active contacts change and reorient until an ultimate state is reached where any further deformation does not alter the nature of active contacts at the same volume (ideally). This tendency for change (hereafter referred to as plastic compressibility) dictates the macroscopic stress–strain response characteristics. The plastic compressibility itself changes as the microstructure is altered. A set of indices that represent the active frictional contacts and the tendency for change in active contacts (compressibility of the sub-matrices) is needed to qualitatively characterize the stress–strain behaviour. Before such indices are proposed, it is prudent to revisit the concepts of critical state soil mechanics and identify the physical meaning of the state variables utilized therein in this framework.

Void ratio—critical state index. Reverting to a rather simpler model, first consider a perfectly arranged (body-centred cubic lattice) system of spherical particles of equal size. When acted upon by an external force, all particles may participate in the force chain transferring and sustaining normal and shear forces. If one considers a perfect face-centred cubic lattice instead, the force chain will be different and so will the void ratio. Hence void ratio could be used as an index of active contacts.

A direct extension of this analogy to sands is not perfect. Sandy soils contain particles of a wide range of size and shape arranged in a heterogeneous form. There is reason to believe that, once acted upon by an external force, some of the grains, by virtue of their size, heterogeneous positions, and availability

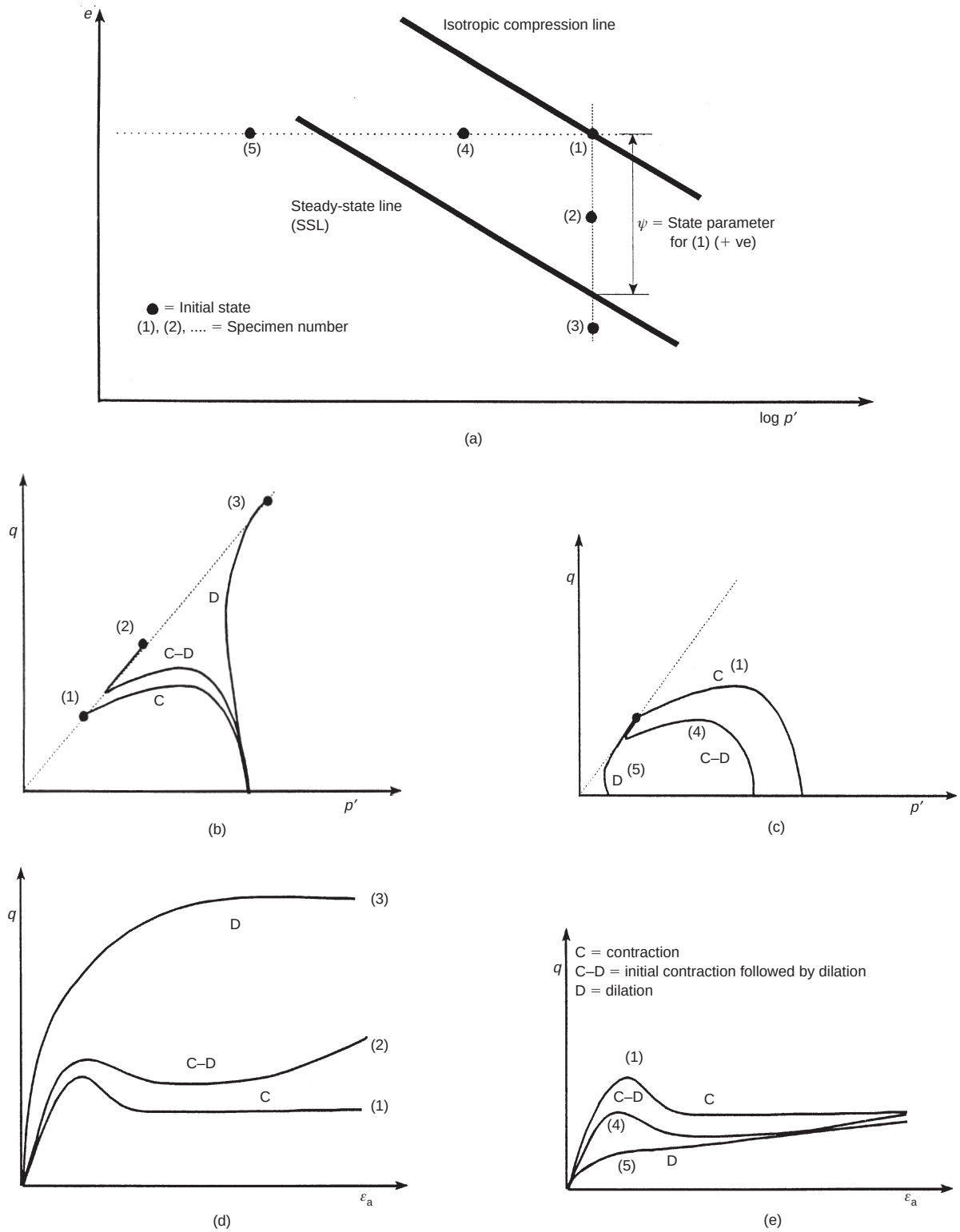

Fig. 1. Undrained stress–strain behaviour—schematic diagram

of void space to adjust their positions without significantly affecting the adjacent particles, may not actively participate in transferring the normal forces or sustain significant shear forces. Only a fraction of the particles may actively participate in sustaining the shear forces along their contacts and form the force chain, while the others remain relatively inactive. Void ratio is only an approximate, imperfect index of active contacts in the force chain. Rather, the void space distribution (or pore size distribution) becomes a better descriptor of active contacts (Altschaeffl & Thevanayagam, 1991; Thevanayagam, 1989). Nevertheless, for many practical applications, one is often left with void ratio as the sole index.

The question is, at what state is void ratio an index of active contact? Limiting the discussion to uniform sands, taking undrained triaxial compression as an example, however, the active contacts cannot remain the same throughout the entire undrained deformation process of a specimen (at the same void ratio). If there exists a unique ultimate steady state, in a more restricted triaxial compression mode, then the void ratio is an approximate index of active contacts at the ultimate steady state

only. The parameters (p_f, q_f, e) refer to the ultimate state where further shear strains do not alter the force chain or the active contacts or cause any further plastic volumetric compression. Void ratio is an index of the microstructure of active particles at critical state.

State parameter—plastic compressibility index. At any other state, the difference between the current state (p', q, e) and the ultimate state (p'_f, q_f, e) signifies the anticipated changes in the active contacts (plastic compressibility) and the associated deformation characteristics of the sand. This difference in states expressed in any form together with void ratio foretells the anticipated behaviour of a soil and the ultimate state. In critical state soil mechanics, using the so-called work-assumption postulate (Roscoe & Burland, 1968), the incremental plastic volumetric compressibility (hence the contractive or dilative behaviour) upon shearing is expressed in terms of the state of stress ($\eta = q/p'$) and the ultimate (critical) state ($M = q_f/p'_f$):

$$\frac{\Delta\varepsilon_v^p}{\Delta\varepsilon_q^p} = \frac{M^2 - \eta^2}{2\eta}; \text{ where } M = \frac{6\sin\phi}{3 - \sin\phi} \tag{1a}$$

where $\Delta\varepsilon_v^p$ = incremental plastic volumetric strain, $\Delta\varepsilon_q^p$ = incremental plastic shear strain, and ϕ = mobilized angle of shearing resistance at critical state. Variations of this formulation incorporating the effects of initial and induced anisotropy can be found elsewhere (Dafalias, 1987, Thevanayagam, 1989; Thevanayagam & Chameau, 1992).

Although not widely recognized in the published literature, the above work assumption can be rewritten simply in terms of the critical state parameters and the state parameter (ψ).

$$\frac{\Delta\varepsilon_v^p}{\Delta\varepsilon_q^p} = \frac{M\left(2 - R^{(1(\psi/\psi_0))}\right)}{2\left(R^{(1(\psi/\psi_0))} - 1\right)^{1/2}} = f(\psi, \psi_0, M, R) \tag{1b}$$

where ψ = state parameter at any stage during loading in triaxial compression, ψ_0 = the initial state parameter at the isotropic normally compressed state (Thevanayagam, 1989), and $R = 2$ according to the work assumption of Roscoe & Burland (1968). Hence, within the framework of critical state soil mechanics, the state parameter ψ has the connotation of a partial measure of plastic volumetric compressibility of the soil, whereas void ratio refers to its ultimate state.

While the 'work assumption' may not accurately describe the internal mechanisms of deformation, using this only as a guide, the parameters (ψ, e) are expected to partially foretell the anticipated deformation characteristics and the ultimate state of the soil. Whether it can be used to foretell comparatively the behaviour of silty sands at different fines contents based on the knowledge gained from studies on clean sands is explored next.

Critical state index and plastic compressibility—silty soils

For silty sands, the direct use of global void ratio and state parameter as a set of unique state variables is expected to break down further. Due to the existence of large intergranular pores of tens of micrometers in size (between the sand grains), there is reason to believe that, during deformation, the micrometre to submicrometre particles (fines) would tend to adjust their positions, moving through the pores without significantly affecting the adjacent particles. Very little opportunity exists for the finer grains to actively participate in transferring the normal forces or sustain significant shear forces, if they are contained within the intergranular void spaces, and their quantity is smaller than a threshold value. Only a fraction of the particles may actively participate in sustaining the shear forces. An analysis of the uniform-sized spherical particle system considered before but containing a small percentage of smaller-sized particles contained in it shows that the minimum size disparity for this to occur is only about 6·5, although practical considerations would demand a much higher size ratio. On the other hand, noticeable participation is possible if the fines fall between the coarser grain contacts or they are in sufficient quantity to fill the intergranular space and begin to displace the coarser grain contacts. Hence, the direct use of critical state mechanics concepts and the associated state variables (e, ψ) as unique indices of active contacts and plastic compressibility of silty soils is difficult. They may not discriminate the differences in the microstructure and therefore may not be directly used to forecast what to expect of a silty soil at different fines contents.

The problem could be simplified by considering the silty sand as a delicate matrix consisting of two sub-matrices, namely, the coarser-grained matrix and the finer-grained matrix, and approximately analysing how they interact with each other. Consideration is given to the differences in compressibility of the respective individual matrices. For this purpose, in the remainder of this paper, the finer grains are defined as those whose size is significantly less than that of the voids that would be present in the soil, if it were to contain only the coarser grains at the same void ratio. In the case of a silty sand or clayey sand, the finer grain size is conveniently chosen as that passing sieve number 200 (0·074 mm), although logically the choice should be made on the basis of the pore size distribution of the coarser-grained matrix. In the case of a sandy gravel, sand sizes (or less) may be considered to be the finer grains as long as the size disparity is large.

Intergranular void ratio—critical state index. At low fines content less than a threshold value, it is assumed that the finer grains do not actively participate in the transfer of contact frictional forces, or their contribution is secondary. The rationale is that at such low fines contents the finer-grains matrix is highly compressible unless the fines are located at the contact points between the coarser grains or when they are trapped in the intergranular void spaces at a compacted state. With this assumption, as a first-order approximation, the volume of fines is considered to be a part of the voids between the coarser grains. Neglecting the differences in specific gravity of the finer and coarser grains in a silty sand, for a unit volume of solids (without the fluid/gas phases) containing both sizes of grains at a fines content FC (as a percentage of the total weight of the solids), the volume of fines would be FC/100 and the volume of coarser grains would be (1 − FC/100). Accordingly, the intergranular (coarser-grains) void ratio e_s is defined as the volume of the voids plus the finer grains per unit volume of the coarser grains:

$$e_s = \frac{[e + (\mathrm{FC}/100)]}{[1 - (\mathrm{FC}/100)]} \tag{2}$$

where e is the global void ratio of the silty sand.

Intergranular steady-state line. By analogy, the intergranular void ratio, e_s, is considered to be an index of active coarser granular frictional contacts that sustain the normal and shear forces at the ultimate state. Then, for the same host sand, a unique intergranular steady-state line (ISSL, the locus of steady-state points in e_s versus $\log(p'_f)$ plane; Fig. 2(a)) is expected for silty sands at all fines contents (until a threshold is reached). The ISSL is expected to coincide with the SSL for the host sand, except for the cases where the finer grains may also participate in the force chain, as discussed before. The traditional SSLs (e versus $\log(p')$) are expected to be different at different fines contents. Equation (2) indicates that each SSL is expected to lie progressively lower in the e versus $\log(p')$ plane with an increase in fines content (up to the threshold). A traditional SSL for a silty sand at a particular fines content $\mathrm{FC} = \mathrm{FC}_1$ is shown in Fig. 2(a). The SSL lines are expected to be, not necessarily but practically, nearly parallel to the ISSL.

Intergranular state parameter—plastic compressibility index. If indeed the intergranular contact is the primary mechanism contributing to the stress–strain behaviour, then the compressibility of the material must also be attributed to intergranular contacts. Extending the work assumption (equation (1)) and the

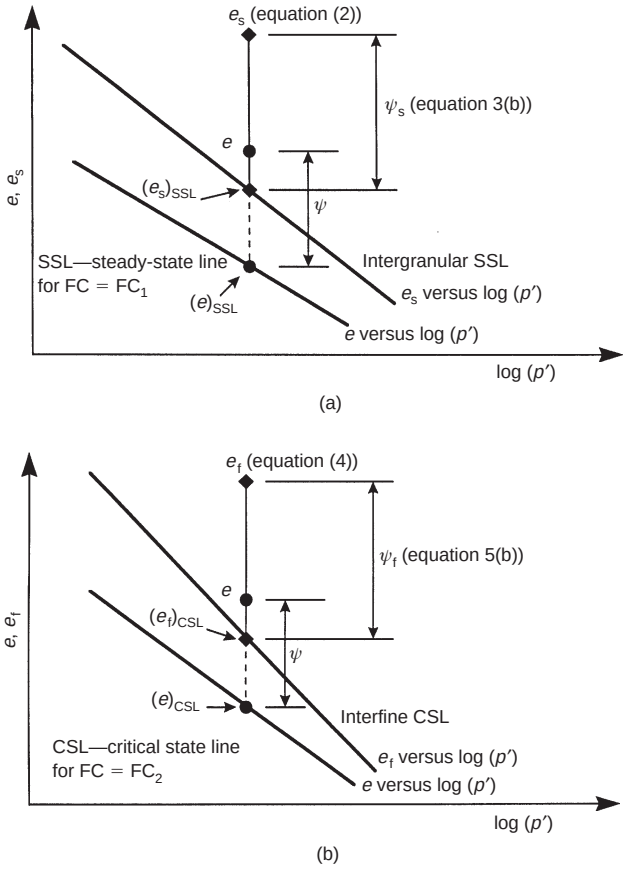

Fig. 2. Intergranular and interfine state parameters—schematic diagram: (a) low fines content; (b) high fines content

critical state soil mechanics concepts, the corresponding dilatancy equation is

$$\frac{\Delta\varepsilon_v^p}{\Delta\varepsilon_q^p} = \frac{M\left(2 - R^{(1(\psi_s/\psi_{so}))}\right)}{2\left(R^{(1(\psi_s/\psi_{so}))} - 1\right)^{1/2}} = f(\psi_s, \psi_{so}, M, R) \tag{3a}$$

where $\psi_s(= e_s - (e_s)_{SSL})$ = intergranular state parameter as defined in Fig. 2(a), $(e_s)_{SSL}$ = the intergranular void ratio at the ISSL corresponding to the intergranular void ratio e_s, and ψ_{so} = the intergranular state parameter at the isotropic compression state (or the reference state). Also shown in Fig. 2(a) is the traditional state parameter ψ. Based on equation (2), it turns out that ψ_s can be related to the more familiar state parameter ψ:

$$\psi_s = e_s - (e_s)_{SSL} = \frac{e - (e)_{SSL}}{[1 - (FC/100)]} = \frac{\psi}{[1 - (FC/100)]} \tag{3b}$$

where $(e)_{SSL}$ = void ratio at the SSL corresponding to the intergranular void ratio e_s (Fig 2(a)).

Equations 1(a) and (1b), 3(a) and 3(b) imply that whether one uses the state parameter or intergranular state parameter, qualitatively, a nearly similar stress–strain response would be anticipated, provided that the fines content does not exceed the threshold. Exceptions are expected due to minor contributions by the finer grains, as discussed later. Similar stress–strain behaviour may be expected at the same e_s and confining stress.

Interfine void ratio—critical state index. If the fines content far exceeds the threshold, the soil begins to be primarily governed by the contacts between the fines. The coarser grains float within the finer-grains matrix. The presence of coarser grains has little or no effect on the force chain, except perhaps serving as a medium of contact (providing some reinforcement) between the many finer grains around it. Since it is not a void and its volume does not affect the nature of the force chain in the finer grains, the volume of the coarser-grain solids may be safely ignored. Contrary to the earlier case, where the finer grains were considered to be voids, in the present case the coarser grains are considered to be of zero volume. The soil may behave similarly to the host finer-grained soil at an effective interfine void ratio e_f defined as the volume of voids per unit volume of the finer-grained solids:

$$e_f = \frac{e}{[(FC/100)]} \tag{4}$$

Interfine critical state line. In a manner similar to the ISSL for silty sands in Fig. 2(a), one could also define an interfine critical state line (ICSL, the locus of steady-state points in e_f versus $\log(p')$ plane) for sandy silt, as shown in Fig. 2(b). For the same host silt, a unique ICSL is expected for sandy silts at all fines contents. Since there exists a transition fines content zone where the soil is governed by the finer grains while the coarser grains are still active, a unique ICSL is expected only when FC exceeds a limiting fines content. The ICSL is expected to coincide with the critical state line (CSL) for the pure silt. It is expected to be different from the ISSL unless the SSL for the sand grains and the critical state line for the silt coincide for other reasons (e.g. self-similar grains with negligible physico-chemical interactions). Different CSLs would be expected for sandy silts at different sand contents. Equation (4) indicates that each CSL is expected to lie progressively higher in the e versus $\log(p')$ plane with an increase in fines content. Fig. 2(b) shows one CSL corresponding to a particular fines content FC = FC$_2$.

The different symbols (SSL in Fig. 2(a), and CSL in Fig. 2(b)) are intended to signify that these steady-state lines (SSL and CSL) do not refer to the same soils. Fig. 2(a) (and SSL) is relevant for soils at low fines contents, where intergranular contacts are dominant. Fig. 2(b) (and CSL) refers to soils at high fines contents, where finer grain contacts are dominant. Physically, they are different lines referring to different soils dominated by different parent granules. No other implied meaning is intended for the different symbols.

Interfine state parameter—plastic compressibility index. At high FC, the plastic compressibility and hence the stress–strain behaviour are derived from interfine contacts. Extending equation (1), similar to equation (3a), the corresponding dilatancy equation is given by

$$\frac{\Delta\varepsilon_v^p}{\Delta\varepsilon_q^p} = \frac{M\left(2 - R^{(1(\psi_f/\psi_{fo}))}\right)}{2\left(R^{(1(\psi_f/\psi_{fo}))} - 1\right)^{1/2}} = f(\psi_f, \psi_{fo}, M, R) \tag{5a}$$

where $\psi_f[= e_f - (e_f)_{CSL}]$ = interfine state parameter as defined in Fig. 2(b), $(e_f)_{CSL}$ = the interfine void ratio at the ICSL corresponding to the interfine void ratio e_f and ψ_{fo} = the interfine state parameter at the isotropic compression state (or the reference state). Based on equation (4), it also turns out that the interfine state parameter ψ_f is related linearly to the more familiar state parameter ψ:

$$\psi_f = e_f - (e_f)_{CSL} = \frac{e - (e)_{CSL}}{[(FC/100)]} = \frac{\psi}{[(FC/100)]} \tag{5b}$$

where $(e)_{CSL}$ = void ratio at the CSL corresponding to the interfine void ratio e_f (Fig. 2(b)).

Equations 1(a), 1(b), 5(a) and 5(b) indicate that similar stress–strain behaviour may be anticipated at the same ψ_f or at the same ψ, if FC far exceeds the threshold value. Similar stress–strain behaviour may also be observed at the same e_f and confining stress.

Summary

At the same void ratio e, with increase in fines content, e_s increases, starting from $e_s = e$; e_f decreases towards $e_f = e$; ψ_s increases, starting from $\psi_s = \psi$; and ψ_f decreases towards $\psi_f = \psi$. At low fines content, when e_f is high, the fines matrix

is highly compressible and the intergranular parameters (e_s, ψ_s) may predominantly affect the stress–strain behaviour. At large fines content, when e_s is high, the compressibility of the finer-grain matrix plays a major role in the stress–strain response; the interfine parameters (e_f, ψ_f) may predominantly affect the response. The transition from coarser-grained behaviour to finer-grained behaviour depends on both the fines content and the void ratio e. With this conceptual framework, assuming that the variables (e_s, ψ_s) and (e_f, ψ_f) are qualitative indices of the behaviour of the sub-matrices at low and high fines contents, and using the modified concepts of critical state soil mechanics summarized in equations (1)–(5) as a guide to develop intuition, one could explore the anticipated behaviour of a silty sand in terms of the behaviour of the host sand and/or in terms of the behaviour of the host silt.

First, the anticipated behaviour of a silty sand with an increase in void ratio at a constant low fines content is presented. This is followed by a discussion of the anticipated behaviour with increase in the fines content at a constant void ratio.

ANTICIPATED STRESS–STRAIN BEHAVIOUR

Intergranular matrix diagram—silty sand

Figure 3(a) shows a tripartite plot of void ratio e, equi-intergranular void ratio ($e_s = \text{const.}$) and equi-interfine void ratio ($e_f = \text{const.}$) lines obtained from equations (2) and (4), as a function of fines content. Also shown in this figure is a profile of the maximum and minimum void ratio of silty sands prepared at different fines content using the same host sand. The $e_{max,HS}$ and $e_{min,HS}$ of the host sand (denoted by subscript HS) in this case are 1·0 and 0·6, respectively. A demarcation line corresponding to $e_s = e_{max,HS}$ is also shown in this figure (to be discussed later). Using this matrix phase diagram, one could determine e_s and e_f at any void ratio e and fines content. This is used to illustrate the matrix effects on the behaviour of silty sands prepared at different void ratios and at different fines contents.

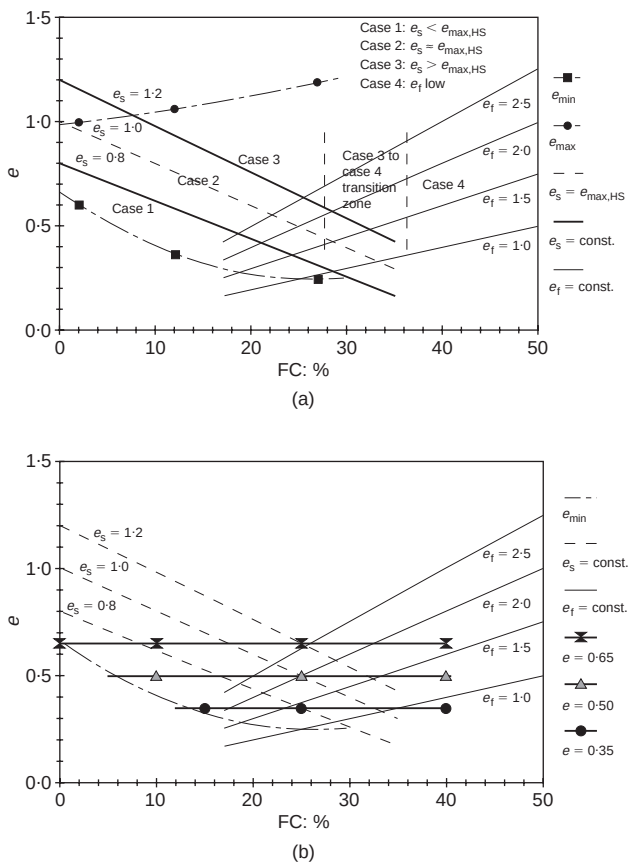

Fig. 3. Intergranular matrix phase diagram—host sand A: (a) cases 1–4; (b) effect of fines on soil matrix at constant *e*

Low fines content. First consider the effect of fines at a constant low fines content with increasing void ratio. As void ratio increases, both e_s and e_f increase. For convenience, silty sand in this group is categorized into three subgroups (cases 1, 2 and 3) in Fig. 3(a). The matrix effects and the anticipated behaviour for each category are as follows.

Case 1. At low void ratios (high densities) where $e_s < e_{max,HS}$, due to the relatively highly compressible nature of the finer-grain matrix (when e_f is very high) compared with the compressibility of the coarser-grain skeleton (at $e_s < e_{max,HS}$), most of the fines are expected to be confined to the intergranular voids, while some of the fines may play the role of a separator between some of the coarser grains. The active contacts sustaining shear forces are expected to be those of the coarser grains. The stress–strain response is expected to be primarily derived from friction along the host sand grain contacts, with some influence of the fines. In a restricted mode of deformation of triaxial compression, a unique SSL may be observed for all specimens when considered in terms of intergranular void ratio. Different SSLs may be observed if plotted on a global void ratio (e) versus $\log(p')$ plane. The parameters (e_s and ψ_s) may be used to unify these differences and determine the anticipated stress–strain characteristics. If the fines content is small, the difference between ψ and ψ_s is very small. Use of either ψ or ψ_s would be satisfactory. Exceptions to this may be expected when e_f is low.

Case 2. At intermediate void ratios (intermediate densities) where e_s is close to $e_{max,HS}$, the sand skeleton would be nearly unstable if there were no support by the fines. The compressibility of the 'loose' coarser-grain skeleton is not expected to be much different from the compressibility of the finer-grain matrix. Whether or not the fines actually lie within the intergranular voids or play the role of the separator between some of the coarser grains dictates the anticipated soil behaviour. If the fines lie within the intergranular voids, then the stress–strain characteristics and shear strength are governed by the intergranular friction between the coarser grains. Therefore, the stress–strain characteristics may resemble those of the host sand at the same e_s. However, if some of the fines play the role of the separator between a fair amount of coarser-grain contacts, then the fines will also impart an influence on the anticipated soil behaviour. Due to the sensitivity of the fines to confining stress, the behaviour may depend on the confining stress. Neither a unique SSL nor unique stress–strain characteristics may be found for a given e_s. Depending on the contact structure, different and erratic stress–strain and shear strength behaviour may be observed. In particular, a clean sand in this case may exhibit very small strength and a flatter SSL due to highly collapsible and unstable structure. At the same e_s, a silty sand, due to support by the finer grains, may exhibit somewhat greater strength and relatively stable behaviour compared to the host sand. The intergranular SSL would begin to deviate from that of the host sand. Two silty sands may exhibit similar stress–strain behaviour, but different from that of the host sand, at the same ψ or ψ_s.

Case 3. At high void ratios (low densities) corresponding to $e_s > e_{max,HS}$, the coarser-grain structure would be very unstable if the fines were not present. The fines may actively play the role of separators between most of the coarser grains. Hence, the soil behaviour may resemble that of the finer grains. The stress–strain behaviour may be significantly affected by shear along the fines. It may be sensitive to confining stress. A unique SSL may not be found due to pressure sensitivity of the fine-grained contacts separating the coarser grains. Similar stress–strain behaviour is expected at the same ψ or ψ_s.

High fines content. Second, consider the case of increase in fines

content at a constant void ratio (Fig. 3(a)). In this case, e_s increases whereas e_f decreases. When e_s is less than $e_{max,HS}$, the soil may behave similar to case 1. However, as e_s approaches $e_{max,HS}$, the soil behaviour may be characterized by case 2. As it exceeds $e_{max,HS}$, the behaviour may be characterized by case 3. As the fines content increases further and further, e_s becomes very high and therefore the influence of coarser grains diminishes. However, as e_f becomes low, the soil is primarily governed by the compressibility of the fines and shearing along the fines. The soil behaviour may be characterized by e_f and ψ_f. This latter case is categorized as case 4 in Fig. 3(a).

As shown in Fig. 3(a), the regions at which the transition between case 1 and case 2 or case 3 and case 4 occurs depend on the void ratio and the fines content. They also depend on the characteristics of the host sand and the silt. For the same silt, a silty sand prepared using a host sand with higher ($e_{max,HS}$ and $e_{min,HS}$) is expected to show transition at a different fines content than a silty sand prepared using a host sand with low ($e_{max,HS}$ and $e_{min,HS}$). Transition between cases 1 and 3 is expected to occur near $e_s = e_{max,HS}$. At this stage, the coarser grains would begin to be separated by the finer grains to such an extent that the coarser-grain skeleton would not be stable without the finer grains. When the fines content is sufficiently high, transition between case 3 and case 4 occurs. From an intuitive point of view, the transition from case 3 to case 4 is expected to occur when e_f falls below $e_{max,HF}$ (the maximum void ratio of the pure silt). At this point, the finer grains would be close enough to make contact among themselves.

Hypothetical examples

For the example shown in Fig. 3(b), at $e = 0{\cdot}65$, as the fines content increases, e_s increases from 0·65 (at 0 fines content) to $e_s = 0{\cdot}83$ at FC = 10% (case 1), $e_s = 1{\cdot}2$ at FC = 25% (case 2 or case 3), and $e_s = 1{\cdot}75$ at FC = 40% fines. On the other hand, e_f decreases to $e_f = 6{\cdot}5$ at 10%, to $e_f = 2{\cdot}6$ at 25%, and to $e_f = 1{\cdot}625$ at 40% (probably case 4). The soil at 10% fines content is expected to behave as a soil described in case 1. The soil at 25% fines may behave as described in case 2 or case 3. Soil at 40% fines is expected to behave as described in case 3 or begin transition into case 4.

At $e = 0{\cdot}5$, as the fines content increases, e_s increases from $e_s = 0{\cdot}67$ at 10% fines content (case 1), to $e_s = 1{\cdot}0$ at 25% (case 2), and to $e_s = 1{\cdot}5$ at 40% fines. On the other hand, e_f decreases to $e_f = 5{\cdot}0$ at 10%, to $e_f = 2{\cdot}0$ at 25%, and to $e_f = 1{\cdot}25$ at 40%. Since the host sand at $e_s = 1{\cdot}5$ ($\gg e_{max,HS}$) is weak and unstable, most probably the coarser-grain contacts are separated by the fines at 40% fines content. The silty sand at 40% fines content is anticipated to behave like a fine-grained soil at $e_f = 1{\cdot}25$ (case 4).

At $e = 0{\cdot}35$, as the fines content increases, e_s increases from $e_s = 0{\cdot}59$ at 15% (case 1), to $e_s = 0{\cdot}80$ at 25% (case 1), and to $e_s = 1{\cdot}25$ at 40% fines (case 4). On the other hand, e_f decreases to $e_f = 2{\cdot}3$ at 15%, to $e_f = 1{\cdot}4$ at 25%, and to $e_f = 0{\cdot}88$ at 40% (case 4). The soil at 40% fines content would be anticipated to behave as a silt at $e_f = 0{\cdot}88$, with some influence of the coarser grains. The transition between the above different cases is much less clear when the soil is very dense.

Effects of fines on steady-state strength

At a constant void ratio (e.g. $e = 0{\cdot}5$) (Fig. 3(b)), e_s increases with increase in fines content. Therefore, the steady-state strength is expected to decrease initially with increase in fines content until it reaches case 2. Erratic behaviour may be observed in case 2 (as discussed before). As the soil reaches case 3, the effect of consolidation stress on strength must also be considered. With further increase in fines content, the soil moves into case 4. It is governed primarily by fines. At that point, as e_f becomes smaller and smaller with increase in fines content at the same global void ratio e, the strength begins to increase beyond a certain limit of fines content.

This hypothesis, based on the matrix phase diagram, can be used to explain the experimentally observed trend in steady-state strength of silty sands with increase in fines content at a constant void ratio (Pitman *et al.*, 1994; Zlatovic & Ishihara, 1995; Thevanayagam *et al.*, 1996a). It can also be used to explain the transition behaviour observed for the cyclic behaviour of silty sands (Singh, 1994; Vaid, 1994).

Effect of fines on collapse potential

At a constant low void ratio (e.g. $e = 0{\cdot}5$ or less for the example in Fig. 3(b)), e_s increases with increase in fines content. Specimens prepared at the same void ratio and at the same confining stress are expected to become more and more contractive. However, since e_f decreases, at some point, the confining stress is partially carried by the fines when e_f becomes sufficiently low. Less stress is sustained by the coarser grains. Therefore, even though the contractive nature may prevail, the degree of contractiveness of the silty sand is expected to reach a transition point. With further increase in fines content, the soil may reach case 4 when e_f becomes low. The soil behaviour is governed by the fines. Depending on the characteristics of the silt, the silty sand may dilate with further increase in fines content (due to decrease in e_f).

However, if one considers a 'looser' specimen ($e = 0{\cdot}65$), the interfine void ratio e_f remains high up to a larger fines content than in the case of a 'denser' ($e = 0{\cdot}5$) specimen. Therefore, in a looser specimen the increase in the tendency to contract will prevail up to a larger fines content. The transition fines content from contractive to dilative behaviour will be larger for the looser specimens than for the denser specimens.

Furthermore, with increase in fines content, a 'loose' soil, at a constant e, passes through cases 2 and 3 before it reaches case 4. In cases 2 and 3, typically the values of e_f are very high. During shear, the probability of dislocating the finer grains separating the coarser grains is very high. Hence a loose specimen in case 2 or case 3 may reach a very unstable stage compared to a specimen in case 4 or case 1. In addition, the strength in cases 2 or 3 is sensitive to the confining stress. Loose silty sand at fines content less than about 20–30% at low confining stresses may be more prone to flow failures than the host sand at the same e and low confining stress. The host sand may dilate and gain strength and therefore experience only a limited deformation. Care is necessary when comparisons are made at the same e_s, when the soil is in case 2.

The above qualitative explanations can be used to explain the experimentally observed contractive/dilative behaviour of silty sand specimens prepared at different fines contents using Toyoura sand (Zlatovic & Ishihara, 1995), as discussed later.

Comparison in terms of ψ and ψ_s

Considering that ψ is linearly related to ψ_s, the contractive nature of a silty sand can be determined using either ψ or ψ_s. At low fines content, the differences between ψ and ψ_s is negligible. One may use either ψ or ψ_s to compare a silty sand with the host sand at the same ψ. Similarly, one may use either ψ or ψ_s to compare two silty sands with one another, if the fines contents for the two soils are not very different. At the same ψ or ψ_s, the stress–strain behaviour is anticipated to be similar (not identical).

However, as the fines content increases, the difference between ψ and ψ_s increases. On the other hand, due to low e_f, the compressibility of the finer-grained matrix begins to be influential. Silty sand and the host sand prepared at the same ψ will have significantly different ψ_s values. One may not always expect similar stress–strain behaviour at the same ψ or at the same ψ_s, especially when the fines content is high (case 4), at which point e_f is low and the silt primarily controls the soil behaviour. One cannot compare the behaviour of silty sand in case 4 with that in case 1 at the same ψ without taking into account the compressibility characteristics of the fines. When the soil falls in case 1, one may use ψ_s to compare the soil behaviour with other case 1 samples. Similar observations hold

within case 3. Exceptions are expected when the soil falls in case 2 (as discussed before). When it falls within case 4, one may use ψ_f to compare the soil behaviour within case 4.

EXPERIMENTAL STUDY

Experimental programme

To investigate the above hypothesis, as a simple approximate unified theme to explain the behaviour of silty sands compared with that of the host sand, an experimental programme was developed. The experimental study, however, was limited to a maximum of 27% fines content and therefore applies to cases 1–3 only. Data from the literature are used to highlight the soil behaviour in case 4. Undrained triaxial compression (TC) tests were performed on large specimens (typically 100 mm dia. and 200 mm height). Specimens were prepared using a single host sand (Fig. 4(a)) mixed with different amounts of fines: (*a*) 10% ground silica fines (GS) (Sil co sil #40, US Silica Company, Ottawa, Illinois, USA); (*b*) 10% kaolin silt fines (KS) (Thiele Co., Georgia, USA), and (*c*) 25% KS. The host sand contained 2% fines naturally found as part of that sand. These test specimens are denoted as A2, indicating 2% fines content in the relevant figures throughout this paper. In essence, the soils described in (*a*), (*b*) and (*c*) had total fines contents of 12%, 12% and 27%, respectively (Tables 1 and 2). The above fines showed no plasticity. Four of the specimens of the host sand (S1.1, S1.3, S1.6 and S1.7) were prepared after washing the host sand. Hence these specimens contained 0% of fines content. These are denoted as A0 on the corresponding figures. The e_{max} and e_{min} for each soil were determined using ASTM D4254 (even though this method is recommended only up to 15% fines content) and ASTM D1557 methods, respectively.

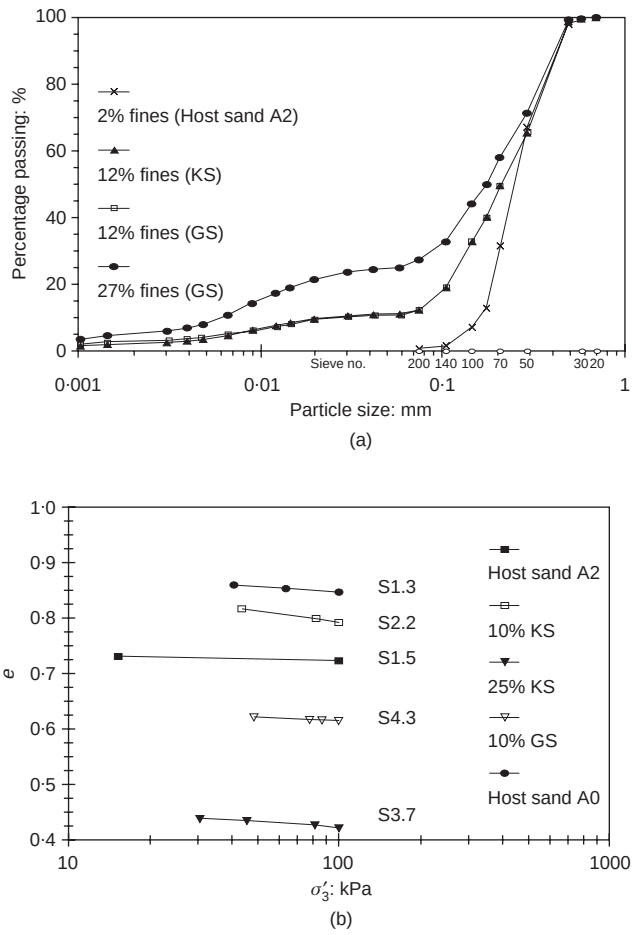

Fig. 4. Gradation curves and compression lines for the specimens

Fig. 4(a) shows the grain size data for the host sand and the silty sands.

The triaxial test specimens were prepared by a dry air pluviation method. First, one fourth of the mould was filled with the soil and it was compacted by tamping until reaching a specified void ratio. Similarly, every one fourth of the mould was filled with the soil and compacted. Then the specimen was placed on the MTS machine (Micro Console Number 458·20) and the sample was saturated using a back pressure until the *B*-value exceeded about 0·98. The target void ratio of the silty sand specimens were selected over a wide range to encompass intergranular void ratios e_s ranging from greater than $e_{max,HS}$ to near $e_{min,HS}$. Saturation was conducted at an effective confining stress of about 25–35 kPa for various specimens. Typical back pressure values were about 500–600 kPa.

Two sets of tests were done (Tables 1 and 2), each at a different initial confining stress. The first set of specimens were isotropically compressed to an effective confining stress of 100 kPa (Table 1). In total, 25 tests were done in the first set. In order to evaluate the effects of confining stress on the stress–strain behaviour in cases 1–3, a second set of specimens was consolidated to 400 kPa (Table 2). Six tests were performed in the second set. For 25% KS soil, one test (S3.8) was done at $e_s > e_{max,HS}$, two tests (S3.9, S3.10) were done at an e_s nearly the same as the $e_{max,HS}$, and one test (S3.11) was done at $e_s < e_{max,HS}$. Two tests (S1.6, S1.7) were done for the host sand. In order to further evaluate the effect of initial confining stress on the host sand, one more test (S1.8) was done at a confining stress of 200 kPa (Table 1).

The final void ratio of each specimen was calculated based on the weight of the soil grains in the specimen, the total volume of water introduced into the specimen, and the measured volume change data (drainage water) during consolidation. Fig. 4(b) shows the consolidation data for a few specimens. Strain controlled monotonic undrained TC tests were done at a strain rate of 0·6%/min. The pore pressure, axial load and axial deformation were recorded using a built-in data acquisition system in the MTS machine. Fig. 5 shows the state of all specimens in the matrix phase diagram. Based on the hypothesis presented before, one may predict the anticipated behaviour of each specimen.

Results

Figures 6–8 show the deviatoric stress ($= \sigma'_1 - \sigma'_3$) versus axial strain, pore pressure versus axial strain, and stress path data, respectively, for a few specimens tested in this study. Fig. 9 shows the steady-state points on an e versus $\log(p')$ and intergranular void ratio (e_s) versus $\log(p')$ plane where p' = mean principal effective stress at steady state ($= (\sigma'_1 + 2\sigma'_3)/3$). There is a variety of opinions on the definition of the steady state present in the literature (Poulos, 1981; Mohamad & Dobry, 1986; Alarcon-Guzman *et al.*, 1988; Vaid *et al.*, 1990; Ishihara, 1993), as schematically shown in Fig. 1. While there is little difference in opinion as to what is steady state when a specimen shows contractive behaviour only, there is much disagreement on the definition of steady state when a specimen shows partially contractive or dilative behaviour. While this question deserves further study, perhaps with particular attention to the field problem for which the strength is to be used, the points designated as steady state in this paper refer to the large strain response at an axial strain level of 20–25%. Tables 1 and 2 present a summary of the index properties, the steady-state strength S_{us}, the corresponding angle of shearing resistance ϕ (at large strain), e_s, and e_f, and the case (1, 2 and 3) that each specimen belongs to. The type of stress–strain curve observed for each specimen is also qualitatively summarized in Tables 1 and 2 with reference to Figs 1(b)–1(e). Only very few specimens were still dilating at large strains as high as 20–25% range. More detailed analysis of the steady-state strength data in terms of void ratio, intergranular void ratio and confining stress is presented and its practical implications are discussed elsewhere (Thevanayagam, 1998).

Table 1. Summary of laboratory tests—stage I (σ'_{vo} = 100 kPa)

Soil	Fines: %	e_{max}	e_{min}	Test no.	ϕ: degree	e	D_r: %	e_s	D_{rs}: %	S_{us}: kPa	Case	Stress–strain behaviour[b]		
												Contractive/dilative	ε_a: %	Stress–strain
Host sand A	0	0·980	0·600	S1.1	30	0·893	23	0·893	23	257	1	CD	23	Y
	2			S1.2	37	0·854	33	0·892	23	261	1	D	23	Y
	0			S1.3	30	0·849	34	0·849	34	290	1	D	24	Y
	2			S1.4	37	0·780	53	0·816	43	346	1	D	25	Y
	2			S1.5	37	0·725	67	0·760	58	459	1	D	18	Y
	2			S1.8[a]	30	0·900	21	0·939	11	141	1	D	20	Y
10% KS	12	1·064	0·369	S2.1	33	0·880	26	1·136	−41	53(7)[c]	3	CD	22	Y
				S2.2	30	0·795	39	1·040	−16	56(11)[c]	3	CD	22	Y
				S2.3	33	0·724	49	0·959	6	174	2	D	22	N
				S2.4	32	0·634	62	0·857	32	185	1	D	22	N
				S2.5	32	0·521	78	0·728	66	315	1	D	21	N
				S2.6	35	0·551	74	0·763	57	255	1	D	20	Y/N
25% KS	27	1·190	0·248	S3.1	33	0·612	61	1·208	−60	26	3	C	17	Y
				S3.2	29	0·593	63	1·182	−53	32	3	C	18	Y
				S3.3	32	0·589	64	1·177	−52	32	3	C	20	Y
				S3.4	29	0·544	69	1·115	−36	55	3	CD	22	Y
				S3.5	30	0·442	79	0·975	1	105	2	CD	22	Y
				S3.6	29	0·437	80	0·968	3	90	2	CD	19	Y
				S3.7	33	0·420	82	0·945	9	174	2	CD	25	Y
				S3.12	30	0·574	65	1·156	−46	37	3	CD	20	Y
10% GS	12	1·000	0·425	S4.1	30	0·808	33	1·055	−20	17	3	C	20	Y
				S4.2	30	0·777	39	1·019	−10	91	2	CD	23	Y
				S4.3	36	0·615	67	1·835	38	332	1	D	18	Y
				S4.4	33	0·555	77	0·767	56	432	1	D	20	Y
				S4.5	36	0·523	83	0·731	66	581	1	D	17	Y
				S4.6	36	0·484	90	0·686	77	720	1	D	20	Y

[a] Specimen S1.8 was tested at 200 kPa.
[b] Refer to Fig. 1.
[c] Specimens S2.1 and S2.2 showed an unusual drop in shear stress at 5–10% axial strain level; ε_a = axial strain level corresponding to steady-state strength.
C, fully contractive; CD, contraction followed by dilation; D, fully dilative; Y, deviator stress reached a plateau at large strains (20–25%); N, plateau was not reached at large strains (20–25%), i.e. continued dilation; e = void ratio at the end of consolidation.

Table 2. Summary of laboratory tests—stage II (σ'_{vo} = 400 kPa)

Soil	Fines: %	Test no.	ϕ: degree	e	D_r: %	e_s	D_{rs}: %	S_{us}: kPa	Case	Stress–strain behaviour[a]		
										Contractive/dilative	ε_a: %	Stress–strain
Host sand A0	0	S1.6	33	0·825	41	0·825	41	440	1	D	20	Y
		S1.7	36	0·718	69	0·718	69	661	1	D	20	Y
25% KS	27	S3.8	30	0·557	67	1·133	−40	129	3	CD	22	Y
		S3.9	30	0·498	73	1·052	−19	166	3	D	24	Y
		S3.10	30	0·472	76	1·016	−10	194	2	CD	22	N
		S3.11	30	0·434	80	0·964	4	217	2	CD	24	Y

[a] Refer to Fig. 1.
CD, contraction followed by dilation; D, fully dilative; Y, deviator stress reached a plateau at large strains (20–25%); N, plateau was not reached at large strains (20–25%), i.e. continued dilation; e = void ratio at the end of consolidation; ε_a = axial strain level corresponding to steady-state strength.

OBSERVED STRESS–STRAIN BEHAVIOUR

Steady state and intergranular steady-state lines

The following observations can be made based on Fig. 9(a). First, the SSL for the host sand is relatively insensitive to confining stress. Second, comparing the host sands tested at 2% fines content and 0% fines content, a small amount of fines appears to be sufficient to shift the position of the SSL from that of the host sand tested at 0% fines content. Third, the steady-state points for each silty sand fall in separate narrow bands, with the exception of the 25% KS soil, which was subjected to two different initial confining stresses. Fourth, as discussed before, at the same void ratio, the steady-state strength decreases as the fines content increases. Since the maximum fines content was limited to 27%, the transition behaviour (from case 3 to case 4) discussed before is not observed in Fig. 9(a). Fifth, for the 25% KS soil, the steady state is dependent on the void ratio and the initial confining stress; as the void ratio decreases, the differences between the SSLs corresponding to confining stresses at 100 kPa and 400 kPa decrease.

The above data are analysed in terms of ISSL for cases 1–3 next using Fig. 9(b). Referring to Fig. 3(a), the steady-state behaviour shown in Fig. 9(b) depends on the state of the soil in the matrix phase diagram. When $e_s < e_{max,HS}$ (case 1), all data fall in a narrow band (ISSL) independent of the fines content. The steady state is dependent primarily on e_s, with very little influence of the initial confining stress. When e_s is near $e_{max,HS}$ (case 2), the SSL for the host sand is very flat. The ISSL for the silty sands deviates from the SSL for the host sand. This may be due to the unstable coarser-grain structure, especially at zero (or very low) fines content, which is created when the soil is in the vicinity of $e_{max,HS}$, whereas in silty soils the loose coarser-grain structure is supported by the finer grains. Thus a stronger steady state is reached for silty sands. When

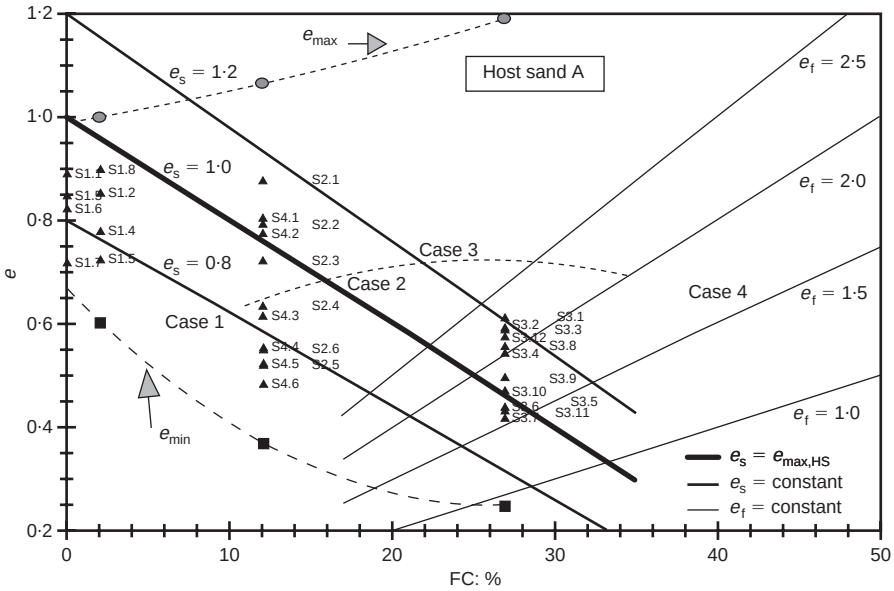

Fig. 5. Intergranular matrix phase diagram of the test specimens

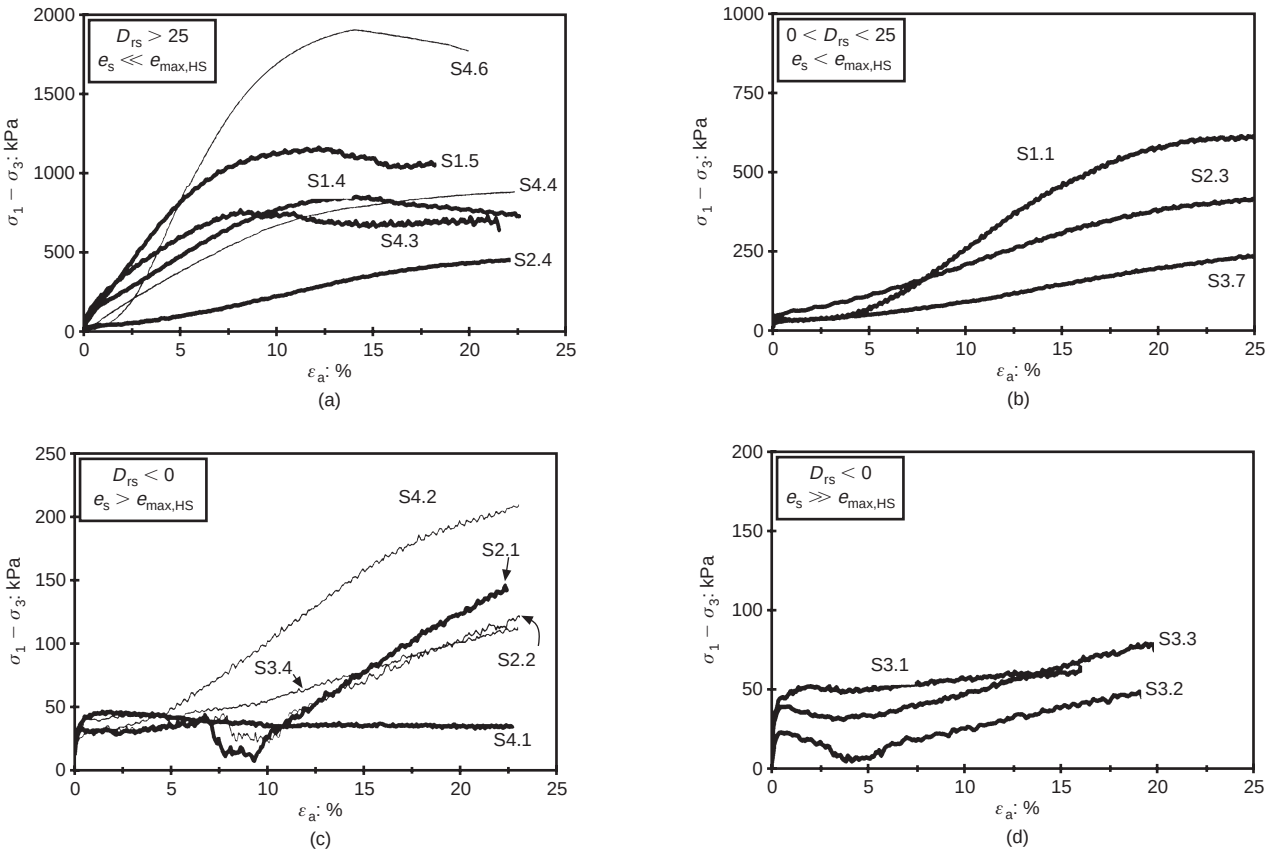

Fig. 6. Effect of intergranular void ratio on stress–strain behaviour (confining stress = 100 kPa): (a) $e_s \ll e_{max,HS}$; (b) $e_s < e_{max,HS}$; (c) $e_s > e_{max,HS}$; (d) $e_s \gg e_{max,HS}$

$e_s > e_{max,HS}$ (case 3), the steady state is dependent on the initial confining stress and e_s. The shear strength decreases with increase in e_s. The shear strength increases with increase in confining stress (for case 3). This dependence on confining stress is significant when silty sand is in case 2 or case 3. The strength of specimen S3.8 ($e_s > e_{max,HS}$), consolidated to 400 kPa, is about three times higher than the strength of specimen S3.12 or S3.4 ($e_s > e_{max,HS}$), consolidated to 100 kPa, although the e_s values for all three specimens are nearly the same. As observed in Fig. 9(b) and Tables 1 and 2 for the 25% KS soil, the dependence of ISSL on initial confining stress diminishes as the soil reaches case 1.

Effect of fines on collapse potential

The stress–strain data for silty sands are compared at: (*a*) nearly the same global void ratio (Fig. 10), (*b*) nearly the same relative density (Fig. 11), and (*c*) nearly the same intergranular void ratio e_s (Fig. 12). Each specimen referred to in

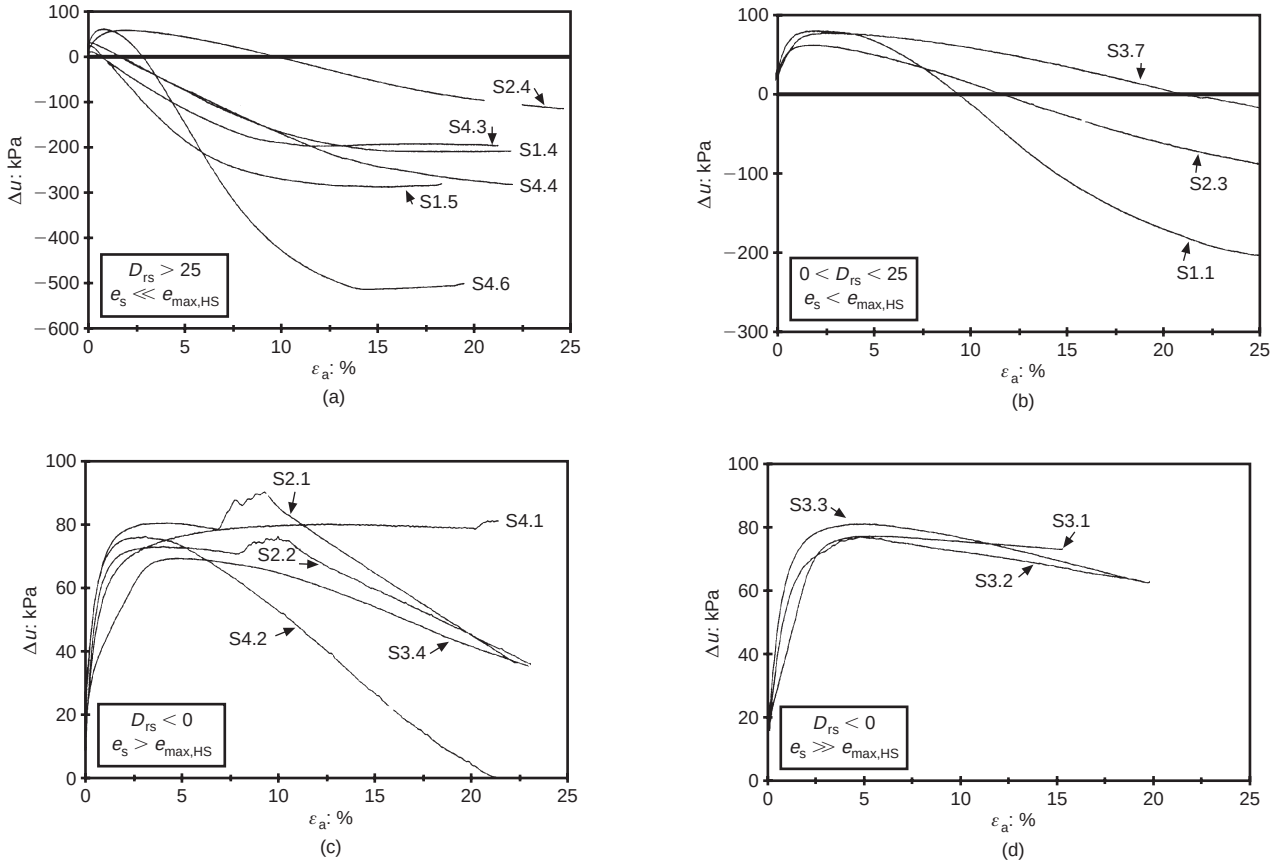

Fig. 7. Effect of intergranular void ratio on pore pressure response (confining stress = 100 kPa): (a) $e_s \ll e_{max,HS}$; (b) $e_s < e_{max,HS}$; (c) $e_s > e_{max,HS}$; (d) $e_s \gg e_{max,HS}$

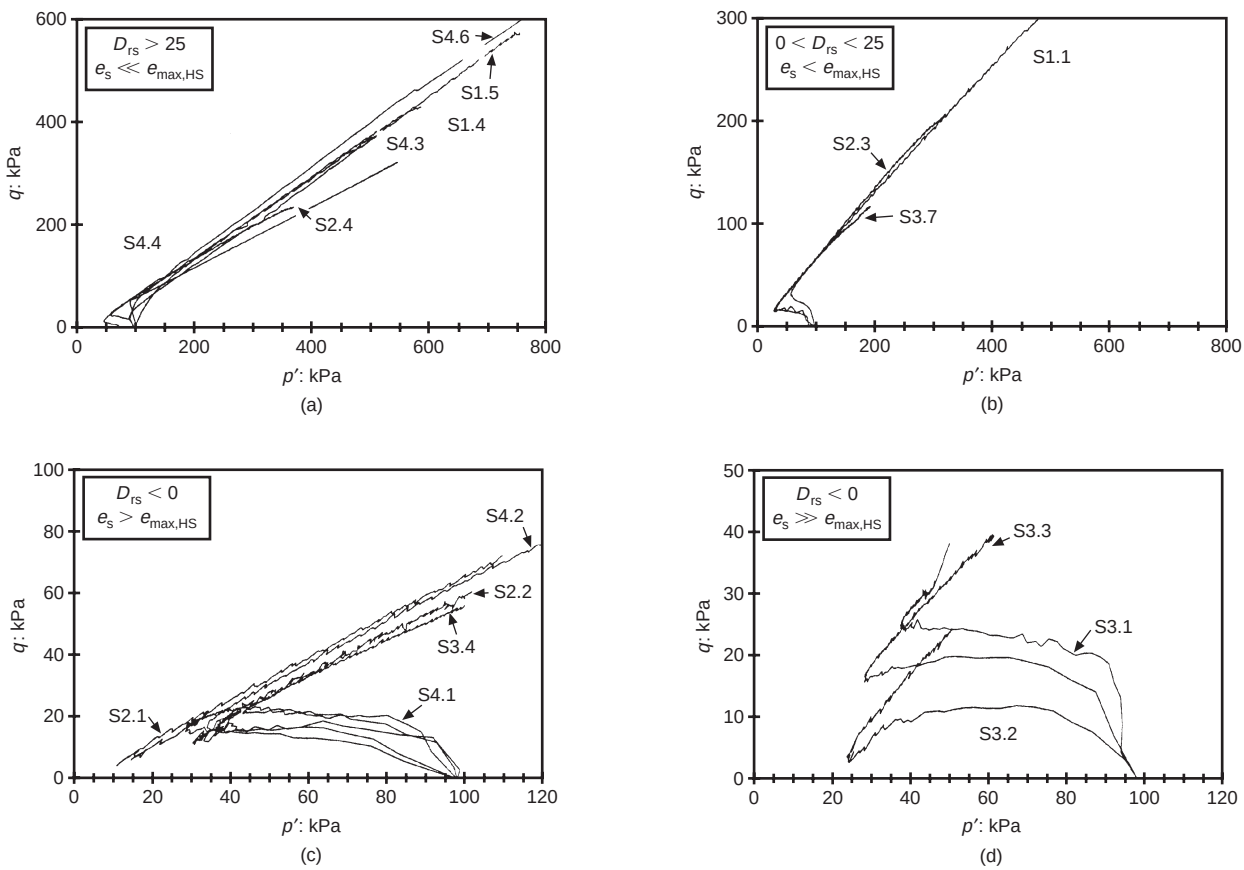

Fig. 8. Effect of intergranular void ratio on effective stress path in triaxial compression (confining stress = 100 kPa): (a) $e_s \ll e_{max,HS}$; (b) $e_s < e_{max,HS}$; (c) $e_s > e_{max,HS}$; (d) $e_s \gg e_{max,HS}$

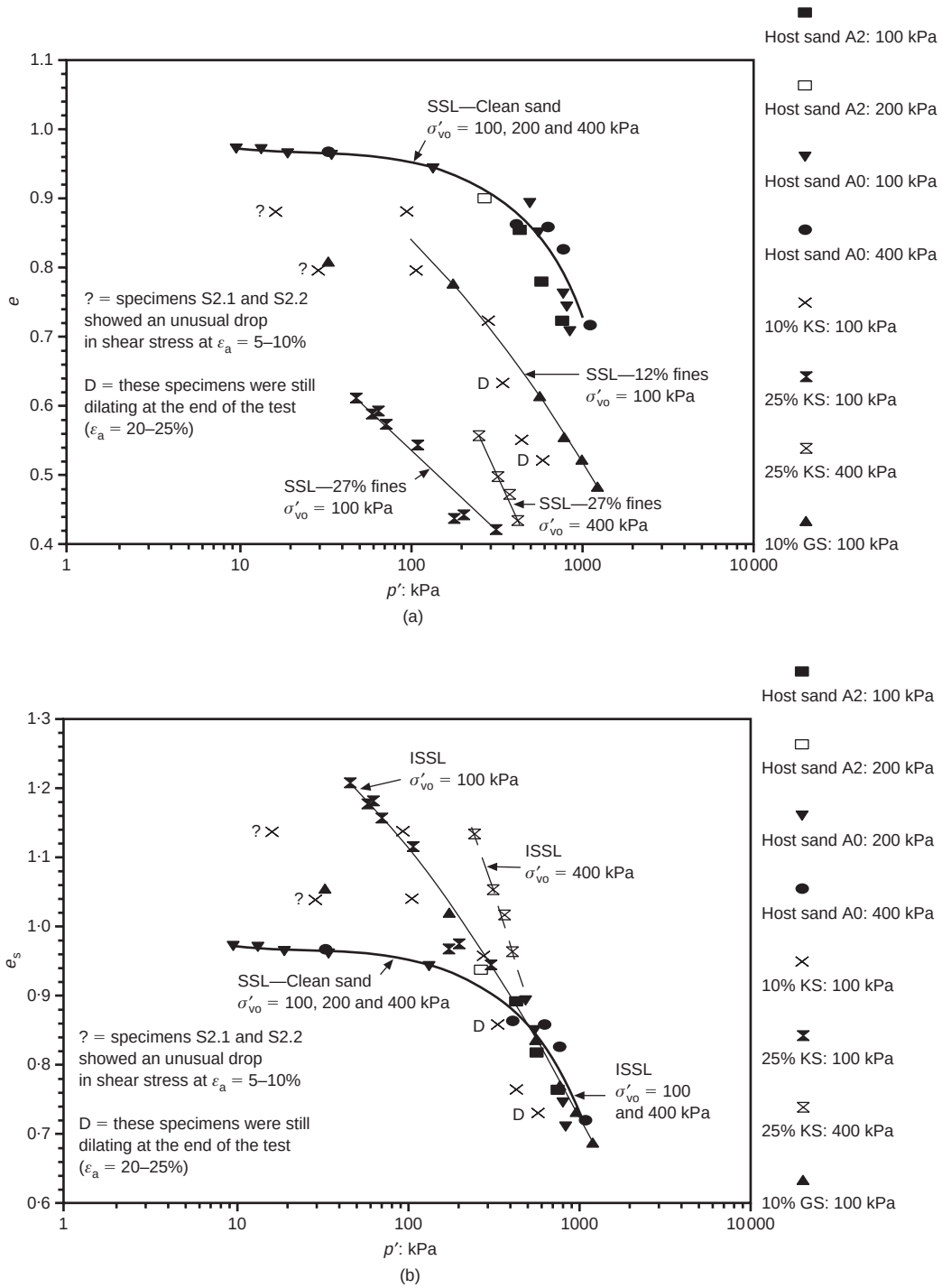

Fig. 9. Steady state versus mean effective stress: (a) e versus p'; (b) e_s versus p'

Figs 10–12 was consolidated to the same initial confining stress of 100 kPa.

As hypothesized before when referring to the matrix phase diagram in Fig. 3(a), when compared at nearly the same void ratio (Fig. 10), the tendency to contract increases with increase in fines content up to a threshold. For example, the specimen S3.1 (27% fines) at $e = 0{\cdot}612$ in Figs 10(c) and 10(f) is relatively contractive compared to S4.3 (12% fines) at $e = 0{\cdot}615$. A similar observation holds for S2.3 (12% fines) at $e = 0{\cdot}724$ in Fig. 10(b) compared with S1.5 (2% fines) at $e = 0{\cdot}725$. The state parameters are also presented in each figure. With increase in fines content, the state parameters also increase, indicating the tendency to contract more. As the fines content increases, the compressibility increases (since e_s increases), and therefore the tendency for contractive behaviour increases. Similar observations hold for Fig. 11. At the same D_r, the relative tendency to contract increases with increase in fines content. Since the fines content in this study was limited to 27% the transition behaviour discussed before (case 3 to case 4; from contractive to dilative behaviour at low e_f) is not observed in these figures. This is discussed later by reinterpreting the data obtained from the literature (Zlatovic & Ishihara, 1995).

An interesting observation is made in Fig. 12. When compared at nearly the same e_s, the stress–strain curves are nearly similar (not identical), relatively, in comparison with the significantly different stress–strain behaviour observed at the same void ratio (in Fig. 10). One reason for the differences in stress–strain response in Fig. 12 is the minor differences in e_s. Further, even if the comparisons are restricted to case 1 and the same e_s, identical stress–strain behaviour is not expected due to the

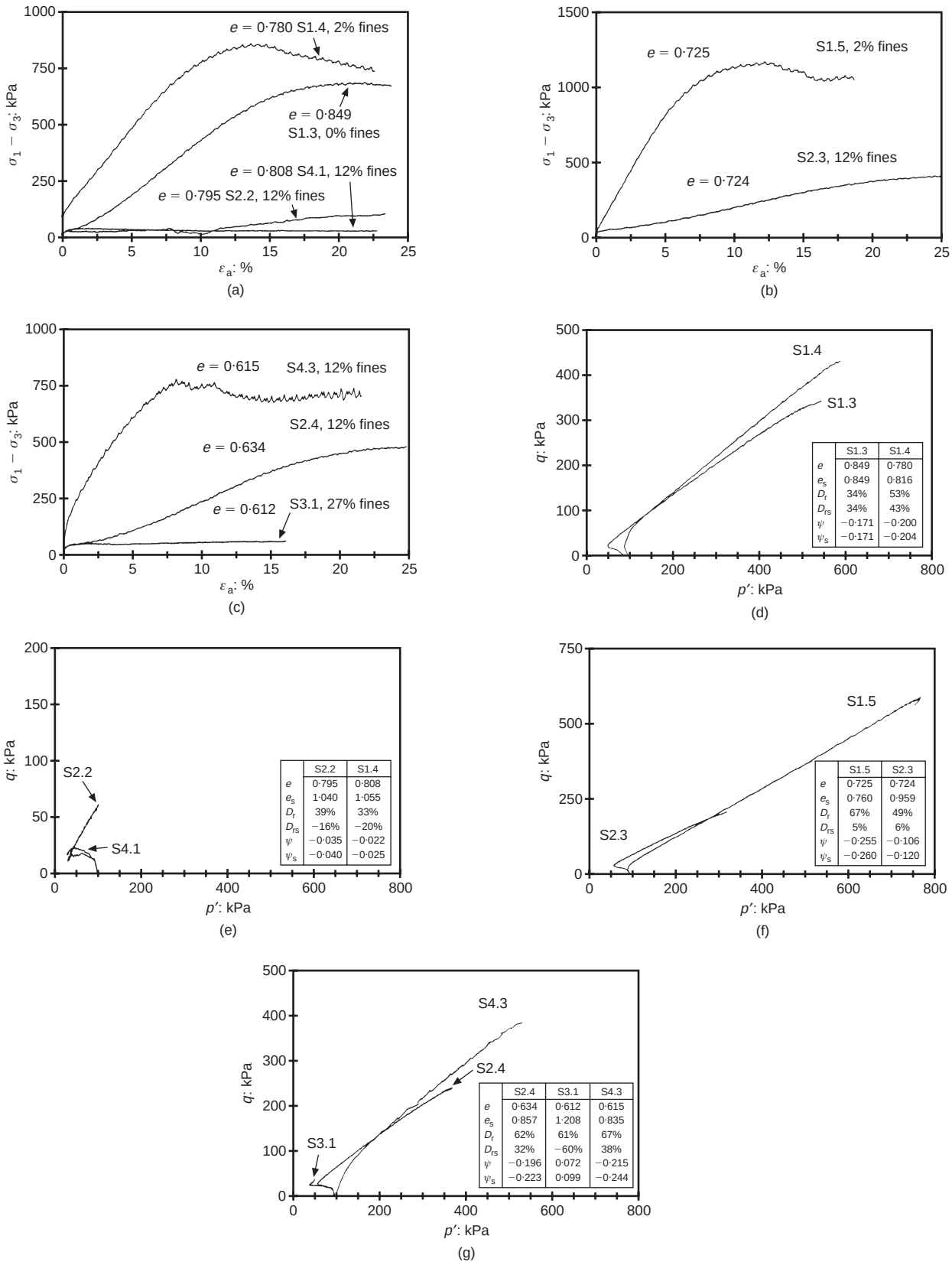

	S1.3	S1.4
e	0·849	0·780
e_s	0·849	0·816
D_r	34%	53%
D_{rs}	34%	43%
ψ	−0·171	−0·200
ψ_s	−0·171	−0·204

	S2.2	S1.4
e	0·795	0·808
e_s	1·040	1·055
D_r	39%	33%
D_{rs}	−16%	−20%
ψ	−0·035	−0·022
ψ_s	−0·040	−0·025

	S1.5	S2.3
e	0·725	0·724
e_s	0·760	0·959
D_r	67%	49%
D_{rs}	5%	6%
ψ	−0·255	−0·106
ψ_s	−0·260	−0·120

	S2.4	S3.1	S4.3
e	0·634	0·612	0·615
e_s	0·857	1·208	0·835
D_r	62%	61%	67%
D_{rs}	32%	−60%	38%
ψ	−0·196	0·072	−0·215
ψ_s	−0·223	0·099	−0·244

Fig. 10. Comparisons at the same initial confining stress and nearly same void ratios: (a–c) stress–strain; (d–g) effective stress path

minor changes in compressibility introduced into the specimens because of the presence of silt (even at high e_f) compared with the host sand. Incidentally, at nearly the same e_s, the intergranular state parameter ψ_s (and ψ) are also nearly the same (not identical). The parameter ψ_s (and ψ) reflects, to some extent, the compressibility of the soil, and e_s reflects, to some extent, the active contacts constituting the force chain referred to before. The combined effect gives nearly the same stress–strain behaviour. Even though the stress–strain curves are not identical, they merge at large strains. This indicates that, even though the stress–strain behaviour is affected by minor differences in the soil matrix compressibility, the strength is governed primarily by e_s, for case 1.

Further observations can be made if the data are grouped

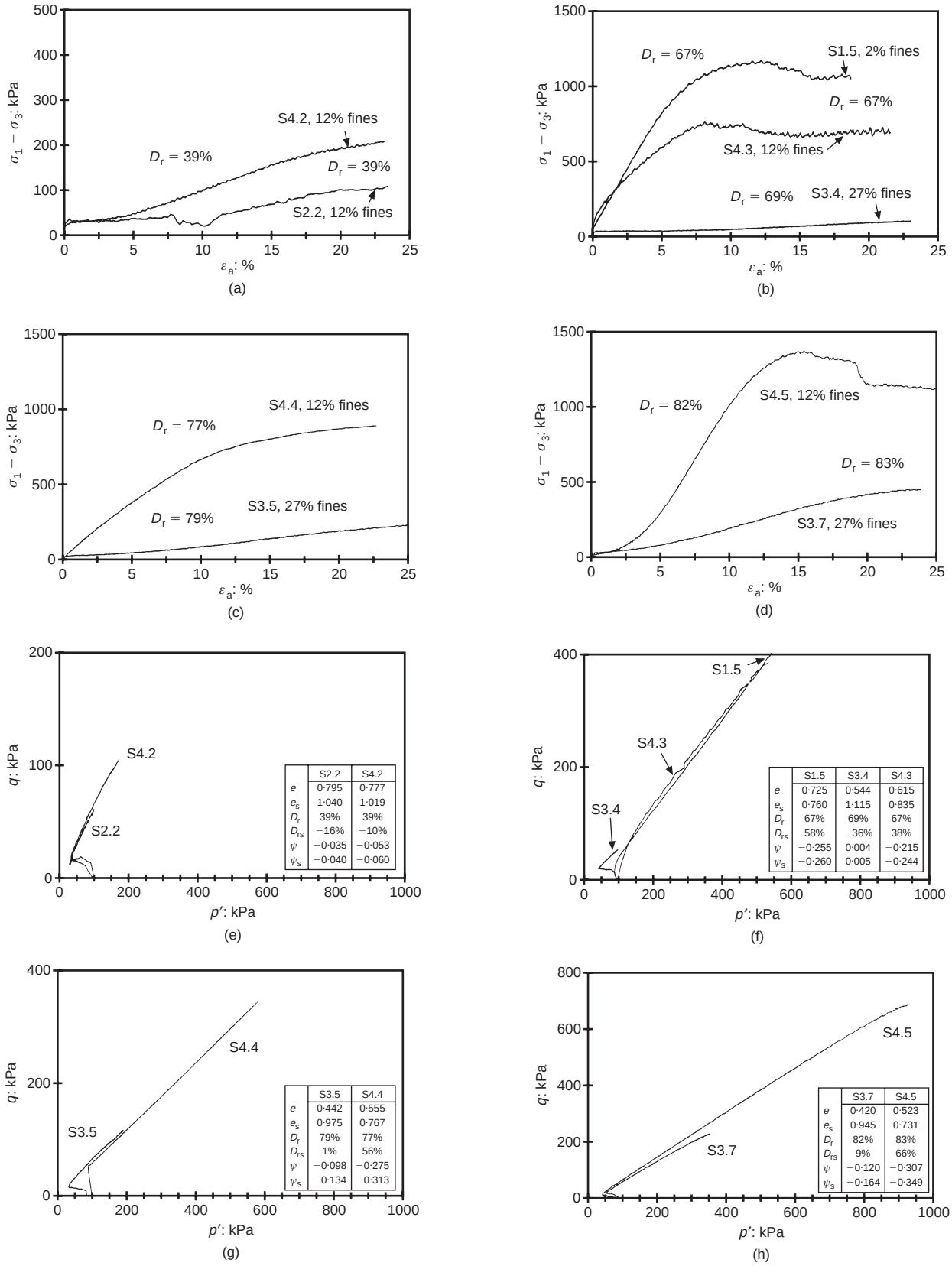

	S2.2	S4.2
e	0·795	0·777
e_s	1·040	1·019
D_r	39%	39%
D_{rs}	−16%	−10%
ψ	−0·035	−0·053
ψ_s	−0·040	−0·060

	S1.5	S3.4	S4.3
e	0·725	0·544	0·615
e_s	0·760	1·115	0·835
D_r	67%	69%	67%
D_{rs}	58%	−36%	38%
ψ	−0·255	0·004	−0·215
ψ_s	−0·260	0·005	−0·244

	S3.5	S4.4
e	0·442	0·555
e_s	0·975	0·767
D_r	79%	77%
D_{rs}	1%	56%
ψ	−0·098	−0·275
ψ_s	−0·134	−0·313

	S3.7	S4.5
e	0·420	0·523
e_s	0·945	0·731
D_r	82%	83%
D_{rs}	9%	66%
ψ	−0·120	−0·307
ψ_s	−0·164	−0·349

Fig. 11. Comparisons at the same initial confining stress and nearly the same relative densities: (a–d) stress–strain; (e–h) effective stress path

into cases 1–3 as follows. The data corresponding to $e_s < e_{max,HS}$ (case 1) are shown in Figs 6(a), 7(a), and 8(a). The data corresponding to e_s near $e_{max,HS}$ (case 1) but less than $e_{max,HS}$ are shown in Figs 6(b), 7(b) and 8(b). The data corresponding to e_s near $e_{max,HS}$ (cases 2–3) but greater than $e_{max,HS}$ are shown in Figs 6(c), 7(c) and 8(c). The data corresponding to case 3 ($e_s > e_{max,HS}$) are shown in Figs 6(d), 7(d) and 8(d). At the same confining stress, as e_s increases, the stress–strain behaviour shown in Figs 6(a)–6(d) (also see Figs 7(a)—7(d) and Figs 8(a)—8(d)) becomes more contractive. The samples in Fig. 7a ($e_s < e_{max,HS}$) develop large negative pore pressures, indicating significant dilation. Conversely, those in Fig. 7(d)

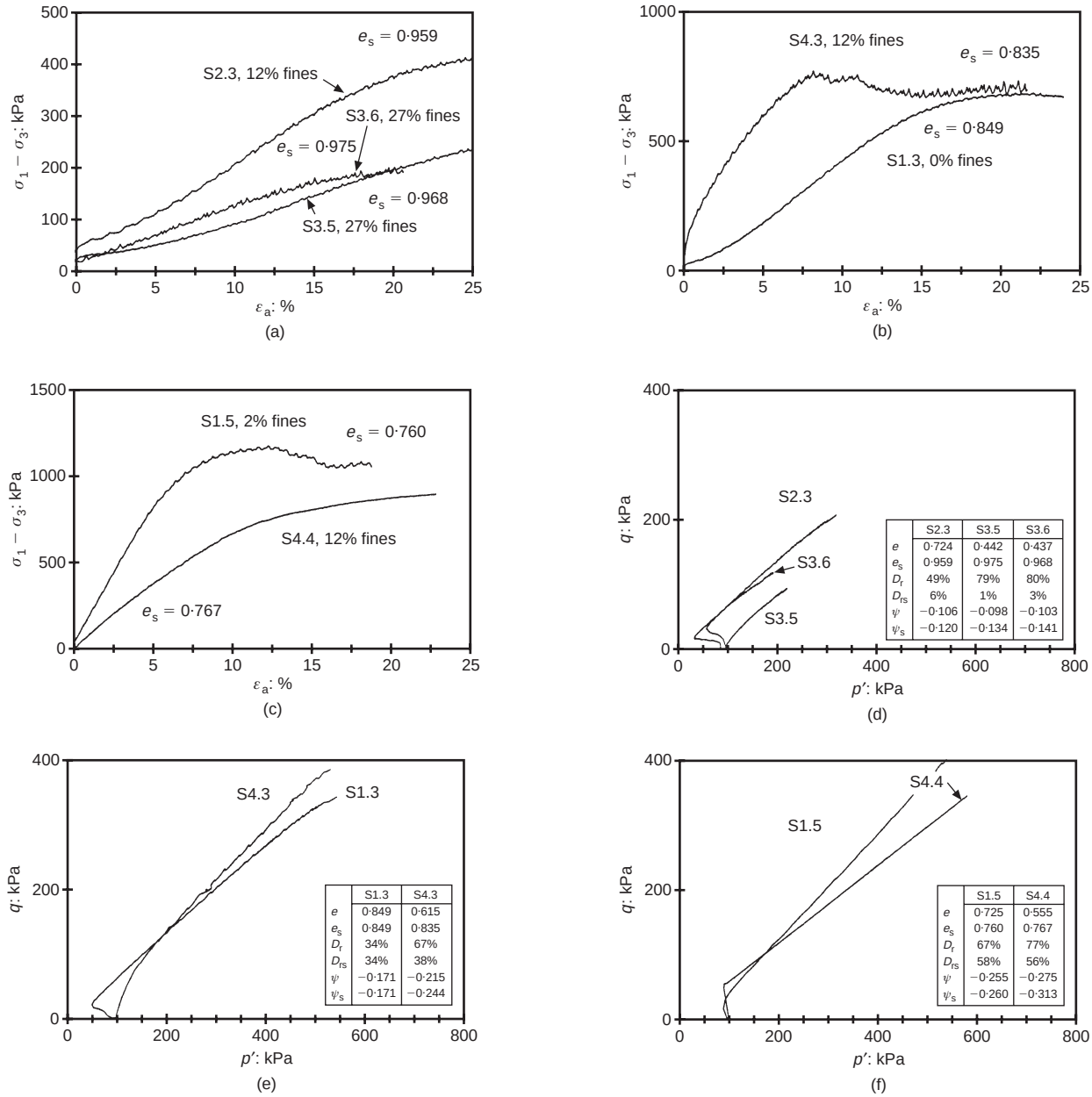

	S2.3	S3.5	S3.6
e	0·724	0·442	0·437
e_s	0·959	0·975	0·968
D_r	49%	79%	80%
D_{rs}	6%	1%	3%
ψ	−0·106	−0·098	−0·103
ψ_s	−0·120	−0·134	−0·141

	S1.3	S4.3
e	0·849	0·615
e_s	0·849	0·835
D_r	34%	67%
D_{rs}	34%	38%
ψ	−0·171	−0·215
ψ_s	−0·171	−0·244

	S1.5	S4.4
e	0·725	0·555
e_s	0·760	0·767
D_r	67%	77%
D_{rs}	58%	56%
ψ	−0·255	−0·275
ψ_s	−0·260	−0·313

Fig. 12. Comparisons at the same initial confining stress and nearly the same intergranular void ratios: (a–c) stress–strain; (d–f) effective stress path

($e_s > e_{max,HS}$) develop positive pore pressures indicating contractive behaviour. The same applies to Fig. 8(a) compared with Fig. 8(d). Although not shown for each specimen in these figures, from Fig. 8(a) to 8(d), the parameters ψ and ψ_s also increase, signifying increased compressibility and hence increased tendency for contractive behaviour. As the soil reaches case 2, some specimens (e.g. S2.1 and S2.2 in Figs 6(c)) show an initial increase in shear stress with axial strain followed by a tendency for sudden collapse and subsequent mild dilation. The pore pressure response data corresponding to these specimens shown in Fig. 7(c) show a sudden rise in pore pressure concurrent with the sudden decrease in shear strength (in the same range of strain) observed in Fig. 6(c). Subsequently, the pore pressure decreases with further strain, indicating dilation. As hypothesized earlier, with reference to Fig. 3, such behaviour of a sudden drop in shear strength observed for case 2 may be due to a sudden shear-induced loss of coarser-grain contacts that remained, initially, separated by the fines. With further straining, new contacts are made and the strength increases.

Other specimens (S3.4, S4.2 in Fig. 6(c); S3.1, 3.2, 3.3 in Fig. 6(d)) that also fall into the category of case 2 (or case 3) show a mild drop in shear strength followed by a mild dilation. As observed for specimens S3.1 to S3.4 (fines content = 27%, e_f nearly 2·0) in case 3 compared with S2.1 and S2.2 (fines content 12%, e_f nearly 7·0) in case 2, as e_f begins to play a role with increase in fines content, such a tendency for a sudden collapse in shear strength diminishes. The variations in the stress–strain behaviour observed for specimens S3.1 to S3.4, prepared at nearly the same e_s, may be partly due to the minor differences in the soil matrix. With further increase in fines content, the collapse potential may be reversed due to further reduced e_f, signifying the increased role of fines. This is discussed next.

Transition collapse potential

Figure 13(a) shows the intergranular matrix phase diagram prepared using the data for silty sands tested by Zlatovic & Ishihara (1995). Figs 13(b) and 13(c) show the stress–path and stress–strain curves for four specimens at 5%, 10%, 15% and 30% fines content (denoted as DD-5, DD-10, DD-15 and DD-30 in Fig. 13(a)) prepared by a dry deposition method. Figs

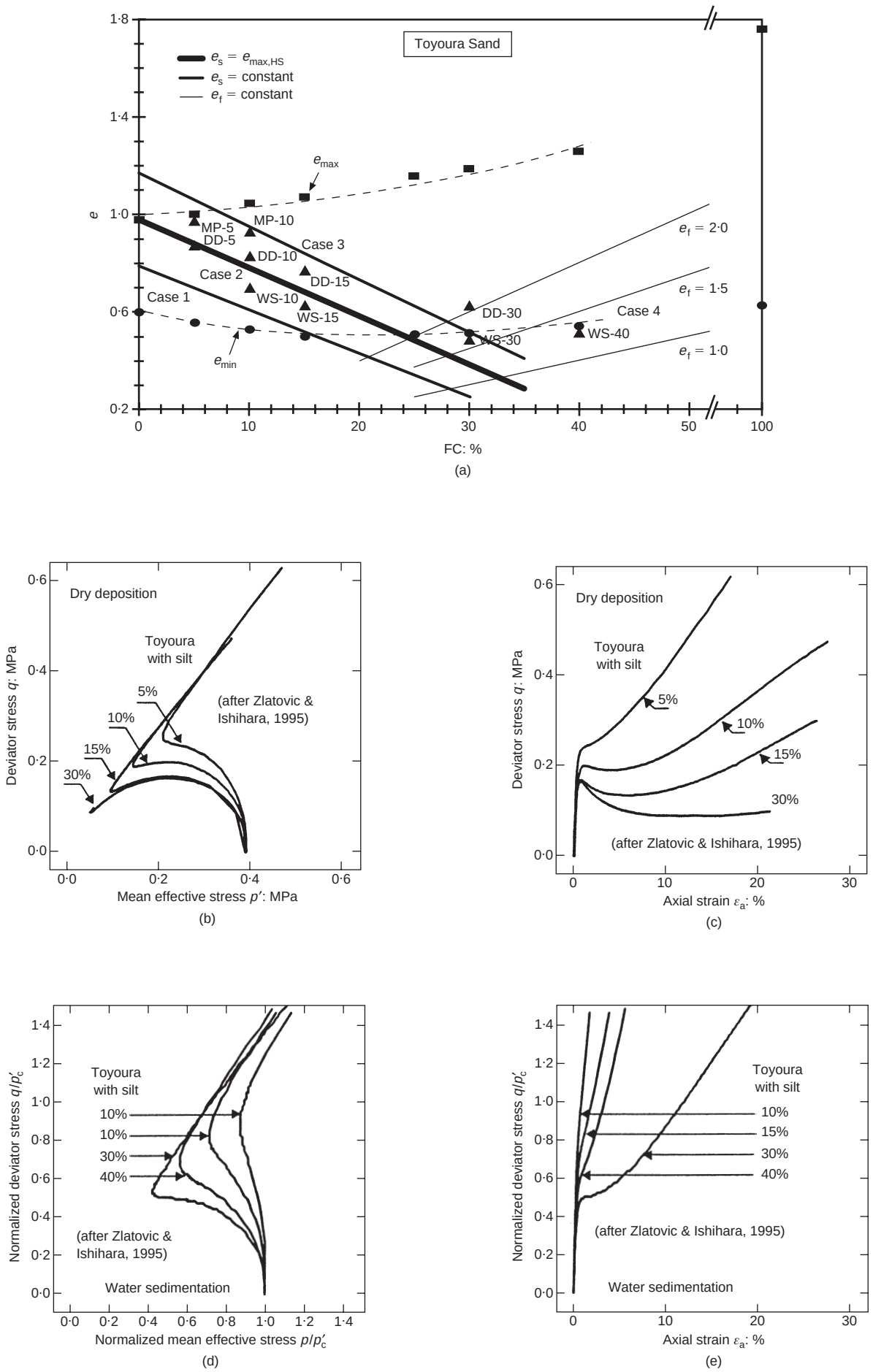

Fig. 13. Effect of intergranular matrix on collapse potential of toyoura sand–silt mix: (a) intergranular matrix diagram; (b–e) stress–strain and effective stress path

13(d) and 13(e) show similar data for specimens prepared at 10%, 15%, 30% and 40% fines content by a water sedimentation method (WS-10, WS-15, WS-30 and WS-40 in Fig. 13(a)). As one moves from DD-5 to DD-30, e_s increases while e_f remains high. The specimens move from case 1 to case 3. Hence, at the same confining stress, the tendency to contract increases as observed in Fig. 13(b) and 13(c). DD-30 may be near the transition point between case 3 and case 4. No data are available for the dry deposition method beyond 30% fines to study the expected tendency for reversal of collapse potential as the soil moves further into case 4.

For water-sedimented specimens, as one moves from WS-10 to WS-30, e_s increases; e_f remains high. Hence, at the same confining stress, the tendency to contract is expected to increase. However, as one moves from WS-30 ($e_f = 1{\cdot}6$) to WS-40 ($e_f = 1{\cdot}3$), e_f decreases. The soil moves from case 3 to case 4. The reported maximum and minimum void ratios for the 100% fines silt are 1·754 and 0·62, respectively. The magnitude of e_f (1·3) in WS-40 is sufficiently low to begin to impart a greater influence on the soil behaviour. Hence, due to a decrease in e_f, the tendency to contract decreases for WS-40 compared to WS-30, as observed in Figs 13(d) and 13(e). The effect of the initial confining stress must also be taken into account in determining the absolute contractive/dilative behaviour. Similar reasoning can be offered to explain the contractive/dilative behaviour observed by Pitman *et al.* (1994) on Ottawa sand specimens prepared at different fines content (10–40%). More detailed studies are needed to further refine this hypothesis in terms of state parameters.

Effect of confining stress

Returning to the experiments conducted in the present study, as the specimen reaches case 3, the behaviour is different from case 1. It becomes more sensitive to the initial confining stress. Figs 14(a) and 14(b) show the effect of confining stress on stress–strain curves for S3.8, consolidated to 400 kPa, versus S3.4, consolidated to 100 kPa, and for S3.7 (100 kPa) versus S3.11 (400 kPa), respectively, for the 25% KS soil. Figs 15(a) and 15(b) show the same data normalized with respect to the initial effective confining stress. Specimens S3.4 and S3.8 are at nearly the same e_s in case 3. Specimens S3.7 and S3.11 are also at nearly the same e_s but in case 1.

For case 3, at the same e_s, the stress–strain characteristics of the silty sand strongly depend on the initial confining stress over a wide range of strain (0–25%) (Fig. 14(a)). The normalized stress–strain curves are nearly the same at the same e_s (Fig. 15(a)). The state parameters for S3.8 and S3.4 are not identical. For the same 25% KS soil in case 1, only the initial stress–strain response for S3.7 and S3.11, at the same e_s, depends on the initial confining stress (Figs 14(b) and 15(b)); the overall stress–strain response is different. However, at large strains, the stress–strain curves asymptotically converge (Fig. 14(b)).

State parameters ψ and intergranular state parameter ψ_s

The earlier discussion tacitly included the state parameter. It is very difficult to accurately estimate the state parameters for clean sands at low confining stresses. This is because the SSL for the host sand is rather flat and very sensitive to void ratio at low confining stress level (Figs 9(a) and 9(b)). On the other hand, the SSL and ISSL for the silty sands depend on the confining stress for $e_s > e_{max,HS}$. Therefore, the reference frame needs to be used for the determination of the state parameter for silty sands. Within these limitations, Figs 16(a)–16(j) show the stress–strain data at nearly the same ψ and ψ_s, respectively. The e_s values are also shown for each specimen in these figures. As is evident, for silty sand specimens, nearly the same stress–strain trend is observed at nearly the same ψ or ψ_s. The degree of agreement or discrepancy is not very different, regardless of whether one considers ψ or ψ_s, (in Figs 16(a)–16(j)) or e_s and confining stress (in Fig. 12) as the basis. There are some

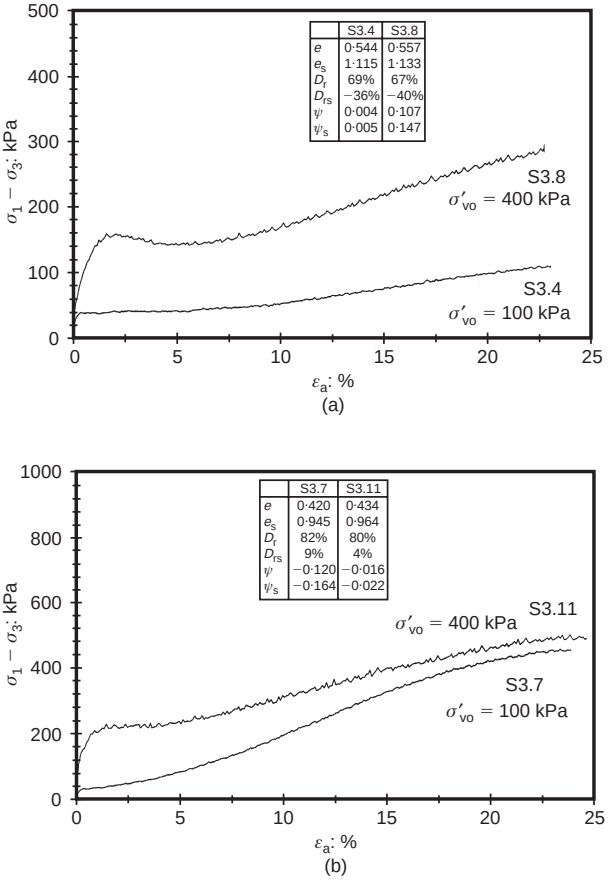

Fig. 14. Effect of initial confining stress on stress–strain behaviour of silty sands at nearly the same e_s: (a) case 3; (b) case 2

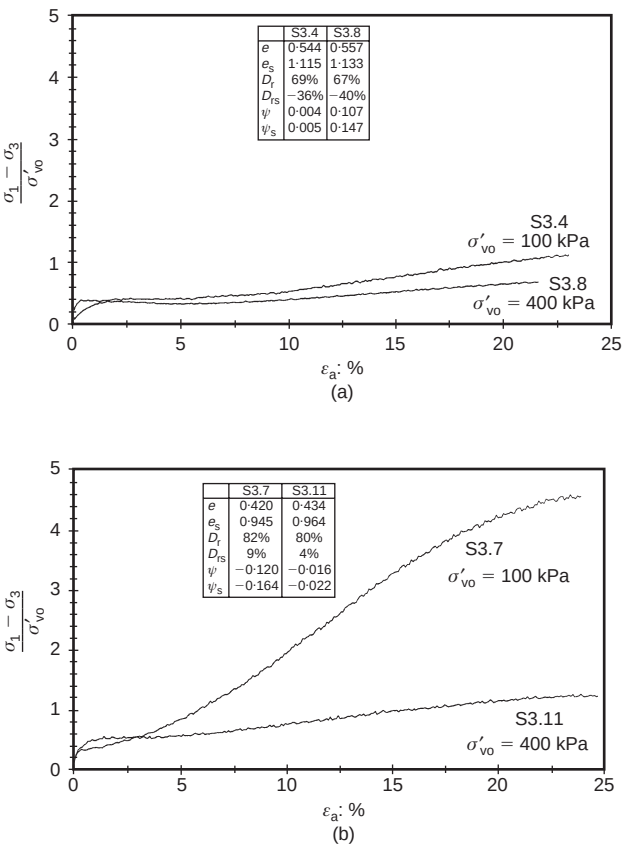

Fig. 15. Normalized stress–strain behaviour of silty sands at nearly the same e_s: (a) case 3; (b) case 2

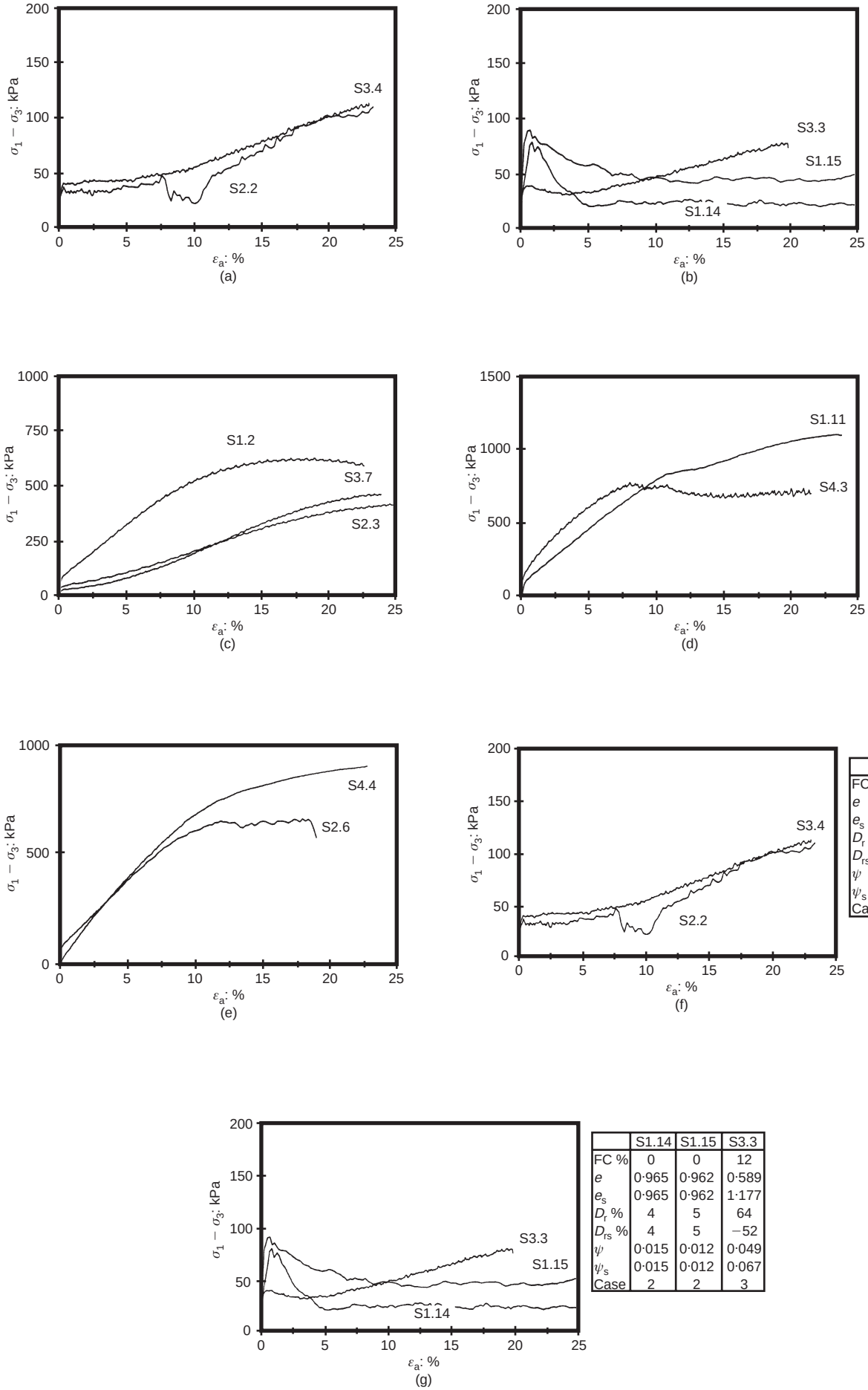

	S2.2	S3.4
FC %	12	27
e	0·795	0·544
e_s	1·040	1·115
D_r %	39	69
D_{rs} %	−16	−36
ψ	−0·035	0·004
ψ_s	−0·040	0·005
Case	3	3

	S1.14	S1.15	S3.3
FC %	0	0	12
e	0·965	0·962	0·589
e_s	0·965	0·962	1·177
D_r %	4	5	64
D_{rs} %	4	5	−52
ψ	0·015	0·012	0·049
ψ_s	0·015	0·012	0·067
Case	2	2	3

Fig. 16. Comparison of stress–strain data: (a–e) at nearly the same state parameters; (f–j) at nearly the same intergranular state parameters; (k–n) at nearly the same modified intergranular state parameters

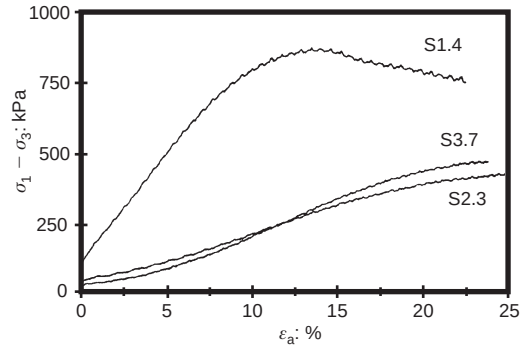

(h)

	S1.2	S1.4	S2.3	S3.7
FC %	2	2	12	27
e	0·854	0·780	0·724	0·442
e_s	0·892	0·816	0·959	0·975
D_r %	33	53	49	79
D_{rs} %	23	43	6	1
ψ	−0·096		−0·106	−0·098
ψ_s		−0·173	−0·120	−0·134
Case	1	1	2	2

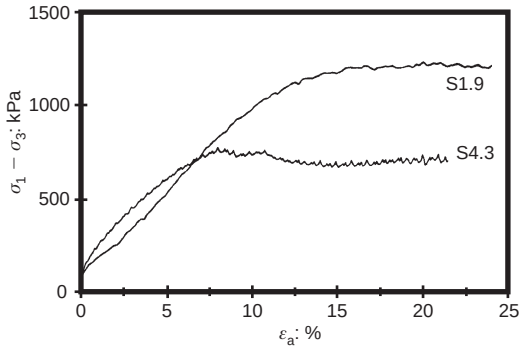

(i)

	S1.9	S1.11	S4.3
FC %	0	0	12
e	0·709	0·744	0·615
e_s	0·709	0·744	0·835
D_r %	71	62	67
D_{rs} %	71	62	38
ψ		−0·206	−0·215
ψ_s	−0·241		−0·244
Case	1	1	1

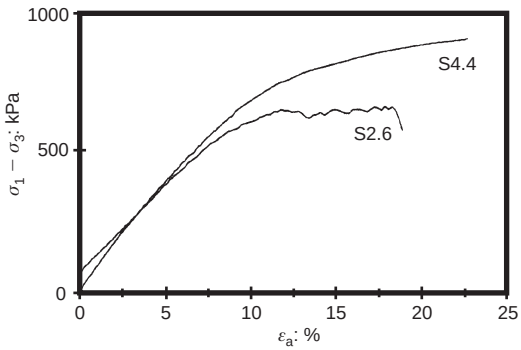

(j)

	S2.6	S4.4
FC %	12	12
e	0·551	0·555
e_s	0·763	0·767
D_r %	74	77
D_{rs} %	57	56
ψ	−0·279	−0·275
ψ_s	−0·317	−0·313
Case	1	1

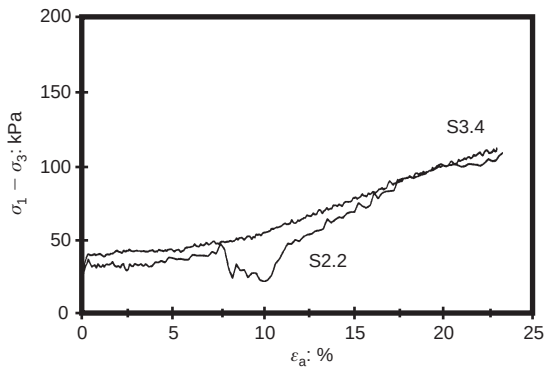

(k)

	S2.2	S3.4
FC %	12	27
e	0·795	0·544
e_s	1·040	1·115
D_r %	39	69
D_{rs} %	−16	−36
ψ_{ms}	−0·040	0·005
Case	3	3

Fig. 16. (*cont*).

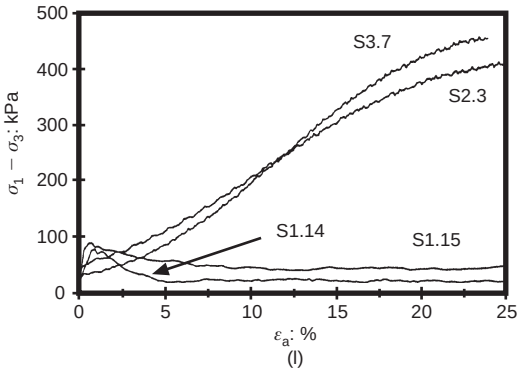

(l)

	S1.14	S1.15	S2.3	S3.7
FC %	0	0	12	27
e	0·965	0·962	0·724	0·442
e_s	0·965	0·962	0·959	0·975
D_r %	4	5	49	79
D_{rs} %	4	5	6	1
ψ_{ms}	−0·155	−0·158	−0·120	−0·134
Case	2	2	2	2

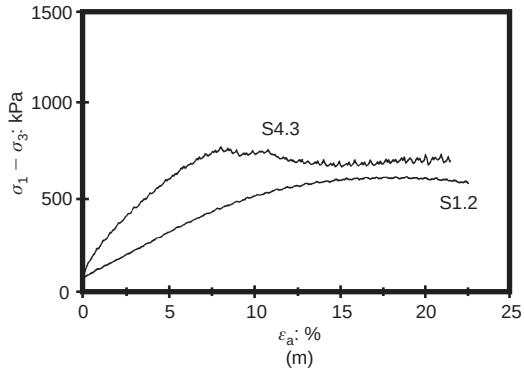

(m)

	S4.3	S1.2
FC %	12	2
e	0·615	0·854
e_s	0·835	0·892
D_r %	67	33
D_{rs} %	38	23
ψ_{ms}	−0·244	−0·228
Case	1	1

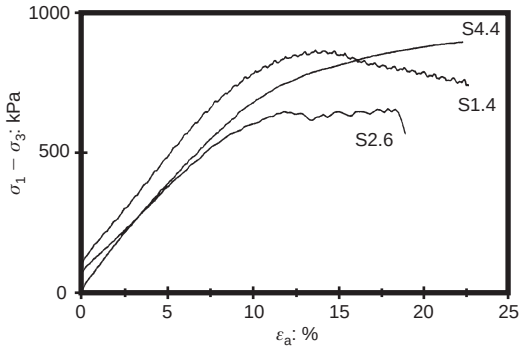

(n)

	S1.4	S2.6	S4.4
FC %	2	12	12
e	0·780	0·551	0·555
e_s	0·816	0·763	0·767
D_r %	53	74	77
D_{rs} %	43	57	56
ψ_{ms}	−0·304	−0·317	−0·313
Case	1	1	1

Fig. 16. (*cont*).

discrepancies when the stress–strain trend is compared with those for the host sand at nearly the same ψ or ψ_s. In Fig. 16(b) and 16(g) (S1.14 and S1.15 versus S3.3), clean sand shows more collapse potential than silty sand. In Figs 16(c), 16(d), 16(h) and 16(i) (S3.7 and S2.3 versus S1.2 or S1.4; S4.3 versus S1.11 or S1.9), the reverse is found.

The specimens S1.14 and S1.15 in Fig. 16(b) and 16(g) are clean sands. The state parameters for S1.14 and 1.15 are positive and are smaller than the state parameters for the silty sand specimen S3.3. Yet, S1.14 and S1.15 show more collapse than S3.3. These specimens are at e_s near $e_{max,HS}$. In the vicinity of $e_{max,HS}$, a clean sand is expected to be more collapsible than silty sands in this case, as explained before.

In Fig. 16(i) the ψ_s values for S1.9 and S4.3 are negative and are nearly the same. Yet, the clean sand specimen S1.9 dilates more than the silty sand specimen S4.3. This discrepancy is due to the difference in the frame of reference used for the determination of ψ_s for the host sand at low confining stress. The SSL is rather flat for the host sand compared to the ISSL for the silty sands (Fig. 9(b)). As a result, at the same e_s and (low) confining stress, the ψ_s values are different for the silty sand and the host sand. In other words, at the same ψ_s, the e_s values are slightly different for the silty sand and the host sand. Hence different stress–strain behaviour is expected. If the ISSL for the silty sands (at 100 kPa) is taken as the common reference line for defining (modified) intergranular state parameters (ψ_{ms}) for both the host sand and silty sands, then the agreement is better as shown in Figs 16(k)–16(n). This also allows comparison of the behaviour in each case (1–3) separately. Obviously, for other reasons discussed before, the discrepancy is now limited to case 2 only (Fig. 16(l)), where, at the same ψ_s, the silty sand specimens dilate, whereas the host sand specimens exhibit softening.

In general, while ψ or ψ_s may be used to deduce the expected behaviour qualitatively, one cannot rely solely on these parameters to quantitatively compare the stress–strain behaviour of different silty sands. ψ or ψ_s is only an approximate index of compressibility of the soil. Qualitative agreement is expected within case 1 or case 3; exceptions are expected within case 2. With further increase in fines content, ψ_f and e_f will begin to have a significant influence on the stress–strain behaviour.

PRACTICAL APPLICATIONS

Practical application of the concepts described in this paper requires reduction of the intergranular matrix phase diagram (Fig. 3(a)) into a more manageable classification chart, either in terms of in situ test parameters (CPT, SPT, etc.), relative

percentage compaction ($PC = 100(1 + e_{min})/(1 + e)\%$), relative density ($D_r$), etc. For the latter purpose, the void ratio e of a silty sand at $e_s = e_{max,HS}$ is termed the transition void ratio $e_{trans,SM}$; D_r and PC at $e_s = e_{max,HS}$ are termed the transition relative density $D_{r(trans)}$ and transition relative percentage compaction $PC_{(trans)}$, respectively. $D_{r(trans)}$ or $PC_{(trans)}$ provides a demarcation between case 1 ($e_s < e_{max,HS}$, $D_r > D_{r(trans)}$, $PC > PC_{(trans)}$), case 2 (e_s near $e_{max,HS}$, D_r near $D_{r(trans)}$, PC near $PC_{(trans)}$), and case 3 ($e_s > e_{max,HS}$, $D_r < D_{r(trans)}$, $PC < PC_{(trans)}$). Using equation (2), the transition void ratio $e_{trans,SM}$ is given by

$$e_{trans,SM} = e_{max,HS}\left(1 - \frac{FC}{100}\right) - \frac{FC}{100} \tag{6}$$

$D_{r(trans)}(= (e_{max,SM} - e_{trans,SM})/(e_{max,SM} - e_{min,SM})]$ and $PC_{(trans)}$ $(= (1 + e_{min,SM})/(1 + e_{trans,SM}))$ are given by

$$D_{r(trans)} = \frac{[e_{max,SM} - e_{max,HS}[1 - (FC/100)] + (FC/100)]}{(e_{max,SM} - e_{min,SM})}\ 100\% \tag{7}$$

$$PC_{(trans)} = \frac{(1 + e_{min,SM})}{\{1 + e_{max,HS}[1 - (FC/100)] - (FC/100)\}}\ 100\% \tag{8}$$

where $e_{max,SM}$ and $e_{min,SM}$ are the maximum (ASTM D4254) and minimum (ASTM D1557) global void ratios of the silty sand, respectively, at a fines content FC. Figs 17 and 18 show the $D_{r(trans)}$ and $PC_{(trans)}$ versus the fines content data for the six silty sands and one clayey sand. $D_{r(trans)}$ is about 40–50% for FC = 12%. It exceeds 80–90% for FC = 20–30%. It exceeds 100% at a fines content of about 30%. $PC_{(trans)}$ values are about 78–87% at FC = 12% and 85–100% at FC = 20–30%. It exceeds 100% at a fines content of about 30%.

At low FC, less than about 20–30%, at $D_r > D_{r(trans)}$ or $PC > PC_{(trans)}$, a silty sand behaves like the host sand at the same e_s (or ψ or ψ_s). At D_r near or less than $D_{r(trans)}$ (or PC near or less than $PC_{(trans)}$), the behaviour is pressure sensitive. At D_r near $D_{r(trans)}$ (or PC near $PC_{(trans)}$), the behaviour of two silty sands at the same e_s and confining stress (or ψ or ψ_s) is similar, but different from that of host sand. The host sand behaviour is expected to be weaker and more collapsible. At $D_r < D_{r(trans)}$ (or $PC < PC_{(trans)}$), the behaviour of two silty sands at the same e_s and confining stress (or ψ or ψ_s) is similar. A host sand specimen may not be constituted at such loose states.

For practical purposes, 30% fines content may be used as a demarcation point to differentiate a silty sand from a silt (case 4). At that stage, the soil behaviour is primarily affected by the fines, with a little secondary influence of the coarser grains. Interfine void ratio and confining stress (or ψ or ψ_s) may be used to characterize the behaviour.

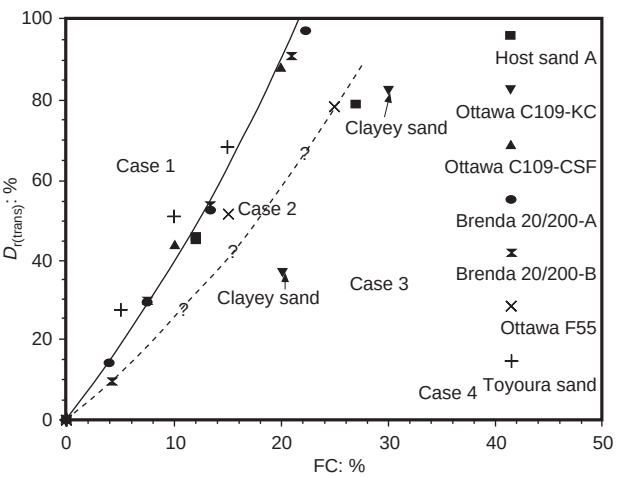

Fig. 17. Transition relative density ($D_{r(trans)}$) versus fines content

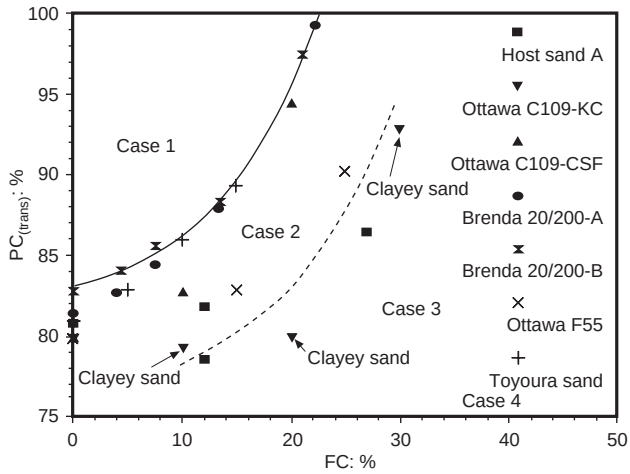

Fig. 18. Transition relative percentage compaction ($PC_{(trans)}$) versus fines content

The regions corresponding to the four cases discussed before are shown in Figs 17 and 18.

Another way to approximately study the behaviour of silty sands is to reduce the discussions presented before in terms of e_s to what is introduced as intergranular relative density D_{rs}. Since $e_{max,HS}$ and $e_{min,HS}$ are different for different host sands. One may normalize the intergranular void ratio to obtain the intergranular relative density, defined as

$$D_{rs} = \frac{e_{max,HS} - e_s}{e_{max,HS} - e_{min,HS}} \tag{9}$$

In essence, the term D_{rs} is an index of the density of the coarser-grain structure in a silty sand normalized using the maximum and minimum void ratio of the host sand as the frames of reference. Since it is possible to have $e_s > e_{max,HS}$ in a silty sand, it is possible to have $D_{rs} < 0$. The discussions presented before in terms of cases 1–3 reduce to $D_{rs} > 0$, D_{rs} near 0, and $D_{rs} < 0$, respectively. Case 4 cannot be categorized using D_{rs}, except for the fact that $D_{rs} < 0$ can be within case 4. One may compare the behaviour of a silty sand with another in terms of D_{rs}. But the effect of confining stress must also be taken into consideration. One may use ψ_s and D_{rs} to comparatively study the behaviour of silty sands within the limitations discussed in this paper.

The discussions contained in this paper hold for freshly deposited gap-graded silty sands. Exceptions are expected when physico-chemical effects, ageing, etc. are present. In the presence of the latter, a silt particle may not be free to move between pores as hypothesized. The soil may behave as a weakly cemented sandstone. A similar limitation prevails when the deposition results in layering.

CONCLUDING REMARKS

A careful reanalysis of the basic concepts of critical state soil mechanics is presented. It is extended to silty sands. A new set of intergranular and interfine state variables (ψ_s, e_s and ψ_f, e_f) are introduced to characterize the stress–strain behaviour of silty soils. The new formulation is used as an intuitive framework to study the behaviour of silty sands compared with that of the host sand. Experimental data indicating the influence of intergranular void ratio and intergranular state parameter on the stress–strain behaviour of silty sands are presented. Results indicate that, in general, when $e_s < e_{max,HS}$, the soil behaviour is governed by the coarser grain contacts. The stress–strain behaviour of a silty sand specimen at an intergranular void ratio $e_s(< e_{max,HS})$ is similar to that of the host sand at a void ratio e equal to e_s. Similar stress–strain behaviour is observed at the same ψ or ψ_s.

Even though it may be difficult to constitute a clean sand at states looser than $e_{max,HS}$, in the case of silty sands, it is possible to reach intergranular void ratios larger than $e_{max,HS}$.

At low fines content, when $e_s > e_{max,HS}$, the stress–strain response of the silty sand is weak. The weak response appears to be caused by significantly reduced sand grain contacts; at such very loose states the stress–strain response normalized with respect to the initial confining stress is nearly the same for the same e_s (or ψ or ψ_s). However, at e_s in the vicinity of $e_{max,HS}$, silty sands exhibit similar stress–strain behaviour, but different from the host sand, at the same e_s and the same confining stress (or at the same ψ or ψ_s).

At the same void ratio and the same confining stress, addition of fines makes the stress–strain response weaker and more contractive. This occurs up to a threshold value in the vicinity of about 30% fines content. However, with further increase in fines content, the soil is expected to become less contractive and stronger again. The behaviour is governed primarily by the fines. The above transition fines content depends on the void ratio and the characteristics of the host sand and the silt.

For practical field applications, the matrix diagram (Fig. 3(a)) can be depicted as relative density or relative percentage compaction versus fines content relation, as shown in Figs 17 and 18. If the fines content exceeds about 30%, then $D_{r(trans)}$ and $PC_{(trans)}$ are greater than 100%. Beyond this fines content the behaviour of that silty sand would be entirely different from that of the host sand; it behaves primarily as a silt with some reinforcement effect by the sand grains. If the fines content is less than 30%, however, a silty sand at $D_r > D_{r(trans)}$ (or $PC > PC_{(trans)}$) behaves like the host sand at the same intergranular void ratio (or the same ψ or ψ_s); if $D_r < D_{r(trans)}$ (or $PC < PC_{(trans)}$), the stress–strain–strength behaviour is expected to be weak and is dependent on the initial effective confining stress. Two silty sands would have similar behaviour when compared at the same e_s (or ψ or ψ_s). However, at D_r near $D_{r(trans)}$ (or PC near $PC_{(trans)}$), silty sands exhibit similar stress–strain behaviour, but different from the host sand, at the same e_s and the same confining stress (or at the same ψ or ψ_s).

ACKNOWLEDGEMENTS

zThe authors would like to thank the reviewers and the advisory panel of *Géotechnique* for their constructive comments and suggestions for improvement that greatly enhanced the value of this paper. The financial support for this research program by the National Science Foundation is greatly acknowledged.

NOTATION

D_r	global relative density
D_{rs}	intergranular relative density
$D_{r(trans)}$	transition relative density
e	global void ratio
e_f	interfine void ratio
$e_{max,HF}$	maximum void ratio of the host fines
$e_{max,HS}$	maximum void ratio of the host sand
$e_{min,HS}$	minimum void ratio of the host sand
$e_{max,SM}$	maximum void ratio of the silty sand
$e_{min,SM}$	minimum void ratio of the silty sand
e_s	intergranular void ratio
e_{trans}	transition void ratio
FC	fines content (percentage passing through No. 200 (0·074 mm) sieve) by total weight of solids
p'	mean effective stress $= (\sigma'_1 + 2\sigma'_3)/3$
p'_f	mean effective stress at steady state
PC	relative percentage compaction
$PC_{(trans)}$	transition percentage compaction
q	$(\sigma'_1 - \sigma'_3)/2$
S_{us}	steady-state undrained shear strength at large axial strain (20–25%)
σ'_{vo}	initial effective confining stress
σ'_c	initial effective confining stress
ψ	state parameter
ψ_f	interfine state parameter
ψ_s	intergranular state parameter
ψ_{ms}	modified intergranular state parameter
φ	angle of shearing resistance at large strains

REFERENCES

Alarcon-Guzman, A., Leonards, G. A. & Chameau, J.-L. (1988). Undrained monotonic and cyclic strength of sands. *J. Geotech. Engng Div., ASCE* **114**, No. 10, 1089–1109.

Altschaeffl, A. G. & Thevanayagam, S. (1991). Characterization of clay fabric. In *Microstructure of fine-grained sediments* (eds. R. H. Bennet, W. R. Bryant and M. H. Hulbert), pp. 291–295. New York: Springer-Verlag.

Been, K. & Jefferies, M. G. (1985). A state parameter for sands. *Géotechnique* **35**, No. 2, 99–112.

Chameau, J. L. & Sutterer, K. (1994). Influence of fines in liquefaction potential and steady state considerations. *Proceedings of the 13th international conference of soil mechanics and foundation engineering*, 183–184.

Chang, N. Y. (1990). Influence of fines content and plasticity on earthquake-induced soil liquefaction. Contract Report, MS Cont. No. DACW3988-C-0078. Vicksburg: US Army WES.

Dafalias, Y. F. (1987). An anisotropic critical state clay plasticity model. In *Constitutive laws for engineering materials–theory and applications*, Vol. 1 (ed C. S. Desai *et al*), pp. 513–522, Elsevier Press

Drescher, A. & De Josselin de Jong, G. (1972). Photoelastic verification of a mechanical model for the flow of a granular material. *J. Mech. Phys. Solids* **20**, 337–351.

Finn, L. W. D., Ledbetter, R. H. & Guoxi Wu (1994). Liquefaction in silty soils: design and analysis. *ASCE Geotech. Special Publication* **44**, 51–76.

Georgiannou, V. N., Hight, D. W. & Burland, J. B. (1990). The undrained behaviour of clayey sands in triaxial compression and extension. *Géotechnique* **40**, No. 3, 431–449.

Georgiannou, V. N., Hight, D. W. & Burland, J. B. (1991a). Undrained behaviour of natural and model clayey sands. *Soils Found.* **31**, No. 3, 17–29.

Georgiannou, V. N., Hight, D. W. & Burland, J. B. (1991b). Behaviour of clayey sands under undrained cyclic triaxial loading. *Géotechnique* **41**, No. 3, 383–393.

Ishihara, K. (1993). Liquefaction and flow failure during earthquakes. *Géotechnique* **43**, No. 3, 351–415.

Jefferies, M. G. and Been, K. (1987). Use of critical state representations of sand in the method of stress characteristics. *Can. Geotech. J.* **24**, No. 3, 441–446.

Kenney, T. C. (1977). Residual strength of mineral mixtures. *Proc. 9th Int. Conf. Soil Mech., Tokyo* **1**, 155–160.

Koester, J. P. (1994). The influence of fines type and content on cyclic strength. *ASCE Geotech. Special Publication* **44**, 17–32.

Kuerbis, R., Nagussey, D. & Vaid, Y. P. (1989). Effect of gradation and fines content on the undrained response of sand. *ASCE Geotech. Special Publication* **21**, 330–345.

Mitchell, J. K. (1993). *Fundamentals of soil behavior*, 2nd edn. John Wiley Interscience: New York.

Mohamad, R. & Dobry, R. (1986). Undrained monotonic and cyclic triaxial strength of sand. *J. Geotech. Engng Div., ASCE* **112**, No. 10, 941–958.

Pitman, T. D., Robertson, P. K. & Sego, D. C. (1994). Influence of fines on the collapse of loose sands. *Can. Geotech. J.* **31**, 728–739.

Poulos, S. J. (1981). The steady state of deformation. *J. Geotech. Engng. Div., ASCE* **107**, No. 5, 553–562.

Roscoe, K. H. & Burland, J. B. (1968). On the generalized stress–strain behaviour of 'wet' clay. In *Engineering Plasticity* (eds. J. Heyman & F. A. Leckie), pp. 535–609. Cambridge University Press, Cambridge.

Roscoe, K. H., Schofield, A. N. & Wroth, C. P. (1958). On the yielding of soils. *Géotechnique* **8**, No. 1, 22–52.

Roscoe, K. H., Schofield, A. N. & Thurairajah, A. (1963). Yielding of clays in states wetter than critical. *Géotechnique* **13**, No. 3, 211–240.

Seed, H. B. (1987). Design problems in soil liquefaction. *J. Geotech. Engng. Div., ASCE* **113**, No. 8, 827–845.

Seed, H. B., Idriss, I. M. & Arango, I. (1983). Evaluation of liquefaction potential using field performance data. *J. Geotech. Engng Div., ASCE* **109**, No. 3, 458–482.

Seed, R. B. and Harder, L. F. Jr (1990). SPT-based analysis of cyclic pore pressure generation and undrained residual strength. Proc. Seed Memorial Symposium, Berkeley, 2, 351–376.

Singh, S. (1994). Liquefaction characteristics of silts. *ASCE Geotech. Special Publication* **44**, 105–116.

Stark, T. D. & Olson, S. M. (1995). Liquefaction resistance using CPT and field case histories. *J. Geotech. Engng Div., ASCE* **121**, No. 12, 856–869.

Thevanayagam, S. (1989). *A fundamental frame work for strain–space soil modeling*. PhD dissertation, Purdue University, Indiana.

Thevanayagam, S. (1997). Dielectric dispersion of porous media as a fractal phenomenon. *J. Appl. Phys., Am. Inst. Phys.* **82**, No. 5, 2538–2547.

Thevanayagam, S. (1998). Effect of fines and confining stress on undrained shear strength of silty sands. *J. Geotech. Geoenviron. Engng Div., ASCE* **124**, No. 6, 479–491.

Thevanayagam, S. & Chameau, J.-L. (1992). Modelling anisotropy of clays at critical state. *J. Eng. Mech. Div., ASCE* **118** No. 4, 786–806.

Thevanayagam, S. & Nesarajah, S. (1998). Fractal model for flow through saturated soils. *J. Geotech. Geoenviron. Engng Div., ASCE* **124**, No. 1, 53–66.

Thevanayagam, S., Ravishankar, K., & Nesarajah, S. (1995). Steady state versus residual strength. Unpublished report, Polytechnic University, Brooklyn, New York.

Thevanayagam, S., Ravishankar, K., & Mohan, S. (1996a). Steady state strength, relative density and fines content relationship for sands. *Transportation Res. Board, TRR* **1547**, 61–67.

Thevanayagam, S., Wang, C. C., & Ravishankar, K. (1996b). Determination post-liquefaction strength of sands: steady state versus residual strength. *ASCE Geotech. Special Publication* **58**, 1210–1223.

Vaid, Y. P. (1994). Liquefaction of silty soils. *ASCE Geotech. Special Publication* **44**, 1–16.

Vaid, Y. P., Chung, E. K. F., & Keurbis, R. H. (1990). Stress path and steady state. *Can. Geotech. J.* **27**, No. 1, 1–7.

Yasuda, S., Wakamatsu, K. & Nagase, H. (1994). Liquefaction of artificially filled silty sands. *ASCE Geotech. Special Publication* **44**, 91–104.

Zlatovic, S. & Ishihara, K. (1995), On the influence of nonplastic fines on residual strength. *Proceedings of IS-TOKYO'95, first international conference on earthquake geotechnical engineering* (ed. K. Ishihara), pp. 239–244. Rotterdam: A. A. Balkema.

Corrigendum

The following equations were published incorrectly in Géotechnique Vol. 50, No. 1 1–23 (S. Thevanayagam and S. Mohan).

$$\frac{\Delta\varepsilon_v^p}{\Delta\varepsilon_q^p} = \frac{M(2 - R^{(1-(\psi/\psi_0))})}{2(R^{(1-(\psi/\psi_0))} - 1)^{1/2}} = f(\psi, \psi_0, M, R) \tag{1b}$$

$$\frac{\Delta\varepsilon_v^p}{\Delta\varepsilon_q^p} = \frac{M(2 - R^{(1-(\psi_s/\psi_{so}))})}{2(R^{(1-(\psi_s/\psi_{so}))} - 1)^{1/2}} = f(\psi_s, \psi_{so}, M, R) \tag{3a}$$

$$\frac{\Delta\varepsilon_v^p}{\Delta\varepsilon_q^p} = \frac{M(2 - R^{(1-(\psi_f/\psi_{fo}))})}{2(R^{(1-(\psi_f/\psi_{fo}))} - 1)^{1/2}} = f(\psi_f, \psi_{fo}, M, R) \tag{5a}$$

5.2 Undrained cyclic behavior of sand and non-plastic silty soils

5.2.1 Technical Articles

Analyses of undrained cyclic behavior of sand and non-plastic silty soils are presented in the following technical articles.

5.2.1.1 Thevanayagam, S. (2001) "Relative role of coarse and fine grains on mechanical behavior of granular mixes", *ASCE J. Geotech and Geoenv. Eng.*, *in review*.

5.2.1.2 Thevanayagam, S. (1999) "Liquefaction and shear wave velocity characteristics of silty/gravely soils – implications for bridge foundations." *Proc. 15th US-Japan Bridge Workshop*, PWRI, Tsukuba City, Japan, pp.133-147.

5.2.1.3 Thevanayagam, S., Fiorillo, M., and Liang, J. (2000) "Effect of non-plastic fines on undrained cyclic strength of silty sands." *Soil dynamics and liquefaction 2000, Proc. ASCE Conference*, GSP. 107, R.Y.S. Pak and J. Yamamura, eds., ASCE, Denver, CO, pp.77-91.

5.2.1.4 Thevanayagam, S., Liang, J., and Shenthan, T. (2000) "A contact index for liquefaction potential analysis of silty/gravely soils," In Tassoulas (ed.). *EM2000, Proc. 14th ASCE EMD Spec. Conf.* Austin, Texas.

5.2.1.5 Thevanayagam, S. (2000) "Liquefaction potential and undrained fragility of silty soils." *Proc. 12WCEE Conference*, Auckland, New Zealand, ed. R. Park, paper # 2383.

5.2.1.6 Thevanayagam, S., Liang, J., and Kanagalingam, T. (2001) "Effects of nonplastic fines on the liquefaction resistance of sands," Discussion to paper#20854, *ASCE J. Geotech and Geoenv. Eng.*, submitted for publication.

5.2.1.7 Thevanayagam, S. (2001) "Role of intergranular contacts on mechanisms causing liquefaction and slope failures in silty sands," *http://erp-web.er.usgs.gov/reports/annsum/vol43/pt/pt_vol43.htm*. USGS web. (not included in this report)

5.2.1.8 Thevanayagam, S., G.R. Martin, J. Liang, T. Kanagalingam, and T. Shenthan. (2001) "Undrained cyclic resistance of sands, silty sands, and sandy silts", *Canadian Geotechnical Journal*, *in review*. (not included in this report)

5.2.1.9 Liang, J. (2003) "Undrained monotonic and cyclic behavior of sand-silt mixes in triaxial compression", *PhD dissertation*, SUNY at Buffalo, *In preparation*. (not included in this report)

Articles 5.2.1.1 to 5.2.1.6 are presented following Sec. 5.2.2.

5.2.2 Conclusions

The main conclusions from this analysis are as follows:

- Liquefaction potential or undrained cyclic strength of silty sands ($FC<FC_{th}$) and sandy silts ($FC>FC_{th}$) are controlled by equivalent intergranular void ratios [$(e_c)_{eq}$ and $(e_f)_{eq}$, respectively]. In addition to the laboratory experiments carried out as a part of this study, reinterpretation of other data collected from literature also confirms this finding as well.
- It was found that at the same global void ratio, e, and the same confining stress, liquefaction potential of silty sands increases with an increase in FC up to FC_{th} due to a reduction in intergranular contact between the coarse grains. Beyond this threshold fines content, this trend reverses as the interfine contact friction becomes significant, and the soil becomes stronger.

- In silty sands ($FC<FC_{th}$), when compared at the same e_c, an increase in fines reduces the liquefaction potential. In sandy silts ($FC>FC_{th}$), when compared at same e_f, an increase in fines content increases the liquefaction potential.

5.2.1.1 RELATIVE ROLE OF COARSE AND FINE GRAINS ON MECHANICAL BEHAVIOR OF GRANULAR MIXES

By: S. Thevanayagam[1], Member, ASCE

ABSTRACT: The stress-strain behavior of granular mixes containing coarse and fine grains is derived from a combination of inter-coarse grain and interfine grain contacts and interactions thereof. A simple analysis of a two-sized particle system with large size disparity is presented to highlight when and how coarse and/or fine grain contacts become dominant, depending on the fine grains content (FC) and void ratio. Two equivalent intergranular $(e_c)_{eq}$ and interfine $(e_f)_{eq}$ void ratios are introduced as primary indices of intergrain contact density (per grain), at FC below and above a certain threshold fines content (FC_{th}), respectively. Beyond a certain limiting fine grains content FC_L, the interfine void ratio e_f is introduced as the contact density index. Global void ratio is identified as the secondary index of active contacts. Depending on the magnitudes of $(e_c)_{eq}$ and $(e_f)_{eq}$ relative to the minimum and maximum void ratios of the host grains and FC relative to the FC_{th} and FC_L, a granular mix is classified into a few sub groups. Based on $(e_c)_{eq}$ and $(e_f)_{eq}$ and FC, the mechanical behavior of a granular mix can be related to the behavior of either the host coarse grain or the host fine grain medium. Anticipated general trends for cyclic strength behavior of a granular mix, with an increase in FC, relative to the host coarse or fine grain medium is presented. This framework presents a mechanistic understanding of possible relative roles of coarse and fine grains on the mechanical behavior of granular mixes.

Key words: silt, silty sand, sand, liquefaction, strength

INTRODUCTION

Recent earthquake case histories indicate that natural soils and man-made sandy deposits containing a significant amount of fine grains (silty sands, clayey sands) and/or gravel do liquefy and cause lateral spreading (Seed et al. 1983, Seed and Harder 1990, JGS 1996). Experience gained from past studies on clean sands does not always directly translate to such broadly graded granular soil mixes. Recognition of this has lead to several laboratory and field studies to evaluate the effects of increasing silt or gravel content on: (a) cyclic strength, (b) collapse potential, (c) steady state strength, (d) shear wave velocity, etc. Results from laboratory studies on clean sands mixed with non-plastic silts or plastic fines show that, at the same (global) void ratio, the steady state strength and cyclic strength of silty sand decreases with an increase in fines content (Chang 1990, Chameau and Sutterer 1994, Georgiannou et al. 1990,91a-b, Vaid 1994, Koester 1994, Finn et al. 1994, Pitman et al. 1994, Singh 1994, Yamamuro et al. 1999, Zlatovic and Ishihara 1995, 1997). Beyond a certain transition range this trend reverses and the strength increases with a further increase in fines content. The transition fines content range is about 20 to 30% for non-plastic fines (Vaid 1994, Kuerbis et al. 1988, Singh 1994, Koester 1994). It is less than 20% for clayey fines (Georgiannou et al. 1990, 1991a-b). The physical meaning of the transition fines content is not clear. The conclusions in the literature on whether the presence of fines is beneficial or not is contentious. No consensus exists on how to characterize liquefaction resistance, collapse resistance, and post-liquefaction strength of silty sands and sandy silts. Similar concerns prevail regarding gravely soils (Evans and Zhou 1995).

Taking a different approach, field performance studies have sought to solve this problem by correlating SPT blow counts, CPT data, and shear wave velocity measurements with observations of liquefied sites and back-calculated post-liquefaction residual strength of failed embankments. Their use in practice relies on such intuitive reasoning as the impeding drainage effect of fines on SPT blow counts and/or their relation with relative density (Seed et al. 1983, Seed 1987, Seed and Harder 1990, Robertson et al. 1997, Andrus and Stokoe 1997). There are variations as well on the nature of such relationships (Stark and Mesri 1992, Ishihara 1993, Baziar and Dobry 1995). Questions prevail among practicing engineers on broad applicability of the field correlations to all (new) sites.

Recently, new and/or additional thoughts concerning the relative roles of various particles in silty/gravely soils have been put forward to explain the observed behavior of such granular mixes (Thevanayagam 1998, Thevanayagam and Mohan 2000). The underlying idea is that the physical nature of silty sands and gravely sands is entirely different from clean sand. As the void ratio and proportion of the coarse and fine grains content of these soils change the nature of their microstructure also changes. The relative participation of the particles of very different sizes in the internal *interparticle contact force chain* also changes. The global void ratio can be a reasonably good state parameter only if it correlates well with the internal force chain within the soil mass. Although it has been used as one of the primary state variables, starting from as early as Terzaghi, in the critical state soil mechanics theories (Roscoe et al. 1958, 1963), its broader application for all soils ranging from clean sands to sandy silts and gravely soils is not fully satisfactory. Due to the particle size disparity and availability of pores larger than some particles, some particles may remain inactive or move between pores without significantly affecting or contributing to the force chain. Yet they contribute to the global void ratio. Alternately, when there are sufficient fine grains, the coarse grains are dispersed and contribute much less to the force chain than to the global void ratio. Global void ratio turns out to be a weak parameter to represent the internal force chain. In general, the stress-strain behavior is affected by a critical combination of *intergranular and interfine contacts* and the physical and physico-chemical *interactions* thereof. The combined effects of intergranular and interfine contacts must be delineated in dealing with silty sands and gravely soils in understanding their mechanical response and mechanisms leading to liquefaction and post-liquefaction deformation.

The present paper focuses on the nature of the microstructure of granular mixes containing coarse and fine grains. A simple approach for classification of the mechanical behavior of such soils, with due consideration for relative frictional contributions at the intergranular and interfine grain contact level, is presented. A set of contact density indices, namely equivalent intergranular $(e_c)_{eq}$, equivalent interfine $(e_f)_{eq}$, and interfine (e_f) void ratios is proposed as the primary indices of contact density for mixes containing low, intermediate, and high fine grain contents, respectively. The approach is rather simple allowing its application to address practical problems. It can be used as a guideline for interpretation of the behavior of gap-graded granular

[1] Associate Prof., Dept. of Civil, Struct. and Envir. Eng., 212 Ketter Hall, SUNY at Buffalo, Buffalo, NY 14260

mixes. Detailed experimental evaluation of the proposed framework is presented elsewhere (Thevanayagam et al. 2001a-c, Thevanayagam et al. 2000, Thevanayagam 1999).

CONCEPTUAL FRAMEWORK

Microstructure

Consider a two-sized granular mix (Fig.1). The microstructure of this granular mix can be constituted by many different ways. Each one of them leads to a different internal force chain network among particles and hence each exhibits a different stress-strain response during shear. Among many variations, a few extreme limiting categories of microstructure are as follows:

Case i: The first category in Fig.1a occurs when the fine grains are fully confined within the void spaces between the coarse-grains with no contribution whatsoever in supporting the coarser grain skeleton. This requires that the fine grain particle size (d) is much smaller than the pore size between the coarse grains (R_d=D/d>>6.5, Appendix III). It is also essential that the fine grain content (FC) is less than a certain threshold value (FC_{th}) such that the inter-coarser granular voids are not completely filled with the fine grains making it not possible to make contact force chain among the fine grains themselves. The threshold state occurs when FC is sufficiently high so that direct fine-grain-to-fine-grain contacts begin to constitute a strong force chain. Soil microstructure that satisfies the two constraints ($FC \ll FC_{th}$ and $R_d \gg 6.5$) is categorized as case i in this paper. FC_{th} is given by (Appendix IV):

$$FC_{th} \leq \frac{100\ e}{e_{\max,\ HF}}\% \qquad (1)$$

where $e_{max,HF}$ is the void ratio of the host fine grain soil above which it has no appreciable strength.

Consider changing the microstructure shown for case i in two ways: (1) alter the position of some of the fine grains, or (2) add more fine grains. The consequences are significant.

Cases-ii and iii: If one alters the position of some of the fine grains, while maintaining the fine grain content, the microstructure corresponding to cases ii and iii in Fig.1a are obtained with a concurrent increase in global void ratio. Essentially, the microstructure for these cases is made up of a coarse grain skeleton where some of the coarse grain contacts are separated by the fine grains while some fine grains are confined within the voids between the coarse grains. Hence, a portion of the fine grains becomes active participants in the internal contact force chain. These fine grains are termed the 'separating fines'.

Case-iv: If FC exceeds sufficiently beyond FC_{th}, the fourth category (Fig.1b) occurs naturally. The fine grains make active contacts among themselves while the coarse grains become gradually dispersed and act as embedded reinforcement elements within the fine grain matrix until they are separated sufficiently apart. This imposes a limiting fines content FC_L (Appendix V). Beyond FC_L, the behavior of the soil mix is entirely governed by the fine-grain-to-fine-grain contact. The transition zone between FC_{th} and FC_L is called case iv-2 and the zone corresponding to $FC>FC_L$ is called case iv-1. The FC_L is given by (Appendix V):

$$FC_L \geq 100\left[1-\frac{\pi(1+e)}{6s^3}\right]\% > FC_{th} \qquad (2)$$

where s=1+a(d/D)=1+a/R_d, and a=10 (approximately). The fifth category (Fig.1c) occurs when the coarse and fine grains constitute a fully layered system. This is called case-v. It is also possible to create a composite system that contains some of the cases i through v.

CONTACT DENSITY INDICES

First Order Indices of Active Contacts

Contact is the mechanism by which particles in granular media compose the internal force chain network, in the absence of inter-particle gravitational and physico-chemical force fields. The latter is relevant for soils containing plastic fines. Stress-strain response, strength, compressibility, and modulus are dictated by the nature of this network. A primary index parameter that represents the density of active contacts (per grain) is essential to deduce the mechanical response of granular mixes. Physics imposes certain space constraints to the motion of particles. Two objects cannot occupy the same space at the same time. This imposes a kinematic constraint on how the contacts and therefore the internal force chain would evolve with subsequent deformation involving motion of particles. Although the particles that are actively in contact constitute the force chain, the inactive grains also have a secondary influence on the evolution of the force chain by imposing kinematic space constraints to the motion of the active grains. Physically, void ratio is an index of mass (solid volume) density. It is a good index for space constraints. Only for certain arrays of spherical particles of equal size it also becomes an index of active contact density. For other particle shapes and packing it is only a crude index of active contacts. It is not expected to hold as a unifying index from one sand to another either. It is only a secondary index of active contacts.

Intergranular (e_c) and interfine (e_f) void ratios: A first order solution would be to consider a granular mix as a composite matrix consisting of two skeletons, the coarse grain skeleton and fine grain skeleton, identify the particles that do not actively participate in the force chain (in Fig.1), and define an index void ratio of active contacts excluding the aforementioned particles. For the cases i through iii ($FC<FC_{th}$), if all fine grains are considered to be inactive and voids, the resulting intergranular void ratio e_c (Mitchell 1993, Vaid 1994) is given by:

$$e_c = \frac{e+fc}{1-fc} \qquad (3)$$

where fc=FC/100. The e_c is also known as the *sand skeleton void ratio* in the literature (Kuerbis et al. 1988). For case iv ($FC>FC_{th}$), if the effect of coarse grain is completely neglected, the relevant intefine contact void ratio (Thevanayagam 1998) is given by:

$$e_f = \frac{e}{fc} \qquad (4)$$

In both cases, the specific gravities of the coarse and fine grains are assumed to be nearly the same. The underlying tenet is that the soil behavior is governed by the coarse grain skeleton alone in cases i through iii and it is governed by the fine grain skeleton alone in case iv. But this tenet is fundamentally flawed because the neglected fine and coarse grains in cases i through iii and iv, respectively, do influence the global mechanical response. For cases i through iii, although it may be possible to use e_c as an index of active contacts, it is expected the mechanical behavior of such mixes would be stronger than that of the host coarse grain soil *at the same* e_c. Similarly, for case iv, the mechanical response of a granular mix is expected to be stronger than that of the host fine grain soil at the same e_f. The magnitude of e_f in cases i through iii, and e_c in case iv may be used as the secondary indices to assess the degree of such secondary influences. A set of equivalent contact indices $(e_c)_{eq}$ and $(e_f)_{eq}$ that reflect the primary and secondary influences together is necessary for characterization of granular mixes.

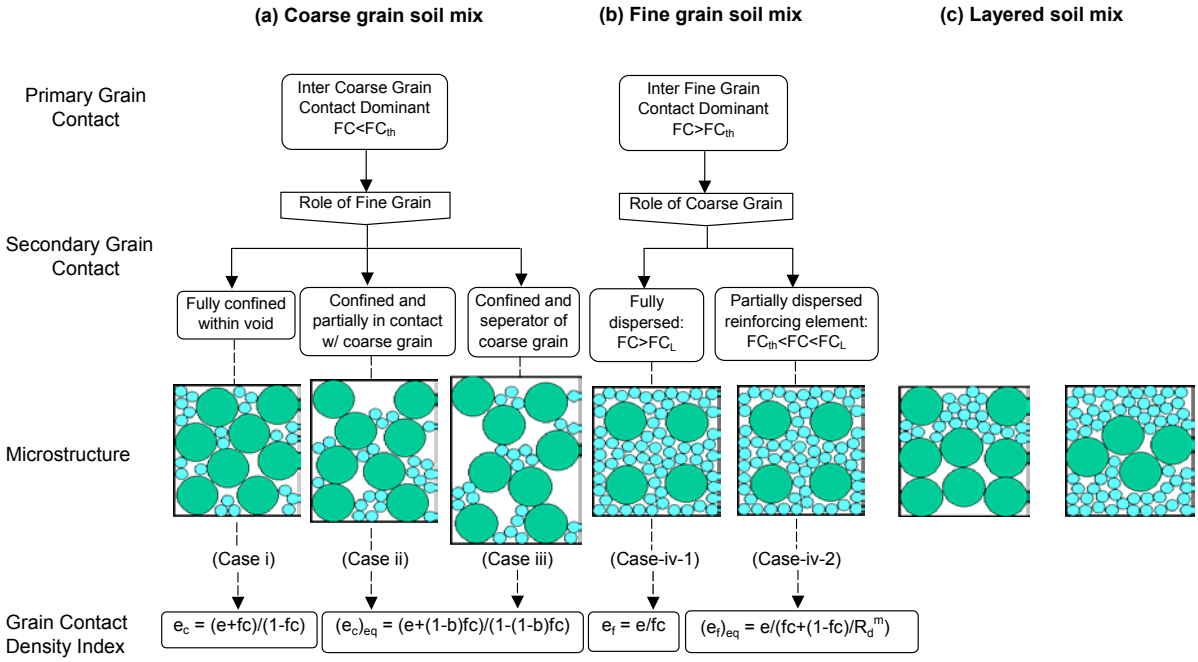

b=portion of the fine grains that contribute to the active intergrain contacts; e=global void ratio; FC=fine grains content; FC_{th}=threshhold fine grains content; FC_L=limit fines content; m: reinforcement factor; R_d=D/d=particle size disparity ratio

Fig.1 Intergranular Soil Mix Classification

Second Order Indices of Active Contacts

Equivalent intergranular void ratio, $(e_c)_{eq}$: At $FC<FC_{th}$, the influence of fine grains supporting the coarse grain skeleton and the kinematic constraints that the fine grains confined within the voids impose on the deformation of the coarse grain skeleton must be accounted for in devising an equivalent index of active contacts. The amount of fine grains that contributes to the force chain would depend on pore size distribution within the coarse grain skeleton, particle shape characteristics, and the size disparity ratio R_d. Denoting the portion of the fine grains contributing to the force chain by 'b', the relevant equivalent intergranular contact index void ratio $(e_c)_{eq}$ is given by

$$(e_c)_{eq} = \frac{e + (1-b)\,fc}{1-(1-b)\,fc} \qquad (5)$$

where 0<b<1. From a physical point of view, b=0 means that none of the fine grains contribute to the force chain and b=1 means that all fine grains contribute to the force chain. Also, when R_d=1, b would be 1 and when R_d is very large, b would tend to be zero. For broadly graded mix, b depends on R_d and gradation of the fine and coarse grain soils contained in the mix. Theoretical development of an expression for b is ongoing, but it is most desirably obtained experimentally.

Equivalent interfine void ratio $(e_f)_{eq}$: At $FC_{th}<FC<FC_L$, the global void ratio e *overestimates* the actual density of active contacts in the granular mix. This is so because the dispersed coarse grains in the mix do not contribute as many active contacts as if the soil was prepared at the same void ratio by substituting each coarse grain by an equal (solid) volume of fine grains. The reason is that solid volume of a dispersed coarse grain, which directly influences the global void ratio, grows in proportion to the power of three of particle size. Surface area, which influences the nature of contacts with the surrounding fine grains, grows in proportion to the power of only two. For equal solid volume, the substituted fine grains have a larger surface for contact than a dispersed coarse grain of equal (solid) volume embedded in the fine grain medium. The density of contacts in the mix is smaller than that in the fine grain soil at the same e. The use of e_c as an index of active contacts is also not valid since it completely ignores the existence of interfine grain contacts. It grossly underestimates the active contacts. Similarly, the interfine void ratio e_f also *underestimates* the active contacts, since it completely ignores the contribution by the dispersed coarse grains to the contact force chain.

One way to theoretically quantify the effect of each dispersed coarse grain on the macro response of the mix is to estimate the *effective* number of active contacts it makes with the fine grains surrounding it and simply replace each dispersed coarse grain in the mix by an equivalent number of fine grains that will make the same number of active contacts made by the coarse grains. The equivalent void ratio $(e_f)_{eq}$ of the resulting equivalent fine grain medium is taken as the index of active contacts, leading to (Appendix VI):

$$(e_f)_{eq} = \left[\frac{e}{fc + \dfrac{(1-fc)}{R_d^{\,m}}}\right] < e_f \le e_{max,\ HF} \quad ;\ e_c > e_{max,HC} \qquad (6)$$

where m= a coefficient satisfying 0<m<1 and it depends on grain size and shape characteristics, gradation, and packing. An expression for m for a few special cases of spherical or disc shaped particles is presented in Appendix VI. An experimental determination of m is most preferred.

GRANULAR MIX CLASSIFICATION

Intergranular Matrix Classification

Conceptually, Fig.2 shows the regions belonging to the four cases i through iv and the transition boundaries, namely the lines corresponding to FC_{th}, FC_L, upper bound for the e_{max} and lower bounds for the e_{min} (corresponding to a standard compaction energy) of the granular mix. Note that FC_{th} and FC_L depend on e. The boundaries (lines) between the cases are transitional zones.

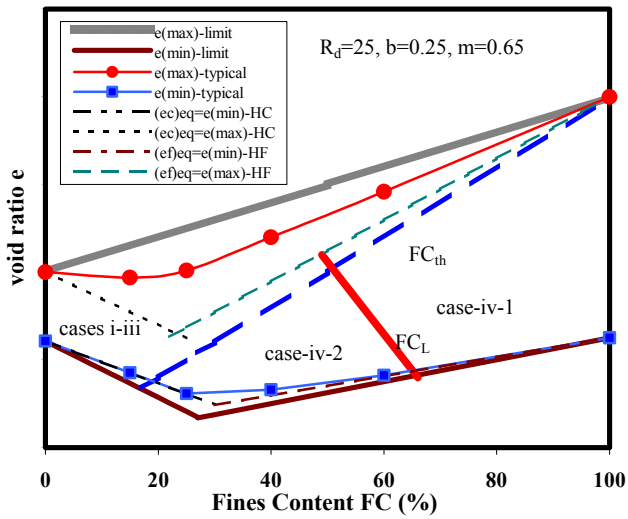

Fig.2 Intergranular Matrix Classification – Schematic

If the conditions setforth for case i were to hold, theoretically, up to FC=FC_{th}, the e_{min} of the soil mix is governed by the minimum void ratio of the coarse grains ($e_{min,HC}$). The e_{min} profile is expected to follow $e_c = e_{min,HC}$ line up to FC=FC_{th}. But due to the contributions by the fine grains to the force chain the actual e_{min} profile is expected to be higher than the line corresponding to $e_c = e_{min,HC}$. The actual e_{min} profile may be expected to most likely follow the line corresponding to $(e_c)_{eq} = e_{min,HC}$

$$e_{\min} = e_{\min,HC}[1-(1-b)fc]-(1-b)fc \qquad (7)$$

Once FC_{th} is reached, the magnitude of e_f drops below $e_{max,HF}$. Hence the contribution by the fine grains would increase and therefore the e_{min} profile would deviate from the above line. With further increase in FC, the soil moves into case iv-2. The e_{min} profile most likely follows the line corresponding to $(e_f)_{eq} = e_{min,HF}$ until FC exceeds FC_L:

$$e_{\min} = e_{\min,HF}\left[fc + \frac{(1-fc)}{R_d^m}\right] \qquad 8)$$

where $e_{min,HF}$ is the minimum void ratio of the host fine grain soil. Beyond FC_L, the e_{min} profile is expected to follow the $e_f = e_{min,HF}$ line.

If the fine grains in the soil mix are fully confined within the intergranular voids or if the coarse grains are fully dispersed, the e_{max} for such a soil mix is governed by the maximum void ratio of the coarse grains ($e_{max,HC}$) and $e_{max,HF}$ at FC<FC_{th} and FC>FC_{th}, respectively. Hence the e_{max} profile may be expected to follow the lines corresponding to $e_c = e_{max,HC}$ and $e_f = e_{max,HF}$ at FC<FC_{th} and FC>FC_{th}, respectively. If the soil mix is a fully layered system, the e_{max} profile is given by the line connecting the coordinates ($e_{max,HC}$,0) and ($e_{max,HF}$,100) in Fig.2. However, due to similar explanation given before for the most likely e_{min} profile, in most cases the e_{max} profile is expected to lie between these two upper limits, and likely follow the lines corresponding to $(e_c)_{eq} = e_{max,HC}$ and $(e_f)_{eq} = e_{max,HF}$, respectively:

$$e_{\max} = e_{\max,HC}[1-(1-b)fc]-(1-b)fc \qquad (9)$$

$$e_{\max} = e_{\max,HF}\left[fc + \frac{(1-fc)}{R_d^m}\right] \qquad (10)$$

In the above derivations it is tacitly assumed that the e_{max} and e_{min} profiles represent constant energy lines and that they represent certain grain contact density values. The e_{min} and e_{max} profiles corresponding to Eqs.7 to 10 are also shown in Fig.2.

Mechanical Response Correlation Indices

Considering that contact density is the primary factor that affects the mechanical stress-strain response of a granular mix, the index parameters $(e_c)_{eq}$, $(e_f)_{eq}$ and e_f may be used to study the mechanical response of a granular mix, at the relevant ranges of FC, in comparison against the behavior of the host coarse grain soil or the host fine grain soil. When comparing the behavior of a mix with other soil mixes prepared by mixing other host grains, the equivalent intergranular and interfine contact relative densities, $(D_{rc})_{eq}$ and $(D_{rf})_{eq}$, may be used as the contact indices at the respective FC ranges.

$$(D_{rc})_{eq} = \left[\frac{(e_{\max,HC}-(e_c)_{eq})}{(e_{\max,.HC}-e_{\min,HC})}\right] \quad \text{for FC<FC}_{th} \qquad (11)$$

$$(D_{rf})_{eq} = \left[\frac{(e_{\max,HF}-(e_f)_{eq})}{(e_{\max,.HF}-e_{\min,HF})}\right] \quad \text{for FC>FC}_{th} \qquad (12)$$

Substituting Eqs. 7 to 10 in Eq.11 and 12, it can be shown that, independent of b and m,

$$(D_{rc})_{eq} = \left[\frac{(e_{\max,HC}-(e_c)_{eq})}{(e_{\max,HC}-e_{\min,HC})}\right] = \left[\frac{(e_{\max}-e)}{(e_{\max}-e_{\min})}\right] = D_r \quad \text{for FC<FC}_{th} \ (13)$$

$$(D_{rf})_{eq} = \left[\frac{(e_{\max,HF}-(e_f)_{eq})}{(e_{\max,HF}-e_{\min,HF})}\right] = \left[\frac{(e_{\max}-e)}{(e_{\max}-e_{\min})}\right] = D_r \quad \text{for FC>FC}_{th} \ (14)$$

where e_{max} and e_{min} are the respective maximum and minimum void ratios of a mix at the relevant FC. Hence, according to the framework presented herein, the traditional relative density D_r is still a valuable index for comparison, given that the soil is divided into two groups depending on FC relative to FC_{th}. Nevertheless, in practice it is difficult to determine e_{max} for silty soils accurately as it is significantly affected by slight variations in procedure (energy input). The e_{max} measured in a laboratory is expected to deviate from Eqs.9-10. The traditional D_r may, but not always expected to, be the same as $(D_r)_{eq}$. Hence, the use of Eqs.11 and 12 is more desirable than D_r for comparison of the mechanical responses of different mixes together, unless the e_{max} is determined based on standardized energy input or strength considerations (such as very slow penetration of a standard cone to a certain distance into the soil mix).

DISCUSSION

Experimental Evaluation

Recent preliminary evaluations of the aforementioned classification scheme indicate that it works well for many silty sands, sandy silts, sandy gravel, and gravely sand. The contact indices correlate well with cyclic strength, steady state strength (Thevanayagam, 2000a, Thevanayagam et al. 2001b-c), shear wave velocity (Thevanayagam 1999), and post-liquefaction volumetric strain (Thevanayagam et al. 2001a). It has also been used to make an assessment of the influence of fines on in situ SPT blow counts, CPT resistance and shear wave velocity in silty soils and possible implications on the use of such parameters for liquefaction screening (Thevanayagam 2000b). This section presents a few of the above correlations observed (Table 1). The raw data were obtained from the cited references and

reinterpreted using the above framework.

Table 1: Soils used for evaluation – An Example

Coarse grain soil	Fine grain soil	Test type	FC %	d_{50} mm	R_d	b	m	Raw Data	Reinterpreted Results
OS-F55 sand	Crushed Silica Fines (Non-plastic)	CIU-TC and CIU-CT	0 to 100	0.25	25.0	0.25 0.35	0.65	Thevanayagam et al. 2001b-c	Thevanayagam et al. 2001b-c
FJ#80 sand	Crushed Silica Fines (Non-plastic)	CIU-TC and CIU-CT	0 to 100	0.18	18.0	0.30 0.65	-	Thevanayagam et al. 2001b-c	Thevanayagam et al. 2001b-c
Monterey 0/30 sand	Yatesville Silt (Non-plastic)	CIU-CT	0 to 100	0.43	14.3	0.25	0.45	Polito and Martin 2001	Thevanayagam et al. 2001c
Yatesville sand	Yatesville Silt (Non-plastic)	CIU-CT	0 to 100	0.18	6.0	0.60	0.60	Polito and Martin 2001	Thevanayagam et al. 2001c
Medium sand	Silt PI=4	CIU-CT	0 to 60	0.48	N/A	N/A	N/A	Chang (1990)	Thevanayagam 2000a
Gravel	Tone River Sand	Shear wave velocity	25 to 100	N/A	25	N/A	0.55	Kokusho et al. 1995	Thevanayagam 1999

Note: CIU-TC = istropic consolidated undrained triaxial compression, CIU-CT = isotropic consolidated undrained cyclic triaxial. Different b values are reported for CIU-TC and CIT-CT.

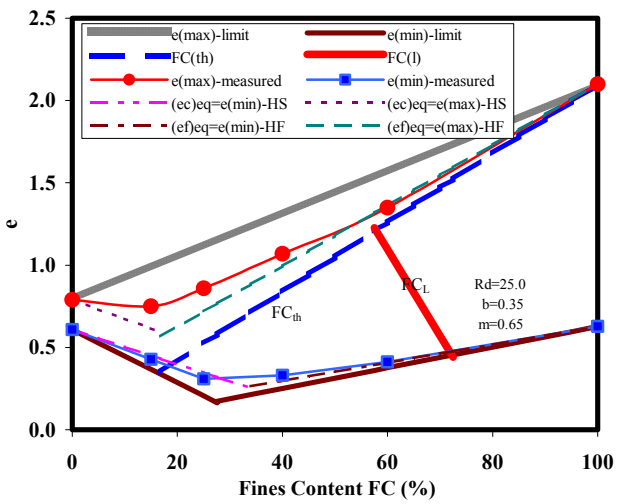

Fig.3 Intergranular Matrix Diagram: OS-F55 Sand-Silt Mix

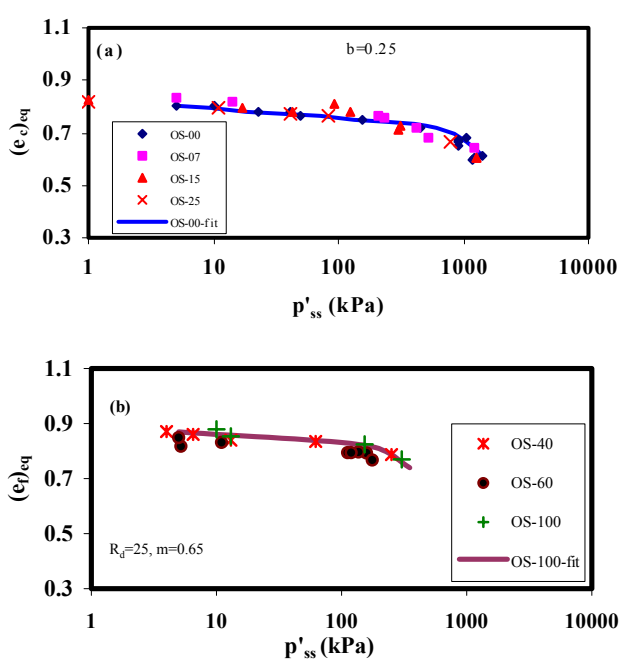

Fig.4 p'_{ss} vs $(e_c)_{eq}$ and $(e_f)_{eq}$: (a) FC<FC_{th} and (b) FC>FC_{th}
(OS-15=OS-F55 Sand with 15% Silt, after Thevanayagam et al. 2001b)

Steady State: Fig.3 shows the intergranular matrix diagram for OS-F55, the theoretical profiles for FC_{th}, FC_L, e_{min}, and e_{max}, and the measured e_{max} and e_{min} data. Figs.4a-b present the steady state data ($p'_{ss} = (\sigma'_1+2\sigma'_3)/3$) obtained from triaxial compression tests on initially isotropic consolidated specimens for OS-F55 sand-silt mixes, split into two groups at FC<FC_{th} and FC>FC_{th} and plotted against $(e_c)_{eq}$ and $(e_f)_{eq}$, respectively. The data for all silty sands up to FC_{th} fall in the vicinity of the data for the respective host clean sands. The data for sandy silts (FC>FC_{th}) falls in the vicinity of the host silt. No unique relationship was found when these data were plotted against e. Figs.5a-b show the steady state data for OS-F55 sand-silt mix and FJ#80 sand-silt mix plotted against $(D_{rc})_{eq}$ and $(D_{rf})_{eq}$ for FC<FC_{th} and FC>FC_{th}, respectively. The data for both mixes fall in a narrow band surrounding the data for the respective host coarse and fine grain soils. The steep curve found in Fig.5b compared to Fig.5a is due to the very high values for $e_{max,HF}$ for silts obtained using the same method (ASTM D4254) developed for coarse-grained soils.

Cyclic Strength: Figs. 6a-b show the energy per unit volume of soil (E_L at 5% double amplitude axial strain) required to cause liquefaction versus $(e_c)_{eq}$ and $(e_f)_{eq}$ for FC<FC_{th} and FC>FC_{th}, respectively, for the OS-F55 sand-silt mix. The specimens were initially isotropically consolidated to 100 kPa and subjected to stress-controlled cyclic triaxial tests at a cyclic stress ratio (CSR) of 0.2. Similar data, in terms of CSR required to trigger liquefaction in 15 cycles, for the Monterey 0/30 and Yatesville sand-silt mixes are shown in Figs. 7a-b plotted against $(D_{rc})_{eq}$ and $(D_{rf})_{eq}$ at FC<FC_{th} and FC>FC_{th}, respectively. The specimens in this case were also initially isotropically consolidated. The data for both sandy silts (FC>FC_{th}) fall in the vicinity of the host silt (Yatesville silt) irrespective of the sand grain characteristics. The data for silty sands at FC<FC_{th} fall in a narrow band corresponding to the respective host sands, except for a few data points. Each of the few latter points (e.g. one data point for each Y-17, M-0, M-10 in Fig.7a) deviates from the trend line formed by the other data points belonging to the same mix and they may have been affected by other experimental factors.

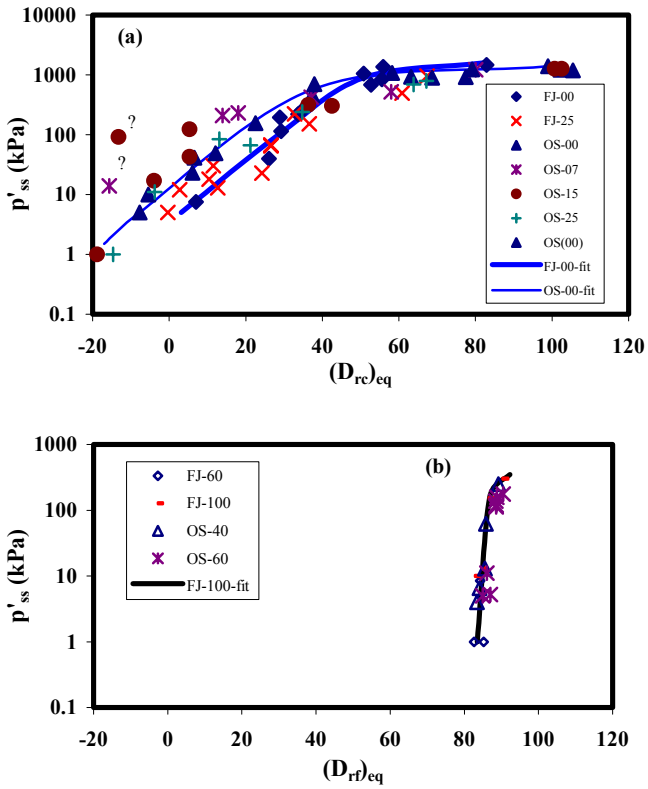

Fig.5 p'_{ss} vs $(D_{rc})_{eq}$ and $(D_{rf})_{eq}$: (a) FC<FC_{th} and (b) FC>FC_{th}
(FJ-60=FJ#80 Sand with 60% Silt)

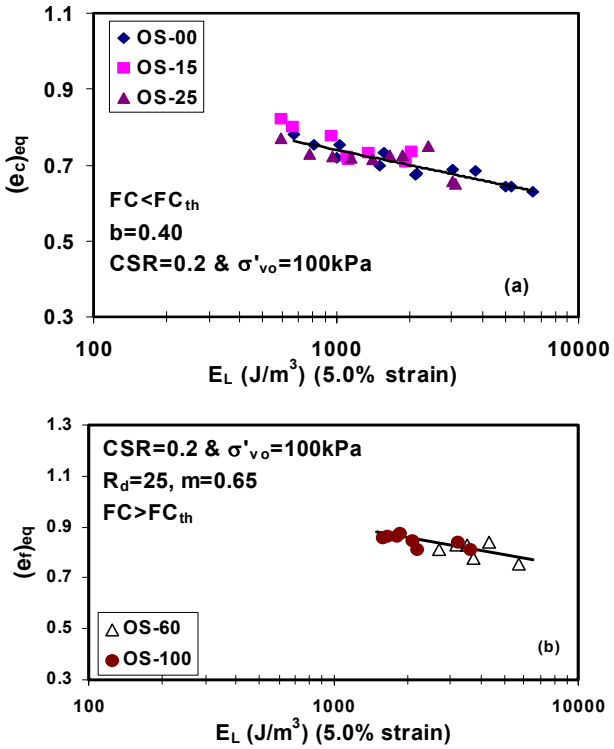

Fig.6 E_L vs $(e_c)_{eq}$ and $(e_f)_{eq}$ at CSR=0.2

Shear Wave Velocity: Fig.8 shows the normalized shear wave velocity corresponding to 100 kPa confining stress for gravelly sands containing up to 75% gravel plotted against $(e_f)_{eq}$ (Thevanayagam 1999). In this case, sand was considered as the fine grain and gravel as the coarse grain. The data fall in a narrow band surrounding the data for sand.

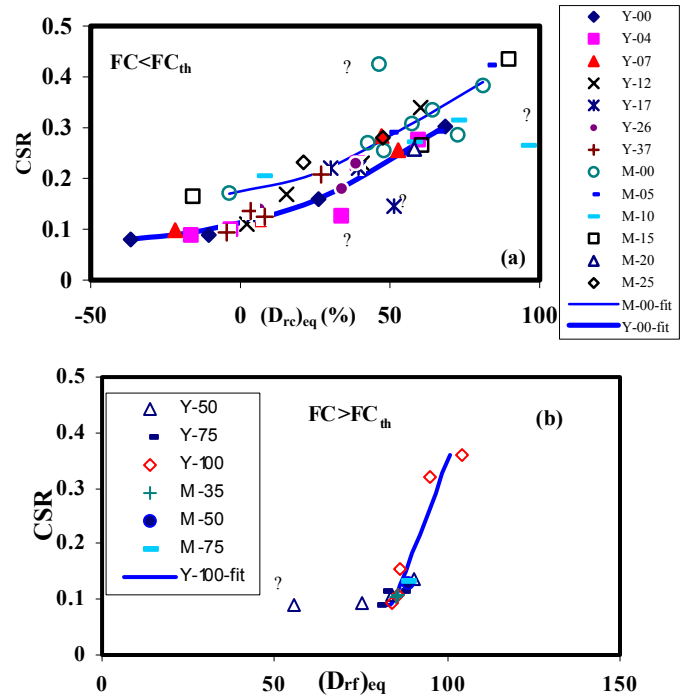

Fig.7 CSR vs $(D_{rc})_{eq}$ and $(D_{rf})_{eq}$

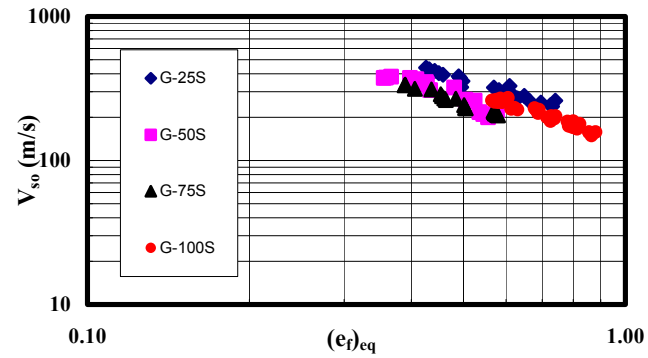

Fig.8 Shear wave velocity - v_{so} versus $(e_f)_{eq}$
(G-25S=Gravel with 25% TRS sand)

Secondary contact parameters b and m: Fig.9 shows the relationship for b and m with C_{uc}, C_{uf}, and R_{d50} (=D_{50}/d_{50}), where C_{uc} and C_{uf} are the coefficients of uniformity of the respective coarse and fine grain soils contained in the mix. It may be used as a guide to determine b and m. Initial theoretical considerations (Appendix VI), limiting to R_d>6.5, indicate that, in general, b and m are expected to increase with an increase in C_{uc} and C_{uf} and decrease in R_d. When R_d decreases, the fine particle size to pore throat size increases allowing participation by more number of finer grains in the contact force chain. Hence, b increases. When C_{uc} increases, the pore throat size decreases, and hence b increases. When C_{uf} increases, the fine-grained soil contains a greater number of larger particles than a case where C_{uf} is small. Hence, the contribution of the fine grains to the contact force chain increases. For the same soil mix, b tends to be slightly higher for cyclic response than for monotonic response (Fig.9). It was also different for post-liquefaction volumetric densification. Such differences may be caused by the differing degrees of influence imparted by fine grains during different mechanical processes such as skeletal collapse during liquefaction and particle rearrangement during post-liquefaction densification as opposed to steady state deformation during monotonic shear.

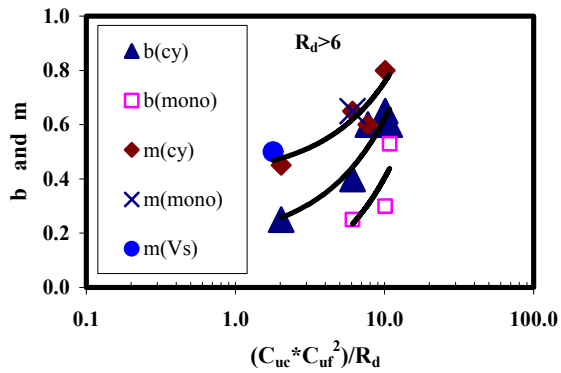

Fig.9 b and m versus $C_{uc}C_{uf}^2/R_{d50}$
(cy=cyclic shear; mono=monotonic shear, Vs= shear wave velocity)

Collapse Potential: Fig.10a shows the cyclic strength data for a sand/silt mix prepared at nearly constant global void ratio (0.558) but at different fines content (0, 5, 12.5, 20, 40, and 60% by weight) (Chang 1990). The plasticity index of the silt was 4. The specimens were initially istropically consolidated to 104 kPa and subjected to cyclic triaxial tests at a constant CSR. Table 2 shows the equivalent index void ratios for each specimen. Fig.11 shows the intergranular matrix diagram for this sand-silt mix. For qualitative discussion purposes, the FC_{th} and FC_L profiles in Fig.11 were estimated assuming typical values of $e_{max,HF}$ =1.5, $e_{min,HF}$ =0.6, and R_d=40, based on a typical value for d_{50} of silts.

Table 2: Intergrain Contact Index Void ratios

Parent Sand	Silt %	e_f	$(e_c)_{eq}$	$(e_f)_{eq}$
Medium Sand	0		0.558	
D_{50}=0.48mm,	5		0.619	
e_{max}=0.675,	12.5		0.719	
e_{min}=0.441	20	2.790	0.833	
C_u=1.8, C_c=2.2	45	1.240		1.006
Poorly Graded	60	0.930		0.825

Notes: D_{50} in mm, Silt d_{50}=not available, assumed d_{50}=0.012mm; b=0.25, m=0.45; e=0.558 and FC_{th}=37%.

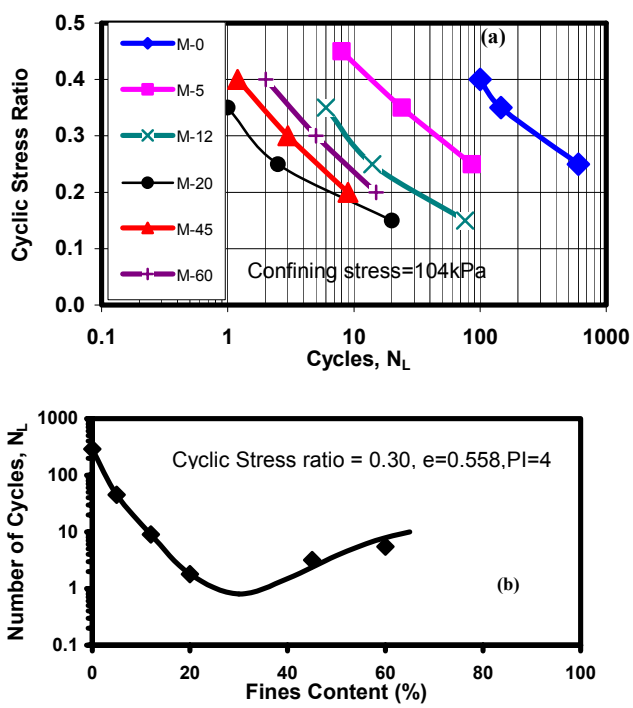

Fig.10 Cyclic strength (M-20 = Medium Sand with 20% Silt)

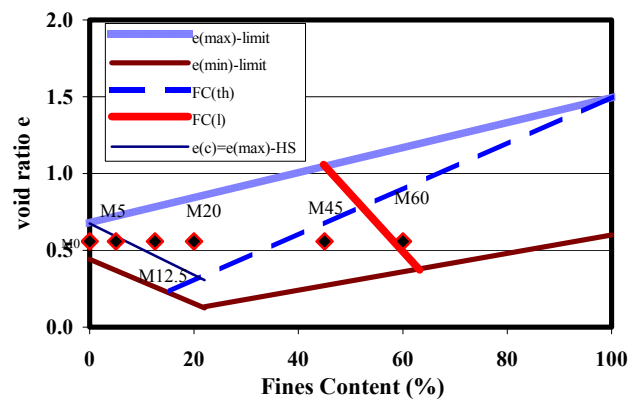

Fig.11 Intergranular Matrix Diagram - Medium Sand-Silt Mix

Fig.10b shows the variation of N_L versus silt content corresponding to CSR=0.3. The N_L decreases with an increase in silt content and then increases with a further increase in silt content. This can be qualitatively explained using the index void ratios shown in Table 2. Initially, $(e_c)_{eq}$ steadily increases with an increase in silt content up to FC_{th}. Hence the strength decreases up to FC=FC_{th}. Thereafter the soil strength is primarily governed by the fines with secondary influences by the sand grains. The relevant contact index $(e_f)_{eq}$ steadily decreases with further increase in silt content leading to a corresponding increase in strength.

Anticipated Relative Trends

Finally, based on the insights gained from experimental evaluations of the framework presented herein, the anticipated trends in mechanical response of a granular mix, relative to the behavior of host sand and the host silt, can be deduced. Many contentious issues on the nature of the influence of fine grains on the mechanical response of granular mixes can be addressed.

As an example, consider a set of hypothetical specimens prepared at the same void ratio (0.64) but different FC (specimens 4,2,5,6,7,13 in Fig.12a], consolidated at a constant confining stress, and subjected to undrained cyclic triaxial shear test at a constant CSR. Fig.12b shows the contact indices, $(e_c)_{eq}$ and $(e_f)_{eq}$, for these specimens plotted against FC. Initially, $(e_c)_{eq}$ increases steadily with an increase in FC. The magnitude of $(e_f)_{eq}$ is very large indicating only a secondary influence by the fine grains. Hence, the strength of such a soil mix is expected to decrease with an increase in FC, at the same e. Beyond FC=FC_{th}, $(e_f)_{eq}$ is sufficiently small and steadily decreases with further increase in FC. The $(e_c)_{eq}$ is large (and further increases with an increase in FC) indicating only a secondary diminishing influence by the coarse grains. Hence, the strength of a soil mix in this range of FC is expected to be governed primarily by the fine grains, and is expected to increase with further increase in FC, at the same e. Taking cyclic strength as an example, this anticipated trend is schematically depicted in Fig.12c. A similar relative trend is expected for other mechanical parameters such as undrained strength, modulus, etc., and in a generic form, the stress-strain behavior that depend primarily on contact density.

Similar analyses could be done for a variety of scenarios. A few scenarios are depicted below: (a) an increase in global void ratio e at the same FC [specimens 1,2,3 in Fig.12a], (b) an increase in FC at the same e_c [8,1,9 or 3,10 in Fig.12a; FC<FC_{th}], and (c) an increase in coarse grain content at the same e_f [11,7,12; Fig.12a; FC>FC_{th}]. Again considering the variation trend for $(e_c)_{eq}$ and $(e_f)_{eq}$ as the guide as FC and e change, Fig.12c shows the N_L versus FC for those specimens prepared at the same global void

ratio. Figs.13a-b show the relative trend in N_L versus e_c and N_L versus $(e_c)_{eq}$, respectively, for soils at $FC<FC_{th}$. Figs.13c-d show the relative trend for N_L versus e_f and $(e_f)_{eq}$, respectively, for soils at $FC>FC_{th}$. Experimental data supporting such trends are reported in Thevanayagam et al. 2001b and c.

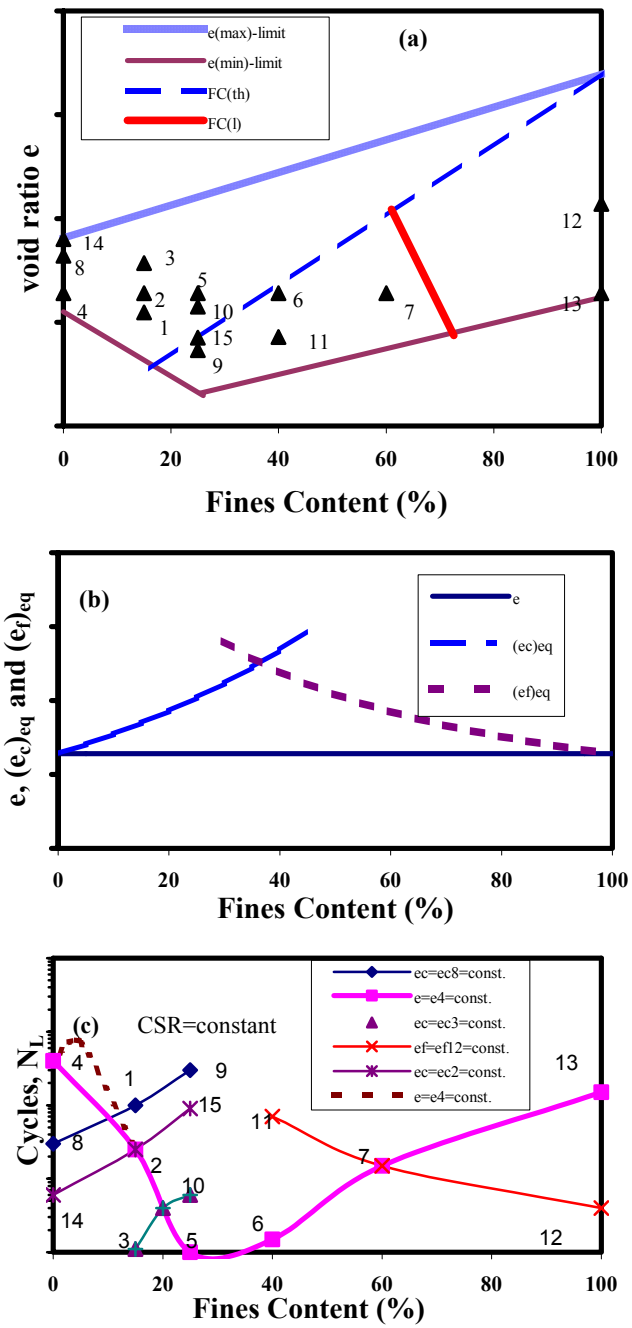

Fig.12 Trend-Cyclic Strength (a) hypothetical specimens, (b) e, $(e_c)_{eq}$ and $(e_f)_{eq}$ vs FC at e=const., and (c) N_L vs FC
(e4 = e of spec. #4, ec2 = e_c of spec. #2, ef12 = e_f of spec. #12)

Effect of Fines on Collapse Potential

Whether the presence of silt in a silty sand increases or decreases its collapse potential is a contentious issue. The conceptual framework and the results presented before can be used to develop a logical answer to this question. The intergranular contacts and its evolution affect collapse potential of a soil. The influence of silt content on undrained collapse potential of a granular mix should be addressed based on grain contact density. The answer turns out to be that the fines can beneficially and/or adversely affect collapse potential depending on the intergranular matrix status of the soil as shown in Figs.10b and 12c.

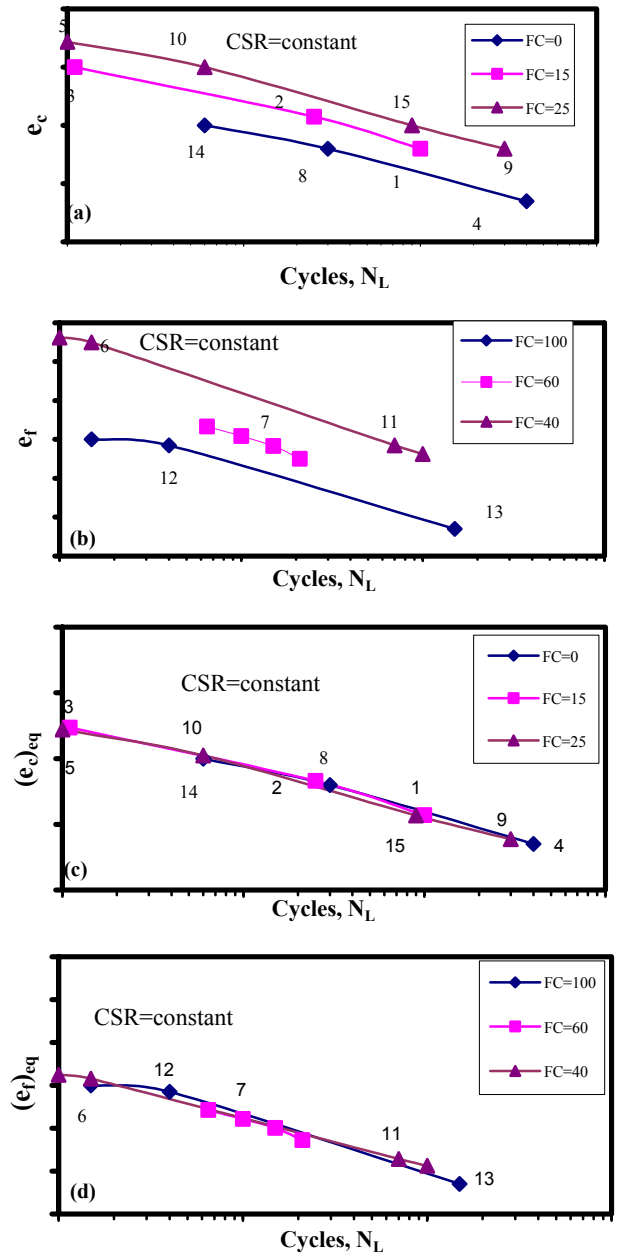

Fig.13 Anticipated trend – Contact Index Void Ratios versus Cyclic Strength, N_L (a) e_c ($FC<FC_{th}$), (b) e_f ($FC>FC_{th}$), (c) $(e_c)_{eq}$ ($FC<FC_{th}$), and (d) $(e_f)_{eq}$ ($FC>FC_{th}$) a

At a given void ratio, collapse potential increases with an increase in silt content up to a threshold value FC_{th}. The reason for this is that the coarse grain skeleton becomes loose (increase in e_c and $(e_c)_{eq}$), if one were to maintain the same void ratio while increasing the silt content. Beyond FC_{th}, for reasons explained before the collapse potential begins to decrease with a further increase in FC. If one were to compare at the same e_c (at $FC<FC_{th}$), collapse potential decreases with an increase in silt content. In this case, while the coarse grain skeleton is maintained (at the same e_c), the increase in fine grains content increases the degree of secondary participation by the fine grains and leads to a reduction in $(e_c)_{eq}$. The equivalent coarse grain skeleton, represented by $(e_c)_{eq}$, is denser than the host sand at the same e_c. At $FC>FC_{th}$ a comparison cannot be made at the same e_c, since the soil response in that range of FC is affected primarily by the

finer grains. At $FC>FC_{th}$, if one were to compare the collapse potential at the same e_f, then collapse potential increases with an increase in FC. The reason for this is the gradual reduction in the influences by the coarse grains (indicated by an increase in $(e_f)_{eq}$). The equivalent silt skeleton at a given FC ($FC_{th}<FC<FC_L$) is stronger than the host silt at the same e_f. Lower is the FC, stronger is the equivalent silt skeleton, at the same e_f.

Physically, at $FC<FC_{th}$, at the same e, the adverse effect stems from the fines that separate some of the coarse grain contacts. They help to create larger intergranular voids than in the host sand at the same e with no fines. This creates a weaker sand skeleton. Furthermore, during shear, the fine grains separating the coarse grains can fall into the relatively larger pore openings and contribute to (or facilitate) the collapse of the coarse grain skeleton. The beneficial effect comes from the fines that are already within the intergranular pore space. At the same e_c, an increase in fines content is somewhat similar to filling more of the physical space in the intergranular voids. The space available for a coarse grain particle to fall into, in the event the conditions for instability develops, is reduced. The degree of collapse is reduced.

The foregoing discussions illustrate that a question on the influence of fines on the mechanical response of a soil mix has to be addressed with reference to grain contact density, among other factors.

CONCLUDING REMARKS

Based on rational reasoning on the nature of the microstructure of a granular mix with large disparities in grain sizes a framework for understanding the mechanical response of granular mixes relative to that of the host coarse and fine grain soils is presented. The relative contributions by the coarse and fine grains to the mechanical response depend on fines content, size disparity between fines and coarse grains, and void ratio. Broadly there exist three zones of soil behavior:

(a) one that is governed primarily by the coarse grain skeleton with a little contributions by the fine grains at FC less than a threshold value FC_{th},

(b) one that is governed by the fine grain skeleton at fines content above a limiting value FC_L, and

(c) one that is governed primarily by the fine grains with a little contribution by the coarse grain at an intermediate range of FC between FC_{th} and FC_L.

The relevant contact index void ratios for these cases are $(e_c)_{eq}$, e_f, and $(e_f)_{eq}$, respectively. In general, the mechanical response of a granular mix is similar to that of the host coarse or fine grained soil behavior at the same $(e_c)_{eq}$ or $(e_f)_{eq}$, respectively, or the relevant equivalent intergranular and intefine relative densities $(D_{rc})_{eq}$ and $(D_{rf})_{eq}$, respectively.

The framework presented herein pertains to gap-graded soil with large particle size disparity. Therefore, any extrapolations to well graded soils must be done carefully. Furthermore this framework does not explicitly include such effects as cementation that may be found in field soils. It may be modified accordingly using appropriate values for the parameters b and m.

ACKNOWLEDGMENTS

The author wishes to thank the ASCE reviewers for the critical reading and thoughtful suggestions for improvement. Financial support for the ongoing research by the National Science Foundation and USGS is gratefully appreciated. This research also benefited from other ongoing research on liquefaction mitigation sponsored by MCEER and FHWA. T. Kanagalingam, University at Buffalo, helped preparing the figures.

APPENDIX I: REFERENCES

Andrus, R., and Stokoe, K. (1997) "Liquefaction resistance based on shear wave velocity", NCEER Report, 97-0022, National Center for Earthq. Eng. Res., State Univ. of New York at Buffalo, NY, 89-128.

Baziar, M.H. and Dobry, R. (1995), "Residual strength and large-deformation potential of loose silty sands", J. Geotech. Eng. Div., ASCE, 121(12), 896-906

Chameau, J.L. and Sutterer, K. (1994), "Influence of fines in liquefaction potential and steady state considerations", 13th Intl. Conf. Soil Mech. and Found Eng., India, 183-84.

Chang, N.Y. (1990) "Influence of fines content and plasticity on earthquake-induced soil liquefaction", Contract Rep. DACW3988-C-0078, US Army WES, Vicksburg,MS.

Evans, M. D. and Zhou, S. (1995) "Liquefaction behavior of sand-gravel composites", ASCE, J. Geotech. Eng., 121(3), 287-298.

Finn, L.W.D., Ledbetter, R.H. and Guoxi Wu (1994), "Liquefaction in silty soils: Design and analysis", Proc. ASCE National Conv., Atlanta, Geotech. Sp. Pub. 44, 51-76

Georgiannou, V.N, Hight, D.W and Burland, J.B (1990), "The undrained behaviour of clayey sands in triaxial compression and extension", Geotechnique, 40(3), 431-49

Georgiannou, V.N, Hight, D.W and Burland, J.B (1991a), "Undrained behaviour of natural and model clayey sands", Soils and Foundations, 31(3), 17-29

Georgiannou, V.N, Hight, D.W and Burland, J.B (1991b), "Behaviour of clayey sands under undrained cyclic triaxial loading", Geotechnique, 41(3), 383-93.

Ishihara, K. (1993), "Liquefaction and flow failure during earthquakes", Geotechnique, 43(3), 351-41.

JGS (1996) "Special issue on geotechnical aspects of the January 17 1995 Hyogoken-Nambu Earthquake", Soils and Foundations, Japanese Soc. Geotech. Eng.

Kenny, T.C. (1977) "Residual strength of mineral mixtures", Proc. 9th Int. Conf. Soil Mech., Tokyo, 1, 155-160.

Koester, J.P. (1994), "The influence of fines type and content on cyclic strength", Proc. ASCE Conv., Atlanta, Geotech. Spec. Pub. 44, 17-32.

Kuerbis, R., Nagussey, D. and Vaid, Y.P. (1989), "Effect of gradation and fines content on the undrained response of sand", Proc. Conf. on Hyd. Fill Struc., ASCE Geotech. Spec. Publ. 21, 330-45.

Kokusho, T., Yoshida, Y. and Tanaka, Y. (1995) "Shear wave velocity in gravelly soils with different particle gradings", ASCE Geotech. STP 56, 92-106

Mitchell, J. K. (1993) *Fundamentals of soil behavior*, second ed. Wiley Interscience Publ.

NRC (1985) "Liquefaction of soils during earthquakes", Committee on Earthq. Eng., National Res. Council, Washington, DC, Rept. No. CETS-EE-001.

Pitman, T.D., Robertson, P.K. and Sego, D.C. (1994), "Influence of fines on the collapse of loose sands", Can. Geotech. J., 31, 728-39

Polito, C. P. and Martin II, J. R, (2001) "Effects of nonplastic fines on the liquefaction resistance of sands" J. Geotech. Engrg. Div., ASCE, 127(5), 408-415.

Poulos, S. J. (1981). "The steady state of deformation," J. Geotech. Engrg. Div., ASCE, 107(5), 553-562.

Reynolds, O. (1885) Philos. Mag. 20, 469.

Robertson, P. K. and Wride, C. E. (1997) "Evaluation of cyclic liquefaction potential based on the CPT", Seismic Behavior of Ground and Geotech Structures, ed. P.S. Pinto, Balkema Publs., 269-278.

Roscoe, K. H., Schofield, A.N. and Wroth, C.P. (1958). "On the yielding of soils," Geotechnique 8, 22-52.

Roscoe, K. H., Schofield, A.N. and Thurairajah, A. (1963). "Yielding of clays in states wetter than critical," Geotechnique 13, 211-240.

Roscoe, K. H. (1970), "The influence of strains in soil mechanics," Geotechnique, 20(2), 129-170.

Seed, H. B., Idriss, I.M. and Arango, I. (1983) "Evaluation of liquefaction potential using field performance data", J. Geotech. Eng., ASCE, 109(3), 458-482

Seed, R. B. and Harder, L. F. Jr. (1990), "SPT-based analysis of cyclic pore pressure generation and undrained residual strength", Proc. Seed Mem. Symp., Berkeley, 2, 351-76

Seed, H.B. (1987), "Design problems in soil liquefaction", J. Geot.. Eng. Div. , ASCE, 113(8), 827-45.

Singh, S. (1994), "Liquefaction characteristics of silts", ASCE Geotech. Sp. Pub. 44, 105-16.
Stark, T. D. and Mesri, G. (1992), "Undrained shear strength of liquefied sands for stability analysis", J. of Geotech. Eng., ASCE, 118(11), 1727-47.
Thevanayagam, S. (1998) "Effect of fines and confining stress on undrained shear strength of silty sands," J. Geotech. & Geoenv. Engrg. Div., ASCE, 124(6), 479-491.
Thevanayagam, S. (1999) "Liquefaction and shear wave velocity characteristics of silty/gravely soils", Proc.15th US-Japan Workshop on Bridge Eng., Public Works Res. Institute, Tsukuba City, Tokyo, Japan, 133-147.
Thevanayagam, S. and Mohan, S. (2000) "Intergranular state variables and stress-strain behavior of silty sands" Geotechnique, vol.1, 1-24.
Thevanayagam, (2000a) "Liquefaction potential and undrained fragility of silty sands", Proc. 12th World Conf. Earthq. Eng., Auckland, New Zealand, eds. R. Park., paper#2383
Thevanayagam, S. (2000b) "Liquefaction in silty soils: considerations for screening and retrofit strategies" Proc. 2nd international workshop on mitigation of seismic effects on transportation structures, NCREE, Taipei, Taiwan. Eds. C. Loh and I. Buckle, 374 -385.
Thevanayagam, S., Liang, J., and Shenthan, T. (2000) "Contact index and liquefaction potential of silty and gravely soils": CD-ROM Proc. 14th ASCE Eng. Mech. Conf., eds. Tassoulas, J.S., Univ. of Texas, Austin.
Thevanayagam, S., Martin, G.R., Shenthan, T. and Liang, J. (2001a) "Post-liquefaction pore pressure dissipation and densification in silty soils", CD-ROM Proc. 4th Intl. Conf. Soil Dyn. & Earthq. Eng., San Diego. Eds. S. Prakash, Univ. of Missouri-Rolla.
Thevanayagam, S., Liang, J., Shenthan, T., and Mohan, S. (20001b) "Undrained fragility of clean sands, silty sands, and sandy silts", tentatively accepted, ASCE J. Geotech and Geoenv Eng. Div.
Thevanayagam, S. Kanagalingam, T., Martin, G. R., and. Liang, J (2001c) "Undrained cyclic strength of sands, silty sands, and sandy silts" in review, Can. Geot.J.
Vaid, Y.P. (1994). "Liquefaction of silty soils", ASCE Geotech. Spec. Publ. 44, 1-16
Yamamuro, J.A. and Lade, P.V. (1998). "Steady-state concepts and static liquefaction of silty sands", J. Geotech. and Geoenv. Engrg. Div., ASCE, 124(9), 868-877.
Yamamuro, J.A., Covert, K. M., and Lade, P.V. (1999) "Static and cyclic liquefaction of silty sands", Proc. workshop, Physics and mechanics of soil liquefaction, Balkema press.
Zlatovic, S. and Ishihara, K. (1995). "On the influence of nonplastic fines on residual strength," Proc. IS-TOKYO'95, First Intl. Conf. Earthquake Geotechnical Engrg., Tokyo, eds. K. Ishihara, publs. A. A. Balkema, 239-244.
Zlatovic, S. and Ishihara, K. (1997). "Normalized behavior of very loose non-plastic soils: effects of fabric" Soils and Foundations, 37(4), 47-56.

APPENDIX II: NOTATIONS

The following symbols are used in this paper.

CPT= cone penetration test
C_{uc} = uniformity coefficient of coarse-grained soil
C_{uf} = uniformity coefficient of fine-grained soil
d= diameter of fine grains
D= diameter of coarse grains
D_r= relative density
$(D_{rc})_{eq}$= equivalent intergranular relative density
$(D_{rf})_{eq}$= equivalent interfine relative density
E_L = energy required to cause liquefaction per unit vol of soil.
e = global void ratio
e_f= interfine void ratio
e_c = inter-coarse granular void ratio
$(e_c)_{eq}$= equivalent intergranular void ratio
$(e_f)_{eq}$= equivalent interfine void ratio
$(e_c)_{th}$= threshold inter-coarse granular void ratio
e_{max}= maximum void ratio
$e_{max,HC}$= maximum void ratio of the host coarse grains
$e_{max,HF}$= maximum void ratio of the host fine grains
e_{min}= minimum void ratio
$e_{mix,HC}$= minimum void ratio of the host coarse grains
$e_{mix,HF}$= minimum void ratio of the host fine grains
FC = fine grains content
FC_{th}= threshold fine grains content
FC_L= limiting fine grains content
N_L= number of cycles to cause initial liquefaction
p= mean effective stress
q= deviatoric stress
R_d= particle size disparity ratio
SPT = standard penetration test

Appendix III: Particle Size Disparity Constraint (R_d)

Consider a two-size spherical particulate system with size disparity R_d. If the fine grains were to remain confined within the coarse grain skeleton (case i), d must be smaller than the minimum possible pore throat opening between the coarse grains (Fig.III-1) for all packing configurations:

$$R_d = \frac{D}{d} > \frac{1}{(4/3)\sin(\pi/3) - 1} \approx 6.46 \qquad \text{(III-1)}$$

For real soils, however, for a number of reasons (shape, angularity, interlocking, packing, gradation, etc.) R_d must be much larger than 6.46.

Appendix IV: Threshold Fines Content, FC_{th}

If the voids within the coarse grain skeleton in Fig.1a are not completely filled with the fine grains and R_d is large enough, then during deformation, the fine grains can move from one void space to another. For this to happen rather freely, the apparent interfine void ratio e_f (=e/fc) in each pore space must be higher than a possible the $e_{max,HF}$ value corresponding to the loosest packing possible where the fine grains cannot sustain any shear stress; viz. $e/fc_{th} > e_{max,HF}$:

$$FC_{th} \le \frac{100\ e_c}{1 + e_c + e_{max,HF}}\% = \frac{100\ e}{e_{max,HF}}\% \qquad \text{(IV-1)}$$

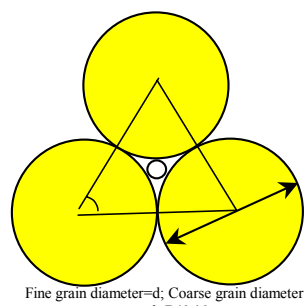

Fine grain diameter=d; Coarse grain diameter = D
d<D/6.46

Fig.III-1 Fully confined fines

Once the interfine grain void ratio drops below $e_{max,HF}$ the fine grains begin to make active contacts among themselves and begin to compose a strong internal force chain.

An accurate determination of FC_{th} requires a detailed knowledge of pore geometry and the number of fine grain particles that could be placed loosely within each inter-coarse granular pore space. An approximate way to estimate FC_{th} is to start with a unit solid volume of fine grain matrix packed at its loosest state ($e_{max,HF}$) and introduce coarse grains into it at the desired coarse grain packing (and the corresponding e_c) and remove the fine grains that each coarse grain displaces, without altering the fine grain packing and the total volume of the mix ($1+e_{max,HF}$). The e is altered as a result. The number of (full) fine grains N_d that each coarse grain displaces is an integer number between the number of (full) fine grains that can be contained at the loosest packing within a sphere of its size (D) and a sphere of size (D+2d).

If the FC at the end of the above process is FC_{th}, global void ratio is e, and the total volume of the mix is ($1+e_{max,HF}$), then the solid volumes of the fine and coarse grains are $[FC_{th}(1+e_{max,HF})/(1+e)]$ and $[(1-FC_{th})(1+e_{max,HF})/(1+e)]$, respectively. The total loss of fine grain solid volume from the initial state is $[1- FC_{th}(1+e_{max,HF})/(1+e)]$. On the other hand, each coarse grain (solid volume=$\pi D^3/6$) replaces a solid volume of $[N_d \pi d^3/6]$ of the fine grains. Hence, the amount of solid volume of fine grains replaced by coarse grains is $\{[(1-FC_{th})(1+e_{max,HF})/(1+e)][N_d \pi d^3/6]/[\pi D^3/6]\}[=N_d/(R_d)^3][(1-FC_{th})(1+e_{max,HF})/(1+e)]$. This must be equal to the total loss of fine grains $\{=[1- FC_{th}(1+e_{max,HF})/(1+e)]\}$, leading to:

$$FC_{th}=100\left[\frac{(1+e)-(1+e_{\max,HF})\frac{N_d}{R_d^3}}{(1+e_{\max,HF})-(1+e_{\max,HF})\frac{N_d}{R_d^3}}\right]\% \qquad \text{(IV-2)}$$

Theoretically, for a simple cubic array of uniform sized spherical particles, the maximum void ratio $e_{max,HF}$ is 0.91 (=6/π–1). The magnitude of N_d/R_d^3, estimated laboriously, is about 0.689 and 0.582 for R_d=16 and 32, respectively, and approaches π/6 for very large R_d. For other particle shapes N_d/R_d^3 asymptotically approaches $1/(1+e_{max,HF})$. FC_{th} increases with an increase in e and R_d and decreases with an increase in $e_{max,HF}$. Hence, FC_{th} can be smaller for silty sand prepared by mixing silt with a fine sand than a coarse sand. For plastic fines, the $e_{max,HF}$ can be high compared to a non plastic silt. FC_{th} can be smaller for clayey sands compared to silty sands.

Appendix V: Limiting Fines Content, FC_L

If the coarse grains were to play an insignificant role on the behavior of the granular mix, the spacing between the coarse-grains must be greater than a minimum value so that they do not influence the shearing along the fine grains. At spacing less than this, the coarse grains can have a reinforcing effect on the behavior of the granular mix somewhat similar to inclusion of short fibers in (clean) sand. The minimum spacing is governed by many constraints including: (1) microgeometry of the locus of motion of a fine grain, (2) thickness of the zone that a fine grain in motion influences, and (3) stress concentrations within the fine grain matrix in the vicinity of the coarse grains. Based on Roscoe's observations (1970), the limiting center-to-center spacing between the coarse grains is about (D+10d). Let the FC at this state be FC_L.

Assume that coarse grains are dispersed uniformly, in a simple cubic array within the fine-grain matrix, at a center-to-center spacing of sD. Consider a cube of size sD. The solid volume of the coarse grains in this cube $=\pi D^3/6$. The total volume of the mix is $(sD)^3$ and the global void ratio is e. Using a simple phase diagram relationship, $[\pi D^3/6]/(sD)^3=(1-fc_L)/(1+e)\}$ where $fc_L= FC_L/100$, leading to:

$$FC_l \geq 100\left[1-\frac{\pi(1+e)}{6s^3}\right]\%=100\left[\frac{\frac{6s^3}{\pi}-1}{\frac{6s^3}{\pi}+e_f}\right]\% \geq FC_{th};\ e_f \leq e_{\max,HF} \qquad \text{(V-1)}$$

where $s=1+a(d/D)=1+a/R_d$ where a=10 (approximately). Slightly different expressions may be found for different arrays. Simple cubic array, however, yields the largest spacing and therefore yields the largest FC_L. Also, the corresponding limiting inter-coarse granular void ratio $(e_c)_l$ is given by:

$$(e_c)_l=\frac{6s^3}{\pi}-1 \qquad \text{(V-2)}$$

The $(e_c)_l$ is the limiting coarse grain intergranular void ratio beyond which the coarse grains have little effect on the behavior of the fine grain matrix.Also note that case iii was defined as a state where the coarse grains are essentially separated by the fine grains, but the fine grains are still not dense enough. By setting s=1 in Eq.V-2, the corresponding threshold inter-coarse granular void ratio $(e_c)_{th}$ is given by:

$$(e_c)_{th}=\frac{6}{\pi}-1=0.91 \qquad \text{(V-3)}$$

Theoretically this is also the maximum theoretical void ratio $e_{max,HC}$ for spherical particles arranged in a simple cubic array (p139, Mitchell 1993). For real soils, the $e_{max,HC}$ varies in the vicinity of 0.90±0.1 for other reasons and hence the magnitude of $(e_c)_{th}$ would be equal to the corresponding $e_{max,HC}$.

Appendix VI: Interfine Contact Index $(e_f)_{eq}$

The $(e_f)_{eq}$ is defined as the void ratio of the equivalent fine grain soil obtained by replacing each coarse grain in the granular mix by an equivalent number of fine grains (N_e) such that the total number of contacts in the medium remains the same. This void ratio is taken as the index of active contact density in the medium.

For spherical particles, the equivalent fine grain solid volume added to the mix per unit solid volume of coarse grain removed from the matrix = $(N_e\pi d^3/6)/(\pi D^3/6)=[N_e/(R_d)^3]$. Neglecting the differences in specific gravities of solids, the *net* equivalent fine grain solid volume= $[fc+(1-fc)N_e/(R_d)^3]$ per unit total solid volume of coarse and fine grains in the mix. It leads to $(e_f)_{eq}$:

$$(e_f)_{eq}=\left[\frac{e}{fc+\frac{(1-fc)N_e}{R_d^3}}\right]<e_f\leq e_{\max,HF} \qquad \text{(VI-1)}$$

N_e depends on void ratio e, R_d, packing of the fine grain skeleton, and proximity between coarse grains.

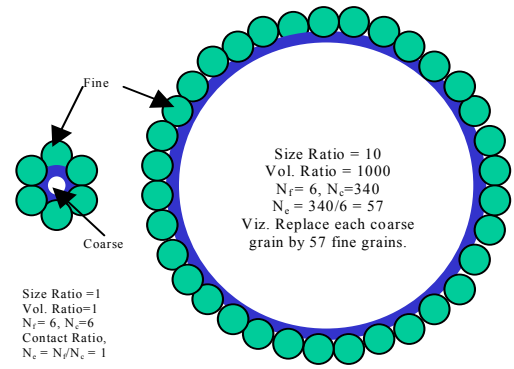

(a) R_d = 1 (b) R_d = 10

Fig.VI-1 Contact Ratio-N_e vs R_d: Disc-like Particle Mix

Consider a disc-like two-size particle arrangement shown in Fig.VI-1. The size disparity ratio is R_d [=diameter ratio (D/d)] and thickness ratio is (T/t)= R_t. Let N_f be the number of contacts that a fine grain (far from the coarse grain) makes with other fine grains surrounding it. Let N_c be the number of contacts that a dispersed coarse grain makes with the fine grains surrounding it. Neglect the influence of the larger disc on the packing of the smaller discs located away from the larger disc. Then $N_e=N_c/N_f$. For the case shown in Fig.VI-1, the angle, made by two adjacenet fine grains in contact with a coarser grain, at the center of the coarse grain is $Arcsin[2/(R_d+1)]$. N_c approaches $2\pi R_t/Arcsin[2/(R_d+1)]$. $N_c=[\pi R_t(R_d+1)]$ for large R_d. N_f=6. Hence, N_e approaches $[\pi R_t(R_d+1)/6 = \beta R_t R_d$, $\beta=\pi/6(1+1/R_d)<1.0$ approaching π/6 for large R_d]. Assuming $R_d = R_t$, the equivalent fine grain solid volume per unit actual solid volume of the dispersed coarse grain is given by $N_e(d/D)^2(t/T)=\pi(R_d+1)/(6R_d^2)$ $[=\beta/R_d]$, leading to $(e_f)_{eq}$:

$$(e_f)_{eq}=\left[\frac{e}{fc+\frac{(1-fc)\beta}{R_d}}\right]<e_f\leq e_{\max HF} \qquad \text{(VI-2)}$$

Consider spherical particles arranged in a simple cubic array. The corresponding N_f=6. The locus of the centers of the fine grains in contact with a dispersed coarse grain is given by a sphere of diameter $(R_d+1)d$ with its center coinciding with the center of the dispersed coarse grain. Accordingly N_c is approximately given by $[\pi(R_d+1)^2]$, for large R_d. N_e is approximately given by $[\pi(R_d+1)^2/6 =\beta R_d^2$, $\beta<1]$. The equivalent fine grain solid volume per unit solid volume of the dispersed coarse grain is given by $N_e(d/D)^3=\pi(R_d+1)^2/(6R_d^3)$ $[=\beta/R_d$, $\beta<1$, β approaches π/6 for large R_d], leading to the same expression as Eq.VI-2 for $(e_f)_{eq}$.

In reality, however, the reinforcement effect of a coarse grain embedded in a fine grain matrix is due to more reasons than mere contacts in its immediate vicinity. Mechanical response depends on the active contacts as well as the kinematic constraints for deformation. A coarse grain also influences contacts beyond its immediate vicinity and introduces kinematic constraints for deformation of other fine particles beyond its immediate vicinity. The *effective* N_e must be larger than βR_d^2. But it must be smaller than $(R_d)^3$ for the reasons discussed before. Physically this means that N_e grows faster than the growth rate of surface area growth ratio $(R_d)^2$ but slower than solid volume growth ratio $(R_d)^3$. To account for this deficiency in Eq.VI-2, N_e is approximated to be $(R_d)^{3-m}$, where 0<m<1.0, leading to Eq.6.

5.2.1.2

LIQUEFACTION AND SHEAR WAVE VELOCITY CHARACTERISTICS OF SILTY/GRAVELY SOILS - IMPLICATIONS FOR BRIDGE FOUNDATIONS

Sabanayagam Thevanayagam[1]

Abstract

Cyclic shear strength, post-liquefaction strength, and shear wave velocity v_s and damping characteristics are important parameters required for both static and dynamic response analyses of earth structures. Traditional indirect methods for estimation of these parameters based on void ratio, relative density, and mean effective stress have been successful for rather narrowly graded soils, but not for the most commonly found silty and gravelly soils. A simple array of two-sized particle system with large size disparity is presented to highlight the relative roles of intercoarser and interfiner grain contacts on mechanical response of such granular mixes. New parameters, namely intergranular void ratio e_c, interfine void ratio e_f, equivalent intergranular void ratio $(e_c)_{eq}$, and equivalent interfine void ratio $(e_f)_{eq}$ are introduced as indices of active intergrain contacts. They are related to v_s, cyclic strength, and post-liquefaction strength for silty and gravely soils.

Introduction

Dynamic stress-strain behavior, shear wave velocity (v_s) and damping characteristics of soils are important parameters required for dynamic response analysis, design, and performance evaluation of earth structures and both shallow and deep foundations associated with transportation facilities and bridges. Shear wave velocity characteristics influence attenuation characteristics and the level of ground accelerations anticipated as well as the shear stresses induced in the ground due to an input earthquake motion at the bedrock. When combined with monotonic and cyclic undrained stress-strain characteristics it foretells the expected performance of the ground in terms of its potential for liquefaction, ground settlement, displacement, sliding, etc in sandy soils. While often engineers resort to sophistication in analysis, the fact that the proper choice of the input soil parameters dictates the design/performance outcome much more than the sophistication in the analysis is not well ingrained. A few examples of the difficulties in estimating these parameters are presented followed by practical geotechnical insights to overcome these difficulties. It can help judicious design choices leading to successful foundation performances during earthquakes.

Soil Parameters: Several indirect methods have been developed, based on theoretical and laboratory studies on (clean) sands and/or field observations, to determine v_s (Duffy and Mindlin 1957, Hardin and Richart 1963, Hardin and Drenevich 1972, Seed et al. 1986, Goddard 1990, Lo Presti and Jamiolkowski 1999), liquefaction potential (Seed et al. 1983, Robertson et al. 1997, Andrews and Stokoe 1997), post-liquefaction strength (Seed 1987,

[1] Associate Professor, Dept. of Civil, Struct. and Env. Eng., SUNY at Buffalo, Buffalo, NY 14260, USA; Email: theva@eng.buffalo.edu; *15th US-Japan Bridge Workshop, PWRI, Tsukuba City, Japan C:\mceer\usjap-nov99-1.doc*

Seed and Harder 1990), etc. which are required for such analyses. There are variations as well (Stark and Mesri 1992, Ishihara 1993, Baziar and Dobry 1995). These methods relate the above material characteristics to void ratio, relative density or some insitu parameters such as SPT blow counts, CPT resistance which are considered to be related to relative density. For example, widely used relationship for v_s (m/s) is of the form:

$$v_s = v_{so}\left(\frac{\sigma'}{p_a}\right)^{\alpha} \quad where \quad v_{so} = Ap_a^{\alpha}(e_m - e) \quad \text{or} \quad v_{so} = Be^{-x} \tag{1}$$

where A=9.1 for rounded grains and 6.2 for angular grains, α=0.25, e_m=2.17 for rounded grains and 2.97 for angular grains, σ'=mean normal stress (N/m$^{2)}$; v_{so}= normalized shear wave velocity [v_s at $\sigma'=p_a$=atmospheric pressure=100,000 N/m^2]; x=1.3 for sands, all approximately. The underlying tenet has been that global void ratio e (or relative density) is an index of active contacts among the soil grains, and hence refers to the resistance they can offer.

While such relationships and methods have proven successful for rather clean sands their wide spread applicability to natural soils, which often contain silty and gravely sandy soils, have proven detrimental. Observations from recent earthquake case histories indicate that, despite rather broadly graded nature of grain size distribution and relatively high density (low void ratio), such soils are often fragile, do liquefy, and experience vertical settlement and lateral spreads (Seed et al. 1983, Seed and Harder 1990, JGS 1996) defying conventional wisdom. Experience gained from past studies on clean sands does not always directly translate to such broadly graded soils. Recognition of this has lead to several laboratory and field studies to evaluate the effects of increasing silt or gravel content on: (a) cyclic strength and liquefaction potential, (b) post-liquefaction strength, (c) shear wave velocity, etc.

Liquefaction Potential: Results from laboratory studies on clean sands mixed with non-plastic silts show that, at the same (global) void ratio, monotonic undrained (steady state) strength and cyclic strength of silty sand decreases with an increase in silt content (Chang 1990, Georgiannou et al. 1990, Vaid 1994, Koester 1994, Pitman et al. 1994, Singh 1994, Zlatovic and Ishihara 1995, 1997). An example is shown in Fig.1a for a soil prepared by mixing a sand with a silt (PI=4) at nearly constant global void ratio (e=0.558) and confining stress (104 kPa) but at different silt contents (0 to 60% by weight, M-0 to M-60). Fig.1b shows the number of cycles to reach initial liquefaction versus silt content for the same sand-silt mix, along with the data for two other sands mixed with the same silt. As observed in Figs.1a-b, beyond a certain transition range of silt content the trend in decrease of strength reverses and the strength increases with further increase in silt content. The transition silt content range is about 20 to 30%.

Undrained (steady state) Strength: Fig.2 shows the mean stress at steady state for another sand/silt mix at different silt contents (00,07,15,25,40,60, and 100%) obtained from undrained monotonic triaxial tests (Thevanayagam et al. 1999). The specimens were initially isotropically consolidated to 100 kPa confining stress. The steady state line for each mix falls below that of the (clean) sand (os00) progressively until reaching fines content range of 25 to 40%. A transition occurs in this range and the trend reverses thereafter.

Shear Wave Velocity: Experimental data for v_s for silty sands and gravely soils (e.g.

Kokusho et al. 1995, Brignoli et al. 1997, Rollins et al. 1998) indicate that shear wave velocity for gravely soils [and silty soils] are often significantly smaller than the respective values for 'pure' sand, silt, or gravel at the same e. An example is shown in Figs.3a-b. It shows the v_{so} data for Tone river sand (TRS) and three other gravely soils prepared by mixing TRS with 25, 50 and 75% gravel by weight.

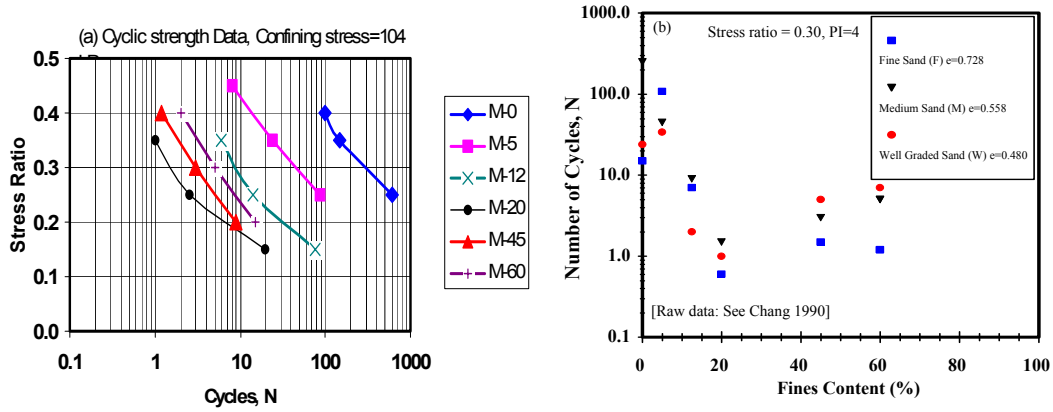

Fig.1 Influence of silt content on cyclic strength (a) Medium sand/silt, (b) Three sands/silt

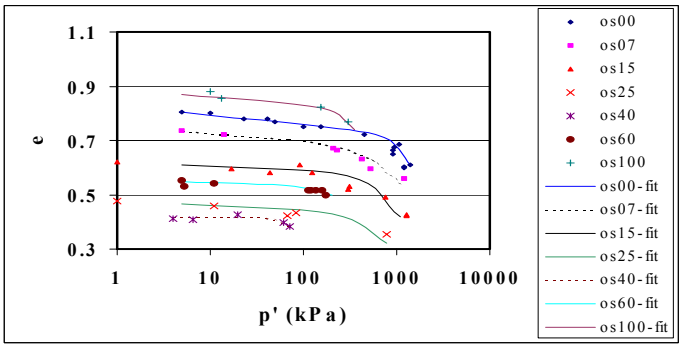

Fig.2 Influence of silt content on steady state

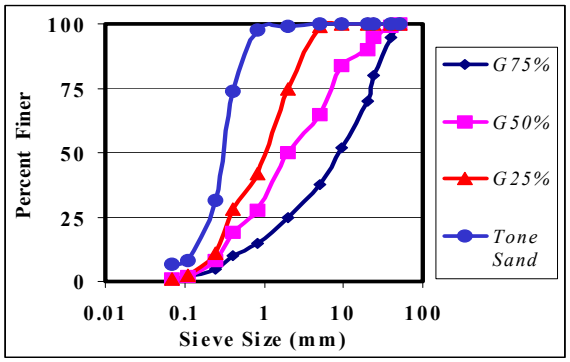

Fig.3a Grain size data – Sand-gravel mixes

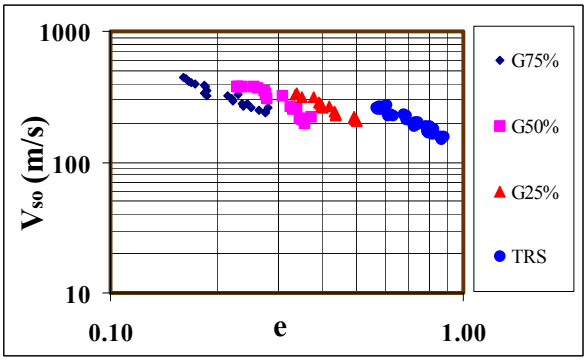

Fig.3b Influence of gravel content on V_{so}

The non-uniqueness of void ratio to correlate with the cyclic strength is clear. Low void ratio does not necessarily mean better mechanical properties. The physical meaning of the transition silt content is not clear. The conclusions in the literature on whether the presence of silt is beneficial or not is contentious. Similar concerns prevail regarding gravely soils (Evans and Zhou 1995). For the same reasons, questions also prevail among practicing

engineers on broad applicability of the field SPT or CPT based correlations to all (new) sites.

Possible Reasons: Recently, it has been brought to the attention that physical nature of silty sands and gravely sands are entirely different from clean sand, silt or gravel (Thevanayagam 1998a-b, 1999a-d, Thevanayagam and Mohan 1998). As the void ratio and proportion of the coarser and finer grains content of these soils change the nature of their microstructure also changes. The relative participation of the particles of very different sizes in the *internal interparticle contact force chain* also changes. Due to particle size disparity and availability of pores larger than some particles, at low finer grains content (FC) some of the finer particles may remain inactive or move between pores without significantly affecting or contributing to the force chain. Yet they contribute to the global void ratio. Alternately when there is a sufficient amount of finer grains the coarser grains become dispersed contributing much less to the force chain than to the global void ratio. Global void ratio e ceases to be an index to represent the nature of *contact density* of active particles. The traditional use of e to compare and correlate with the behavior of soils containing different amounts of finer grains content ceases to be valid. The same holds for relative density. In general the stress-strain behavior, liquefaction potential, and v_{so} of granular mixes are affected by a critical combination of *intergranular and interfine contacts*. New *indices of active contacts* are needed to represent the nature of intergrain contacts in order to characterize the behavior of such soils.

Using a two-sized particle mix as a model, this paper highlights the nature of the microstructure of granular mixes. Based on this such granular mixes are classified into certain groups (Fig.4) depending on the relative frictional contributions at the intergranular and interfine grain contact level. Intergranular (e_c), interfine (e_f), equivalent intergranular $(e_c)_{eq}$, and equivalent interfine $(e_f)_{eq}$ void ratios (Fig.5) are introduced as primary indices of contact density for the various groups. Global void ratio is introduced as a secondary index. These new indices are related to v_s and undrained strength of young silty/gravely soils at different silt or gravel contents. Details are presented elsewhere (Thevanayagam 1999c-d, Thevanayagam et al. 1999). The underlying theme is that contact is the mechanism by which a granular medium responds to external excitations. The density of contacts may be expressed using the above indices.

Conceptual Microstructure

Consider a two-sized granular mix (Fig.4). The microstructure of this granular mix can be constituted by infinite different ways. Each one of them leads to a different internal force chain network among particles and hence each exhibits a different stress-strain response during shear. Among infinite variations, a few extreme limiting categories of microstructure and the relevant roles of coarser and finer grains are as follows.

Case-i: The first category (Fig.4a) is when the finer grains are fully confined within the void spaces between the coarser-grains with no contribution whatsoever in supporting the coarser grain skeleton. Finer grains are inactive (or secondary) in the transfer of inter particle forces. They may largely play the role of "filler" of intergranular voids. The mechanical behavior is affected primarily by the coarser grain contacts. During deformation the finer

grains may move from one pore space to another without significantly contributing to the mechanical response of the soil. This requires that the finer grain particle size (d) is much smaller than the pore size between the coarser grains and that the intergranular pore space is not completely filled with the finer grains. Typically this requires that the coarser grain size (D) is at least 6.5 times larger than the finer grain size, and that the finer grain content (FC) is less than a certain threshold value (FC_{th}). This category is called *case-i*. Even at low FC, if the size disparity R_d (=D/d) is not very large, the finer grains cannot freely move through the inter-coarser granular voids; They also tend to participate in the force chain and actively contribute to the stress-strain response.

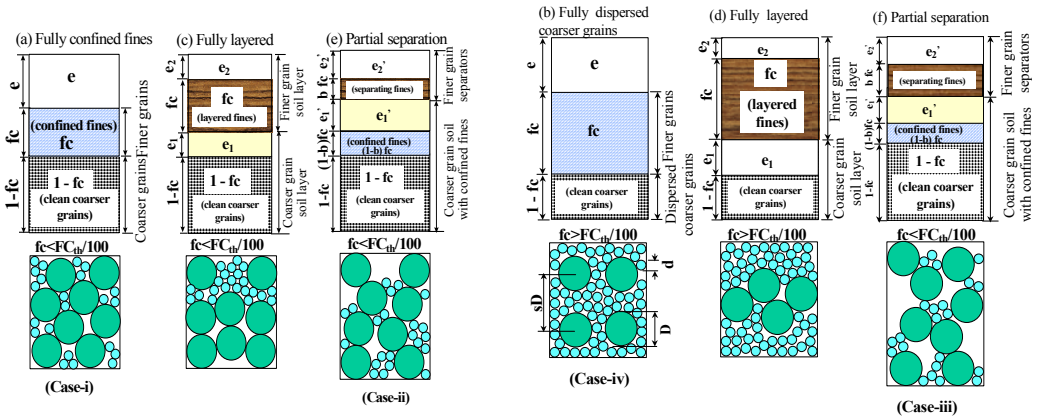

Fig.4 Microstructure and intergranular matrix phase diagram

Cases-ii and iii: Consider changing the microstructure shown in Fig.4a in two ways: (1) alter the position of some of the finer grains, or (2) add more finer grains. The consequences are significant. If one alters the position of some of the finer grains, while maintaining the finer grain content the same, the microstructure corresponding to the second and third categories shown in Figs.4e and f are obtained with a concurrent increase in global void ratio. Essentially, the microstructure in Figs.4e-f is made up of partial layering and partial separation of coarser grains by the finer grains along with confined finer grains within the voids between the coarser grains. Some of the finer grains become active participants in the internal force chain. These finer grains are termed the *'separating fines'* in Figs.4e and f. In Fig.4e, the finer grains may be supporting the coarser-grain skeleton that is otherwise unstable. They act as a load transfer vehicle between "some" of the coarse-grain particles in the soil-matrix while the remainder of the fines play the role of "filler" of voids. They may dominate the initial stress-strain behavior depending on the type of finer grains (plastic or non-plastic). In Fig.4f, the finer grains may play an active role of *"separator"* between a significant number of coarse-grain contacts and therefore begin to dominate the strength characteristics. Coarser grain skeleton is virtually unstable without the finer grains. These categories of microstructure are called case ii and iii, respectively. Case-ii is a transition between cases i and iii. Theoretically case-iii occurs at an intergranular void ratio exceeding the maximum void ratio ($e_{max,HC}$) achievable for the 'pure' host coarser grain soil.

Cases-iv-1 and iv-2: On the other hand if one increases the finer grains content sufficiently, one gets the fourth category (Fig.4b). It occurs naturally when sufficient finer grains are present making active contacts among themselves. The coarser grains begin to disperse in the finer grain matrix. Transition from Fig.4a to Fig.4b occurs when the finer

grains content (FC) exceeds beyond the threshold fines content (FC_{th}). When $FC>FC_{th}$ the finer grains begin to play a rather important role while the role of coarser grains begin to diminish. The fines may carry the contact and shear forces while the coarser grains may act as *reinforcing elements* embedded within the finer grain matrix. The effect of coarser grains cannot be completely neglected until they are separated sufficiently apart. This imposes a limiting fines content FC_l. There exists a transition zone between FC_{th} and FC_l before the behavior of the soil mix is entirely governed by the finer grains. This is called case-iv-2 whereas the case corresponding to $FC>FC_l$ is called case-iv-1. The size disparity constraint discussed before for cases i to iii needs not be satisfied.

The fifth category (Figs.4c-d) is when the coarser and finer grains constitute a fully layered system where the coarser grain layers have no fines contained in them and vice versa. This is called case-v. It is also possible to create a composite system that contains some of the cases i through v. The figures 4a, c, e and f are more relevant at low finer grains content. Figs.4b and d are relevant at high finer grains content.

Intergranular Contact Indices

Case-i: Up to $FC=FC_{th}$ the finer grains can, but not necessarily, remain within the intergranular voids. Provided that the size disparity is large and the coarser granular skeleton is dense whether or not some of the finer grains fall between the coarser grain contacts or remain fully confined within the intergranular voids does not significantly affect the shear strength of the soil. Primarily the intergranular contacts between the coarser grains affect the mechanical behavior with secondary effects by the finer grains. Hence, neglecting the effects of fines, the *inter-coarser grain void ratio* e_c (Fig.5c) may be used as an index of active contacts. The magnitude of e_f (Fig.5b) may be used as an index to assess the secondary effects by the finer grains.

$$e_c = \frac{e + fc}{1 - fc}; \qquad e_f = \frac{e}{fc}; \qquad fc = FC/100 \tag{2}$$

Cases-ii and iii: For these cases, still the inter-coarser grain contact plays a significant role. However, the influence of finer grains supporting the coarser grains must also be accounted for in devising an index of active contacts. The relevant contact index void ratio would be $(e_c)_{eq}$ (Figs.4e-f); 'b' refers to the finer grains contributing to active contacts. Although it may be possible to use e_c as an index of active contacts for these cases, it is expected the mechanical behavior of such mixes would be different and generally stronger than that of the host coarser grain soil at the same e_c.

$$(e_c)_{eq} = \frac{e + (1-b)fc}{1 - (1-b)fc}; \qquad 0 \le b \le 1 \tag{3}$$

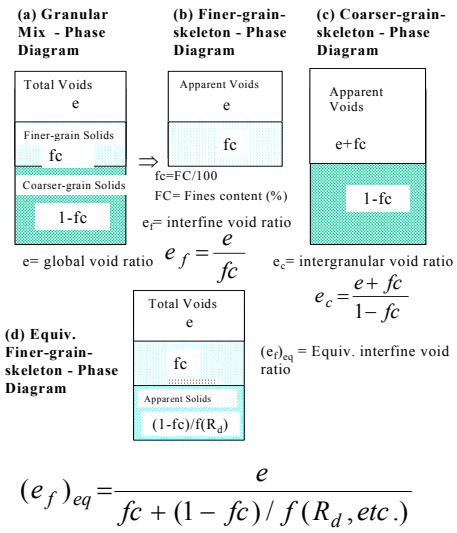

Fig.5 Intergranular contact indices

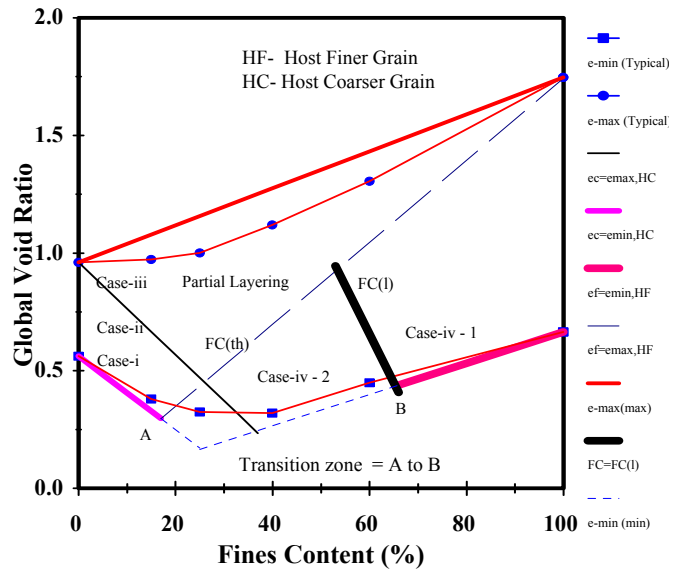

Fig.6 Intergranular matrix diagram – Mix classification

Case-iv: When FC>FC_l, for case-iv-1, neglecting the effects of dispersed coarser grains, the *interfine void ratio* e_f may be used as an index of active contacts. At FC_{th}<FC<FC_l, neither e, e_c, nor e_f can sufficiently represent the active contacts, alone, although all of them together can be used to deduce the mechanical response. Devising a primary index of active contacts in this range is useful, however.

For a granular mix in this range the global void ratio e overestimates the actual density of active contacts in the granular mix. This is so because the dispersed coarser grains in the mix do not contribute as many active contacts as if the soil was prepared at the same void ratio by substituting each coarser grain by an equal (solid) volume of finer grains. The reason is that solid volume of a dispersed coarser grain, which directly influences the global void ratio, grows in proportion to the power of three of size. Whereas its surface area, which influences the nature of contacts with the surrounding finer grains, grows in proportion to the power of only two. For equal solid volume, the substituted finer grains have a larger surface for contact than a dispersed coarser grain of equal (solid) volume embedded in the finer grain medium. The density of contacts in the mix is smaller than that in the finer grain soil at the same e. Hence e overestimates the active contacts in the mix.

The use of e_c as an index of active contacts is not valid since it ignores entirely the existence of interfiner grain contacts. It grossly underestimates the active contacts. Similarly, the interfine void ratio e_f also underestimates the active contacts, since it completely ignores the presence of the dispersed coarser grains. The latter do make contact with the surrounding finer grains and participate in the force chain. The effects of such contacts may not be negligible unless the spacing between the dispersed coarser grains is very large. The reinforcement effect by the coarser grains must also be introduced to obtain an *equivalent* interfine void ratio index $(e_f)_{eq}$ as the index of active contacts. The equation for e_f must be modified accordingly. Combining the above arguments, after simplifications, theoretically $(e_f)_{eq}$ (Fig.5d) is (Thevanayagam 1999c).

$$\left(e_f\right)_{eq}=\frac{e}{[fc+(1-fc)/R_d^m]};\qquad R_d=\frac{D}{d};\qquad 0<m<1;\qquad e_c>e_{\max,HC} \tag{4}$$

Conceptually, Fig.6 shows the regions belonging to the four cases i through iv confined by various transition boundaries. The transition lines corresponding to the theoretical threshold and limiting finer grains contents (Thevanayagam 1999c) are given by:

$$FC_{th}\leq\frac{100e_c}{1+e_c+e_{\max,HF}}\%=\frac{100e}{e_{\max,HF}}\%;\ FC_l\geq 100\left[1-\frac{\pi(1+e)}{6s^3}\right]\%=100\left[\frac{\frac{6s^3}{\pi}-1}{\frac{6s^3}{\pi}+e_f}\right]\%\geq FC_{th} \tag{5}$$

where $s=1+a(d/D)=1+a/R_d$ where a=10 (approximately). The various boundaries refer to the maximum and minimum void ratio profiles: $e=e_{max,HC}+(e_{max,HF}-e_{max,HC})fc$; $e_c=e_{max,HC}$; $e_f=e_{max,HF}$; $e_c=e_{min,HC}$; and $e_f=e_{min,HF}$ where $e_{max,HC}$ and $e_{max,HF}$=maximum void ratio of the host coarser and finer grains, respectively, beyond which they have no appreciable strength, $e_{min,HC}$ and $e_{min,HF}$ = minimum void ratio of the host coarser and finer grains, respectively.

The aforementioned contact indices and the location of a soil mix in Fig.6 can be used to predict the trends for stress-strain characteristics and v_s of silty or gravely soils *relative* to that of the host coarser grain soil or the host finer grain soil as reference.

Mechanical Behavior

Fig.7a shows a schematic diagram for *hypothetical* specimens satisfying the following specific constraints. (1) An increase in e at the same FC [specimens 1,2,3], (2) An increase in FC at the same e [4,2,5,6,7,13], (3) An increase in FC at the same e_c [8,1,9 or 3,10 or 14,2,15; $FC<FC_{th}$], or (4) An increase in coarser grain content at the same e_f [11,7,12; $FC>FC_{th}$]. For reasons discussed below the mechanical response parameters (v_s, and shear strength) for the four categories above is expected to be of the form shown in Fig.7b, although it refers only to cyclic strength.

Relative Trends -- Cyclic Strength: The anticipated trends in number of cycles (N) required to cause initial liquefaction at the same cyclic stress ratio are *schematically* shown in Fig.7b [N versus FC]. In (1) both intergranular and interfine void ratios increase with concurrent reduction in inter-coarser grain contacts. Therefore the soil becomes weaker. In (2) while e_c increases e_f decreases. Viz. the inter-coarser granular contacts decrease while the interfine contacts increase. Hence initially the soil is expected to weaken [4,2,5] followed by a transition in the vicinity of $e_f=e_{max,HF}$ ($FC=FC_{th}$). The soil becomes stronger beyond that [6,7,13]. In (3), the increase in a cushioning effect by the finer grains contained in the intergranular void spaces is manifested leading to a slight increase in strength [3,10, case-iii]. In (4) when the soil is at $FC_{th}<FC<FC_l$ [11,7,12] the reinforcement effect of the coarser grain 'inclusions' affect the stress- strain behavior. The specimen 11 is expected to be stronger than 7. Once FC exceeds FC_l the reinforcement effect is expected to be small. Primarily the interfine contacts and e_f are expected to affect the soil behavior [7,12].

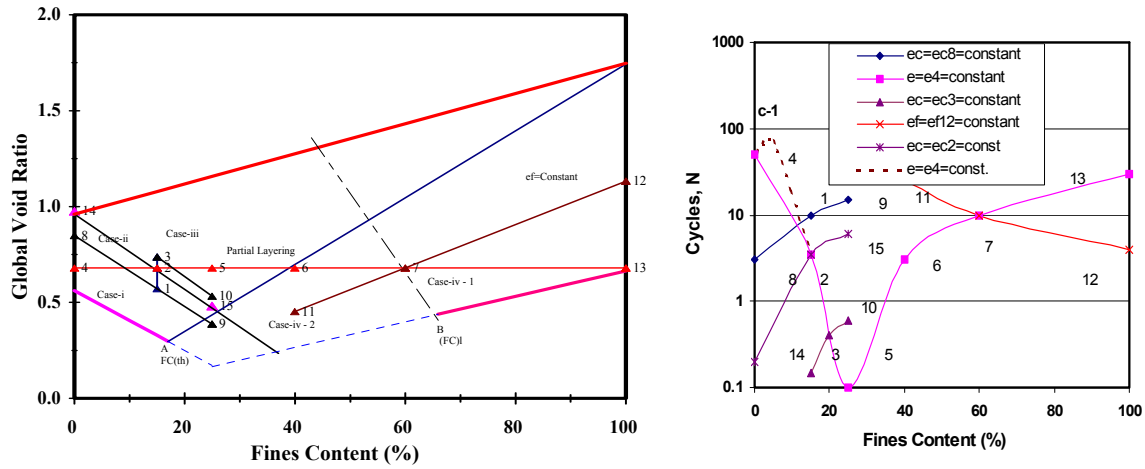

Fig.7 Relative trend in cyclic strength – Schematic

Shear wave velocity: Based on the above considerations, with due consideration for the dependence of v_s on the nature of contacts (Duffy and Mindlin 1957, Goddard 1990, Thevanayagam 1999d), v_s of granular mixes may be given by the following, reflecting its dependence on contact index e_{eq}:

$$v_s = v_{so}\left(\frac{\sigma'}{p_a}\right)^{\alpha}; \qquad v_{so} = Ap_a^{\alpha}\,(e_m - e_{eq}) \qquad \text{or} \quad v_{so} = Be_{eq}^{-x} \tag{6}$$

where $e_{eq}=(e_c)_{eq}$ for FC< FC_{th}; $e_{eq}=(e_f)_{eq}$ for FC>FC_{th}. Eq.6 may also be conveniently presented in terms of e by substituting the proposed expressions for e_{eq}:

$$v_{so} = A_{eq}\,p_a^{\alpha}\,((e_m)_{eq} - e) \tag{7a}$$

$$\text{or } v_{so} = B_{eq}e^{-x} \text{ for FC>FC}_{th} \text{ and } v_{so} = B(1-(1-b)fc)^{x}(e+(1-b)fc)^{-x} \text{ for FC< FC}_{th} \tag{7b}$$

where A_{eq}=A/(1-(1-b)fc) and $(e_m)_{eq}$ =e_m(1-(1-b)fc)-(1-b)fc for FC<FC_{th}; A_{eq}=A/[fc+(1-fc)/$(R_d)^m$] and $(e_m)_{eq}$ =e_m [fc+(1-fc)/$(R_d)^m$] for FC>FC_{th}; B_{eq}=B[fc+(1-fc)/$(R_d)^m$] for for FC>FC_{th}. It is readily apparent that Eq.7 is similar to Eq.1 but with different coefficients depending on FC. The differences are manifestations of differences in contacts in granular mixes containing different proportions of coarser and finer grains. Direct use of Eq.1, without due consideration for the dependence of the coefficients in Eq.1 on FC can be misleading. Details are presented elsewhere (Thevanayagam 1999d).

Observations - Reinterpretations

A limited set of experimental data is available in support of the above conceptual framework. The following sections present one example each for cyclic strength, undrained steady state strength, and shear wave velocity.

Cyclic Strength: The data shown in Fig.1b is recalled again in Figs.9-10. Figs.8a-c show the intergranular matrix diagram for the three host sands [(1) Fine (F), (2) Medium (M), and (3) Well graded (W)] mixed with a low plasticity silt (PI=4) reported in Figs.1a-b. The locations of the specimens are also shown. Each sand mix was tested at 0, 5, 12, 20, 45,

and 60% silt content (FC). The specimens were prepared by moist tamping method and tested at nearly constant e=0.728 for F, e=0.558 for M, and e=0.480 for W, respectively. No data were available for $e_{max,HF}$ and $e_{min,HF}$ for the silt. FC_{th} was estimated assuming typical values of $e_{max,HF}$ =1.5 and $e_{min,HF}$ =0.6 for the silt. R_d (defined as D_{50}/d_{50}) for the soils F, M, and W were estimated to be about 15, 40, and 40 based on a typical value for d_{50} of silts.

An examination of Fig.8 and calculated index void ratios (shown in Fig.9) would readily reveal the cases each specimen belongs to and the expected behavior of each granular mix relative to one another. As the fines content increases, at the same e, e_c increases and e_f decreases. Initially e_f remains high indicating the lack of significant interfine contacts. With increase in FC the soil mixes move gradually from Case-i to Case-ii to Case-iii and then cross over to Case-iv-2. So is the behavior of the soils (Fig.9). Initially the strength decreases due to reduced intergranular contacts with increase in e_c with little or secondary contribution from the silt. As the soil moves beyond the threshold transition zone (FC_{th} at e_f= $e_{max,HF}$) and enters the zone for Case-iv-2 the influence of e_f becomes important with some reinforcement effect by the coarser grains. The $(e_f)_{eq}$ becomes the primary contact index void ratio. The trend reverses and the strength begins to increase with further increase in fines content.

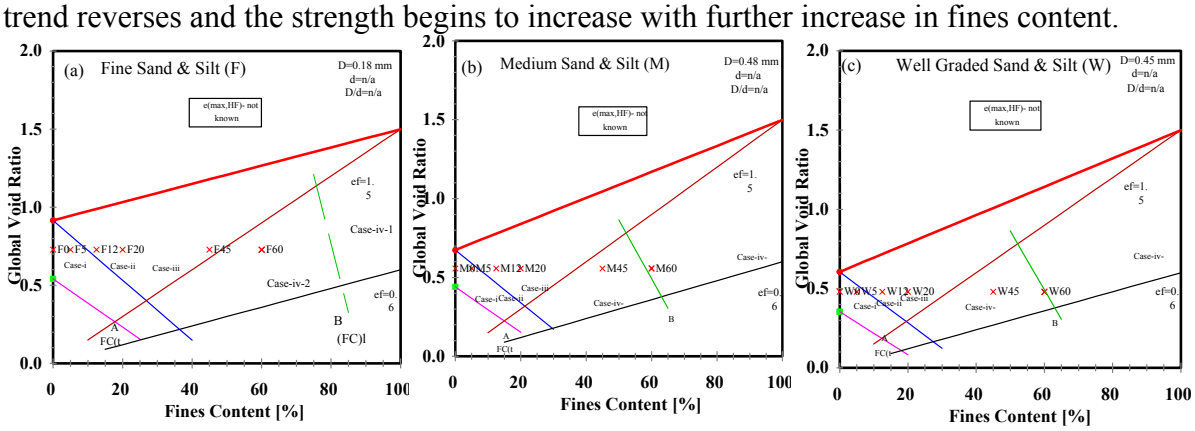

Fig.8 Intergranular matrix diagrams – Three Sand – Silt Mixes

Fig.10a shows the same data in a different format: Number of cycles to initial liquefaction versus e_c for Cases-i to iii [$FC<FC_{th}$]. For this case, a different cyclic strength profile is obtained for each mix depending on the parent sand type (F,M,W). Cyclic strength (N) is affected primarily by the parent sand type. e_c becomes the primary index of active contacts. The fines have a secondary role.

Fig.10b shows N versus e_f data for Case-iv ($FC>FC_{th}$). N data show significant dependency on e_f. The data for each fines content (45% and 60% separately) correlates well with e_f and fall in a (separate for 45% and 60%) narrow band regardless of the parent sand type. The separate narrow bands for the soils mixed with 45% fines and 60% fines are due to the differences in the degree of reinforcement effect. At the same e_f, the cyclic strength is higher for the soil with higher sands content. The reinforcement effect is higher at 45% fines content than at 60%. Fig.10c shows the same data, plotted against $(e_f)_{eq}$ [calculated assuming m=0.45). Interestingly the number of cycles required to cause liquefaction correlates with $(e_f)_{eq}$ for all three mixes. The reason for this is that all sands were mixed with the *same silt*. Hence, once FC exceeds the threshold value, all soil mixes are affected by the same silt

except for the minor differences due to the presence of different size coarser grains (F,M,W). Hence a single narrow band is obtained in Fig.10c.

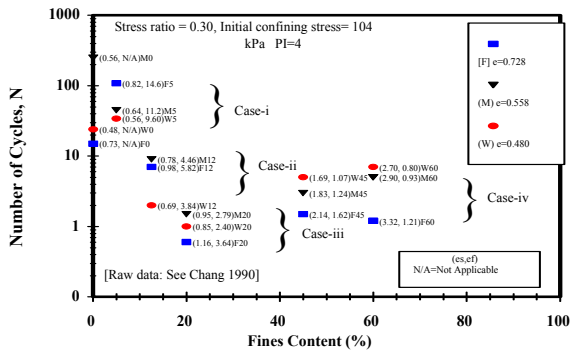

Fig.9 Effect of silt content on cyclic strength

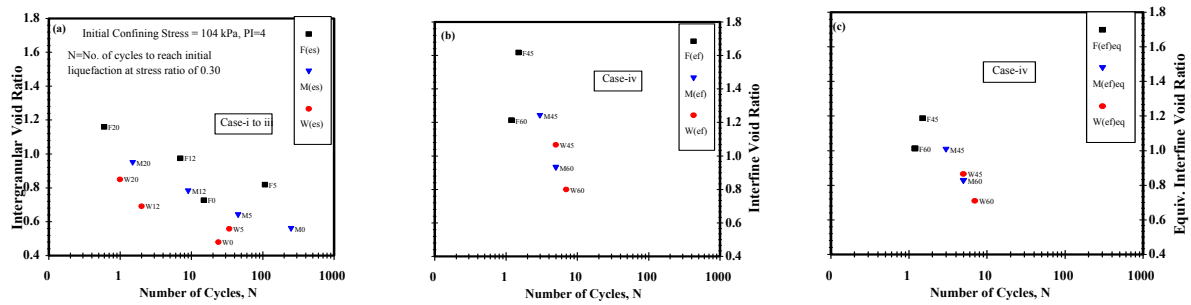

Fig.10 Influence of intergrain contacts on cyclic strength: (a) e_c, (b) e_f, and (c) $(e_f)_{eq}$

Undrained (steady state) Strength: Fig.11 shows the intergranular matrix diagram for the sand/silt mix reported before in Fig.2. Figs.12-13 show the same data plotted against $(e_c)_{eq}$ and $(e_f)_{eq}$, respectively, for up to silt content (FC) of 25% and beyond that. The values of 'b' and 'm' were 0.25 and 0.65, respectively. The data in each case fall in a narrow band surrounding the data for clean sand and silt, respectively. This is indicative of the primary role of inter coarser grain contacts at $FC<FC_{th}$ and interfiner grain contacts at $FC>FC_{th}$. The direct use of e to characterize steady state strength can be misleading (Fig.2). Further care is necessary due to possible dependence of undrained shear strength on confining stress (Thevanayagam 1998a).

Shear Wave Velocity: Fig.14 shows the intergranular matrix diagram for the sand/gravel mixes shown before in Figs.3a-b. In this case sand is the finer grain and gravel is the coarser grain. The gradation data (Fig.3a) was decomposed into gravel and sand and the respective D_{50} and d_{50} were determined (Table 1). FC_{th} was estimated for each specimen assuming $e_{max,HF}$=0.966 (TRS). FC exceeded FC_{th} for most specimens. They belong to case-iv-2. The relevant contact index void ratio $(e_f)_{eq}$ was calculated using assuming m=0.45. Fig.15 shows the same data shown in Fig.3b, but plotted against $(e_f)_{eq}$. v_{so} correlates well with $(e_f)_{eq}$. It also shows clearly that addition of gravel to sand did not contribute to the v_{so} as much as it did to e. Direct use of e to estimate v_{so} can be very unconservative. Indirect methods of estimating v_{so} may use the relationships of the type Eqs.6-7. Further results are reported in Thevanayagam (1999d).

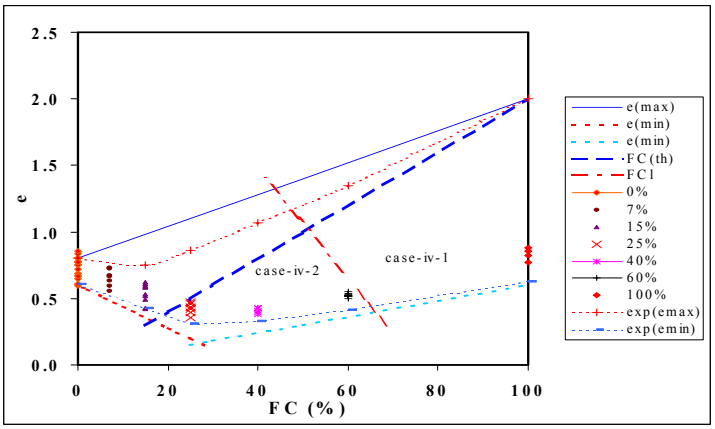

Fig.11: Intergranular matrix diagram

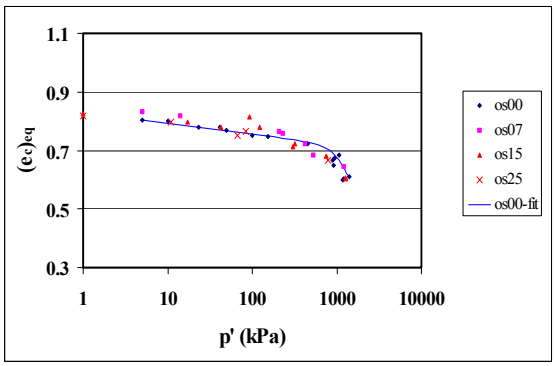

Fig.12: $(e_c)_{eq}$ vs p' –sand and silty sands

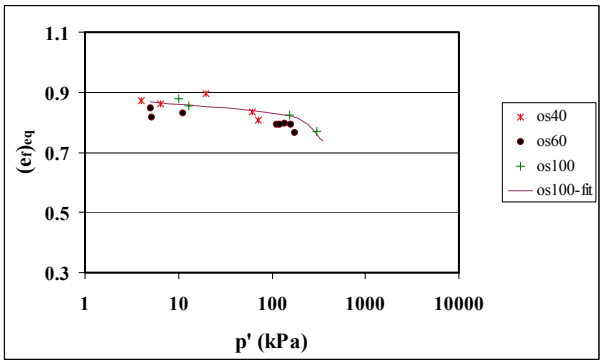

Fig.13: $(e_f)_{eq}$ vs p' – Sandy silts and silt

Table 1: Sand-gravel mix data

Soil	*D_{50} (mm)*	*d_{50} (mm)*	*R_d*	Range e	FC (%)	FC_{th} (%)	*Remarks*
Tone River Sand	---	0.34	---	0.55-0.90	100		Case-iv
G25 Gravel	3	0.7	4.3	0.33-0.50	75	35-52	Case-iv
G50 Gravel	7	0.7	10	0.22-0.37	50	24-38	Case-iv
G75 Gravel	15	0.6	25	0.16-0.28	25	17-29	Case-iv

Note: Data obtained from Fig.3a.

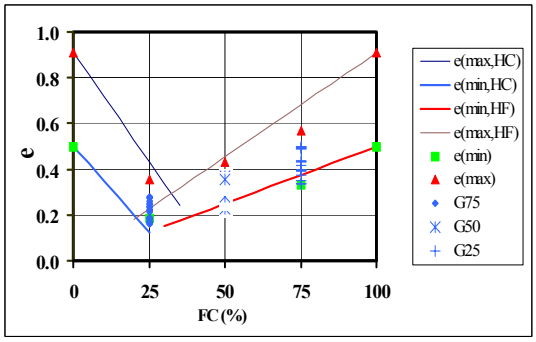

Fig.14 Intergranular matrix diagram-Sand-gravel Mix

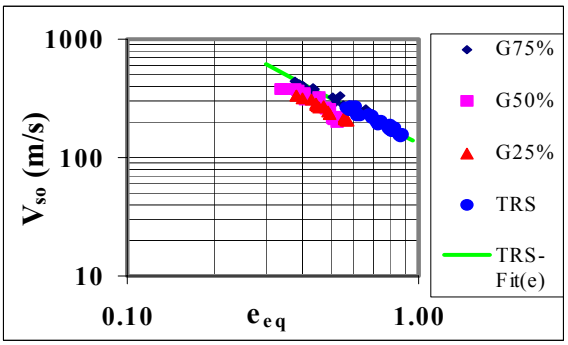

Fig.15: v_{so} versus $(e)_{eq}$ relations

<u>Implications & Conclusions</u>

The above analyses illustrate the differences in the relative contribution of coarser and finer grains in a soil to its mechanical response parameters. Indirect methods of estimating material parameters, even for preliminary design purposes, based on density or void ratio of a soil can yield often unconservative values for v_s, and shear strength. The reason for this is that void ratio or density of a soil is indeed an index of volume or mass density. Mechanical soil parameters are primarily affected by contact density (per grain).

A simple framework is presented to modify the relevant indirect methods to obtain more realistic input soil parameters. With this framework, one may deduce the behavior of granular mix soils at various finer grain contents and void ratios *relative* to the behavior of the host coarser grain soil or the finer grain soil as reference.

In general, (a) for soils containing low finer grains content less than a threshold value (FC_{th}), when compared at the same $(e_c)_{eq}$, the mechanical response is similar to that of the host coarser grain soil at the same void ratio, and (b) for soils containing large finer grains content, when compared at the same $(e_f)_{eq}$, the response is similar to that of the host finer grain soil at the same void ratio. Further work is needed to examine the applicability of these contact indices for different soils.

The above results indicate that the choice of soil parameters for dynamic analysis of earth structures, liquefaction potential evaluation, determination of post-liquefaction ground damage, foundation performance, etc. should consider a method that reflects the nature of active grain contacts. Insitu parameters such as SPT blow counts, CPT resistance, and field shear wave velocity do reflect this to some extent. But how well do they reflect this, on the face of the several uncertainties involved in the development of the empirical correlations of such parameters with soil parameters based on observed performances, remains the subject of an engineer's judgement. It is hoped that the geotechnical insights presented herein help engineers in judicious choice of soil parameters for foundation design involving young silty/gravely soils against seismic events.

Acknowledgments

Financial support by the USGS/NSF/MCEER for the various aspects of this ongoing research work is gratefully appreciated. Thanks are also due to J. Liang and T. Shenthan, SUNY at Buffalo, for their assistance in the laboratory triaxial tests on silty soils.

References

Andrus, R., and Stokoe, K. H. II (1997) "Liquefaction resistance based on shear wave velocity", NCEER Report, 97-0022, State University of New York at Buffalo, NY, 89-128.

Baziar, M.H. and Dobry, R. (1995), "Residual strength and large-deformation potential of loose silty sands", J. Geotech. Eng. Div., ASCE, 121(12), 896-906.

Brignoli, E., Fretti, C., Jamiolkowski, M. and Stokoe, K.H. II (1997) "Stiffness of gravelly soils to small strains", Proc. 14th Intl. Conf. SMFE, Germany, vol.1, 37-40.

Chang, N.Y. (1990) "Influence of fines content and plasticity on earthquake-induced soil liquefaction", Contract Rep., US Army WES, Vicksburg, MS Contract No. DACW3988-C-0078

Duffy, J. and Mindlin, R.D. (1957) "Stress-strain relations of a granular medium", Transactions, ASME, 585-593.

Evans, M. D. and Zhou, S. (1995) "Liquefaction behavior of sand-gravel composites", ASCE, J. Geotech. Eng., 121(3), 287-298.

Georgiannou, V.N, Hight, D.W and Burland, J.B (1990), "The undrained behaviour of clayey sands in triaxial compression and extension", Geotechnique, 40(3), 431-49.

Goddard, J. D. (1990) "Nonlinear elaasticity and pressure-dependent wave speeds in granular media", Proc. Royal Soc. London, A, 430, 105-131.

Hardin, B.O., and Richart, F. E. Jr. (1963). "Elastic wave velocities in granular soils" J. Soil Mech. and Found. Div., ASCE, 89(SM1), 33-65.

Hardin, B. O., and Drnevich, V. P. (1972). "Shear modulus and damping in soils: Measurements and parameter effects", *J. Soil Mech. Found. Div*., ASCE, 98(6), 603-624.

Ishihara, K. (1997) "Terzaghi oration: Geotechnical aspects of 1995 Kobe earthquake", Proc. 14th Itnl. Conf. SMFE, vol.4, 2047-2073.

Ishihara, K. (1993), "Liquefaction and flow failure during earthquakes", Geotechnique, 43(3), 351-41.

JGS (1996) "Soils and Foundations - Special issue on geotechnical aspects of the January 17 1995 Hyogoken-Nambu Earthquake", Japanese Soc. Geotech. Eng.

Koester, J.P. (1994), "The influence of fines type and content on cyclic strength", ASCE Geotech. STP 44, 17-32.

Kokusho, T., Yoshida, Y. and Tanaka, Y. (1995) "Shear wave velocity in gravelly soils with different particle gradings", ASCE Geotech. STP 56, 92-106.

Kuerbis, R., Nagussey, D. and Vaid, Y.P. (1989), "Effect of gradation and fines content on the undrained response of sand", Proc. Conf. on Hyd. Fill Struc., ASCE Geotech. STP 21, 330-45.

Lo Presti, C.F. and Jamiolkowski, M. (1998) "SPT N-value and S-wave velocity for gravelly soils with different grain size distributions" Discussion, Soils and Foundation, 39(2), 138-140.

Mitchell, J. K. (1993) *Fundamentals of soil behavior*, 2nd ed. Wiley Interscience Publ.

Pitman, T.D., Robertson, P.K. and Sego, D.C. (1994), "Influence of fines on the collapse of loose sands", Can. Geotech. J., 31, 728-39

Robertson, P. K. and Wride, C. E. (1997) "Evaluation of cyclic liquefaction potential based on the CPT", Seis. Behavior of Ground & Geotech Struct., ed. P.S. Pinto, Balkema Publs., 269-278.

Rollins, K., Evans, M., Diehl, N. B., and Daily W.D. (1998) "Shear modulus and damping

relationships for gravels" J. Geotech. and Geoenv. Eng., 124(5), 396-405.
Seed, H.B., Wong, R.T., Idriss, I.M., and Tokimatsu, K. (1986). "Moduli and damping factors for dynamic analysis of cohesionless soils", J. Geot. Eng. Div., ASCE, 112(11), 1-17.
Seed, H. B., Idriss, I.M. and Arango, I. (1983) "Evaluation of liquefaction potential using field performance data", J. Geotech. Eng., ASCE, 109(3), 458-482
Seed, R. B. and Harder, L. F. Jr. (1990), "SPT-based analysis of cyclic pore pressure generation and undrained residual strength", Proc. Seed Memorial Symp., Berkeley, 2, 351-76
Seed, H.B. (1987), "Design problems in soil liquefaction", J. Geotech. Eng. Div., ASCE, 113(8), 827-45.
Singh, S. (1994), "Liquefaction characteristics of silts", ASCE Geotech. STP 44, 105-16.
Stark, T. D. and Mesri, G. (1992), "Undrained shear strength of liquefied sands for stability analysis", J. of Geotech. Eng., ASCE, 118(11), 1727-47.
Thevanayagam, S. (1998a) "Effect of fines and confining stress on steady state strength of silty sands," J. Geotech. & Geoenv. Engrg. Div., ASCE, 124(6), 479-491.
Thevanayagam, S. (1998b) "Role of intergrain contacts, friction, and interactions on undrained response of granular mixes", Proc. Intl. Workshop on *The Physics and Mechanics of Liquefaction*, Baltimore, ed. Lade, P. V., Balkema Publishiers.
Thevanayagam, S. (1999a) "Intergrain contact and shear modulus of non-plastic granular mixes", CD-ROM Proc. 13th ASCE Conf. on Eng. Mech., Eds. Jones, N. and Ghanem, R., Johns Hopkins Univ., Maryland, June 13-16, 1999.
Thevanayagam, S. (1999b) "Effect of fines and confining stress on steady state strength of silty sands," *Closure*, J. Geotech. & Geoenv. Engrg. Div., ASCE, 125(11), *in press*.
Thevanayagam, S. (1999c) "Relative roles of coarser and finer grains on undrained behavior of granular mixes", *in review*, J. Geotech. & Geoenv. Eng. Div., ASCE.
Thevanayagam, S. (1999d) "Contact indices - shear wave velocity - shear modulus for granular mixes" to be submitted, J. Geotech. & Geoenv. Engrg. Div., ASCE.
Thevanayagam, S. and Mohan, S. (1998) "Intergranular void ratio - steady state strength relations for silty sands" ASCE Geotech. STP 75, ed. P. Dakoulas et al., IIIrd Conf. on Geot. Earthq. Eng.
Thevanayagam, S. and Mohan, S. (1999) "Intergranular state variables and stress-strain behaviour of silty sands", Geotechnique, *in press*.
Thevanayagam, S., Liang, J., Mohan, S., and Shenthan, T. (1999) "Undrained fragility of clean sands, silty sands and sandy silts," *in review*, J. Geotech. & Geoenv. Engrg. Div., ASCE
Vaid, Y.P. (1994), "Liquefaction of silty soils", Proc. ASCE Conv., Geotech. Spec. Publ. 44, 1-16.
Zlatovic, S. and Ishihara, K. (1995). "On the influence of nonplastic fines on residual strength," Proc. IS-TOKYO'95, First Intl. Conf. Earthq. Geotech. Eng., Tokyo, eds. K. Ishihara, publs. A. A. Balkema, 239-244.
Zlatovic, S. and Ishihara, K. (1997). "Normalized behavior of very loose non-plastic soils: effects of fabric" Soils and Foundations, 37(4), 47-56.

5.2.1.3

Effect of Non-Plastic Fines on Undrained Cyclic Strength of Silty Sands

S. Thevanayagam[1], M. ASCE, M. Fiorillo[2] and J. Liang[2]

Abstract

Whether the presence of silt adversely or beneficially affects liquefaction and the collapse potential of silty soils is a contentious issue. The purpose of this work is to investigate this question. Stress controlled undrained cyclic triaxial tests were conducted on specimen prepared by mixing the silt and sand in different proportions. The cyclic stress ratio and confining pressure were maintained constant. A framework for analysis of the undrained stress-strain behavior, shear strength and collapse potential of granular mixes ranging from clean sands to pure silts (or gravel) in terms of intergranular and interfine friction is presented. New intergrain contact indices are presented to evaluate the liquefaction potential and large undrained deformation characteristics at various silt/gravel contents. The usefulness of the intergrain contact indices is evaluated using the experimental data.

Introduction

Recent earthquake case histories indicate that natural soils and man-made sandy deposits that contain a significant amount of finer-grains (silty sands, clayey sands) and/or gravel do liquefy and cause lateral spreads (Seed et al. 1983, Seed and Harder 1990, JGS 1996). Experience gained from past studies on clean sands does not always directly translate to such broadly graded soils. Recognition of this has lead to several laboratory and field studies to evaluate the effects of increasing silt or gravel content on: (a) cyclic strength, (b) collapse potential, (c) steady state strength, (d) shear wave velocity, etc. Results from laboratory studies on clean sands mixed with non-plastic silts or plastic fines show that, at the same (global) void ratio, the steady state strength and cyclic strength of silty sand decreases with an increase in fines content (Chang 1990, Chameau and Sutterer 1994, Georgiannou et al. 1990,91a-b, Vaid 1994, Koester 1994, Pitman et al. 1994, Singh 1994, Zlatovic and Ishihara 1995, 1997, Thevanayagam et al. 1996). An example is shown in Fig.1a for a soil prepared

[1] *Assoc. Prof., Dept. of Civil, Struct., & Env. Eng., State Univ. of New York, 212 Ketter, Buffalo, NY 14260; Email: theva@eng.buffalo.edu*
[2] *Graduate student, Dept. of Civil, Struct., & Env. Eng., State Univ. of New York*

by mixing a sand [M = Medium Sand] with a silt (PI=4) at nearly constant global void ratio (e=0.558) and confining stress (104 kPa) but at different silts content (0 to 60% by weight). Fig.1b shows the number of cycles to reach initial liquefaction versus silts content for the same sand-silt mix, along with the data for two other sands [F = Fine Sand, W = Well Graded Sand] mixed with the same silt. [Fig.1b can also be expressed in the form of Fig. 8d, which will be discussed later]. As observed in these figures, beyond a certain transition range the trend in decrease of strength reverses and the strength increases with further increase in silts content. The transition fines content range is about 20 to 30% for non-plastic fines (Vaid 1994, Kuerbis et al. 1988, Singh 1994, Koester 1994). It is less than 20% for clayey (plastic) fines (Georgiannou et al. 1991a-b). The physical meaning of the transition fines content is not clear. The conclusions in the literature on whether the presence of fines is beneficial or not is contentious. Similar concerns prevail regarding gravely soils (Evans and Zhou 1995). No consensus exists on how to characterize liquefaction resistance of silty sands, sandy silts, and gravely soils.

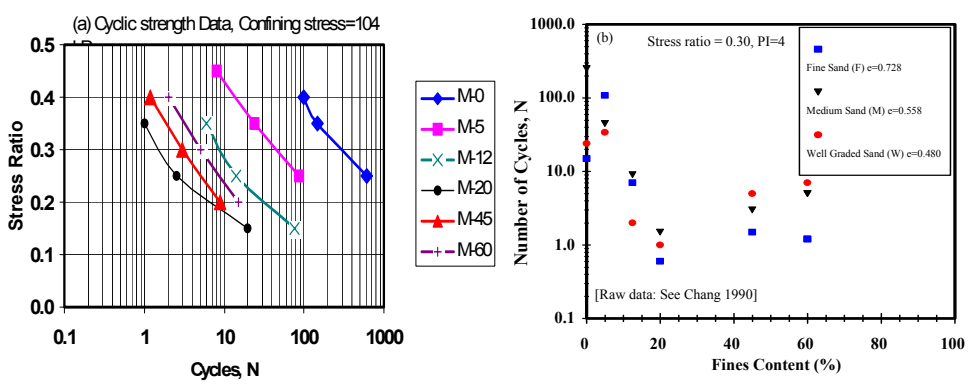

Fig.1. Influence of finer grain content on cyclic strength – (a) Medium Sand, (b) Three Sands

In this regard, recently, it has been noted that physical nature of silty sands and gravely sands is entirely different from clean sand (Thevanayagam 1998a-b, 1999, Thevanayagam and Mohan 1998). As the void ratio and proportion of the coarser and finer grains content of these soils change the nature of their microstructure also changes. The relative participation of the particles of very different sizes in the *internal interparticle contact force chain* also changes. Due to particle size disparity and availability of pores larger than some particles, at low finer grains content some of the finer particles may remain inactive or move between pores without significantly affecting or contributing to the force chain. Yet they contribute to the global void ratio. Alternately when there are sufficient amount of finer grains the coarser grains become dispersed contributing much less to the force chain than to the global void ratio. Global void ratio *e* ceases to be an index to represent the nature of contact density of active particles. The traditional use of *e* to compare the behavior of soils containing different amounts of fines content ceases to be valid. The same holds for relative density.

In general the stress-strain behavior, liquefaction potential, and fragility of granular mixes are affected by a critical combination of *intergranular and interfine contacts* and the physical and physico-chemical interactions thereof. The combined effects of intergranular and interfine contacts must be delineated in dealing with silty sands and gravely soils in understanding the mechanisms leading to liquefaction and post-liquefaction deformation, and the mechanical response of the media in general. New indices of active contacts are needed to represent the nature of intergrain contacts in order to characterize the behavior of such soils. It is thought that recognition of these factors may help to bring about a rational method for liquefaction potential assessment of silty and gravely soils.

Using a two-sized particle mix as a model, this paper highlights the nature of the microstructure of granular mixes. Based on this such granular mixes are classified into certain groups (Fig.2) depending on the relative frictional contributions at the intergranular and interfine grain contact level. Intergranular (e_c) (Mitchell 1993), interfine (e_f) (Thevanayagm 1998a), and equivalent intergranular $(e_c)_{eq}$ and interfine $(e_f)_{eq}$ (Thevanayagam 1998b) void ratios (Fig.3) are introduced as primary indices of contact density for granular mixes at various ranges of finer grain contents. Global void ratio *e* is introduced as a secondary index. The range of void ratio and fines content where each group (Fig.2) belongs to is conveniently shown in a global void ratio versus fines content diagram (Fig.4). The usefulness of these indices to characterize the observed cyclic strength behavior of granular mixes is evaluated.

Conceptual Framework

Microstructure

Consider a two-sized granular mix. The microstructure of this granular mix can be constituted by infinite different ways. Each one of them leads to a different internal force chain network among particles and hence each exhibits a different stress-strain response during shear. Among infinite variations, a few extreme limiting categories of microstructure and the relevant roles of coarser and finer grains are as follows.

Case-i: The first category (Fig.2a) is when the finer grains are fully confined within the void spaces between the coarser-grains with no contribution whatsoever in supporting the coarser grain skeleton. Finer grains are inactive (or secondary) in the transfer of inter particle forces. They may largely play the role of "filler" of intergranular voids. The mechanical behavior is affected primarily by the coarser grain contacts. During deformation the finer grains may move from one pore space to another without significantly contributing to the mechanical response of the soil. This requires that the finer grain particle size (d) is much smaller than the pore size between the coarser grains and that the intergranular pore space is not completely filled with the finer grains. Typically this requires that the coarser grain size (D) is at least 6.5 times larger than the finer grain size, and that the finer grain content (FC) is less than a certain threshold value (FC_{th}). This category is called *case-i*. Even at low

FC, if the size disparity R_d (=D/d) is not very large, the finer grains cannot freely move through the inter-coarser granular voids; They also tend to participate in the force chain and actively contribute to the stress-strain response.

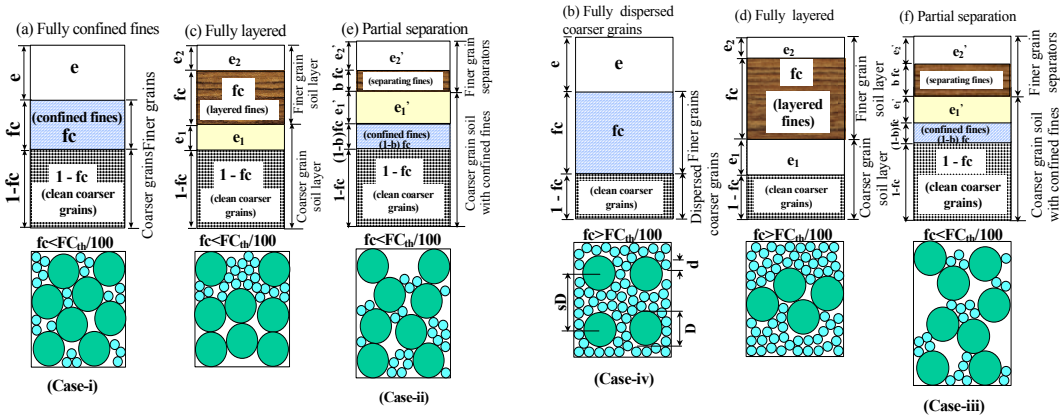

Fig.2 Microstructure and intergranular matrix phase diagram

Cases-ii and iii: Consider changing the microstructure shown in Fig.2a in two ways: (1) alter the position of some of the finer grains, or (2) add more finer grains. The consequences are significant. If one alters the position of some of the finer grains, while maintaining the finer grain content the same, the microstructure corresponding to the second and third categories shown in Figs.2e and f are obtained

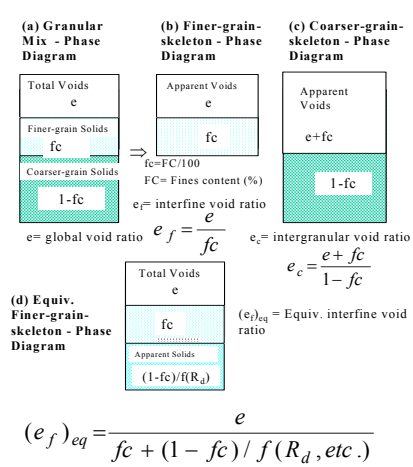

$$e_f = \frac{e}{fc}$$

$$e_c = \frac{e + fc}{1 - fc}$$

$$(e_f)_{eq} = \frac{e}{fc + (1 - fc)/f(R_d, etc.)}$$

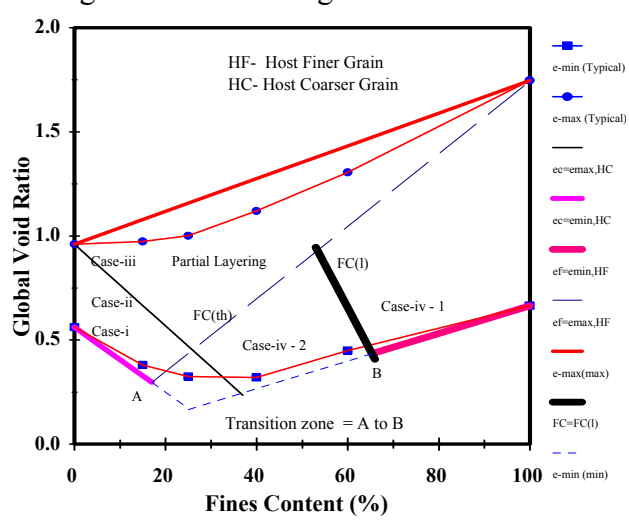

Fig.3 Intergranular contact indices **Fig. 4 Intergranular matrix diagram – Mix Classification**

with a concurrent increase in global void ratio. Essentially, the microstructure in Figs.2e-f is made up of partial layering and partial separation of coarser grains by the finer grains along with confined finer grains within the voids between the coarser grains. Some of the finer grains become active participants in the internal force chain. These finer grains are termed the *'separating fines'* in Figs.2e and f. In Fig.2e, the finer grains may be supporting the coarser-grain skeleton that is otherwise unstable. They act as a load transfer vehicle between "some" of the coarse-grain particles in the

soil-matrix while the remainder of the fines play the role of "filler" of voids. They may dominate the initial stress-strain behavior depending on the type of finer grains (plastic or non-plastic). In Fig.2f, the finer grains may play an active role of *"separator"* between a significant number of coarse-grain contacts and therefore begin to dominate the strength characteristics. Coarser grain skeleton is virtually unstable without the finer grains. These two categories of microstructure are called cases ii and iii, respectively. Case-ii is a transition between cases i and iii. Theoretically case-iii occurs at an intergranular void ratio exceeding the maximum void ratio ($e_{max,HC}$) achievable for the 'pure' coarser grain soil.

Cases-iv-1 and iv-2: On the other hand if one increases the finer grains content sufficiently, one gets the fourth category (Fig.2b). It occurs naturally when sufficient finer grains are present making active contacts among themselves. The coarser grains begin to disperse in the finer grain matrix. Transition from Fig.2a to Fig.2b occurs when the finer grains content (FC) exceeds beyond the threshold fines content (FC_{th}). When $FC>FC_{th}$ the finer grains begin to play a rather important role while the role of coarser grains begin to diminish. The fines may carry the contact and shear forces while the coarser grains may act as *reinforcing elements* embedded within the finer grain matrix. The effect of coarser grains cannot be completely neglected until they are separated sufficiently apart. This imposes a limiting fines content FC_l. There exists a transition zone between FC_{th} and FC_l before the behavior of the soil mix is entirely governed by the finer grains. This is called case-iv-2 whereas the case corresponding to $FC>FC_l$ is called case-iv-1. The size disparity constraint discussed before for cases i to iii needs not be satisfied for case-iv.

The fifth category (Figs.2c-d) is when the coarser and finer grains constitute a fully layered system where the coarser grain layers have no fines contained in them and vice versa. This is called case-v. It is also possible to create a composite system that contains some of the cases i through v. The figures 2a, c, e and f are more relevant at low finer grains content. Figs. 2b and d are relevant at high finer grains content.

Conceptually Fig.4 shows the regions belonging to the four cases i through iv confined by various transition boundaries. The transition lines corresponding to the threshold FC_{th} and limiting FC_l fines contents may be estimated using:

$$FC_{th} \le \frac{100 e_c}{1 + e_c + e_{\max,HF}}\% = \frac{100\, e}{e_{\max,HF}}\% \; ; \qquad FC_l \ge 100\left[1 - \frac{\pi(1+e)}{6 s^3}\right]\% = 100\left[\frac{\frac{6s^3}{\pi} - 1}{\frac{6s^3}{\pi} + e_f}\right]\% \ge FC_{th};\; e_f \le e_{\max,HF} \quad (1)$$

where $e_c=(e+fc)/(1-fc)$, $e_f=e/fc$, $fc=FC/100$, $s=1+a(d/D)=1+a/R_d$ where a=10 (approximately). The rationale behind the equation for FC_{th} is that once the interfiner grain void ratio e_f drops below $e_{max,HF}$ (the maximum void ratio achievable for the 'pure' finer grain soil) the finer grains begin to make active contacts among themselves and contribute to the force chain. The reasons leading to the derivation of the expression for FC_l may be attributed to the observations of Roscoe (1970) that the zone of influence of shear is about 10 times the diameter of particles. The various

other boundaries refer to the maximum and minimum void ratio profiles: e=$e_{max,HC}$ +($e_{max,HF}$ –$e_{max,HC}$) fc; e_c=$e_{max,HC}$; e_f =$e_{max,HF}$; e_c =$e_{min,HC}$; and e_f = $e_{min,HF}$.

Contact Indices and Mechanical Behavior

Recently the nature of the microstructure of such granular mixes have been studied in some detail. Results show that up to FC=FC_{th} the finer grains can, but not necessarily, remain within the intergranular voids. Primarily the intergranular contacts between the coarser grains affect the mechanical behavior with secondary effects by the finer grains. Hence, neglecting the effects of fines, the *inter-coarser grain void ratio* e_c (Fig.3c) may be used as an index of active contacts. The magnitude of e_f may be used as an index to assess the secondary effects by the finer grains. If the secondary effects are included, the relevant *equivalent intergranular contact index void ratio* would be of the form $(e_c)_{eq}$ (=[e+(1-b)fc)]/[1-fc+bfc]) (Fig.2).

At very high FC (>FC_{th}), neglecting the effects of dispersed coarser grains, the *interfine void ratio* e_f (=e/fc, Fig.3b) may be used as an index of active contacts. If the secondary effect of the coarser grains are included, recent work shows that the relevant *equivalent interfine contact index void ratio* is of the form $(e_f)_{eq}$ =e/[fc+(1-fc)/$(R_d)^m$], Figs.2b and 3d, m=a coefficient satisfying 0<m<1, e_c>$e_{max,HC}$ (Thevanayagam 1998b, Thevanayagam 2000).

The aforementioned contact indices and the location of a soil mix in Fig.4 can be used as aids to predict the trends of the stress-strain characteristics, liquefaction potential, and fragility of silty or gravely soils (prepared by the same method at the same confining stress) *relative* to that of the host coarser grain soil or the finer grain soil. Fig.5 shows a schematic diagram for *hypothetical* specimens satisfying the following specific constraints: (1) an increase in global void ratio e at the same fines content [specimens 1,2,3], (2) an increase in fines content at a constant global void ratio e [4,2,5,6,7,13], (3) an increase in fines content at the same intergranular void ratio e_c [8,1,9 or 3,10 or 14,2,15; FC<FC_{th}], or (4) an increase in coarser grain content at the same interfine void ratio e_f [11,7,12; FC>FC_{th}].

Cyclic Strength and Fragility: The anticipated trends in number of cycles (N) required to cause initial liquefaction at the same cyclic stress ratio are *schematically* shown in Fig.5 [N versus FC]. In (1) both intergranular and interfine void ratios increase with concurrent reduction in inter-coarser grain contacts. Therefore the soil becomes weaker. In (2) while e_c increases e_f decreases. Viz. the inter-coarser granular contacts decrease while the interfine contacts increase. Hence initially the soil is expected to weaken [4,2,5] followed by a transition in the vicinity of e_f=$e_{max,HF}$ (FC=FC_{th}). The soil becomes stronger beyond that [6,7,13]. In (3), the increase in cushioning effect by the fines is manifested leading to a slight increase in strength [3,10, case-iii]. The specimen 10 is expected to be somewhat more resistant to collpase than the specimen 3. This effect, however, diminishes gradually if the soil becomes denser in terms of e_c [case-ii]. The reason is that when e_c is small (dense coarser grains) the relative effect of fines is less appreciable compared to the direct coarser-coarser grain contact resistance until e_f becomes sufficiently low. In (4) when

the soil is at a fines content less than FC_l but greater than FC_{th} [11,7,12] the reinforcement effect of the coarser grain 'inclusions' may affect the stress strain behavior. The specimen 11 is expected to be stronger than 7. Again this reinforcement effect may become relatively small compared to the direct finer-grain-to-finer-grain contact resistance when e_f is small (dense interfine contacts). Once FC exceeds FC_l the reinforcement effect is expected to be small. Primarily the interfine contacts and e_f are expected to affect the soil behavior [7,12]. Without elaboration, the remaining figures show the relative trends for N for various cases i through iv plotted against the relevant contact indices (e_c, e_f, and $(e_f)_{eq}$).

Experimental Evaluation

This section presents an experimental evaluation of the above conceptual framework. For this purpose the experimental data reported by Chang (1990, Figs.1a-b) and additional new experimental data generated as a part of this study are used. The latter experiments involve undrained triaxial cyclic tests on large size specimens (typically 74 mm diameter and 150 ~ 160 mm height) prepared using a single host sand (OS55) (OS-F55, Foundry Sand from US Silica Company, Illinois, e_{max}=0.80, e_{min}=0.60, d_{50}=0.24mm) mixed with different amounts of non-plastic crushed silica fines (Sil co sil #40, 99.9% passing sieve #200, d_{50}=0.007mm) at (a) 0%, (b) 15%, (c) 25%, and (d) 60% fines by dry weight.

Cylindrical specimens were prepared by placing soils in four layers or eight layers in a trixial mold using dry air deposition method or moisture tamping method. The mold (75 mm diameter and 175 mm height) was filled with the soil by layers and compacted by gentle tamping until reaching a specified target void ratio. The procedure was similar for each layer until a specified target void ratio was reached.

Following initial preparation, the specimens were percolated with carbon dioxide for about 5 minutes. After that, deaired water was allowed to flow from the bottom of the specimen towards the top if the specimen was prepared by dry deposition method (If the specimen was prepared by moist tamping method, this step was omitted). Then the specimen was then back-pressure saturated. Initially about 20 to 30 kPa effective confining pressure (σ'_c) was applied to the specimen. Then the cell pressure and the pore water pressure were slowly increased in equal increments simultaneously. The net volume of the water introduced into the specimen was measured accurately. Finally the specimen was set up on the triaxial test apparatus to continue the saturation until the B-value ($=\Delta u/\Delta\sigma_c$) was typically greater than 0.95. Following this, the specimens were isotropically consolidated to a constant effective consolidation stress (σ'_c) of 100 kPa.

Stress ratio ($[\pm\Delta\sigma_1/(2\sigma'_c)]$=0.2) controlled undrained triaxial cyclic tests were done at a frequency of 0.2 Hz or 1 Hz. The pore pressure, axial load, and axial deformation were recorded using a built-in data acquisition system. The final void ratio of each specimen was calculated based on the weight of the dry solid grains in

the specimen, the net volume of water introduced into the specimen during saturation, and the measured volume change data during consolidation.

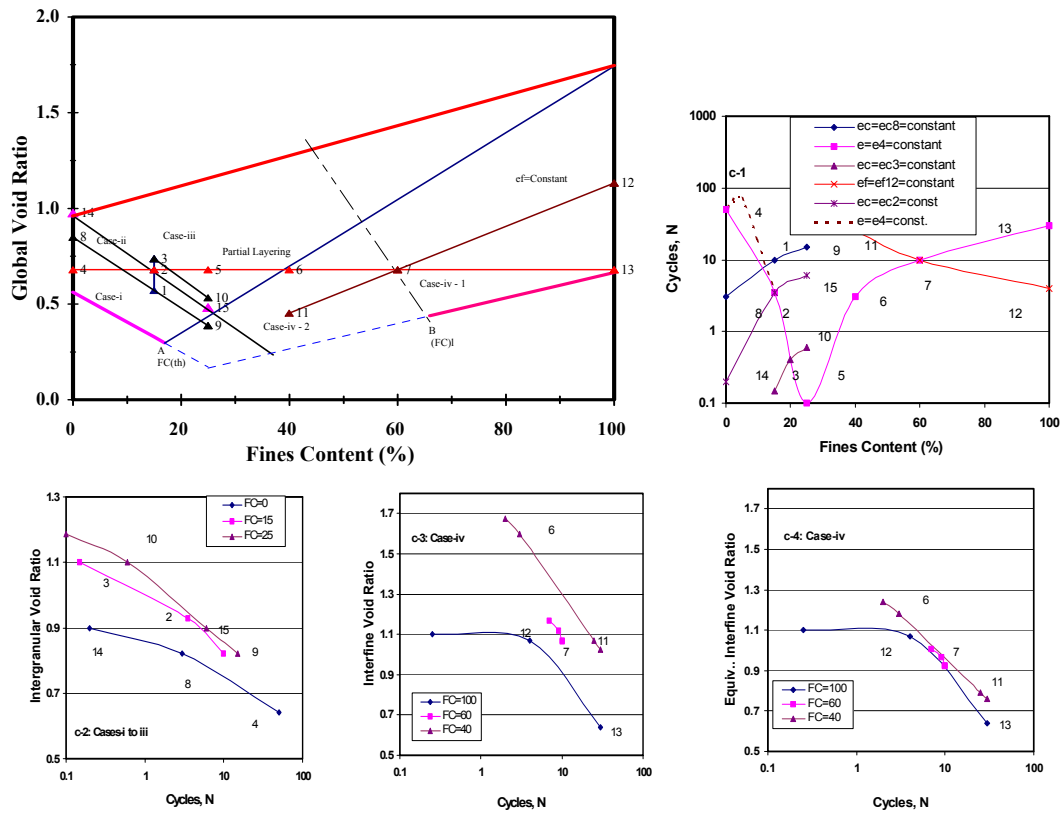

Fig.5 Relative trend in cyclic strength – Schematic.

Reinterpretation of Existing Data

Intergranular Matrix Diagram: Figs.6a-c show the intergranular matrix diagram for three host sands [(1) Fine (F), (2) Medium (M), and (3) Well graded (W)] mixed with a low plasticity fines (PI=4) tested by Chang (1990), reported in Figs.1a-b. The locations of the specimens are also shown. Each sand mix was tested at 0, 5, 12, 20, 45, and 60% fines content. The specimens were prepared by moist tamping method. All specimens were consolidated to the same initial confining stress (104kPa). The specimens for each soil mix were tested at nearly constant global void ratio: e=0.728 for F, e=0.558 for M, and e=0.480 for W, respectively. These void ratios correspond to about 50% relative density of the respective parent sands. No data were available for $e_{max,HF}$ and $e_{min,HF}$ for the silt. For qualitative discussion purposes the threshold boundary may be estimated assuming typical values of $e_{max,HF}$ =1.5 and $e_{min,HF}$ =0.6. Also for illustration purposes the R_d (defined as D_{50}/d_{50}) values for the soils F, M, and W were estimated to be about 15, 40, and 40 based on a typical value for d_{50} of silts. An examination of Fig.6 and calculated index void ratios e_c, e_f, $(e_f)_{eq}$ would readily reveal the cases each specimen belongs to and the expected behavior of each granular mix relative to one another.

Cyclic Strength variation with Increase in FC: Fig.7d shows the same cyclic strength data shown in Fig.1b. The e_c and e_f values for each specimen and the respective cases each specimen belongs to are also shown in this figure. As the fines content increases, at the same global void ratio e, the e_c increases and e_f decreases. Initially the e_f remains high to be of any significance, alone. With increase in FC the soil mixes move gradually from Case-i to Case-ii to Case-iii and then cross over to Case-iv-2. So is the behavior of the soils. Initially the strength decreases due to reduced intergranular contacts with increase in e_c with little or secondary contribution from the fines. As the soil moves beyond the threshold transition zone (FC_{th} at $e_f = e_{max,HF}$) and enters the zone for Case-iv-2 the influence of e_f becomes important with some reinforcement effect by the coarser grains. The $(e_f)_{eq}$ becomes the primary contact index void ratio. The trend reverses and the strength begins to increase with further increase in fines content.

The transition fines content FC_{th} is slightly different for each soil mix. Theoretically it corresponds to the intersection of the constant global void ratio line with the $e_{max,HF}$ line. For the same host fines, typically a soil mix at a smaller global void ratio (Fig.6c) will cross the $e_{max,HF}$ line and reach Case-iv-2 at a smaller fines content than a soil mix at a higher global void ratio (Fig.6a). Hence, the soil W (at e=0.480) reaches this transition at smaller fines content than the soil F (at e=0.728).

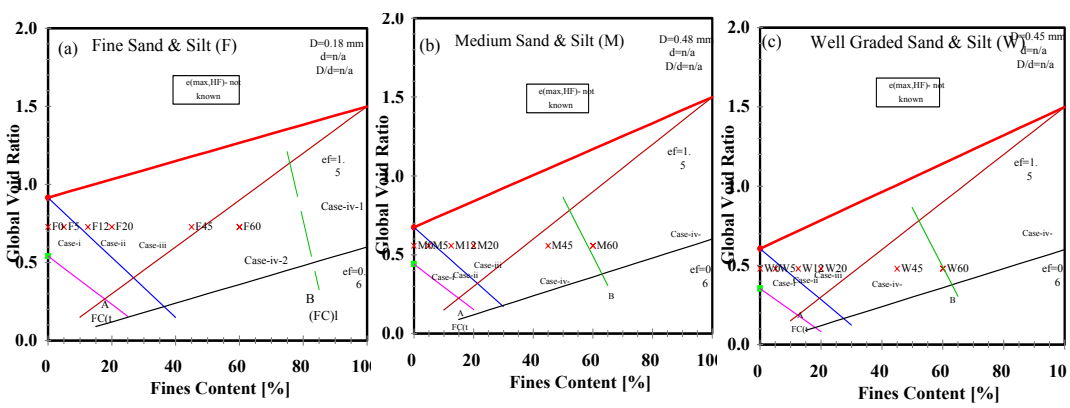

Fig.6 Intergranular matrix diagrams – Three Sand – Silt Mixes

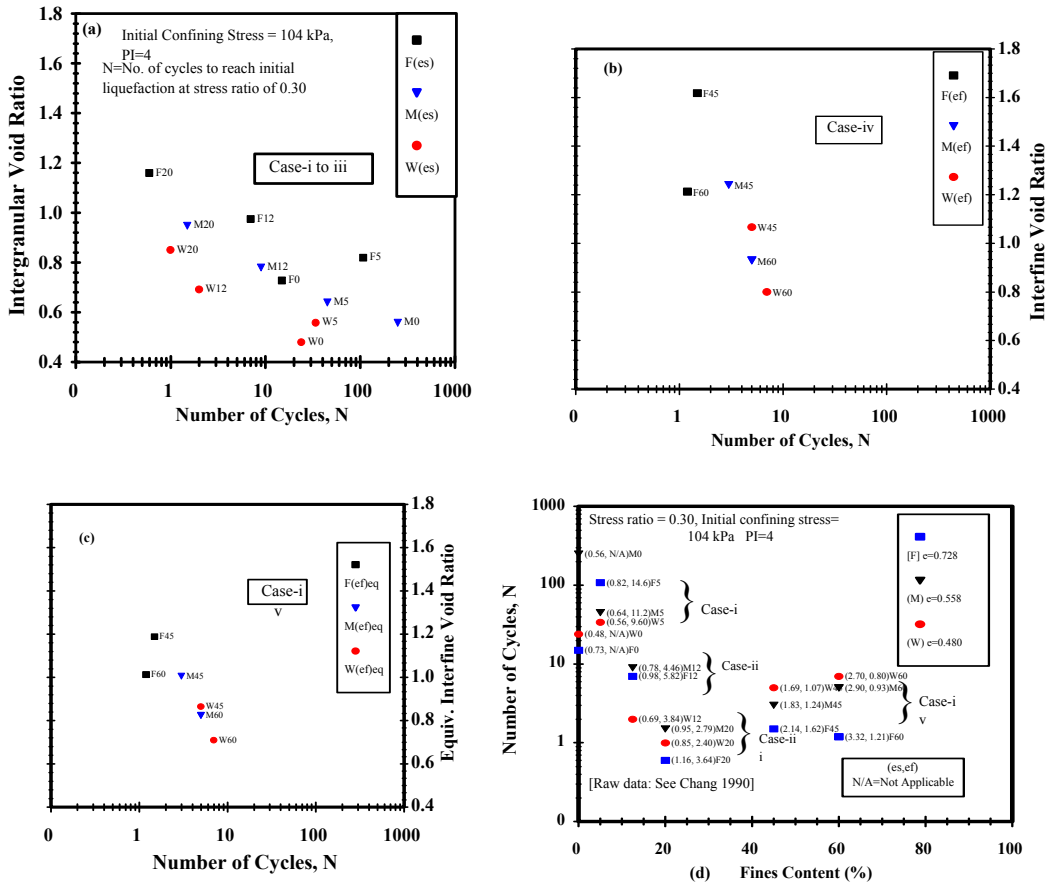

Fig.7 Influence of intergrain contacts on cyclic strength: (a) e_c, (b) e_f, (c) $(e_f)_{eq}$ and (d) FC

FC<FC$_{th}$: Fig.7a show the same data in a different format: Number of cycles to initial liquefaction versus e_c for Cases-i to iii [FC<FC$_{th}$]. For this case, a different cyclic strength profile is obtained for each mix depending on the parent sand type (F,M,W). N is affected primarily by the parent sand type. e_c becomes the primary index of active contacts. The fines have a secondary role. It would be more revealing if (if available) the data for each host sand are superimposed in this figure permitting a comparison of the kind shown in Fig.5 (e_c versus N).

FC>FC$_{th}$: Fig.7b show the N versus e_f data for Case-iv. N data show significant dependency on interfine void ratio e_f. The data for each fines content (45% and 60% separately) correlates well with e_f and fall in a (separate for 45% and 60%) narrow band regardless of the parent sand type. The separate narrow bands for the soils mixed with 45% fines and 60% fines are due to the differences in the degree of reinforcement effect. At the same e_f, the cyclic strength is higher for the soil with higher sands content. The reinforcement effect is higher at 45% fines content than at 60% which is approaching the limiting fines content FC$_l$. Nevertheless, at low e_f (dense interfine contacts) the relative effect of reinforcement becomes less appreciable compared to direct interfine contact friction. The separate bands for 45 and 60% merge together at low e_f. Fig.7c shows the same data, plotted against

equivalent interfine void ratio $(e_f)_{eq}$ [calculated assuming m=0.45). Interestingly the number of cycles required to cause liquefaction correlates with $(e_f)_{eq}$ for all cases of iv. The reason for this is that all sands were mixed with the *same silt*. Hence, once FC exceeds the threshold value, all soil mixes are affected by the same silt except for the minor differences due to the presence of different size coarser grains (F,M,W). Hence a single narrow band is obtained in Fig.7c. It would be more revealing if (if available) the data for the silt is superimposed in this figure permitting a comparison of the kind shown in Fig.5 [$(e_f)_{eq}$ versus N].

Ottawa Sand – Silt Mix: Fig. 8 shows the locations of the specimens in the intergranular matrix diagram. Figs. 9 and 10a-b show the number of cycles to liquefaction (±5% double amplitudes of axial strain) versus e, e_c and $(e_c)_{eq}$, Respectively. In the e versus N plane a distinct trend is observed as FC increases (Fig. 9). At low FC ($<FC_{th}$) and at the same e, N required to cause liquefaction (at $[\pm\Delta\sigma_1/(2\sigma'_c)]=0.2$) becomes smaller and smaller as the fines content increases. As FC increases beyond FC_{th}, the trend reverses. This is because at low FC, the undrained cyclic strength of the soil is characterized largely by intergranular contact indices (e_c or $(e_c)_{eq}$). Beyond FC_{th}, the interfine contact indices (e_f or $(e_f)_{eq}$) control the undrained cyclic strength. This can be further illustrated when the data are plotted on a e_c versus N or $(e_c)_{eq}$ (assuming b=0.35) versus N plane (Figs. 10a-b). The data points for all soils at $FC < FC_{th}$ collapse into a narrow band in Fig. 10b. This indicates that the undrained cyclic strength of these soils can be characterized by the equivalent intergranular void ratio $(e_c)_{eq}$. Further data are required to evaluate whether the soils at $FC > FC_{th}$ could be characterized by the equivalent interfine void ratio $(e_f)_{eq}$.

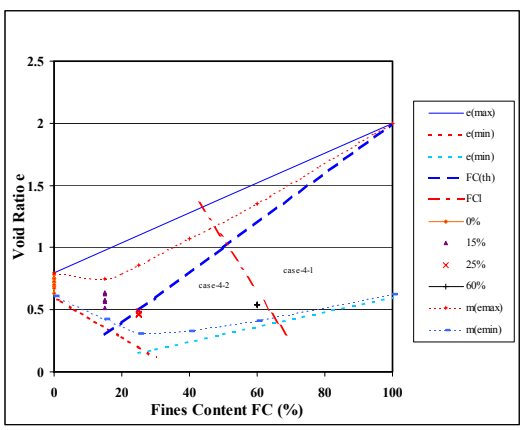

Fig. 8 Intergranular matrix diagram – Ottawa Sand–Silt Mixes

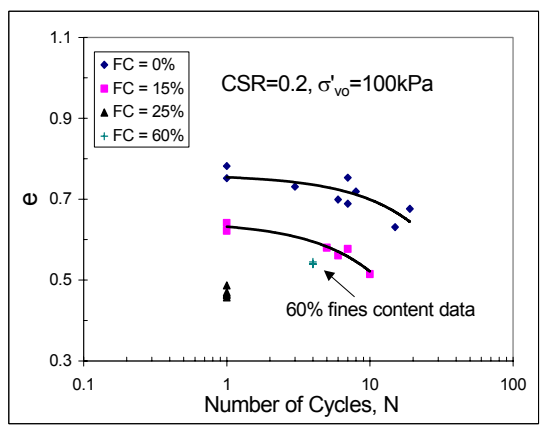

Fig. 9 Effects of *e* on undrained cyclic strength

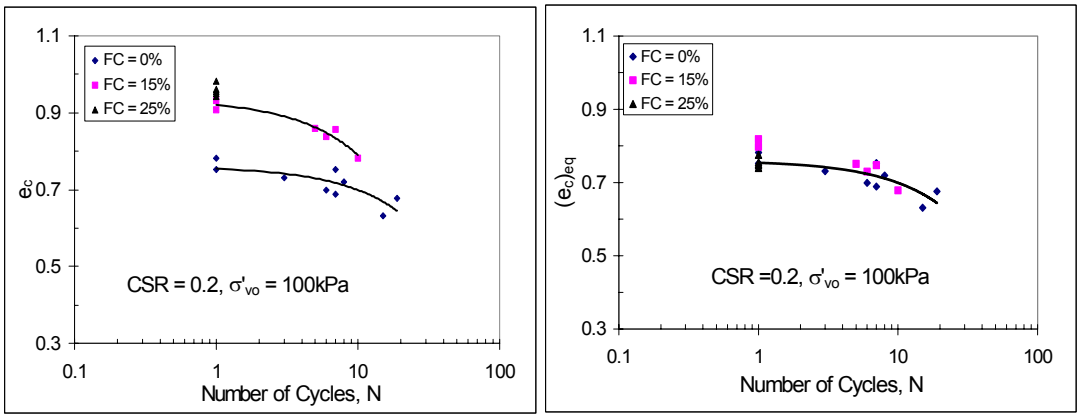

Fig. 10a-b Effects of e_c *and* $(e_c)_{eq}$ on undrained cyclic strength

Concluding Rrmarks

A simple framework for analysis of the relative effects of inter-coarser granular and interfine contacts on cyclic undrained strength of granular mixes is presented. Intergranular and interfine contact indices (e_c, $(e_c)_{eq}$, e_f, *and* $(e_f)_{eq}$) are introduced as parameters that control undrained cyclic strength of sand – silt mixes. With this framework, one may deduce the behavior of granular mixes at various finer grains contents and void ratios relative to the behavior of the host coarser grain soil or finer grain soil.

Based on this framework, new reinterpretation of some existing data from the literature, and interpretation of a limited amount of experimental data generated as a part of this study, the following observations could be made about the liquefaction potential of a granular mix prepared at the same initial confining stress. (a) When compared at the same global void ratio e, the collapse potential increases with an increase in finer grains content up to a certain threshold value FC_{th}. Beyond that the collapse potential decreases. FC_{th} depends on the host fines, size disparity ratio, and the global void ratio, (b) At low FC ($<FC_{th}$), when compared at the same e_c, an increase in finer grains content reduces the collapse potential, (c) At high FC ($>FC_{th}$), when compared at the same e_f, an increase in finer grains content increases the collapse potential, (d) When FC $<$ FC_{th}, equivalent intergranular void ratio $(e_c)_{eq}$ could be a useful index to characterize the undrained cyclic, and (e) At high FC ($>FC_{th}$), when compared at the same $(e_f)_{eq}$, an increase in finer grains content slightly increases the collapse potential. The question remains on the possible differences on the nature of field deposits relevant for built environment versus what is studied in the laboratory.

Acknowledgements

Financial support by the NSF for the ongoing research is gratefully appreciated.

References

Andrus, R.D. and Stokoe, K.H. (1997), "Liquefaction Resistance Based on Shear Wave Velocity", Technical Rep. NCEER-97-0022, NCEER Highway Project Task No. 112-D-4.2, FHWA Contact No. DTFH61-92-C-00112, 89-128

Baziar, M.H. and Dobry, R. (1995), "Residual strength and large-deformation potential of loose silty sands", J. Geotech. Eng. Div., ASCE, 121(12), 896-906

Chameau, J.L. and Sutterer, K. (1994), "Influence of fines in liquefaction potential and steady state considerations", 13th Intl. Conf., New Delhi, India, 183-84

Chang, N. Y. (1990). "Influence of fines content and plasticity on earthquake-induced soil liquefaction," Contract Rep., US Army WES, Vicksburg, MS contract No. DACW3988-C-0078

Evans, M. D. and Zhou, S. (1995), "Liquefaction behavior of sand-gravel composites", ASCE, J. Geoech. Eng., 121(3), 287-298

Georgiannou, V.N., Burland, J.B. and Hight, D.W. (1990), "The undrained behaviour of clayey sands in triaxial compression and extension", Geotechnique 40, No.3, 431-449

Georgiannou, V.N., Hight, D.W. and Burland, J.B. (1991), "Undrained behaviour of natural and model clayey sands", Soils and Foundations 31, No.3, 17-29

Ishihara, K. (1993), "Liquefaction and flow failure during earthquakes", Geotechnique, 43(3), 351-41

JGS (1996) "Soils and Foundations - Special issue on geotechnical aspects of the January 17, 1995 Hyogoken-Nambu Earthquake", Japanese Soc. Geotechnical Eng.

Koester, J.P. (1994), "The influence of fines type and conent on cyclic strength", Proc. ASCE Conv., Atlanta, Geotech. Spec. Pub. 44, 17-32

Kuerbis, R., Nagussey, D. and Vaid, Y.P. (1988), "Effect of gradation and fines content on the undrained response of sand", Proc. Conf. Hyd. Fill Struc., ASCE Geot. Spec. Publ. 21, 330-45

Mitchell, J.K. (1993). *Fundamentals of soil behavior,* 2nd Ed., John Wiley & Sons, Inc., New York, N.Y.

Pitman, T.D., Robertson, P.K. and Sego, D.C. (1994), "Influence of fines on the collapse of loose sands", Can. Geotech. J., 31, 728-39

Robertson, P.K and Wride, C.E. (1997), "Cyclic Liquefaction and its Evaluation based on the SPT and CPT", Technical Rep. NCEER-97-0022, NCEER Highway Project Task No. 112-D-4.2, FHWA Contact No. DTFH61-92-C-00112, 41-87

Roscoe, K. H. (1970), "The influence of strains in soil mechanics," Geotechnique, 20(2), 129-170

Seed, H.B., Idriss, I.M. & Arango, I. (1983). "Evaluation of liquefaction potential using field performance data", J. Geot.. Eng. Div., ASCE, 109, GT3, 458-482

Seed, H.B. (1987), "Design Problems in Soil Liquefaction", J. Geot.. Eng. Div., ASCE, 113(8), 827-45

Seed, R.B., and Harder, L. F. Jr. (1990). “SPT-based analysis of cylcic pore pressure generation and undrained residual strength.” *Proc., Seed Memorial Symp.*, 2, 351-376.

Singh, S. (1994). “Liquefaction characteristics of silts.” *Ground failures under seismic conditions*. *Proc., ASCE Nat. Convention, Geotech Spec. Publ.* 44, S. Prakash and P. Dakoulas, eds., ASCE, Reston, Va., 105-116

Stark, T. D. and Mesri, G. (1992), "Undrained shear strength of liquefied sands for stability analysis", J. of Geotech. Eng., ASCE, 118(11), 1727-47

Thevanayagam, S., Ravishankar, K., and Mohan, S. (1996). "Steady state strength, relative density and fines content relationship for sands," TRB Transp. Research Record 1547, 61-67

Thevanayagam, S. (1998a) "Effect of fines and confining stress on steady state strength of silty sands,” J. Geotech. & Geoenv. Eng., ASCE, 124(6), 479-491

Thevanayagam, S. (1998b) "Relative role of coarser and finer grains on undrained behavior of granular mixes" in review, J. Geotech. & Geoenv. Eng., ASCE

Thevanayagam, S. and Mohan, S. (1999) “Intergranular state variables and stress-strain behavior of silty sands" in press, Geotechnique

Thevanayagam, S. (1999) "Role of intergrain contacts, friction, and interactions on undrained response of granular mixes" Proc. workshop *Physics and mechanics of soil liquefaction*, A.A. Balkema press

Vaid, Y.P. (1994), "Liquefaction of silty soils", Proc. ASCE Conv., Geotech. Spec. Publ. 44, 1-16

Zlatovic, S. and Ishihara, K. (1997). "Normalized behavior of very loose non-plastic soils: effects of fabric” Soils and Foundations, 37(4), 47-56

14th ASCE Engineering Mechanics Conference, Austin, Texas, May 2000

Contact Index and Liquefaction Potential of Silty and Gravely Soils

S. Thevanayagam, J. Liang, and T. Shenthan
State University of New York, Buffalo, NY 14260
theva@eng.buffalo.edu

Abstract

A framework for analysis of liquefaction potential of granular mixes ranging from clean sands to pure silts (or gravel) with due consideration for intergranular and interfine friction within a granular mix is presented. New intergrain contact density indices $(e_c)_{eq}$ and $(e_f)_{eq}$ are presented to evaluate their liquefaction potential. The usefulness of these indices is evaluated using stress controlled undrained cyclic triaxial tests conducted on specimens prepared by mixing a silt and clean sand in different proportions. They correlate well with cyclic strength data.

Key words: *Liquefaction, cyclic strength, sand, silt, silty sand, intergranular void ratio.*

Introduction

Natural soils and man-made sandy deposits do contain a significant amount of finer-grains and/or gravel. Recent earthquake case histories indicate that such soils do liquefy and cause lateral spreads (JGS 1996). Experience gained from past studies on clean sands does not always directly translate to such broadly graded soils. Recognition of this has lead to several laboratory and field studies to evaluate the effects of increasing silt or gravel content on liquefaction potential of such soils (Chang 1990, Georgiannou et al. 1990, Vaid 1994, Koester 1994, Pitman et al. 1994, Singh 1994, Zlatovic and Ishihara, 1997). Results indicate that at a given global void ratio, an increase in silt content has a tendency to increase the liquefaction potential up to a certain transition silt content range. Beyond that the trend reverses and the strength increases with further increase in silt content. The transition silt content range is about 20 to 30% for non-plastic fines. It is less than 20% for clayey (plastic) fines. The physical meaning of the transition fines content is not clear. Whether the presence of fines is beneficial or not is contentious. Similar concerns prevail regarding gravely soils (Evans and Zhou 1995). What soil parameter, if not global void ratio or relative density, is a suitable intergrain contact index to characterize liquefaction potential of silty soils is unclear. This paper investigates this question.

Conceptual Development

Recently, it has been noted that physical nature of silty sands and gravely sands is entirely different from clean sand (Thevanayagam 1998,2000, Thevanayagam and Mohan 2000). As the void ratio and proportion of the coarser and finer grains content of these soils change the nature of their microstructure also changes. The relative participation of the particles of very different sizes in the *internal interparticle contact force chain* also changes. Due to particle size disparity and availability of pores larger than some particles,

at low finer grains content some of the finer particles in a granular mix may remain inactive within the pores between the coarser grains or move between pores without significantly affecting or contributing to the force chain. Yet they contribute to the global void ratio. Alternately when there are sufficient amount of finer grains the coarser grains become dispersed contributing much less to the force chain than to the global void ratio. Global void ratio *e* ceases to be an index to represent the nature of contact density of active particles. The traditional use of *e* or relative density to compare and characterize the behavior of soils containing different amounts of fines content ceases to be valid.

In general the stress-strain behavior, liquefaction potential, and fragility of granular mixes are affected by a critical combination of *intergranular and interfine contacts* and the physical and physico-chemical interactions thereof. The latter is important for plastic silty soils. The combined effects of intergranular and interfine contacts must be delineated in dealing with non-plastic silty sands and gravely soils in understanding the mechanisms leading to liquefaction and post-liquefaction deformation, and the mechanical response of the media in general.

Recently, the nature of the microstructure of granular mixes has been studied in some detail using a two-sized particle mix model. Based on this a granular mix is classified into certain groups (Fig.1) depending on the makeup of the soil microstructure and the relative frictional contributions at the intergranular and interfine grain contact level to its mechanical response. Table 1 presents the rationale behind this recent development and the contact void ratios relevant for the various cases. The range of void ratio and fines content relevant for each case is conveniently shown in a global void ratio e versus fines content (FC) diagram (Fig.3). Equivalent intergranular $(e_c)_{eq}$ (=$[e+(1-b)fc)]/[1-(1-b)fc]$, fc=FC/100, 0<b<1), and equivalent interfine void ratios $(e_f)_{eq}$ (=$e/[fc+(1-fc)/(R_d)^m]$, R_d= D/d, D=diameter of sand, d=diameter of silt, m=a coefficient, 0<m<1) (Thevanayagam 1998,2000) (Fig.2) have been introduced as primary indices of contact density for granular mixes at low (FC < FC_{th}) and high (FC>FC_{th}) finer grain contents, respectively. This paper evaluates the usefulness of these indices to characterize liquefaction potential of granular mixes.

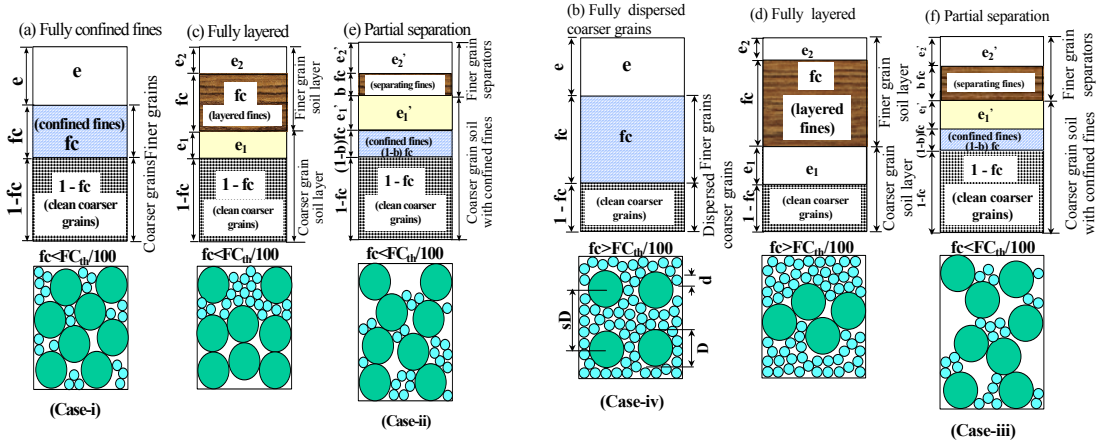

Fig.1 Microstructure and intergranular matrix phase diagram

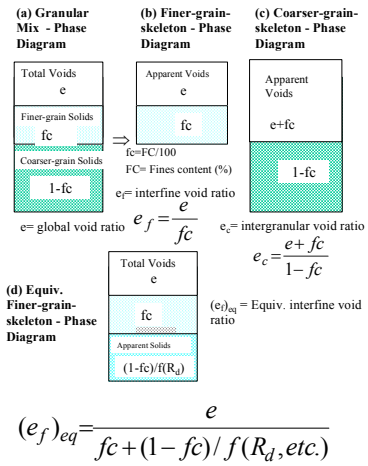

Fig.2 Intergranular contact indices

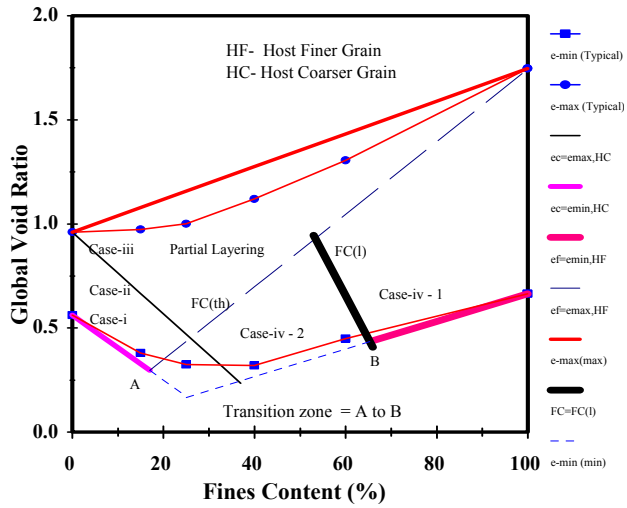

Fig. 3 Intergranular matrix diagram – Mix Classification

Table 1: Granular Mix Classification (Ref. Fig. 3)

Case	FC	e_c	e_f	Roles of coarser-grains and finer-grains	Contact Void Ratio	Fig.
i		$e_c<e_{max,Hc}$	$e_f>e_{max,HF}$	Finer grains are inactive (or secondary) in the transfer of inter particle forces. They may largely play the role of "filler" of intergranular voids. The mechanical behavior is affected primarily by the coarser grain contacts.	$(e_c)_{eq}$	1a
ii	$FC<FC_{th}$	e_c *near* $e_{max,Hc}$		Finer grains support the coarser-grain skeleton that is otherwise unstable. They act as a load transfer vehicle between "some" of the coarse-grain particles in the soil-matrix while the remainder of the fines play the role of "filler" of voids.	$(e_c)_{eq}$	1e
iii		$e_c>e_{max,Hc}$		Finer grains play an active role of "separator" between a significant number of coarse-grain contacts and therefore begin to dominate the strength characteristics.	$(e_c)_{eq}$	1f
iv-2	$FC_{th}<FC<FC_l$		$e_f<e_{max,HF}$	The fines carry the contact and shear forces while the coarser grains may act as reinforcing elements embedded within the finer grain matrix.	$(e_f)_{eq}$	1b
iv-1	$FC_l<FC$	$e_c>>e_{max,Hc}$	$e_f<e_{max,HF}$	The fines carry the contact and shear forces while the coarser grains are fully dispersed.	$(e_f)_{eq}$	1b

Notes: $e_{max,Hc}$, $e_{max,HF}$ = maximum void ratio of the host sand (coarser grains) and host fines (finer grains) media, respectively. They are the limiting void ratios beyond which each soil (clean coarser grained soil, pure fine grained soil) has no appreciable strength. FC_{th}=Threshold finer grains content, and FC_l = limiting finer grains content. The magnitudes of FC_{th} and FC_l depend on the size disparity ratio (R_d=D/d) of the size of the coarser (D) and finer (d) grains, shape, packing, $e_{max,Hc}$, and $e_{max,HF}$ as shown elsewhere (Thevanayagam 1998). Intergranular void ratio (e_c) =[e+fc]/[1-fc], (fc=FC/100, FC=finer grain content by weight). Interfine void ratio (e_f) =e/fc.

$$FC_{th} \le \frac{100 e_c}{1 + e_c + e_{\max,HF}}\% = \frac{100\, e}{e_{\max,HF}}\% \;; \qquad FC_l \ge 100\left[1 - \frac{\pi(1+e)}{6 s^3}\right]\% = 100\left[\frac{\frac{6 s^3}{\pi} - 1}{\frac{6 s^3}{\pi} + e_f}\right]\% \ge FC_{th}\,;\; e_f \le e_{\max,HF}$$

s=1+a(d/D)=1+a/R_d, where a=10 (approximately)

Experimental Evaluation

To investigate the effectiveness of the above contact indices to characterize the liquefaction potential of sand-silt mix soils, an experimental program was developed. Undrained triaxial cyclic tests were performed on large size specimens (typically 74 mm diameter and 150 ~ 160 mm height) prepared using a single host sand (OS55) (OS-F55, Foundry Sand from US Silica Company, Illinois, e_{max}=0.80, e_{min}=0.60, d_{50}=0.24mm) mixed with different amounts of non-plastic crushed silica fines (Sil co sil #40, 99.9% passing sieve #200, d_{50}=0.007mm) at (a) 0%, (b) 15%, (c) 25%, (d) 60% and (e) 100% fines by dry weight.

Cylindrical specimens were prepared by placing soils in four layers or eight layers in a triaxial mold using dry air deposition method or moist tamping method. The specimens were percolated with carbon dioxide for about 5 minutes. After that, deaired water was allowed to flow from the bottom of the specimen towards the top if the specimen was prepared by dry deposition method (If the specimen was prepared by moist tamping method, this step was omitted). The specimen was then backpressure saturated until the B-value ($=\Delta u/\Delta\sigma_c$) was typically greater than 0.95. Following this, the specimens were isotropically consolidated to a constant effective consolidation stress (σ'_c) of 100 kPa. The final void ratio of each specimen was calculated based on the weight of the dry solid grains in the specimen, the net volume of water introduced into the specimen during saturation, and the measured volume change data during consolidation. Stress ratio ($[\pm\Delta\sigma_1/(2\sigma'_c)]$=0.2) controlled undrained triaxial cyclic tests were done at a frequency of 0.2 Hz or 1 Hz. The pore pressure, axial load, and axial deformation were recorded using a built-in data acquisition system.

Results

Fig. 4 shows the locations of the specimens in the intergranular matrix diagram. Fig. 5 shows the number of cycles (N) to cause liquefaction (±5% double amplitude axial strain) versus *e.* Although there is no unique relationship for N versus e for all soils, a distinct trend is observed as FC increases. At low FC ($<FC_{th}$) and at the same *e*, N decreases as the fines content increases. Beyond FC_{th} the trend reverses. This is because at low FC, cyclic strength is governed primarily by intergranular contacts. Beyond $FC_{th,}$ primarily the interfine contacts control the cyclic strength. The respective cyclic strengths are expected to correlate with appropriate intergranular and interfine contact density indices rather than e. This was examined further. The same data are plotted on $(e_c)_{eq}$ (b=0.35) versus N plane and $(e_f)_{eq}$ (m=0.65) versus N plane (Figs. 6a-b). The data points for all soils at $FC < FC_{th}$ fall in a narrow band in Fig. 6a. This indicates that the cyclic strength of these soils can be characterized by the equivalent intergranular void ratio $(e_c)_{eq}$. A similar observation is made in Fig.6b for all soils at $FC>FC_{th}$. The soils at $FC > FC_{th}$ can be characterized by the equivalent interfine void ratio $(e_f)_{eq}$.

Figs. 7a-b examine further the effectiveness of $(e_c)_{eq}$ in a different way using energy required to cause liquefaction (±5% double amplitude axial strain) for $FC>FC_{th}$. No unique relationship exists for e versus energy. At the same e, the energy required to reach

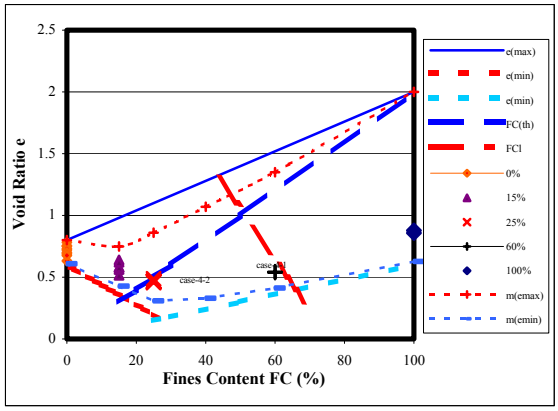

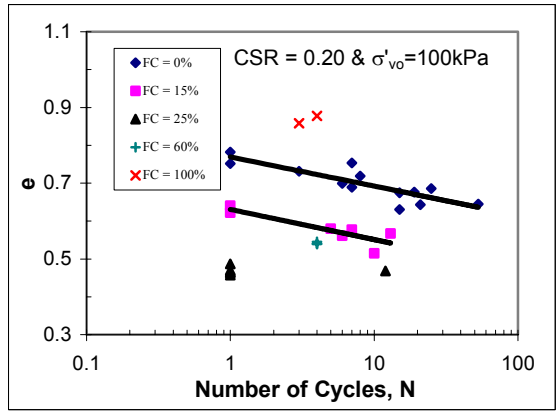

Fig. 4 Intergranular matrix diagram – Ottawa Sand–Silt Mixes

Fig. 5 *e* Vs N (Liquefaction)

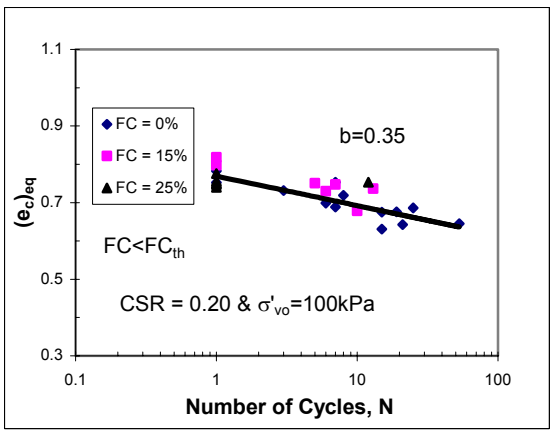

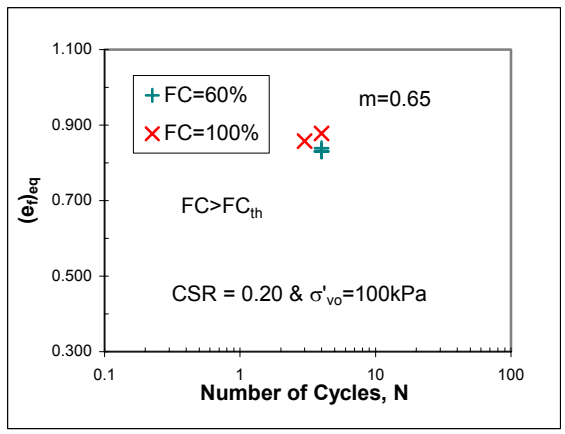

Fig. 6a-b $(e_c)_{eq}$ and $(e_f)_{eq}$ Vs N required to cause liquefaction

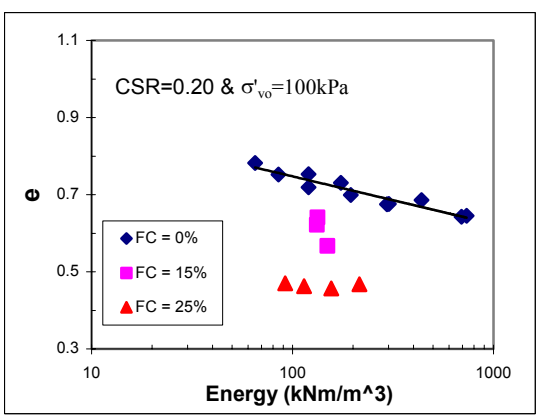

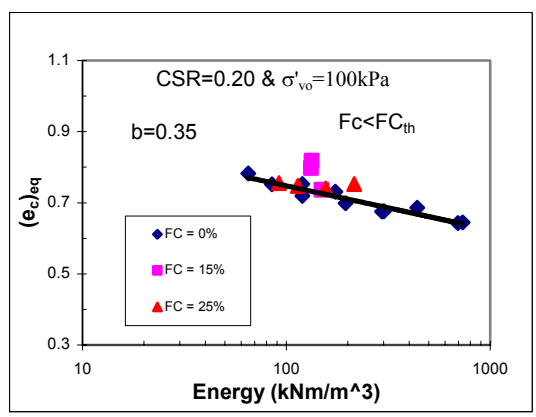

Fig. 7a-b *e* and $(e_c)_{eq}$ Versus Energy required to cause liquefaction ($FC<FC_{th}$)

liquefaction decreases as FC increases. When plotted against $(e_c)_{eq}$, all data for clean sand and silty sand collapse into a narrow band in Fig. 7b similar to Fig.6a.

Conclusions

A simple framework for liquefaction potential analysis of granular mixes with due consideration for the relative influences of inter-coarser granular and interfine contacts is presented. Two equivalent intergranular and interfine contact indices $(e_c)_{eq}$ *and* $(e_f)_{eq}$) are introduced as parameters that control undrained cyclic strength of sand – silt mixes at low FC (< FC_{th}) and high FC (>FC_{th}), respectively. The observations in Figs.6 and 7 together suggest that the proposed contact indices $(e_c)_{eq}$ and $(e_f)_{eq}$ are very useful to characterize the liquefaction potential of granular mixes in a rational way.The present study is limited to gap graded granular mixes. Extrapolations to well graded granular mixes need care. Furthermore, possible influences by differences on the nature of field deposits relevant for built environment versus laboratory also need to be considered.

Acknowledgements

Financial support by the NSF and USGS for this research is gratefully appreciated.

References

Chang, N. Y. (1990). “Influence of fines content and plasticity on earthquake-induced soil liquefaction,” US Army WES, Vicksburg, DACW3988-C-0078

Evans, M. D. and Zhou, S. (1995), “Liquefaction behavior of sand-gravel composites”, ASCE, J. Geoech. Eng., 121(3), 287-298

Georgiannou, V.N., Burland, J.B. and Hight, D.W. (1990), “The undrained behaviour of clayey sands in triaxial compression and extension”, Geotechnique 40, No.3, 431-449

JGS (1996) “Soils and Foundations - Special issue on geotechnical aspects of the January 17, 1995 Hyogoken-Nambu Earthquake”, Japanese Soc. Geotechnical Eng.

Koester, J.P. (1994), "The influence of fines type and conent on cyclic strength", ASCE, Geotech. Spec. Pub. 44, 17-32

Pitman, T.D., Robertson, P.K. and Sego, D.C. (1994), "Influence of fines on the collapse of loose sands", Can. Geotech. J., 31, 728-39

Singh, S. (1994). “Liquefaction characteristics of silts.” ASCE, *Geotech Spec. Publ.* 44, 105-116

Thevanayagam, S. (1998) "Relative role of coarser and finer grains on undrained behavior of granular mixes" in review, J. Geotech. & Geoenv. Eng., ASCE

Thevanayagam, S. and Mohan, S. (2000) “Intergranular state variables and stress-strain behavior of silty sands", Geotechnique, 50(1), 1-23.

Thevanayagam, S. (2000) “Liquefaction potential and undrained fragility of silty soils.” Proc. 12WCEE 2000 Conference, Auckland, New Zealand.

Vaid, Y.P. (1994), "Liquefaction of silty soils", ASCE , Geotech. Sp. Publ. 44, 1-16

Zlatovic, S. and Ishihara, K. (1997). "Normalized behavior of very loose non-plastic soils: effects of fabric” Soils and Foundations, 37(4), 47-56

Addendum

The following changes have been made in the paper: Thevanayagam, S., Liang, J., and Shenthan, T. (2000) "A contact index for liquefaction potential analysis of silty/gravely soils," *EM2000, Proc. 14th ASCE EMD Spec. Conf.*

- In Fig. 7a-b, the X-axis title should be read as E_L (10 J/m^3)

LIQUEFACTION POTENTIAL AND UNDRAINED FRAGILITY OF SILTY SOILS

Sabanayagam THEVANAYAGAM[1]

SUMMARY

Observations from recent earthquake case histories indicate that natural and man made fills containing a mix sands, silt, and/or gravel do liquefy and cause lateral spreads, defying conventional wisdom. The knowledge gained from past three decades of research on clean sands does not directly translate to such soils. Whether the presence of silt adversely or beneficially affects liquefaction and the collapse potential of silty soils is a contentious issue. The mechanisms leading to liquefaction and large deformation in such soils are more complex. This requires a greater understanding of the soil microstructure and the contributions of soil particles of different sizes to its mechanical response. A framework for analysis of the undrained stress-strain behavior, shear strength and collapse potential of granular mixes ranging from clean sands to pure silts (or gravel) in terms of intergranular and interfine friction is presented. The primary mechanisms affecting the mechanical response of silty (or gravely) soils are identified. New intergrain contact indices are presented to evaluate the liquefaction potential and large undrained deformation characteristics at various silt/gravel contents. This is followed by experimental evaluation of the framework. The behavior of such granular mixes deserves a greater detailed study.

INTRODUCTION

Recent earthquake case histories indicate that natural soils and man-made sandy deposits that contain a significant amount of finer-grains (silty sands, clayey sands) and/or gravel do liquefy and cause lateral spreads (Seed et al. 1983, Seed and Harder 1990, JGS 1996). Experience gained from past studies on clean sands does not always directly translate to such broadly graded soils. Recognition of this has lead to several laboratory and field studies to evaluate the effects of increasing silt or gravel content on: (a) cyclic strength, (b) collapse potential, (c) steady state strength, (d) shear wave velocity, etc. Results from laboratory studies on clean sands mixed with non-plastic silts or plastic fines show that, at the same (global) void ratio, the steady state strength and cyclic strength of silty sand decreases with an increase in fines content (Chang 1990, Chameau and Sutterer 1994, Georgiannou et al. 1990,91a-b, Vaid 1994, Koester 1994, Finn et al. 1994, Pitman et al. 1994, Singh 1994, Zlatovic and Ishihara 1995, 1997, Thevanayagam et al. 1996). An example is shown in Fig.1a for a soil prepared by mixing a sand with a silt (PI=4) at nearly constant global void ratio (e=0.558) and confining stress (104 kPa) but at different fines content (0 to 60% by weight). Fig.1b shows the number of cycles to reach initial liquefaction versus fines content for the same sand-silt mix, along with the data for two other sands mixed with the same silt. [Fig.1c which is the same as Fig.1b will be discussed later]. As observed in these figures, beyond a certain transition range the trend in decrease of strength reverses and the strength increases with further increase in fines content. The transition fines content range is about 20 to 30% for non-plastic fines (Vaid 1994, Kuerbis et al. 1988, Singh 1994, Koester 1994). It is less than 20% for clayey fines (Georgiannou et al. 1991a-b). The physical meaning of the transition fines content is not clear. The conclusions in the literature on whether the presence of fines is beneficial or not is contentious. Similar concerns prevail regarding gravely soils (Evans and Zhou 1995).

[1] *Dept. Civil, Struct., & Env. Eng., State Univ. of New York, 212 Ketter ,Buffalo, NY 14260; Email: theva@eng.buffalo.edu*

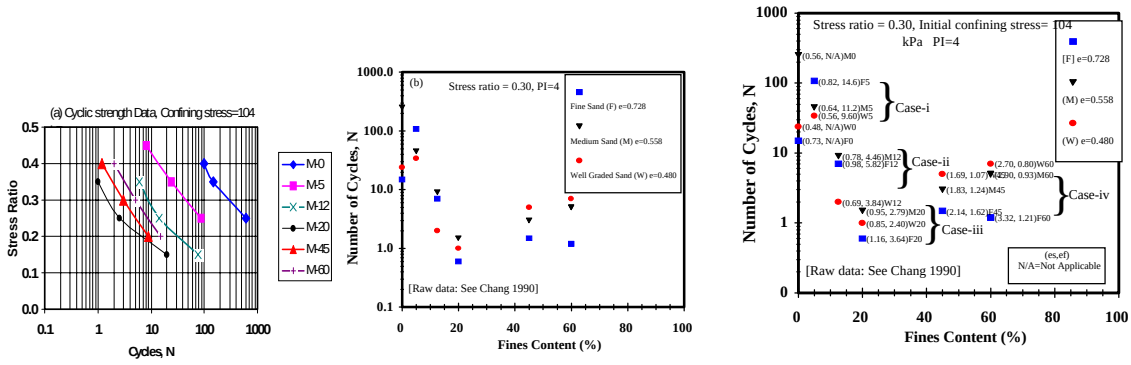

Fig.1. Influence of finer grain content on cyclic strength – (a) Medium Sand, (b,c) Three Sands

Taking a different approach, field performance studies have sought to solve this problem by correlating SPT blow counts, CPT data, and shear wave velocity measurements with liquefaction potential in a binary fashion based on observations of liquefied sites. Such correlations have also been developed for post-liquefaction strength based on back-analysis of failed embankments. Various corrective procedures have been incorporated to account for the influence of fines (Seed et al. 1983, Seed 1987, Seed and Harder 1990, Robertson et al. 1997, Andrews and Stokoe 1997). Their use in practice relies on such intuitive reasoning as the impeding drainage effect of fines on such field measurements and/or their relation with relative density. There are variations as well (Stark and Mesri 1992, Ishihara 1993, Baziar and Dobry 1995) on the nature of such relationships. Questions also prevail among practicing engineers on broad applicability of the field correlations to all (new) sites.

No consensus exists on how to characterize liquefaction resistance, collapse resistance, and post-liquefaction strength of silty sands, sandy silts, and gravely soils.

In this regard, recently, it has been brought to the attention that physical nature of silty sands and gravely sands is entirely different from clean sand (Thevanayagam 1998a-b, 1999, Thevanayagam and Mohan 1998). As the void ratio and proportion of the coarser and finer grains content of these soils change the nature of their microstructure also changes. The relative participation of the particles of very different sizes in the *internal interparticle contact force chain* also changes. Due to particle size disparity and availability of pores larger than some particles, at low finer grains content some of the finer particles may remain inactive or move between pores without significantly affecting or contributing to the force chain. Yet they contribute to the global void ratio. Alternately when there are sufficient amount of finer grains the coarser grains become dispersed contributing much less to the force chain than to the global void ratio. Global void ratio e ceases to be an index to represent the nature of contact density of active particles. The traditional use of e to compare the behavior of soils containing different amounts of fines content ceases to be valid. The same holds for relative density.

In general the stress-strain behavior, liquefaction potential, and fragility of granular mixes are affected by a critical combination of *intergranular and interfine contacts* and the physical and physico-chemical interactions thereof. The combined effects of intergranular and interfine contacts must be delineated in dealing with silty sands and gravely soils in understanding the mechanisms leading to liquefaction and post-liquefaction deformation, and the mechanical response of the media in general. New indices of active contacts are needed to represent the nature of intergrain contacts inorder to characterize the behavior of such soils. It is thought that recognition of these factors may help to bring about a rational method for liquefaction potential assessment of silty and gravely soils.

Using a two-sized particle mix as a model, this paper highlights the nature of the microstructure of granular mixes. Based on this such granular mixes are classified into certain groups (Fig.2) depending on the relative frictional contributions at the intergranular and interfine grain contact level. Intergranular (e_c) (Mitchell 1993), interfine (e_f) (Thevanayagm 1998a), and equivalent interfine $(e_f)_{eq}$ (Thevanayagam 1998b) void ratios (Fig.3) are introduced as primary indices of contact density for the various groups. Global void ratio is introduced as a secondary index. The range of void ratio and fines content where each group (Fig.2) belongs to is conveniently shown in a global void ratio versus fines content diagram (Fig.4). This is followed by reanalysis of observed cyclic behavior of silty soils at various silt contents using the above indices. Detailed theoretical developments and experimental evaluations are presented elsewhere (Thevanayagam et al. 1999, Thevanayagam 1998a-b, 1999).

CONCEPTUAL FRAMEWORK

Microstructure

Consider a two-sized granular mix. The microstructure of this granular mix can be constituted by infinite different ways. Each one of them leads to a different internal force chain network among particles and hence each exhibits a different stress-strain response during shear. Among infinite variations, a few extreme limiting categories of microstructure and the relevant roles of coarser and finer grains are as follows.

Case-i: The first category (Fig.2a) is when the finer grains are fully confined within the void spaces between the coarser-grains with no contribution whatsoever in supporting the coarser grain skeleton. Finer grains are inactive (or secondary) in the transfer of inter particle forces. They may largely play the role of "filler" of intergranular voids. The mechanical behavior is affected primarily by the coarser grain contacts. During deformation the finer grains may move from one pore space to another without significantly contributing to the mechanical response of the soil. This requires that the finer grain particle size (d) is much smaller than the pore size between the coarser grains and that the intergranular pore space is not completely filled with the finer grains. Typically this requires that the coarser grain size (D) is atleast 6.5 times larger than the finer grain size, and that the finer grain content (FC) is less than a certain threshold value (FC_{th}). This category is called *case-i*. Even at low FC, if the size disparity R_d (=D/d) is not very large, the finer grains cannot freely move through the inter-coarser granular voids; They also tend to participate in the force chain and actively contribute to the stress-strain response.

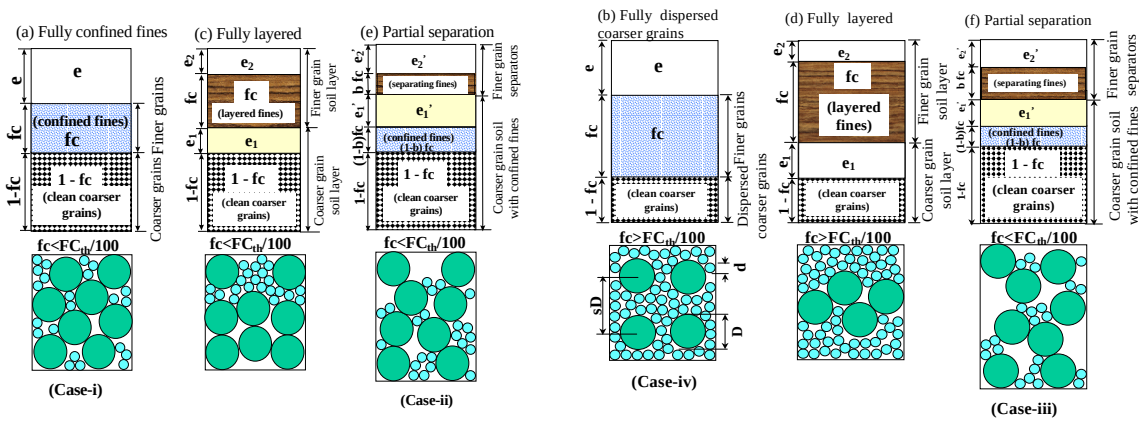

Fig.2 Microstructure and intergranular matrix phase diagram

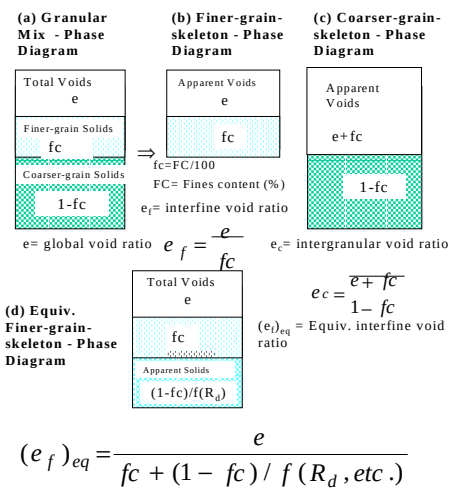

$$e_f = \frac{e}{fc}$$

$$e_c = \frac{e + fc}{1 - fc}$$

$$(e_f)_{eq} = \frac{e}{fc + (1 - fc)/f(R_d, etc.)}$$

Fig.3 Intergranular contact indices

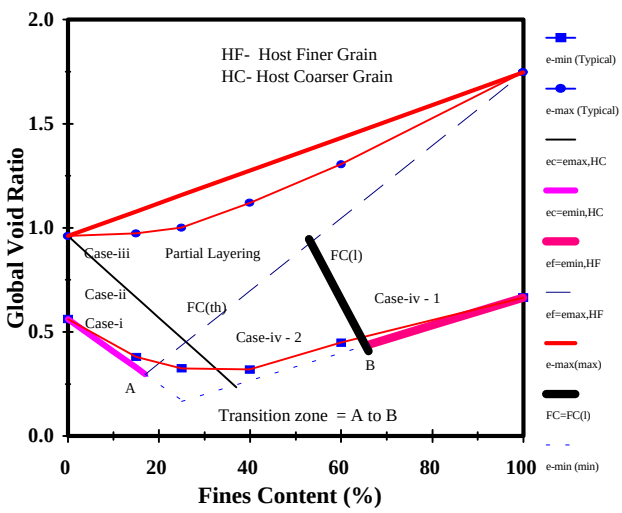

Fig.4 Intergranular matrix diagram – Mix Classification

Cases-ii and iii: Consider changing the microstructure shown in Fig.2a in two ways: (1) alter the position of some of the finer grains, or (2) add more finer grains. The consequences are significant. If one alters the position of some of the finer grains, while maintaining the finer grain content the same, the microstructure corresponding to the second and third categories shown in Figs.2e and f are obtained with a concurrent increase in global void ratio. Essentially, the microstructure in Figs.2e-f is made up of partial layering and partial separation of coarser grains by the finer grains along with confined finer grains within the voids between the coarser grains. Some of the finer grains become active participants in the internal force chain. These finer grains are termed the *'separating fines*' in Figs.2e and f. In Fig.2e, the finer grains may be supporting the coarser-grain skeleton that is otherwise unstable. They act as a load transfer vehicle between "some" of the coarse-grain particles in the soil-matrix while the remainder of the fines play the role of "filler" of voids. They may dominate the initial stress-strain behavior depending on the type of finer grains (plastic or non-plastic). In Fig.2f, the finer grains may play an active role of *"separator"* between a significant number of coarse-grain contacts and therefore begin to dominate the strength characteristics. Coarser grain skeleton is virtually unstable without the finer grains. These two categories of microstructure are called cases ii and iii, respectively. Case-ii is a transition between cases i and iii. Theoretically case-iii occurs at an intergranular void ratio exceeding the maximum void ratio (emax.HC) achievable for the 'pure' coarser grain soil.

Cases-iv-1 and iv-2: On the other hand if one increases the finer grains content sufficiently, one gets the fourth category (Fig.2b). It occurs naturally when sufficient finer grains are present making active contacts among themselves. The coarser grains begin to disperse in the finer grain matrix. Transition from Fig.2a to Fig.2b occurs when the finer grains content (FC) exceeds beyond the threshold fines content (FC_{th}). When $FC>FC_{th}$ the finer grains begin to play a rather important role while the role of coarser grains begin to diminish. The fines may carry the contact and shear forces while the coarser grains may act as *reinforcing elements* embedded within the finer grain matrix. The effect of coarser grains cannot be completely neglected until they are separated sufficiently apart. This imposes a limiting fines content FC_l. There exists a transition zone between FC_{th} and FC_l before the behavior of the soil mix is entirely governed by the finer grains. This is called case-iv-2 whereas the case corresponding to $FC>FC_l$ is called case-iv-1. The size disparity constraint discussed before for cases i to iii needs not be satisfied for case-iv.

The fifth category (Figs.2c-d) is when the coarser and finer grains constitute a fully layered system where the coarser grain layers have no fines contained in them and vice versa. This is called case-v. It is also possible to create a composite system that contains some of the cases i through v. The figures 2a, c, e and f are more relevant at low finer grains content. Figs. 2b and d are relevant at high finer grains content.

Contact Indices

Case-i: Up to $FC=FC_{th}$ the finer grains can, but not necessarily, remain within the intergranular voids. Provided that the size disparity is large and the coarser granular skeleton is dense whether or not some of the finer grains fall between the coarser grain contacts or remain fully confined within the intergranular voids does not significantly affect the shear strength of the soil. Primarily the intergranular contacts between the coarser grains affect the mechanical behavior with secondary effects by the finer grains. Hence, neglecting the effects of fines, the *inter-coarser grain void ratio* e_c (=[e+fc]/[1-fc], fc=FC/100, Fig.3c) may be used as an index of active contacts. The magnitude of e_f (=e/fc) may be used as an index to assess the secondary effects by the finer grains.

Cases-ii and iii: For these cases, still the inter-coarser grain contact plays a significant role. However, the influence of finer grains supporting the coarser grains must also be accounted for in devising an index of active contacts. The relevant contact index void ratio would be [e+(1-b)fc)]/[1-fc+bfc] (Fig.2). Hence, although it may be possible to use e_c as an index of active contacts for these cases, it is expected the mechanical behavior of such mixes would be different and generally stronger than that of the host coarser grain soil at the same *ec*.

Case-iv: When $FC>FC_l$, for case-iv-1, neglecting the effects of dispersed coarser grains, the *interfine void ratio* e_f (=e/fc, Fig.3b) may be used as an index of active contacts. At $FC_{th}<FC<FC_l$, neither e, e_c, nor e_f can sufficiently represent the active contacts, alone, although all of them together can be used to deduce the mechanical response. Devising a primary index of active contacts in this range is useful, however.

For a granular mix in this range the global void ratio e overestimates the actual density of active contacts in the granular mix. This is so because the dispersed coarser grains in the mix do not contribute as many active contacts as if the soil was prepared at the same void ratio by substituting each coarser grain by an equal (solid) volume of finer grains. The reason is that solid volume of a dispersed coarser grain, which directly influences the global void ratio, grows in proportion to the power of three of size. Whereas its surface area, which influences the

nature of contacts with the surrounding finer grains, grows in proportion to the power of only two. For equal solid volume, the substituted finer grains have a larger surface for contact than a dispersed coarser grain of equal (solid) volume embedded in the finer grain medium. The density of contacts in the mix is smaller than that in the finer grain soil at the same e. Hence e overestimates the active contacts in the mix.

The use of e_c as an index of active contacts is not valid since it ignores entirely the existence of interfiner grain contacts. It grossly underestimates the active contacts. Similarly, the interfine void ratio e_f also underestimates the active contacts, since it completely ignores the presence of the dispersed coarser grains. The latter do make contact with the surrounding finer grains and participate in the force chain. The effects of such contacts may not be negligible unless the spacing between the dispersed coarser grains is very large. The reinforcement effect by the coarser grains must also be introduced to obtain an equivalent interfine void ratio $(e_f)_{eq}$ as the index of active contacts. The equation for e_f must be modified accordingly.

Combining the above arguments e_f should be modified by accounting for the contacts made by the coarser grains with the surrounding finer grains. Theoretically, after simplifications, this leads to a form of the type, $(e_f)_{eq} = e/[fc+(1-fc)/(R_d)^m]$ (Figs.2b and 3d, exponential m), and m=a coefficient satisfying $0<m<1$, $e_c>e_{max,HC}$ (Thevanayagam 1998b). The value of m ranges between about 0.4 to 0.5 for non-plastic granular mixes.

Intergranular Matrix Diagram: Conceptually Fig.4 shows the regions belonging to the four cases i through iv confined by various transition boundaries. The transition lines corresponding to the threshold and limiting fines contents are given by:

$$FC_{th} \le \frac{100 e_c}{1+e_c+e_{max,HF}}\% = \frac{100\,e}{e_{max,HF}}\% \;; \qquad FC_l \ge 100\left[1-\frac{\pi(1+e)}{6s^3}\right]\% = 100\left[\frac{\frac{6s^3}{\pi}-1}{\frac{6s^3}{\pi}+e_f}\right]\% \ge FC_{th};\; e_f \le e_{max,HF} \qquad (1)$$

where $s=1+a(d/D)=1+a/R_d$ where a=10 (approximately). The rationale behind the equation for FC_{th} is that once the interfiner grain void ratio drops below $e_{max,HF}$ (the maximum void ratio achievable for the 'pure' finer grain soil) the finer grains begin to make active contacts among themselves and contribute to the force chain. The reasons leading to the derivation of the expression for FC_l may be attributed to the observations of Roscoe (1970) that the zone of influence of shear is about 10 times the diameter of particles. The various other boundaries refer to the maximum and minimum void ratio profiles: $e=e_{max,HC}+(e_{max,HF}-e_{max,HC})\,fc$; $e_c=e_{max,HC}$; $e_f=e_{max,HF}$; $e_c=e_{min,HC}$; and $e_f=e_{min,HF}$.

Mechanical Behavior

The aforementioned contact indices and the location of a soil mix in Fig.4 can be used as aids to predict the trends of the stress-strain characteristics, liquefaction potential, and fragility of silty or gravely soils (prepared by the same method at the same confining stress) *relative* to that of the host coarser grain soil or the finer grain soil. Fig.5 shows a schematic diagram for *hypothetical* specimens satisfying the following specific constraints: (1) an increase in global void ratio e at the same fines content [specimens 1,2,3], (2) an increase in fines content at a constant global void ratio e [4,2,5,6,7,13], (3) an increase in fines content at the same intergranular void ratio e_c [8,1,9 or 3,10 or 14,2,15; $FC<FC_{th}$], or (4) an increase in coarser grain content at the same interfine void ratio e_f [11,7,12; $FC>FC_{th}$].

Relative Trends -- Cyclic Strength and Fragility: The anticipated trends in number of cycles (N) required to cause initial liquefaction at the same cyclic stress ratio are *schematically* shown in Fig.5 [N versus FC]. In (1) both intergranular and interfine void ratios increase with concurrent reduction in inter-coarser grain contacts. Therefore the soil becomes weaker. In (2) while e_c increases e_f decreases. Viz. the inter-coarser granular contacts decrease while the interfine contacts increase. Hence initially the soil is expected to weaken [4,2,5] followed by a transition in the vicinity of $e_f=e_{max,HF}$ ($FC=FC_{th}$). The soil becomes stronger beyond that [6,7,13]. In (3), the increase in cushioning effect by the fines is manifested leading to a slight increase in strength [3,10, case-iii]. The specimen 10 is expected to be somewhat more resistant to collpase than the specimen 3. This effect, however, diminishes gradually if the soil becomes denser in terms of e_c [case-ii]. The reason is that when e_c is small (dense coarser grains) the relative effect of fines is less appreciable compared to the direct coarser-coarser grain contact resistance until e_f becomes sufficiently low. In (4) when the soil is at a fines content less than FC_l but greater than FC_{th} [11,7,12] the reinforcement effect of the coarser grain 'inclusions' may affect the stress strain behavior. The specimen 11 is expected to be stronger than 7. Again this reinforcement effect may become relatively small compared to the direct finer-grain-to-finer-grain contact resistance when e_f is small (dense

interfine contacts). Once FC exceeds FC_l the reinforcement effect is expected to be small. Primarily the interfine contacts and e_f are expected to affect the soil behavior [7,12]. Without elaboration, the remaining figures show the relative trends for N for various cases i through iv plotted against the relevant contact indices (e_c, e_f, and $(e_f)_{eq}$).

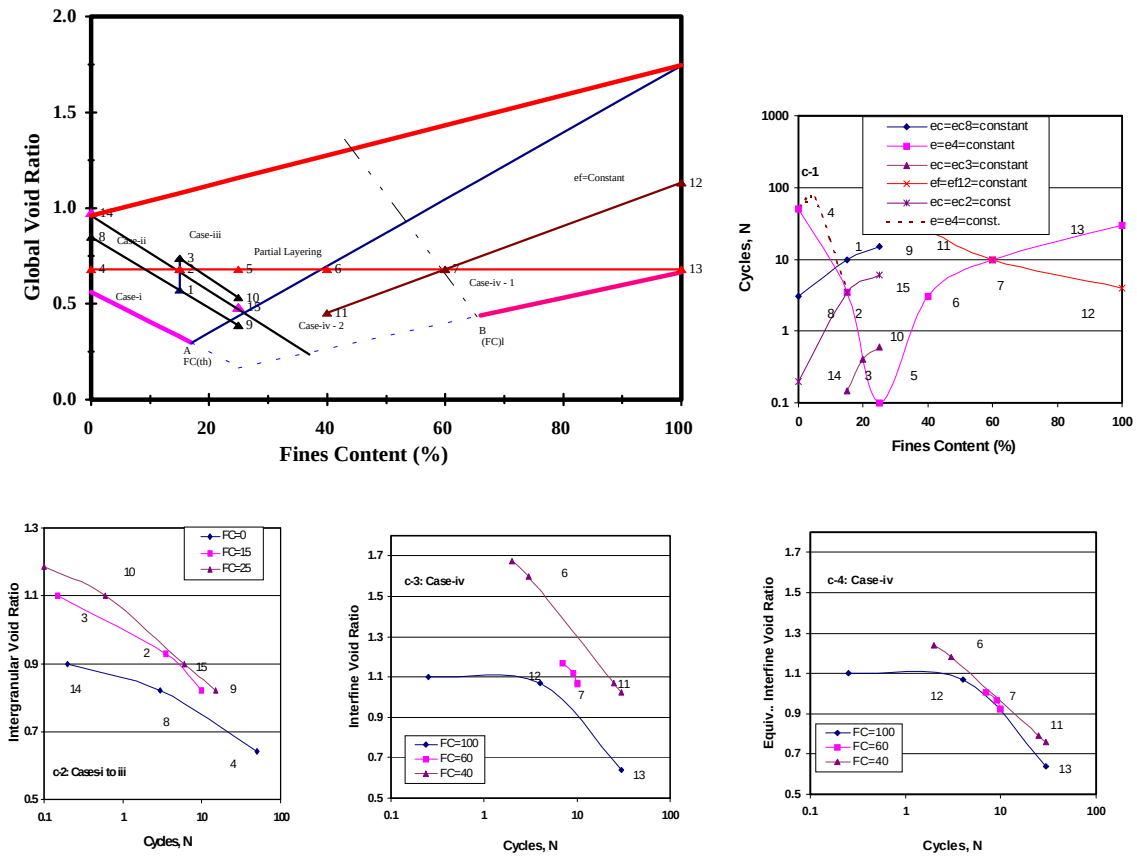

Fig.5 Relative trend in cyclic strength – Schematic.

EXPERIMENTAL EVALUATION

A limited set of experimental data is available in support of the above conceptual framework. In order to save space, only the data shown in Fig.1b is recalled again in Fig.1c, 6 and 7 to illustrate the various roles of coarser and finer grains on the behavior of granular mixes. A series of other papers (Thevanayagam et al. 1999, Thevanayagam 1999) present the results of detailed analyses of other experimental data.

Intergranular Matrix Diagram: Figs.6a-c show the intergranular matrix diagram for three host sands [(1) Fine (F), (2) Medium (M), and (3) Well graded (W)] mixed with a low plasticity fines (PI=4) tested by Chang (1990), reported in Fig.1. The locations of the specimens are also shown. Each sand mix was tested at 0, 5, 12, 20, 45, and 60% fines content. The specimens were prepared by moist tamping method. All specimens were consolidated to the same initial confining stress (104kPa). The specimens for each soil mix were tested at nearly constant global void ratio: e=0.728 for F, e=0.558 for M, and e=0.480 for W, respectively. These void ratios correspond to about 50% relative density of the respective parent sands. No data were available for $e_{max,HF}$ and $e_{min,HF}$ for the silt. For qualitative discussion purposes the threshold boundary may be estimated assuming typical values of $e_{max,HF}$ =1.5 and $e_{min,HF}$ =0.6. Also for illustration purposes the R_d (defined as D50/d50) values for the soils F, M, and W were estimated to be about 15, 40, and 40 based on a typical value for d50 of silts. An examination of Fig.6 and calculated index void ratios would readily reveal the cases each specimen belongs to and the expected behavior of each granular mix relative to one another.

Cyclic Strength variation with Increase in FC: Fig.1c shows the same cyclic strength data shown in Fig.1b. The e_c and e_f values for each specimen and the respective cases each specimen belongs to are also shown in this figure. As the fines content increases, at the same global void ratio e, the e_c increases and e_f decreases. Initially the ef remains high to be of any significance, alone. With increase in FC the soil mixes move gradually from

Case-i to Case-ii to Case-iii and then cross over to Case-iv-2. So is the behavior of the soils. Initially the strength decreases due to reduced intergranular contacts with increase in e_c with little or secondary contribution from the fines. As the soil moves beyond the threshold transition zone (FC_{th} at $e_f = e_{max,HF}$) and enters the zone for Case-iv-2 the influence of e_f becomes important with some reinforcement effect by the coarser grains. The $(e_f)_{eq}$ becomes the primary contact index void ratio. The trend reverses and the strength begins to increase with further increase in fines content.

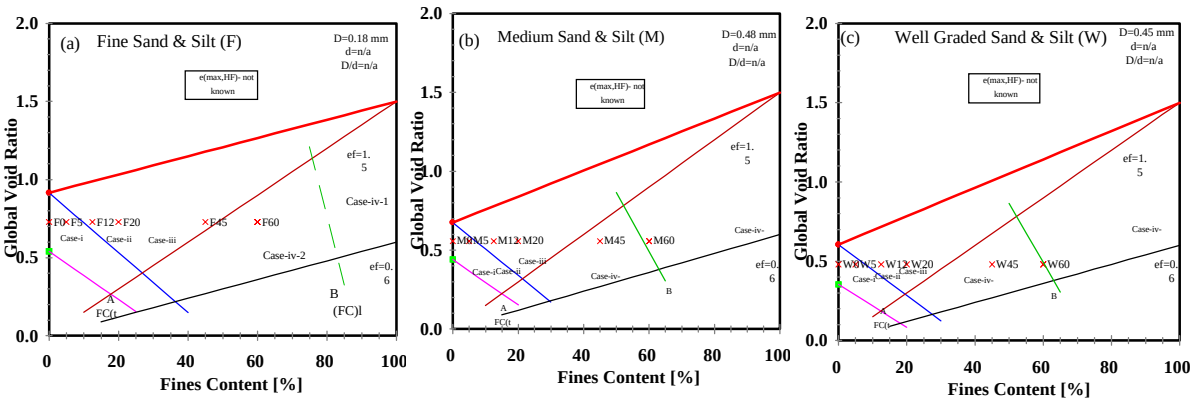

Fig.6 Intergranular matrix diagrams – Three Sand – Silt Mixes

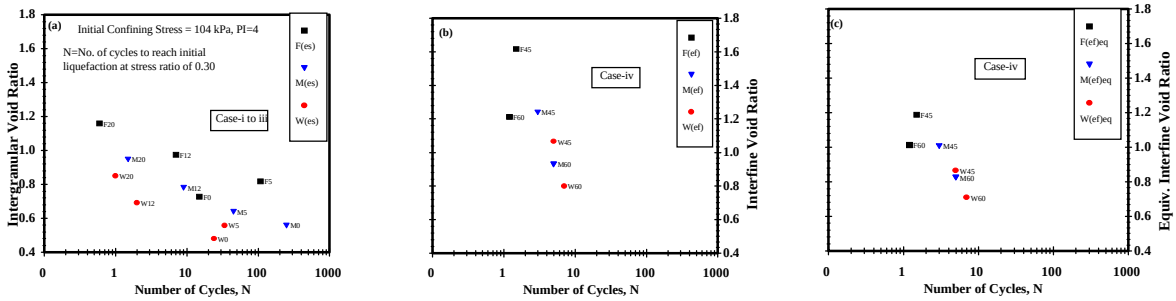

Fig.7 Influence of intergrain contacts on cyclic strength: (a) e_c, (b) e_f, and (c) $(e_f)_{eq}$

The transition fines content FC_{th} is slightly different for each soil mix. Theoretically it corresponds to the intersection of the constant global void ratio line with the $e_{max,HF}$ line. For the same host fines, typically a soil mix at a smaller global void ratio (Fig.6c) will cross the $e_{max,HF}$ line and reach Case-iv-2 at a smaller fines content than a soil mix at a higher global void ratio (Fig.6a). Hence, the soil W (at e=0.480) reaches this transition at smaller fines content than the soil F (at e=0.728).

$FC<FC_{th}$: Fig.7a show the same data in a different format: Number of cycles to initial liquefaction versus e_c for Cases-i to iii [$FC<FC_{th}$]. For this case, a different cyclic strength profile is obtained for each mix depending on the parent sand type (F,M,W). N is affected primarily by the parent sand type. e_c becomes the primary index of active contacts. The fines have a secondary role. It would be more revealing if (if available) the data for each host sand are superimposed in this figure permitting a comparison of the kind shown in Fig.5 (e_c versus N).

$FC>FC_{th}$: Fig.7b show the N versus e_f data for Case-iv. N data show significant dependency on interfine void ratio e_f. The data for each fines content (45% and 60% separately) correlates well with e_f and fall in a (separate for 45% and 60%) narrow band regardless of the parent sand type. The separate narrow bands for the soils mixed with 45% fines and 60% fines are due to the differences in the degree of reinforcement effect. At the same e_f, the cyclic strength is higher for the soil with higher sands content. The reinforcement effect is higher at 45% fines content than at 60% which is approaching the limiting fines content FC_l. Nevertheless, at low e_f (dense interfine contacts) the relative effect of reinforcement becomes less appreciable compared to direct interfine contact friction. The separate bands for 45 and 60% merge together at low e_f. Fig.7c shows the same data, plotted against equivalent interfine void ratio $(e_f)_{eq}$ [calculated assuming m=0.45). Interestingly the number of cycles required to cause liquefaction correlates with $(e_f)_{eq}$ for all cases of iv. The reason for this is that all sands were mixed with the *same silt*. Hence, once FC exceeds the threshold value, all soil mixes are affected by the same silt except for the minor differences due to the presence of different size coarser grains (F,M,W). Hence a single narrow band is obtained in Fig.7c. It would be more revealing if (if available) the data for the silt is superimposed in this figure permitting a comparison of the kind shown in Fig.5 [$(e_f)_{eq}$ versus N].

CONCLUDING REMARKS

A simple framework for analysis of the relative effects of inter-coarser granular and interfine contacts on the undrained behavior of granular mixes is presented. Intergranular and interfine void ratios are introduced as indices of active contacts. For a granular mix with large size disparities between grain sizes, at low finer grains content less than a threhold value, if and when the finer-grains are fully confined to the void spaces without providing any support to the coarser grain skeleton the stress-strain behavior of that soil can be deduced using the coarser-grain skeleton void ratio (e_c) as an index with secondary beneficial effects derived from the fines. FC_{th} occurs when the intergranular voids are filled with finer grains at the loosest possible packing of the fines. At $e_c << e_{max,HC}$ and FC<FC th the soil mix is categorized as case-i. The secondary beneficial effect of fines is the least when the soil is dense (low e_c). The beneficial effect is the highest when the intergranular skeleton is loose and the intergranular void ratio is close to its maximum void ratio possible for the host coarser grains ($e_{max,HC}$). This is categorized as case-ii behavior. In reality, however, even at $FC<FC_{th}$ the finer grains are not confined strictly within the intergranular voids. The fines can also play the role of separator of coarser grain contacts and constitute a loose and metastable structure. This occurs typically when $e_c>e_{max,HC}$. This is denoted as Case-iii behavior. When FC exceeds FC_{th} the finer grains begin to exert a major role on the stress-strain response of the soil. The coarser grains act as reinforcements embedded within the finer grain matrix. This occurs until FC exceeds a limiting fines content FC_l. Beyond this, the behavior of sandy silt is primarily governed by the interfine void ratio e_f. This is categorized as case-iv-1 behavior. In the intermediate range ($FC_{th}<FC<FC_l$) both interfine void ratio and coarser grains influence the soil behavior. Neither the intergranular nor the interfine void ratio alone can be the sole index of the behavior of a silty sand and sandy silt in this range. This is categorized as case-iv-2 behavior. An equivalent interfine void ratio $(e_f)_{eq}$ may be used as an index. Obviously the zones of these behaviors (Fig.4) are not rigid, but rather consist of smooth transitions embedded between them.

With this framework, one may deduce the behavior of granular mixes at various finer grains contents and void ratios relative to the behavior of the host coarser grain soil or the finer grain soil. Based on this framework and reinterpretation of a limited amount of experimental data the following observations could be made about the liquefaction potential and fragility of granular mix prepared at the same initial confining stress. (a) When compared at the same e_c, an increase in finer grains content reduces the collapse potential, (b) When compared at the same e_f, an increase in finer grains content increases the collapse potential, (c) When compared at the same $(e_f)_{eq}$, an increase in finer grains content slightly increases the collapse potential, and (d) When compared at the same global void ratio e the collapse potential increases with an increase in finer grains content up to a certain threshold value FC_{th}. Beyond that the collapse potential decreases. FC_{th} depends on the host fines, size disparity ratio, and the global void ratio. The question remains on the possible differences on the nature of field deposits relevant for built environment versus what is studied in the laboratory.

These considerations need to be rationally incorporated in evaluating observed field performances at past earthquake sites and its extrapolations to predict the anticipated field performance at other sites. Correlations of SPT, CPT, and shear wave velocity data versus observed seismic response of ground need to be studied further beyond the traditional consideration for impeding drainage effects.

Acknowledgements: Financial support for the ongoing research by the NSF is gratefully appreciated. Thanks are also due to J. Koester of US Army Corps of Engineers for providing some of the data included in this paper.

REFERENCES

Due to space limitations only a few refernces are cited herein. Details of these references may be found in (1) Thevanayagam, S. (1998a) "Effect of fines and confining stress on steady state strength of silty sands," J. Geotech. & Geoenv. Eng., ASCE, 124(6), 479-491; (2) Thevanayagam, S. (1998b) "Relative role of coarser and finer grains on undrained behavior of granular mixes" in review, J. Geotech. & Geoenv. Eng., ASCE; (3) Thevanayagam, S. and Mohan, S. (1999) "Intergranular state variables and stress-strain behavior of silty sands" in press, Geotechnique; (4) Thevanayagam, S. (1999) "Role of intergrain contacts, friction, and interactions on undrained response of granular mixes" Proc. workshop *Physics and mechanics of soil liquefaction*, A.A. Balkema press; (5) Chang, N.Y. (1990) "Influence of fines content and plasticity on earthquake-induced soil liquefaction", Contract Rep., US Army WES, Vicksburg, MS Contract No. DACW3988-C-0078.

5.2.1.6 EFFECTS OF NONPLASTIC FINES ON THE LIQUEFACTION RESISTANCE OF SANDS[a]

Discussion by: S. Thevanayagam[2], M. ASCE, J. Liang[3] and T. Kanagalingam[3]

The authors are to be congratulated for presenting a valuable set of cyclic triaxial test data for two sands (Monterey sand and Yatesville sand) each mixed with non-plastic silt (Yatesville silt) and the implications of their finding on field liquefaction screening using penetrations resistance.This discussion raises some questions on the authors' interpretation of the data, offers an intergrain contact density based interpretation, and discusses further effects of fines that needs to be considered in liquefaction screening using penetration resistance.

Fig.6 shows the cyclic resistance required to cause initial liquefaction in 15 cycles of loading versus void ratio data for Monterey sand – silt mix. Defining the "sand skeleton void ratio" as "the void ratio that would exist in a silty sand if all of the silt particles were removed, leaving only the sand grains and voids to form the soil skeleton", the authors re-plot the same data against sand skeleton void ratio in Fig.9. The writers believe that there is ambiguity as to how the authors calculated the sand skeleton void ratio. For example, according to the authors' definition, the sand skeleton void ratio for one of the 35% silt content specimen tested at a void ratio of 0.471 should be about 1.263 (=(0.471+0.35)/(1-0.35)) and 2.092 (=(0.546+0.5)/(1-0.5)) for one of the specimens at 50% silt content shown in Fig.6. The magnitudes of sand skeleton void ratios shown in Fig.9 are significantly different for these and many other specimens. An examination of Polito (1999) shows that the calculations for sand skeleton void ratios are sometimes correct (Fig.4.8, Polito 1999), and sometimes not (Fig.4.7, Polito 1999). Fig. A shows the same data plotted against sand skeleton void ratio, recalculated according to the authors' definition. Fig.A significantly differs from Fig.9.

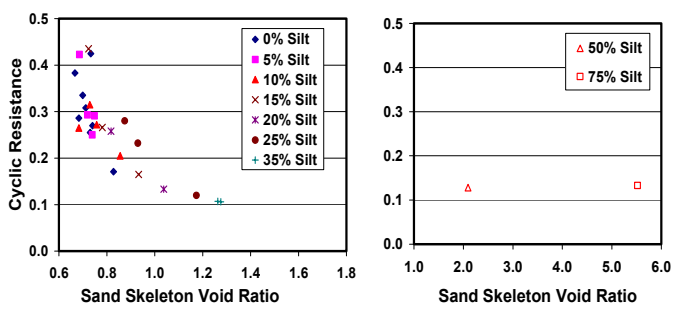

Fig.A Cyclic Resistance Vs Sand Skeleton Void Ratio

The writers have conducted a detailed study on the relative influences of the coarse and fine grains on the mechanical response of a gap graded granular mix (Thevanayagam 1999, Thevanayagam 2000a, Thevanayagam et al. 2000). A scrutiny of the authors' data using this framework is very useful. How and when coarse and fine grains contribute to the mechanical response of a granular mix is a complex problem. It depends on a number of factors, including fines content, void ratio, size disparity, particle shape, and gradation of the host coarse and fine grain soils.

Consider a two-sized granular mix containing coarse and fine particles of size D and d, respectively (Fig.B). The microstructure of this granular mix can be constituted by many different ways. Each one of them leads to a different internal force chain network among particles and hence each exhibits a different stress-strain response during shear. Among many variations, a few extreme limiting categories of microstructure are as follows. The first category in Fig.B-a occurs when the fine grains are fully confined within the void spaces between the coarse-grains with no contribution whatsoever in supporting the coarser grain skeleton. This requires that the fine grain particle size (d) is much smaller than the pore size between the coarse grains (R_d=D/d>>6.5). It is also essential that the fine grain content (FC) is less than a certain threshold value (FC_{th}) such that the inter-coarser granular voids are not completely full of fine grains so that they do not constitute a contact force chain among the fine grains themselves. The threshold state occurs when FC is sufficiently high so that direct fine-grain-to-fine-grain contacts begin to constitute a strong force chain. Soil microstructure that satisfies the two constraints ($FC<<FC_{th}$ and R_d>>6.5) is categorized as case i. FC_{th} is given by 100e/ $e_{max,HF}$, where $e_{max,HF}$ is the void ratio of the host fine grain soil above which it has no appreciable strength.

Consider changing the microstructure shown for case i in two ways: (a) alter the position of some of the fine grains while maintaining the fine grain content, or (b) add more fine grains. In (a), a microstructure corresponding to case ii or iii in Fig.B-a forms with a concurrent increase in global void ratio. Essentially, the microstructure for these cases is made of a coarse grain skeleton where some of the coarse grain contacts form via fine grains while some fine grains remain confined within the voids between the coarse grains. The portion of the fine grains that actively participate in the internal contact force chain is termed the 'separating fines'. If FC exceeds sufficiently beyond FC_{th}, the fourth category (Fig.B-b) occurs naturally. The fine grains make active contacts among themselves while the coarse grains disperse and act as embedded reinforcement elements within the fine grain matrix until they disperse sufficiently far from each other. This imposes a limiting fines content FC_I. Beyond FC_I, fine-grain-to-fine-grain contact governs the behavior of the soil mix. The transition zone between FC_{th} and FC_I is case iv-2 and the zone corresponding to $FC>FC_I$ is case iv-1. The fifth category (Fig.B-c) occurs when the coarse and fine grains constitute a fully layered system. This is case-v. It is also possible to create a composite system that contains some of the cases i through v.

Fig.B presents a simple scheme for mechanical behavior classification of such granular mixes. Based on contact density (per grain) considerations, equivalent intergranular void ratios have been developed as indices of active grain contact density for each of the above cases as shown in Fig.B. Neglecting differences in specific gravities between the coarse and fine grains, e_c is the coarse grain (sand) skeleton void ratio. It is applicable when the fine grains remain fully confined within the coarse grain skeleton with no contribution to the contact force chain within the mix. For reasons discussed before, however, fine grains do contribute to the contact force chain. In such cases, an equivalent intergranular void ratios $(e_c)_{eq}$ has been defined as the contact density index. The term b in $(e_c)_{eq}$ refers to the contribution by fine grains to the force chain. Similarly, for case iv-1, an equivalent interfine void ratio $(e_f)_{eq}$ has been defined as the contact density index. The term m in $(e_f)_{eq}$ refers to the contribution by dispersed coarse grains to the force chain. At $FC>FC_I$, an interfine void ratio e_f has been defined as the contact density index. e_f is the void ratio of the fine-grained soil, assuming that the coarse grains are absent.

[a] May 2001, Vol. 127, No. 5, by C.P. Polito and J.R. Martin II (Paper 20854)

[2] Assoc. Prof., Dept. of Civil, Struct. and Envir. Eng., 212 Ketter Hall, SUNY, Buffalo, NY 14260
[3] Graduate student, Dept. of Civil, Struct. and Envir. Eng., 212 Ketter Hall, SUNY, Buffalo, NY 14260

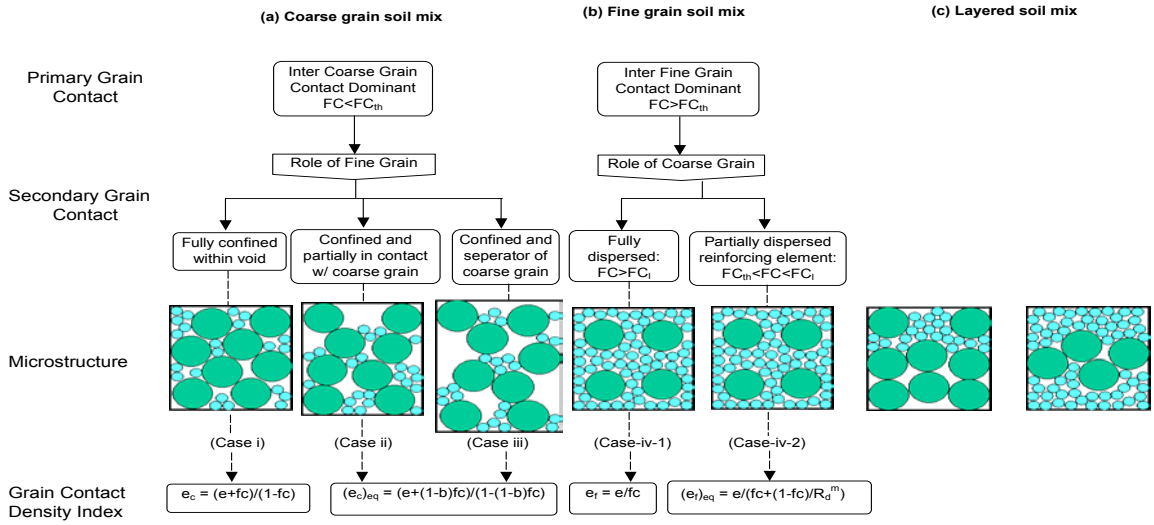

b=portion of the fine grains that contribute to the active intergrain contacts; e=global void ratio; FC=fine grains content; FC_{th}=threshhold fine grains content, $FC_{th}<(100e/e_{max,HF})\%$; FC_l=limit fines content, $FC_l>100(1-\pi(1+e)/(6s^3))\%>FC_{th}$; m: reinforcement factor; R_d=D/d=particle size disparity ratio; $s=1+a/R_d$, a=10; $e_{max,HF}$: the maximum void ratio of host fine

Fig.B Intergranular Soil Mix Classification

Using these equivalent intergranular void ratios, the mechanical behavior of a granular mix at $FC<FC_{th}$ or $FC>FC_{th}$ may be compared with the behavior of the host coarse-grained or host fine-grained soil, respectively. It is also possible to derive equivalent contact relative densities using the above equivalent void ratios. For granular mixes containing graded coarse and fine-grained soils, the same relationships may be applicable, by replacing R_d by D_{50}/d_{50} in the equations shown in Fig.B. b and m depend on the gradation of the coarse and fine-grained soils contained in the mix.

Based on this framework, the data shown in Fig.6 can be re-plotted against $(e_c)_{eq}$ ($FC<FC_{th}$) and equivalent interfine void ratio [$(e_f)_{eq}$ for $FC_{th}<FC<FC_L$ and e_f for $FC>FC_L$) as shown in Figs. C-a and C-b, respectively. All the data for silt content up to FC_{th} fall in a narrow band surrounding the data for the host sand (Fig.C-a). Similar observation holds for the soils at silt content greater than FC_{th} in Fig.C-b. Similar observation holds for the Yatesville sand-Yatesville silt mix (b=0.6, m=0.6), and a number of other sand-silt mixes, although the corresponding figures are not presented herein due to space limitations. The data for all sand-silt mixes fall in a narrow band when compared against equivalent relative density in terms of the above void ratio indices. These reinterpretations indicate that when compared at the same intergrain contact density index, relevant for the silt content, the *undrained* cyclic resistance of granular mix containing nonplastic fines compares well against the resistance of the host (coarse or fine-grained) medium.

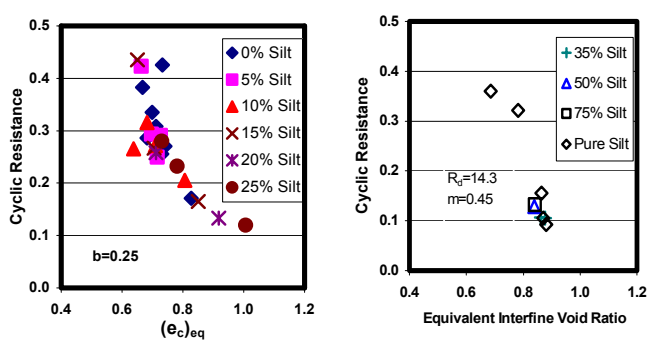

(a) $FC<FC_{th}$ (b) $FC>FC_{th}$

Fig.C Cyclic Resistance – Equivelent intergranular density indices

However, at the same intergrain contact density index, due to the presence of fines and the associated reduction in pore size, hydraulic conductivity and coefficient of consolidation a granular mix is very different from those of the host coarse-grained medium (Thevanayagam et al. 2001). Therefore, unless partial drainage that occurs around the penetrating tip of an SPT sampler or CPT cone during testing is prevented, the penetration resistance of a granular mix containing fines is expected to be different from that of the host coarse-grained medium at the same intergrain contact density index. Therefore, any modifications to the current liquefaction screening methods using insitu penetration data or shear wave velocity versus cyclic resistance relationships, should, at the least, involve an analysis of the combined effects of fines on mechanical and flow characteristics of a granular mix on insitu penetration resistance, accounting for partial drainage effects during testing (Thevanayagam 2000b). The method based on shear wave velocity holds a slight advantage since shear wave velocity is little affected by drainage effects during testing but primarily by contact density (Thevanayagam 1999), and therefore less sensitive to fines content than penetration resistance is.

References

Polito, C. P. (1999) "The effects of nonplastic and plastic fines on the liquefaction of sandy soils." Ph.D Dissertation, Virginia Polytech. Inst. and State Univ., Blacksburg, Va., 270p

Thevanayagam, S. (1999) "Liquefaction and shear wave velocity characteristics of silty/gravely soils – implications for bridge foundations", Proc. of 15th US-Japan Bridge Workshop, Tech. Memorandum #3694, PWRI, Tsukuba City, Japan, ed. K. Nishikawa, 133-147.

Thevanayagam, S. (2000a) "Liquefaction potential and undrained fragility of silty soils." Proc. 12WCEE 2000 Conference, Auckland, New Zealand, ed. R. Park, Paper# 2383.

Thevanayagam, S. (2000b) "Liquefaction in silty soils: considerations for screening and retrofit strategies" Proc. 2nd intl workshop on mitigation of seismic effects on transportation structures, NCREE, Taipei, Taiwan. Eds. C. Loh, K. Kawashima, and I. G. Buckle, 374-385.

Thevanayagam, S., Fiorillo, M. and Liang, J. (2000). "Effect of non-plastic fines on undrained cyclic strength of silty sands." ASCE, GSP 107, 77-91

Thevanayagam, S., Martin, G.R., Shenthan, T. and Liang, J. (2001) "Post-liquefaction pore pressure dissipation and densification in silty soils", Proc. 4th Intl Conf. Geot. Earthq. Eng. & Soil Dyn., eds. S. Prakash, UMR, Missouri, Paper# 4.28

5.3 Undrained cyclic behavior of sand and non-plastic silty soils based on energy principles

5.3.1 Technical Articles

Analyses of undrained cyclic behavior of sand and non-plastic silty soils based on energy principles are presented in the following technical articles.

5.3.1.1 Thevanayagam, S., Kanagalingam, T., and Shenthan, T. (2003) "Intergrain friction, Contact density, and cyclic resistance of sands," *Proc., 2003 Pacific Conf. on Earthquake Engineering,* Univ. of Canterbury, Christchurch, New Zealand: Paper# 115.

5.3.1.2 Thevanayagam, S., Kanagalingam, T., and Shenthan, T. (2003) "Intergrain friction, Contact density, and cyclic resistance of silty sands," *Proc., 12th Panamerican Conference on Soil Mechanics and Geotechnical Engineering/39th U.S. Rock Mechanics Symposium,* pp. 1007-1012.

5.3.1.3 Thevanayagam, S., Kanagalingam, T., and Shenthan, T. (2002) "Contact density – confining stress – energy to liquefaction", *Proc. 15th ASCE Eng. Mech Conf.* Columbia Univ., Paper 428. (not included in this report)

5.3.1.4 Kanagalingam, T. (2003) "Role of contacts and fines on resistance to liquefaction of granular mixes", *MS Thesis*, SUNY at Buffalo, 132p. (not included in this report)

5.3.1.5 Kanagalingam, T. (2004) "Energy based liquefaction analysis and modeling of granular mixes", *PhD dissertation*, SUNY at Buffalo, *In preparation*. (not included in this report)

Articles 5.3.1.1 and 5.3.1.2 are presented following Sec. 5.3.2.

5.3.2 Conclusions

The main conclusions from this analysis are as follows:

- The recently proposed equivalent intergranular void ratios [$(e_c)_{eq}$ and $(e_f)_{eq}$] or equivalent relative densities [$(D_{r,c})_{eq}$ and $(D_{r,f})_{eq}$] are useful parameters to characterize the energy required to liquefy granular mix soils (silty sands and sandy silts, respectively). The energy E_L required to cause liquefaction increases linearly with initial effective confining stress and increases log-linearly with intergrain contact density
- Cyclic pore pressure ratio increases log-linearly with E/E_L, independent of contact density, E is the cumulative energy dissipated in the soil.
- Theoretically estimated internal frictional energy loss W based on intergrain friction at contacts during cyclic loading of granular soils agrees fairly well with the experimentally measured external energy input E_L required to cause liquefaction.
- Intergrain contact friction increases with strain and reaches limiting value in the vicinity of 0.4% shear strain. The mobilized friction coefficient evaluated from experimental data agrees well with that of theoretical values for sand. A reasonable degree of agreement is observed for silty soils as well.

5.3.1.1

2003 Pacific Conference on Earthquake Engineering

Intergrain friction, contact density, and cyclic resistance of sands

S. Thevanayagam, T. Kanagalingam & T. Shenthan

Dept. of Civil, Struct. & Env. Eng., University at Buffalo, SUNY, Buffalo, USA.

ABSTRACT: Soil liquefaction phenomenon involves progressive intergrain contact deformation, slip, reorganization of contacts, and eventual collapse of soil skeleton. During this process frictional energy is lost along contacts. Resistance to liquefaction depends on the density of active intergrain contacts, contact friction, and confining stress. Higher the density of active intergrain contacts (per grain) more resistant is the soil to liquefaction. Higher is the confining stress higher is the energy loss along contacts and higher is the resistance to liquefaction. This paper presents an analysis of the evolution of intergrain contact friction, slip, and energy loss during undrained cyclic loading in sand. A theoretical framework for estimation of an index of active contact density for sands is presented. Theoretical results for mobilized intergrain friction and frictional energy loss are compared with experimental data. A new expression is presented for porewater pressure generated during undrained cyclic loading as a function of energy loss.

1 INTRODUCTION

Liquefaction, lateral spreading due to temporary loss of strength, and post-liquefaction settlement are major causes of ground failures during earthquakes. Soil liquefaction is a process leading to structural collapse of the soil skeleton due to shear, with a concurrent frictional loss of energy along active intergrain contacts due to rolling and sliding friction and local yielding at contact zones. The net energy loss is equal to the frictional energy loss W_L plus energy released from the intergrain contact force network minus the energy gained due to increase in porewater pressure. The latter two components are small. There has been several studies on the use of W_L to study liquefaction potential of soils (Nemat-Nasser & Shokooh 1979, Berrill & Davis 1985, Okada & Nemat-Nasser 1994, Figureuoa et al. 1994, Kayen & Mitchell 1997, Thevanayagam 2000, and Thevanayagam et al. 2000). A complete quantitative understanding of the relationship for the cumulative energy loss W_L per unit volume of soil required to liquefy the soil is still far from grasp.

Consider a regular array of uniform spherical particles. Frictional energy loss per unit volume of this array subjected to shear is primarily a function of the coefficient of friction μ, intergrain contact normal force N, number of slipping contacts per grain n_g, number of grains per unit volume m_g, and the magnitude of slip between contacts $\Delta\delta$. N is a function of n_g and m_g, and effective confining stress σ'. m_g is a function of void ratio e of the soil and grain size D. n_g and m_g depend on soil structure. $\Delta\delta$ is a function of incremental shear strain $\Delta\gamma$ and D. The energy loss at small strains prior to full slip between particles is also dependent on the elastic properties of the grains (Mindlin & Deresiewicz 1953). However, liquefaction is a large strain problem and the energy loss prior to full slip between contacts is small, and hence the influence of the elastic properties is negligible.

During drained loading the soil volume changes and, if the volume change is disallowed (undrained), pore water pressure changes. During cyclic loading these processes continue with concurrent accumulation of frictional energy loss, eventually leading to cessation of further volume change or pore pressure changes. For loose soils subjected to undrained shear, such a state is called liquefaction. Intuitively, as a first order approximation, W_L may be expressed as a function of intergrain contact density, initial effective confining stress σ_c', and frictional characteristics of the soil.

What would be the form of the relationship for W_L, and what would be a suitable index of active intergrain contact density are difficult questions. For practical purposes, for rather uniform granular arrays, void ratio may be a useful index. Except for such regular arrays, there exist particles that do not actively participate in the internal contact force network within the medium. e is not a valid index. The relative density D_r may be useful in such cases. For a broadly graded granular mix containing coarse grains and fine grains of different sizes and shapes with large size disparity, like silty sands and gravelly sands, there exist many particles that do not actively participate in the intergrain contact force chain. Neither e nor D_r is useful. For such soils, a set of equivalent intergrain contact void ratios $(e_c)_{eq}$ (and equivalent relative density $(D_{rc})_{eq}$) and $(e_f)_{eq}$ (and equivalent relative density $(D_{rf})_{eq}$) have been introduced as useful indices of active intergrain contact density (Appendix I). This paper examines the form of W_L and the influence of intergrain contact density and confining stress on W_L for granular soils.

2 THEORY

2.1 External Energy E and E_L

The external energy dissipated per unit volume of soil (E Nm/m^3) is the cumulative area inside each hysteretic loop developed during cyclic loading, given by:

$$E = \sum_{i=1}^{n-1} \frac{1}{2}(\tau_i + \tau_{i+1})(\gamma_{i+1} - \gamma_i) \tag{1}$$

where τ = shear stress; γ = shear strain; n = number of points recorded up to γ. Definition of liquefaction in terms of pore pressure is difficult, as the excess pore pressure ratio r_u ($\Delta u/\sigma_c$') may reach unity only momentarily. It is customary to define liquefaction as a state where the soil experiences ±5% double amplitude axial strain during undrained shear. E at ±5% axial strain is termed as the energy spent E_L to cause liquefaction, in this paper.

2.2 Internal Frictional Energy Loss W and W_L

Consider a granular array (Table 1), initially at a confining stress σ_c'. The normal contact force is N. During shear, the magnitudes of confining stress σ', N, contact tangent force, and contact slip vary from contact to contact, except for very small strains. Initially slip occurs along an annular region of the contact area and grows to full-slip condition after a threshold magnitude strain (Mindlin and Deresiewicz 1953). Exact relationship for these parameters depends on loading history and the evolution of the granular skeleton. As a first order approximation, in this paper, neglecting the variations in the internal contact normal forces N and the magnitude of slip $\Delta\delta$ at each active contact in a grain, W (Nm/m^3) per unit volume of soil, for all packing, is:

$$W = \sum (N\mu^*(\Delta\delta)(n_g m_g)/2) = 1.5\mu^* \sum (\sigma'(\Delta\gamma)) \tag{2}$$

where $\Delta\gamma$= incremental shear strain amplitude, σ'= mean effective confining stress $(\sigma_1'+\sigma_2'+\sigma_3')/3$ during the incremental cyclic loading, and μ^* = effective coeff. of friction. W is given by $1.5\mu^*$ times the cumulative area under the σ' versus γ diagram during cyclic loading. At small strains, however, due to lack of full slip, W given by Eq.2 would be higher than actual value. For small strains less than a threshold value, a magnitude of $\mu^*<\mu$ should be used to account for this error (μ=mobilized contact friction at full slip). $\mu^*=\mu$ at large strains. W at ±5% axial strain is termed as the internal frictional loss W_L required to cause liquefaction, in this paper. Neglecting other energy losses, E = W.

Table 1. Intergrain contact parameters – spherical array

Packing	Contact Normal, N	Active Contact Slips/grain, n_g	Active Grains/unit vol., m_g	Energy Loss/Unit vol. $N\mu^*(\Delta\delta)(n_g m_g)/2$
Simple cubic	$D^2\sigma'$	6	$1/D^3$	$1.5\mu^*\sigma'\Delta\gamma$
Cubical-tetrahedral	$(D^2/3^{1/2})\sigma'$; $(3^{1/2}D^2/2)\sigma'$	2; 6	$2/(3^{1/2}D^3)$	$1.5\mu^*\sigma'\Delta\gamma$
Face centered cubic	$(D^2/8^{1/2})\sigma'$	12	$2^{1/2}/D^3$	$1.5\mu^*\sigma'\Delta\gamma$
Body centered cubic	$(D^2/3^{1/2})\sigma'$	8	$27^{1/2}/(4D^3)$	$1.5\mu^*\sigma'\Delta\gamma$

3 EXPERIMENTAL PROGRAM

The experimental program involved undrained cyclic triaxial tests on three sands (OS, FJ#80, and WG), and sand-silt mixes prepared by mixing the above sands with a non-plastic silt (Sil co sil #40, US Silica Company, Illinois). The OS sand-silt mixes at silt contents of 0%, 15%, 25%, 60, and 100% by dry weight are named OS-00, OS-15, OS-25, OS-60, and OS-100, respectively. The FJ#80 sand-silt mixes containing 0%, 25%, and 60% silt are termed FJ-00, FJ-25, and FJ-60, respectively. Similarly the WG sand-silt mixes are termed WG-00, WG-25, WG-60, respectively. Figure 3 shows the grain size data for two soils (Thevanayagam 2001).

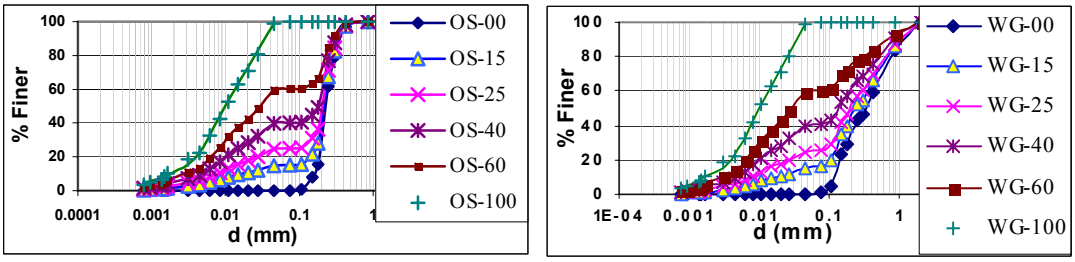

(a) Ottawa sand (OS) – silt mix (b) Well-graded sand (WG) – silt mix

Figure 1 Grain Size Distribution

Cylindrical specimens (typically 75 mm diameter and 175 mm height) were prepared using moist-tamping or dry pluviation method. Following initial preparation, the specimens were percolated with carbon dioxide to displace the air in the void space of the specimens to facilitate full saturation by water. After that, deaired water was allowed to flow from the bottom of the specimen towards the top. The net volume of the water introduced into the specimen was measured accurately. Finally, the specimen was set up on the triaxial test apparatus to continue the saturation until the B-value ($=\Delta u/\Delta\sigma_c$) was typically greater than 0.95. Following this, the specimens were isotropically consolidated to σ_c'=100kPa or 400kPa. The final void ratio of each specimen was calculated based on the weight of the dry solid grains in the specimen, the net volume of water introduced into the specimen during saturation, and the measured volume change data during consolidation. Following consolidation, the drainage valves were closed and cyclic stress ratio ($CSR=[\pm\Delta\sigma_1/(2\sigma_c')]$=0.1, 0.2, and 0.3) controlled undrained cyclic triaxial tests were done at a frequency of 0.2 Hz or 1 Hz. The pore pressure, axial load, and axial deformation were recorded using a built-in data acquisition system.

4 ANALYSIS

4.1 E versus W

Figure 2a shows E and W versus axial strain amplitude reached during each cycle for OS-00 at 3 different void ratios. W was calculated using Eq.2 assuming μ^*=0.32 (a reasonable μ for silica sand grains). At low strains less than about 0.1%, the calculated magnitude of W is consistently higher than E. The reason for this is that Eq.2 is based on the assumption that full-slip occurs along contacts whereas full-slip can occur only at large strains beyond a threshold slip-strain. This error in W was corrected by assigning a lower value for μ^* (=0.08) up to about 0.1% strain (typical range of threshold strain) and μ^*=0.32 thereafter. The results are shown in Figure 2b. When such small-strain corrections are made, E and W agree well through out the cyclic loading up to liquefaction (±5% axial strain). Figure 3 shows E versus W from the beginning of cyclic loading up to liquefaction for OS-00 at 5 different e. W was calculated assuming μ^*=0.08 for ε<0.1% and μ^*=0.32 for ε>0.1%. Results show a very close 1:1 relationship between E and W for all contact densities.

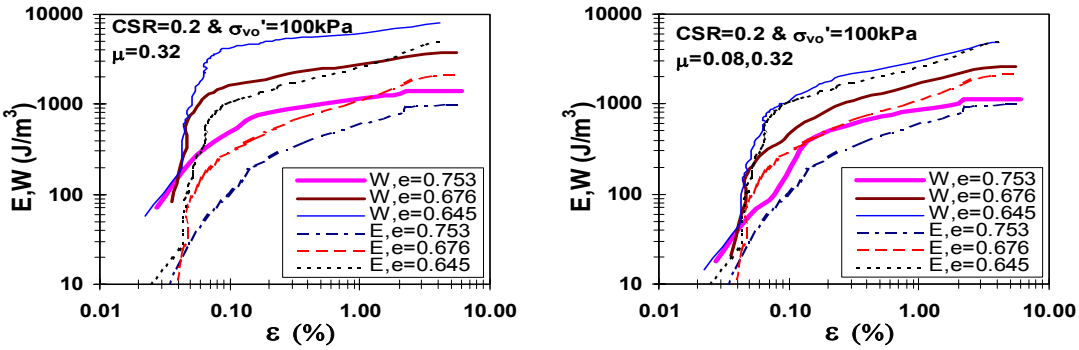

(a) μ=0.32 (b) μ=0.08 for ε<0.1%; μ=0.32 for ε>0.1%

Figure 2 E and W versus axial strain ε

The same observation held for all specimens, including the granular mixes, although the magnitudes of μ differed slightly, depending on the soil grain type. This indicates the validity of the theory and that W_L is a function of contact density, confining stress, and intergrain friction. For spherical array (Table 1), $n_g m_g = 5e^{-x}/D^3$, x=1±0.2. This and Eq.2 imply that, in general:

$$W_L = A\mu\sigma_c^{'}(e)_{eq}^{-\alpha} \tag{3}$$

where A, μ and α may depend on the gradation and other soil characteristics. $(e)_{eq}$ is defined in Appendix I.

4.2 Pore Pressure and Energy Loss

Figure 4 shows the pore pressure ratio r_u ($\Delta u/\sigma'_c$) versus normalized cumulative energy loss E/E_L for the OS sand. Results indicate that, except for the initial stage corresponding to very small strain level, r_u is log-linearly related to E/E_L, independent of contact density index, approximately following $r_u=0.5\log_{10}(100E/E_L)$, $E/E_L>0.05$. Such a relationship was found to hold for all specimens. The confining stress ratio (σ'/σ'_c) that can be sustained by the soil skeleton at any stage of cyclic loading depends on the cumulative energy loss ratio E/E_L up to that stage, where E_L is the cumulative energy loss required to fully reorganize the soil skeleton and liquefy the soil.

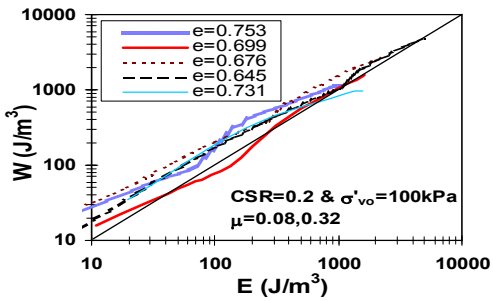

Figure 3 E versus W

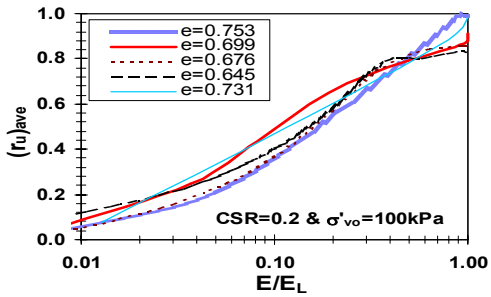

Figure 4 $(r_u)_{ave}$ (=Δu/σ'$_c$) versus E/E_L

4.3 Effect of contact density on E_L

Figures 5a-c show E_L versus e for the three types of sand-silt mixes consolidated to σ'_{vo}=100kPa and sheared at CSR = 0.2. For each soil-mix, at the same silt content FC, there exists a log-linear relationship for E_L versus e ($E_L=A_1\mu e^{-\alpha}$). There is no unique relationship for E_L versus e for all mixes. The relationship depends on FC for a given sand-silt mix, and sand type for a given silt type and silt content. Even though e is a reasonably good intergrain contact index for a given soil mix at the same FC, it is not a valid contact index for all soils. For each type of sand-silt mix, at the same e, E_L decreases with increasing FC up to a threshold value (FC_{th}). Beyond FC_{th} the trend reverses. The reason for this is that at low FC, the intergrain contact force network is made of inter coarse grain contacts with only a secondary influence by the (confined) fine grains, and hence soil resistance is governed primarily by the inter coarse grain contacts (Figure I, Appendix I). Beyond FC_{th}, the intergrain force network is primarily made of the interfine contacts with only a secondary influence by the (dispersed) coarse grains, and hence soil resistance is governed primarily by the inter fine grain contacts. Void ratio is not a good index to account for such different roles by the coarse and fine grains. If such differing roles are accounted for using the indices $(e_c)_{eq}$ and $(e_f)_{eq}$, E_L correlates with $(e_c)_{eq}$ and $(e_f)_{eq}$ at FC<FC_{th} and FC>FC_{th}, respectively, as shown in Figures 6a-c and 7, respectively ($E_L=A_1\mu(e)_{eq}^{-\alpha}$). A log-linear relationship is observed for E_L with $(e_c)_{eq}$ and $(e_f)_{eq}$. The relationships in Figures 6a-c depend on the sand type (gradation and shape effects). When the same data are plotted against $(D_{rc})_{eq}$, the shape and gradation effects of different sands is reduced; all data fall in a narrow band (Fig.8) and follows the form $E_L=B_1\mu(1-(D_{rc})_{eq}/100)^{-\beta}$.

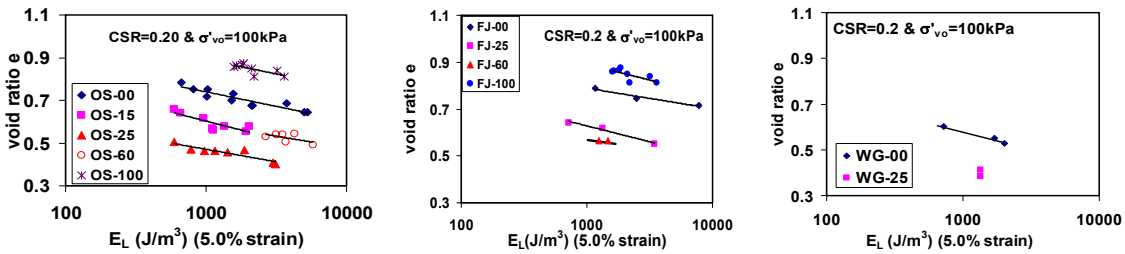

(a) OS-silt mix (b) FJ#80-silt mix (c) WG-silt mix

Figure 5 E_L at σ_c'=100 kPa and CSR=0.2

4.4 Effect of CSR and σ'$_c$ on E_L

The above test data (Figs 5-8) correspond to CSR=0.2. To investigate the influence of CSR on E_L versus contact density relationships, several additional cyclic tests were conducted at CSR=0.1 and 0.3 on specimens consolidated at σ'_c=100kPa. Figure 9 shows the data for the OS-silt mixes. The results indicate that E_L versus contact density index relationship is insensitive to CSR. Additional tests were conducted to study the effect of σ'_c on E_L. Figure10 shows the normalized energy E_{L1} (=E_L*100/σ'_c) versus $(e_c)_{eq}$ for FC<FC_{th} for the OS-silt specimens tested at σ'_c=100kPa and 400kPa, and at CSR =1, 0.2 and 0.3. Results indicate that there exists a log-linear relationship for E_{L1} versus $(e_c)_{eq}$. E_L increases linearly with σ'_c, and follows the form $E_L=A\mu\sigma'_c(e)_{eq}^{-\alpha}$.

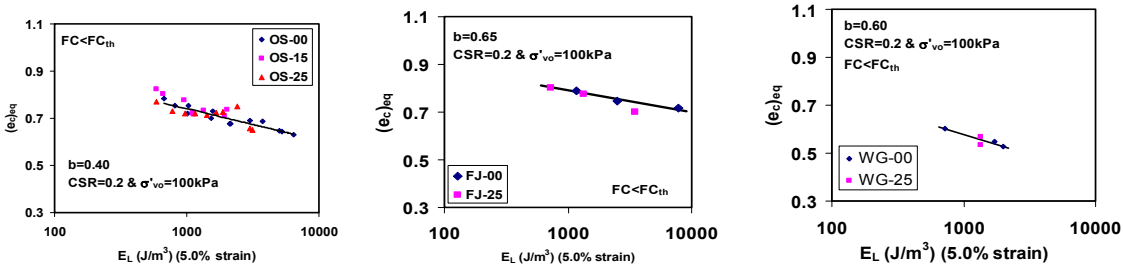

(a) OS-silt mix (b) FJ#80-silt mix (c) WG-silt mix

Figure 6 E_L versus $(e_c)_{eq}$: FC<FC_{th}

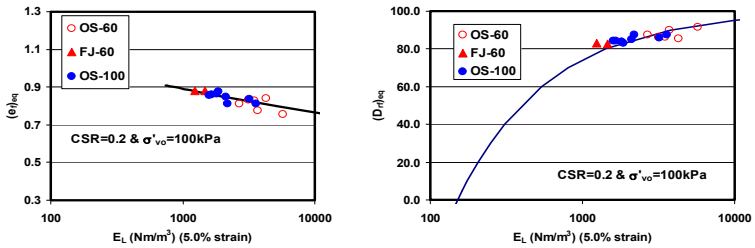

(a) E_L versus $(e_f)_{eq}$ (b) E_L versus $(D_{rf})_{eq}$

Figure 7 E_L versus $(e_f)_{eq}$ and $(D_{rf})_{eq}$: FC>FC_{th}

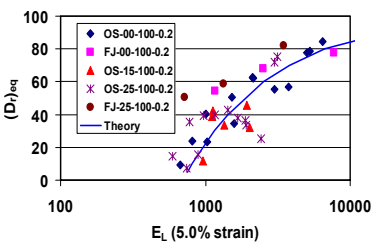

Figure 8 E_L versus $(D_{rc})_{eq}$

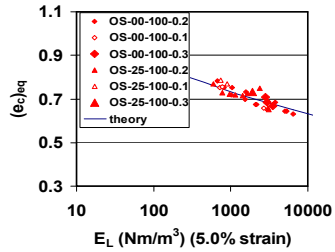

Figure 9 Effect of CSR

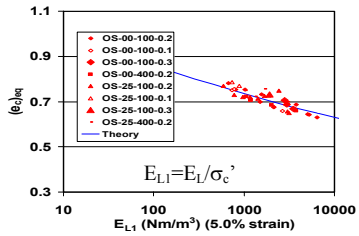

Figure 10 Effect of σ_c' and CSR

5 CONCLUSIONS

Semi-theoretical and experimental analyses of key factors that influence the frictional energy loss along active grain contacts during cyclic loading of granular soils indicate the following. The internal frictional energy loss W estimated based on intergrain friction at contacts agrees fairly well with the external energy input E. Cyclic pore pressure ratio increases log-linearly with E/E_L, independent of contact density. The energy E_L required to cause liquefaction increases linearly with initial effective confining stress (Fig. 10) and increases log-linearly with intergrain contact density. The recently proposed equivalent intergranular void ratios (or equivalent relative densities) are useful parameters to characterize the liquefaction resistance of granular mix soils (e.g. silty sands). Further research is needed to fully develop an understanding of the key factors affecting energy loss during cyclic loading, and better characterize liquefaction behavior of soil.

6 ACKNOWLEDGEMENTS

Financial support for this research by grants from NSF, NEHRP/USGS, and MCEER is gratefully appreciated.

REFERENCES:

Berrill, J.B. and Davis, R.O. 1985. Energy dissipation and seismic liquefaction of sands: revised model. *Soils and Foundations*. 25 (2): 106-118.

Kayen, R.E. & Mitchell, J.K. 1997. Assessment of liquefaction potential during earthquakes by arias intensity. *ASCE, J. Geotech. & Geoenv. Eng.* 123 (12): 1162-1174.

Mindlin, R.D. & Deresiewicz, H. 1953. Elastic spheres in contact under varying oblique forces. *ASME, J. Appl. Mech*. 74: 327-344.

Figueroa, J.L., Saada, A.S., Liang, L. & Dahisaria, M.N. 1994. Evaluation of soil liquefaction by energy principles. *ASCE, J. Geotech. Eng*. 120 (9): 1554-1569.

Nemat-Nasser, S. & Shokooh, A. 1979. A unified approach for densification and liquefaction of cohesionless sands in cyclic loading. *Can. Geot. J,* 16: 659-678.

Okada, N. & Nemat-Nasser, S. 1994. Energy dissipation in inelastic flow of saturated cohesionless granular media. *Geotechnique*. 44 (1): 1-19.

Thevanayagam, S. 1998. Relative roles of coarse and fine grains on the mechanical response of granular mixes. *ASCE, J. Geotech. & Geoenv. Eng*. in review.

Thevanayagam, S., Shenthan, T., Mohan, S. and Liang, J. 2002. Undrained fragility of sands, silty sands and silt. *ASCE, J. Geotech. & Geoenv. Eng*. 128 (10): 849-859.

Thevanayagam, S. 2000. Liquefaction potential and undrained fragility of silty sands. In R. Park (ed.). *Proc. 12th International Conf. Earthq Eng.* Auckland, New Zealand, paper # 2383.

Thevanayagam, S., Liang, J., and Shenthan, T. 2000. A contact index for liquefaction potential analysis of silty/gravely soils. In Tassoulas (ed.). *EM2000, Proc. 14th ASCE EMD Spec. Conf.* Austin, Texas.

Thevanayagam, S. 2001. Role of intergranular contacts on mechanisms causing liquefaction and slope failures in silty sands. *http://erp-web.er.usgs.gov/reports/annsum/vol43/pt/pt_vol43.htm*. USGS web.

Thevanayagam, S., Kanagalingam, T, Martin, G.R., and Shenthan, T. 2001. Cyclic resistance of sand, silty sand, and silts. *Can. Geo.J.* in review.

APPENDIX I. Contact density Indices

How and when coarse and fine grains contribute to the mechanical response of a granular mix is a complex problem. It depends on a number of factors, including fines content, void ratio, size disparity, particle shape, and gradation of the host coarse and fine grain soils.

Consider a granular mix containing coarse and fine particles of size D and d, respectively (Fig.I, Thevanayagam 2001). The microstructure of this granular mix can be formed in many different ways. Each one of them leads to a different internal force chain network among particles and hence each exhibits a different stress-strain response. Among many variations, the first category in Figure I-a occurs when the fine grains are fully confined within the void spaces between the coarse-grains with no contribution whatsoever in supporting the coarser grain skeleton. This requires that d is much smaller than the pore size between the coarse grains (R_d=D/d>>6.5). It is also essential that the fine grain content (FC) is less than a certain threshold value (FC_{th}) such that the inter coarse-granular voids are not completely full of fine grains so that the fine grains do not constitute a strong contact force chain among themselves nor contribute to the coarse grain force chain. When FC is sufficiently high (>FC_{th}), direct fine-grain-to-fine-grain contacts begin to constitute a strong force chain. Soil microstructure that satisfies the two constraints (FC<<FC_{th} and R_d>>6.5) is categorized as case i. FC_{th} is given by $100e/e_{max,HF}$ where $e_{max,HF}$ = void ratio of the host fine grain soil above which it has no appreciable strength.

At FC<FC_{th}, however, other microstructures are possible. Consider changing the position of some of the fine grains, while maintaining the fine grain content. Microstructure corresponding to case ii or iii in Figure I-a forms. Essentially, the microstructure for these cases is made of a coarse grain skeleton where some of the coarse grain contacts form via fine grains while some fine grains remain confined within the voids between the coarse grains. The 'separating fines' actively participating in the internal contact force chain needs to be accounted for in order to explain the mechanical response of the mix.

If FC exceeds sufficiently beyond FC_{th}, a fourth category (Fig.I-b) occurs naturally. The fine grains make active contacts among themselves while the coarse grains disperse and act as embedded reinforcement elements within the fine grain matrix until they disperse sufficiently far from each other. This imposes a limiting fines content FC_L. Beyond FC_L, fine-grain-to-fine-grain contact governs the behavior of the soil mix. The transition zone between FC_{th} and FC_L is case iv-2 and the zone corresponding to $FC>FC_L$ is case iv-1. The case v (Fig.I-c) occurs when coarse and fine grains constitute a fully layered system. A composite system consisting of these cases is also possible.

Based on contact density (per grain) considerations, equivalent intergranular void ratios $(e_c)_{eq}$ and $(e_f)_{eq}$ have been developed as indices of active grain contact density. Neglecting the differences in specific gravities between the coarse and fine grains, for case i, e_c (=(e+fc)/(1-fc)); fc=FC/100; e=global void ratio) may be used as the contact density index. For reasons discussed before, however, fine grains do contribute to the contact force chain. In such cases, an equivalent intergranular void ratio $(e_c)_{eq}$ (=e+(1-b)fc)/((1-(1-b)fc)) has been defined as the contact density index. The term b in $(e_c)_{eq}$ refers to the contribution by fine grains to the force chain. For case iv-1, an equivalent interfine void ratio $(e_f)_{eq}$ (=e/(fc+(1-fc)/R_d^m) has been defined as the contact density index. The term m refers to the contribution by dispersed coarse grains to the force chain. At $FC>FC_L$, $(e_f)_{eq}$ becomes the interfine void ratio e_f (=e/fc), the void ratio of the fine-grained soil, ignoring the presence of coarse grains. The corresponding equivalent intergranular relative densities are: $(D_{rc})_{eq}=(e_{max.HC}-(e_c)_{eq})/(e_{max.HC}-e_{min,HC})$ for $FC<FC_{th}$ and $(D_{rf})_{eq}=(e_{max.HF}-(e_f)_{eq})/(e_{max.HF}-e_{min,HF})$ for $FC>FC_{th}$, where $e_{max.HC}$=maximum void ratio of the host coarse grain soil; $e_{min.HC}$ and $e_{min.HF}$ = minimum void ratios of the host coarse- grained and host fine-grained soils, respectively. Using the respective equivalent contact density indices at $FC<FC_{th}$ and $FC>FC_{th}$, the mechanical response of a granular mix may be compared with the response of the host coarse-grained or host fine-grained soil, respectively. For granular mixes containing graded coarse and fine-grained soils, the same relationships may be applicable, by replacing R_d by D_{50}/d_{50}. Figure II (Thevanayagam 2001) presents the experimental relationship for b and m as a function of the coefficients of uniformity C_{uc} and C_{uf} of the coarse and fine grained soils, respectively, and D_{50}/d_{50} (=R_{d50}). Further details are found in Thevanayagam (1998) and Thevanayagam et al. (2001, 2002).

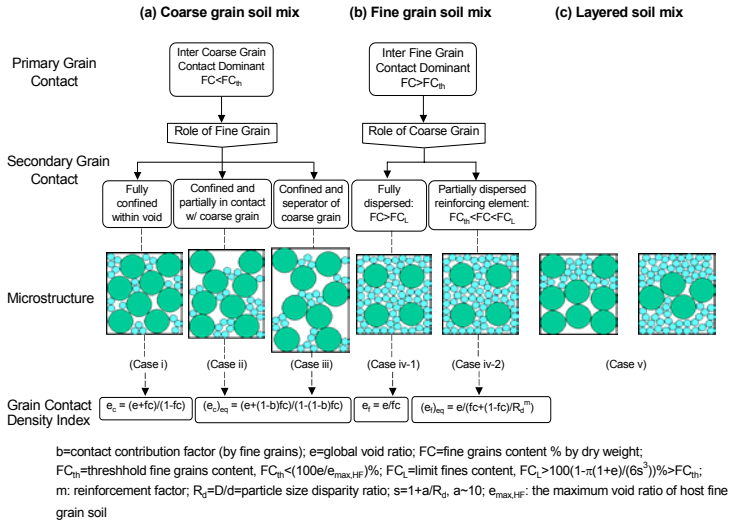

Figure I Intergranular soil mix classification

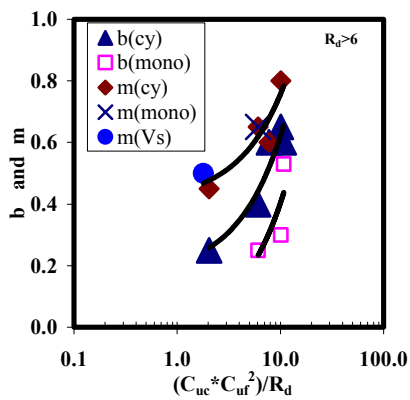

Figure II b and m versus $C_{uc}C_{uf}^2/R_{d50}$
(cy=cyclic shear; mono=monotonic shear, Vs= shear wave velocity)

5.3.1.2

Intergrain Friction, Contact Density, and Cyclic Resistance of Silty Sands

Fricción Intergranular, Densidad de Contactos y Resistencia Cíclica de Arenas Limosas

S. Thevanayagam, T. Kanagalingam, T. Shenthan
SUNY at Buffalo

ABSTRACT

Soil liquefaction phenomenon involves progressive intergrain contact deformation, slip, reorganization of contacts, and eventual collapse of soil skeleton. During this process energy is lost along frictional contacts. Resistance to liquefaction depends on the density of active intergrain contacts, contact friction, and confining stress. This paper examines the effects of contact density, intergrain friction, and confining stress on the energy required to cause liquefaction in silty sands. An analysis of the evolution of intergrain contact friction, slip, and energy loss during undrained cyclic loading in silty sands is presented. A theoretical framework for estimation of an index of active contact density is presented. Theoretical results for mobilized intergrain friction and frictional energy loss are compared with experimental data. A new expression is presented for pore water pressure generated during undrained cyclic loading as a function of energy loss.

RESUMEN

Varios procesos se presentan en el fenómeno de licuefacción de suelos, por ejemplo, deformación intergranular de contacto, deslizamiento, reorganización de contactos y colapso eventual del depósito. Durante este proceso hay pérdida de energía a través de los contactos de fricción. La resistencia a la licuefacción depende de la densidad de contactos intergranulares activos, fricción de contacto y esfuerzo de confinamiento. Este articulo examina los efectos de la densidad de contacto, fricción intergranular y esfuerzo de confinamiento en la energía requerida para causar licuefacción en arenas limosas. Se presenta un análisis de la evolución de la fricción intergranular de contacto, deslizamiento y energía perdida durante cargas cíclicas en condiciones no drenadas para arenas limosas. También se describe un marco teórico para la estimación de un índice de densidad de contacto activo. Se hacen comparaciones de resultados teóricos de la fricción intergranular movilizada y de energía perdida con datos experimentales. Finalmente, se introduce una nueva expresión para la presión generada durante cargas cíclicas en condiciones no drenadas en función de la energía perdida.

1 INTRODUCTION

Liquefaction is one of the most destructive consequences causing ground failures during earthquakes. It has become a matter of great interest in geotechnical engineering over the last few decades. A significant amount of laboratory and field research has been focused on identifying the factors and mechanisms causing liquefaction. Soil liquefaction is a process leading to structural collapse of the soil skeleton due to shear, with a concurrent frictional loss of energy along active intergrain contacts. The frictional energy loss mainly depends on active intergrain contact density, confining stress, and frictional characteristics of the soil. The cumulative energy loss (W_L per unit volume) up to liquefaction has been identified as a useful index for liquefaction potential assessment of soils (Nemat-Nasser and Shokooh 1979, Berrill and Davis 1985, Okada and Nemat-Nasser 1994, Figureuoa et al. 1994, Kayen and Mitchell 1997, Thevanayagam et al. 2000). A complete quantitative understanding of the interrelationships between W_L and the intergrain contact friction, contact density, and confining stress is still far from grasp. This paper presents a relationship for internal frictional energy loss W per unit volume of soil in terms of contact friction coefficient μ, intergrain contact density, and confining stress, with due consideration for interaction between particles. The Mindlin-Deresiewicz (1953) solution for contact-slip behavior between two spherical particles is

studied. This is extended to multi-particle array subjected to shear under undrained conditions. Internal energy loss during shear is obtained as a function of contact normal force N, number of slipping contacts per grain n_g, number of grains per unit volume m_g, and the magnitude of slip between contacts $\Delta\delta$ (Thevanayagam el al. 2002b). A set of equivalent intergrain contact void ratios $(e_c)_{eq}$ and $(e_f)_{eq}$ (Thevanayagam el al. 2002a) has been used as useful indices of active intergrain contact density for silty soils. The energy dissipated per unit volume of soil E_L up to liquefaction is analyzed based on the above indices for different soils having different fines contents (FC). The theoretical results for mobilized friction and cumulative energy are compared with experimental data on sands and silty sands.

2 THEORY

2.1 Internal frictional energy

Consider two identical solid elastic spheres in contact. The normal and tangential forces acting along the contact are N and T respectively. Assuming Hertzian contact, the relative tangential displacement along the contact plane is given by (Mindlin and Deresiewicz 1953):

$$\delta = \frac{3\mu N(2-\nu)[1-\left(1-\mu^*/\mu\right)^{2/3}]}{16Ga} \tag{1}$$

where ν=Poisson's ratio of solid, G=shear modulus of solid, $a=[3(1-\nu)ND/16G]^{1/3}$ = contact radius, D=particle diameter, μ=full-slip contact friction coefficient, and μ^*=T/N=mobilized contact friction. The magnitude of slip is governed by elastic properties of solids, contact friction, and confining stress. Full slip occurs when μ^* reaches μ. The corresponding threshold δ is termed δ_{th}. The corresponding threshold shear strain at full-slip is $\gamma_{th}=1.5\varepsilon_{th}=2\delta_{th}/D$, where ε_{th} = threshold axial strain.

The mobilized friction μ^* may be expressed as a function of shear strain γ:

$$\mu^* = \mu\left[1-\left(1-\frac{8GDa\ \gamma}{3(2-\nu)\mu N}\right)^{3/2}\right] \tag{2a}$$

$$\mu^* = \mu\left[1-\left(1-\frac{4G[3(1-\nu)/2G]^{1/3}}{3(2-\nu)\mu}\left(\frac{D^2}{N}\right)^{2/3}\gamma\right)^{3/2}\right] \tag{2b}$$

where N/D^2 is proportional to σ', and is dependent on packing (Table 1).

Hence, the mobilized friction depends on strain level, shear modulus of solid, confining stress, and packing (Table 1).

Assuming a constant contact normal force N, the incremental frictional energy loss (ΔW) due to an incremental slip Δδ is,

$$\Delta W=\mu^* N(\Delta\delta)/2 \tag{3}$$

Consider a regular array of uniform spherical particles (Table 1). In a regular array, the contact normal forces between all contacts are not the same, except for a few arrays subjected to isotropic confining stress. The contact normal forces continuously change during shear. The effective confining stress also changes, depending on drainage conditions and the imposed stress path. As a first-order approximation, in this paper, it is assumed that the average contact normal force is proportional to the mean effective confining stress. Based on this assumption, Table 1 shows the contact normal forces for a few regular arrays of particles. Assuming that the average contact normal force as representative of the contact forces, the frictional energy loss W per unit volume of this array is:

$$\begin{aligned} W &= \sum [N\mu^*(\Delta\delta)(n_g m_g)/2] \\ &= 1.5\mu^*\sum[\sigma'(\Delta\gamma)] \end{aligned} \tag{4}$$

where n_g=number of slipping contacts per grain, m_g=number of grains per unit volume, Δγ= incremental shear strain amplitude, and σ'= mean effective confining stress given by $(\sigma_1'+\sigma_2'+\sigma_3')/3$. Hence, W is given by 1.5μ* times the cumulative area under the σ' versus γ diagram during cyclic loading. At small strains, due to lack of full slip, a magnitude of μ*<μ should be used to account for the mobilization of friction along the contacts. μ*=μ at large strains.

2.2 Externally supplied energy

Externally supplied energy E is the cumulative area inside each hysteretic loop developed during cyclic loading, given by:

$$E = \sum_{i=1}^{n-1}\frac{1}{2}(\tau_i+\tau_{i+1})(\gamma_{i+1}-\gamma_i) \tag{5}$$

Table 1 Intergrain Contact Parameters for Spherical Arrays

Packing	Contact Normal, N	Active Contact Slips/grain, n_g	Active Grains/ unit vol., m_g	Void Ratio, e	Energy Loss/Unit vol. $N\mu^*(\Delta\delta)(n_g m_g)/2$
Simple cubic (SC)	$D^2\sigma'$	6	$1/D^3$	0.91	$1.5\mu^*\sigma'\Delta\gamma$
Cubical-tetrahedral	$[D^2/3^{1/2}]\sigma'$; $[3^{1/2}D^2/2]\sigma'$	2; 6	$2/[3^{1/2}D^3]$	0.65	$1.5\mu^*\sigma'\Delta\gamma$
Face centered cubic (FCC)	$[D^2/8^{1/2}]\sigma'$	12	$2^{1/2}/D^3$	0.35	$1.5\mu^*\sigma'\Delta\gamma$
Body centered cubic (BCC)	$[D^2/3^{1/2}]\sigma'$	8	$27^{1/2}/[4D^3]$	0.47	$1.5\mu^*\sigma'\Delta\gamma$

where τ = shear stress,. γ= shear strain, and n = number of points recorded up to γ. It is customary to define liquefaction as a state where the soil experiences ±5% double amplitude axial strain during undrained shear. E at ±5% axial strain is termed as the energy (E_L) required to cause liquefaction.

2.3 Equivalent contact density indices

Analyzing all possible microstructural arrangements of a binary granular mix containing two sizes (d and D) of particles in different proportions, Thevanayagam (1998, 1999) proposed the existence of a threshold fines content FC_{th} below which intergranular contact friction plays the primary role, and above FC_{th} inter fine grainfriction plays the primary role. At $FC<FC_{th}$, considering the secondary influence of the fine grains, the equivalent intergranular contact index, $(e_c)_{eq}$, has been shown to be of the form (Thevanayagam 1998, 2000, Thevanayagam el al. 2002a):

$$(e_c)_{eq} = \frac{e+(1-b)fc}{1-(1-b)fc}; \qquad 0<b<1 \qquad (6)$$

where fc=FC/100 and b denotes the portion of the fine grains that contributes to the active intergrain contacts.

Similarly, at $FC_{th}<FC$, there exists a limiting fines content FC_L above which the behavior of soil fully controlled by fine grains (Thevanayagam 1998). At $FC_{th}<FC<FC_L$, considering the reinforcement effect by the coarse grains, equivalent interfine void ratio $(e_f)_{eq}$ is given by (Thevanayagam 1998, 2000, Thevanayagam el al. 2002a):

$$(e_f)_{eq} = \frac{e}{fc + \frac{1-fc}{R_d^m}} \qquad (7)$$

where 0<m<1 and m = a coefficient that depends on grain characteristics and fine grain packing, R_d = D/d, d=fine grain size, and D=coarse grain size. The expressions for FC_{th} and FC_L are presented in Thevanayagam et al (2002a).

It is considered that the energy required to cause liquefaction could be related to these contact density indices and confining stress.

2.4 Mobilized friction coefficient

Based on Eqs. 4 and 5, the evolution of mobilized friction coefficient μ^* with increase in shear strain is given by:

$$\mu^* = \frac{\sum_{i=1}^{i} \frac{1}{2}(\tau_i + \tau_{i+1})(\gamma_{i+1} - \gamma_i)}{1.5\sum_{1}^{i}[\sigma'(\Delta\gamma)]} \qquad (8)$$

The above first-order theoretical developments provide a basis for a better understanding of the relationship between energy loss, contact friction, contact density, shear strain, confining stress and elastic properties of solids in a granular media. This was further evaluated using experimental data.

3 EXPERIMENTAL PROGRAM

The experimental program involved undrained cyclic triaxial tests on three sands (OS, FJ#80, and WG), and sand-silt mixes prepared by mixing the above sands with a non-plastic silt (Sil co sil #40, US Silica Company, Illinois). The OS sand-silt mixes at silt contents of 0%, 15%, 25%, 60, and 100% by dry weight are named OS-00, OS-15, OS-25, OS-60, and OS-100, respectively. The FJ#80 sand-silt mixes containing 0%, 25%, and 60% silt are termed FJ-00, FJ-25, and FJ-60, respectively. Similarly the WG sand-silt mixes are termed WG-00, WG-25, and WG-60, respectively. Fig.3 shows the grain size data for OS sand-silt mix (Thevanayagam 2001).

Cylindrical specimens (typically 75 mm diameter and 175 mm height) were prepared using moist-tamping or dry pluviation method. Following initial preparation, the specimens were percolated with carbon dioxide and then deaired water was allowed to flow from the bottom of the specimen towards the top. The net volume of the water introduced into the specimen was measured accurately. Finally, the specimen was set up on the triaxial test apparatus to continue the saturation until the B-value ($=\Delta u/\Delta\sigma_c$) was typically greater than 0.95. Following this, the specimens were isotropically consolidated to σ_c'=100kPa. The final void ratio of each specimen was calculated based on the weight of the dry solid grains in the specimen, the net volume of water introduced into the specimen during saturation, and the measured volume change data during consolidation. Following consolidation, the drainage valves were closed and cyclic stress ratio ($CSR=[\pm\Delta\sigma_1/(2\sigma_c')]$=0.1, 0.2, and 0.3) controlled undrained cyclic triaxial tests were done at a frequency of 0.2 Hz or 1 Hz. The pore pressure, axial load, and axial deformation were recorded using a built-in data acquisition system.

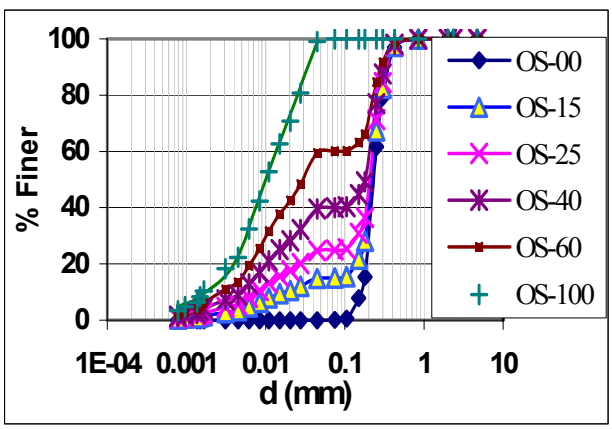

Figure 1 Grain Size: OS sand-silt mixes

4 ANALYSIS

4.1 E and W

Figures 2, 3 and 4 show W versus E plots for sand, silty sand, and sandy silt, respectively, at different void ratios. E was calculated using Eq.5. This is equal to the sum of the area inside each hysteretic loop in a τ versus γ diagram obtained from cyclic triaxial tests. W was calculated using Eq.4, as described in section 2.1, assuming two different friction coefficient values: $\mu^*<\mu$ for $\varepsilon<\varepsilon_{th}$ and $\mu^*=\mu$ for $\varepsilon>\varepsilon_{th}$, respectively. Although the threshold full-slip strain level depends on grain characteristics, elastic properties of solids, and packing, it was assumed to be the same (0.1%) for all soils. Slightly different μ values (0.32 for sand, 0.17 for silty sand, and 0.11 for sandy silt) were used depending on soil characteristics. In each case, results show a very close 1:1 relationship between E and W for all contact densities. This indicates the validity of the theory for W.

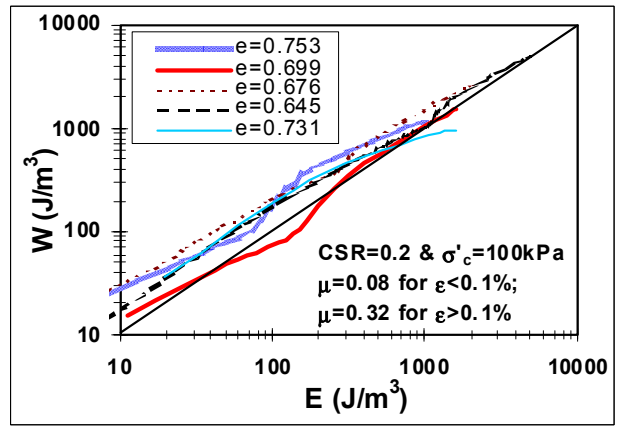

Figure 2 W versus E for OS-00: Sand

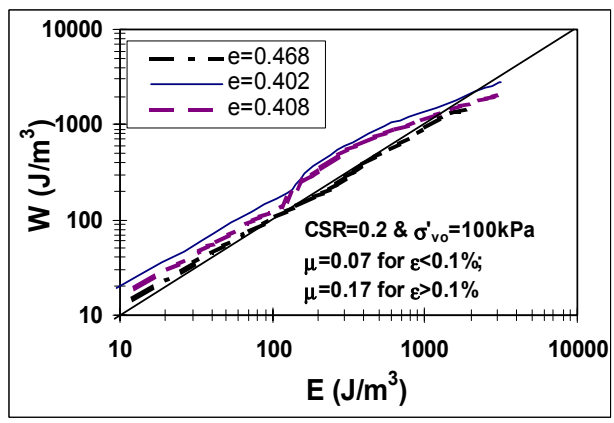

Figure 3 W versus E for OS-25: Silty Sand

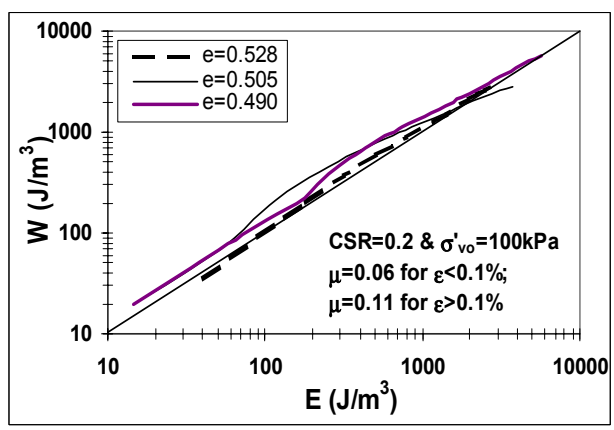

Figure 4 W versus E for OS-60: Sandy silt

4.2 Pore pressure and energy loss

Figure 5 shows the pore pressure ratio r_u ($\Delta u/\sigma'_c$) versus normalized cumulative energy loss E/E_L for OS sand-silt mixes. Results indicate that, except for the initial stage corresponding to very small strain level, r_u is log-linearly related to E/E_L, independent of contact density index, approximately following $r_u=0.5\log_{10}(100E/E_L)$, $E/E_L>0.05$. Such a relationship was found to hold for all specimens.

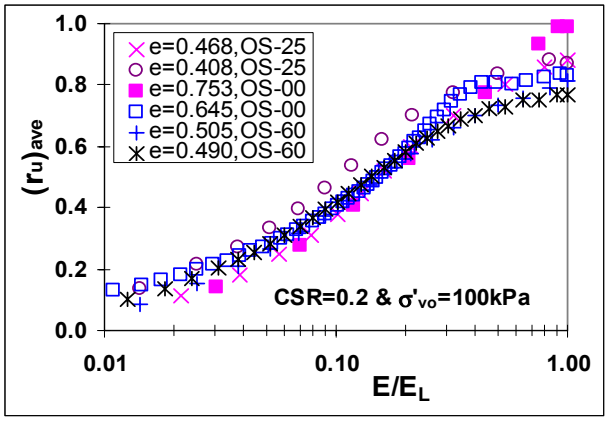

Figure 5 $(r_u)_{ave}$ versus E/E_L for OS sand-silt mixes

4.3 Contact density and energy loss

Figure 6 shows E_L versus e for OS sand-silt mixes consolidated to σ'_{vo}=100kPa and sheared at CSR = 0.2. E_L correlates log-linearly with e for each mix. e is a good measure of contact density when the analysis focuses on a particular soil having same FC. But, at same e, E_L for each mix decreases with increasing FC up to a threshold value (FC_{th}) and then it reverses. This could be accounted by using $(e_c)_{eq}$ and $(e_f)_{eq}$. Figure 7 shows $(e_c)_{eq}$ versus E_L plot for OS sand-silt mixes at $FC<FC_{th}$. This trend was observed for mixes of all three sands. Figure 8 shows $(e_f)_{eq}$ versus E_L plot at $FC>FC_{th}$.

4.4 Mobilized contact friction coefficient

Based on experimental data, the evolution of mobilized friction μ^* with increasing shear strain can be back-calculated using Eq.8. The theoretical relationship for μ^* is given by Eq.2. Theoretical values were calculated assuming three different packings: (a) simple cubic (SC), (b) body centered cube (BCC), and (c) face centered cube (FCC). Elastic properties of solids were assumed to be as follows: ν=0.25, G=30 MPa corresponding to crystal quartz mineral. Confining stress was σ_c'= 100 kPa.

For each full cycle of loading, Eq.8 was used to estimate μ^*. The estimated μ^* is plotted against the maximum shear strain γ (=1.5ε_a, ε_a=axial strain) during that cycle. Figures 9, 10 and 11 show a comparison of the theoretical and back-calculated values of μ^* versus shear strain for sand, silty sand, and sandy silt, respectively. In each case, the full-slip friction coefficients μ are different: μ=0.32 for OS-00, μ=0.17 for OS-25, and μ=0.11 for OS-60. Theoretically, higher the density higher is the mobilized friction coefficient at the same strain level. Full-slip friction is mobilized at a shear strain level of 0.20 to 0.45%. Although not shown in this paper, this strain level corresponded to the onset of significant pore pressure generation during cyclic loading.

In general, the back-calculated values for μ^* agrees well with the theoretical values. The agreement is better for sand (OS-00) than silty sand (OS-25) and sandy silt (OS-60). For a particular μ^* value, the experimental results for silty soils show higher shear strain than theoretical results. The reasons for this may be due to the limitations in the theory, which is applicable only for uniform size particles, as well as the differences in the elastic properties. It is also considered that the presence of fine grains in a coarser grain media may facilitate increased rolling slip and rearrangements, and hence may cause higher shear strains.

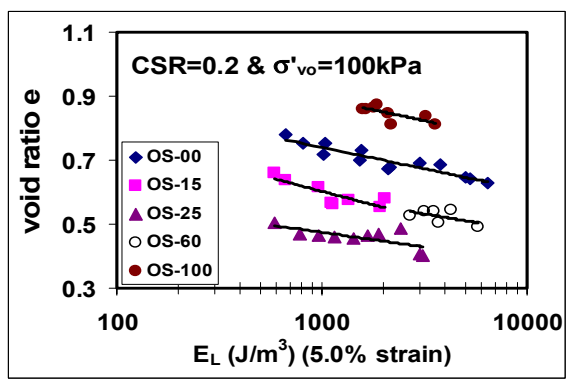

Figure 6 Void ratio versus E_L sand-silt mixes

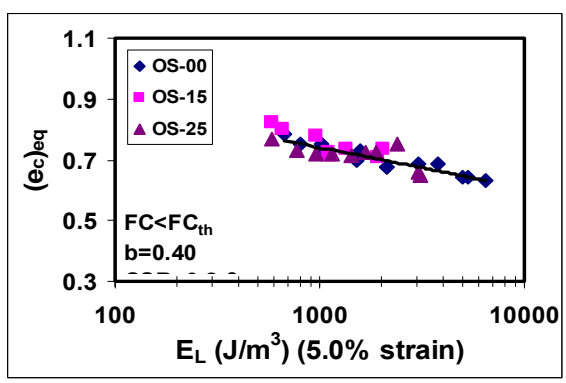

Figure 7 $(e_c)_{eq}$ versus E_L: $FC<FC_{th}$: Silty Sand

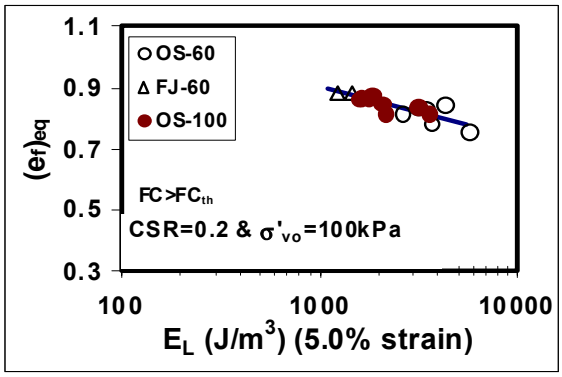

Figure 8 $(e_f)_{eq}$ versus E_L: FC>FC_{th}: Sandy Silt

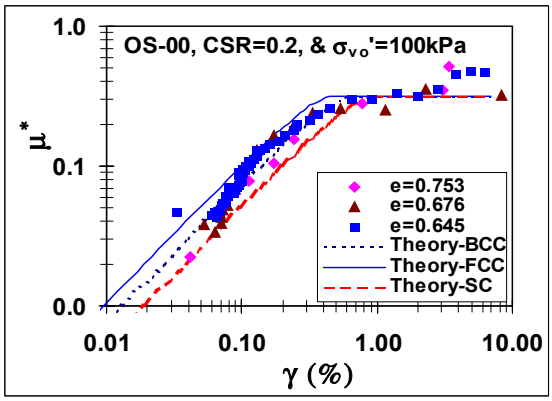

Figure 9 μ* versus γ (%) for OS-00: Sand

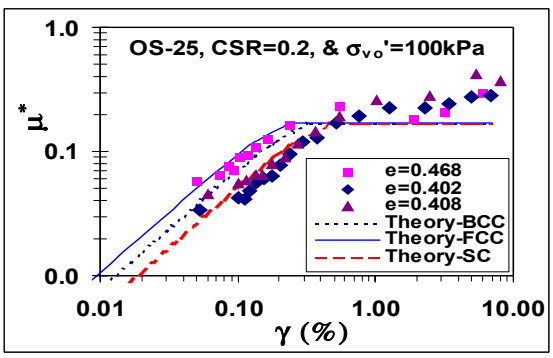

Figure 10 μ* versus γ (%) for OS-25: Silty Sand

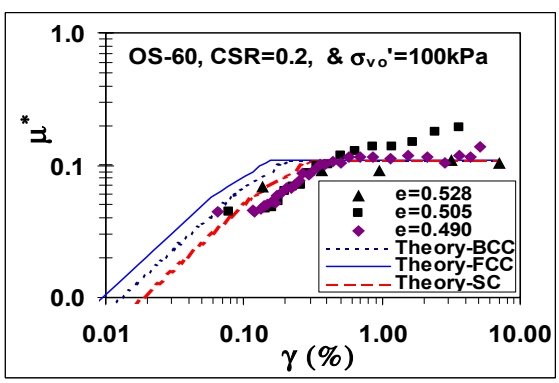

Figure 11 μ* versus γ (%) for OS-60: Sandy Silt

5 CONCLUSIONS

The internal frictional energy loss W estimated based on intergrain friction at contacts agrees fairly well with the external energy input E. Cyclic pore pressure ratio increases log-linearly with E/E_L, independent of contact density. The energy E_L required to cause liquefaction increases log-linearly with intergrain contact density. The mobilized friction coefficient evaluated from experimental data agrees well with that of theoretical values for sand. A limited agreement is observed for silty soils. Further research is needed to fully develop an understanding of the key factors affecting energy loss during cyclic loading, and better characterize liquefaction behavior of soil.

Acknowledgements

Financial support for this research by grants from NSF, NEHRP/USGS, and MCEER is gratefully appreciated.

REFERENCES

Berrill, J. B. and Davis, R. O. (1985). "*Energy dissipation and seismic liquefaction in sands*: *Revised model*" Soils and Found., Tokyo, 25(2), 106-118.

Figueroa, J. L., Saada, A. S., Liang, L., and Dahisaria, M. N. (1994). "*Evaluation of soil liquefaction by energy principles*" ASCE, J. Geotech. Eng., 120(9),1554-1569.

Kayen, R. E. and Mitchell, J. K. (1997). "*Assessment of liquefaction potential during earthquakes by arias intensity*" ASCE, J. Geotech. & Geoenv. Eng., 123(12), 1162-1174.

Mindlin, R. D., and Deresiewicz, H. (1953). "*Elastic spheres in contact under varying oblique forces*" ASME, J. Appl. Mech., 74, 327-344.

Nemat-Nasser, S. and Shokooh, A. (1979). "*A unified approach for densification and liquefaction of cohesionless sands in cyclic loading*" Can. Geot. J., 16, 659-678.

Okada, N. and Nemat-Nasser, S. (1994). "*Energy dissipation in inelastic flow of saturated cohesionless granular media*" Geotechnique, 44(1),1-19.

Thevanayagam, S. (1998). "*Effect of fines and confining stress on undrained shear strength of silty sands*" J. Geotech. & Geoenv. Engrg. Div., ASCE, 124(6), 479-491.

Thevanayagam, S. (1999). "*Effect of fines and confining stress on undrained shear strength of silty sands*" *Closure* of Discussion, J. Geotech. & Geoenv. Engrg. Div., ASCE, 125(11), 1024-1027.

Thevanayagam, S. (2000). "*Liquefaction potential and undrained fragility of silty sands*" *Proc., 12th World Conf. Earthq. Eng.*, R. Park, ed., Auckland, New Zealand, paper # 2383.

Thevanayagam, S., Liang, J., and Shenthan, T. (2000). "*A contact index for liquefaction potential analysis of silty/gravely soils*" *EM2000, Proc. 14th ASCE EMD Spec. Conf.*, Tassoulas, ed., Austin, Texas.

Thevanayagam, S. (2001). "*Role of intergranular contacts on mechanisms causing liquefaction and slope failures in siltysands*",http://erp-web.er.usgs.gov/reports/annsum/ vol43 / pt/pt_vol43.htm; USGS web.

Thevanayagam, S., Shenthan, T., Mohan, S. and Liang, J. (2002a). "*Undrained fragility of sands, silty sands and silt*" *ASCE, J. Geotech. & Geoenv. Eng.* 128 (10): 849-859.

Thevanayagam, S., Kanagalingam, T., and Shenthan, T. (2002b). "*Contact density – confining stress – energy to liquefaction*" *Proc. 15th ASCE Eng. Mech Conf.* Columbia Univ., Paper #428.

5.4 Liquefaction behavior and screening of sand and non-plastic silty soils, remediation, and other issues

5.4.1 Technical Articles

Analyses of liquefaction behavior and screening of sand and non-plastic silty soils, remediation, and other issues are presented in the following technical articles.

5.4.1.1 Thevanayagam, S. and Martin, G. R. (2001) "Liquefaction in Silty Soils – Screening and Remediation Issues", presented at the *12th Conf Soil dynamics and earthquake engineering*, Philadelphia, Oct.7-10, Drexel Univ., Published in J. Soil Dyn. Earthq. Eng. (October 2002 issue).

5.4.1.2 Thevanayagam, S., Martin, G.R., Shenthan, T., and Liang, J. (2001) "Post-liquefaction pore pressure dissipation and densification in silty soils." *Proc. 4th Int. Conf. on Recent Adv. in Geot. Earthq. Eng. and Soil Dyn*., San Diego, CA, Mar.2001, Paper 4.28.

5.4.1.3 Thevanayagam, S. and Liang, J. (2001) "Shear wave velocity relations for silty and gravely soils," Proc. *4th Intl Conf. Recent Adv. Geot. Earthq. Eng. & Soil Dyn*., San Diego, CA, Mar.2001, Paper 1.36.

5.4.1.4 Thevanayagam, S. (1999) "Intergrain contact and shear modulus of non-plastic granular mixes", *CD-ROM Proc. 13th ASCE Conf. on Eng. Mech*., Eds. Jones, N. and Ghanem, R., Johns Hopkins Univ., Maryland, June 13-16, 1999.

5.4.1.5 Thevanayagam, S. (2000). "Liquefaction in silty soils – Considerations for screening and retrofit strategies" *Proc. 2nd international workshop on mitigation of seismic effects on transportation structures*, Eds. C. Loh and I. Buckle, NCREE, Taipei, Taiwan.

5.4.1.6 Shenthan, T. (2001). "Factors affecting liquefaction mitigation in silty soils using stone columns." *MS Thesis*, University at Buffalo, NY, 220p. (not included in this report)

5.4.1.7 Shenthan, T. (2003). "Liquefaction mitigation in silty soils using composite stone columns with wick drains." PhD *Dissertation*, ***in preparation***, University at Buffalo, SUNY, NY. (not included in this report)

Articles 5.4.1.1 to 5.4.1.5 are presented following Sec. 5.4.2.

5.4.2 Conclusions

The main conclusions from this analysis are as follows:

- Laboratory undrained cyclic tests followed by dissipation were conducted to study the pore pressure generation, and post-liquefaction dissipation and densification behavior of silty sands and sandy silts. Pore pressure generation characteristics (r_u vs N/N_L) for sand and silty sand up to about 25% silt content follow the same trend found in literature for sand (e.g. Seed et al. 1976). The generation rate for silt and sandy silt (silt > 25%) is somewhat faster than that of sand at the beginning of the loading, and slows down as considerable amount of pore pressure (r_u of 0.5-0.6) has been built up.
- Soil skeleton is completely remolded during liquefaction and as a result post-liquefaction compression line (e vs. σ_c') almost parallels the pre-liquefaction virgin compression line. Liquefied soil behaves like a freshly deposited soil.
- For the same soil, post-liquefaction volume compressibility (m_v) and coefficient of consolidation (c_v) values are similar to those of the normally consolidated virgin soil at the same stress level.

- Coefficient of consolidation for silty soils is lower by more than one or two orders of magnitude and is primarily affected by the silt content (viz. permeability of the soil). For the same soil, coefficient of consolidation values of soils at low confining stresses (about 10 kPa) immediately following liquefaction are about an order of magnitude less than that at 100 kPa confining stress. It is significantly stress dependent.
- At the same void ratio, a silty sand ($FC<FC_{th}$) densifies more than clean sand following liquefaction. Post-liquefaction volumetric densification of sand and silty sand with silt content up to FC_{th} correlates well with equivalent intergranular void ratio, $(e_c)_{eq}$. Post-liquefaction volumetric compression of silty soils correlates well with equivalent interfine void ratio, $(e_f)_{eq}$.
- Ground improvement schemes for liquefaction mitigation in silty soils based on densification and drainage methods need to take into consideration of the differences in the above behavior characteristics of silts compared to sands. Primarily, permeability (and silt content) affects the dissipation characteristics of silty soils compared to sands. This requires much closer spacing of dynamic compaction grids or stone columns or provision of additional means such as supplementary wick drains to expedite dissipation of pore pressures developed during ground improvement operation in silty soils. Similarly, permeation grouting may be difficult to achieve unless very closer spacing is utilized which may increase the cost significantly.
- A sand and sand-silt mix show similar cyclic resistance (CRR), energy required to cause liquefaction E_L, strength s_{us}, shear wave velocity v_{s1}, m_v, and post-liquefaction densification characteristics when compared at the same $(e_c)_{eq}$, $(e_f)_{eq}$ or equivalent relative densities [$(D_{r,c})_{eq}$ and $(D_{r,f})_{eq}$]. However, there is a major difference between sand and sand-silt mixes when one considers c_v (flow and permeability) and time required to dissipate excess pore pressures.
- Since SPT tests involves partial drainage during the test, although the resistance of a sand and silty sand may be similar at the same contact density, the differences in c_v causes major differences in SPT resistance of sand and silty sand at the same contact density. The same applies to CPT resistance.
- At the same $(e_c)_{eq}$ (up to FC_{th}), c_v decreases and relative dissipation time increases with an increase in silt content. Due to high dissipation time a lower effective stress is maintained near the penetration tip of a cone or SPT sampler in a silty sand compared to sand at the same $(e_c)_{eq}$ resulting in a major reduction in $(N_1)_{60}$ and q_{c1N}. Beyond FC_{th}, at the same $(e_f)_{eq}$, only a slight reduction is observed in c_v. Hence only a small further reduction is expected in $(N_1)_{60}$ and q_{c1N} is expected. There is little change expected for CRR, E_L, s_{us}, and v_{s1} with increase in silt content at the same $(e_f)_{eq}$. Liquefaction screening techniques should account of these differences and need modifications based on these findings.

ELSEVIER

Soil Dynamics and Earthquake Engineering 22 (2002) 1035–1042

SOIL DYNAMICS AND EARTHQUAKE ENGINEERING

www.elsevier.com/locate/soildyn

Liquefaction in silty soils—screening and remediation issues

S. Thevanayagam[a,*], G.R. Martin[b]

[a]Department of Civil, Structural and Environmental Engineering, SUNY at Buffalo, Buffalo, NY 14260, USA
[b]Department of Civil Engineering, University of Southern California, Los Angeles, CA, USA

Abstract

Current techniques for liquefaction screening, ground modification for liquefaction mitigation, and post-improvement verification rely on knowledge gained from extensive research on *clean sands*, field observations of liquefied ground, and judicial correlation of normalized penetration resistance [$(N_1)_{60}$,q_{c1N}] or shear wave velocity (v_{s1}) data with field liquefaction observations. Uncertainties prevail on the direct extrapolation of such techniques for silty soil sites. This paper examines laboratory data on liquefaction resistance, strength, and v_{s1} of sands and silty soils using grain contact density as the basis. Effect of silt content on cyclic resistance, strength, m_v, and c_v is examined in this light. Rational insights on effects of silt content on the current screening techniques based on $(N_1)_{60}$, q_{c1N}, and v_{s1} to silty soils are offered. Recent advances and modifications to the traditional densification, drainage, and permeation grouting techniques to make them viable for silty soils are discussed.
© 2002 Elsevier Science Ltd. All rights reserved.

Keywords: Liquefaction; Sand; Silty sand; Silt; Shear wave velocity

1. Introduction

Saturated, loose granular deposits, when subjected to rapid shear loading, experience a rapid pore pressure increase and temporary loss of strength, which may lead to liquefaction, a stage, when soil looses almost all the strength and behaves like a liquid. Such a stage leads to lateral spreading of gently sloping ground, densification and vertical ground settlements, and slope instability. Case histories indicate that soil types prone to liquefaction are loose sand, silty sands/sandy silts containing mostly non-plastic silt, and gravel. Only rarely clays, except for sensitive clays, do experience loss of strength. Recent liquefaction-induced damages to port, transportation, and lifeline infrastructure at Kobe, Japan, and Taiwan are reminders of the need to develop and transfer prudent liquefaction screening techniques and remedial measures for its mitigation.

Current liquefaction screening techniques [1] rely on extensive laboratory research conducted on clean sands, and extrapolations of observed field performance during past earthquakes. Such observations have been documented in the form of normalized penetration resistance (SPT $(N_1)_{60}$, CPT q_{c1N}) [2,3], and shear wave velocity (v_{s1}) [4] vs. cyclic stress ratio (CSR) induced by the earthquakes (corrected for magnitude) at the relevant liquefied/non-liquefied sites as shown in Fig. 1. Cyclic resistance ratio (CRR) of a soil deposit (at a given $(N_1)_{60}$, q_{c1N} or v_{s1}) subjected to an earthquake of a certain magnitude is derived from demarcation lines drawn between the data points corresponding to those sites that liquefied and those that did not liquefy in Fig. 1. This CRR is compared against the anticipated CSR from a future earthquake of the same magnitude to discern whether or not that site would liquefy (Table 1). Researchers have observed that such a procedure depends on silt content of the soil. Tentative demarcation lines have been developed for fines contents less than 5, 15 and 35%. The rationale for such demarcation strategies needs to be clarified, limitations identified, and such strategies need to be refined.

Soil remediation techniques to mitigate liquefaction and lateral spread hazards primarily rely on densification, drainage, reinforcement, and in some cases on cementation/solidification by grouting [5,6]. They also primarily rely on the understanding of the behavior of clean sands. Their extension to liquefiable silty soils requires an understanding of the behavior of silty soils in general, and during implementation of such techniques, in particular. Where necessary these techniques need to be modified to make them suitable for silty soils (Table 2).

The first part of this paper focuses on recent developments in the understanding of the undrained cyclic

* Corresponding author. Tel.: +1-716-645-2114x2430.
E-mail addresses: theva@eng.buffalo.edu (S. Thevanayagam), geomar@usc.edu (G.R. Martin).

0267-7261/02/$ - see front matter © 2002 Elsevier Science Ltd. All rights reserved.
PII: S0267-7261(02)00128-8

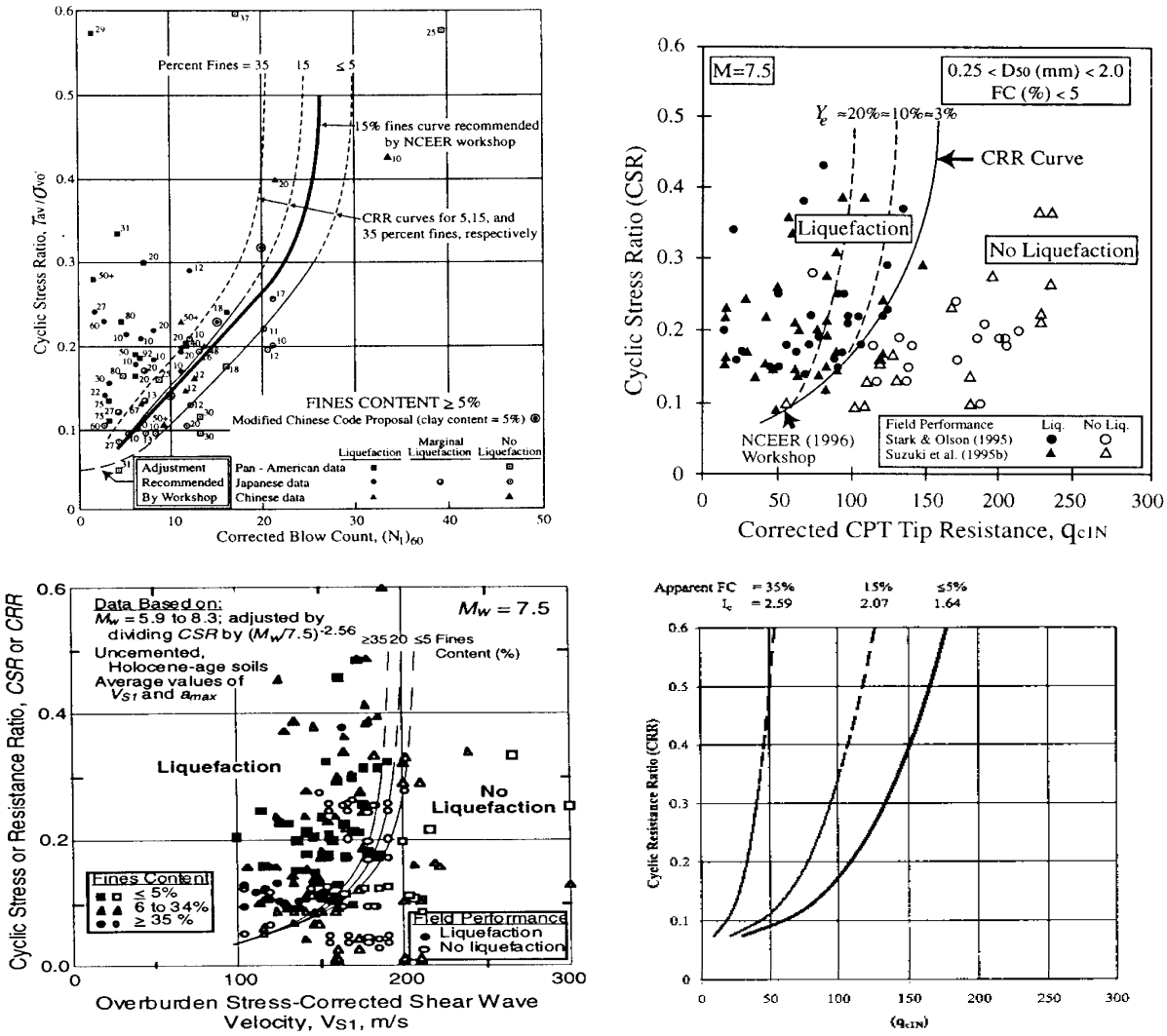

Fig. 1. Field liquefaction screening charts—SPT, CPT, and shear wave velocity [7,8].

resistance and post-liquefaction (densification/dissipation) behavior of silty soils compared to clean sands, based on intergrain contact density (Fig. 2, explained later) and pore size considerations, respectively. The second part extrapolates this understanding to discern how silt content affects the field response parameters such as $(N_1)_{60}$, q_{c1N} and v_{s1} when compared at the same intergrain contact density. Its implications on current liquefaction screening techniques

Table 1
Current liquefaction screening methods

Method	$CRR_{7.5}$	x	FS
SPT	$[a + cx + ex^2 + gx^3]/[1 + bx + dx^2 + fx^3 + hx^4]$	$(N_1)_{60cs} = \alpha + \beta(N_1)_{60}$	$(CRR_{7.5}/CSR)MSF$
CPT	$0.833[x/1000] + 0.05$ for $x < 50$;	$(q_{c1N})_{cs} = K_c q_{c1N}$	
	$93[x/1000]^3 + 0.08$ for $50 < x < 160$		
S-wave	$r(V_{s1}/100)^2 + s[1/(V_{s1c} - V_{s1}) - 1/V_{s1c}]$		

(i) FS = Factor of safety against liquefaction, CSR = stress ratio caused by earthquake, MSF = magnitude scaling factor; (ii) $\alpha = 0$ and $\beta = 1$ for FC < 5; $\alpha = \exp[1.76 - (190/FC^2)]$ and $\beta = [0.99 + (FC^{1.5}/1000)]$ for 5 < FC < 35; $\alpha = 5$ and $\beta = 1.2$ for FC > 35, FC = fines content by weight, $a = 0.048$, $b = -0.1248$, $c = 0.004721$, $d = 0.009578$, $e = 0.0006136$, $f = -0.0003285$, $g = -1.673 \times 10^{-5}$; $h = 3.714 \times 10^{-6}$; (iii) $K_c = 1.0$ for $I_c < 1.64$, $K_c = -0.403I_c^4 + 5.581I_c^3 - 21.63I_c^2 + 33.75I_c - 17.88$ for $I_c > 1.64$; $I_c = [(3.47 - \log Q)^2 + (1.22 + \log F)^2]^{0.5}$, $Q = [(q_c - \sigma_{vo})/P_a][(P_a/\sigma'_{vo})^n]$, $F = 100[f_s/(q_c - \sigma_{vo})]\%$; (iv) $r = 0.022$, $s = 2.8$; $V_{s1c} = 220$ m/s for FC < 5, $V_{s1c} = 210$ m/s for FC = 20, $V_{s1c} = 200$ m/s for FC > 35; (v) $(N_1)_{60}$ and $(N_1)_{60cs}$ = stress − normalized SPT blow count of silty soil, and equivalent clean sand blow count, respectively; q_{c1N} and $(q_{c1N})_{cs}$ = stress − normalized cone penetration resistance of silty soil, and equivalent clean sand resistance, respectively; q_c and f_s = measured cone tip and side resistance, respectively; P_a = atmospheric pressure; σ_{vo} and σ'_{vo} = total and effective vertical overburden stresses at the cone tip, respectively; $n = 1.0$; V_{s1} = stress-normalized shear wave velocity in m/s.

Table 2
Potential methods for liquefaction mitigation in silty soils (emerging new techniques are indicated in italics)

Technique	Soil treated		
	Sand (fines < 5%)	Silty sand	Silt
Permeation grout	Yes	Marginal	No
Compaction grout	Yes	Yes	Marginal
Soil mixing	Yes	Yes	Yes
Jet grout	Yes	Yes	Yes
Electro-kinetic injection	No	*Yes*	*Yes*
Passive grouting	*Yes*	*Marginal*	No
Stone column and dynamic compaction	*Yes*	*Provide drains*	*Provide drains*

are discussed and limitations are identified. Design considerations for liquefaction mitigation are addressed.

2. Soil strength: effect of contact density

Fig. 3 shows the number of cycles required to reach liquefaction vs. void ratio for Ottawa sand/silt mix, tested at a constant stress ratio (CSR) of 0.2. The specimens were prepared by mixing Ottawa sand ($D_{50} = 0.25$ mm) with a non-plastic silt ($d_{50} = 0.01$ mm) at different silt contents (0–100 wt%, [os15 = sand–silt mix at 15% silt content]) [9]. At the same void ratio, cyclic strength of silty sand decreases with an increase in silt content. Beyond a transition silt content (about 20–30%), the trend reverses and the strength increases with further increase in silt content. Similar observation has been elsewhere [10]. This observation, thought to be apparently in contradiction to the screening charts in Fig. 1, has puzzled many researchers.

Recently, Thevanayagam and co-workers [11,12] proposed that mechanical properties of soils are derived from intergrain contact. Therefore, it is not proper to compare silty soil behavior with that of clean sand using global void ratio or any other solid density parameter. Sand and sand–silt mixes are expected to show similar mechanical behavior if compared at a same contact density index. A soil classification system based on contact density has been developed (Fig. 2) and the relevant contact density indices, $(e_c)_{eq}$ and $(e_f)_{eq}$, respectively, for soils at silt content (FC) less than and more than a threshold value FC_{th} have been identified.

Fig. 4(a) and (b) show the same data shown in Fig. 3, but plotted against $(e_c)_{eq}$ [$b = 0.35$] for $FC < FC_{th}$ and $(e_f)_{eq}$ [$m = 0.65$] for $FC > FC_{th}$, respectively. When compared at the same intergrain contact density, cyclic resistance of silty sand is similar to that of host sand; cyclic resistance of sandy silt is similar to that of the host silt. This is also true if the resistance to liquefaction is measured in terms of energy required to cause liquefaction (Fig. 4(c) and (d)).

Similarly Fig. 5(a) and (b) shows the steady state data obtained from undrained monotonic tests on the same sand–silt mix plotted against $(e_c)_{eq}$ [$b = 0.25$] for $FC < FC_{th}$ and $(e_f)_{eq}$ [$m = 0.65$] for $FC > FC_{th}$, respectively [13]. All data points fall in a narrow band correlating well with the relevant contact density indices.

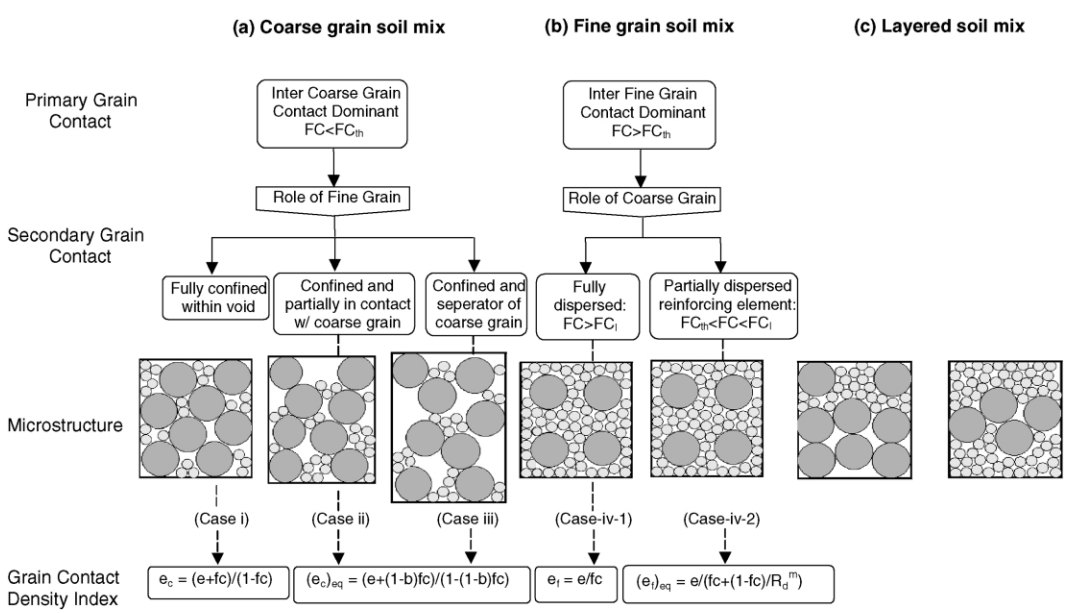

b=portion of the fine grains that contribute to the active intergrain contacts; e=global void ratio; FC=fine grains content; FC_{th}=threshhold fine grains content, $FC_{th}<(100e/e_{max,HF})\%$; FC_l=limit fines content, $FC_l>100(1-\pi(1+e)/(6s^3))\%>FC_{th}$; m: reinforcement factor; R_d=D/d=particle size disparity ratio; $s=1+a/R_d$, a=10; $e_{max,HF}$: the maximum void ratio of host fine

Fig. 2. Granular mix classification and contact density indices.

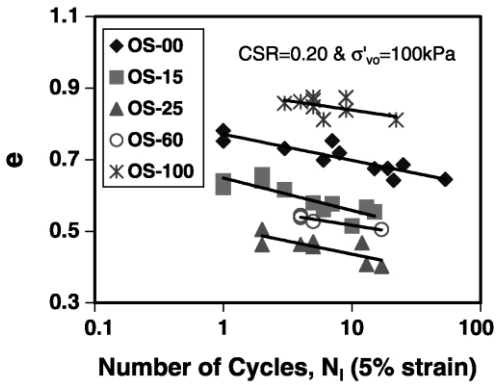

Fig. 3. Void ratio vs. liquefaction potential of silty soils.

3. Shear wave velocity: effect of contact density

Fig. 6(a) shows the normalized shear velocity data (v_{s1}) for tone river sand (TRS) and three other gravely soils prepared by mixing TRS with 25, 50 and 75 wt% of gravel [14]. Designating sand as fine grain and gravel as coarse grain, Fig. 6(b) shows the same data plotted in terms of $(e_f)_{eq}$ [$m = 0.45$] [11]. At the same $(e_f)_{eq}$, sand and gravely sand have similar shear wave velocity.

Fig. 7 shows shear modulus of the Ottawa sand–silt mixes at 0.05% axial strain plotted against $(e_c)_{eq}$ [$b = 0.25$]. At the same $(e_c)_{eq}$, sand and silty sand show similar shear modulus [15]. Similarly, it has been also observed that volume compressibility and post-liquefaction densification characteristics of silty soils are also affected by contact density.

4. Flow and dissipation: effect of silt content

Fig. 8(a) and (b) shows c_v vs. $(e)_{eq}$ [$(e_c)_{eq}$ or $(e_f)_{eq}$] and normalized (c_{vo}/c_v) at nearly the same $(e)_{eq}$ vs. silt content, where c_v and c_{vo} are the coeffecients of consolidation of Ottawa sand–silt mix and clean Ottawa sand, respectively. There is no correlation for c_v with $(e)_{eq}$. The (c_{vo}/c_v) increases rapidly with an increase in silt content up to about FC_{th} and it is less affected at $FC > FC_{th}$. At the same contact density, an increase in silt content significantly affects the pore size and permeability, and hence reduces c_v. At $FC > FC_{th}$, the degree of change in pore size is small with a further increase in FC at the same e_f or $(e_f)_{eq}$. Although the absolute magnitude variation in c_{vo}/c_v shown in Fig. 8(b) depends on the grain size characteristics of the host silt and sand, for other sand–silt mixes, the trend is expected to be the same.

5. Implications

The above observations indicate that a sand and sand–silt mix show similar cyclic resistance (CRR), energy required to cause liquefaction E_l, G, m_v, and v_{s1} as the host sand or silt, when compared at the same $(e_c)_{eq}$ or $(e_f)_{eq}$, respectively. But there is major difference between sand and sand–silt mixes when one considers $c_v(=k/(m_v\gamma_w))$ and the degree of excess pore pressure dissipation achievable in a given time duration. This can be deduced from Fig. 8(b) considering (c_{vo}/c_v) as a relative measure of the time it would take for dissipation of excess pore pressure in a

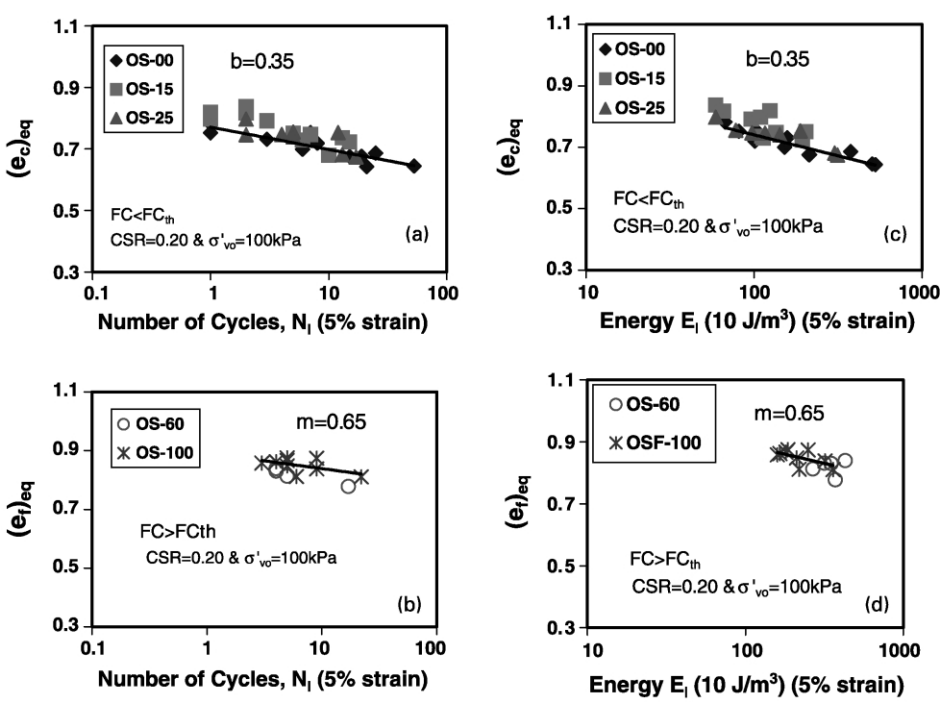

Fig. 4. Influence of contact density: (a and c) $(e_c)_{eq}$; (b and d) $(e_f)_{eq}$.

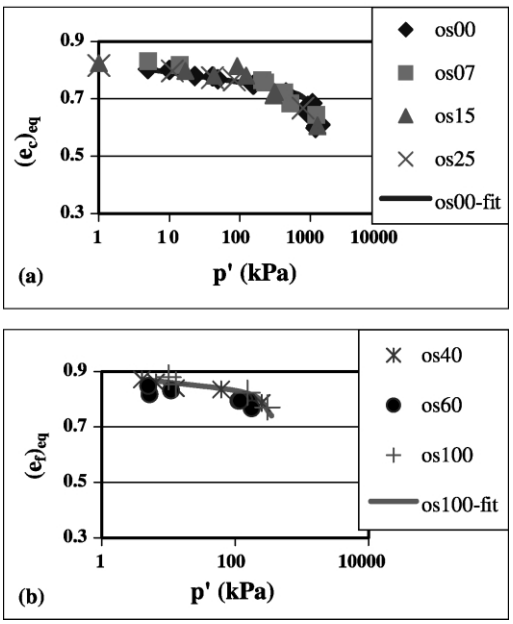

Fig. 5. Influence of contact density: (a) $(e_c)_{eq}$ vs. p'; (b) $(e_f)_{eq}$ vs. p'.

sand–silt mix normalized to clean host sand for the same loading and geometric boundary conditions. The problem under consideration could be the dissipation of excess pore pressure around CPT and SPT during penetration, dissipation and densification around a vibro-compaction stone column or soil under dynamic compaction, pore pressure redistribution during an earthquake, etc. In each case the degree of dissipation achievable in a given duration would be smaller for silty sand, up to FC_{th}, than the host sand at the same $(e_c)_{eq}$.

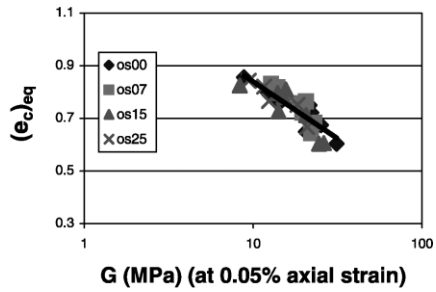

Fig. 7. $(e_c)_{eq}$ vs. $G_{0.05}$.

5.1. Liquefaction screening

Table 3 presents a qualitative summary of the expected degree of influence of silt content on undrained CRR, field measured parameters $(N_1)_{60}$, q_{c1N}, and v_{s1}, and its impact on the expected trend for $(N_1)_{60}$, q_{c1N}, v_{s1} vs. CRR in the field.

First, Table 3 summarizes the effect of increase in silt content on k, c_v, undrained CRR or E_l, v_{s1}, when compared at the same $(e_c)_{eq}$ for $FC < FC_{th}$ and $(e_f)_{eq}$ for $FC > FC_{th}$. It also shows the effect of silt on relative dissipation time for a silty soil compared to sand or silt subjected to the same loading history.

Secondly, based on the relative dissipation time, it summarizes the anticipated relative influence of increase in silt content on field $(N_1)_{60}$, q_{c1N}, and v_{s1} compared at the same $(e_c)_{eq}$ or $(e_f)_{eq}$. At the same $(e_c)_{eq}$ (up to FC_{th}), c_v decreases rapidly and relative dissipation time increases with an increase in silt content. The increase in dissipation time helps to maintain a lower effective stress near the penetration tip of a cone or SPT sampler in a silty sand than

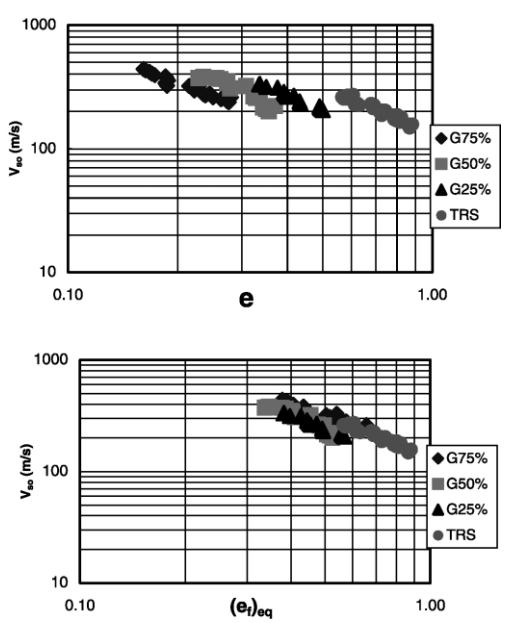

Fig. 6. Influence of gravel content: (a) void ratio e; (b) $(e_f)_{eq}$.

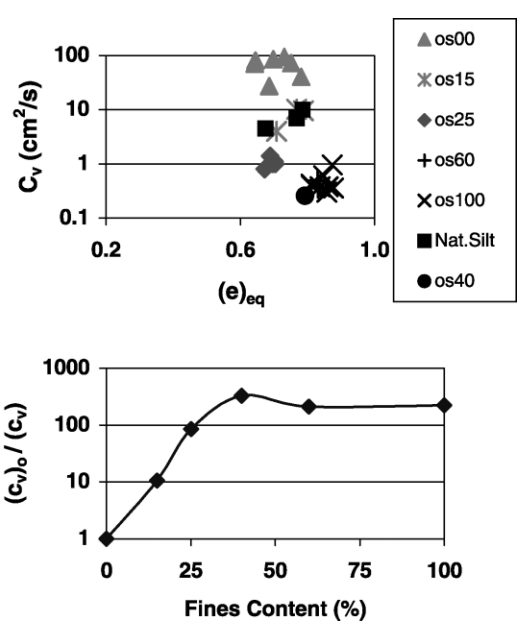

Fig. 8. Relative coefficient of consolidation ratio-fines content.

Table 3
Effect of increase in silt content at constant $(e_c)_{eq}$ or constant $(e_f)_{eq}$

Primary role		Lab measured parameter				Field measured parameter[a]			Liquefaction screening		
Coarse grain	Fine grain	k and c_v	Mono. undr. strength	CRR and energy	V_{s1}	V_{s1}	SPT $(N_1)_{60}$	CPT q_{c1N}	V_{s1} vs. CRR	$(N_1)_{60}$ vs. CRR	q_{c1N} vs. CRR
Primary contact $FC < FC_{th}$, $(e_c)_{eq}$ = constant	Block pores, reduce pore size	Major reduction in k due to decrease in void ratio and pore size compared to sand Rapid increase in dissipation time	Minor change compared to sand	Minor change compared to sand	Minor change compared to sand	Minor change Compared to sand	Reduction in $(N_1)_{60}$ compared to sand due to reduction in k and c_v and rapid increase in dissipation time	Reducion in q_{c1N} compared to sand due to reduction in k and c_v and rapid increase in dissipation time	Minor impact on CSR to cause liquefaction at the same V_{s1}	Higher CSR than sand to cause liquefaction at the same $(N_1)_{60}$	Higher CSR than sand to cause liquefaction at the same q_{c1N}
Reinforcement	Primary contact $FC > FC_{th}$ $(e_f)_{eq}$ = constant	May expect a slight increase in k due to increase in void ratio, but decrease in pore size reduces the k. Minor increase in dissipation time beyond FC_{th} Smaller k and c_v than for sand at comparable $(e_c)_{eq}$	Minor change compared to silt	Minor change compared to silt	Minor change compared to silt	Minor change compared to silt	Minor reduction in $(N_1)_{60}$ for sandy silt compared to silty sand due to reduction in k and c_v and minor increase in dissipation time beyond FC_{th} Major reduction in $(N_1)_{60}$ for sandy silt compared to sand at comparable $(e_c)_{eq}$ due to smaller c_v.	Minor reduction in q_{c1N} for sandy silt compared to silty sand due to reduction in k and c_v and minor increase in dissipation time beyond FC_{th} Major reduction in q_{c1N} for sandy silt compared to sand at comparable $(e_c)_{eq}$ due to smaller c_v.	Negligible impact on CSR to cause liquefaction at the same V_{s1}	Slightly higher CSR than silty sand to cause liquefaction at the same $(N_1)_{60}$	Slightly higher CSR than silty sand to cause liquefaction at the same q_{c1N}

k = permeability, c_v = coefficient of consolidation, s_{us} = undrained shear strength (large strain), CRR = cyclic resistance ratio.
[a] Field CRR is considered to be similar to undrained CRR.

in host sand. Thus a gradual reduction is anticipated for $(N_1)_{60}$ and q_{c1N} in silty sands up to FC_{th} compared to host sand at the same $(e_c)_{eq}$. Beyond FC_{th}, at the same $(e_f)_{eq}$, only a slight change is observed for c_v. Hence, only a small change is expected in $(N_1)_{60}$ and q_{c1N} in a sandy silt with a further increase in silt content at the same $(e_f)_{eq}$.

What would be the influence of silt content on field CRR as opposed to laboratory undrained CRR, when compared at the same relevant $(e)_{eq}$, is the next question. Due to relatively much larger thickness of a soil deposit subjected to seismic excitation in contrast with the small zone of soil influenced by a SPT sampler and CPT cone, the relative influence of c_{vo}/c_v on field CRR (that reflects partial drainage during excitation) is much smaller compared to its effect on SPT and CPT resistance. Therefore, the error in assuming that CRR of a field soil is not significantly different from undrained conditions is smaller, except for special field conditions involving thinly layered soils.

The combined impact of this on CSR required to cause liquefaction at a given $(N_1)_{60}$, q_{c1N}, and v_{s1} is summarized in Table 3. The CSR vs. v_{s1} relationship is affected very little by silt content. The CSR required to cause liquefaction at a given $(N_1)_{60}$ or q_{c1N} is expected to increase with silt content up to FC_{th}. Conversely the $(N_1)_{60}$ and q_{c1N} required to resist liquefaction in silty soils at a given CSR is expected to decrease from that of clean sand with an increase in silt content up to FC_{th}. The magnitude of reduction for $(N_1)_{60}$ and q_{c1N} depends on the relative c_v/c_{vo}. The relative magnitude of reduction is also expected to be different for SPT and CPT due to differences in probe geometry. The $(N_1)_{60}$ or q_{c1N} required to resist liquefaction is expected to be affected further only slightly beyond FC_{th}.

The current screening charts (Fig. 1) based on direct observations do, to some extent, reflect this expected trend. The 35% fines content limit in the SPT and CPT charts also agrees with typical FC_{th} threshold limit values identified before. The weak silt-content dependent corrections introduced in the s-wave chart in Fig. 1 is perhaps unnecessary, except for possible reasons of minor cementation effects.

The same reasoning (Table 3) also indicates that the CRR vs. $(N_1)_{60}$ or q_{c1N} chart should also be sensitive to relative grain size ratio of clean sand and silt. Different relationships would exist for very fine sand and coarse sand [16], even if no silt is present. A unique demarcation line between liquefied and non-liquefied sites may not be possible in Fig. 1 for all soils.

5.2. Liquefaction mitigation

The fact that non-plastic silty soils behave similar to sands when compared at the appropriate contact density index parameters but show silt content dependent c_v has a dramatic impact on liquefaction mitigation in silty soils. Low permeability and c_v render the effectiveness of traditional densification, drainage, and permeation (grouting) techniques limited in silty soils unless modifications are incorporated. Preliminary analyses indicate that closer spacing of dynamic compaction grids and stone columns along with provision of supplementary (wick) drains can expedite the dissipation of excess pore pressures developed during ground improvement operation in silty soils and help to achieve desired densification. Limited field data [17,18] and analyses [19] show that supplementary wick drains do help relieve pore pressures developed during dynamic compaction and stone column installation in silty soils and help densification. Effectiveness of permeation grouting in silty soils is limited due to low permeability and short setting times associated with traditional grouts. Passive permeation techniques using very slow setting grouts pumped into the ground using natural groundwater gradients [20] and electrokinetic injection of grouts [21] also appear attractive means for liquefaction remediation in silty soils. Effective design guidelines for such systems are still lacking and need to be developed.

Acknowledgments

Financial support by the USGS, NSF, MCEER, and FHWA for the various aspects of this work is gratefully appreciated. Thanks are also due to T. Kanagalingam, J. Liang, and T. Shenthan, University at Buffalo, SUNY for their assistance.

References

[1] Youd TL, Idriss IM. editors. Proceedings of the NCEER Workshop on Evaluation of Liquefaction Resistance of Soils. NCEER Technical Report NCEER-97-0022; 1997. p. 276.
[2] Seed HB, Idriss IM, Arango I. Evaluation of liquefaction potential using field performance data. J Geotech Engng, ASCE 1983;109(3): 458–82.
[3] Robertson PK, Wride CE. Evaluation of cyclic liquefaction potential based on the CPT, Seis. Behavior of ground and geotechnical Structures, Rotterdam: Balkema; 1997. p. 269–78.
[4] Andrus RD, Stokoe KH. Liquefaction resistance of soils from shear-wave velocity. J Geotech Geoenviron Engng, ASCE 2000;126(11): 1015–25.
[5] JGS, Remedial measures against soil liquefaction: from investigation and design to implementation. Japan: Port and Harbor Research Institute; 1995.
[6] Cooke HG, Mitchell JK. Guide to remedial measures for liquefaction mitigation at existing highway bridge sites. MCEER-99-0015, SUNY, Buffalo, USA; 1999. p. 168.
[7] Youd TL, Gilstrap SD. Liquefaction and deformation of silty and fine-grained soils. In: Seco e Pinto P, editor. Proceedings of the Second International Conference on Earthquake Geotechnical Engineering, vol. 3. Rotterdam: Balkema; 1999. p. 1013–20.
[8] Stokoe KHII, Darendeli MB, Andrus RD, Brown LT. Dynamic soil properties: laboratory, field and correlation studies. In: Seco e Pinto P, editor. Second International Conference on Earthquake Geotechnical Engineering, vol. 3. Rotterdam: Balkema; 1999. p. 811–45.
[9] Thevanayagam S, Fiorillo M, Liang J. Effect of non-plastic fines on undrained cyclic strength of silty sands. ASCE Geotech Spec Publ 2000;107:77–91.

[10] Zlatovic S, Ishihara K. Normalized behavior of very loose non-plastic soils: effects of fabric. Soils Foundations 1997;37(4):45–56.

[11] Thevanayagam S. Liquefaction and shear wave velocity characteristics of silty/gravely soils—implications for bridge foundations. In: Nishikawa K, editor. Proceedings of 15th US–Japan Bridge Workshop, PWRI, Japan; 1999. p. 133–47.

[12] Thevanayagam S. Liquefaction potential and undrained fragility of silty soils. In: Park R, editor. Proceedings of 12WCEE Conference, Auckland, New Zealand; 2000. Paper# 2383.

[13] Thevanayagam S, Martin GR, Shenthan T, Liang J. Post-liquefaction pore pressure dissipation and densification in silty soils. In: Prakash S, editor. Proceedings of the Fourth International Conference on Recent Advances in Geotechnical Earthquake Engineering and Soil Dynamica, San Diego; 2001. Paper# 4.28.

[14] Kokusho T, Yoshida Y, Tanaka Y. Shear wave velocity in gravelly soils with different particle gradings. ASCE Geotech Spec Publ 1995; 56:92–106.

[15] Thevanayagam S, Liang J. Shear wave velocity relations for silty and gravely soils. In: Prakash S, editor. Proceedings of the Fourth International Conference on Recent Advances in Geotechnical and Earthquake Engnineering and Soil Dyanmics, San Diego; 2001. Paper#1.36.

[16] Mitchell JK, Tseng D-J. Assessment of liquefaction potential by cone penetration resistance. In: Duncan M, editor. Proceedings of the Seed Memorial Symposium; 1991. p. 335–50. Berkeley, CA.

[17] Dise K, Stevens MG, Von Thun JL. Dynamic compaction to remediate liquefiable embankment foundation soils. ASCE Geotech Spec Publ 1994;45:1–25.

[18] Luehring R, Snorteland N, Stevens M, Mejia L. Liquefaction mitigation of a silty dam foundation using vibro-stone columns and drainage wicks: a case history at Salman Lake Dam. Proceedings of the Dam Safety Conference, Colorado; 11–15 September 2001.

[19] Shenthan T. Factors affecting liquefaction mitigation in silty soils using stone columns, MS Thesis, University at Buffalo, SUNY, NY; 2001. p. 129.

[20] Gallagher PM, Mitchell JK. Passive site remediation for mitigation of liquefaction risk. In: Bruneau M, Inman DJ, editors. Proceedings of the MEDAT-2 workshop, MCEER, University at Buffalo, SUNY, NY; 2000. p. 29–36.

[21] Thevanayagam S, Jia W. Liquefaction remediation in silty soils. In: Bruneau M, Inman DJ, editors. Proceedings of the MEDAT-2 Workshop, MCEER, University at Buffalo, SUNY, NY; 2000. p. 23–8.

POST-LIQUEFACTION PORE PRESSURE DISSIPATION AND DENSIFICATION IN SILTY SOILS

S.Thevanayagam
Assoc. Prof., Dept. of Civil, Struc. and Env. Eng.
212 Ketter Hall, SUNY Buffalo
Buffalo, NY 14260
Email: theva@eng.buffalo.edu
Tel: 716 645 2114 Ext:2430
Fax: 716 645 3733

G.R.Martin
Professor, Dept. of Civil and Env. Eng.
USC, Los Angeles, CA 90089-2531

T.Shenthan, and J.Liang
Grad. Students
212 Ketter Hall, SUNY Buffalo
Buffalo, NY 14260

ABSTRACT

Pore pressure generation, and post-liquefaction dissipation and densification characteristics are data essential for detailed analysis of performance of sites containing liquefiable sands during and after earthquakes. These characteristics are also necessary for the design, analysis and choice of appropriate ground modification systems to mitigate liquefaction-induced hazards. Past research has addressed such material characteristics for clean sands. However, there are many sites that comprise non-plastic silts or silty sands have experienced liquefaction-induced damage. This paper presents results from an experimental study on silts and silty sands. Pore pressure generation characteristics are evaluated and compared with that of sands. Pre- and post-liquefaction compressibility and coefficient of consolidation, and densification characteristics are determined from undrained cyclic tests data followed by dissipation. Implications of these findings on the earthquake performance of sites containing non-plastic silts and silty sands are discussed. Their impacts on the choice of ground improvement techniques are also discussed.

INTRODUCTION

Soil liquefaction has been matter of great interest in geotechnical engineering for more than three decades. Apart from its dramatic disasters such as landslides, sand boils, cracks, foundation failures, etc., excessive settlements can be hazardous too. Pore water pressure builds up in saturated soils due to cyclic shearing. At the same time, dissipation of this shear induced pressure takes place at a rate depending on the hydraulic conductivity and volume compressibility of the soil and available drainage paths. When the loading is such that the rate of pore pressure generation is much faster than that of dissipation, a non-plastic soil will temporarily loose a large portion of its strength, which may lead to liquefaction, a stage, when soil looses almost all the strength and behaves like a liquid. Pore pressure dissipation will usually be accompanied by a reduction in volume of voids, hence settlement of ground surface. This kind of settlements are lower for denser soils than that for looser ones. This knowledge is the basic for analysis of earthquake performance of sites and design of soil improvement techniques such as dynamic densification, vibro-stone columns, deep blasting, etc.

Current design guidelines for practice of the above soil improvement techniques to mitigate liquefaction and settlement hazards is mainly based on the extensive research work that has been conducted using clean sands (e.g. Seed et al. 1976, Seed and Booker 1977). However, recent earthquake case histories indicate that sites containing a significant percentage of finer grains, mostly non-plastic, also liquefy due to seismic loading. Only a limited amount of research information is available for silty soils. Current research work indicates that these soils behave differently from clean sands, and that the knowledge gained from past three decades of research on clean sands does not directly translate to silty soils. Further modifications to the traditional ground densification/drainage techniques are needed to mitigate liquefaction effects in silty soils. Installation of supplementary wick drains have been observed to help relieve pore pressures developed during dynamic compaction and stone column installation in silty soils (Dise et al. 1994, and Luehring et al. 2000) and help densification. Therefore, not surprisingly, evaluation of pre- and post-liquefaction characteristics of silty soils, which are important in selecting the appropriate ground improvement technique and in designing such systems with appropriate modifications, has recently attracted attention of researchers (Andrews 1998, Baez and Martin 1995).

This paper presents results from an experimental study on non-plastic sand-silt mixes having silt contents from 0% to

100% by weight, and a natural silt. Undrained cyclic triaxial tests followed by dissipation were carried out in order to determine pore pressure generation, pre- and post-liquefaction compressibility, coefficient of consolidation, and densification characteristics. Observations from this study are summarized.

EXPERIMENTAL PROGRAM

Laboratory tests were carried out using artificial soil mixes of a sand (Foundry sand #55) and a non-plastic silt (Sil-co-sil#40), which are commercially available from U.S.Silica Company. The soils were mixed thoroughly until there was no obvious color difference. Table 1 summarizes the index properties of different mixtures. A limited number of tests were also conducted on a natural silt.

Specimen Preparation: Cylindrical specimens having typical dimensions of 155 mm in height and 75 mm in diameter were prepared using Moist Tamping Method. Each specimen was prepared at a different target void ratio. A known weight of dry solids required to reach the target void ratio was weighed and mixed thoroughly with water at a water content of about 5%. The soil was divided into four equal portions. Each portion was poured into a mold mounted on a triaxial cell, and tamped gently using a wooden rod until the height corresponding to the target void ratio was achieved. The specimen was then percolated with CO_2 and saturated with deaired water using back pressure saturation. The back pressure was increased gradually while maintaining the effective confining pressure at 15 to 20 kPa. This process was continued until the B ($=\Delta u/\Delta\sigma_c$) factor exceeded 0.95. Following saturation, the specimens were consolidated to an effective isotropic consolidation stress of 100 kPa.

Table 1. Index Properties

	Sand / Silt Ratio by weight				
Property	**100/0**	**85/15**	**75/25**	**40/60**	**0/100**
G_s	2.65				2.65
e_{min}	0.608	0.428	0.309	0.413	0.627
e_{max}	0.79	0.75	0.86	1.35	2.10
D_{10} (mm)	0.16	0.018	0.0085	0.0027	0.0015
D_{30} (mm)	0.22	0.19	0.15	0.01	0.006
D_{50} (mm)	0.25	0.235	0.23	0.0285	0.01
D_{60} (mm)	0.27	0.245	0.24	0.07	0.015
C_u	1.69	13.61	28.24	25.93	10.00
C_g	1.12	8.19	11.03	0.53	1.60

e_{min} = minimum void ratios (ASTM D1557), e_{max} = maximum void ratios (ASTM D4254 method C).

In each stage the amount of water flowing into or out of the specimen was recorded. Final void ratio at the end of consolidation of the specimen was calculated using the dry weight of the solids, specific gravity of solids, and net volume of water introduced into the specimen.

Following consolidation phase, a small amount of water was removed from the triaxial cell while the cell pressure was maintained the same as the value at the end of consolidation. This was done to make room for cyclic movement of the axial loading piston into and out of the triaxial cell during the cyclic loading phase without adversely affecting the cell pressure.

Cyclic Loading: Undrained cyclic loading was applied using a triaxial apparatus (GEOCOMP Inc., MA). The tests were conducted at a constant cyclic stress ratio ($CSR=\Delta\sigma_1/2\sigma_c'$) of 0.2 at a frequency of 0.2 Hz. For safety purposes, the maximum axial strain allowable was set at 8%. The axial displacement, cell pressure, and sample pore water pressure were monitored using a built-in data acquisition system. Once the specimen liquefied, cyclic loading phase was terminated.

Pore Pressure Dissipation. Post-liquefaction pore pressure dissipation tests were initiated immediately following the cyclic loading. The bottom end of the specimen was connected to a pressure controlled volume measuring burette. The top end of the specimen was connected to a pore pressure transducer with no drainage allowed from this end. This setup simulated a one-way drainage condition. The dissipation tests were done in three stages. In the first stage the pressure in the burette was set at a value such that the post-consolidation effective stress in the specimen was 25kPa. In the second and third stages, the burette pressure was set at values such that the effective stresses were, 50 and 100 kPa, respectively.

The pore pressure at the top of the specimen and outflow volume of water from the bottom of the specimen versus elapsed time were recorded in each stage. The duration of each stage varied from 16 sec to more than 3 hours, depending on the silt content of the specimen.

ANALYSIS

Pore Pressure Generation: Figure 1 shows pore pressure ratio, (r_u = shear induced pore pressure due to cyclic loading/ σ_c') versus normalized number of cycles to reach liquefaction for a few specimens, at different silt contents. The specimen notations are as follows: os25-408 = Ottawa sand/silt mix at 25% silt content and e=0.408. Also shown in this figure is the best-fit curve for sands proposed by Seed et al. (1976). The data for sand and silty sand up to about 25% silt content follow the pattern found by Seed at al. The pattern for silt and sandy silt at high silt contents appears to deviate from the above trend, and it needs further study.

Compressibility: Pre-liquefaction virgin consolidation lines and post-liquefaction consolidation lines (e vs. σ_3') were drawn from volume change data obtained during the tests. Figures 2a-b show example plots for sand and silt, respectively. The post-liquefaction consolidation line is nearly parallel to the virgin consolidation line. This indicates that during liquefaction the soil skeleton is completely remolded and behaves like a freshly deposited soil. The post-liquefaction compression line follows a new virgin consolidation line differing from a typical recompression line.

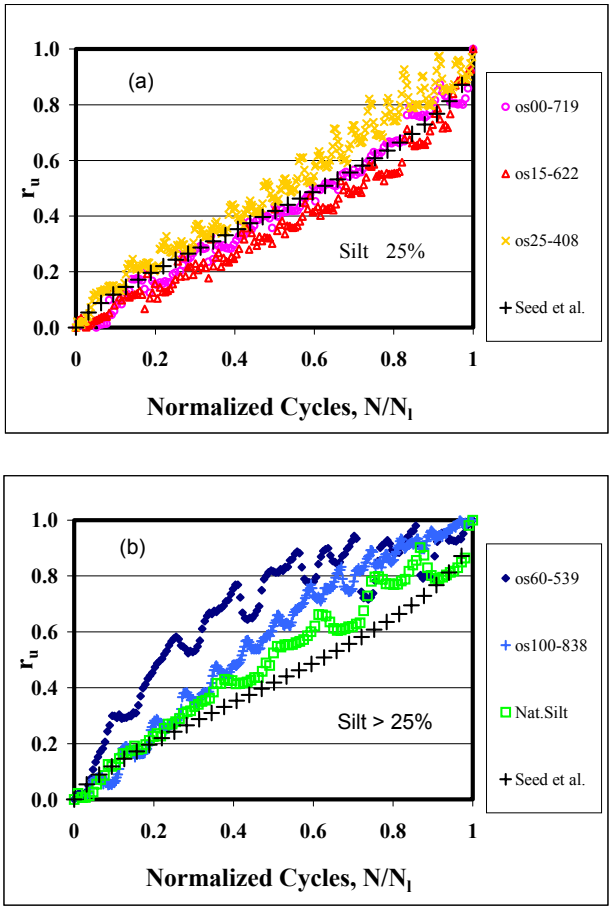

Fig. 1. Pore pressure generation: (a) sands (silt<25%) and (b) silts (silt>25%)

Figures 3a-b show pre- and post-liquefaction volume compressibility data (m_v) for sand, silty sand, and sandy silt specimens. Compressibility values of silt and silty sand are of the same order of magnitude as that of sands at the same effective stress. Also pre- and post-liquefaction compressibility values do not differ significantly from one another.

Coefficient of Consolidation: Pre-liquefaction coefficient of consolidation (c_v) values were calculated based on hydraulic conductivity and volume compressibility data for *virgin loading*. Post-liquefaction c_v values were back calculated using pore pressure and volume change measurements obtained during post-liquefaction dissipation tests. Back calculations were done by fitting the measured pore pressure vs. time data at the closed-end of the specimen to the theoretical solution for pore pressure at that end based on Terzaghi's one dimensional consolidation (Coduto 1999), given by:

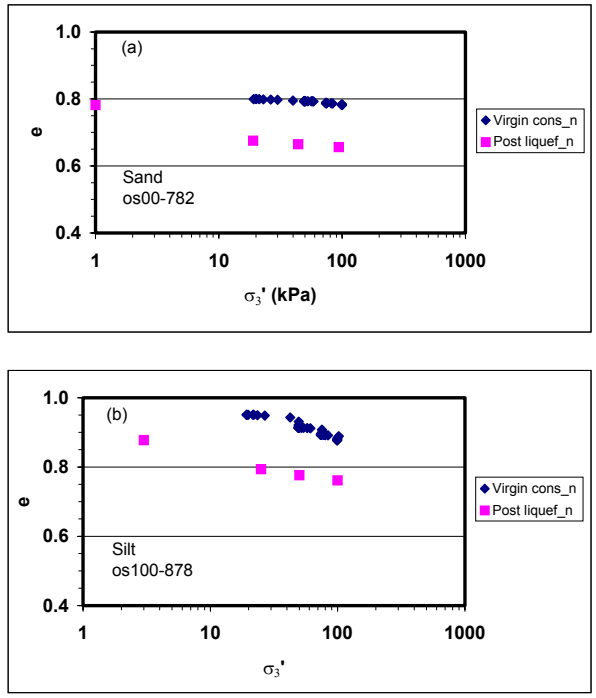

Fig. 2. Pre and post-liquefaction consolidation

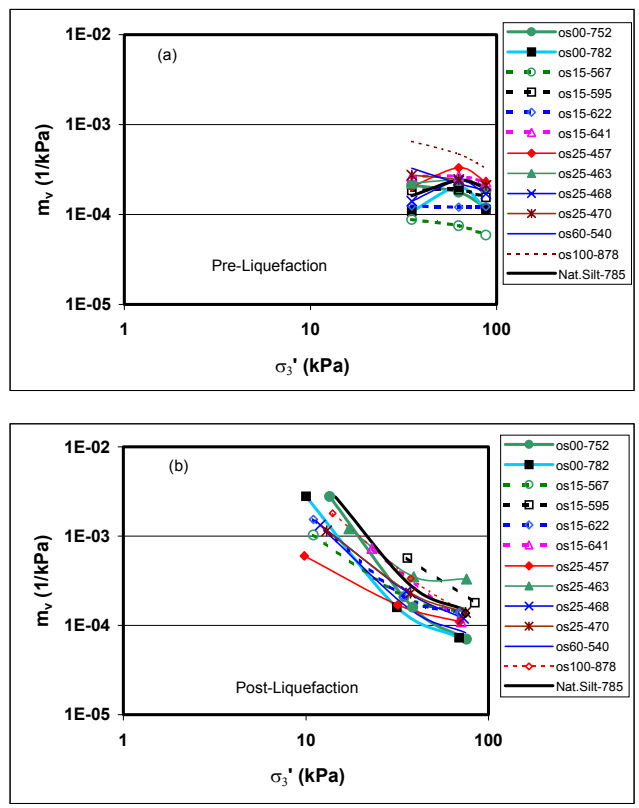

Fig. 3 Pre and post-liquefaction volume compressibility

$$u = \Delta\sigma \sum_{m=0}^{\infty} \{ \frac{4}{(2m+1)\pi} \sin[\frac{(2m+1)\pi}{2} \frac{Z_{dr}}{H_{dr}}] e^{-[\frac{(2m+1)^2\pi^2}{4} T_v]} \} . \quad (1)$$

where H_{dr} = length of longest drainage path, T_v = time factor, u = excess pore pressure, Z_{dr} = nearest distance to the drainage end, and $\Delta\sigma$ = change in total stress.

Similarly, volume change data was also used to back calculate c_v using Terzaghi's one dimensional consolidation theory.

Figures 4a-b show typical plots for each case, respectively, for a 100% silt specimen (os100-838) at void ratio of 0.838. The back calculated values in each case are in close agreement except for minor differences.

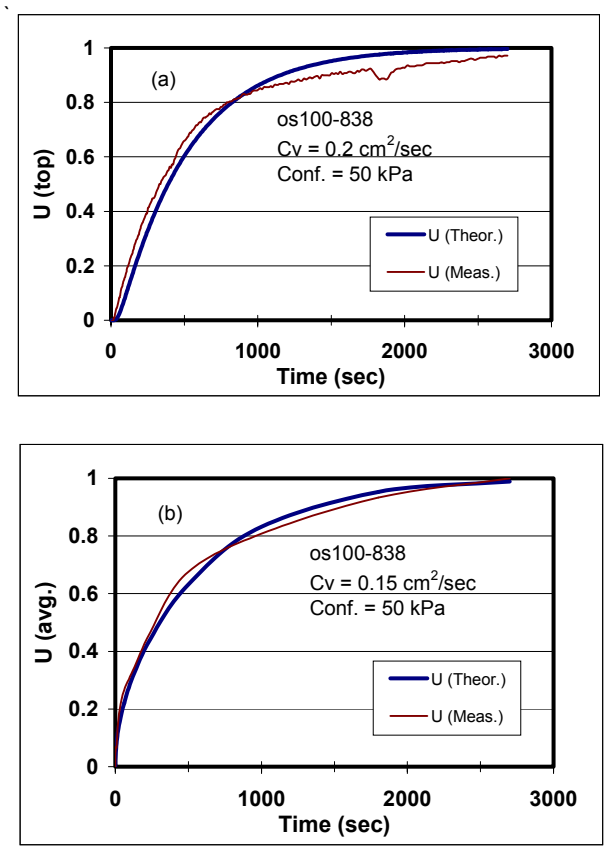

Fig. 4. Back calculation of c_v using (a) pressure measurements, and (b) volume measurements (U = degree of consolidation)

Figures 5a-b show the c_v values as a function of effective confining stress. For the same specimen, at the same effective confining stress, the c_v values for pre-liquefaction consolidation along virgin loading and post-liquefaction c_v values are nearly the same for the same soil. The reason for this is the same as that identified for the prior observation for m_v. The soil is completely remolded following liquefaction and it behaves as a freshly deposited soil. Its consolidation line parallels that of the pre-liquefaction virgin loading.

None of the specimens was subjected to dissipation tests before liquefaction occurred. Hence no direct data exist to determine the applicable c_v value during generation of pore pressure up to liquefaction (viz. before remolding of soil structure). It is thought that the c_v values for such generation/dissipation stages would be similar to the value during unloading/reloading stage of the soil along the recompression line. However, this needs to be verified.

Further, for the same soil, c_v is lower by more than one order of magnitude at an effective confining stress of 10 kPa compared to its value at 100 kPa (Figs.5a-b). This indicates the need for use of confining stress dependent c_v values for post-liquefaction dissipation analyses.

Coupled analysis of pore pressure generation and dissipation requires use of appropriate values adjusted to the status of the soil.

The c_v values are smaller for silty soils by more than one order of magnitude compared to sand. It is predominantly affected by permeability of the soil which is affected by silt content. Hydraulic conductivity of the soil specimens ranged from 0.6 to 1.3×10^{-3} cm/s for the sand, 9×10^{-5} cm/s for 15% silt, 0.6 to 1.2×10^{-5} cm/s for 25% silt, and 3 to 5×10^{-6} cm/s for 60% and 100% silt soils. The c_v values are affected in the same order.

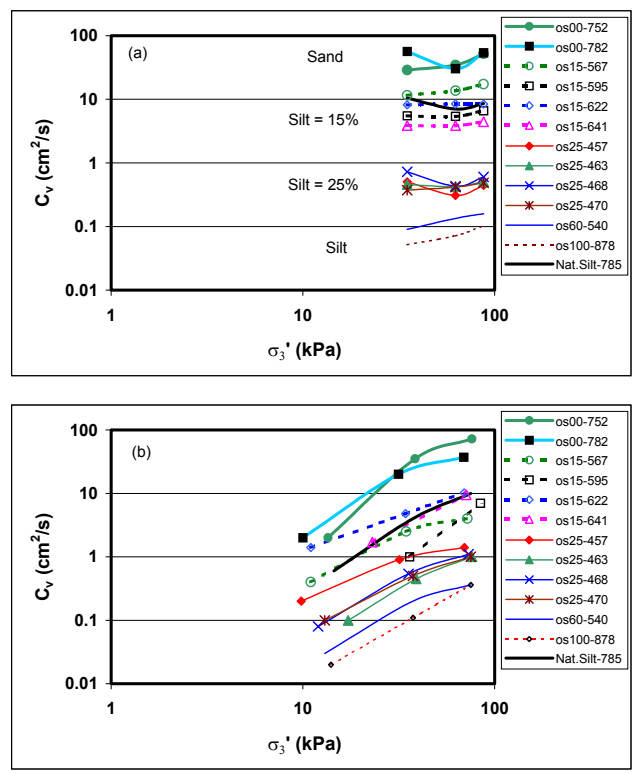

Fig. 5. Coefficient of consolidation: (a) pre-liquefaction and (b) post-liquefaction

The c_v values for the natural silt in Figs.5a-b are somewhat higher than those for artificial silt (Sil-co-sil#40). But the m_v values (Fig.3) are nearly the same. The difference in c_v is due to the difference in grain size and permeability for these two silts. Grain size (d_{50}) for the natural silt is about 38μm versus 10μm for the artificial silt. Hydraulic conductivity values are of the order of $2x10^{-4}$ cm/s for the natural silt versus 3 to $5x10^{-6}$ cm/s for the artificial silt. The difference in hydraulic conductivity is reflected in the c_v values for these two silts.

Post-Liquefaction Densification: Quantification of post-liquefaction densification is an important aspect in performance evaluation of liquefiable soil sites. At present, there is only limited data available on this subject (Lee and Albaisa, 1974, Pyke et al., 1975, Silver and Seed, 1971a,b, Tokimatsu and Seed, 1987). The data are primarily limited to clean sands. The data from the current study sheds further light on this subject.

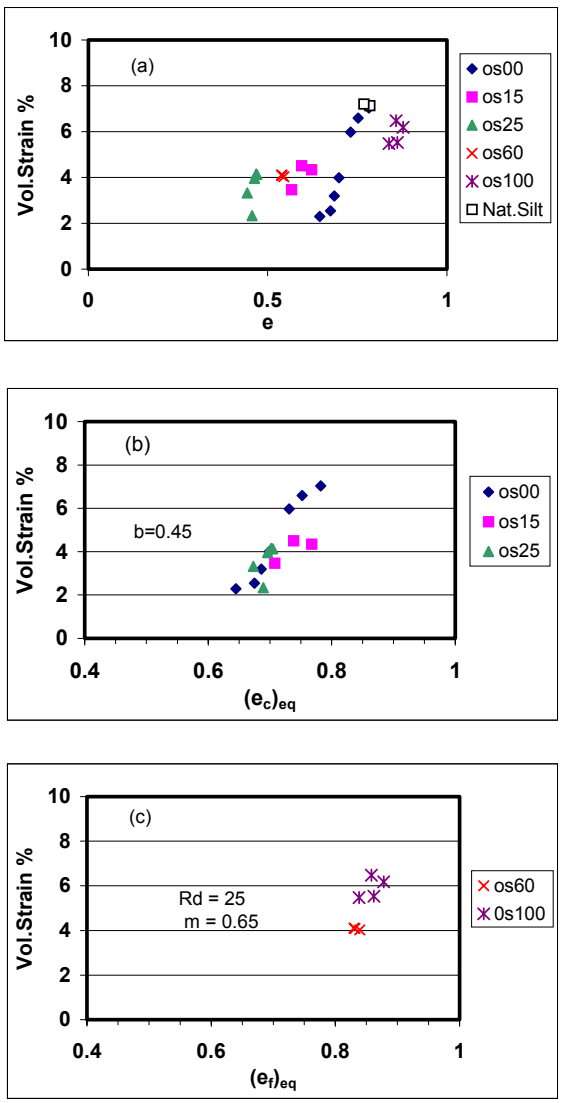

Fig. 6. Post-liquefaction volume change data

Figures 6a-c show the post-liquefaction densification data for the soils tested. There is no single relationship for volumetric compression against void ratio for all soils (Fig.6a). When the data are split into two parts, one for sands and silty sands up to 25% silt content, and the other for sandy silts, and plotted against the equivalent intergranular and interfine void ratios $(e_c)_{eq}$ {= [e+(1-b)fc]/[1-(1-b)fc], e = global void ratio, fc = FC/100, FC = (silt) fine content in percentage, and b = a coefficient}and $(e_f)_{eq}$ {= e/[fc+(1-fc)/R_d^m, m = a coefficient, R_d = D_{50}/d_{50}, D_{50} = 50% passing diameter of sand portion, and d_{50} = 50% passing diameter of fines portion] (Thevanayagam, 2000), respectively, the data for each group fall in a narrow band (Figs. 6b and c).

It is also interesting to note that the above respective equivalent intergranular void ratios have also been found to correlate well with the number of cycles to cause liquefaction (Thevanayagam et al. 2000b) and the energy required to cause liquefaction (Thevanayagam et al. 2000a) for sands and silty sands, and sandy silts and silts, respectively.

CONCLUSION

Laboratory undrained cyclic tests followed by dissipation were conducted to study the pore pressure generation, and post-liquefaction dissipation and densification behavior of silty sands and sandy silts. The limited data show the following.

(a) Pore pressure generation characteristics (r_u vs N/N_l) for sand and silty sand up to 25% silt content follow the same trend found for sand by Seed et al. (1976). The generation rate for silt and sandy silt (silt > 25%) is somewhat faster than that of sand. This needs further study.

(b) Soil skeleton is completely remolded during liquefaction and as a result post-liquefaction compression line (e vs. σ_c') almost parallels the pre-liquefaction compression line. It behaves like a freshly deposited soil.

(c) For the same soil, post-liquefaction volume compressibility (m_v) and coefficient of consolidation (c_v) values are similar to those of the normally consolidated virgin soil at the same stress level.

(d) Coefficient of consolidation for silty soils is lower by more than one or two orders of magnitude and is primarily affected by the silt content (viz. permeability of the soil). For the same soil, coefficient of consolidation values of soils at low confining stresses (10 kPa) immediately following liquefaction are about an order of magnitude less than that at 100 kPa confining stress. It is significantly stress dependent.

(e) At the same void ratio, a silty sand (silt content<25%) densifies more than clean sand following liquefaction. Post-liquefaction volumetric densification of sand and silty sand up to 25% silt content correlates well with equivalent intergranular void ratio, $(e_c)_{eq}$. Post-

liquefaction volumetric compression of silty soils correlates well with equivalent interfine void ratio, $(e_f)_{eq}$.

Ground improvement schemes for liquefaction mitigation in silty soils based on densification and drainage methods need to take into consideration of the differences in the above behavior characteristics of silts compared to sands. Primarily, permeability (and silt content) affects the dissipation characteristics of silty soils compared to sands. This requires much closer spacing of dynamic compaction grids or stone columns or provision of additional means such as supplementary wick drains to expedite dissipation of pore pressures developed during ground improvement operation in silty soils.

ACKNOWLEDGEMENTS

Financial support for this research was provided by MCEER Highway project, sponsored by the FHWA.

REFERENCES

Andrews, D.C.A. (1998). "Liquefaction of silty soils: susceptibility, deformation, and remediation." PhD Dissertation, Dept. of Civil Eng., USC, CA.

Baez, J.I., and G. Martin. (1995). "Permeability and shear wave velocity of vibro-replacement stone columns." Soil improvement for earthquake hazard mitigation, GSP No.49, Proc ASCE Convention, San Diego, CA. pp66-81.

Coduto, D.P. (1999). *Geotechnical Engineering*, Prentice Hall, Inc., Upper Saddle River, NJ.

Dise, K., M.G. Stevens, and J.L. Von Thun. (1994). "Dynamic compaction to remediate liquefiable embankment foundation soils." GSP No.45, ASCE National Convention, Oct.1994.

Lee, K.L., and A. Albaisa. (1974). "Earthquake induced settlements in saturated sands." J. Geotech. Eng. Div., ASCE, Vol.100(4). pp.387-406.

Luehring, R., B. Dewey, L. Mejia, M. Stevens, and J. Baez. (2000). "Liquefaction mitigation of a silty dam foundation using vibro-stone columns and drainage wicks - a test section case history at salmon lake dam." No.00-0748, Unpublished report.

Pyke, R., H.B. Seed and C.K. Chan. (1975). "Settlement of sands under multi directional shaking." J. Geotech. Eng. Div., Vol.101(4). pp.379-397.

Seed, H.B, P.P. Martin and J. Lysmer. (1976). " Pore water pressure change during soil liquefaction." J. Geotech. Eng. Div., ASCE, Vol.102(4). pp.323-346.

Seed, H.B., and J.R. Booker. (1977). "Stabilization of potentially liquefiable sand deposits using gravel drains." J. Geotech. Eng. Div., ASCE, Vol.103(7). pp.757-68.

Silver, M.L., and H.B. Seed. (1971a). "Deformation characteristics of sands under cyclic loading." Journal of the Soil Mechanics and Foundations Div., ASCE, Vol.97, No. SM8, Proc. Paper 8334. pp1081-98.

Silver, M.L., and H.B. Seed. (1971b). "Volume changes in sands during cyclic loading." Journal of the Soil Mech. and Found. Div., ASCE, Vol.97, No. SM9, Proc. Paper 8354. pp1171-82.

Singh, S. (1994). "Liquefaction characteristics of silts." Ground failures under seismic conditions. Proc., ASCE Convention, GSP. 44, S.Prakash and P.Dakoulas, eds., ASCE, Reston, VA. pp.105-116.

Thevanayagam, S. (2000). "Liquefaction potential and undrained fragility of silty soils." Proc. 12th World Conf. Earthq. Eng., New Zealand, Feb.2000.

Thevanayagam, S., J. Liang, and T.Shenthan. (2000a). "Contact index and liquefaction potential of silty and gravely soils." Proc. 14th ASCE Eng. Mech. Conf., Austin, Texas, May 2000.

Thevanayagam, S., M. Fiorillo, and J. Liang (2000b). "Effect of non-plastic fines on undrained cyclic strength of silty sands." Proc. ASCE Conference, Denver, CO, August 2000 (in press).

Tokimatsu, K., and H.B. Seed. (1987). "Evaluation of settlements in sands due to earthquake shaking." J. Geotech. Eng. Div., ASCE, 113(8). pp.861-78.

5.4.1.3

SHEAR WAVE VELOCITY RELATIONS FOR SILTY AND GRAVELY SOILS

S. Thevanayagam
Assoc. Prof., Dept. of Civil , Struc, and Env. Eng.
212 Ketter Hall, SUNY Buffalo
Buffalo, NY 14260, USA
Email: theva@eng.buffalo.edu
Tel: (716) 645-2114 ext. 2430
Fax: (716) 645-3733

J. Liang
Graduate Student, Dept. of Civil , Struc, and Env. Eng
212 Ketter Hall, SUNY Buffalo
Buffalo, NY 14260, USA

ABSTRACT

Shear wave velocity v_s, dynamic shear modulus G_{max}, and damping characteristics are important parameters required for both static and dynamic response analyses of earth structures. Traditional indirect methods for estimation of these parameters based on void ratio, relative density, and mean effective stress have been successful for rather narrowly graded soils, but not for the most commonly found silty and gravelly soils. Their direct application to determine the above characteristics for silty and gravely soils are not satisfactory. A primary reason for this is that global void ratio is not a good measure of intergrain contact density for granular mixes. A simple array of two-sized particle system with large size disparity is presented to highlight the relative roles of intercoarser and interfiner grain contacts on mechanical response parameters of such granular mixes. New parameters, namely equivalent intergranular void ratio $(e_c)_{eq}$, and equivalent interfine void ratio $(e_f)_{eq}$ are introduced as indices of active intergrain contacts. They are related to shear modulus and v_s of silty and gravely soils.

INTRODUCTION

Shear wave velocity (v_s), dynamic shear modulus G_{max}, and damping characteristics of soils are important parameters required for dynamic site response analysis as well as for design and performance evaluation of earth structures and foundations. Proper choice of such input soil parameters is an essential part of ground motion studies and determination of design ground accelerations. Several indirect methods have been developed, based on theoretical studies on uniform spherical arrays, laboratory studies on (clean) sands and/or field observations, to determine v_s and G_{max} (Duffy and Mindlin 1957, Hardin and Richart 1963, Hardin and Drenevich 1972, Seed et al. 1986, Goddard 1990, Lo Presti and Jamiolkowski 1998). Direct field test methods such as cross-hole and SASW techniques (Stokoe and Woods 1972, Stokoe et al. 1988) have also been developed. The indirect methods relate the above material characteristics to void ratio, relative density or some insitu parameters such as SPT blow counts and/or CPT resistance which are considered to be related to relative density. For example, widely used relationship for v_s (m/s) is of the form:

$$v_s = v_{so}\left(\frac{\sigma'}{p_a}\right)^{\alpha} \quad where \quad v_{so} = Ap_a^{\alpha}(e_m - e)$$

or $$v_{so} = Be^{-x} \qquad (1)$$

The dynamic shear modulus G_{max} relationships are of the form:

$$G_{max} = C\frac{(e_m - e)^2}{1+e}\left(\frac{\sigma'}{p_a}\right)^{\beta} \text{MPa}; \qquad (2)$$

$$G_{max} = 219K_{2max}(\sigma')^{0.5}\text{kPa} \quad [\sigma' \text{ in kPa}] \qquad (3)$$

where A=9.1 for rounded grains and 6.2 for angular grains, C= constant (about 70 for rounded grains and 32 for angular grains), α=0.25, β = constant (about 0.5), e = void ratio, e_m=2.17 for rounded grains and 2.97 for angular grains, σ'=mean normal stress (kN/m^2); v_{so}= normalized shear wave velocity [v_s at $\sigma'=p_a$=atmospheric pressure=100 kN/m^2]; x=1.3 for sands, all approximately. The K_{2max} depends on relative density and it varies from about 30 for loose sands and about 75 for dense sands. For gravel it ranges from 80 to 180. Other factors such as aging, cementation (Saxena et al. 1988), packing, anisotropy, etc. also affect v_s and G_{max}.

The underlying tenet has been that global void ratio e (or relative density) is an index of active contacts among the soil grains, and hence it can be correlated with v_s and G_{max}.

OBSERVATIONS

While such indirect correlations have proven successful for rather clean sands their wide spread applicability to natural

soils, which often contain silty and gravely sandy soils, have proven unsatisfactory.

Shear Wave Velocity: Experimental data for v_s for silty sands and gravely soils (e.g. Kokusho et al. 1995, Brignoli et al. 1997, Rollins et al. 1998) indicate that shear wave velocity for gravely soils and silty soils are often significantly smaller than the respective values for 'pure' sand, silt, or gravel at the same e. An example is shown in Figs.1-2. Fig.2 shows the v_{so} (shear wave velocity at 100 kPa confining stress) data for Tone river sand (TRS) and three gravely soils (G25, G50, G75) prepared by mixing TRS with 25, 50 and 75% gravel by weight (Kokusho et al. 1995). The non-uniqueness of void ratio e to correlate with v_{so} is clear. Low void ratio does not necessarily mean larger shear wave velocity. The measured v_{so} is about 200m/s for the dense Gravely Soil G75 at e=0.3 whereas v_{so} is about the same for TRS at a very loose state at e=0.7.

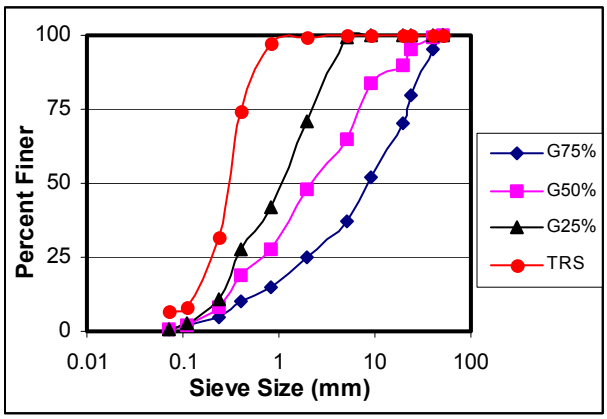

Fig.1 Grain size data – Sand-gravel mixes

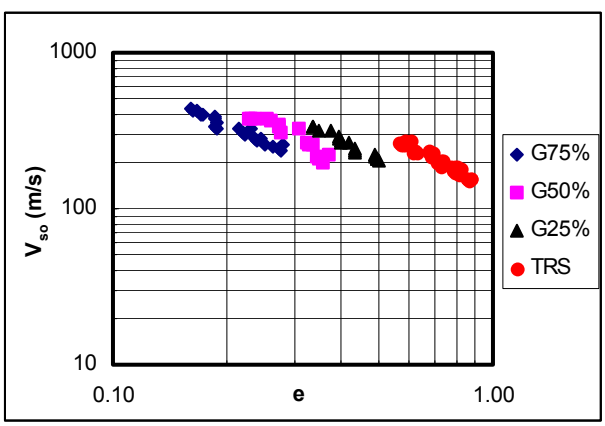

Fig.2 Influence of gravel content on V_{so}

Shear Modulus: Fig.3 shows a comparison of calculated G_{max} (Eq.2) and the measured G_{max} (Borden et al. 1996) for two non-plastic silty soils at 10 and 19% silt content by weight. Each soil was tested at two different confining stresses (50 and 100 kPa). The calculated values of G_{max} using Eq.2 deviate from the measured ones. The deviation increases with an increase in silt content.

Fig.4 shows four sets of secant shear modulus $G_{0.05}$ (measured at 0.05% axial strain) data for a sand-silt mix at different silt contents obtained from a series monotonic triaxial tests on large size specimens (typically 74 mm diameter and 150 ~ 160 mm height) prepared using a single host sand (OS55) (OS-F55, Foundry Sand from US Silica Company, Illinois, e_{max}=0.80, e_{min}=0.60, d_{50}=0.24mm) mixed with different amounts of non-plastic crushed silica fines (Sil co sil #40, 99.9% passing sieve #200, d_{50}=0.007mm) at (a) 0%, (b) 7%, (c) 15%, (d) 25% fines by dry weight (denoted as os00, os07, os15 and os25, respectively) (Thevanayagam et al. 1999). All specimens were consolidated to an initial effective isotropic confining stress of 100 kPa. Again, the silty sand specimens show lower $G_{0.05}$ values when compared against clean sands at the same global void ratio e.

Possible Reasons: Recently, it has been brought to the attention that physical nature of silty sands and gravely sands are entirely different from clean sand, 'pure' silt or gravel (Thevanayagam 1998, 1999a-c). As the void ratio and proportion of the coarser and finer grains content of these soils change the nature of their microstructure also changes.

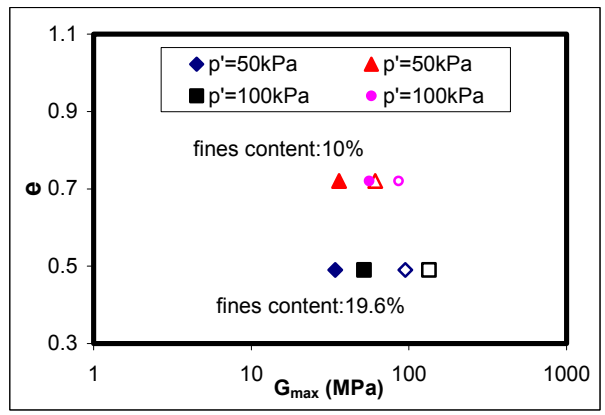

Fig.3 G_{max}: measured vs. estimated (Eq.2) (symbols: solid = measured; open = calculated; p'=eff. confining stress)

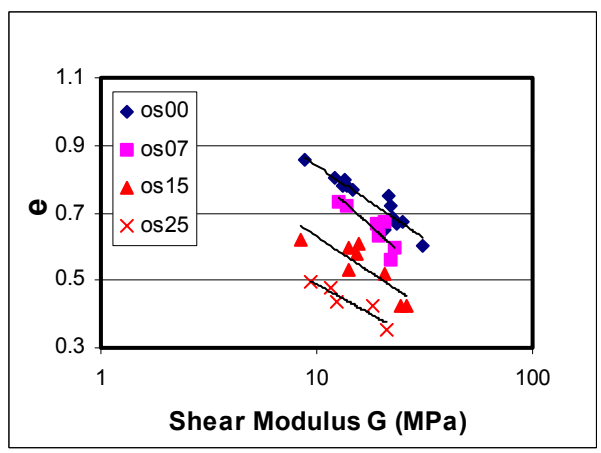

Fig.4 e vs. $G_{0.05}$ -- sand and silty sand (os00=0% fines content; os07=7% fines content)

The relative participation of the particles of very different sizes in the *internal interparticle contact* also changes. Due to particle size disparity and availability of pores larger than

some particles, at low finer grains content (FC) some of the finer particles may remain inactive or move between pores without significantly affecting or contributing to the force chain. Yet they contribute to the global void ratio. Alternately when there is a sufficient amount of finer grains the coarser grains become dispersed contributing much less to the force chain than to the global void ratio. Global void ratio e ceases to be an index to represent the nature of *contact density* of active particles. The traditional use of e to compare and correlate with G_{max} or v_{so} of granular mixes containing different amounts of finer grains content ceases to be valid. The same holds for relative density.

In general the stress-strain behavior of granular mixes are affected by a critical combination of *intergranular and interfine contacts*. New *indices of active contacts* are needed to represent the nature of intergrain contacts in order to characterize the behavior of such soils.

Using a two-sized particle mix as a model, this paper highlights the nature of the microstructure of granular mixes. Based on this such granular mixes are classified into certain groups (Fig.5) depending on the relative frictional contributions at the intergranular and interfine grain contact level. Equivalent intergranular $(e_c)_{eq}$, and equivalent interfine $(e_f)_{eq}$ void ratios (Fig.6) are introduced as primary indices of contact density for the various groups. Global void ratio is introduced as a secondary index. These new indices are related to v_s and G_{max} at different silt or gravel contents. The underlying theme is that contact is the mechanism by which a granular medium responds to external excitations. The density of contacts may be expressed using the above indices.

CONCEPTUAL FRAMEWORK

Soil Microstructure: Consider a two-size gap graded particle system shown in Fig.5. The microstructure of such a granular mix can be constituted by many different ways. Each one of them leads to a different internal contact arrangement and therefore to a different internal force chain structure and different stress-stain response. Among infinite variations, four extreme limiting categories of microstructure are as follows: The first category (Fig.5a) is obtained when the finer grains are fully confined within the void spaces between the coarser grains with no contribution whatsoever in supporting the coarser grain skeleton. The second category (Fig.5b) is applicable when the coarser grains are fully dispersed in the finer grain matrix. The third category (Figs.5c-d) is possible when the coarser and finer grains constitute a fully layered system where the coarser grain layers have no fines contained in them and vice versa. A fourth category (Fig.5e-f) is obtained when partial separation of coarser grains by the finer grains is present. The figures 5a, c, e and f are relevant at low finer grains content (FC). Figs. 5b and d are relevant at high FC. The case of layered soils (Fig.5c-d) is not discussed further.

It is apparent from Fig.5 that global void ratio is not a suitable common index to characterize the mechanical response of the entire spectrum of cases shown. A simple solution may be to consider the various cases as a composite mix of coarser and finer grain skeletons with respective intergranular and interfine void ratios e_c [=(e+fc)/(1-fc)] and e_f [=e/fc] as defined in Fig.6 (Thevanayagam 2000).

Index of Active Contacts: Transition from Fig.5a to Fig.5b occurs naturally with an increase in FC beyond a threshold value (FC_{th}). The category shown in Fig.5a is possible only if: (1) the size of the finer grains is much smaller than the possible minimum pore opening size in the coarser grain skeleton. For spherical particles this implies that D/d>6.5 where d and D=sizes of finer and coarser grains, respectively, and (2) the intergranular voids are not completely filled with the fines ($FC<FC_{th}$). From a conceptual standpoint FC_{th} is expected to occur when the interfine void ratio e_f decreases below $e_{max,HF}$ (Thevanayagam 1999c, 2000):

$$FC_{th} \le FC_{th,\max} = \frac{100e_c}{1+e_c+e_{\max,HF}}\% = \frac{100e}{e_{\max,HF}}\% \qquad (4)$$

where $e_{max,HF}$ = the maximum void ratio of the pure silt beyond which it has no appreciable strength, and e_c = intergranular void ratio (Fig.6). The rationale is that, as e_f reaches below $e_{max,HF}$, the finer grains are packed close enough so that direct finer-grain to finer-grain friction becomes active.

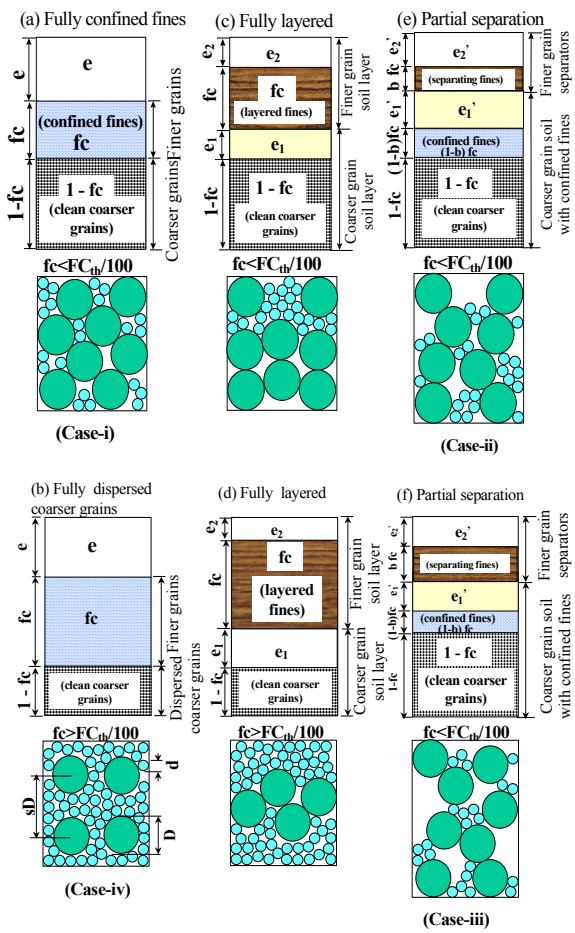

Fig.5 Microstructure and intergranular matrix phase diagram

At FC<FC_{th}, primarily the intergranular contacts between the coarser grains affect the mechanical response. Further, if considering the separating fines' contribution to active contact as "b" (0<b<1) (Fig5e-f), it is expected the mechanical behavior of such mixes would be different and generally stronger than that of the host coarser grain soil at the same e_c. Then relevant contact index would be equivalent intergranular void ratio $(e_c)_{eq}$:

$$(e_c)_{eq} = \frac{e + (1-b)fc}{1-(1-b)fc}; \qquad 0 < b < 1 \qquad (5)$$

When FC>FC_{th} the finer grains begin to play a rather important role. The coarser grains begin to disperse (Fig.5b) and provide a sort of reinforcement effect until they are separated sufficiently apart when FC exceeds a limiting fines content FC_l. The FC_l is given by (Thevanayagam 1999c, 2000):

$$FC_l \geq 100\left[1 - \frac{\pi(1+e)}{6s^3}\right]\% = 100\left[\frac{\frac{6s^3}{\pi} - 1}{\frac{6s^3}{\pi} + e_f}\right]\%; \qquad e_f \leq e_{\max,HF} \qquad (6)$$

where s = 1+a/R_d, R_d = D/d = size disparity ratio, and a =10 (approximately). At FC_{th}<FC<FC_l, the reinforcement effect by the coarser grains must also be introduced to obtain an equivalent interfine void ratio $(e_f)_{eq}$ as the index of active contacts. For a two size particle system with large size disparity, an approximate expression for $(e_f)_{eq}$ can be derived (Thevanayagam 1999c, 2000):

$$(e_f)_{eq} = \frac{e}{fc + \frac{1-fc}{R_d^m}} < e_f \qquad (7)$$

where fc=FC/100, and m = a coefficient. Beyond FC_l the behavior is entirely governed by the finer grains. The interfine void ratio e_f may be considered as an index of active contacts.

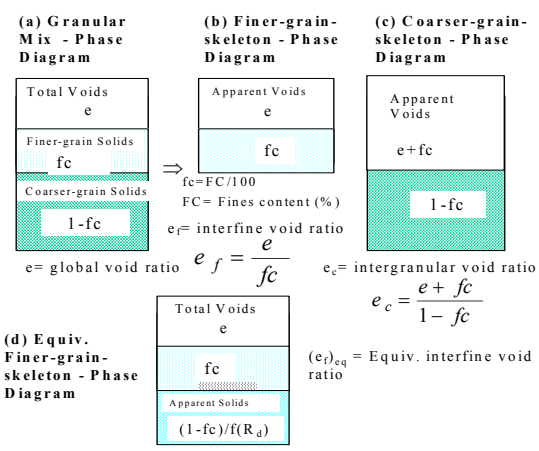

$$e_f = \frac{e}{fc}$$

$$e_c = \frac{e + fc}{1 - fc}$$

$$(e_f)_{eq} = \frac{e}{fc + (1 - fc)/f(R_d, etc.)}$$

$$(e_c)_{eq} = \frac{e + (1-b)fc}{1-(1-b)fc} \qquad 0<b<1$$

Fig.6 Intergranular contact indices

PROPOSED RELATIONS FOR v_s AND G_{max}

Shear wave velocity: Based on the above considerations, with due consideration for the dependence of v_s on the nature of contacts (Duffy and Mindlin 1957, Goddard 1990, Thevanayagam 1999c), v_s of granular mixes may be given by the following, reflecting its dependence on contact index e_{eq}:

$$v_s = v_{so}\left(\frac{\sigma'}{p_a}\right)^{\alpha}; \qquad v_{so} = Ap_a^{\alpha}(e_m - e_{eq})$$

or $v_{so} = Be_{eq}^{-x}$ (8)

where $e_{eq}=(e_c)_{eq}$ for FC< FC_{th}; $e_{eq}=(e_f)_{eq}$ for FC>FC_{th}. Eq.8 may also be conveniently presented in terms of e by substituting the proposed expressions for e_{eq}:

$$v_{so} = A_{eq}p_a^{\alpha}((e_m)_{eq} - e) \qquad (9a)$$

or $v_{so} = B_{eq}e^{-x}$ for FC>FC_{th} and

$$v_{so} = B(1-(1-b)fc)^x(e + (1-b)fc)^{-x} \quad \text{for FC< } FC_{th} \qquad (9b)$$

where A_{eq}=A/(1-(1-b)fc) and $(e_m)_{eq}$ =e_m(1-(1-b)fc)-(1-b)fc for FC<FC_{th}; A_{eq}=A/[fc+(1-fc)/$(R_d)^m$] and $(e_m)_{eq}$ =e_m [fc+(1-fc)/$(R_d)^m$] for FC>FC_{th}; B_{eq}=B[fc+(1-fc)/$(R_d)^m]^x$ for FC>FC_{th}.

It is readily apparent that Eq.9 is similar to Eq.1 but with different coefficients depending on FC. The differences are manifestations of differences in intergrain contact density in granular mixes containing different proportions of coarser and finer grains. Direct use of Eq.1, without due consideration for the dependence of the coefficients in Eq.1 on FC can be misleading. Details are presented elsewhere (Thevanayagam 1999e).

Shear Modulus: Since G_{max} is a mechanical response parameter that is dependent on active contact density of the particles, G_{max} relationship for silty sands (or sandy gravels) and sandy silts (or gravelly sands) could be related to $(e_c)_{eq}$ and $(e_f)_{eq}$, respectively:

$$G_{\max} = C\frac{(e_m - (e_c)_{eq})^2}{1 + (e_c)_{eq}}\left(\frac{\sigma'}{p_a}\right)^b \text{MPa}; \quad \text{for FC<}FC_{th} \qquad (10a)$$

$$G_{\max} = C\frac{(e_m - (e_f)_{eq})^2}{1 + (e_f)_{eq}}\left(\frac{\sigma'}{p_a}\right)^b \text{MPa}; \quad \text{for FC>}FC_{th} \qquad (10b)$$

EVALUATION

Shear Wave Velocity: Consider the sand/gravel mixes shown before in Figs.1-2. In this case sand is the finer grain and gravel is the coarser grain. The gradation data (Fig.1) was decomposed into two gradation curves, one for gravel and the other for sand. Then the respective D_{50} and d_{50} were determined (Table 1). FC_{th} was estimated for each specimen assuming $e_{max,HF}$=0.966 (=e_{max} for TRS). FC (=sand content) exceeded FC_{th} for most specimens. The relevant contact index void ratio $(e_f)_{eq}$ was calculated assuming m=0.45.

Table 1: Sand-gravel mix data

Soil	D_{50} (mm)	d_{50} (mm)	R_d	Range e	FC (%)	FC_{th} (%)	Contact Index
TRS		0.34		0.55-0.90	100		e
G25	3	0.7	4.3	0.33-0.50	75	35-52	$(e_f)_{eq}$
G50	7	0.7	10	0.22-0.37	50	24-38	$(e_f)_{eq}$
G75	15	0.6	25	0.16-0.28	25	17-29	$(e_f)_{eq}$

FC=sand content

Fig.7 shows the same v_{so} data shown in Fig.2, but plotted against $(e_f)_{eq}$. The v_{so} data for all sand/gravel mixes collapse into a single narrow band along with that for TRS sand. It correlates well with $(e_f)_{eq}$ better than with e. It shows clearly that the direct use of e to estimate v_{so} (Eq.1) for gravely soils can be very unconservative.

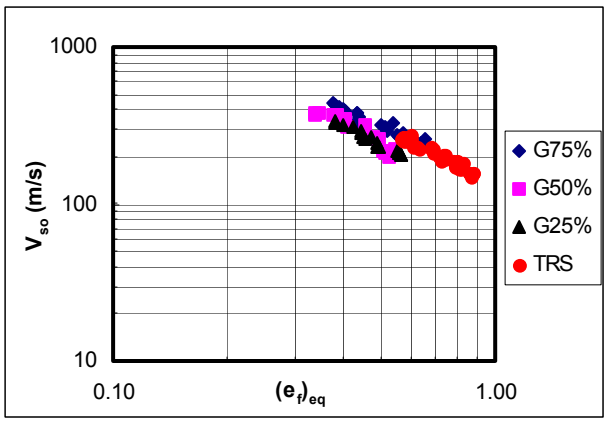

Fig.7 v_{so} versus $(e_f)_{eq}$ relations

Shear Modulus: Fig.8 presents a comparison of the re-calculated G_{max} values for two silty soils using Eq.10 in terms of $(e_c)_{eq}$ against the same measured values shown in Fig.3. The $(e_c)_{eq}$ values were calculated assuming b=0.25. The calculated

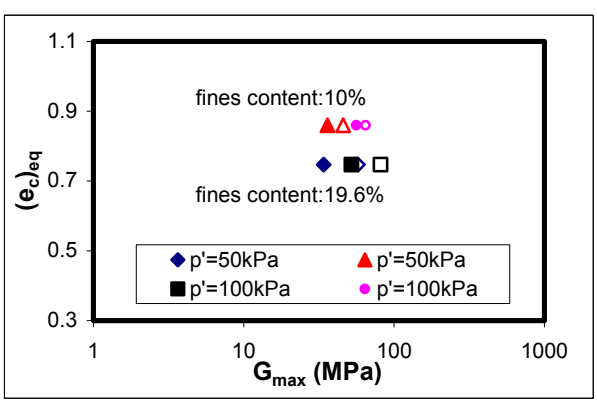

Fig.8 G_{max}: measured vs. estimated (Eq.10a) (symbols: solid = measured; open = calculated; p'=eff. confining stress)

G_{max} values in Fig.8 are in closer agreement with the measured values than those in Fig.3. The equivalent intergranular void ratio $(e_c)_{eq}$ represents more closely the active contacts than global void ratio e. Therefore $(e_c)_{eq}$ appears to correlate with G_{max} better than e versus G_{max}.

The newly proposed active contact indices were also evaluated using the $G_{0.05}$ data shown before in Fig.4. Fig.9 shows the same $G_{0.05}$ data plotted versus $(e_c)_{eq}$ (b=0.25). The data for all soils collapse into a narrow band with that of the host clean sand in Fig. 9, as opposed to the different trend lines for each soil observed in Fig.4. Again, $(e_c)_{eq}$ correlates better with shear modulus than does the global void ratio e.

Although not shown in this paper, the above contact indices [$(e_c)_{eq}$ and $(e_f)_{eq}$] have also been found to correlate with many other mechanical properties of granular mixes (Thevanayagam et al. 2000a, 2000b, 2001).

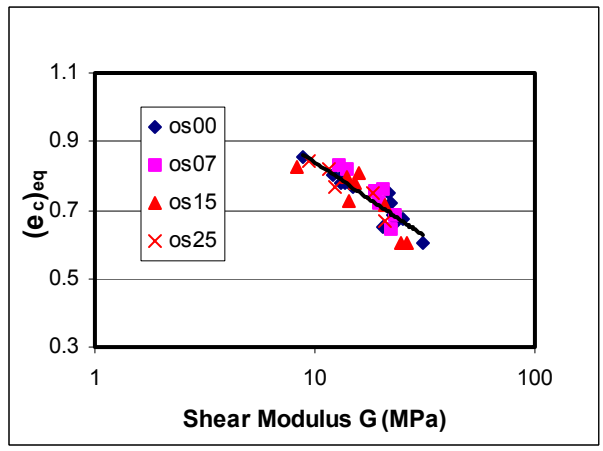

Fig.9 $(e_c)_{eq}$ vs. $G_{0.05}$ -- sand and silty sands (os00=0% fines content; os07=7% fines content)

CONCLUSION

The limitation of indirect methods for estimating shear wave velocity and G_{max} based on global void ratio e is examined. These indirect methods of estimating material parameters, even for preliminary design purposes, based on density or void ratio of a soil can yield unconservative values for v_s and G_{max}. The reason for this is that void ratio or density of a soil is indeed an index of volume or mass density. Mechanical soil parameters are primarily affected by contact density (per grain). A simple framework is presented to take into account the relative contribution of coarser and finer grains in a soil to its shear wave velocity and shear modulus. Based on the above simple framework, two new intergrain contact indices [$(e_c)_{eq}$ and $(e_f)_{eq}$] have been proposed for correlation with v_s and G_{max}. These contact indices correlate well with the measured v_{so} and G_{max} data for silty and gravely soils. For soils containing low finer grains content (FC) less than a threshold value (FC_{th}), v_{so} and G_{max} correlate well with $(e_c)_{eq}$. For soils containing large finer grains content, v_{so} and G_{max} correlate well with $(e_f)_{eq}$. There is no unique correlation with global void ratio e in either case.

Further work is needed to examine the applicability of these contact indices for different soils.

ACKNOWLEDGMENTS

Financial support by the USGS/NSF/MCEER for the various aspects of this ongoing research work is gratefully appreciated. Thanks are also due to M. Pollino, SUNY at Buffalo, sponsored by NSF-REU program, for his assistance in preparing this paper.

REFERENCES

Borden, R. H., Shao, L. and Gupta, A. (1996). "Dynamic properties of Piedmont residual soils", *J. Geotech. Geoenv. Div*., ASCE, **122**(10), 813-821.

Brignoli, E., Fretti, C., Jamiolkowski, M. and Stokoe, K.H. II (1997) "Stiffness of gravelly soils to small strains", Proc. 14th Intl. Conf. SMFE, Germany, vol.1, 37-40.

Duffy, J. and Mindlin, R.D. (1957) "Stress-strain relations of a granular medium", Transactions, ASME, 585-593.

Goddard, J. D. (1990) "Nonlinear elaasticity and pressure-dependent wave speeds in granular media", Proc. Royal Soc. London, A, 430, 105-131.

Hardin, B.O., and Richart, F. E. Jr. (1963). "Elastic wave velocities in granular soils" J. Soil Mech. and Found. Div., ASCE, 89(SM1), 33-65.

Hardin, B. O., and Drnevich, V. P. (1972). "Shear modulus and damping in soils: Measurements and parameter effects", *J. Soil Mech. Found. Div*., ASCE, 98(6), 603-624.

Kokusho, T., Yoshida, Y. and Tanaka, Y. (1995) "Shear wave velocity in gravelly soils with different particle gradings", ASCE Geotech. STP 56, 92-106.

Lo Presti, C.F. and Jamiolkowski, M. (1998) "SPT N-value and S-wave velocity for gravelly soils with different grain size distributions" Discussion, Soils and Foundation, 39(2), 138-140.

Mitchell, J. K. (1993) *Fundamentals of soil behavior*, 2nd ed. Wiley Interscience Publ.

Rollins, K., Evans, M., Diehl, N. B., and Daily W.D. (1998) "Shear modulus and damping relationships for gravels" J. Geotech. and Geoenv. Eng., **124**(5), 396-405.

Saxena, S.K., Avramidis, A.S., and Reddy, K.R. (1988). "Dynamic moduli and damping ratios for cemented sands at low strains", *Can. Geot. J.*, **25**(2), 353-368.

Seed, H.B., Wong, R.T., Idriss, I.M., and Tokimatsu, K. (1986). "Moduli and damping factors for dynamic analysis of cohesionless soils", J. Geot. Eng. Div., ASCE, **112**(11), 1-17.

Stokoe, K.H., and Woods, R.D. (1972). "In situ shear wave velocity by cross-hole method", *J. Soil Mech. Found. Div*., ASCE, **98**(5), 443-460.

Stokoe, K.H., Nazarian, S., Rix, G.J., Salinero, I.S., Sheu, J.C., and Mok, Y.J. (1988). "In situ seismic testing of hard-to-sample soils by surface wave method", *Geot. Spec. Publ. 20, Earthq. Eng. and Soil Dyn. II*, ASCE, NY, 264-278.

Thevanayagam, S. (1998) "Effect of fines and confining stress on steady state strength of silty sands," J. Geotech. & Geoenv. Engrg. Div., ASCE, **124**(6), 479-491.

Thevanayagam, S. (1999a) "Intergrain contact and shear modulus of non-plastic granular mixes", CD-ROM Proc. 13th ASCE Conf. on Eng. Mech., Eds. Jones, N. and Ghanem, R., Johns Hopkins Univ., Maryland, June 13-16, 1999.

Thevanayagam, S. (1999b) "Effect of fines and confining stress on steady state strength of silty sands," *Closure*, J. Geotech. & Geoenv. Engrg. Div., ASCE, 125(11).

Thevanayagam, S. (1999c) "Relative roles of coarser and finer grains on undrained behavior of granular mixes", *in review*, J. Geotech. & Geoenv. Eng. Div., ASCE.

Thevanayagam, S. (1999d) "Liquefaction and shear wave velocity characteristics of silty/gravely soils – implications for bridge foundations", Proc. of 15th US-Japan Bridge Workshop, PWRI, Tsukuba City, Japan

Thevanayagam, S. (1999e) "Contact indices - shear wave velocity - shear modulus for granular mixes" to be submitted, J. Geotech. & Geoenv. Engrg. Div., ASCE.

Thevanayagam, S., Liang, J., Mohan, S., and Shenthan, T. (1999) "Undrained fragility of clean sands, silty sands and sandy silts," *in review*, J. Geotech. & Geoenv. Engrg. Div., ASCE

Thevanayagam, S. (2000) "Liquefaction potential and undrained fragility of silty soils." Proc. 12WCEE 2000 Conference, Auckland, New Zealand

Thevanayagam, S., Liang, J., and Shenthan, T. (2000a). "Contact index and liquefaction potential of silty and gravely soils." Proc. 14th ASCE Eng. Mech. Conf., Austin, Texas, May 2000.

Thevanayagam, S., Fiorillo, M. and Liang, J. (2000b). "Effect of non-plastic fines on undrained cyclic strength of silty sands." ASCE Geot. Spec. Publ., 107, 77-91.

Thevanayagam, S., Martin, G.R., Shenthan, T. and Liang, J. (2001). "Post-liquefaction pore pressure dissipation and densification in silty soils." 4th International Conf. Recent Adv. On Geotech. Earthq. Eng. And Soils Dynamics, San Diego, 2001.

Presented at the 13th ASCE Engineering Mechanics Conference, Baltimore, Maryland, June 1999

Intergrain contacts and shear modulus of non-plastic granular mixes

S. Thevanayagam, M. ASCE
State University of New York, Buffalo, NY 14260
theva@eng.buffalo.edu

Abstract:

A simple array of two-sized particle system with large size disparity is presented to highlight the relative roles of intercoarser and interfiner grain contacts on mechanical response of gap-graded granular mixes. New parameters, namely intergranular void ratio e_s and equivalent interfine void ratio $(e_f)_{eq}$ are introduced as indices of active contacts. A simple expression is presented to determine G_{max} of young non-plastic deposits of granular mixes (silty and gravelly soils) in terms of e_s and $(e_f)_{eq}$. This is experimentally evaluated.

Introduction

Shear modulus and damping characteristics are important parameters required for dynamic response analysis of earth structures. Several direct laboratory and insitu (Stokoe and Woods 1972, Stokoe et al. 1988) measurement technique and indirect empirical estimation methods (Hardin and Black 1968, Hardin and Drnevich 1972, Seed et al. 1986) have been developed for their determination. The underlying tenet for the indirect methods has been that global void ratio e (or relative density) is an index of active contacts while mean stress enhances contact, interlocking, and resistance against deformation. Widely used relationships to estimate the small strain maximum shear modulus G_{max} of a sand are:

$$G_{\max} = A\frac{(e_m - e)^2}{(1+e)}\left(\frac{\sigma'}{p_a}\right)^b MPa; \qquad or \qquad G_{\max} = 1000K_{2\max}(\sigma')^{0.5}\ psf \tag{1}$$

where A=constant (about 70 for rounded grains and 32 for angular grains), b=constant (about 0.5), e= void ratio, e_m=a constant (about 2.17 for rounded grains and 2.97 for angular grains), σ'=mean normal stress in psf, and p_a=atmospheric pressure in psf, and K_{2max} depends on relative density and it varies from about 30 for loose sands and about 75 for dense sands. For gravel it ranges from 80 to 180. Other factors such as aging, cementation (Saxena et al. 1988), packing, anisotropy, etc. also affect the shear modulus.

The indirect methods (Eq.1) were generally derived or inferred from laboratory measurements on rather clean sands and have proven to be successful for such soils. Their widespread applicability to characterize G_{max} of non-plastic silty soils, gravelly soils, or soils containing vastly different grain sizes has not been studied in detail. Such soils are abundant in nature and deserve a greater detailed study.

G_{max} is a mechanical response that is dependent on active contact density of the particles. There is reason to believe that active contact density of particles in a clean sand and a silty sand containing the same host sand and a non-plastic silt at the same void ratio may

not be the same (Thevanayagam 1998a). Indeed the nature of active contacts may be vastly different in such granular mixes depending on the proportion of the mixes and the size distributions of particles. Hence the G_{max} may be significantly different. The direct use of Eq.1 based on global void ratio e may be of little value to estimate G_{max} for silty or gravelly soil mixes. For such young deposits of granular mixes (in the absence of cementation) a parameter that describes the nature and density of active contacts and the internal force chain is needed to estimate G_{max}.

The objective of this paper is to present a simple two-particle size system as a model for gap graded granular mixes and to introduce new indices of active contacts for correlation with G_{max} for non-plastic silty soils. This is experimentally evaluated using limited data available in the literature.

Conceptual Framework

Soil Microstructure: Consider a two-size gap graded particle system shown in Fig.1. The microstructure of such a granular mix can be constituted by many different ways. Each one of them leads to a different internal contact arrangement and therefore to a different internal force chain structure and different stress-strain response. Among infinite variations, four extreme limiting categories of microstructure are as follows: The first category (Fig.1a) is obtained when the finer grains are fully confined within the void spaces between the coarser grains with no contribution whatsoever in supporting the coarser grain skeleton. The second category (Fig.1b) is applicable when the coarser grains are fully dispersed in the finer grain matrix. The third category (Figs. 1c-d) is possible when the coarser and finer grains constitute a fully layered system where the coarser grain layers have no fines contained in them and vice versa. A fourth category (Figs.1e-f) is obtained when partial separation of coarser grains by the finer grains is present. The figures 1a, c, e and f are relevant at low finer grains content (FC). Figs. 1b and d are relevant at high FC. The case of layered soils (Figs.1c-d) is not discussed further.

It is apparent from Fig.1 that global void ratio is not a suitable common index to characterize the mechanical response of the entire spectrum of cases shown. A simple solution may be to consider the various cases as a composite mix of coarser and finer grain skeletons with respective intergranular and interfine void ratios e_s and e_f as defined in Fig.2 (Thevanayagam 1998a).

Index of Active Contacts and Threshold & Limiting Fines Content FC_{th} & FC_l: Transition from Fig.1a to Fig.1b occurs naturally with an increase in FC beyond a threshold value (FC_{th}). The category shown in Fig.1a is possible only if: (1) the size of the finer grains is much smaller than the possible minimum pore opening size in the coarser grain skeleton. For spherical particles this implies that D/d>6.5 where d and D=sizes of finer and coarser grains, respectively, and (2) the intergranular voids are not completely filled with the fines ($FC<FC_{th}$). From a conceptual standpoint FC_{th} is expected to occur when the interfine void ratio e_f decreases below $e_{max,HF}$ (Thevanayagam 1998b,c):

$$FC_{th} \leq FC_{th,\max} = \frac{100 e_s}{1 + e_s + e_{\max,HF}}\% = \frac{100 e}{e_{\max,HF}}\% \qquad (2)$$

where $e_{max,HF}$ = the maximum void ratio of the pure silt beyond which it has no appreciable strength, and e_s=intergranular void ratio (Fig. 2). The rationale is that, as e_f reaches below $e_{max,HF}$, the finer grains are packed close enough so that direct finer-grain-to-finer-grain friction becomes active. At FC< FC_{th}, primarily the intergranular contacts between the coarser grains affect the mechanical response. The intergranular void ratio e_s may be considered as an index of active contacts.

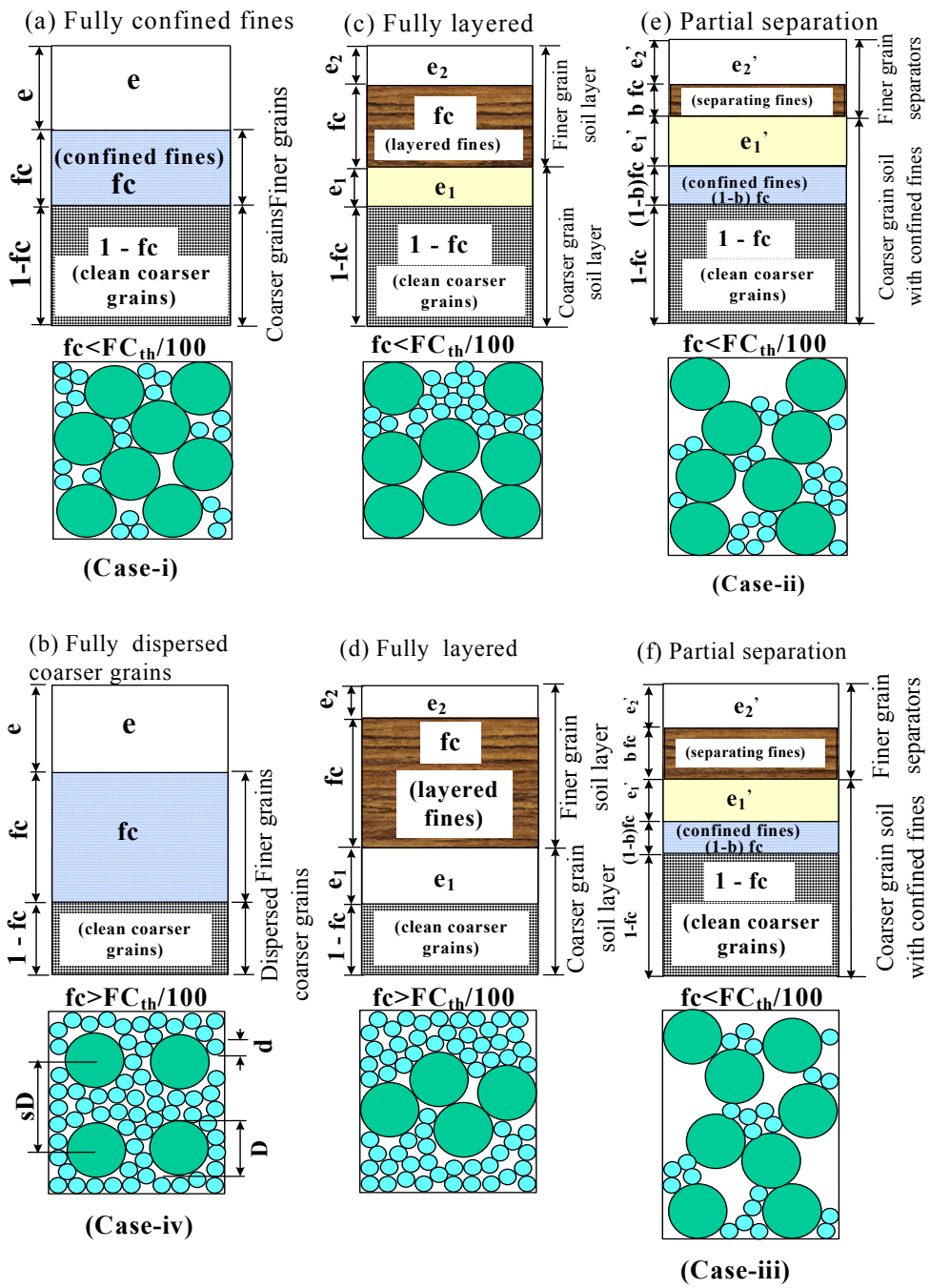

Notes: e=Global Void Ratio; fc=FC/100; FC_{th}=threshold fines content (%)

Fig. 1 Intergranular and Interfine Matrix Phase Diagram

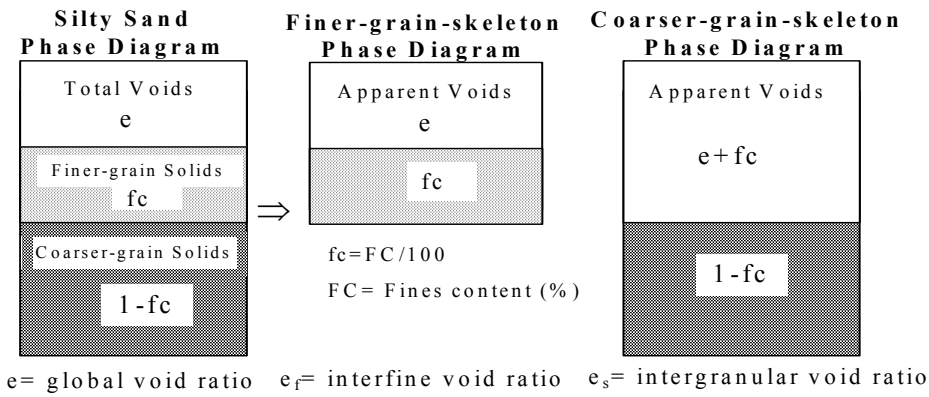

$$e_f = \frac{e}{fc} \qquad e_s = \frac{e + fc}{1 - fc}$$

Fig. 2 Intergranular Phase Diagram and Apparent Void Ratios

When $FC>FC_{th}$ the finer grains begin to play a rather important role. The coarser grains begin to disperse (Fig.1b) and provide a sort of *reinforcement* effect until they are separated sufficiently apart when FC exceeds a limiting fines content FC_l. The FC_l is given by (Thevanayagam 1998b,c):

$$FC_l \geq 100\left[1-\frac{\pi(1+e)}{6s^3}\right]\% = 100\left[\frac{\frac{6s^3}{\pi}-1}{\frac{6s^3}{\pi}+e_f}\right]\%;\ e_f \leq e_{\max,HF} \tag{3}$$

where $s=1+a/R_d$, $R_d=D/d$=size disparity ratio, and a=10. The magnitude of a may be partly attributed to the observations of Roscoe (1970) that the zone of influence of shear is about ten times the particle diameter. At $FC_{th}<FC<FC_l$, neither e_s nor e_f can sufficiently represent the active contacts. The reinforcement effect by the coarser grains must also be introduced to obtain an equivalent interfine void ratio $(e_f)_{eq}$ as the index of active contacts. For a two size particle system with large size disparity, an approximate expression for $(e_f)_{eq}$ can be derived (Thevanayagam 1998c):

$$(e_f)_{eq} = \frac{e}{fc + \frac{1-fc}{R_d^m}} < e_f \tag{4}$$

where fc=FC/100, and m=a coefficient.

Beyond FC_l the behavior is entirely governed by the finer grains. The interfine void ratio e_f may be considered as an index of active contacts.

Eqs.2-4 offer a simple means to delineate the roles of coarser and finer grains of poorly graded silty soils and identify the relevant indices of active contacts affecting their mechanical response. The transition and limiting fines contents are dependent on R_d, global void ratio, and other grain characteristics. Depending on the mix proportion and size disparity the relevant indices may be used to correlate with mechanical response parameters.

Proposed G_{max} Relations

Since G_{max} is a mechanical response that is heavily dependent on active contact density of the particles, plausibly, G_{max} relationship for silty sands (or sandy gravels) and sandy silts (or gravelly sands) could be related to e_s and $(e_f)_{eq}$, respectively:

$$G_{\max} = A\frac{(e_m - e_s)^2}{(1+e_s)}\left(\frac{\sigma'}{P_a}\right)^b \text{ Mpa} \qquad \text{for FC<FC}_{th} \tag{5a}$$

$$G_{\max} = A\frac{(e_m - (e_f)_{eq})^2}{(1+(e_f)_{eq})}\left(\frac{\sigma'}{P_a}\right)^b \text{ Mpa} \qquad \text{for FC>FC}_{th} \tag{5b}$$

Experimental Evaluation

The above conceptual framework and its practical applicability were evaluated using a limited amount of measured G_{max} data available in the published literature for silty sands (Borden et. al. 1996). The measurements were made on undisturbed Piedmont residual silty soils using resonant column and torsional shear test devices. The tests involved both saturated and unsaturated specimens. Only the data corresponding to non-plastic silty soil samples recovered from below the groundwater level (saturated) are included in the present evaluation. Table 1 shows the measured data along with G_{max} values predicted using Eqs.1 and 5a.

Table 1 Measured and calculated G_{max} – Piedmont residual soils

Meas ured								Calcul ated			
Soil Type	e	Sand %	Silt %	Clay %	FC %	σ'_{vo} kPa	G_{max} MPa	e_s	e_f	G_{max} Mpa Eq.1a	G_{max} Mpa Eq.3a
SM	0.49	80.4	18.1	1.5	19.6	50	34	0.853	2.50	95	47
	0.49	80.4	18.1	1.5	19.6	100	52	0.853	2.50	134	66
	0.72	84.7	9.8	0.2	10.0	50	36	0.968	7.20	61	37
	0.72	84.7	9.8	0.2	10.0	100	56	0.968	7.20	86	52

The traditional Eq.1 based on global void ratio e overestimates the G_{max} by more than 150 and 250 percent for fines content of 10 and 20 percent, respectively. The deviations from the measured values increase with an increase in FC.

Predictions using Eq.5a based on intergranular void ratio are closer to the measured values. The intergranular void ratio represents the active contacts better and therefore appears to correlate better with G_{max}.

Conclusions

Two new parameters, namely the intergranular void ratio and equivalent interfine void ratio are proposed as indices of active contacts among particles in non-plastic granular mixes. A simple expression for maximum shear modulus for granular mixes is presented. Validity of the new expression is evaluated against experimental data. Traditional Hardin-Black empirical equations for low strain maximum shear modulus based on global void ratio and mean stress overestimates the G_{max} for silty sands. The estimated values are about 150 to 250% of the measured values for a fines content of about 10 and 20%. The new expressions based on intergranular void ratio and equivalent interfine void ratio and mean effective stress predicts the G_{max} values reasonably well. The experimental data are too limited to draw any final conclusions.

References

Borden, R. H., Shao, L. and Gupta, A. (1996). "Dynamic properties of Piedmont residual soils", *J. Geotech. Geoenv. Div*., ASCE, **122**(10), 813-821.

Hardin, B.O., and Black, W.L. (1968). "Vibration modulus of normally consolidated clays", *J. Soil Mech. Found. Div*., ASCE, **94**(2), 353-369.

Hardin, B. O., and Drnevich, V. P. (1972). "Shear modulus and damping in soils: Measurements and parameter effects", *J. Soil Mech. Found. Div*., ASCE, **98**(6), 603-624.

Roscoe, K. H. (1970). "The influence of strains in soil mechanics". *Geotechnique*, **20**(2),129-170.

Saxena, S.K., Avramidis, A.S., and Reddy, K.R. (1988). "Dynamic moduli and damping ratios for cemented sands at low strains", *Can. Geot. J*., **25**(2), 353-368.

Seed, H.B., Wong, R.T., Idriss, I.M., and Tokimatsu, K. (1986). "Moduli and damping factors for dynamic analysis of cohesionless soils", *J. Geot. Eng. Div*., ASCE, **112**(11), 1-17.

Stokoe, K.H., and Woods, R.D. (1972). "In situ shear wave velocity by cross-hole method", *J. Soil Mech. Found. Div*., ASCE, **98**(5), 443-460.

Stokoe, K.H., Nazarian, S., Rix, G.J., Salinero, I.S., Sheu, J.C., and Mok, Y.J. (1988). "In situ seismic testing of hard-to-sample soils by surface wave method", *Geot. Spec. Publ. 20, Earthq. Eng. and Soil Dyn. II*, ASCE, NY, 264-278.

Thevanayagam, S. (1998a) "Effect of fines and confining stress on undrained shear strength of silty sands", *J. Geotech. Geoenv. Div*., ASCE, **124**(6), 479-491.

Thevanayagam, S. (1998b) "Role of intergrain contacts, friction, and interactions on undrained response of granular mixes", Proc. Intl. Workshop on *The Physics and Mechanics of Liquefaction*, Baltimore, ed. Lade, P. V., Balkema Publishiers, in press.

Thevanayagam, S. (1998c). Relative role of coarser and finer grains on the undrained behavior of granular mixes. *in review*, *J. Geotech. & Geoenv. Engrg. Div*., ASCE

The Second International Workshop on Mitigation of Seismic Effects on Transportation Structures
September 13-15, 2000, Taipei, Taiwan

Liquefaction in Silty Soils – Considerations for Screening and Retrofit Strategies

S. Thevanayagam

Dept. of Civil, Struct. and Env. Eng., SUNY at Buffalo, Buffalo, NY 14260, USA

ABSTRACT

Current techniques for liquefaction screening, ground modification for liquefaction mitigation, and post-improvement verification rely on knowledge gained from extensive research on *clean sands*, field observations of liquefied ground, and judicial correlation of normalized penetration resistance [$(N_1)_{60}$, q_{c1N}] or shear wave velocity (v_{s1}) data with field liquefaction observations. Uncertainties prevail on the direct extrapolation of such techniques for silty soil sites. Many silty soil sites in Kobe, Turkey, and Taiwan did liquefy. They offer a test bed opportunity to study these questions. This paper examines laboratory data on liquefaction resistance, strength, and v_{s1} of sands and silty soils using grain contact density as the basis. Effect of silt content on cyclic resistance, strength, $(N_1)_{60}$, q_{c1N}, v_{s1}, m_v, and c_v is examined in this light. Rational insights for extrapolation of the current screening techniques to silty soils are offered. Thoughts on modifications necessary to the traditional densification, drainage, and permeation grouting techniques to make them viable for silty soils are offered.

INTRODUCTION

Saturated, loose granular deposits, when subjected to rapid shear loading, experience a rapid pore pressure increase and temporary loss of strength, which may lead to liquefaction, a stage, when soil looses almost all the strength and behaves like a liquid. Such a stage leads to lateral spreading of the gently sloping ground, densification and vertical ground settlements, and slope instability. Case histories indicate that soil types prone to liquefaction are loose sand, silty sands/sandy silts containing mostly non-plastic silt, and gravel. Only rarely clays, except for sensitive clays, do experience loss of strength. Saturated alluvial granular deposits prone to liquefaction are very commonly found particularly near river-crossings and water-front harbor facilities and have caused major damage to transportation structures in almost every major

earthquake. Of several such documented examples, during the great Alaskan earthquake many highway and railway bridges were collapsed beyond repair; Buckle (1995) reported of the distress to the bridge superstructure and collapse of several spans caused by lateral movement of several bridge piers due to lateral spread of the ground along the manmade waterfront area in Kobe. Similar waterfront and transportation facility damage has been observed during the most recent Taiwan Chi-Chi and Turkey earthquakes as well. Such damages are reminders of the need to develop and transfer prudent liquefaction screening techniques and remedial measures for its mitigation to retrofit transportation and lifeline infrastructure systems.

Current screening techniques (Table 1, Fig.1) for liquefaction potential evaluation (Youd and Idriss 1997, Youd and Gilstrap1999) rely on extensive laboratory research conducted on clean sands, and extrapolations of that knowledge and geotechnical engineering experience leading to correlations between measured normalized penetration resistance (SPT, CPT) (Idriss, Seed and Arango 1983, Robertson and Wride 1997), and shear wave velocity (v_{s1}) (Andrus and Stokoe 1997, Stokoe et al. 1999) and cyclic stress ratio induced by an earthquake at liquefied/non-liquefied sites. Cyclic resistance ratio (CRR) of a soil deposit is derived from demarcation lines drawn between data points collected from liquefied sites from those from non-liquefied sites (Fig.1). This is compared with the anticipated cyclic stress ratio (CSR) from a future earthquake at a new site to discern whether or not that site would liquefy (Table 1).

Soil improvement techniques to mitigate liquefaction and deformation hazards primarily rely on densification, drainage, reinforcement, and in some cases on cementation/solidification by grouting (JGS 1995, Cooke and Mitchell 1999). They also primarily rely on the understanding of the behavior of clean sands.

A high level of understanding of the behavior of non-plastic silty soils is currently lacking. Practicing engineers question the reliability of direct extrapolations of field observations (Fig.1) for liquefaction screening purposes at other silty soil sites. The rationale for such extrapolation is yet to be developed and its limitations identified. Furthermore the low permeable nature of such sites demand new/modified ground densification/drainage/grouting techniques viable for such soils.

The first part of this paper focuses on recent developments in understanding of the liquefaction and post-liquefaction behavior of silty soils. The second part extrapolates that understanding to make some comments on the current field observation-based liquefaction screening techniques. Particularly a rational basis for extrapolation of current screening techniques for silty soils is developed. Current limitations of these techniques are discussed. This is followed by commentary on design considerations for liquefaction mitigation by densification, drainage and grouting techniques in silty soils.

Table 1. Current Liquefaction Screening Methods

Method	$CRR_{7.5}$=	x =	x =	FS
SPT	$[a+cx+ex^2+gx^3]/[1+bx+dx^2+fx^3+hx^4]$	$(N_1)_{60cs}$	$\alpha + \beta\ (N_1)_{60}$	
CPT	$0.833[x/1000]+0.05$ for $x<50$ $93[x/1000]^3+0.08$ for $50<x<160$	$[(q_{c1N})_{cs}$	$K_c\ q_{c1N}$	$(CRR_{7.5}/CSR)MSF$
S-wave	$r(V_{s1}/100)^2 + s[1/(V_{s1c}- V_{s1})-1/V_{s1c}]$			

Notes for Table 1: (i) FS=Factor of safety against liquefaction, CSR=stress ratio caused by earthquake,

MSF=magnitude scaling factor; (ii) $\alpha = 0$ & $\beta = 1$ for FC<5; $\alpha = \exp[1.76 - (190/FC^2)]$ & $\beta = [0.99 + (FC^{1.5}/1000)]$ for 5<FC<35; $\alpha = 5$ & $\beta = 1.2$ for FC>35, FC= fines content by weight, a= 0.048, b= -0.1248, c= -0.004721, d= 0.009578, e=0.0006136, f= -0.0003285, g= -1.673E-05; h= 3.714E-06; (iii) $K_c=1.0$ for $I_c<1.64$, $K_c = -0.403\, I_c^4 + 5.581\, I_c^3 - 21.63\, I_c^2 + 33.75\, I_c - 17.88$ for $I_c>1.64$; $I_c = [(3.47 - \log Q)^2 + (1.22 + \log F)^2]^{0.5}$, $Q=[(q_c - \sigma_{vo})/ P_a][(P_a/\sigma'_{vo})^n]$, $F=100[f_s/(q_c - \sigma_{vo})]$ %; (iv) r=0.03, s=0.9; V_{s1c}=220m/s for FC<5, V_{s1c}=210m/s for FC=20, V_{s1c} =200m/s for FC>35; (v) $(N_1)_{60}$ and $(N_1)_{60cs}$ =stress-normalized SPT blow count of silty soil, and equivalent clean sand blow count, respectively; q_{c1N} and $(q_{c1N})_{cs}$ = stress-normalized cone penetration resistance of silty soil, and equivalent clean sand resistance, respectively; q_c and f_s =measured cone tip and side resistance, respectively; P_a =atmospheric pressure; σ'_{vo} and σ'_{vo} =total and effective vertical overburden stresses at the cone tip, respectively; n=1.0; V_{s1} =stress-normalized shear wave velocity m/s.

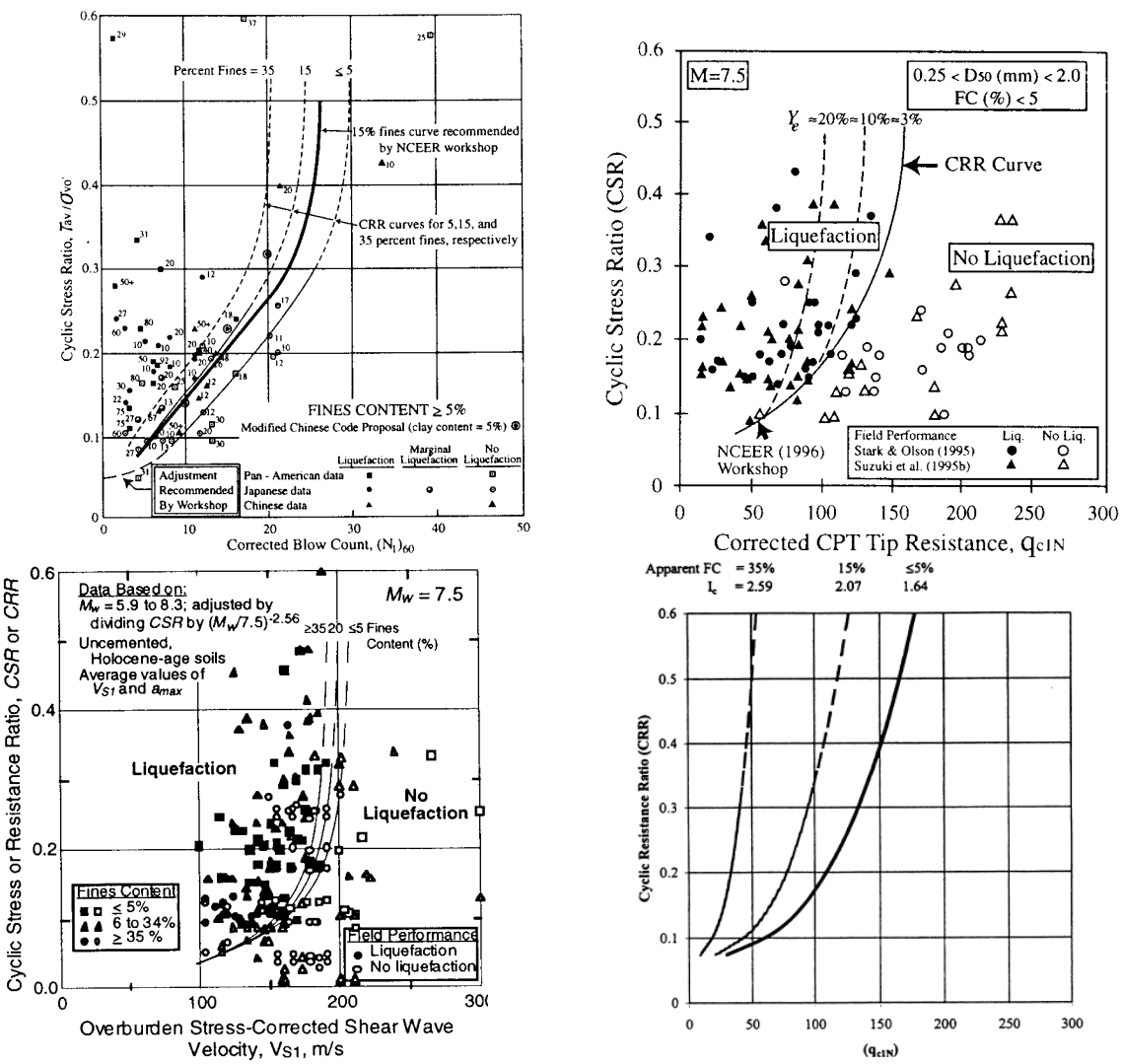

Fig.1 Field Liquefaction Screening Charts – SPT, CPT, and Shear wave velocity

[after Youd and Gilstrap (1999), p1013-1020; Stokoe et al. (1999), p811-856 in *Earthquake Geotechnical Engineering*, eds. P. Seco e Pinto, vol.3, A.A.Balkema Press]

DIFFERENCES AND SIMILARITIES IN BEHAVIOR: SAND AND SAND-SILT MIX

Cyclic Strength and Energy to Liquefaction

Differences: Figs.2a-b show the number of cycles and energy input, respectively, to reach liquefaction versus void ratio for Ottawa sand/silt mix, tested at a constant stress ratio (CSR) of 0.2. Specimens were prepared by mixing Ottawa sand (D_{50}=0.25mm) with a non-plastic silt (d_{50}=0.01mm) at different silt contents (0 to 100% by weight, [os15=sand-silt mix at 15% silt content]) (Thevanayagam et al. 1999). In both cases, at the same void ratio, cyclic strength of silty sand decreases with an increase in silt content. Beyond transition silt content (about 20 to 30%), the trend reverses and the strength increases with further increase in silt content. At the same e, sand and silty sand/sandy silt behave differently.

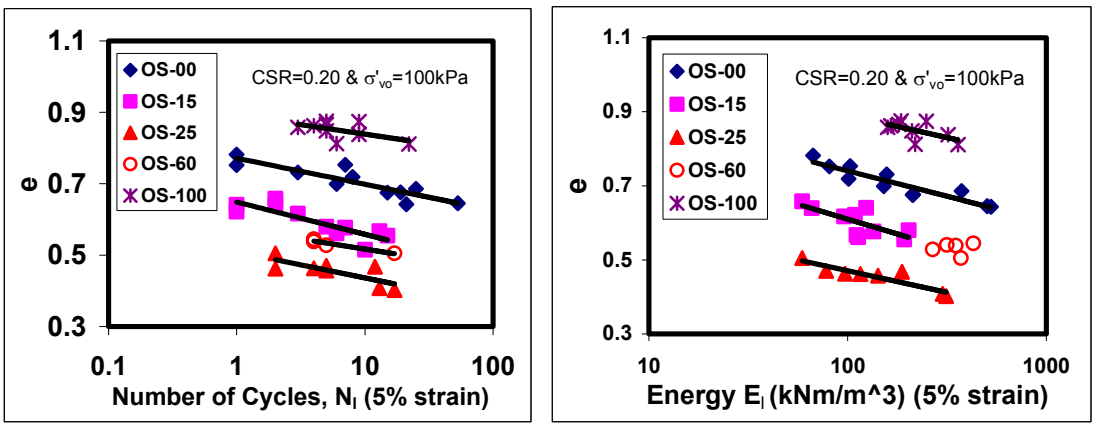

Fig.2 Void ratio vs. liquefaction potential of silty soils: (a) No. of cycles, and (b) Energy

New Basis for Comparison: Recently Thevanayagam and co-workers (1999-2000) proposed that mechanical properties of soils are derived from grain contact. Therefore, sand and sand-silt mixes are expected to show similar mechanical behavior if compared at a same contact density index. Such contact density indices, namely an equivalent inter-coarser grain contact density index void ratio $(e_c)_{eq}$ and equivalent interfine contact density void ratio $(e_f)_{eq}$, respectively, for soils at silt content (FC) less than and more than a threshold value FC_{th} have been identified. Theoretical expressions for these indices are: $(e_c)_{eq}=(e+(1-b)fc)/(1-(1-b)fc)$, $(e_f)_{eq}=e/(fc+(1-fc)/R_d^m)$, $FC_{th}=100e_c/(1+ e_c + e_{max,HF})=100e/e_{max,HF}$ where $0<b<1$, fc=FC/100= finer grain fraction by weight, e=global void ratio, $R_d=D_{50}/d_{50}$, $0<m<1$, and $e_c=(e+fc)/(1-fc)$.

Similarities: Figs.3a-b show the same data shown in Fig.2a, but plotted against $(e_c)_{eq}$ [b=0.35] for silt content less than FC_{th} of about 25% and against $(e_f)_{eq}$ [m=0.65] for silt content greater than 25%, respectively. Figs.3c-d show the same data in terms of energy. At the same $(e_c)_{eq}$ sand and silty sand show similar cyclic strength and require similar input energy to cause liquefaction. At the same $(e_f)_{eq}$, silt and sandy silt have similar cyclic strength.

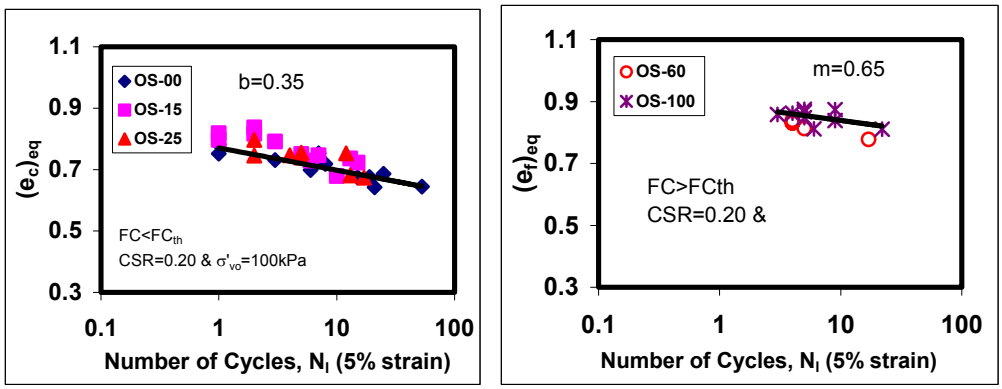

Fig. 3a-b Influence of contact density: (a) $(e_c)_{eq}$ [FC<FC$_{th}$] and (b) $(e_f)_{eq}$ [FC>FC$_{th}$]

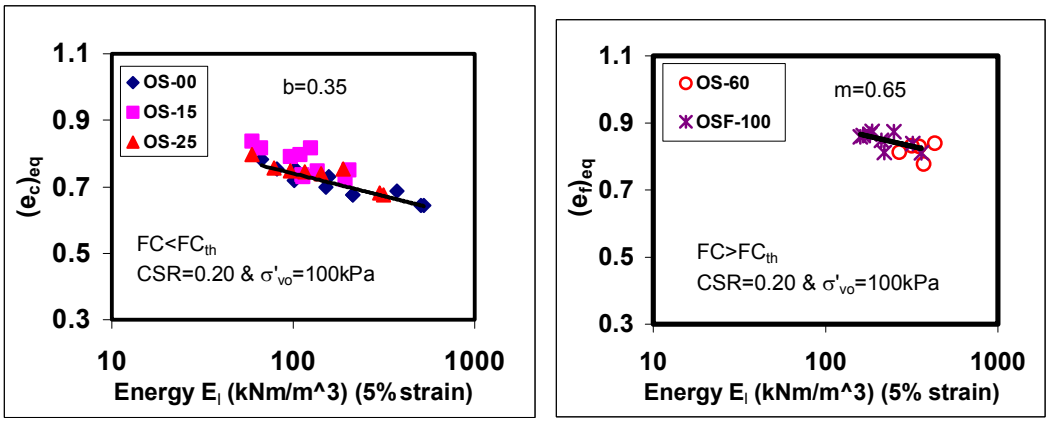

Fig. 3c-d Influence of contact density: (c) $(e_c)_{eq}$ [FC<FC$_{th}$] and (d) $(e_f)_{eq}$ [FC>FC$_{th}$]

Undrained Strength

Fig.6 shows the mean effective stress at steady state for the same Ottawa sand/silt mix obtained from undrained monotonic triaxial tests (Thevanayagam et al. 1999). The steady state line for each mix falls below that of the (clean) sand (os00) progressively until reaching fines content range of 25 to 40%. The trend reverses thereafter. At the same e, sand and silty sand/sandy silt does not behave the same.

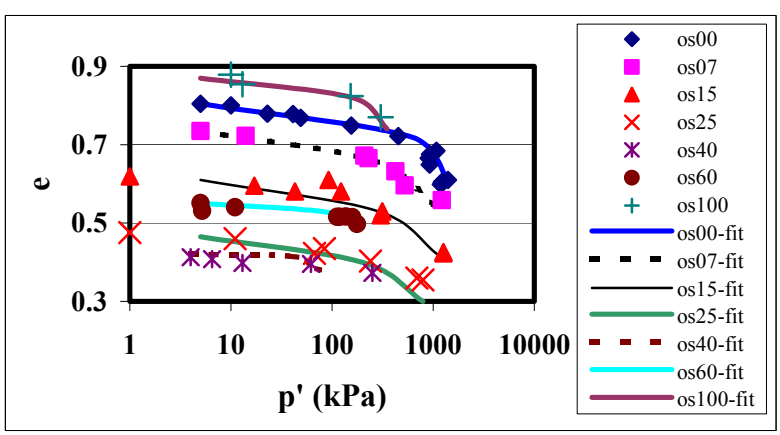

Fig.4 Influence of silt content on steady state

Figs.5a-b show the same data shown in Fig.4, but plotted against $(e_c)_{eq}$ [b=0.25] for silt content less than (FC_{th}) 25% and $(e_f)_{eq}$ [m=0.65] for silt content greater than 25%, respectively. All data points fall in a narrow band correlating well with the relevant contact density indices.

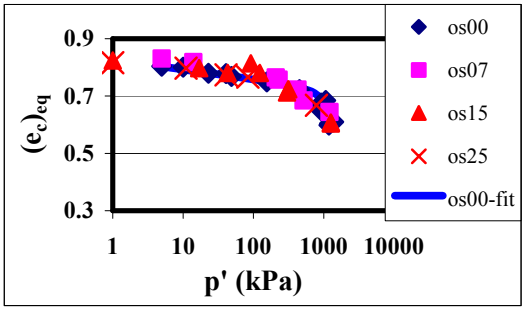

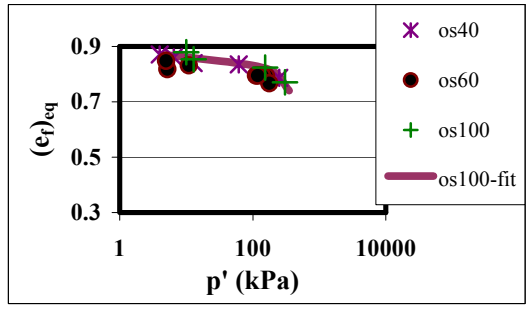

Fig.5a: $(e_c)_{eq}$ vs p' –sand and silty sands **Fig.5b: $(e_f)_{eq}$ vs p' – Sandy silts and silt**

Shear wave velocity and shear modulus

Fig.6a shows one set of normalized shear velocity data (v_{s1}) for Tone river sand (TRS) and three other gravely soils prepared by mixing TRS with 25, 50 and 75% gravel by weight (Kokusho et al. 1995). The data indicate that shear wave velocity for gravely soils are often significantly smaller than the respective values for 'pure' sand at the same e. In this case, designating sand=fine grain and gravel=coarse grain, Fig.6b shows the same data plotted in terms of $(e_f)_{eq}$ [m=0.45] (Thevanayagam 2000). At the same $(e_f)_{eq}$, sand and gravely sand have similar shear wave velocity.

Fig.7a shows shear modulus of the Ottawa sand-silt mixes at 0.05% axial strain plotted against void ratio. Fig.7b shows the same data against $(e_c)_{eq}$ [b=0.25]. At the same e, sand and silty sand does not behave the same. At the same $(e_c)_{eq}$, sand and silty sand show similar shear modulus (Thevanayagam and Liang 2001).

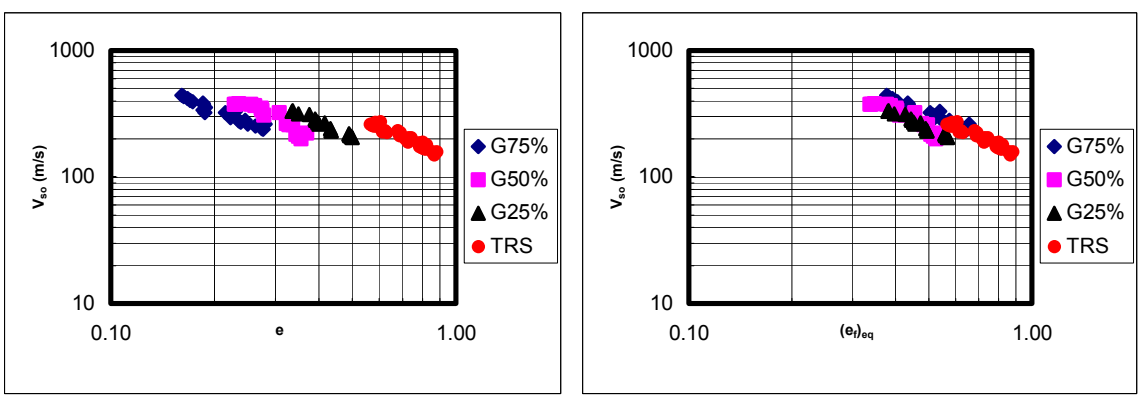

Fig.6 Influence of gravel content on V_{s1}: (a) void ratio e, and (b) $(e_f)_{eq}$

The same behavior holds true for post-liquefaction densification behavior as well as for the Ottawa sand-silt mix (Thevanayagam et al. 2001).

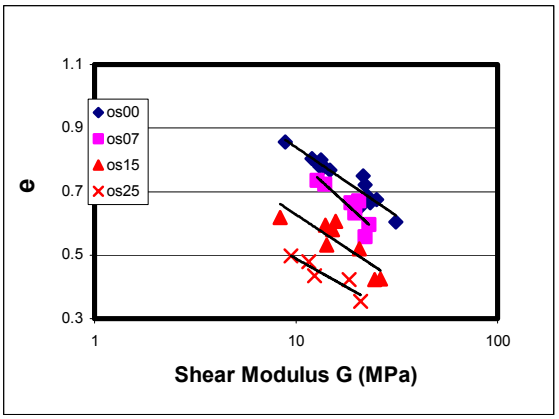

Fig.7a. e vs. $G_{0.05}$

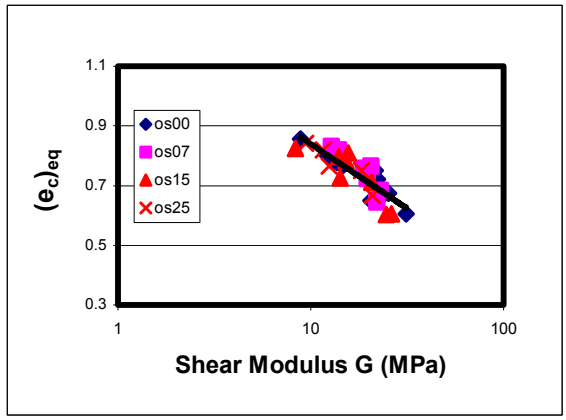

Fig.7b. $(e_c)_{eq}$ vs. $G_{0.05}$

Coefficient of Consolidation

Fig.8 shows the pre- and post-liquefaction coefficient of consolidation (c_v) values for the Ottawa sand-silt mix. Two important observations can be made. At the same effective confining stress, the c_v values for pre-liquefaction consolidation (obtained along virgin loading) and post-liquefaction c_v values are nearly the same for the same soil. Similar observation is made for the volume compressibility m_v (Fig.9). This indicates that the soil is completely remolded following liquefaction and it behaves as a freshly deposited soil. Its consolidation line parallels that of the pre-liquefaction virgin loading.

The m_v values are not significantly dependent on silt content. But, the c_v values are much smaller for the silty soils by more than one order of magnitude compared to sand. It is predominantly affected by the soil permeability depending on the silt content. Hydraulic conductivity (k) of the soil specimens ranged from 0.6 to 1.3×10^{-3} cm/s for the sand, 9×10^{-5} cm/s for 15% silt, 0.6 to 1.2×10^{-5} cm/s for 25% silt, and 3 to 5×10^{-6} cm/s for 60% and 100% silt soils. The c_v values are affected in the same order.

C_{vo}/C_v Ratio and Relative Dissipation Time – Sand and Sand-Silt Mix

Fig.10a-b show the influence of fines content on c_v and normalized (c_{vo}/c_v), where c_v and c_{vo} are the coefficients of consolidation of Ottawa sand-silt mix and clean sand, respectively, compared at nearly the same equivalent contact index void ratio. The parameter (c_{vo}/c_v) is a convenient relative measure of the time it would take for dissipation of excess pore pressure in the sand-silt mix normalized to clean sand for the same geometric boundary conditions. The problem under consideration could be dissipation of excess pore pressure around CPT and SPT during penetration, around a stone column, pore pressure redistribution during an earthquake, or another scenario. The (c_{vo}/c_v) increases and hence rate of dissipation decreases rapidly with an increase in silt content up to a threshold value in the vicinity of FC_{th} and thereafter it decreases only slightly. This has significant implications on the measured $(N_1)_{60}$ and q_{c1N}, but not very much on v_{s1} (Table 2, discussed later). Also it has a significant impact on drainage and densification achievable during vibro-compaction installation, dissipation and densification achievable during dynamic compaction, drainage towards stone-columns during earthquakes. The

magnitude variation in c_{vo}/c_v depends on the grain size characteristics of the silt and sand, and therefore the influences are not the same for each pair of sand and silt. This can be observed by comparing the c_v values for the Ottawa sand with that of a natural silt (d_{50}=0.038mm)(Figs.8 and 10a).

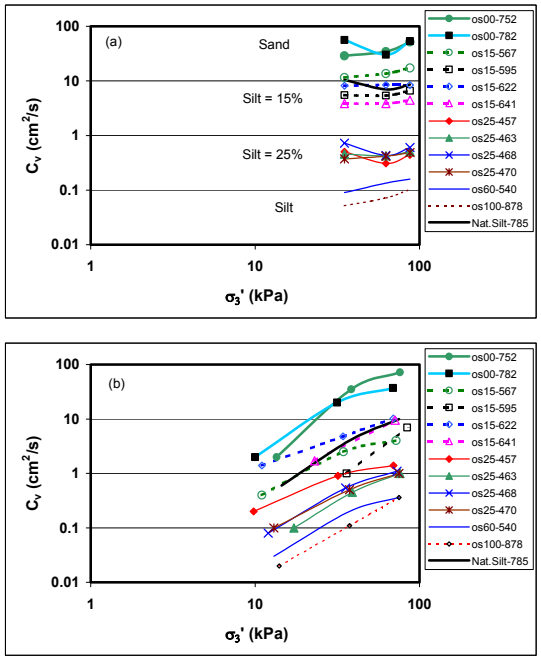

Fig. 8 Pre- and post-liquefaction c_v

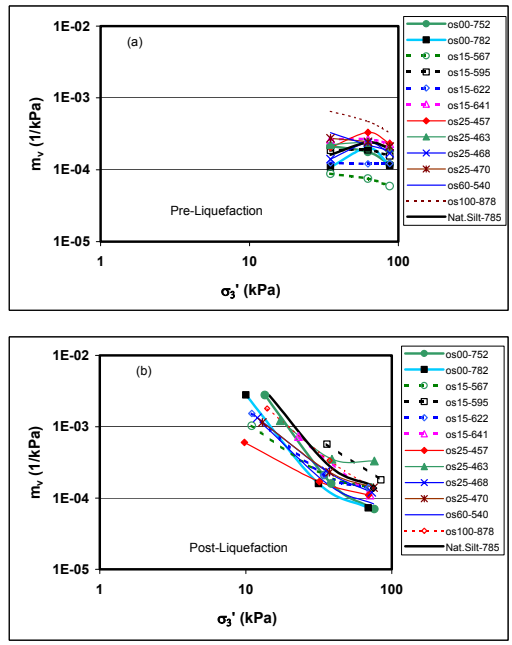

Fig. 9 Pre- and post-liquefaction m_v

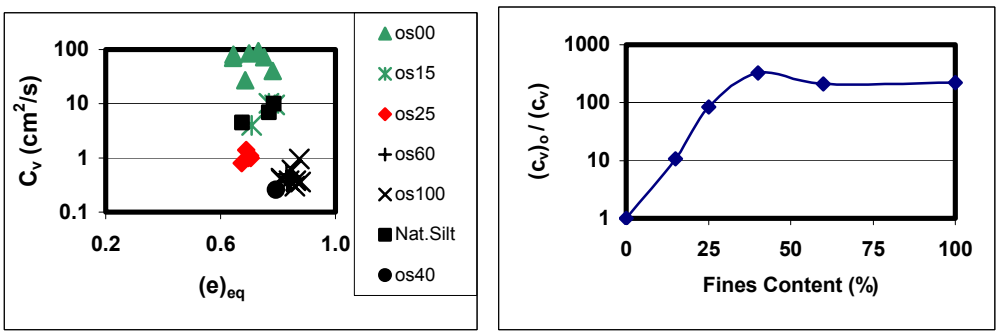

Fig.10 Relative coefficient of consolidation ratio – Fines content

IMPLICATIONS AND CONCLUSIONS

The above observations indicate that a sand and sand-silt mix show similar cyclic resistance (CRR), energy required to cause liquefaction E_l, strength s_{us}, v_{s1}, m_v, and post-liquefaction densification characteristics when compared at the same $(e_c)_{eq}$, $(e_f)_{eq}$ or similar grain contact density index [relative density in terms of $(e_c)_{eq}$, $(e_f)_{eq}$]. But there is major difference between sand and sand-silt mixes when one considers c_v (flow and permeability) and time required to dissipate excess pore pressures, and therefore major differences in $((N_1)_{60}$ and q_{c1N} at the same

$(e_c)_{eq}$ or $(e_f)_{eq}$. When combined together these observations have significant impact on interpretation and use of field liquefaction screening methods using in situ ($(N_1)_{60}$, q_{c1N} and v_{s1}) measurements, and in the choice, modification, and design of appropriate ground improvement techniques to mitigate liquefaction potential in silty soil sites. This can be used to develop a rational explanation for the field observations (Fig.1) and used to refine the screening techniques.

Liquefaction Screening: Implications of the above findings on liquefaction screening using SPT, CPT, and v_{s1} can be analyzed as follows. First, Table 2 summarizes the effect of increase in silt content on k, c_v, CRR, energy to cause liquefaction, v_{s1}, and relative dissipation time at the same $(e_c)_{eq}$ for $FC<FC_{th}$, and at the same $(e_f)_{eq}$ for $FC>FC_{th}$.

Secondly, based on relative dissipation time, this table also summarizes the anticipated relative influence of increase in fines content on field measurements of $(N_1)_{60}$, q_{c1N}, and v_{s1} for silty soils compared to clean sand. At the same $(e_c)_{eq}$ (up to FC_{th}), c_v decreases rapidly and relative dissipation time increases with an increase in silt content as indicated by c_{vo}/c_v (Fig.10). The increase in dissipation time helps maintain a lower effective stress near the penetration tip of a cone or SPT sampler in a silty sand than in sand at the same $(e_c)_{eq}$. Thus a major reduction anticipated for $(N_1)_{60}$ and q_{c1N} in silty soils up to FC_{th} with an increase in silt content compared to sand. Beyond FC_{th}, at the same $(e_f)_{eq}$, only a slight reduction is observed in c_v. Hence only a small further reduction is expected $(N_1)_{60}$ and q_{c1N} in silty soils with further increase in silt content due to only a minor increase in relative dissipation time. But there is little change expected for CRR, E_l, s_{us}, and v_{s1} with increase in silt content at the same $(e_f)_{eq}$.

Taking these reasoning into consideration, the combined effects of increase in silt content on field liquefaction screening using $(N_1)_{60}$, q_{c1N}, and v_{s1} data are summarized in Table 2. In developing this summary it is considered that the relative ratio c_{vo}/c_v does not significantly affect the dissipation of excess pore pressures, due to large thickness of a soil deposit (in contrast with the size of a SPT sampler and CPT cone), during the short duration of the strong motion and therefore CRR of a field soil is not significantly different from undrained conditions. Such a condition may not prevail at all sites.

In essence, for the reasons cited above, there is very little differences expected on CRR versus and v_{s1} between sand and non-plastic silty soils. On the other hand, $(N_1)_{60}$ and q_{c1N} required to resist liquefaction in silty soils up to FC_{th} at a given CSR is expected to decrease rapidly from that of clean sand. The magnitude in reduction depends on the relative c_v/c_{vo}. The magnitude reduction is also expected to be different for SPT and CPT due to differences in probe geometry. The $(N_1)_{60}$ or q_{c1N} required to resist liquefaction is expected to decrease further only slightly beyond FC_{th}. The current screening charts (Fig.1) based on direct observations do, to some extent, reflect this expected trend. The weak silt-content dependent s-wave method in Fig.1 is likely more of a perceptive extension of SPT charts than necessary. The 35% fines content limit in the SPT and CPT charts also agrees with the FC_{th} threshold limit considerations identified before.

The same reasoning also indicates that the CRR versus $(N_1)_{60}$ or q_{c1N} should also be sensitive to relative grain size ratio of clean sand and silt. Different relationships would exist for very fine sand and coarse sand, even if no silt is present. A unique demarcation line between liquefied and non-liquefied sites may not be possible in Fig.1 for all.

The field data are affected by more factors than considered herein. Therefore detailed research and analysis of the observed data (Fig.1) in light of the insights presented is recommended to develop a refined and rational liquefaction screening technique for all soils.

Table 2: Effect of Increase in Silt Content at Constant $(e_c)_{eq}$ or constant $(e_f)_{eq}$

Primary	**Role**		**Lab**	**Measured**	**Parameter**	**Field**	**Measured**	**Parameter***	**Liquefaction**	**Screening**	
Coarse Grain	Fine Grain	k and c_v	Mono. undr. strength	CRR & Energy	V_{s1}	V_{s1}	SPT $(N_1)_{60}$	CPT q_{c1N}	V_{s1} vs. CRR	$(N_1)_{60}$ vs. CRR	q_{c1N} vs. CRR
Primary Contact **$FC<FC_{th}$** **$(e_c)_{eq}$ = constant**	Block pores, reduce pore size	Major reduction in k due to decrease in void ratio and pore size compared to sand. Rapid increase in dissipation time.	Minor change compared to sand	Minor change compared to sand	Minor change compared to sand	Minor change Compared to sand	Reduction in $(N_1)_{60}$ compared to sand due to reduction in k and c_v and rapid increase in dissipation time.	Reducion in q_{c1N} compared to sand due to reduction in k and c_v and rapid increase in dissipation time.	Minor impact on CSR to cause liquefaction at the same V_{s1}	Higher CSR than sand to cause liquefaction at the same $(N_1)_{60}$	Higher CSR than sand to cause liquefaction at the same q_{c1N}
Reinforcement	Primary contact **$FC>FC_{th}$** **$(e_f)_{eq}$ = constant**	May expect a slight increase in k due to increase in void ratio, but decrease in pore size reduces the k. Minor increase in dissipation time beyond FC_{th}. Smaller k and c_v than for sand at comparable $(e_c)_{eq}$.	Minor change compared to silt	Minor change compared to silt	Minor change compared to silt	Minor change compared to silt	Minor reduction in $(N_1)_{60}$ for sandy silt compared to silty sand due to reduction in k and c_v and minor increase in dissipation time beyond FC_{th}. Major reduction in $(N_1)_{60}$ for sandy silt compared to sand at comparable $(e_c)_{eq}$ due to smaller c_v.	Minor reduction in q_{c1N} for sandy silt compared to silty sand due to reduction in k and c_v and minor increase in dissipation time beyond FC_{th}. Major reduction in q_{c1N} for sandy silt compared to sand at comparable $(e_c)_{eq}$ due to smaller c_v.	Negligible impact on CSR to cause liquefaction at the same V_{s1}	Slightly higher CSR than silty sand to cause liquefaction at the same $(N_1)_{60}$	Slightly higher CSR than silty sand to cause liquefaction at the same q_{c1N}

Notes: k=permeability, c_v=coefficient of consolidation, s_{us}=undrained shear strength (large strain), CRR = cyclic resistance ratio, CSR= cyclic stress ratio.
*=Field CRR is considered to be similar to undrained CRR.

Retrofit Strategies: The fact that non-plastic silty soils behave similar to sands when compared at the appropriate contact density index parameters at any silt content, but show significantly low coefficient of consolidation and permeability has a dramatic impact on the choice of ground improvement techniques for liquefaction mitigation in silty soils. Ground improvement schemes based on densification, drainage, and permeation (grouting) have limited application in silty soils unless modifications are incorporated. Since primarily permeability (and silt content) affects the pore pressure dissipation/densification characteristics, closer spacing of dynamic compaction grids and stone columns along with provision of supplementary wick drains can expedite dissipation of pore pressures developed during ground improvement operation in silty soils and help achieve desired densification. Limited field data shows that such supplementary wick drains do help relieve pore pressures developed during dynamic compaction and stone column installation in silty soils (Dise et al. 1994, and Luehring et al. 2000) and help densification. Furthermore recent research indicates that reinforcement effect by stone columns may be another important factor that needs to be considered more carefully in the design of stone columns (Baez and Martin 1995). Permeation grouting may be difficult to achieve unless very closer spacing is utilized which may increase the cost significantly. Ongoing work at SUNY Buffalo indicates that other alternatives such as introduction of chemical ionic constituent of chemicals/cementing agents using electrokinetics may become attractive and more cost-effective than permeation grouting. Effective design guidelines for such systems are still lacking and needs to be developed.

The above results indicate that extrapolation of methods developed for liquefaction potential evaluation and mitigation schemes for sands to silty soil sites should consider the differences and similarities between silty soils and sand. A method that reflects the nature of active grain contacts while recognizing the major differences in flow/consolidation characteristics is essential for liquefaction screening in silty soils. As shown in this paper, in situ parameters such as SPT blow counts, CPT resistance, and field shear wave velocity do reflect this to some extent. But how well do they reflect this, on the face of the several uncertainties involved in the development of the empirical correlations of such parameters based on observed performances, remains the subject of an engineer's judgement. It is hoped that the geotechnical insights presented herein help engineers in judicious choice of soil parameters for foundation design involving young silty/gravely soils against seismic events.

ACKNOWLEDGMENTS

Financial support by the USGS/NSF/MCEER/FHWA for the various aspects of this ongoing research work is gratefully appreciated. Thanks are also due to J. Liang and T. Shenthan, SUNY at Buffalo, for their assistance in the laboratory triaxial tests on silty soils.

REFERENCES

Andrus, R., and Stokoe, K. H. II (1997) "Liquefaction resistance based on shear wave velocity", NCEER Report, 97-0022, State University of New York at Buffalo, NY, 89-128.

Baez, J.I., and G. Martin. (1995). “Permeability and shear wave velocity of vibro-replacement stone columns.” ASCE, GSP 49, 66-81.

Buckle, I. G. (1995) “Highways and Bridges“, in the Hanshin-Awaji Earthquake of January 17, 1995 Performance of Lifelines, M. Shinozuka, ed., NCEER-95-0015, 7-22 to 7-23.

Chien, L-K, Oh, Y-N., and Chang, C-H. (2000) “Evaluation of liquefaction resistance induced settlement for reclaimed soil”, Proc. 12WCEE, New Zealand.

Cooke, H.G., and Mitchell, J. K. (1999) “Guide to remedial measures for liquefaction mitigation at existing highway bridge sites”, Tech Report-MCEER-99-0015, SUNY, Buffalo, USA, 168p.

Dise, K., M.G. Stevens, and J.L. Von Thun. (1994). “Dynamic compaction to remediate liquefiable embankment foundation soils.” ASCE, GSP 45.

JGS (1995) *Remedial measures against soil liquefaction – From investigation and design to implementation*, Port and Harbor Research Inst., Japan.

Kokusho, T., Yoshida, Y. and Tanaka, Y. (1995) "Shear wave velocity in gravelly soils with different particle gradings", ASCE, Geot. Spec. Pub (GSP 56), 92-106.

Luehring, R., B. Dewey, L. Mejia, M. Stevens, and J. Baez. (2000). “Liquefaction mitigation of a silty dam foundation using vibro-stone columns and drainage wicks - a test section case history at salmon lake dam.” No.00-0748, Unpublished report, USBR, USA.

Robertson, P. K. and Wride, C. E. (1997) “Evaluation of cyclic liquefaction potential based on the CPT”, Seis. Behavior of Ground & Geotech Struct., Balkema Publs., 269-278.

Seed, H. B., Idriss, I.M. and Arango, I. (1983) "Evaluation of liquefaction potential using field performance data", J. Geotech. Eng., ASCE, 109(3), 458-482

Thevanayagam, S. (1999b) "Effect of fines and confining stress on steady state strength of silty sands,” *Closure*, J. Geotech. & Geoenv. Engrg. Div., ASCE, **125**(11) and **124**(6).

Thevanayagam, S. (1999c) “Liquefaction and shear wave velocity characteristics of silty/gravely soils – implications for bridge foundations”, Proc. 15th US-Japan Bridge Workshop, Japan

Thevanayagam, S. (1999d) "Relative roles of coarser and finer grains on undrained behavior of granular mixes", *in review*, J. Geotech. & Geoenv. Eng. Div., ASCE.

Thevanayagam, S., Liang, J., Mohan, S., and Shenthan, T. (1999) “Undrained fragility of clean sands, silty sands and sandy silts,” *in review*, J. Geot. & Geoenv. Engrg. Div., ASCE

Thevanayagam, S. and Mohan, S. (2000) “Intergranular state variables and stress-strain behaviour of silty sands", Geotechnique, **50**(1), 1-24.

Thevanayagam, S. (2000) “Liquefaction potential and undrained fragility of silty soils.” Proc. 12WCEE 2000 Conference, Auckland, New Zealand

Thevanayagam, S., Liang, J., and Shenthan, T. (2000). “Contact index and liquefaction potential of silty and gravely soils.” Proc. 14th ASCE Eng. Mech. Conf., Austin, Texas.

Thevanayagam, S., Fiorillo, M. and Liang, J. (2000). “Effect of non-plastic fines on undrained cyclic strength of silty sands.” ASCE GSP 107, 77-91.

Thevanayagam, S., Martin, G.R., Shenthan, T. and Liang, J. (2001). “Post-liquefaction pore pressure dissipation and densification in silty soils.” 4th Intl Conf. Recent Adv. Geot. Earthq. Eng. & Soil Dyn., San Diego, in press.

Thevanayagam, S. and Liang, J. (2001) “Shear wave velocity relations for silty and gravely soils.” 4th Intl Conf. Recent Adv. Geot. Earthq. Eng. & Soil Dyn., San Diego, in press.

Wang, M-H, Chen, M-H., and Loh, C-H. (2000) “Liquefaction potential study of Taiwan”, Proc. 12WCEE, New Zealand.

Youd, T. L., and Idriss, I. M. eds. (1997) Proc. NCEER workshop on Evaluation of liquefaction resistance of soils, NCEER Tech. Report NCEER-97-0022, 276p.

Youd, T. L. (1999) "Screening guide for rapid assessment of liquefaction hazard at highway bridge sites." Tech Report-MCEER-99-0005, SUNY, Buffalo, NY, USA, 58p.

Addendum

The following changes have been made in the paper: Thevanayagam, S. (2000). "Liquefaction in silty soils – Considerations for screening and retrofit strategies" *Proc. 2nd international workshop on mitigation of seismic effects on transportation structures*

- In Figs. 2(b), 3(c), and 3(d), the X-axis title should be read as E_L (10 J/m^3)

Appendix A

Monotonic Triaxial Compression Tests Data

Appendix A: Monotonic Triaxial Compression Tests Data

Table A.1 summarizes the monotonic triaxial tests data.

Table A.1 Summary of Monotonic Triaxial Compression Tests

Test No.	File Name	Soil Type	FC (%)	Prep. Mtd.	σ_c' (kPa)	B Value	e	P_f' (kPa)	q_f' (kPa)	U_{sh}' (kPa)	p_{ss}' (kPa)	p_{qss}' (kPa)	CP	RFD	max. ε_a (%)
M01	r031299	OS-00	0	DD	100	0.96	0.684	1073	1397	7	1073	93	0.07	0.91	7
M02	r060799	OS-00	0	MT	100	0.92	0.800	10	4	95	10	5	0.95	0.50	23
M03	r060999	OS-00	0	MT	100	0.91	0.804	5	0	98	5	2	0.98	0.60	22
M04	r061099	OS-00	0	MT	100	0.91	0.779	23	15	91	23	9	0.91	0.61	23
M05	r061199	OS-00	0	DD	100	0.90	0.649	920	1101	19	920	81	0.19	0.91	20
M06	r062199	OS-00	0	MT	100	0.94	0.778	41	38	87	41	13	0.87	0.68	23
M07	r062399	OS-00	0	MT	100	0.92	0.749	155	165	43	155	57	0.43	0.63	22
M08	r062599	OS-00	0	DD	100	0.95	0.604	1215	1741	2	1215	98	0.02	0.92	9
M09	r062899	OS-00	0	MT	100	0.92	0.768	49	47	80	49	20	0.80	0.59	22
M10	r070199	OS-00	0	DD	100	0.93	0.675	928	1152	7	928	93	0.07	0.90	21
M11	r070299	OS-00	0	DD	100	0.92	0.665	900	1036	17	900	83	0.17	0.91	20
M12	r070799	OS-00	0	MT	100	0.92	0.722	452	509	19	452	81	0.19	0.82	21
M13	r070999	OS-00	0	DD	100	0.99	0.598	1188	1670	9	1188	91	0.09	0.92	7
M14	r071699	OS-00	0	DD	100	0.97	0.610	1397	1954	10	1397	90	0.10	0.94	7
M15	i073099	OS-00	0	DD	100	0.95	0.672	1345	1650	2	1345	98	0.02	0.93	20
M16	i080199	OS-00	0	MT	100	0.93	0.611	949	1096	0	949	100	0.00	0.89	15
M17	i080299	OS-00	0	MT	100	0.93	0.751	412	475	11	412	89	0.11	0.78	20
M18	i080399	OS-00	0	MT	100	0.94	0.730	146	171	30	146	70	0.30	0.52	19
M19	i080499	OS-00	0	MT	100	0.94	0.710	507	620	24	507	76	0.24	0.85	16
M20	i020701	OS-00	0	DD	100	0.97	0.646	1239	1954	1	1239	99	0.01	0.92	5
M21	i020901	OS-00	0	MT	100	0.96	0.721	696	826	12	696	88	0.12	0.87	19
M22	r072899	OS-07	7	MT	100	0.95	0.665	230	305	1	230	99	0.01	0.57	21
M23	r073199	OS-07	7	MT	100	0.93	0.596	521	632	1	521	99	0.01	0.81	20
M24	r080199	OS-07	7	MT	100	0.94	0.672	209	272	6	209	94	0.06	0.55	21
M25	r080299	OS-07	7	MT	100	0.95	0.723	14	7	89	14	11	0.89	0.21	21
M26	r080399	OS-07	7	MT	100	0.92	0.632	424	528	2	424	98	0.02	0.77	20
M27	r080499	OS-07	7	MT	100	0.93	0.735	5	0	98	5	2	0.98	0.60	20
M28	r081299	OS-07	7	MT	100	0.97	0.558	1218	1719	1	1218	99	0.01	0.92	19
M29	i110299	OS-07	7	DP	400	0.88	0.520	1320	1920	40	1320	360	0.10	0.73	6
M30	i110499	OS-07	7	MT	400	0.95	0.688	115	140	285	115	115	0.71	0.00	21
M31	r032999	OS-15	15	DD	100	0.966	0.580	123	142	49	123	51	0.49	0.59	17
M32	r040299	OS-15	15	DD	100	0.95	0.530	315	373	23	315	77	0.23	0.76	21
M33	r051999	OS-15	15	DD	100	0.92	0.610	92	100	29	92	71	0.29	0.23	22
M34	r053099	OS-15	15	DD	100	0.91	0.580	43	42	68	43	32	0.68	0.26	20
M35	r060199	OS-15	15	MT	100	0.94	0.619	1	0	99	1	1	0.99	0.10	18
M36	r071299	OS-15	15	MT	100	0.95	0.520	302	366	1	302	99	0.01	0.67	23
M37	r071999	OS-15	15	MT	100	0.98	0.423	1266	2601	1	1266	99	0.01	0.92	5
M38	r080599	OS-15	15	MT	100	0.92	0.595	17	15	92	17	8	0.92	0.53	22
M39	r081199	OS-15	15	MT	100	0.94	0.426	1267	2012	1	1267	99	0.01	0.92	5
M40	i111699	OS-15	15	MT	400	0.98	0.575	68	47	332	68	68	0.83	0.00	20
M41	i120199	OS-15	15	MT	400	0.97	0.601	60	40	340	60	60	0.85	0.00	19
M42	i011100	OS-15	15	MT	400	0.92	0.602	55	39	345	55	55	0.86	0.00	20

Table A.1 Summary of Monotonic Triaxial Compression Tests (Cont.)

Test No.	File Name	Soil Type	FC (%)	Prep. Mtd.	σ_c' (kPa)	B Value	e	P_f' (kPa)	q_f' (kPa)	U_{sh}' (kPa)	p_{ss}' (kPa)	p_{qss}' (kPa)	CP	RFD	max. ε_a (%)
M43	r033199	OS-25	25	DD	100	0.91	0.476	1	5	99	1	1	0.99	0.10	23
M44	r060399	OS-25	25	MT	100	0.94	0.460	11	4	91	11	9	0.91	0.18	20
M45	r060499	OS-25	25	MT	100	0.92	0.435	84	94	60	84	40	0.60	0.52	21
M46	r071599	OS-25	25	MT	100	0.93	0.423	67	75	55	67	45	0.55	0.33	21
M47	i101199	OS-25	25	DP	100	0.95	0.403	240	300	40	240	60	0.40	0.75	21
M48	i101399	OS-25	25	DP	100	0.93	0.360	690	915	12	690	88	0.12	0.87	19
M49	i100799	OS-25	25	DP	400	0.93	0.372	593	720	150	593	250	0.38	0.58	20
M50	i100899	OS-25	25	MT	400	0.93	0.439	110	50	290	110	110	0.73	0.00	17
M51	i102099	OS-25	25	MT	400	0.94	0.441	41	40	359	41	41	0.90	0.00	19
M52	i102599	OS-25	25	MT	400	0.99	0.458	40	40	360	40	40	0.90	0.00	19
M53	i102799	OS-25	25	MT	400	0.96	0.474	42	27	358	42	42	0.90	0.00	20
M54	i081699	OS-40	40	MT	100	0.99	0.408	7	0	94	7	6	0.94	0.08	11
M55	r092499	OS-40	40	MT	100	0.93	0.396	62	80	56	62	44	0.56	0.29	18
M56	r100499	OS-40	40	MT	100	0.93	0.413	4	0	96	4	4	0.96	0.00	19
M57	r102299	OS-40	40	MT	100	0.88	0.373	250	310	25	250	75	0.25	0.70	21
M58	g112399	OS-40	40	MT	100	0.9	0.398	13	13	87	13	13	0.87	0.00	18
M59	i011300	OS-40	40	MT	400	0.99	0.412	37	6	363	37	37	0.91	0.00	19
M60	i011800	OS-40	40	MT	400	1.04	0.394	74	10	326	74	74	0.82	0.00	19
M61	r081999	OS-60	60	MT	100	0.95	0.515	158	189	32	158	68	0.32	0.57	18
M62	r082099	OS-60	60	MT	100	0.96	0.517	137	172	38	137	62	0.38	0.55	20
M63	r082599	OS-60	60	MT	100	0.95	0.516	112	130	40	112	60	0.40	0.46	21
M64	r082699	OS-60	60	MT	100	0.90	0.498	176	216	42	176	58	0.42	0.67	21
M65	i081899	OS-60	60	MT	100	0.98	0.551	5	8	96	5	5	0.96	0.10	15
M66	i090399	OS-60	60	MT	100	0.99	0.531	5	9	95	5	5	0.95	0.08	20
M67	i091499	OS-60	60	MT	100	0.95	0.540	11	5	89	11	11	0.89	0.00	19
M68	i020100	OS-60	60	MT	400	0.99	0.610	51	22	349	51	51	0.87	0.00	18
M69	i020900	OS-60	60	MT	400	0.98	0.559	15	7	385	15	15	0.96	0.00	22
M70	i021600	OS-60	60	MT	400	0.98	0.549	33	15	367	33	33	0.92	0.00	22
M71	i021800	OS-60	60	MT	400	1.00	0.532	88	41	312	88	88	0.78	0.00	22
M72	i090999	OS-100	100	MT	100	0.99	0.879	10	8	90	10	10	0.90	0.00	19
M73	i091399	OS-100	100	MT	100	0.99	0.854	13	12	87	13	13	0.87	0.00	19
M74	i091999	OS-100	100	DP	100	0.98	0.770	303	417	17	303	83	0.17	0.73	21
M75	g092799	OS-100	100	DP	100	0.97	0.824	153	200	26	153	74	0.26	0.52	16
M76	i022300	OS-100	100	MT	400	1.00	0.879	31	10	369	31	31	0.92	0.00	22
M77	i031500	OS-100	100	MT	400	1.00	0.813	115	43	285	115	115	0.71	0.00	9

Table A.1 Summary of Monotonic Triaxial Compression Tests (Cont.)

Test No.	File Name	Soil Type	FC (%)	Prep. Mtd.	σ_c' (kPa)	B Value	e	P_f' (kPa)	q_f' (kPa)	U_{sh}' (kPa)	p_{ss}' (kPa)	p_{qss}' (kPa)	CP	RFD	max. ε_a (%)
M78	r100600	FJ-00	0	MT	100	0.97	0.785	839	964	11	839	89	0.11	0.89	23
M79	r101000	FJ-00	0	MT	100	0.97	0.868	114	129	53	114	47	0.53	0.59	22
M80	i031301	FJ-00	0	MT	100	0.96	0.699	1457	2000	16	1457	84	0.16	0.94	11
M81	i032101	FJ-00	0	MT	100	0.96	0.784	1360	1723	15	1360	85	0.15	0.94	20
M82	i032301	FJ-00	0	MT	100	0.97	0.800	1055	1269	35	1055	65	0.35	0.94	20
M83	i032601	FJ-00	0	MT	100	0.98	0.794	683	813	17	683	83	0.17	0.88	20
M84	i032801	FJ-00	0	MT	100	0.97	0.851	249	319	34	249	66	0.34	0.74	20
M85	i033001	FJ-00	0	MT	100	0.98	0.869	194	218	25	194	75	0.25	0.61	20
M86	i052401	FJ-00	0	MT	100	0.965	0.854	221	269	32	221	68	0.32	0.69	20
M87	i052501	FJ-00	0	MT	100	0.98	0.938	8	12	93	8	8	0.93	0.00	20
M88	i071901	FJ-00	0	MT	100	0.98	0.878	40	46	76	40	25	0.76	0.39	20
M89	i071900	FJ-25	25	MT	100	0.99	0.590	18	20	82	18	18	0.82	0.00	21
M90	i072400	FJ-25	25	MT	100	0.9	0.618	5	3	95	5	5	0.95	0.00	21
M91	i080100	FJ-25	25	MT	100	0.97	0.610	12	14	88	12	12	0.88	0.00	20
M92	i081100	FJ-25	25	MT	100	0.99	0.584	13	17	87	13	13	0.87	0.00	21
M93	i101100	FJ-25	25	MT	100	0.98	0.442	950	1246	15	950	85	0.15	0.91	21
M94	i101900	FJ-25	25	MT	100	0.97	0.587	30	41	78	30	22	0.78	0.27	21
M95	i122200	FJ-25	25	MT	100	0.96	0.548	67	92	75	67	25	0.75	0.63	20
M96	i122700	FJ-25	25	DP	100	0.97	0.459	496	644	25	496	75	0.25	0.85	20
M97	i010501	FJ-25	25	DP	100	0.95	0.522	152	208	52	152	48	0.52	0.68	21
M98	r101300	FJ-25	25	MT	100	0.98	0.554	23	29	84	23	16	0.84	0.28	23
M99	r122900	FJ-25	25	MT	100	0.99	0.532	223	285	12	223	88	0.12	0.60	23
M100	r011801	FJ-25	25	MT	100	0.99	0.548	65	80	66	65	34	0.66	0.48	22
M101	i072500	FJ-25	25	MT	400	0.97	0.576	75	50	325	75	75	0.81	0.00	18
M102	i081500	FJ-25	25	MT	400	0.98	0.551	73	77	327	73	73	0.82	0.00	20
M103	i100900	FJ-25	25	MT	400	0.98	0.559	102	114	298	102	102	0.75	0.00	20
M104	i102000	FJ-25	25	MT	400	0.97	0.491	1375	1910	212	1375	288	0.53	0.79	12
M105	i102700	FJ-25	25	MT	400	1	0.441	1381	1820	71	1381	329	0.18	0.76	20
M106	i010201	FJ-25	25	DP	400	0.95	0.500	623	735	55	623	345	0.14	0.45	19
M107	i011201	FJ-25	25	MT	400	0.95	0.562	165	130	263	165	137	0.66	0.17	19
M108	i011601	FJ-25	25	MT	400	0.97	0.613	90	70	321	90	79	0.80	0.13	20
M109	i011801	FJ-25	25	MT	400	0.96	0.550	159	162	275	159	125	0.69	0.21	18
M110	i013001	FJ-25	25	MT	400	0.98	0.576	132	106	310	132	90	0.78	0.32	22
M111	i020101	FJ-25	25	MT	400	0.97	0.548	143	154	303	143	97	0.76	0.32	19
M112	r102700	FJ-25	25	MT	400	0.97	0.537	85	102	315	85	85	0.79	0.00	20
M113	r110700	FJ-25	25	MT	400	0.98	0.546	126	158	298	126	102	0.75	0.19	24
M114	r111300	FJ-25	25	MT	400	0.97	0.569	67	79	343	67	57	0.86	0.15	24
M115	r111400	FJ-25	25	MT	400	0.98	0.616	74	87	343	74	58	0.86	0.23	24
M116	r011401	FJ-25	25	MT	400	1	0.564	109	132	332	109	68	0.83	0.37	22
M117	r011701	FJ-25	25	MT	400	0.99	0.553	111	131	331	111	69	0.83	0.37	22
M118	r012401	FJ-25	25	MT	400	1	0.569	33	38	378	33	22	0.95	0.34	21
M119	r012501	FJ-25	25	MT	400	1	0.554	81	97	331	81	69	0.83	0.14	22
M120	r012901	FJ-25	25	MT	400	1	0.557	82	100	343	82	57	0.86	0.31	21
M121	r013001	FJ-25	25	MT	400	1	0.568	86	104	343	86	57	0.86	0.34	22
M122	r020501	FJ-25	25	MT	400	1	0.546	112	136	327	112	73	0.82	0.35	22
M123	i072800	FJ-60	60	MT	100	0.98	0.640	12	3	88	12	12	0.88	0.00	19
M124	i051701	FJ-60	60	MT	100	0.98	0.641	2	3	100	2	0	1.00	1.00	22
M125	i051801	FJ-60	60	MT	100	0.98	0.623	9	10	92	9	8	0.92	0.11	22
M126	i052001	FJ-60	60	MT	100	0.98	0.615	21	7	82	21	18	0.82	0.14	22
M127	i052601	FJ-60	60	MT	100	0.97	0.613	3	10	97	3	3	0.97	0.00	22
M128	i100400	FJ-60	60	MT	400	1	0.616	64	10	336	64	64	0.84	0.00	20

Table A.1 Summary of Monotonic Triaxial Compression Tests (Cont.)

Test No.	File Name	Soil Type	FC (%)	Prep. Mtd.	σ_c' (kPa)	B Value	e	P_f' (kPa)	q_f' (kPa)	U_{sh}' (kPa)	p_{ss}' (kPa)	p_{qss}' (kPa)	CP	RFD	max. ε_a (%)
M129	i061401	WG-00	0	MT	100	0.97	0.586	24	31	92	24	8	0.92	0.66	22
M130	i061501	WG-00	0	MT	100	0.98	0.633	6	6	98	6	2	0.98	0.63	18
M131	i061601	WG-00	0	MT	100	0.975	0.569	105	136	20	105	80	0.20	0.24	17
M132	i061701	WG-00	0	MT	100	0.955	0.556	271	328	3	271	97	0.03	0.64	22
M133	i061801	WG-00	0	MT	100	0.96	0.646	11	6	91	11	9	0.91	0.11	22
M134	i062701	WG-00	0	MT	100	0.97	0.644	11	10	90	11	10	0.90	0.06	21
M135	i062701-2	WG-00	0	MT	100	0.965	0.604	27	44	91	27	10	0.91	0.65	21
M136	i062801	WG-00	0	MT	100	0.98	0.501	1350	1685	1	1350	99	0.01	0.93	21
M137	i070101	WG-00	0	MT	100	0.96	0.481	1578	1951	100	1578	0	1.00	1.00	22
M138	i070201	WG-00	0	MT	100	0.985	0.642	4	5	99	4	1	0.99	0.77	21
M139	i070501	WG-00	0	MT	100	0.98	0.631	8	9	93	8	7	0.93	0.10	22
M140	i070501-2	WG-00	0	MT	100	0.975	0.629	18	23	83	18	17	0.83	0.08	22
M141	i070601	WG-25	25	MT	100	0.98	0.427	25	31	87	25	13	0.87	0.48	22
M142	i071001	WG-25	25	MT	100	0.98	0.423	27	12	74	27	26	0.74	0.06	22
M143	i071101	WG-25	25	MT	100	0.98	0.440	16	12	92	16	8	0.92	0.47	22
M144	i071201	WG-25	25	MT	100	0.98	0.415	11	12	91	11	9	0.91	0.19	22
M145	i071601	WG-25	25	MT	100	0.99	0.441	14	13	87	14	13	0.87	0.04	18
M146	i071701	WG-25	25	MT	100	0.98	0.426	22	14	79	22	21	0.79	0.05	22
M147	i072001	WG-25	25	MT	100	0.98	0.448	1	8	100	1	0	1.00	1.00	22
M148	i072301	WG-25	25	MT	100	0.965	0.415	31	18	70	31	31	0.70	0.00	22
M149	i072501	WG-25	25	MT	100	0.97	0.442	7	10	96	7	4	0.96	0.51	22
M150	i072601	WG-25	25	MT	100	0.96	0.364	615	911	98	615	3	0.98	1.00	6

Notes: * = sedimentation by layers

- Preparation Method: DD = dry deposition; DP = dry pluviation; MT = moisture tamping
- σ_c' = initial effective confining pressure; p_f' = final mean effective conf. pressure; q_f' = final deviatoric stress; U_{sh}' = max. positive shear induced pressure; p_{ss}' = mean eff. Conf. pressure at steady state; p_{qss}' = mean eff. Conf. pressure at quasi steady state
- CP = collapse potential (=U_{sh}'/ σ_c'); RFD = resistance to further deformation (= 1- p_{qss}'/ p_{ss}')

Test Information Summary Table

Test Date: 3/12/99

Test Mode:	Geocomp		
File Name:	r031299	Fine Content (%):	0
Soil Type:	OSF55-40	Preparation Method:	DD
Dry Soil Weight (g):	1023.1	Initial Water in Sample (g) (preparation):	264.2
Sample Height (cm):	155	Final Water in Sample (g) (shear phase):	264.1
Final B Value:	0.96	Void Ratio:	0.684
Intergranular Void Ratio:	0.684	Interfine Void Ratio:	
Final Consolidation Confining Stress (kPa):	100	Final Strain (%):	7
Final Cell Pressure (kPa):	590	Calculated Friction Angle:	32
Final Back Pressure (kPa):	-17	Young's Modulus E (0.05%) (kPa):	68065
Final Shear Induced Pore Pressure (kPa):	-507	Shear Modulus G (0.05%) (kPa):	22688
Final Effective Mean Stress p' (kPa):	1074	Final Effective Sigma1 (kPa):	2005
Final Effective Deviatoric Stress q' (kPa):	1398	Final Effective Sigma3 (kPa):	608

sig3' vs strain

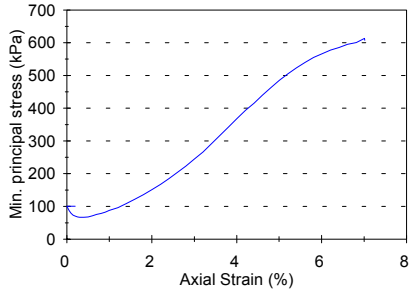

dev stress vs strain (overall)

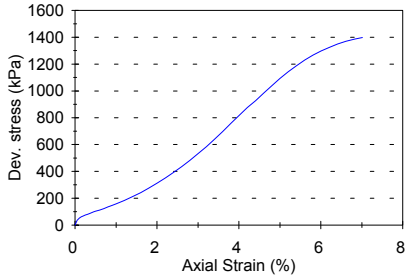

p(3)-q

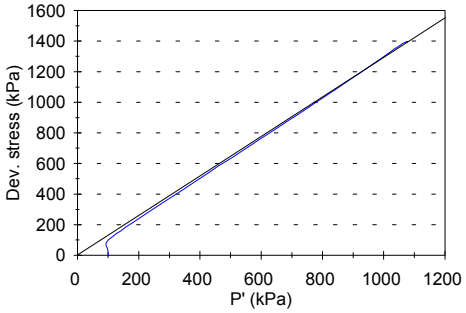

dev stress vs strain (2%)

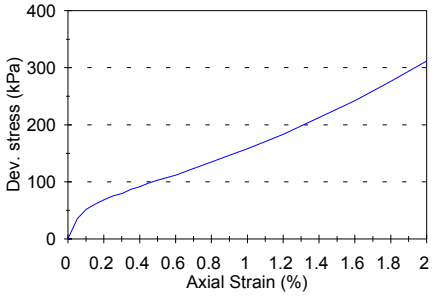

U (sh)

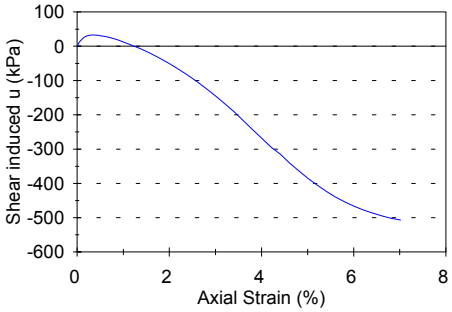

Test Information Summary Table

Test Date: 6/07/99

Test Mode:	Geocomp		
File Name:	r060799	Fine Content (%):	0.001
Soil Type:	OSF55-40	Preparation Method:	MT
Dry Soil Weight (g):	941.5	Initial Water in Sample (g) (preparation):	291.4
Sample Height (cm):	15.2	Final Water in Sample (g) (shear phase):	284.4
Final B Value:	0.92	Void Ratio:	0.800
Intergranular Void Ratio:	0.800	Interfine Void Ratio:	**********
Final Consolidation Confining Stress (kPa):	100	Final Strain (%):	23
Final Cell Pressure (kPa):	650	Calculated Friction Angle:	
Final Back Pressure (kPa):	641	Young's Modulus E (0.05%) (kPa):	40033
Final Shear Induced Pore Pressure (kPa):	91	Shear Modulus G (0.05%) (kPa):	13344
Final Effective Mean Stress p' (kPa):	10	Final Effective Sigma1 (kPa):	13
Final Effective Deviatoric Stress q' (kPa):	4	Final Effective Sigma3 (kPa):	9

sig3' vs strain

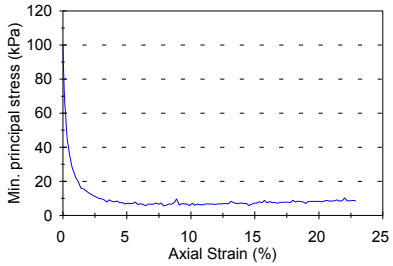

dev stress vs strain (overall)

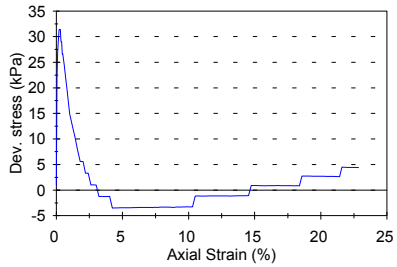

p(3)-q

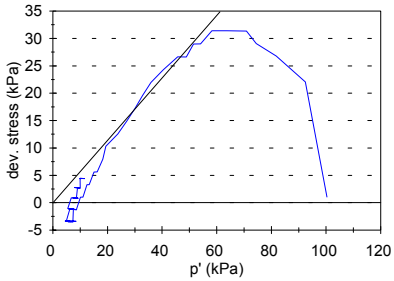

dev stress vs strain (2%)

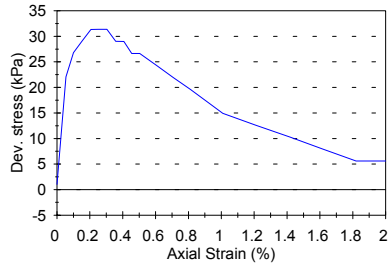

U (sh)

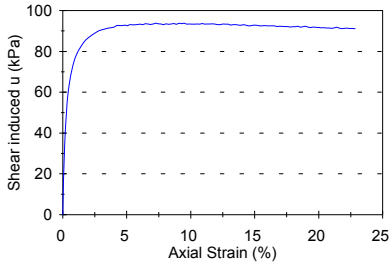

Test Information Summary Table

Test Date: 6/09/99

Test Mode:	Geocomp		
File Name:	r060999	Fine Content (%):	0.001
Soil Type:	OSF55-40	Preparation Method:	MT
Dry Soil Weight (g):	953.3	Initial Water in Sample (g) (preparation):	297.8
Sample Height (cm):	15.5	Final Water in Sample (g) (shear phase):	289.3
Final B Value:	0.91	Void Ratio:	0.804
Intergranular Void Ratio:	0.804	Interfine Void Ratio:	**********
Final Consolidation Confining Stress (kPa):	100	Final Strain (%):	22
Final Cell Pressure (kPa):	625	Calculated Friction Angle:	14
Final Back Pressure (kPa):	620	Young's Modulus E (0.05%) (kPa):	35994
Final Shear Induced Pore Pressure (kPa):	95	Shear Modulus G (0.05%) (kPa):	11998
Final Effective Mean Stress p' (kPa):	5	Final Effective Sigma1 (kPa):	5
Final Effective Deviatoric Stress q' (kPa):	0	Final Effective Sigma3 (kPa):	5

sig3' vs strain

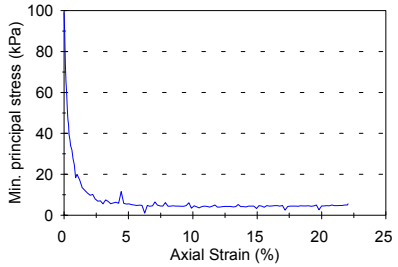

dev stress vs strain (overall)

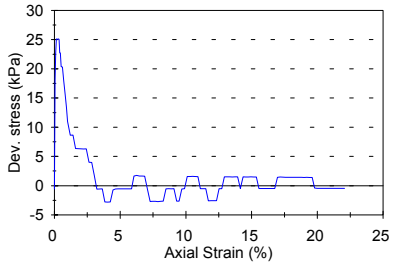

p(3)-q

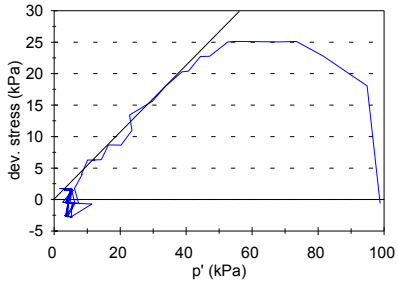

dev stress vs strain (2%)

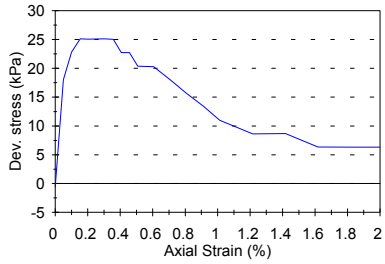

U (sh)

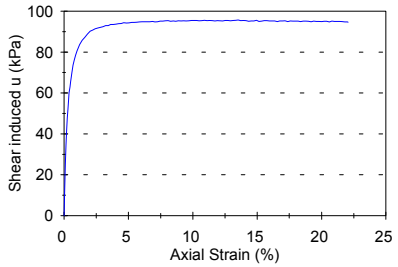

Test Information Summary Table

Test Date: 6/10/99

Test Mode:	Geocomp		
File Name:	r061099	Fine Content (%):	0.001
Soil Type:	OSF55-40	Preparation Method:	MT
Dry Soil Weight (g):	960	Initial Water in Sample (g) (preparation):	290.0
Sample Height (cm):	15.1	Final Water in Sample (g) (shear phase):	282.3
Final B Value:	0.91	Void Ratio:	0.779
Intergranular Void Ratio:	0.779	Interfine Void Ratio:	**********
Final Consolidation Confining Stress (kPa):	100	Final Strain (%):	23
Final Cell Pressure (kPa):	605	Calculated Friction Angle:	15
Final Back Pressure (kPa):	587	Young's Modulus E (0.05%) (kPa):	39295
Final Shear Induced Pore Pressure (kPa):	82	Shear Modulus G (0.05%) (kPa):	13098
Final Effective Mean Stress p' (kPa):	23	Final Effective Sigma1 (kPa):	33
Final Effective Deviatoric Stress q' (kPa):	15	Final Effective Sigma3 (kPa):	18

sig3' vs strain

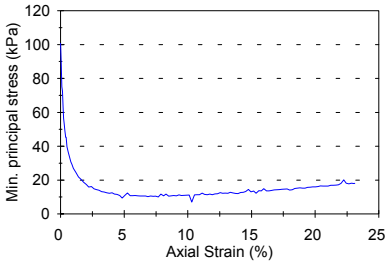

dev stress vs strain (overall)

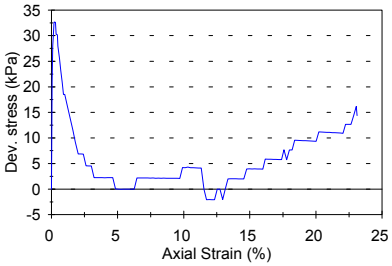

p(3)-q

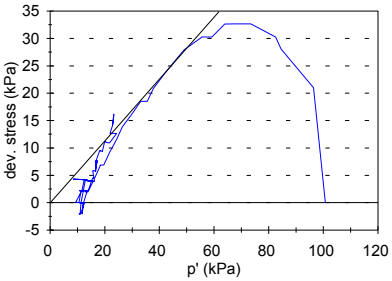

dev stress vs strain (2%)

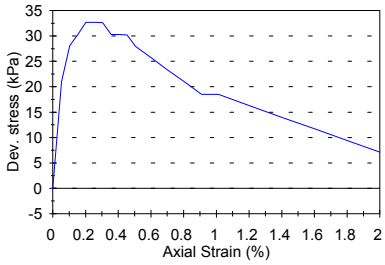

U (sh)

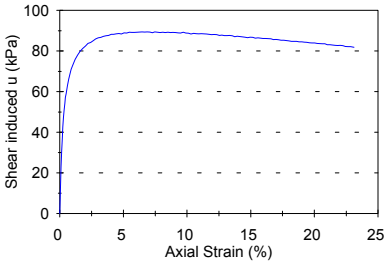

Test Information Summary Table

Test Date: 6/11/99

Test Mode:	Geocomp		
File Name:	r061199	Fine Content (%):	0.001
Soil Type:	OSF55-40	Preparation Method:	DD
Dry Soil Weight (g):	1048	Initial Water in Sample (g) (preparation):	260.4
Sample Height (cm):	15.2	Final Water in Sample (g) (shear phase):	256.6
Final B Value:	0.90	Void Ratio:	0.649
Intergranular Void Ratio:	0.649	Interfine Void Ratio:	**********
Final Consolidation Confining Stress (kPa):	100	Final Strain (%):	20
Final Cell Pressure (kPa):	605	Calculated Friction Angle:	33
Final Back Pressure (kPa):	53	Young's Modulus E (0.05%) (kPa):	61665
Final Shear Induced Pore Pressure (kPa):	-452	Shear Modulus G (0.05%) (kPa):	20555
Final Effective Mean Stress p' (kPa):	920	Final Effective Sigma1 (kPa):	1654
Final Effective Deviatoric Stress q' (kPa):	1101	Final Effective Sigma3 (kPa):	553

sig3' vs strain

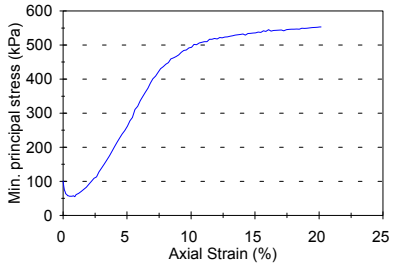

dev stress vs strain (overall)

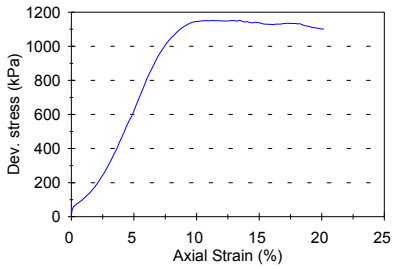

p(3)-q

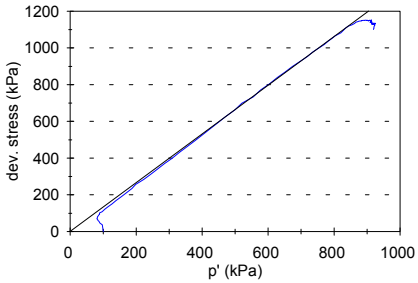

dev stress vs strain (2%)

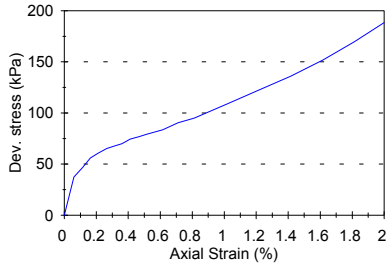

U (sh)

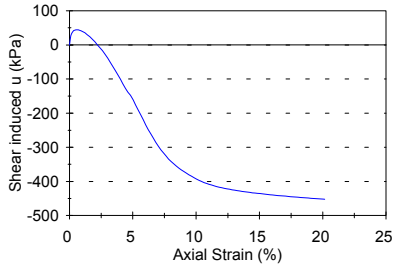

Test Information Summary Table

Test Date: 6/21/99

Test Mode:	Geocomp		
File Name:	r062199	Fine Content (%):	0.001
Soil Type:	OSF55-40	Preparation Method:	MT
Dry Soil Weight (g):	966	Initial Water in Sample (g) (preparation):	289.7
Sample Height (cm):	15.2	Final Water in Sample (g) (shear phase):	283.7
Final B Value:	0.94	Void Ratio:	0.778
Intergranular Void Ratio:	0.778	Interfine Void Ratio:	**********
Final Consolidation Confining Stress (kPa):	100	Final Strain (%):	23
Final Cell Pressure (kPa):	605	Calculated Friction Angle:	24
Final Back Pressure (kPa):	576	Young's Modulus E (0.05%) (kPa):	41269
Final Shear Induced Pore Pressure (kPa):	71	Shear Modulus G (0.05%) (kPa):	13756
Final Effective Mean Stress p' (kPa):	41	Final Effective Sigma1 (kPa):	68
Final Effective Deviatoric Stress q' (kPa):	39	Final Effective Sigma3 (kPa):	29

sig3' vs strain

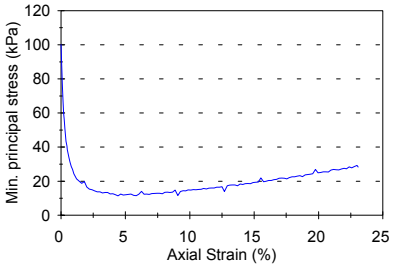

dev stress vs strain (overall)

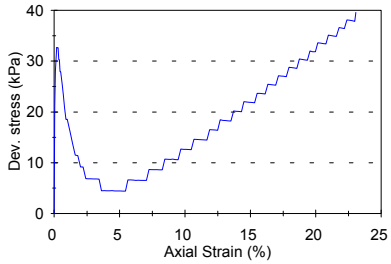

p(3)-q

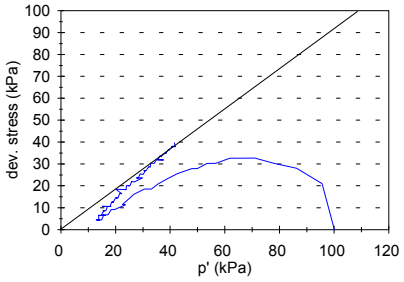

dev stress vs strain (2%)

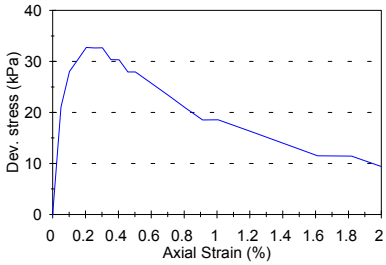

U (sh)

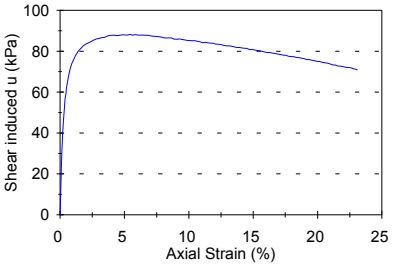

Test Information Summary Table

Test Date: 6/23/99

Test Mode:	Geocomp		
File Name:	r062399	Fine Content (%):	0.001
Soil Type:	OSF55-40	Preparation Method:	MT
Dry Soil Weight (g):	1021	Initial Water in Sample (g) (preparation):	292.4
Sample Height (cm):	15.6	Final Water in Sample (g) (shear phase):	288.8
Final B Value:	0.92	Void Ratio:	0.749
Intergranular Void Ratio:	0.749	Interfine Void Ratio:	**********
Final Consolidation Confining Stress (kPa):	100	Final Strain (%):	22
Final Cell Pressure (kPa):	650	Calculated Friction Angle:	27
Final Back Pressure (kPa):	550	Young's Modulus E (0.05%) (kPa):	64715
Final Shear Induced Pore Pressure (kPa):	0	Shear Modulus G (0.05%) (kPa):	21572
Final Effective Mean Stress p' (kPa):	155	Final Effective Sigma1 (kPa):	266
Final Effective Deviatoric Stress q' (kPa):	165	Final Effective Sigma3 (kPa):	101

sig3' vs strain

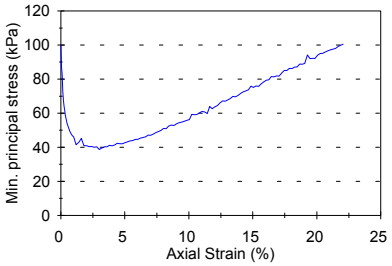

dev stress vs strain (overall)

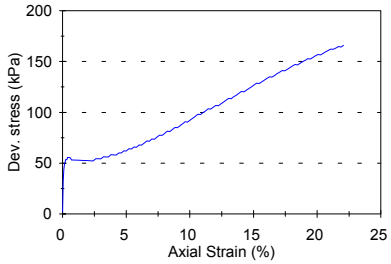

p(3)-q

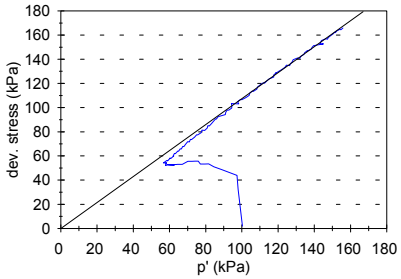

dev stress vs strain (2%)

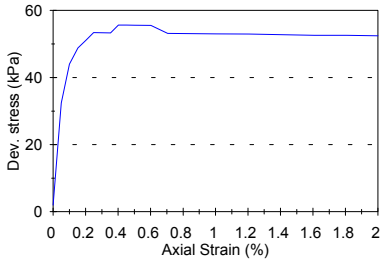

U (sh)

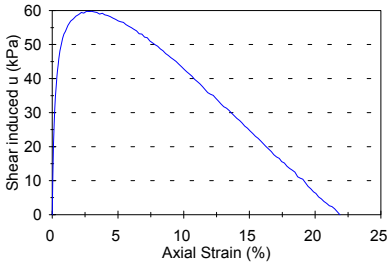

Test Information Summary Table

Test Date: 6/25/99

Test Mode:	Geocomp		
File Name:	r062599	Fine Content (%):	0.001
Soil Type:	OSF55-40	Preparation Method:	DD
Dry Soil Weight (g):	1108	Initial Water in Sample (g) (preparation):	255.3
Sample Height (cm):	15.5	Final Water in Sample (g) (shear phase):	252.6
Final B Value:	0.95	Void Ratio:	0.604
Intergranular Void Ratio:	0.604	Interfine Void Ratio:	**********
Final Consolidation Confining Stress (kPa):	100	Final Strain (%):	9
Final Cell Pressure (kPa):	621	Calculated Friction Angle:	36
Final Back Pressure (kPa):	-14	Young's Modulus E (0.05%) (kPa):	93782
Final Shear Induced Pore Pressure (kPa):	-534	Shear Modulus G (0.05%) (kPa):	31261
Final Effective Mean Stress p' (kPa):	1215	Final Effective Sigma1 (kPa):	2375
Final Effective Deviatoric Stress q' (kPa):	1741	Final Effective Sigma3 (kPa):	635

sig3' vs strain

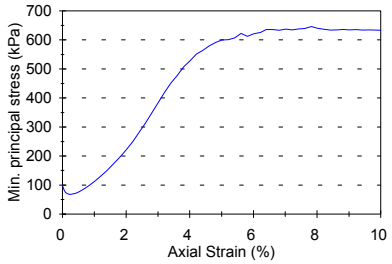

dev stress vs strain (overall)

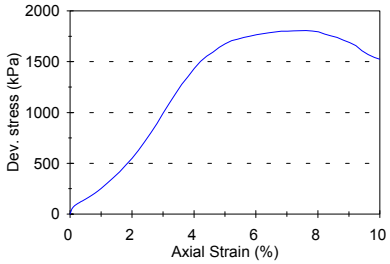

p(3)-q

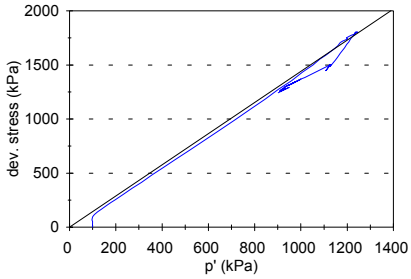

dev stress vs strain (2%)

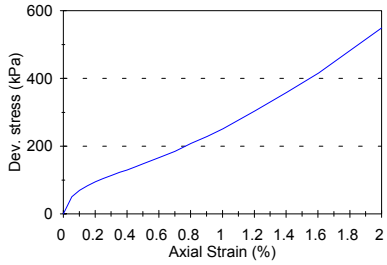

U (sh)

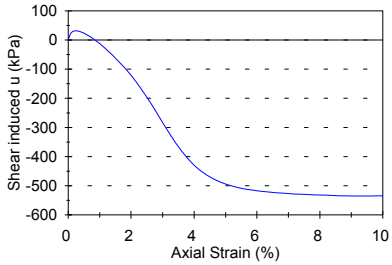

Test Information Summary Table

Test Date: 6/28/99

Test Mode:	Geocomp		
File Name:	r062899	Fine Content (%):	0.001
Soil Type:	OSF55-40	Preparation Method:	MT
Dry Soil Weight (g):	982.4	Initial Water in Sample (g) (preparation):	289.4
Sample Height (cm):	15.2	Final Water in Sample (g) (shear phase):	284.6
Final B Value:	0.92	Void Ratio:	0.768
Intergranular Void Ratio:	0.768	Interfine Void Ratio:	**********
Final Consolidation Confining Stress (kPa):	100	Final Strain (%):	22
Final Cell Pressure (kPa):	635	Calculated Friction Angle:	25
Final Back Pressure (kPa):	601	Young's Modulus E (0.05%) (kPa):	44271
Final Shear Induced Pore Pressure (kPa):	66	Shear Modulus G (0.05%) (kPa):	14757
Final Effective Mean Stress p' (kPa):	49	Final Effective Sigma1 (kPa):	80
Final Effective Deviatoric Stress q' (kPa):	47	Final Effective Sigma3 (kPa):	33

sig3' vs strain

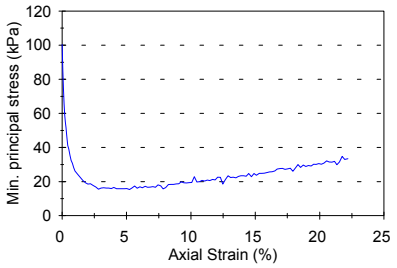

dev stress vs strain (overall)

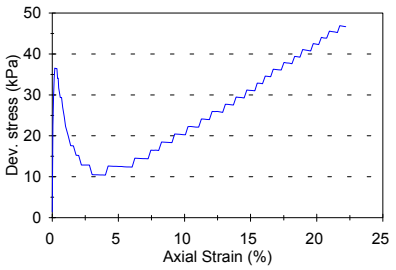

p(3)-q

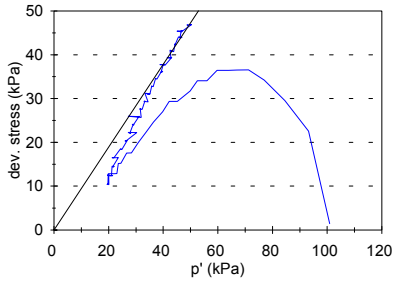

dev stress vs strain (2%)

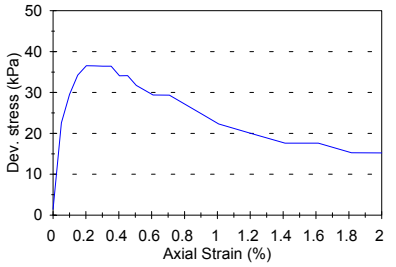

U (sh)

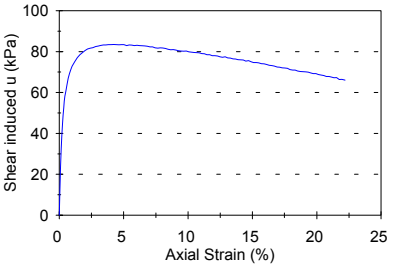

Test Information Summary Table

Test Date: 7/01/99

Test Mode:	Geocomp		
File Name:	r070199	Fine Content (%):	0.001
Soil Type:	OSF55-40	Preparation Method:	DD
Dry Soil Weight (g):	1028	Initial Water in Sample (g) (preparation):	263.7
Sample Height (cm):	15.5	Final Water in Sample (g) (shear phase):	261.8
Final B Value:	0.93	Void Ratio:	0.675
Intergranular Void Ratio:	0.675	Interfine Void Ratio:	**********
Final Consolidation Confining Stress (kPa):	100	Final Strain (%):	21
Final Cell Pressure (kPa):	590	Calculated Friction Angle:	32
Final Back Pressure (kPa):	46	Young's Modulus E (0.05%) (kPa):	75629
Final Shear Induced Pore Pressure (kPa):	-444	Shear Modulus G (0.05%) (kPa):	25210
Final Effective Mean Stress p' (kPa):	928	Final Effective Sigma1 (kPa):	1696
Final Effective Deviatoric Stress q' (kPa):	1152	Final Effective Sigma3 (kPa):	544

sig3' vs strain

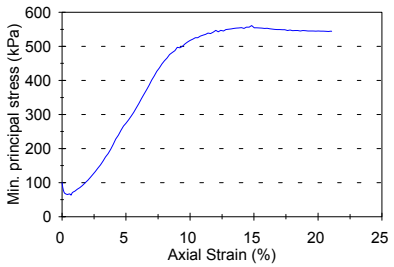

dev stress vs strain (overall)

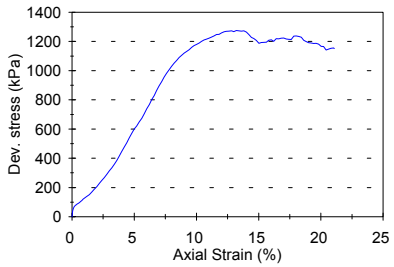

p(3)-q

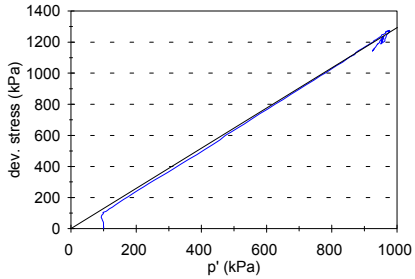

dev stress vs strain (2%)

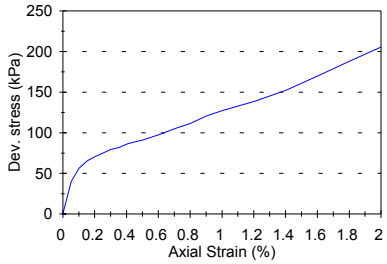

U (sh)

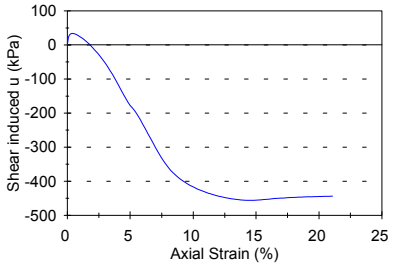

Test Information Summary Table

Test Date: 7/02/99

Test Mode:	Geocomp		
File Name:	r070299	Fine Content (%):	0.001
Soil Type:	OSF55-40	Preparation Method:	DD
Dry Soil Weight (g):	1020	Initial Water in Sample (g) (preparation):	257.8
Sample Height (cm):	15.0	Final Water in Sample (g) (shear phase):	256.1
Final B Value:	0.92	Void Ratio:	0.665
Intergranular Void Ratio	0.665	Interfine Void Ratio:	**********
Final Consolidation Confining Stress (kPa):	100	Final Strain (%):	20
Final Cell Pressure (kPa):	650	Calculated Friction Angle:	32
Final Back Pressure (kPa):	95	Young's Modulus E (0.05%) (kPa):	70110
Final Shear Induced Pore Pressure (kPa):	-455	Shear Modulus G (0.05%) (kPa):	23370
Final Effective Mean Stress p' (kPa):	900	Final Effective Sigma1 (kPa):	1591
Final Effective Deviatoric Stress q' (kPa):	1036	Final Effective Sigma3 (kPa):	555

sig3' vs strain

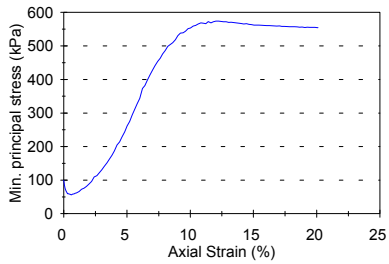

dev stress vs strain (overall)

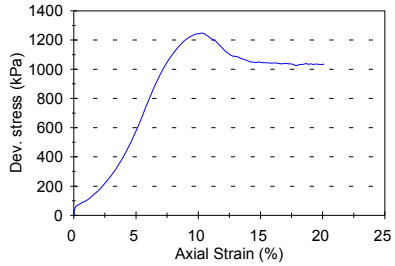

p(3)-q

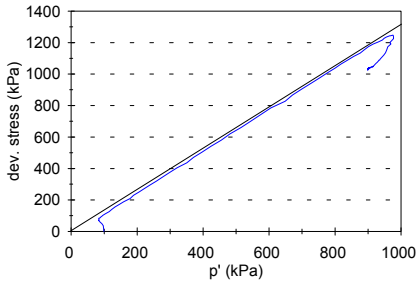

dev stress vs strain (2%)

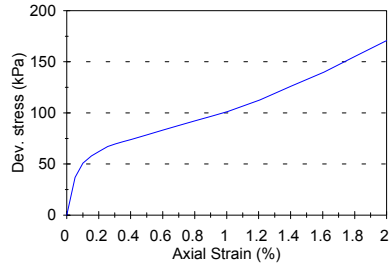

U (sh)

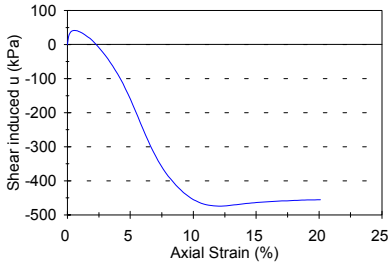

Test Information Summary Table

Test Date: 7/07/99

Test Mode:	Geocomp		
File Name:	r070799	Fine Content (%):	0.001
Soil Type:	OSF55-40	Preparation Method:	MT
Dry Soil Weight (g):	1004.9	Initial Water in Sample (g) (preparation):	276.5
Sample Height (cm):	15.1	Final Water in Sample (g) (shear phase):	273.9
Final B Value:	0.92	Void Ratio:	0.722
Intergranular Void Ratio:	0.722	Interfine Void Ratio:	**********
Final Consolidation Confining Stress (kPa):	100	Final Strain (%):	21
Final Cell Pressure (kPa):	630	Calculated Friction Angle:	29
Final Back Pressure (kPa):	348	Young's Modulus E (0.05%) (kPa):	66273
Final Shear Induced Pore Pressure (kPa):	-182	Shear Modulus G (0.05%) (kPa):	22091
Final Effective Mean Stress p' (kPa):	452	Final Effective Sigma1 (kPa):	791
Final Effective Deviatoric Stress q' (kPa):	509	Final Effective Sigma3 (kPa):	282

sig3' vs strain

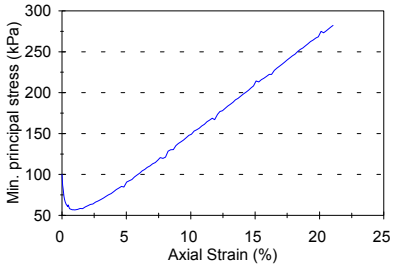

dev stress vs strain (overall)

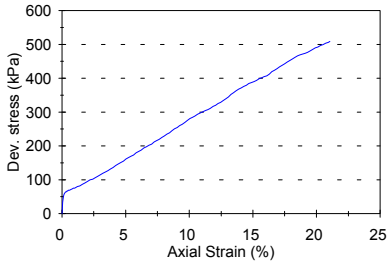

p(3)-q

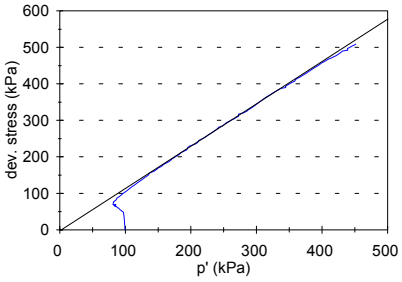

dev stress vs strain (2%)

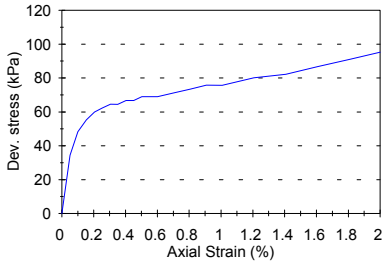

U (sh)

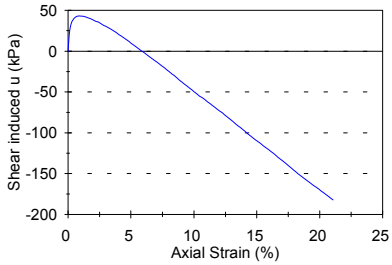

Test Information Summary Table

Test Date: 7/09/99

Test Mode:	Geocomp		
File Name:	r070999	Fine Content (%):	0.001
Soil Type:	OSF55-40	Preparation Method:	DD
Dry Soil Weight (g):	1120	Initial Water in Sample (g) (preparation):	255.8
Sample Height (cm):	15.6	Final Water in Sample (g) (shear phase):	252.7
Final B Value:	0.99	Void Ratio:	0.598
Intergranular Void Ratio:	0.598	Interfine Void Ratio:	**********
Final Consolidation Confining Stress (kPa):	100	Final Strain (%):	7
Final Cell Pressure (kPa):	614	Calculated Friction Angle:	35
Final Back Pressure (kPa):	-17	Young's Modulus E (0.05%) (kPa):	42076
Final Shear Induced Pore Pressure (kPa):	-527	Shear Modulus G (0.05%) (kPa):	14025
Final Effective Mean Stress p' (kPa):	1188	Final Effective Sigma1 (kPa):	2301
Final Effective Deviatoric Stress q' (kPa):	1670	Final Effective Sigma3 (kPa):	631

sig3' vs strain

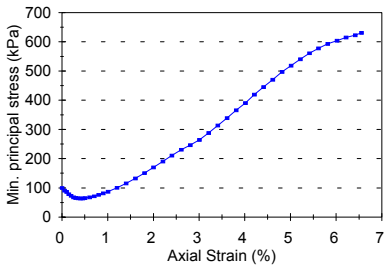

dev stress vs strain (overall)

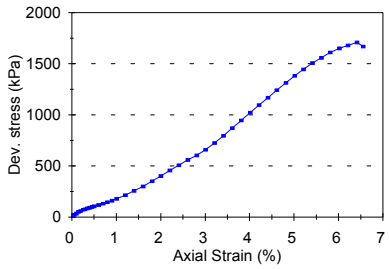

p(3)-q

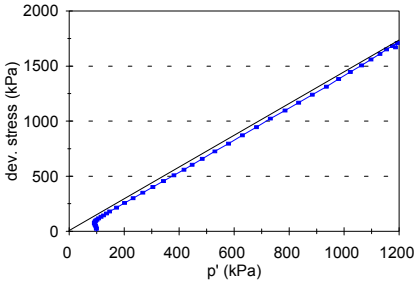

dev stress vs strain (2%)

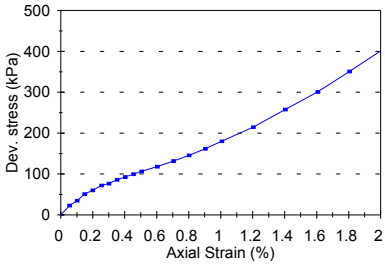

U (sh)

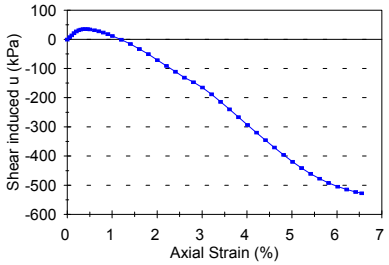

Test Information Summary Table

Test Date: 7/16/99

Test Mode:	Geocomp		
File Name:	r071699	Fine Content (%):	0.001
Soil Type:	OSF55-40	Preparation Method:	DD
Dry Soil Weight (g):	1108	Initial Water in Sample (g) (preparation):	258.6
Sample Height (cm):	15.6	Final Water in Sample (g) (shear phase):	255.1
Final B Value:	0.97	Void Ratio:	0.610
Intergranular Void Ratio:	0.610	Interfine Void Ratio:	**********
Final Consolidation Confining Stress (kPa):	100	Final Strain (%):	7
Final Cell Pressure (kPa):	730	Calculated Friction Angle:	35
Final Back Pressure (kPa):	-11	Young's Modulus E (0.05%) (kPa):	77447
Final Shear Induced Pore Pressure (kPa):	-641	Shear Modulus G (0.05%) (kPa):	25816
Final Effective Mean Stress p' (kPa):	1397	Final Effective Sigma1 (kPa):	2699
Final Effective Deviatoric Stress q' (kPa):	1954	Final Effective Sigma3 (kPa):	745

sig3' vs strain

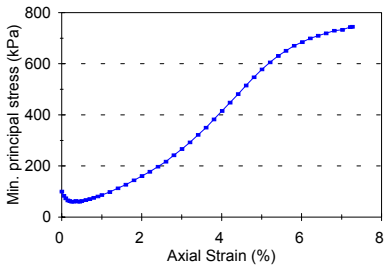

dev stress vs strain (overall)

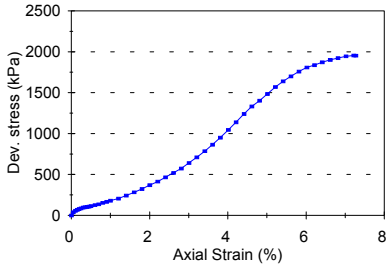

p(3)-q

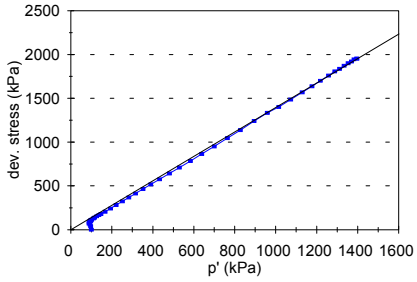

dev stress vs strain (2%)

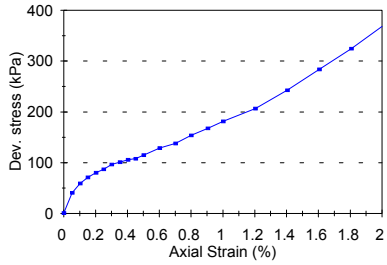

U (sh)

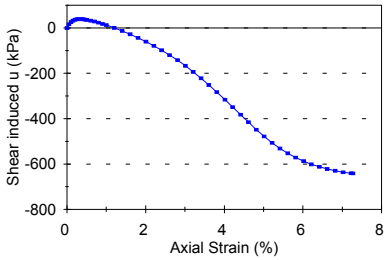

GDS OS#55

Date: 7/30/99 Fines= 0 e= 0.672 ec= 0.672 ef= n.a.

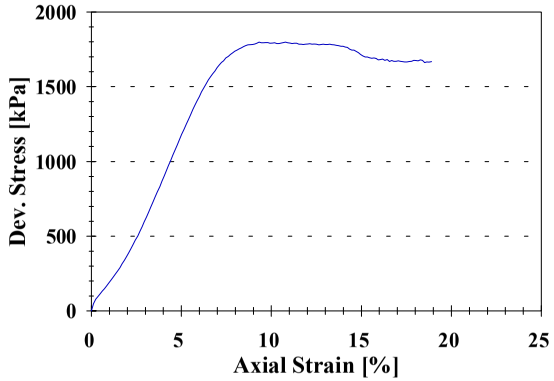

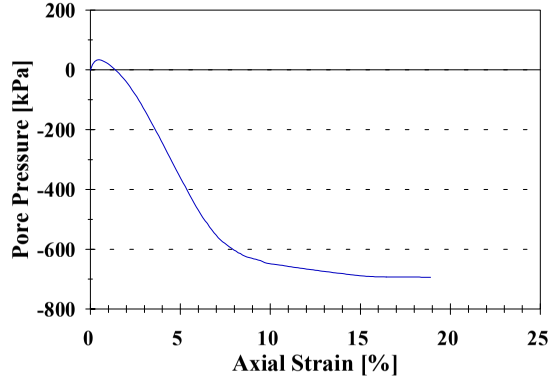

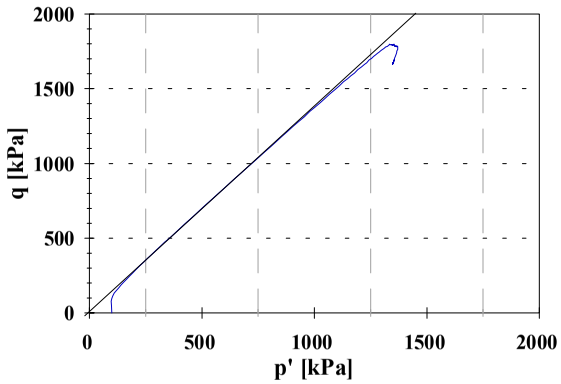

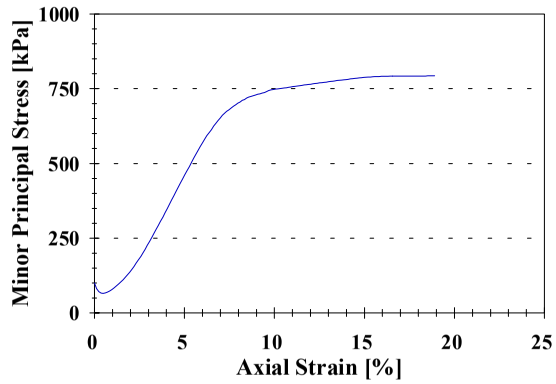

ϕ= 34.0 Confining stress = 100 kPa

GDS OS#55

Date: 08/01/99 Fines= 0 e= 0.611 ec= 0.611 ef= n.a.

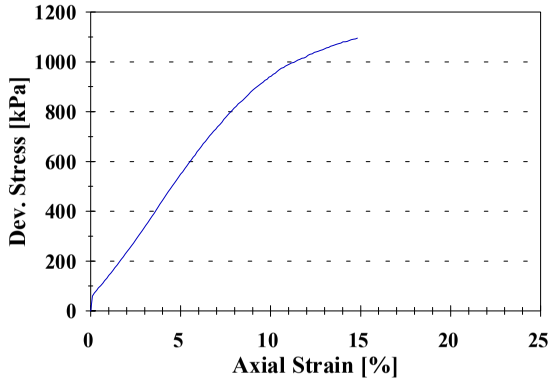

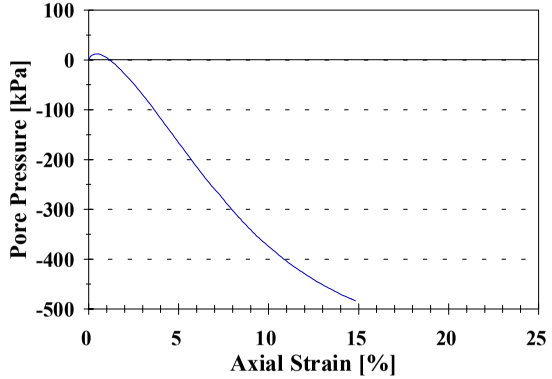

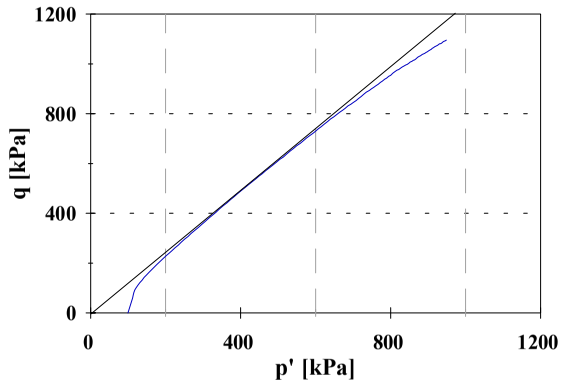

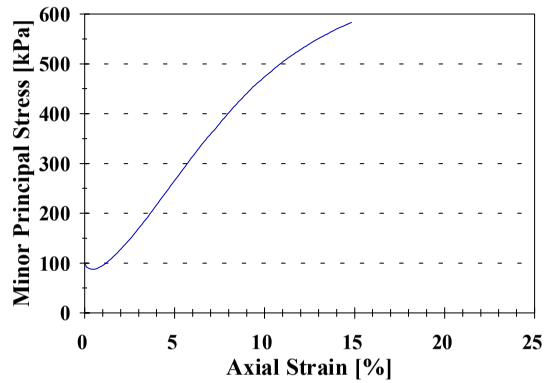

ϕ= 30.0 Confining stress = 100 kPa

GDS OS#55

Date: 08/02/99 Fines= 0 e= 0.751 ec= 0.751 ef= n.a.

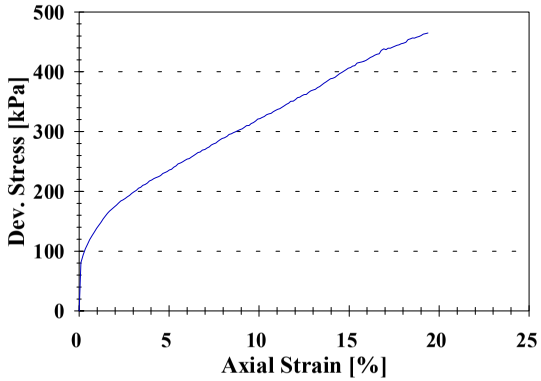

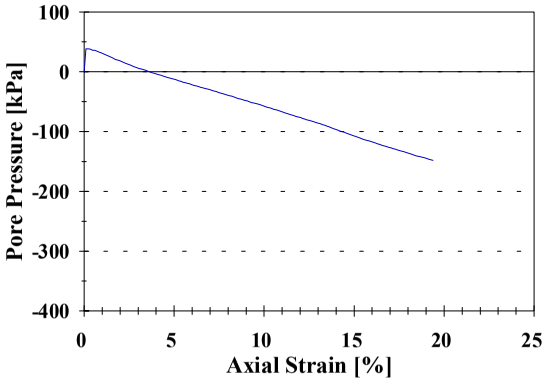

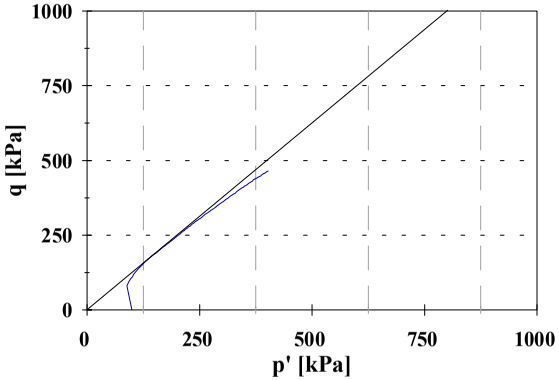

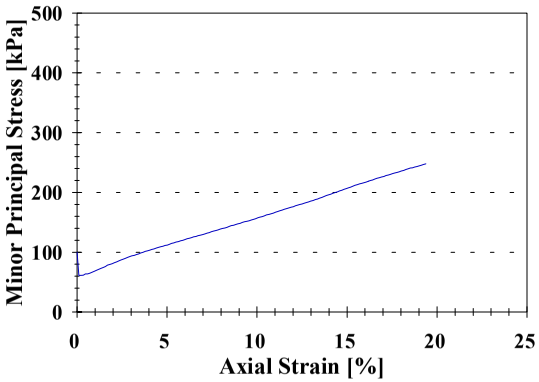

ϕ= 31.1 Confining stress = 100 kPa

GDS OS#55 GS#40

Date: 08/03/99 Fines= 0 e= 0.730 ec= 0.730 ef= n.a.

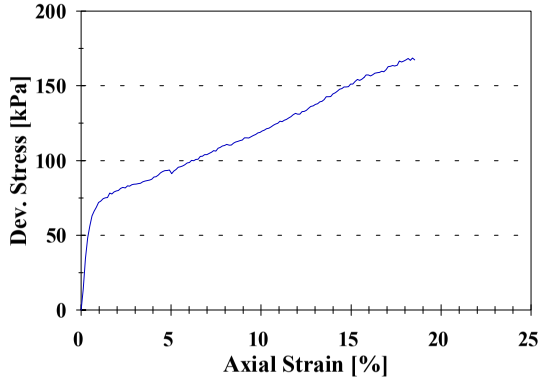

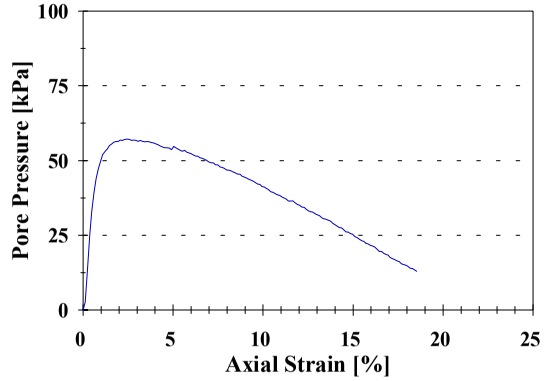

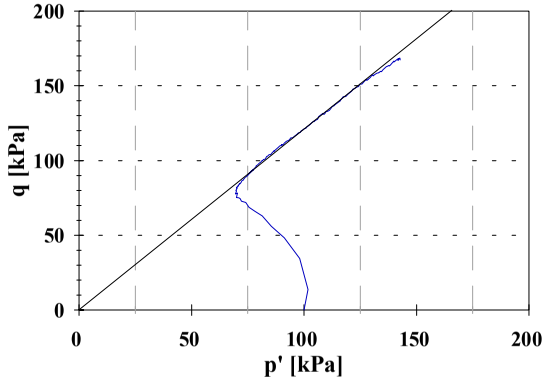

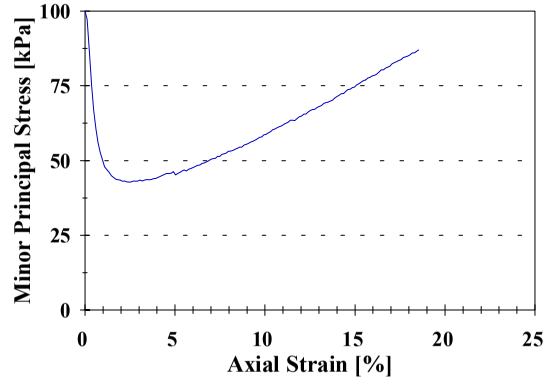

ϕ = 30.3 Confining stress = 100 kPa

GDS OS#55

Date: 08/04/99 Fines= 0 e= 0.710 ec= 0.710 ef= n.a.

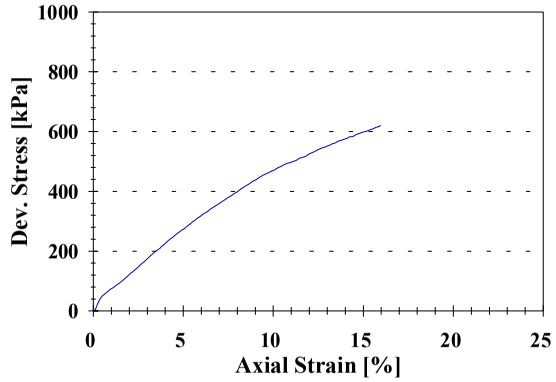

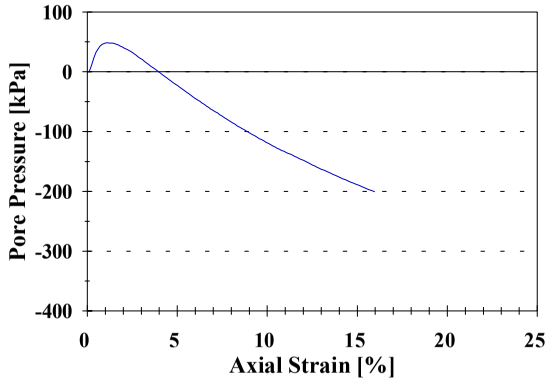

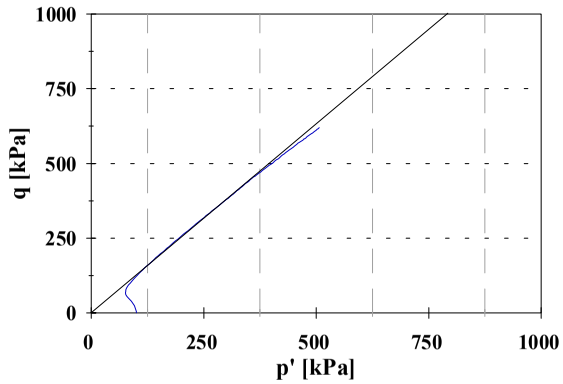

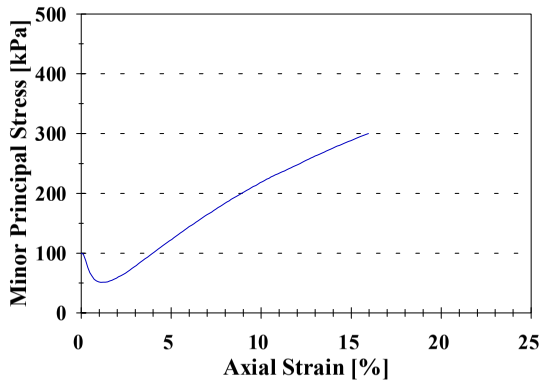

ϕ= 31.1 Confining stress = 100 kPa

GDS OS#55

Date: 36929	Fines= 0	e= 0.646	ec= 0.646	ef= n.a.	(ef)eq= n.a.	(ec)eq= 0.646

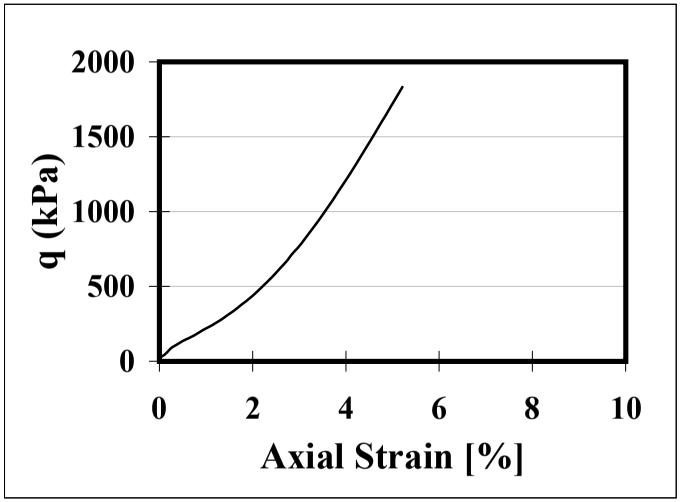

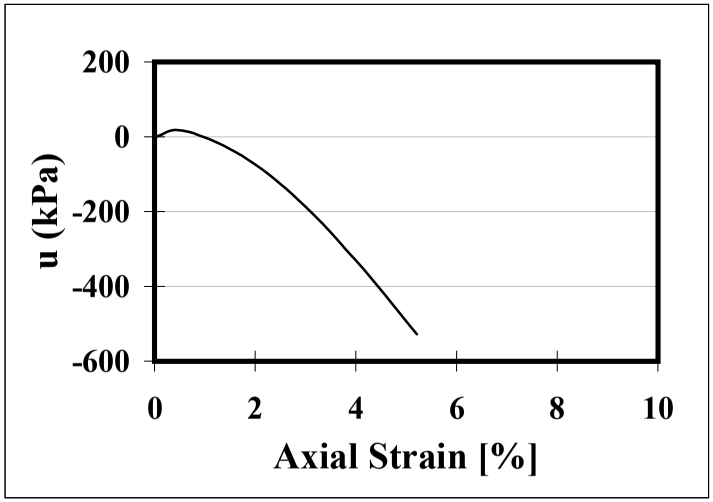

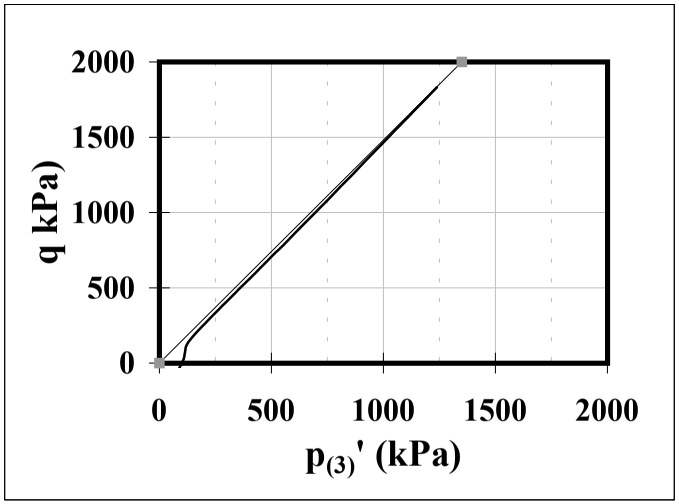

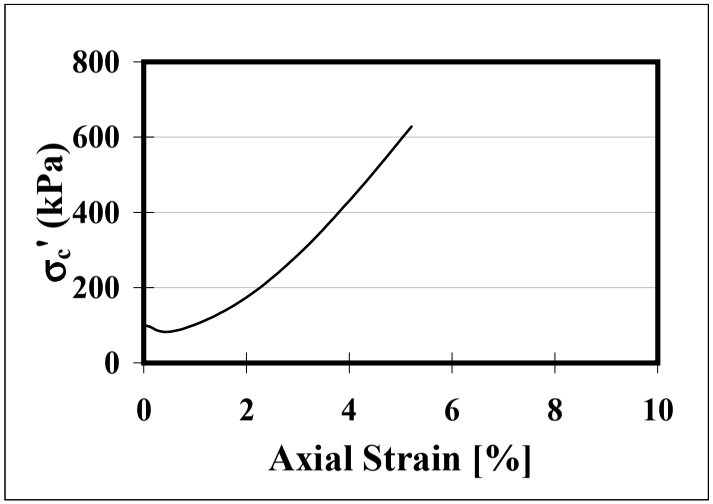

ϕ = 36.4 Confining stress = 100 kPa

GDS OS#55

Date: 36931	Fines= 0	e= 0.721	ec= 0.721	ef= n.a.	(ef)eq= n.a.	(ec)eq= 0.721

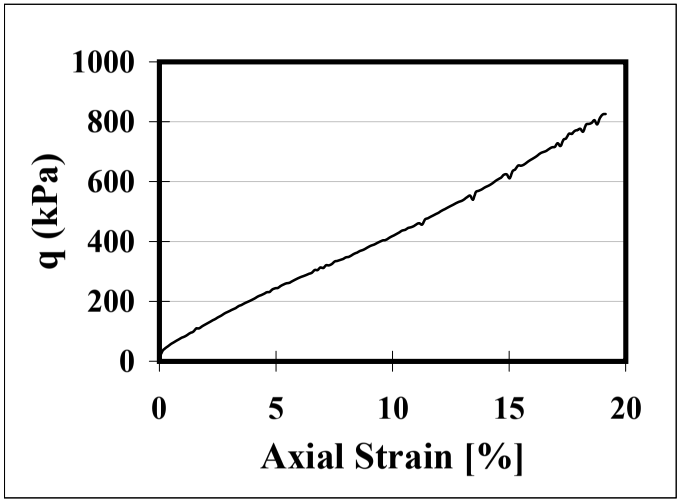

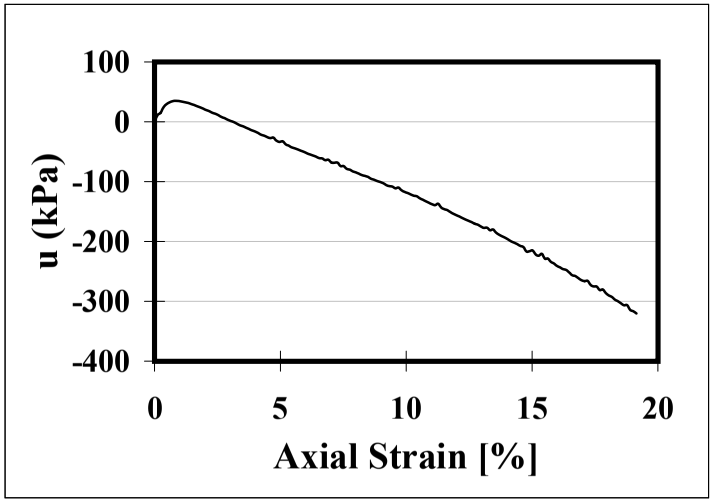

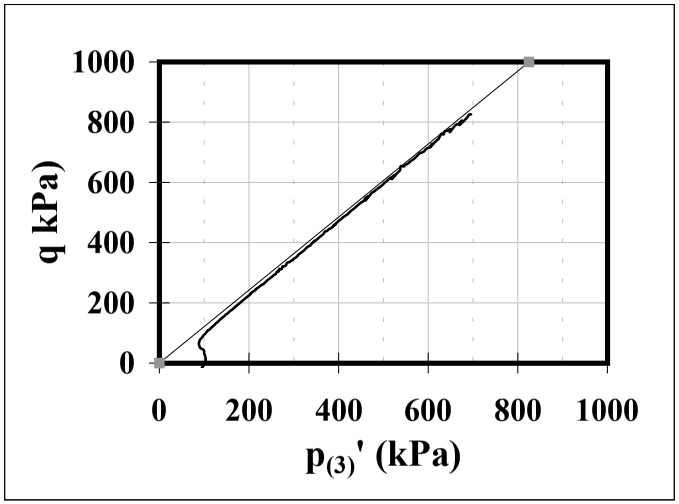

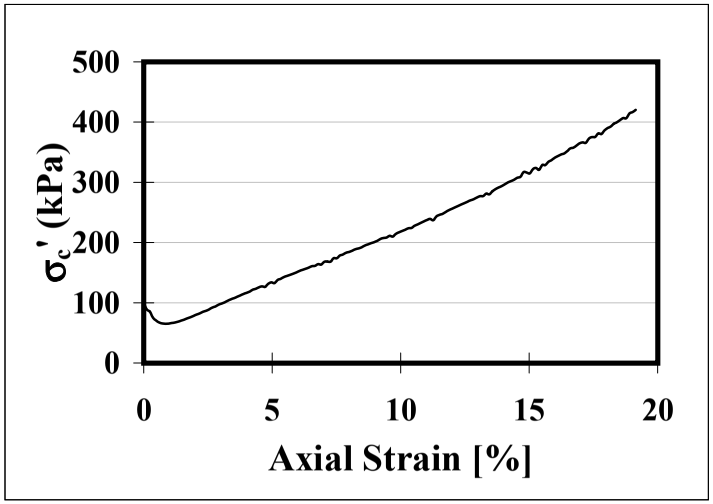

ϕ = 30.3 Confining stress = 100 kPa

Test Information Summary Table

Test Date: 7/28/99

Test Mode:	Geocomp		
File Name:	r072899	Fine Content (%):	7
Soil Type:	OSF55-40	Preparation Method:	MT
Dry Soil Weight (g):	1041.5	Initial Water in Sample (g) (preparation):	264.7
Sample Height (cm):	15.2	Final Water in Sample (g) (shear phase):	261.5
Final B Value:	0.95	Void Ratio:	0.665
Intergranular Void Ratio:	0.790	Interfine Void Ratio:	9.500
Final Consolidation Confining Stress (kPa):	100	Final Strain (%):	21
Final Cell Pressure (kPa):	602	Calculated Friction Angle:	34
Final Back Pressure (kPa):	473	Young's Modulus E (0.05%) (kPa):	56391
Final Shear Induced Pore Pressure (kPa):	-27	Shear Modulus G (0.05%) (kPa):	18797
Final Effective Mean Stress p' (kPa):	230	Final Effective Sigma1 (kPa):	433
Final Effective Deviatoric Stress q' (kPa):	305	Final Effective Sigma3 (kPa):	128

sig3' vs strain

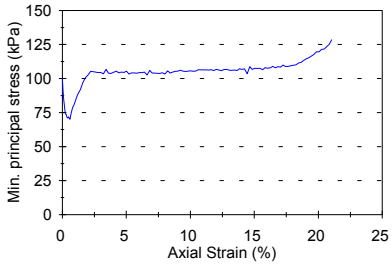

dev stress vs strain (overall)

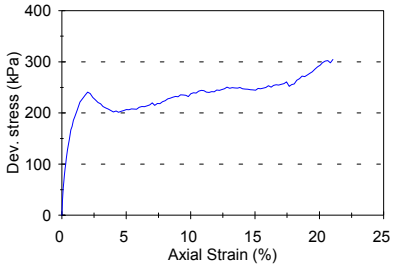

p(3)-q

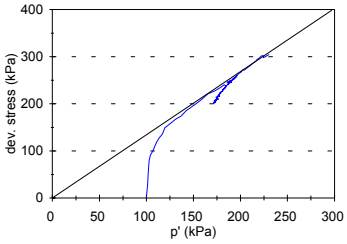

dev stress vs strain (2%)

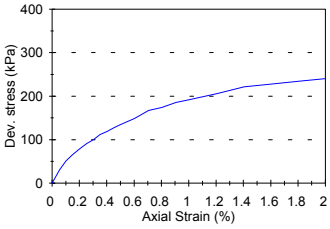

U (sh)

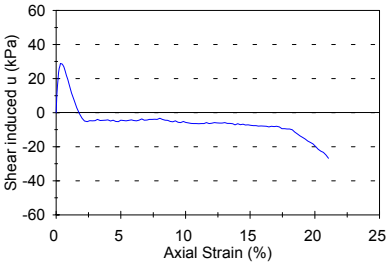

Test Information Summary Table

Test Date: 7/31/99

Test Mode:	Geocomp		
File Name:	r073199	Fine Content (%):	7
Soil Type:	OSF55-40	Preparation Method:	MT
Dry Soil Weight (g):	1125	Initial Water in Sample (g) (preparation):	255.5
Sample Height (cm):	15.6	Final Water in Sample (g) (shear phase):	252.9
Final B Value:	0.93	Void Ratio:	0.596
Intergranular Void Ratio:	0.716	Interfine Void Ratio:	8.514
Final Consolidation Confining Stress (kPa):	100	Final Strain (%):	20
Final Cell Pressure (kPa):	641	Calculated Friction Angle:	34
Final Back Pressure (kPa):	330	Young's Modulus E (0.05%) (kPa):	69177
Final Shear Induced Pore Pressure (kPa):	-210	Shear Modulus G (0.05%) (kPa):	23059
Final Effective Mean Stress p' (kPa):	521	Final Effective Sigma1 (kPa):	943
Final Effective Deviatoric Stress q' (kPa):	632	Final Effective Sigma3 (kPa):	311

sig3' vs strain

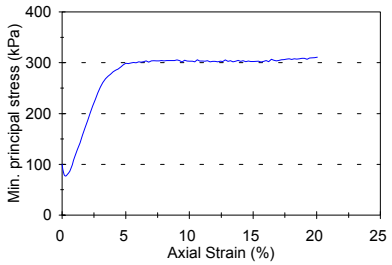

dev stress vs strain (overall)

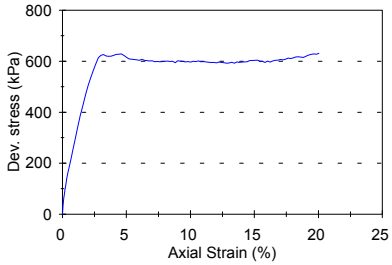

p(3)-q

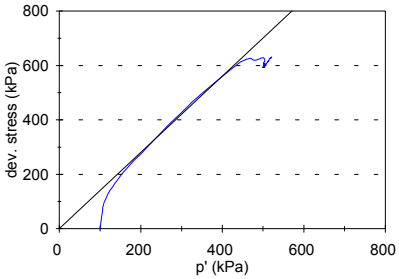

dev stress vs strain (2%)

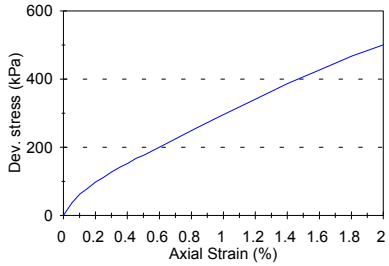

U (sh)

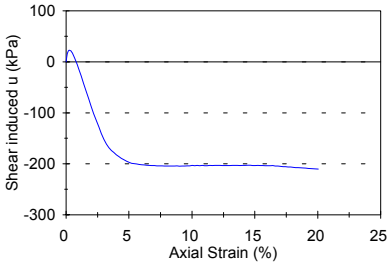

Test Information Summary Table

Test Date: 8/01/99

Test Mode:	Geocomp		
File Name:	r080199	Fine Content (%):	7
Soil Type:	OSF55-40	Preparation Method:	MT
Dry Soil Weight (g):	1021.7	Initial Water in Sample (g) (preparation):	262.6
Sample Height (cm):	15.1	Final Water in Sample (g) (shear phase):	258.9
Final B Value:	0.94	Void Ratio:	0.672
Intergranular Void Ratio:	0.798	Interfine Void Ratio:	9.600
Final Consolidation Confining Stress (kPa):	100	Final Strain (%):	21
Final Cell Pressure (kPa):	620	Calculated Friction Angle:	32
Final Back Pressure (kPa):	503	Young's Modulus E (0.05%) (kPa):	61554
Final Shear Induced Pore Pressure (kPa):	-17	Shear Modulus G (0.05%) (kPa):	20518
Final Effective Mean Stress p' (kPa):	207	Final Effective Sigma1 (kPa):	388
Final Effective Deviatoric Stress q' (kPa):	271	Final Effective Sigma3 (kPa):	116

sig3' vs strain

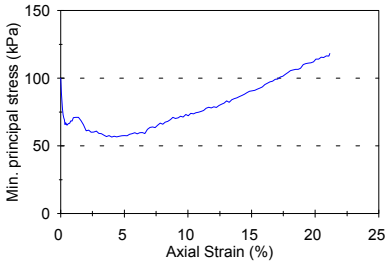

dev stress vs strain (overall)

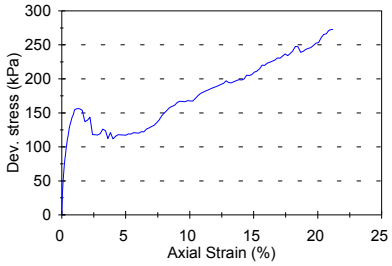

p(3)-q

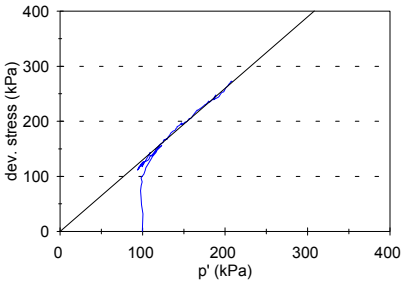

dev stress vs strain (2%)

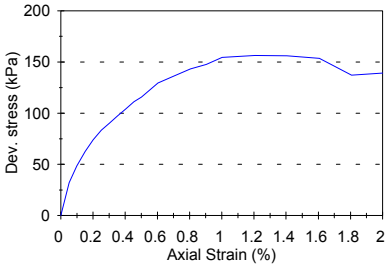

U (sh)

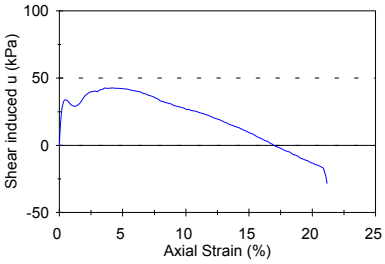

Test Information Summary Table

Test Date: 8/02/99

Test Mode:	Geocomp		
File Name:	r080299	Fine Content (%):	7
Soil Type:	OSF55-40	Preparation Method:	MT
Dry Soil Weight (g):	1016	Initial Water in Sample (g) (preparation):	281.7
Sample Height (cm):	15.6	Final Water in Sample (g) (shear phase):	277.1
Final B Value:	0.95	Void Ratio:	0.723
Intergranular Void Ratio:	0.853	Interfine Void Ratio:	10.329
Final Consolidation Confining Stress (kPa):	100	Final Strain (%):	21
Final Cell Pressure (kPa):	721	Calculated Friction Angle:	22
Final Back Pressure (kPa):	709	Young's Modulus E (0.05%) (kPa):	41710
Final Shear Induced Pore Pressure (kPa):	89	Shear Modulus G (0.05%) (kPa):	13903
Final Effective Mean Stress p' (kPa):	14	Final Effective Sigma1 (kPa):	18
Final Effective Deviatoric Stress q' (kPa):	7	Final Effective Sigma3 (kPa):	11

sig3' vs strain

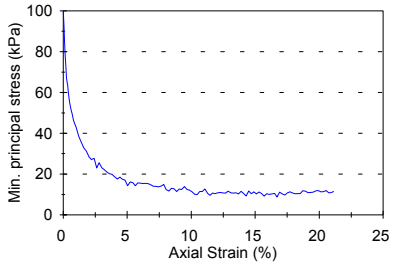

dev stress vs strain (overall)

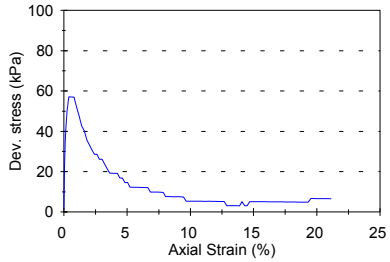

p(3)-q

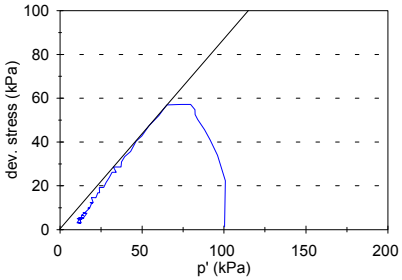

dev stress vs strain (2%)

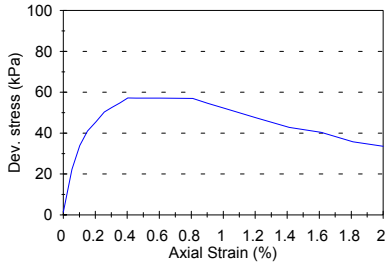

U (sh)

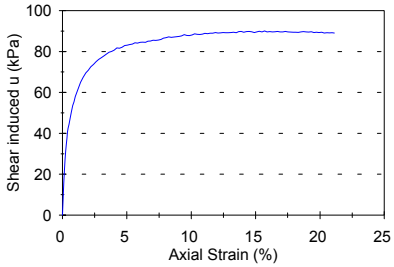

Test Information Summary Table

Test Date: 8/03/99

Test Mode:	Geocomp		
File Name:	r080399	Fine Content (%):	7
Soil Type:	OSF55-40	Preparation Method:	MT
Dry Soil Weight (g):	1097.3	Initial Water in Sample (g) (preparation):	264.6
Sample Height (cm):	15.6	Final Water in Sample (g) (shear phase):	261.7
Final B Value:	0.92	Void Ratio:	0.632
Intergranular Void Ratio:	0.755	Interfine Void Ratio:	9.029
Final Consolidation Confining Stress (kPa):	100	Final Strain (%):	20
Final Cell Pressure (kPa):	700	Calculated Friction Angle:	32
Final Back Pressure (kPa):	452	Young's Modulus E (0.05%) (kPa):	58666
Final Shear Induced Pore Pressure (kPa):	148	Shear Modulus G (0.05%) (kPa):	19555
Final Effective Mean Stress p' (kPa):	424	Final Effective Sigma1 (kPa):	776
Final Effective Deviatoric Stress q' (kPa):	528	Final Effective Sigma3 (kPa):	248

sig3' vs strain

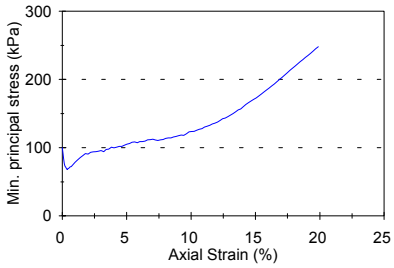

dev stress vs strain (overall)

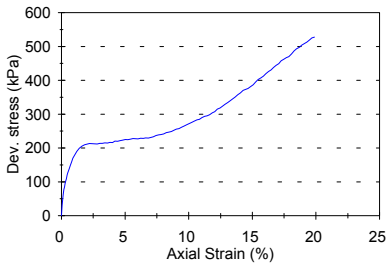

p(3)-q

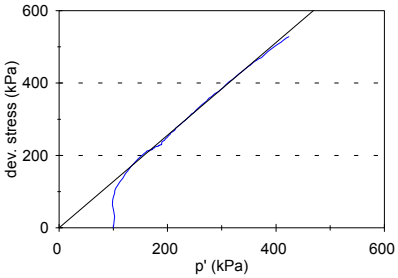

dev stress vs strain (2%)

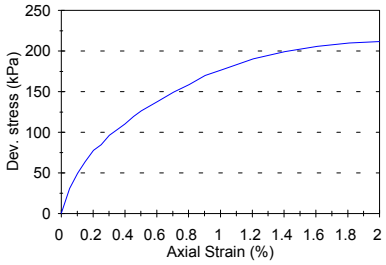

U (sh)

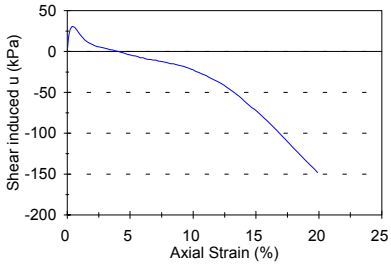

Test Information Summary Table

Test Date: 8/04/99

Test Mode:	Geocomp		
File Name:	r080499	Fine Content (%):	7
Soil Type:	OSF55-40	Preparation Method:	MT
Dry Soil Weight (g):	958	Initial Water in Sample (g) (preparation):	270.8
Sample Height (cm):	15.2	Final Water in Sample (g) (shear phase):	265.8
Final B Value:	0.93	Void Ratio:	0.735
Intergranular Void Ratio	0.866	Interfine Void Ratio:	10.500
Final Consolidation Confining Stress (kPa):	100	Final Strain (%):	20
Final Cell Pressure (kPa):	661	Calculated Friction Angle:	20
Final Back Pressure (kPa):	656	Young's Modulus E (0.05%) (kPa):	38229
Final Shear Induced Pore Pressure (kPa):	96	Shear Modulus G (0.05%) (kPa):	12743
Final Effective Mean Stress p' (kPa):	6	Final Effective Sigma1 (kPa):	6
Final Effective Deviatoric Stress q' (kPa):	1	Final Effective Sigma3 (kPa):	5

sig3' vs strain

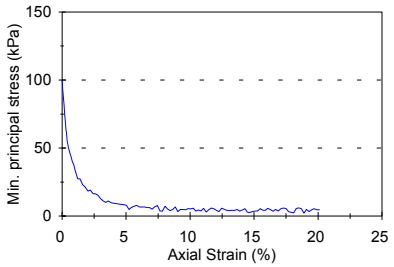

dev stress vs strain (overall)

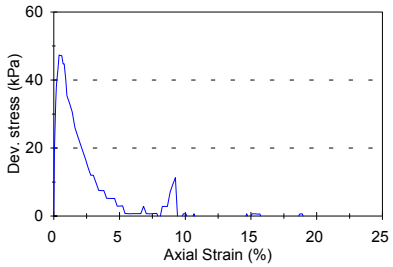

p(3)-q

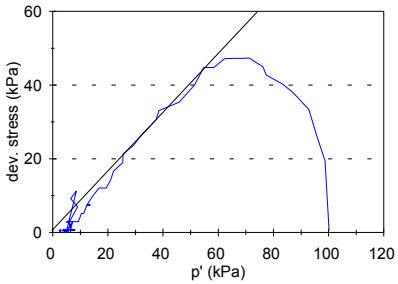

dev stress vs strain (2%)

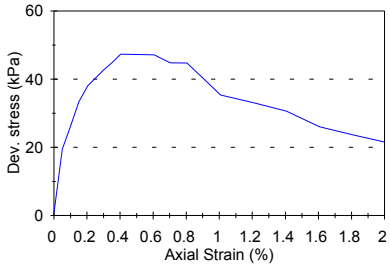

U (sh)

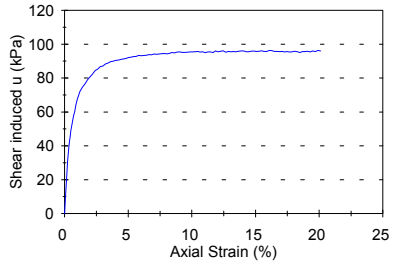

Test Information Summary Table

Test Date: 8/12/99

Test Mode:	Geocomp		
File Name:	r081299	Fine Content (%):	7
Soil Type:	OSF55-40	Preparation Method:	MT
Dry Soil Weight (g):	1110	Initial Water in Sample (g) (preparation):	235.7
Sample Height (cm):	15.2	Final Water in Sample (g) (shear phase):	233.8
Final B Value:	0.97	Void Ratio:	0.558
Intergranular Void Ratio:	0.675	Interfine Void Ratio:	7.971
Final Consolidation Confining Stress (kPa):	100	Final Strain (%):	19
Final Cell Pressure (kPa):	710	Calculated Friction Angle:	35
Final Back Pressure (kPa):	65	Young's Modulus E (0.05%) (kPa):	66043
Final Shear Induced Pore Pressure (kPa):	-545	Shear Modulus G (0.05%) (kPa):	22014
Final Effective Mean Stress p' (kPa):	1218	Final Effective Sigma1 (kPa):	2364
Final Effective Deviatoric Stress q' (kPa):	1719	Final Effective Sigma3 (kPa):	645

sig3' vs strain

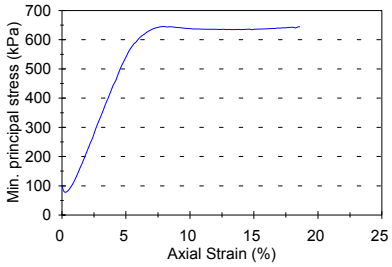

dev stress vs strain (overall)

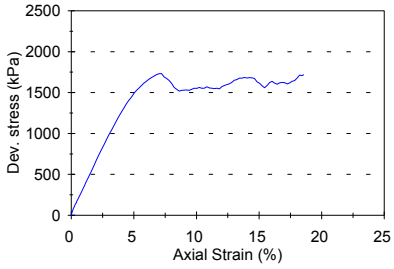

p(3)-q

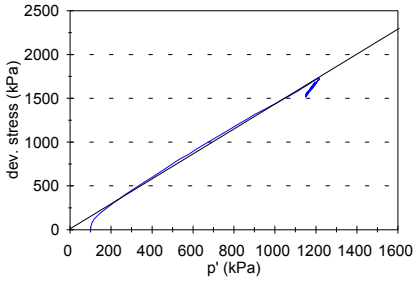

dev stress vs strain (2%)

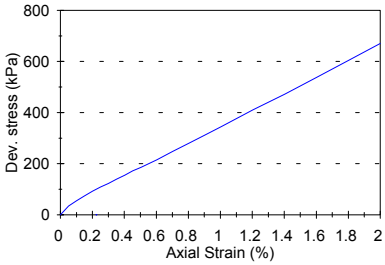

U (sh)

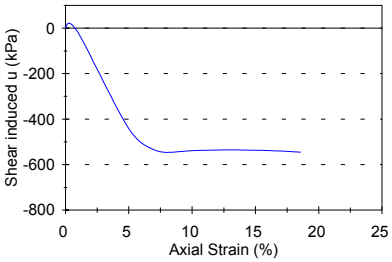

GDS OS#55 GS#40

Date: 11/02/99 Fines= 7 e= 0.520 ec= 0.634 ef= n.a. (ef)eq= n.a. (ec)eq= 0.604

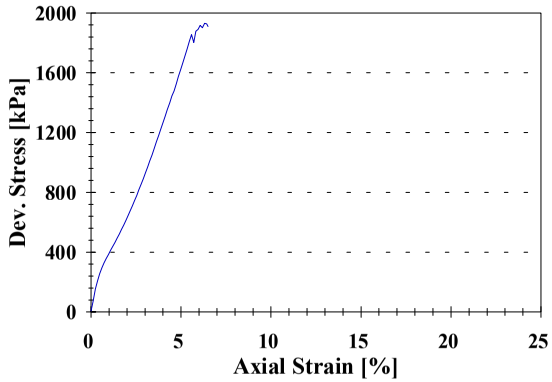

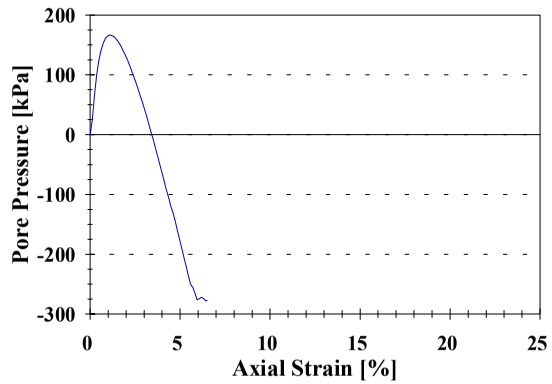

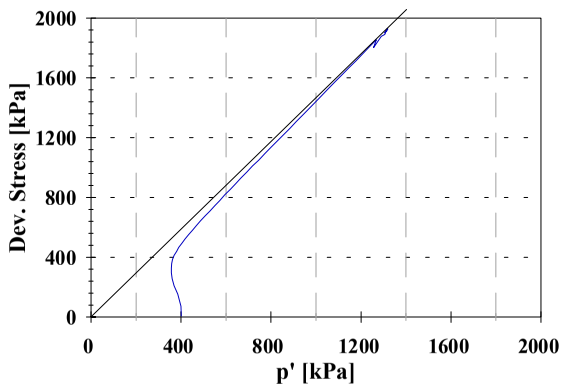

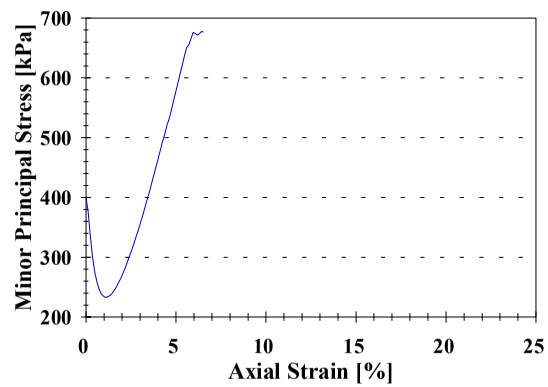

ϕ = 36.2 Confining stress = 400 kPa

GDS OS#55 GS#40

Date: 11/04/99 Fines= 7 e= 0.688 ec= 0.816 ef= n.a. (ef)eq= n.a. (ec)eq= 0.782

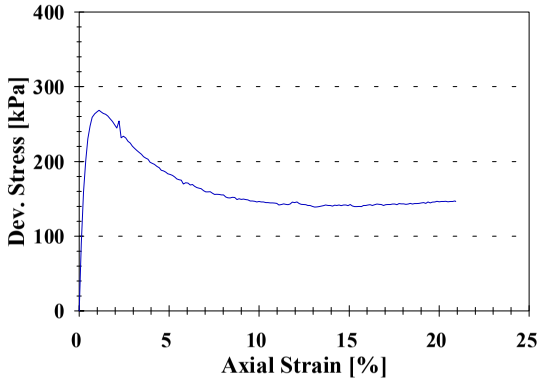

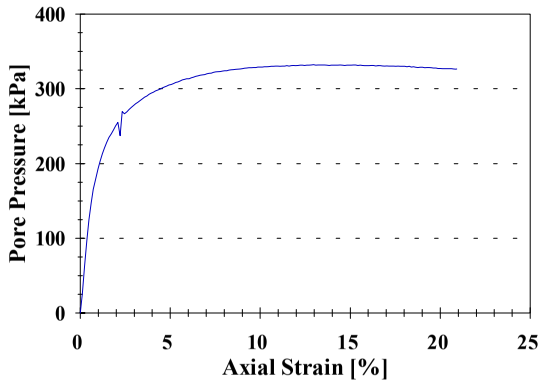

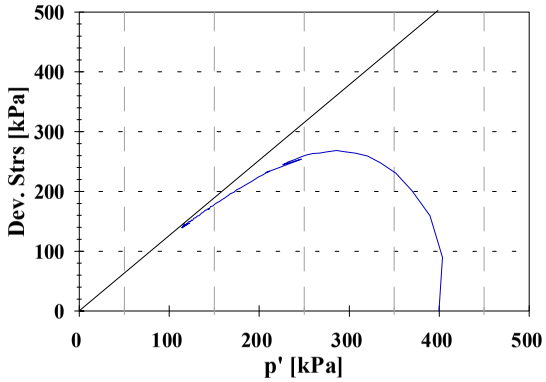

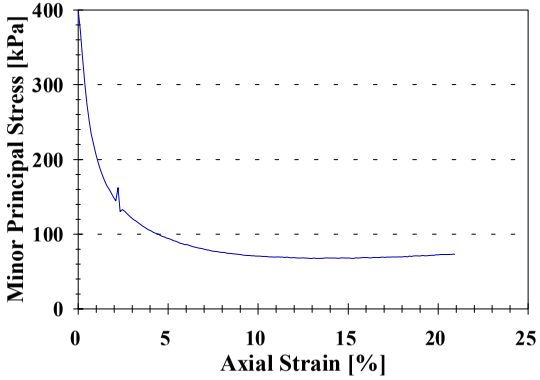

ϕ = 31.1 Confining stress = 400 kPa

Test Information Summary Table

Test Date: 3/29/99

Test Mode:	Geocomp		
File Name:	r032999	Fine Content (%):	15
Soil Type:	OSF55-40	Preparation Method:	DD
Dry Soil Weight (g):	1010.7	Initial Water in Sample (g) (preparation):	229.0
Sample Height (cm):	152	Final Water in Sample (g) (shear phase):	221.6
Final B Value:	0.97	Void Ratio:	0.581
Intergranular Void Ratio:	0.860	Interfine Void Ratio:	3.873
Final Consolidation Confining Stress (kPa):	100	Final Strain (%):	17
Final Cell Pressure (kPa):	770	Calculated Friction Angle:	29
Final Back Pressure (kPa):	695	Young's Modulus E (0.05%) (kPa):	45474
Final Shear Induced Pore Pressure (kPa):	24	Shear Modulus G (0.05%) (kPa):	15158
Final Effective Mean Stress p' (kPa):	123	Final Effective Sigma1 (kPa):	218
Final Effective Deviatoric Stress q' (kPa):	142	Final Effective Sigma3 (kPa):	76

sig3' vs strain

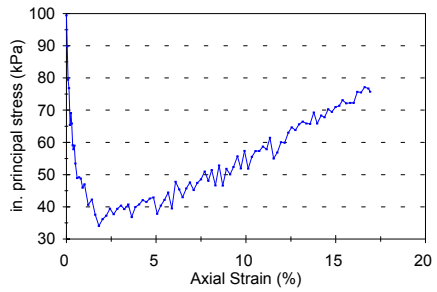

dev stress vs strain (overall)

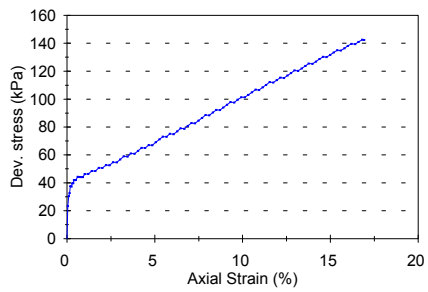

p(3)-q

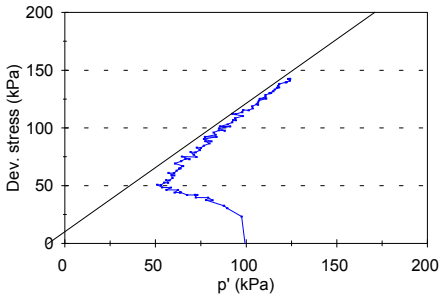

dev stress vs strain (2%)

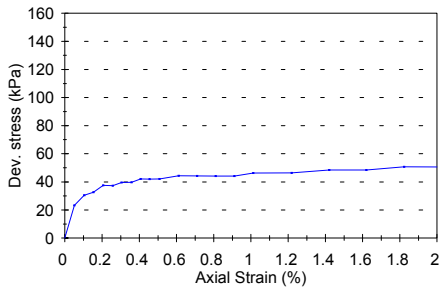

U (sh)

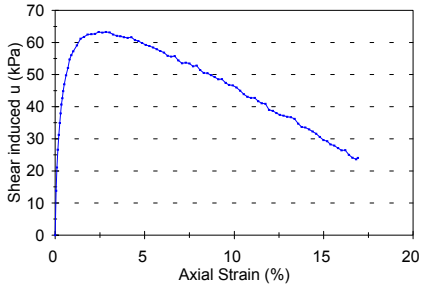

Test Information Summary Table

Test Date: 4/2/99

Test Mode:	Geocomp		
File Name:	r040299	Fine Content (%):	15
Soil Type:	OSF55-40	Preparation Method:	DD
Dry Soil Weight (g):	1081.2	Initial Water in Sample (g) (preparation):	225.5
Sample Height (cm):	150	Final Water in Sample (g) (shear phase):	216.8
Final B Value:	0.95	Void Ratio:	0.531
Intergranular Void Ratio:	0.801	Interfine Void Ratio:	3.540
Final Consolidation Confining Stress (kPa):	100	Final Strain (%):	21
Final Cell Pressure (kPa):	555	Calculated Friction Angle:	29.6
Final Back Pressure (kPa):	365	Young's Modulus E (0.05%) (kPa	42152
Final Shear Induced Pore Pressure (kPa):	-90	Shear Modulus G (0.05%) (kPa):	14050
Final Effective Mean Stress p' (kPa):	316	Final Effective Sigma1 (kPa):	565
Final Effective Deviatoric Stress q' (kPa):	374	Final Effective Sigma3 (kPa):	191

sig3' vs strain

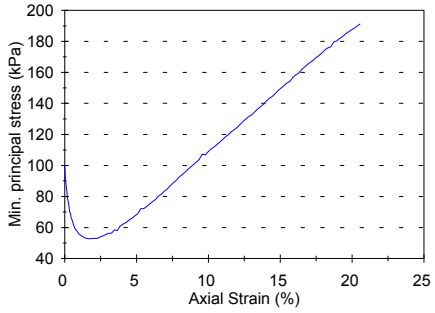

dev stress vs strain (overall)

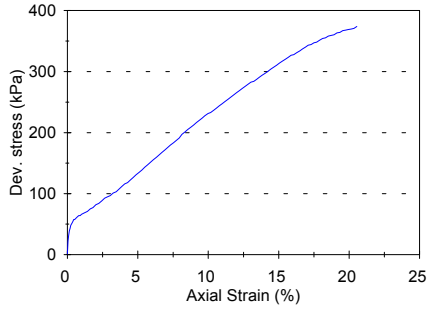

p(3)-q

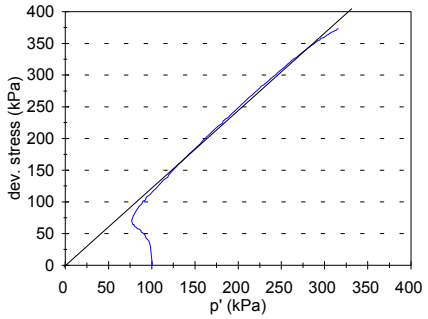

dev stress vs strain (2%)

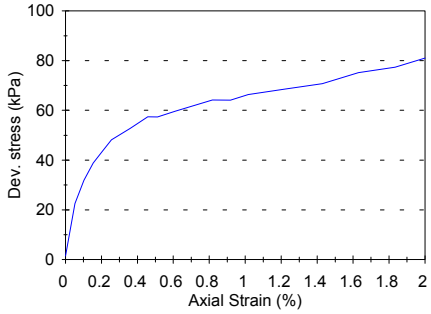

U (sh)

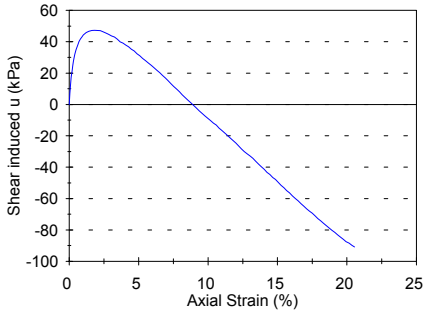

Test Information Summary Table

Test Date: 5/19/99

Test Mode:	Geocomp		
File Name:	r051999	Fine Content (%):	15
Soil Type:	OSF55-40	Preparation Method:	DD
Dry Soil Weight (g):	941.3	Initial Water in Sample (g) (preparation):	218.1
Sample Height (cm):	139	Final Water in Sample (g) (shear phase):	215.3
Final B Value:	0.92	Void Ratio:	0.606
Intergranular Void Ratio:	0.889	Interfine Void Ratio:	4.040
Final Consolidation Confining Stress (kPa):	100	Final Strain (%):	22
Final Cell Pressure (kPa):	685	Calculated Friction Angle:	27.4
Final Back Pressure (kPa):	626	Young's Modulus E (0.05%) (kPa):	47059
Final Shear Induced Pore Pressure (kPa):	41	Shear Modulus G (0.05%) (kPa):	15686
Final Effective Mean Stress p' (kPa):	93	Final Effective Sigma1 (kPa):	160
Final Effective Deviatoric Stress q' (kPa):	101	Final Effective Sigma3 (kPa):	59

sig3' vs strain

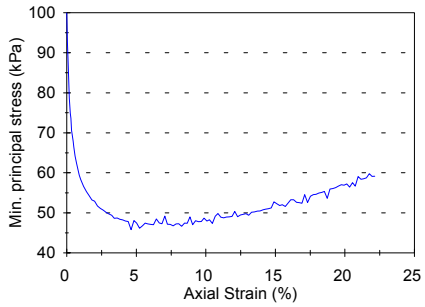

dev stress vs strain (overall)

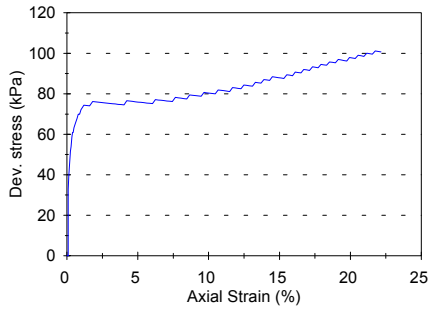

p(3)-q

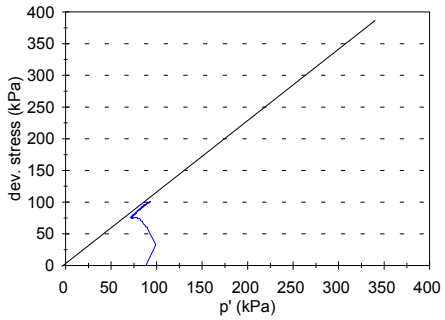

dev stress vs strain (2%)

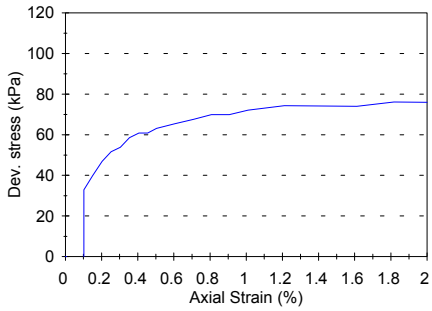

U (sh)

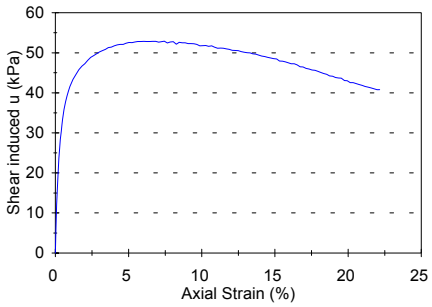

Test Information Summary Table

Test Date: 5/30/99

Test Mode:	Geocomp		
File Name:	r053099	Fine Content (%):	15
Soil Type:	OSF55-40	Preparation Method:	DD
Dry Soil Weight (g):	960	Initial Water in Sample (g) (preparation):	216.9
Sample Height (cm):	14	Final Water in Sample (g) (shear phase):	211.5
Final B Value:	0.91	Void Ratio:	0.584
Intergranular Void Ratio:	0.864	Interfine Void Ratio:	3.893
Final Consolidation Confining Stress (kPa):	100	Final Strain (%):	20
Final Cell Pressure (kPa):	575	Calculated Friction Angle:	25
Final Back Pressure (kPa):	546	Young's Modulus E (0.05%) (kPa):	18672
Final Shear Induced Pore Pressure (kPa):	71	Shear Modulus G (0.05%) (kPa):	6224
Final Effective Mean Stress p' (kPa):	43	Final Effective Sigma1 (kPa):	71
Final Effective Deviatoric Stress q' (kPa):	42	Final Effective Sigma3 (kPa):	29

sig3' vs strain

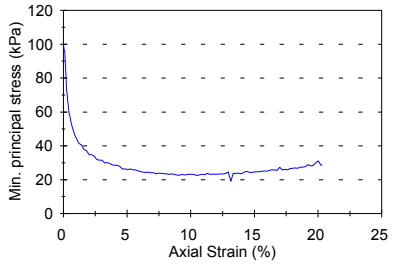

dev stress vs strain (overall)

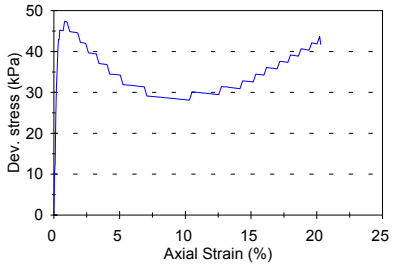

p(3)-q

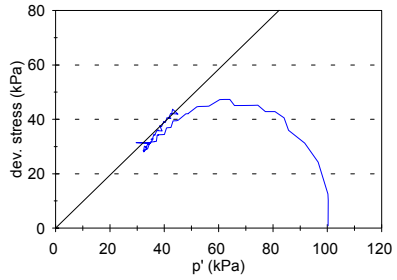

dev stress vs strain (2%)

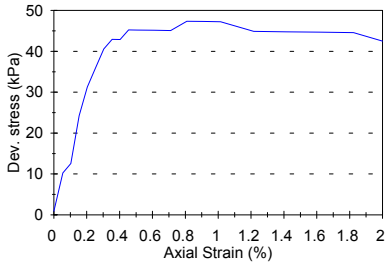

U (sh)

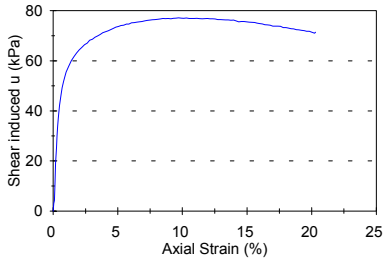

Test Information Summary Table

Test Date: 6/01/99

Test Mode:	Geocomp		
File Name:	r060199	Fine Content (%):	15
Soil Type:	OSF55-40	Preparation Method:	MT
Dry Soil Weight (g):	957.8	Initial Water in Sample (g) (preparation):	237.7
Sample Height (cm):	15.1	Final Water in Sample (g) (shear phase):	223.7
Final B Value:	0.94	Void Ratio:	0.619
Intergranular Void Ratio:	0.905	Interfine Void Ratio:	4.127
Final Consolidation Confining Stress (kPa):	100	Final Strain (%):	18
Final Cell Pressure (kPa):	555	Calculated Friction Angle:	
Final Back Pressure (kPa):	551	Young's Modulus E (0.05%) (kPa):	25046
Final Shear Induced Pore Pressure (kPa):	96	Shear Modulus G (0.05%) (kPa):	8349
Final Effective Mean Stress p' (kPa):	1	Final Effective Sigma1 (kPa):	0
Final Effective Deviatoric Stress q' (kPa):	0	Final Effective Sigma3 (kPa):	4

sig3' vs strain

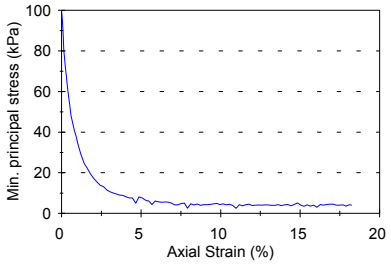

dev stress vs strain (overall)

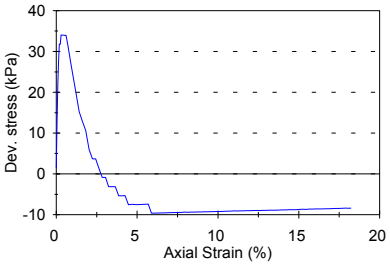

p(3)-q

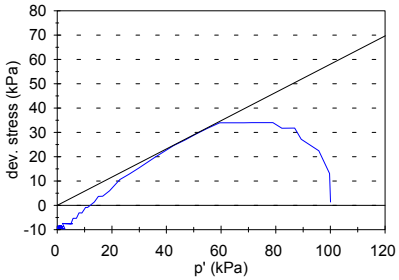

dev stress vs strain (2%)

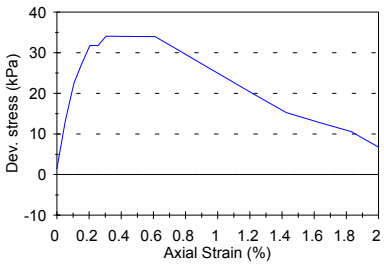

U (sh)

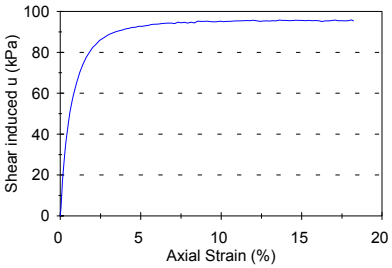

Test Information Summary Table

Test Date: 7/12/99

Test Mode:	Geocomp		
File Name:	r071299	Fine Content (%):	15
Soil Type:	OSF55-40	Preparation Method:	MT
Dry Soil Weight (g):	1194	Initial Water in Sample (g) (preparation):	237.9
Sample Height (cm):	15.9	Final Water in Sample (g) (shear phase):	234.1
Final B Value:	0.95	Void Ratio:	0.520
Intergranular Void Ratio:	0.788	Interfine Void Ratio:	3.467
Final Consolidation Confining Stress (kPa):	100	Final Strain (%):	23
Final Cell Pressure (kPa):	625	Calculated Friction Angle:	31
Final Back Pressure (kPa):	446	Young's Modulus E (0.05%) (kPa):	61848
Final Shear Induced Pore Pressure (kPa):	-80	Shear Modulus G (0.05%) (kPa):	20616
Final Effective Mean Stress p' (kPa):	302	Final Effective Sigma1 (kPa):	546
Final Effective Deviatoric Stress q' (kPa):	366	Final Effective Sigma3 (kPa):	180

sig3' vs strain

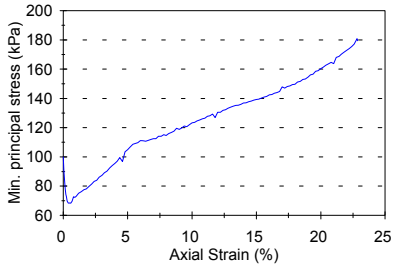

dev stress vs strain (overall)

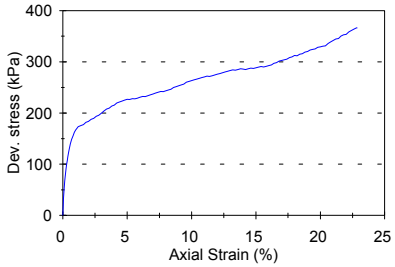

p(3)-q

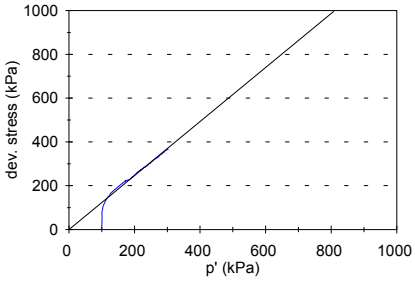

dev stress vs strain (2%)

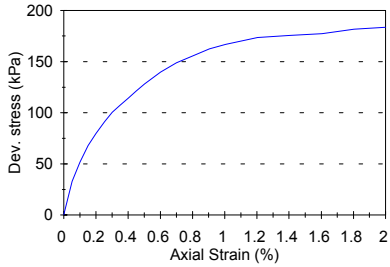

U (sh)

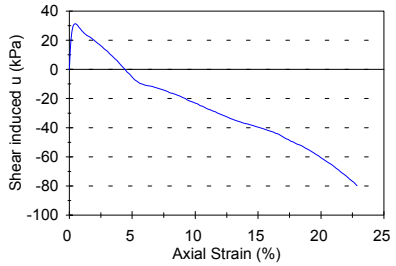

Test Information Summary Table

Test Date: 7/19/99

Test Mode:	Geocomp		
File Name:	r071999	Fine Content (%):	15
Soil Type:	OSF55-40	Preparation Method:	MT
Dry Soil Weight (g):	1258	Initial Water in Sample (g) (preparation):	201.4
Sample Height (cm):	15.6	Final Water in Sample (g) (shear phase):	200.9
Final B Value:	0.98	Void Ratio:	0.423
Intergranular Void Ratio:	0.674	Interfine Void Ratio:	2.820
Final Consolidation Confining Stress (kPa):	100	Final Strain (%):	5
Final Cell Pressure (kPa):	751	Calculated Friction Angle:	39
Final Back Pressure (kPa):	153	Young's Modulus E (0.05%) (kPa):	73692
Final Shear Induced Pore Pressure (kPa):	-497	Shear Modulus G (0.05%) (kPa):	24564
Final Effective Mean Stress p' (kPa):	1266	Final Effective Sigma1 (kPa):	2601
Final Effective Deviatoric Stress q' (kPa):	2002	Final Effective Sigma3 (kPa):	599

sig3' vs strain

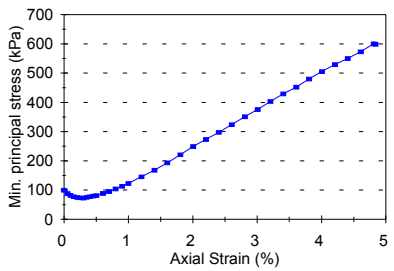

dev stress vs strain (overall)

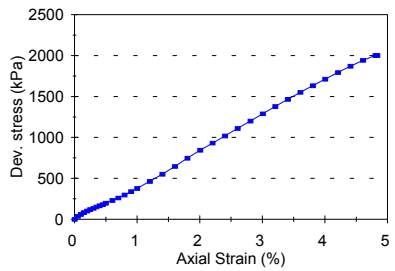

p(3)-q

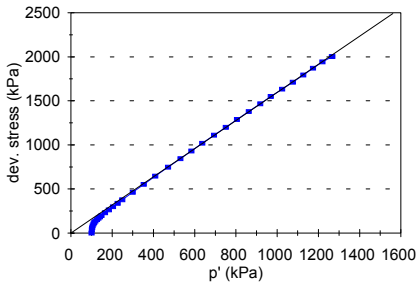

dev stress vs strain (2%)

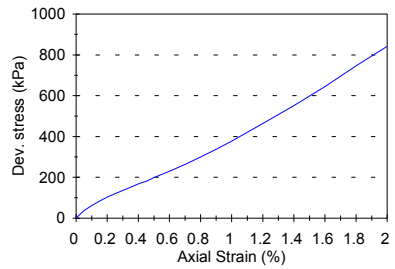

U (sh)

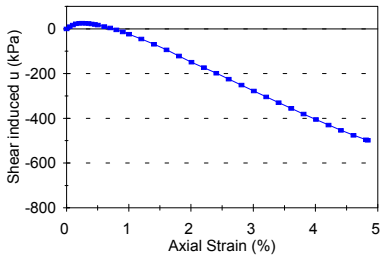

Test Information Summary Table

Test Date: 8/05/99

Test Mode:	Geocomp		
File Name:	r080599	Fine Content (%):	15
Soil Type:	OSF55-40	Preparation Method:	MT
Dry Soil Weight (g):	1108.1	Initial Water in Sample (g) (preparation):	255.8
Sample Height (cm):	15.7	Final Water in Sample (g) (shear phase):	248.6
Final B Value:	0.92	Void Ratio:	0.595
Intergranular Void Ratio:	0.876	Interfine Void Ratio:	3.967
Final Consolidation Confining Stress (kPa):	100	Final Strain (%):	22
Final Cell Pressure (kPa):	680	Calculated Friction Angle:	22
Final Back Pressure (kPa):	668	Young's Modulus E (0.05%) (kPa):	41865
Final Shear Induced Pore Pressure (kPa):	88	Shear Modulus G (0.05%) (kPa):	13955
Final Effective Mean Stress p' (kPa):	17	Final Effective Sigma1 (kPa):	27
Final Effective Deviatoric Stress q' (kPa):	15	Final Effective Sigma3 (kPa):	12

sig3' vs strain

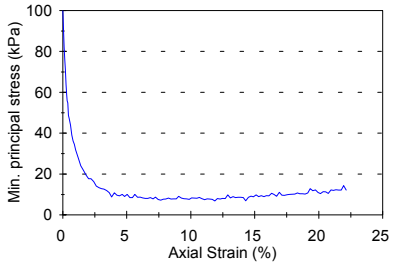

dev stress vs strain (overall)

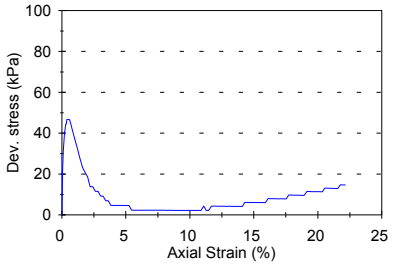

p(3)-q

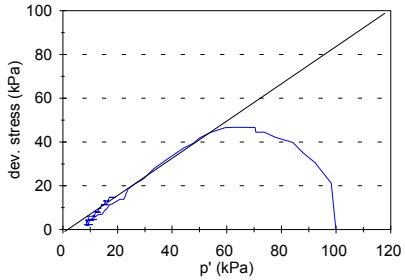

dev stress vs strain (2%)

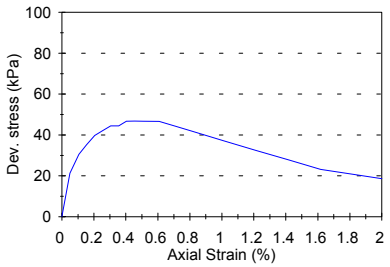

U (sh)

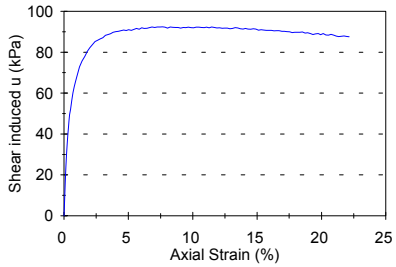

Test Information Summary Table

Test Date: 8/11/99

Test Mode:	Geocomp		
File Name:	r081199	Fine Content (%):	15
Soil Type:	OSF55-40	Preparation Method:	MT
Dry Soil Weight (g):	1272	Initial Water in Sample (g) (preparation):	205.7
Sample Height (cm):	15.8	Final Water in Sample (g) (shear phase):	204.3
Final B Value:	0.94	Void Ratio:	0.426
Intergranular Void Ratio:	0.678	Interfine Void Ratio:	2.840
Final Consolidation Confining Stress (kPa):	100	Final Strain (%):	5
Final Cell Pressure (kPa):	740	Calculated Friction Angle:	41
Final Back Pressure (kPa):	165	Young's Modulus E (0.05%) (kPa):	78749
Final Shear Induced Pore Pressure (kPa):	-475	Shear Modulus G (0.05%) (kPa):	26250
Final Effective Mean Stress p' (kPa):	1239	Final Effective Sigma1 (kPa):	2568
Final Effective Deviatoric Stress q' (kPa):	1992	Final Effective Sigma3 (kPa):	575

sig3' vs strain

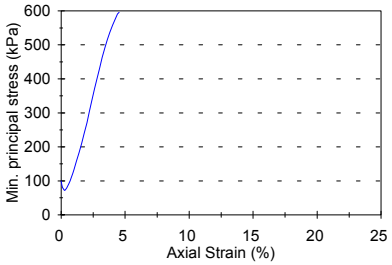

dev stress vs strain (overall)

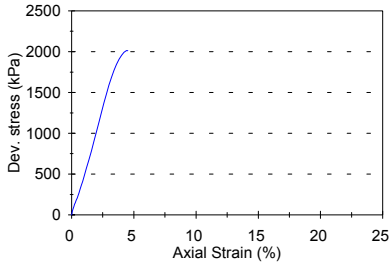

p(3)-q

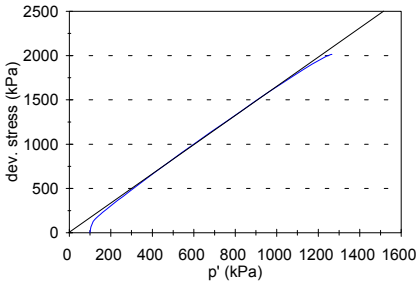

dev stress vs strain (2%)

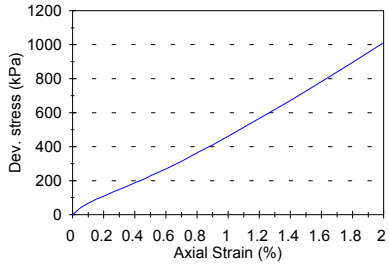

U (sh)

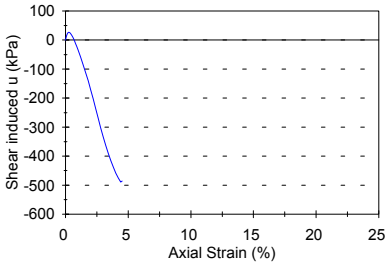

GDS OS#55 GS#40

Date: 11/16/99 Fines= 15 e= 0.575 ec= 0.853 ef= n.a. (ef)eq= n.a. (ec)eq= 0.775

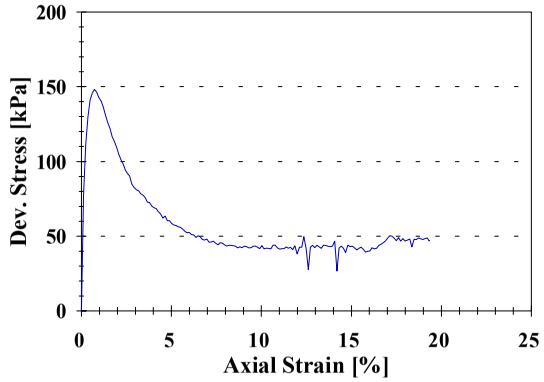

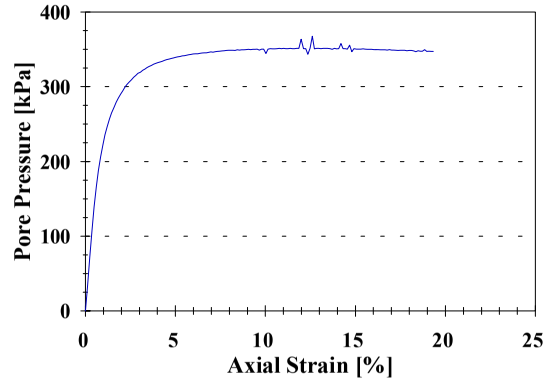

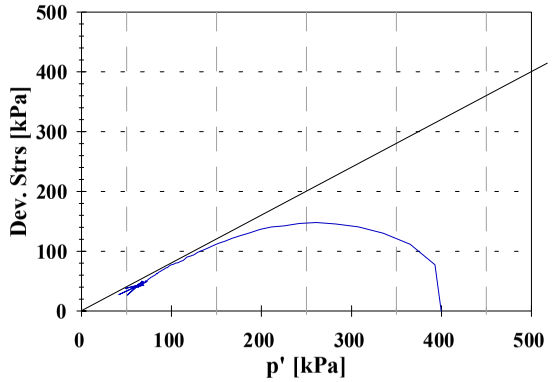

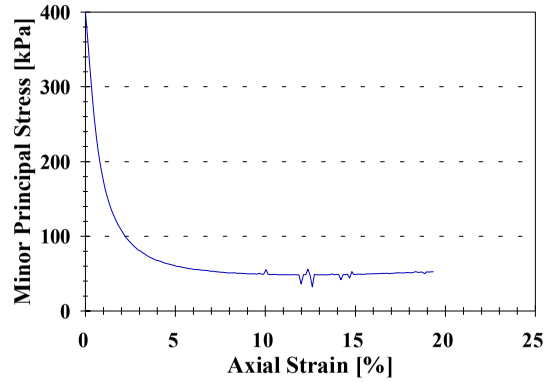

$\phi =$ 20.7 Confining stress = 400 kPa

GDS OS#55 GS#40

Date: 12/01/99 Fines= 15 e= 0.601 ec= 0.884 ef= n.a. (ef)eq= n.a. (ec)eq= 0.804

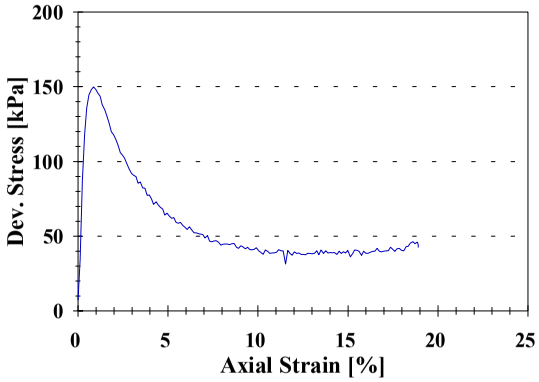

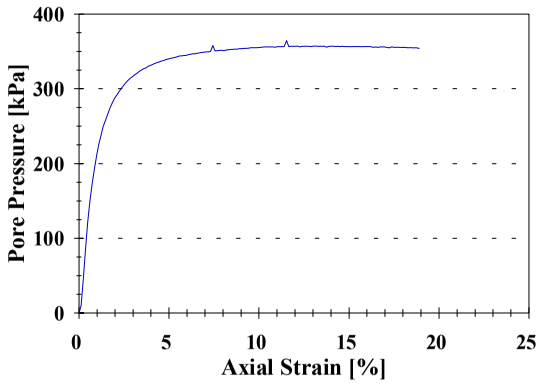

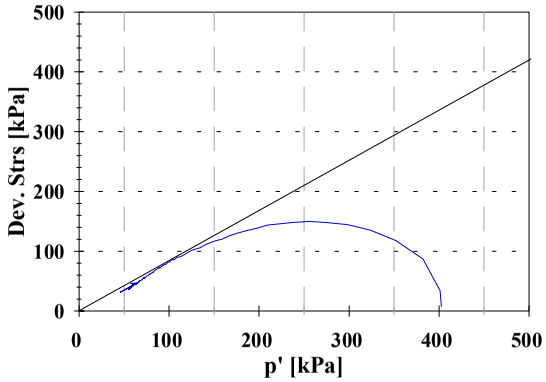

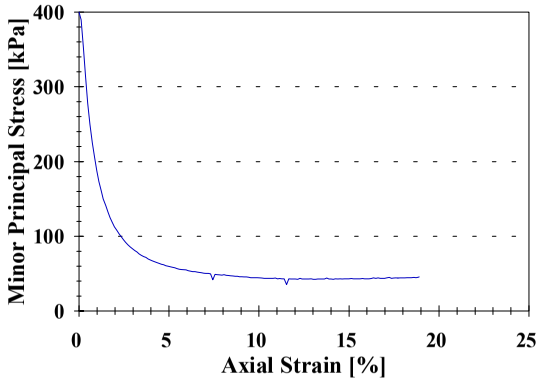

ϕ = 21.5 Confining stress = 400 kPa

GDS OS#55 GS#40

Date: 01/11/00 Fines= 15 e= 0.602 ec= 0.885 ef= n.a. (ef)eq= n.a. (ec)eq= 0.805

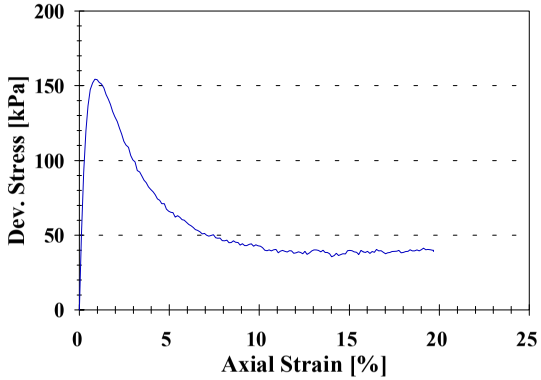

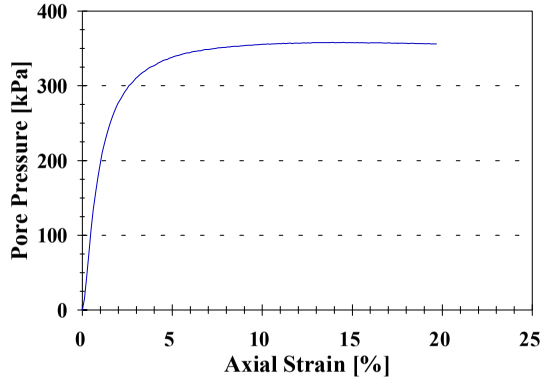

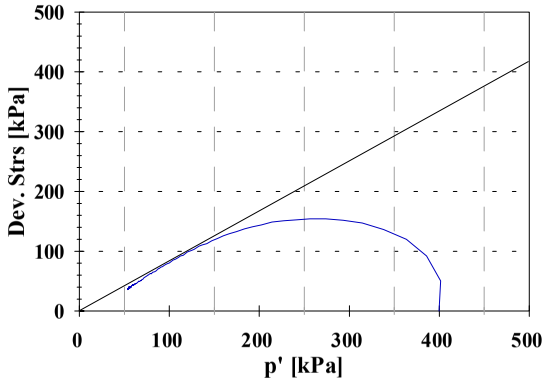

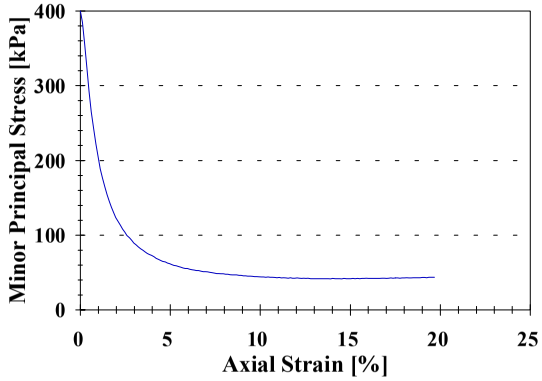

ϕ = 21.6 Confining stress = 400 kPa

Test Information Summary Table

Test Date: 3/31/99

Test Mode:	Geocomp		
File Name:	r033199	Fine Content (%):	25
Soil Type:	OSF55-40	Preparation Method:	DD
Dry Soil Weight (g):	1012.6	Initial Water in Sample (g) (preparation):	186.1
Sample Height (cm):	155	Final Water in Sample (g) (shear phase):	182.0
Final B Value:	0.91	Void Ratio:	0.476
Intergranular Void Ratio:	0.968	Interfine Void Ratio:	1.904
Final Consolidation Confining Stress (kPa):	100	Final Strain (%):	23
Final Cell Pressure (kPa):	680	Calculated Friction Angle:	
Final Back Pressure (kPa):	674	Young's Modulus E (0.05%) (kPa)	
Final Shear Induced Pore Pressure (kPa):	84	Shear Modulus G (0.05%) (kPa):	
Final Effective Mean Stress p' (kPa):	6	Final Effective Sigma1 (kPa):	6
Final Effective Deviatoric Stress q' (kPa):	0	Final Effective Sigma3 (kPa):	6

sig3' vs strain

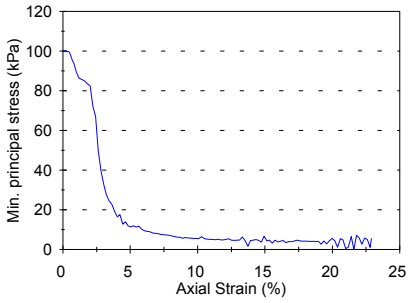

dev stress vs strain (overall)

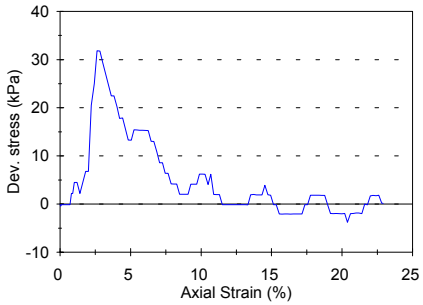

p(3)-q

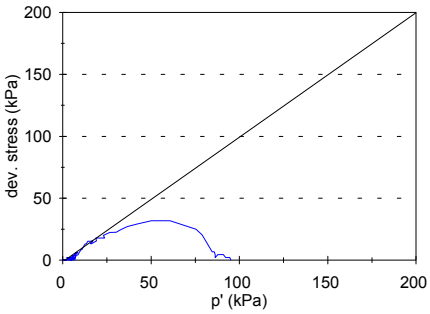

dev stress vs strain (2%)

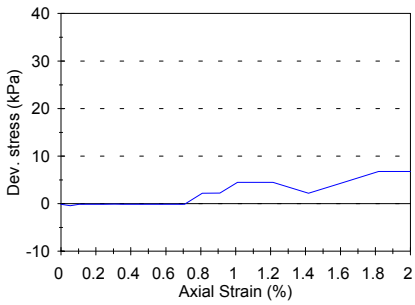

U (sh)

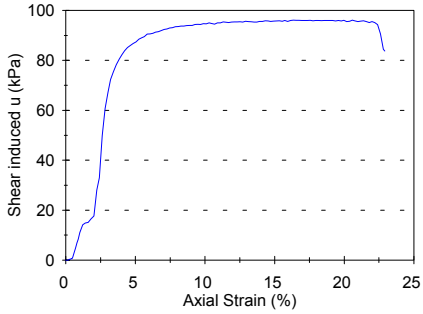

Test Information Summary Table

Test Date: 6/03/99

Test Mode:	Geocomp		
File Name:	r060399	Fine Content (%):	25
Soil Type:	OSF55-40	Preparation Method:	MT
Dry Soil Weight (g):	1011.3	Initial Water in Sample (g) (preparation):	193.1
Sample Height (cm):	15.8	Final Water in Sample (g) (shear phase):	175.5
Final B Value:	0.94	Void Ratio:	0.46
Intergranular Void Ratio:	0.947	Interfine Void Ratio:	1.840
Final Consolidation Confining Stress (kPa):	100	Final Strain (%):	20
Final Cell Pressure (kPa):	610	Calculated Friction Angle:	14
Final Back Pressure (kPa):	600	Young's Modulus E (0.05%) (kPa):	31137
Final Shear Induced Pore Pressure (kPa):	90	Shear Modulus G (0.05%) (kPa):	10379
Final Effective Mean Stress p' (kPa):	11	Final Effective Sigma1 (kPa):	14
Final Effective Deviatoric Stress q' (kPa):	4	Final Effective Sigma3 (kPa):	10

sig3' vs strain

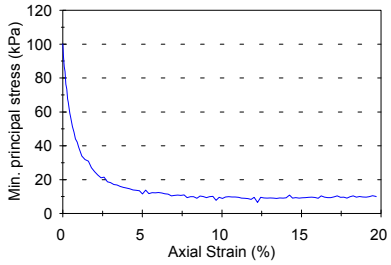

dev stress vs strain (overall)

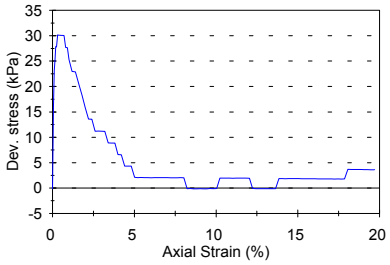

p(3)-q

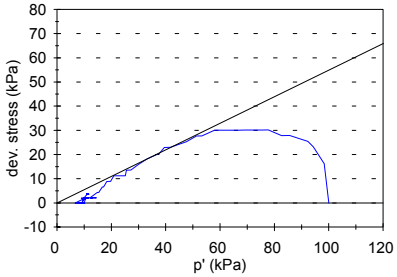

dev stress vs strain (2%)

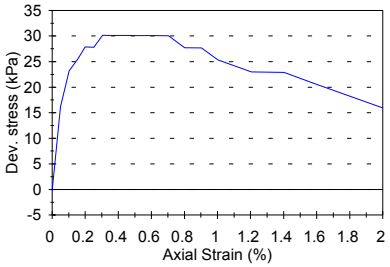

U (sh)

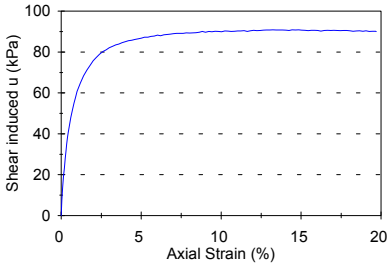

Test Information Summary Table

Test Date: 6/04/99

Test Mode:	Geocomp		
File Name:	r060499	Fine Content (%):	25
Soil Type:	OSF55-40	Preparation Method:	MT
Dry Soil Weight (g):	960.4	Initial Water in Sample (g) (preparation):	192.2
Sample Height (cm):	14.8	Final Water in Sample (g) (shear phase):	157.7
Final B Value:	0.92	Void Ratio:	0.435
Intergranular Void Ratio:	0.913	Interfine Void Ratio:	1.740
Final Consolidation Confining Stress (kPa):	100	Final Strain (%):	21
Final Cell Pressure (kPa):	650	Calculated Friction Angle:	27
Final Back Pressure (kPa):	598	Young's Modulus E (0.05%) (kPa):	37214
Final Shear Induced Pore Pressure (kPa):	48	Shear Modulus G (0.05%) (kPa):	10379
Final Effective Mean Stress p' (kPa):	84	Final Effective Sigma1 (kPa):	149
Final Effective Deviatoric Stress q' (kPa):	94	Final Effective Sigma3 (kPa):	55

sig3' vs strain

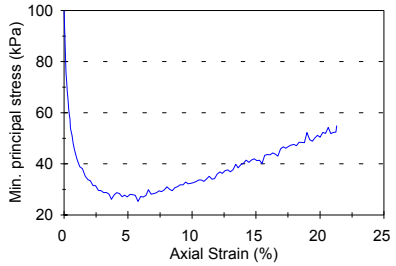

dev stress vs strain (overall)

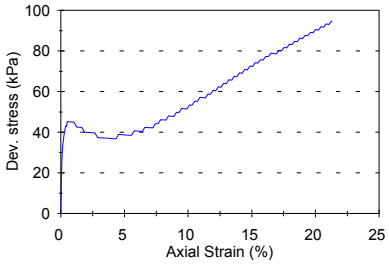

p(3)-q

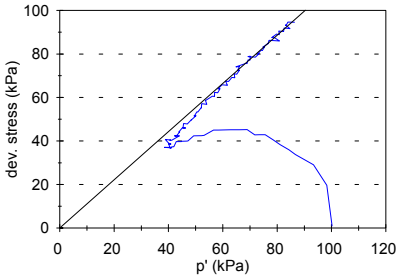

dev stress vs strain (2%)

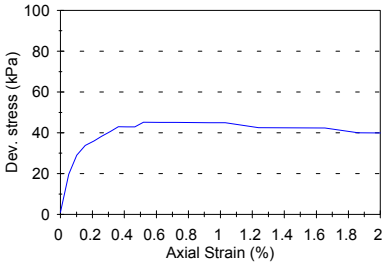

U (sh)

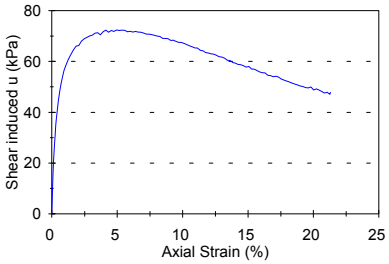

Test Information Summary Table

Test Date: 7/15/99

Test Mode:	Geocomp		
File Name:	r071599	Fine Content (%):	25
Soil Type:	OSF55-40	Preparation Method:	MT
Dry Soil Weight (g):	1285	Initial Water in Sample (g) (preparation):	208.8
Sample Height (cm):	15.8	Final Water in Sample (g) (shear phase):	205.0
Final B Value:	0.93	Void Ratio:	0.423
Intergranular Void Ratio:	0.897	Interfine Void Ratio:	1.692
Final Consolidation Confining Stress (kPa):	100	Final Strain (%):	23
Final Cell Pressure (kPa):	710	Calculated Friction Angle:	27
Final Back Pressure (kPa):	668	Young's Modulus E (0.05%) (kPa):	72924
Final Shear Induced Pore Pressure (kPa):	58	Shear Modulus G (0.05%) (kPa):	24308
Final Effective Mean Stress p' (kPa):	67	Final Effective Sigma1 (kPa):	117
Final Effective Deviatoric Stress q' (kPa):	75	Final Effective Sigma3 (kPa):	42

sig3' vs strain

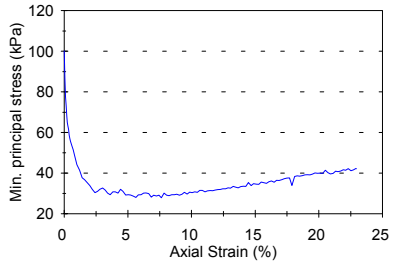

dev stress vs strain (overall)

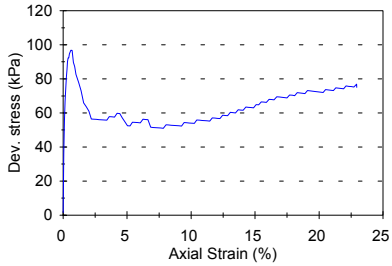

p(3)-q

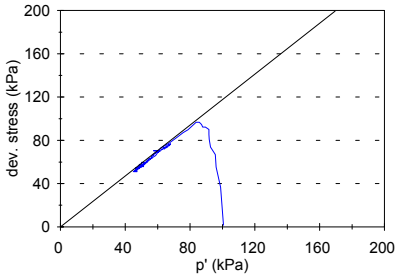

dev stress vs strain (2%)

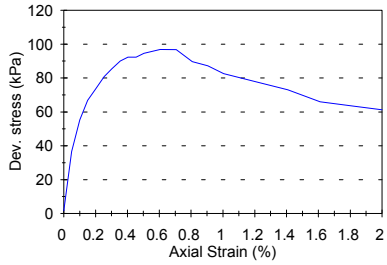

U (sh)

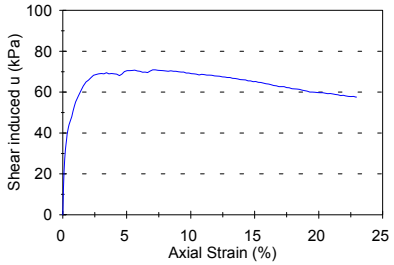

GDS OS#55 GS#40

Date: 10/11/99 Fines= 25 e= 0.403 es= 0.871 ef= n.a. (ef)eq= n.a. (ec)eq= 0.727

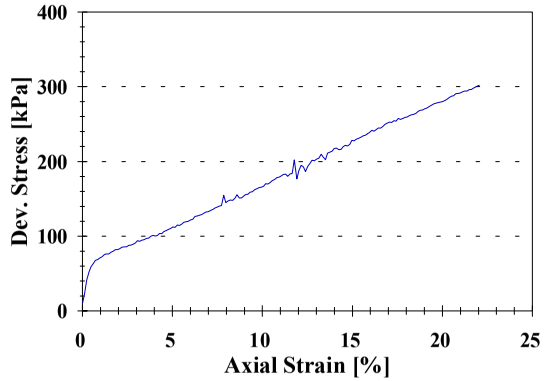

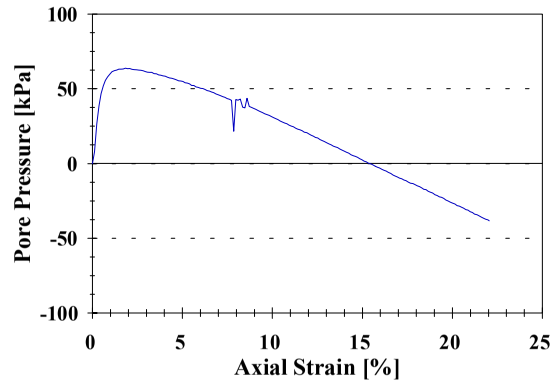

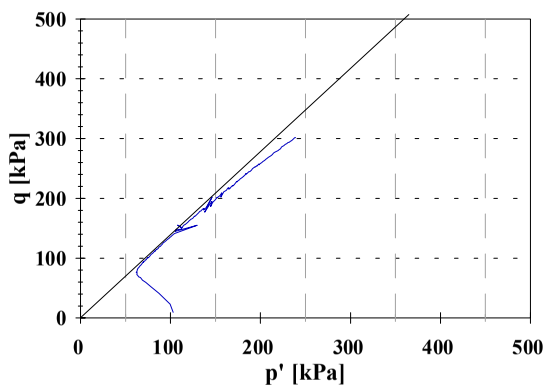

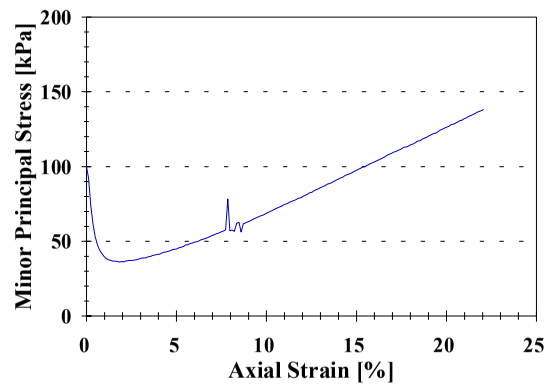

$\phi =$ 34.3 Confining stress = 100 kPa

GDS OS#55 GS#40

Date: 10/13/99 Fines= 25 e= 0.360 ec= 0.813 ef= n.a. (ef)eq= n.a. (ec)eq= 0.673

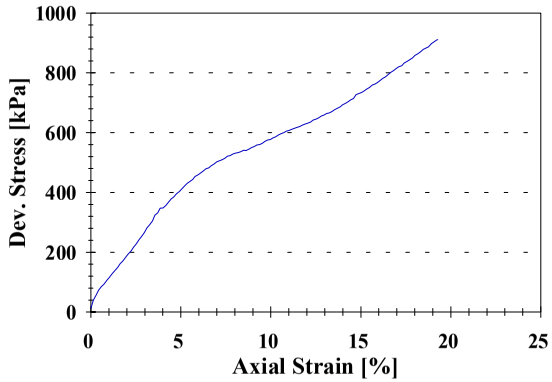

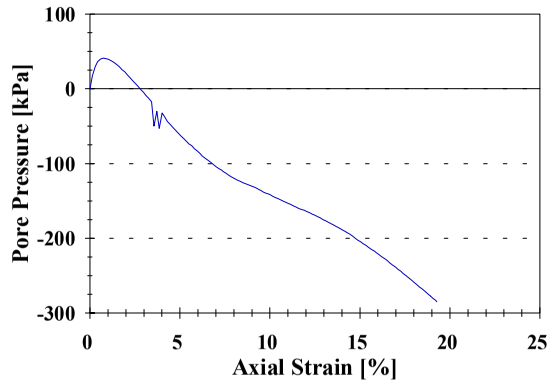

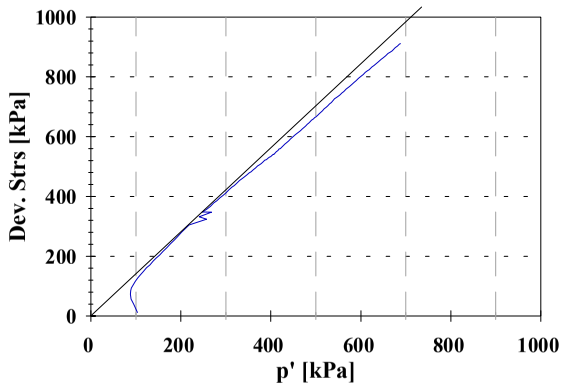

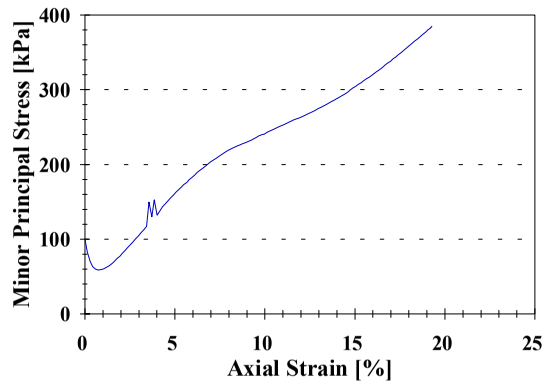

ϕ = 34.3 Confining stress = 100 kPa

GDS OS#55 GS#40

Date: 10/07/99 Fines= 25 e= 0.372 ec= 0.829 ef= n.a. (ef)eq= n.a. (ec)eq= 0.688

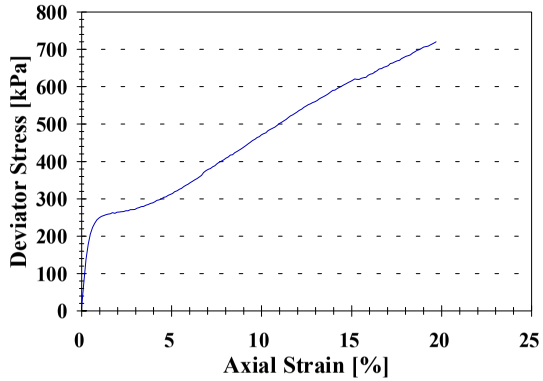

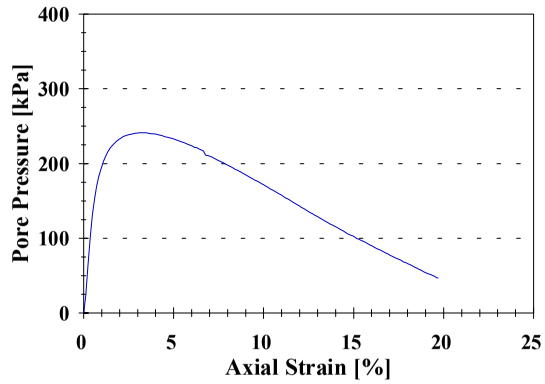

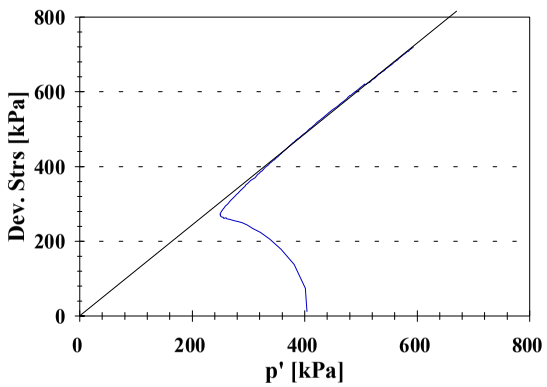

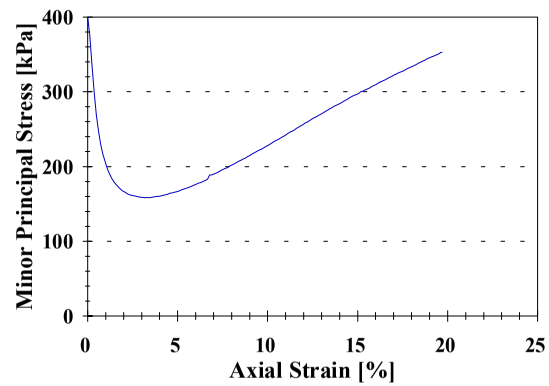

$\phi =$ 30.7 Confining Stress = 400 kPa

GDS OS#55 GS#40

Date: 10/08/99 Fines= 25 e= 0.439 ec= 0.918 ef= 1.754 (ef)eq= 1.087 (ec)eq 0.770

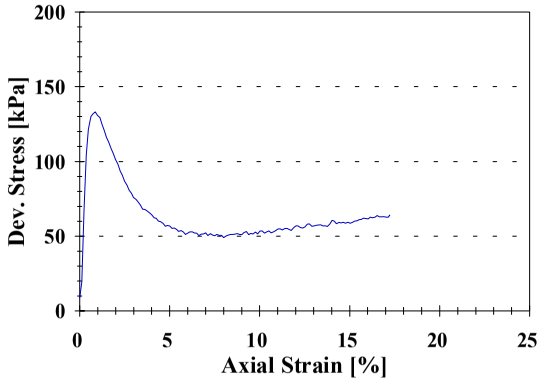

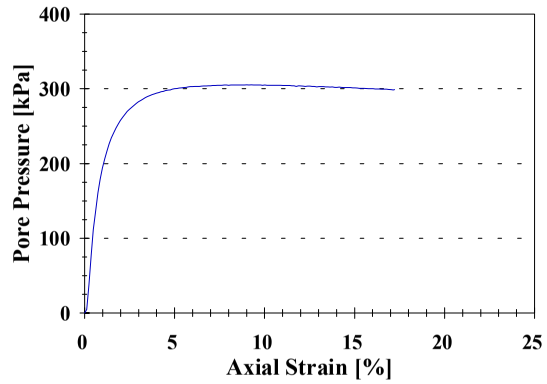

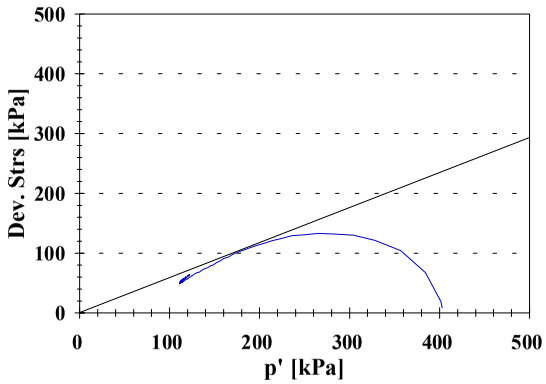

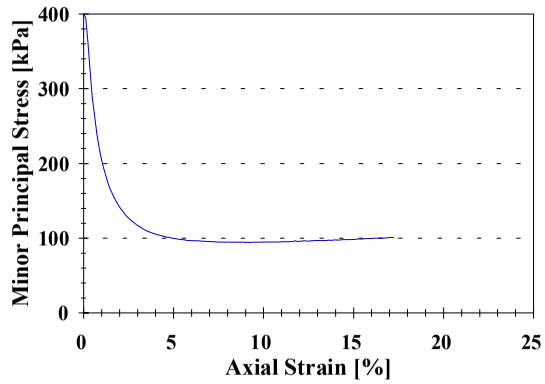

$\phi =$ 15.5 Confining Stress = 400 kPa

GDS OS#55 GS#40

Date: 10/20/99 Fines= 25 e= 0.441 ec= 0.922 ef= n.a. (ef)eq= n.a. (ec)eq= 0.774

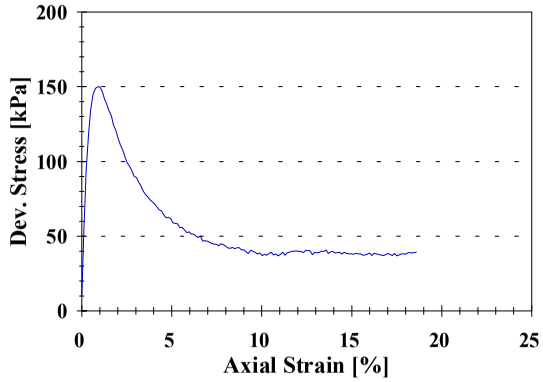

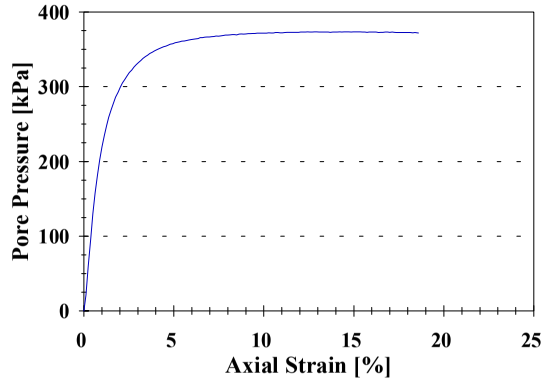

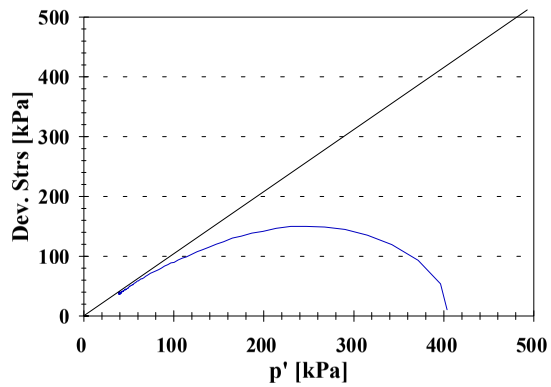

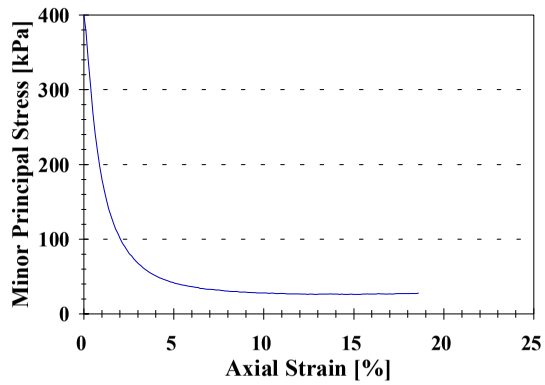

$\phi =$ 22.9 Confining Stress= 400 kPa

GDS OS#55 GS#40

Date: 10/25/99 Fines= 25 e= 0.458 es= 0.944 ef= n.a. (ef)eq= n.a. (ec)eq= 0.794

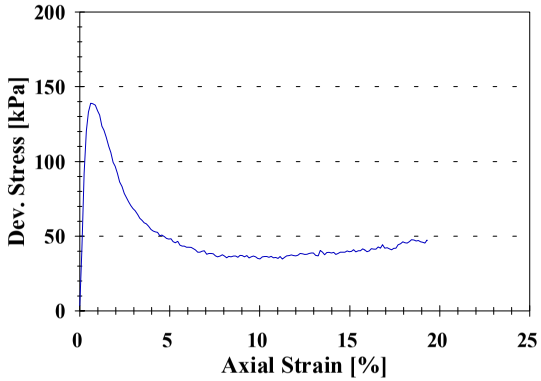

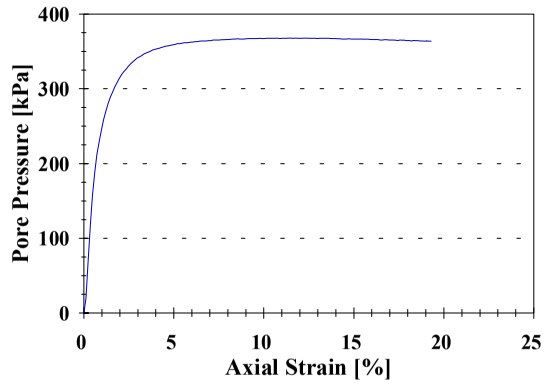

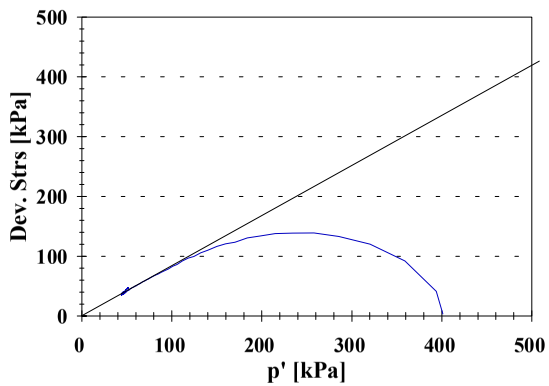

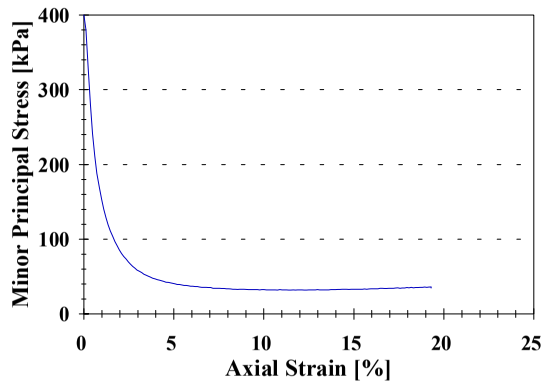

$\phi =$ 21.5 Confining Stress = 400 kPa

GDS OS#55 GS#40

Date: 10/27/99 Fines= 25 e= 0.474 ec= 0.966 ef= n.a. (ef)eq= n.a. (ec)eq= 0.815

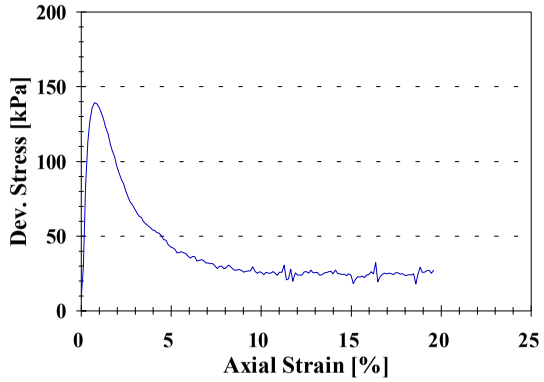

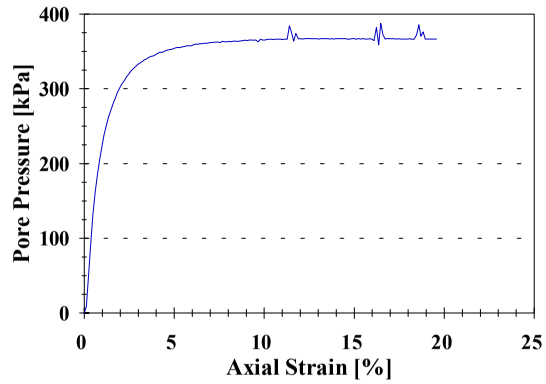

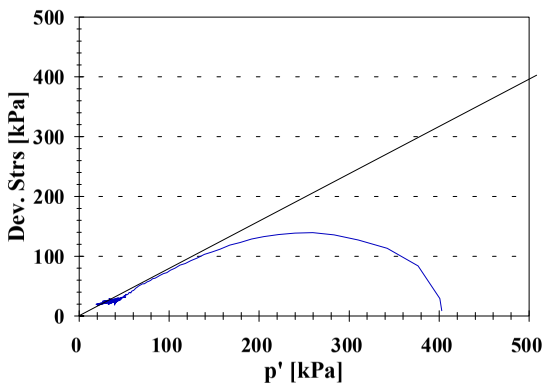

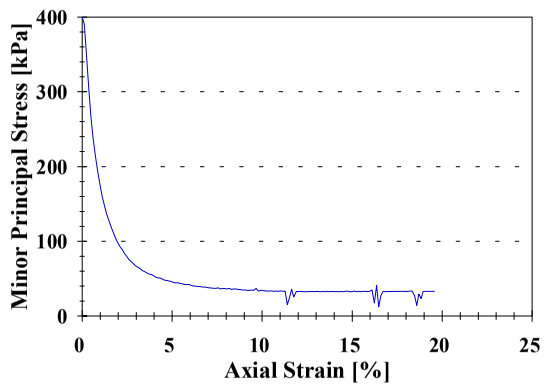

ϕ = 20.7 Confining stress = 400 kPa

GDS OS#55 GS#40

Date: 08/16/99 Fines= 40 e= 0.408 ec= n.a. ef= 1.019 (ef)eq= 0.780

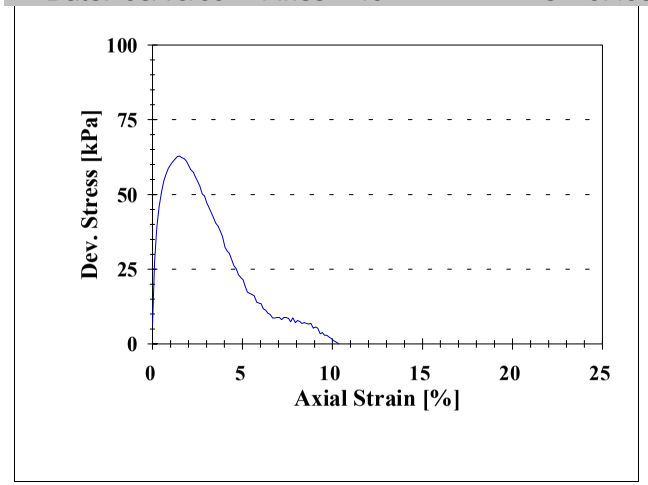

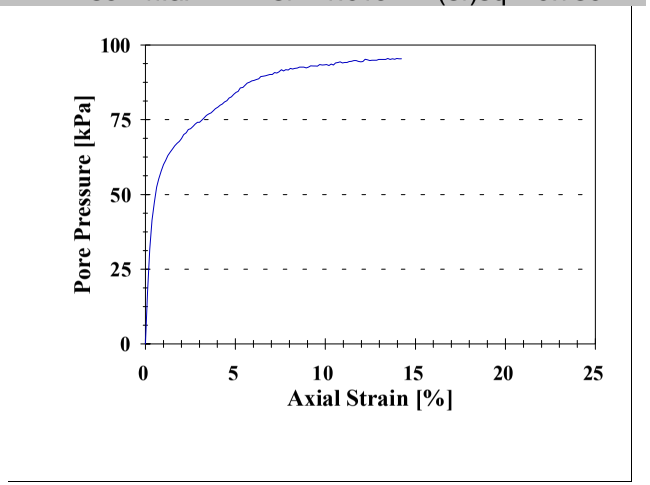

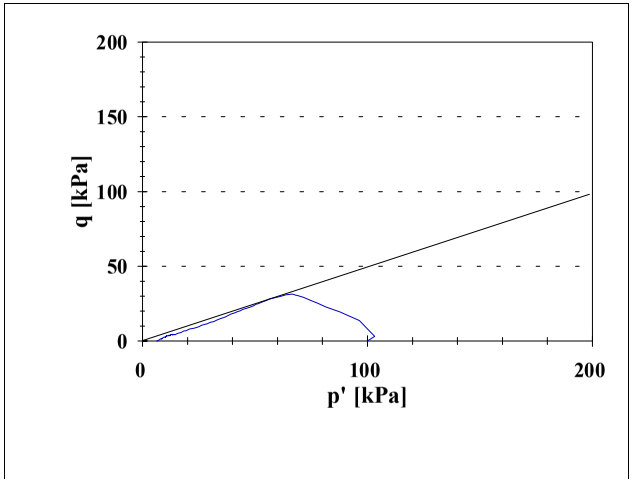

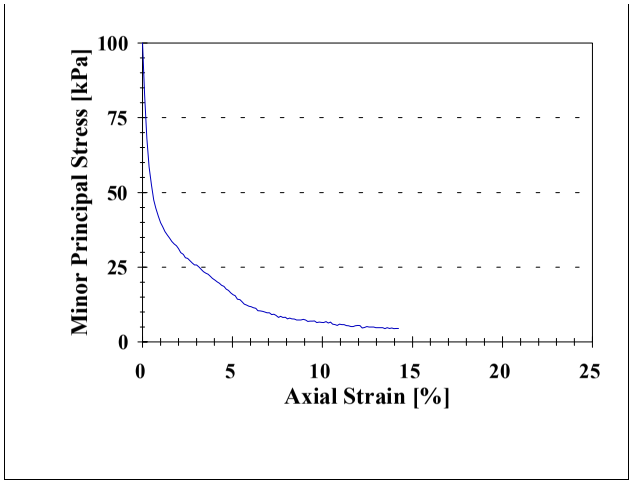

ϕ= 30.0 Confining stress = 100 kPa

Test Information Summary Table

Test Date: 9/24/99

Test Mode:	Geocomp		
File Name:	r092499	Fine Content (%):	40
Soil Type:	OSF55-40	Preparation Method:	MT
Dry Soil Weight (g):	1140	Initial Water in Sample (g) (preparation):	180.1
Sample Height (cm):	157	Final Water in Sample (g) (shear phase):	170.2
Final B Value:	0.93	Void Ratio:	0.396
Intergranular Void Ratio:	1.327	Interfine Void Ratio:	0.990
Final Consolidation Confining Stress (kPa)	100	Final Strain (%):	18
Final Cell Pressure (kPa):	655	Calculated Friction Angle:	29
Final Back Pressure (kPa):	627	Young's Modulus E (0.05%) (kPa):	29687
Final Shear Induced Pore Pressure (kPa):	72	Shear Modulus G (0.05%) (kPa):	9896
Final Effective Mean Stress p' (kPa):	44	Final Effective Sigma1 (kPa):	77
Final Effective Deviatoric Stress q' (kPa):	49	Final Effective Sigma3 (kPa):	28

sig3' vs strain

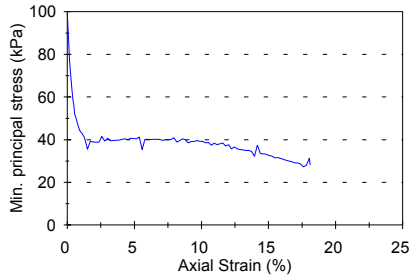

dev stress vs strain (overall)

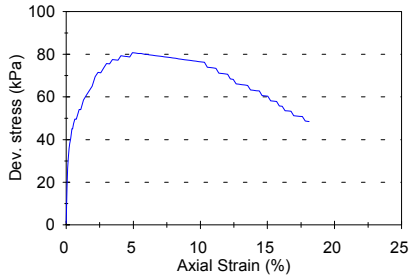

p(3)-q

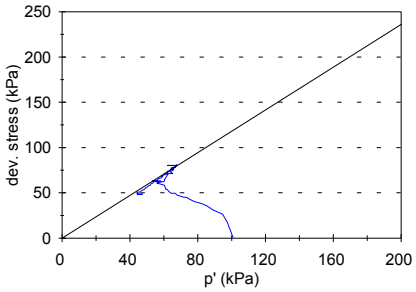

dev stress vs strain (2%)

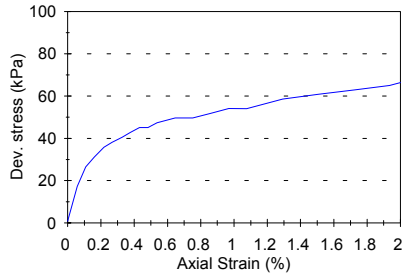

U (sh)

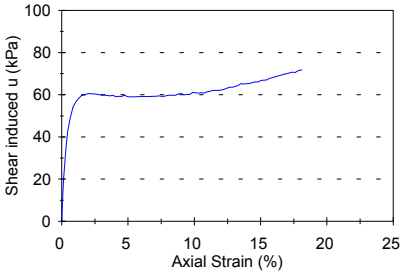

Test Information Summary Table

Test Date: 10/04/99

Test Mode:	Geocomp		
File Name:	r100499	Fine Content (%):	40
Soil Type:	OSF55-40	Preparation Method:	MT
Dry Soil Weight (g):	1103.8	Initial Water in Sample (g) (preparation):	182.7
Sample Height (cm):	157	Final Water in Sample (g) (shear phase):	172.0
Final B Value:	0.93	Void Ratio:	0.413
Intergranular Void Ratio:	1.355	Interfine Void Ratio:	1.033
Final Consolidation Confining Stress (kPa):	100	Final Strain (%):	19
Final Cell Pressure (kPa):	680	Calculated Friction Angle:	28
Final Back Pressure (kPa):	676	Young's Modulus E (0.05%) (kPa):	34014
Final Shear Induced Pore Pressure (kPa):	95	Shear Modulus G (0.05%) (kPa):	11338
Final Effective Mean Stress p' (kPa):	4	Final Effective Sigma1 (kPa):	4
Final Effective Deviatoric Stress q' (kPa):	0	Final Effective Sigma3 (kPa):	4

sig3' vs strain

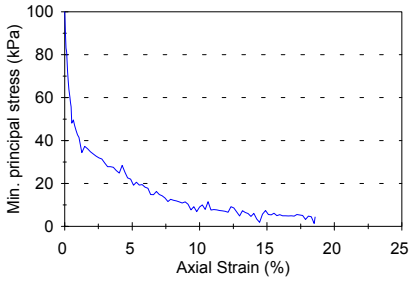

dev stress vs strain (overall)

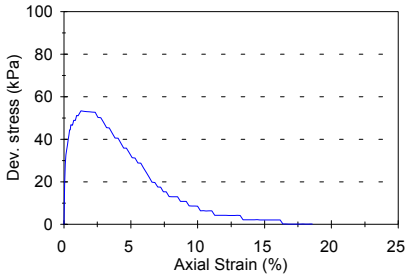

p(3)-q

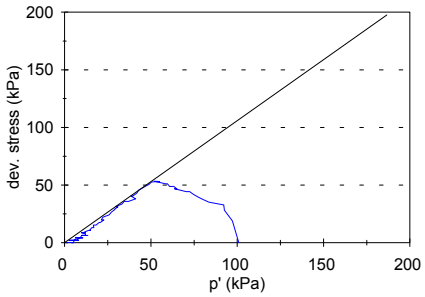

dev stress vs strain (2%)

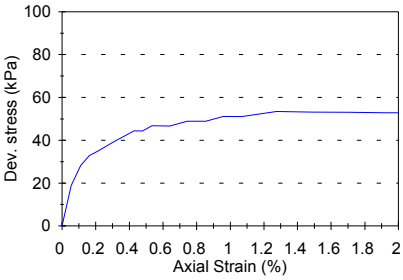

U (sh)

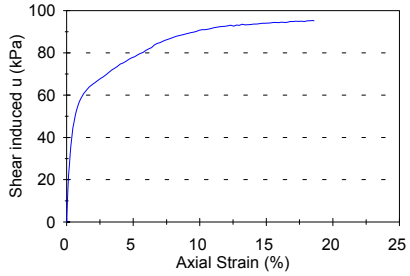

Test Information Summary Table

Test Date: 10/22/99

Test Mode:	Geocomp		
File Name:	r102299	Fine Content (%):	40
Soil Type:	OSF55-40	Preparation Method:	MT
Dry Soil Weight (g):	984.6	Initial Water in Sample (g) (preparation):	149.9
Sample Height (cm):	148	Final Water in Sample (g) (shear phase):	138.4
Final B Value:	0.90	Void Ratio:	0.373
Intergranular Void Ratio:	1.288	Interfine Void Ratio:	0.932
Final Consolidation Confining Stress (kPa):	100	Final Strain (%):	21
Final Cell Pressure (kPa):	790	Calculated Friction Angle:	33
Final Back Pressure (kPa):	643	Young's Modulus E (0.05%) (kPa):	37439
Final Shear Induced Pore Pressure (kPa):	-48	Shear Modulus G (0.05%) (kPa):	12480
Final Effective Mean Stress p' (kPa):	246	Final Effective Sigma1 (kPa):	443
Final Effective Deviatoric Stress q' (kPa):	297	Final Effective Sigma3 (kPa):	147

sig3' vs strain

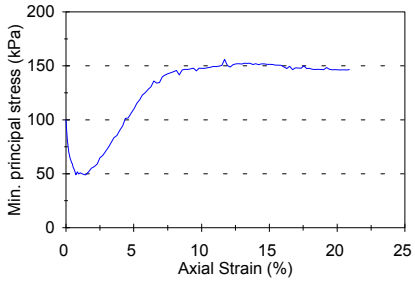

dev stress vs strain (overall)

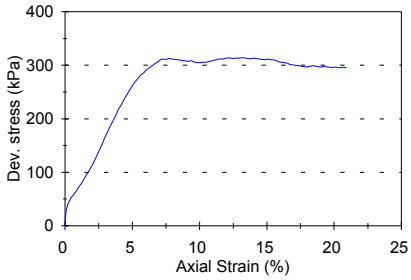

p(3)-q

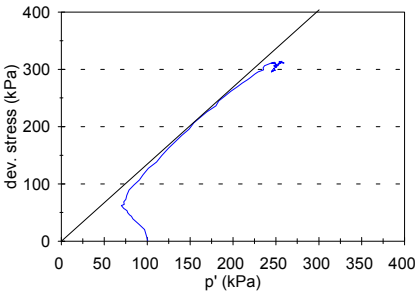

dev stress vs strain (2%)

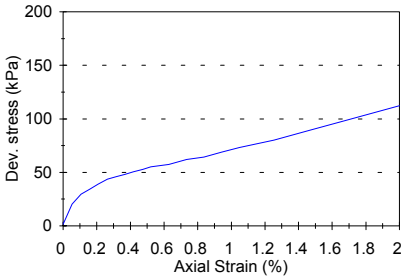

U (sh)

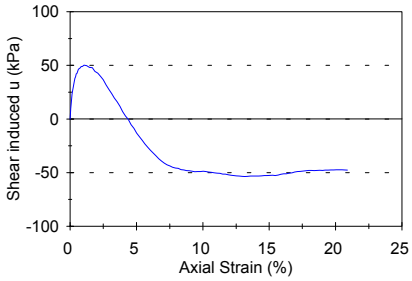

GEOCOMP OS#55 GSF#40

Date: 11/23/99 e = 0.398 ec= n.a. ef = 0.995 (ef)eq= 0.761

sig3' vs strain

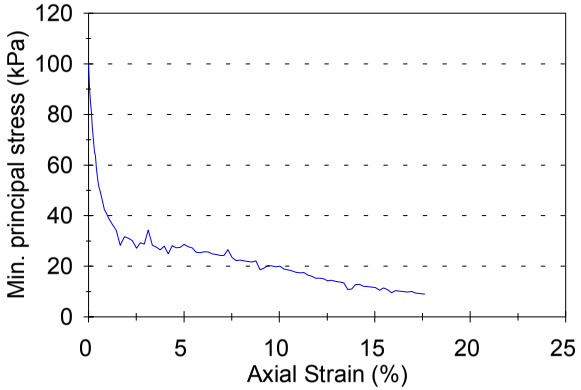

dev stress vs strain

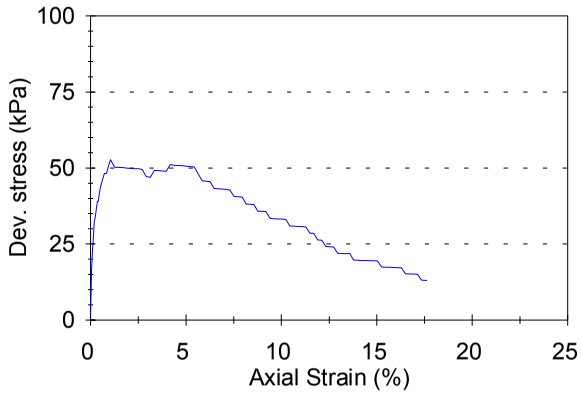

U(sh)

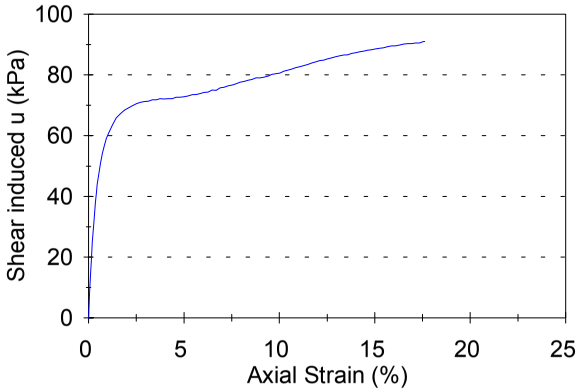

p(3)-q

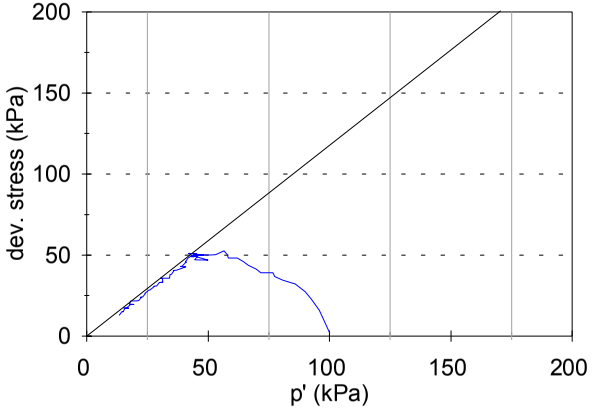

Fines = 40% Confining stress = 100 kPa ϕ = 29.5

GDS OS#55 GS#40

Date: 01/13/00 Fines= 40 e= 0.412 ec= n.a. ef= 1.031 (ef)eq= 0.789 (ec)eq= n.a.

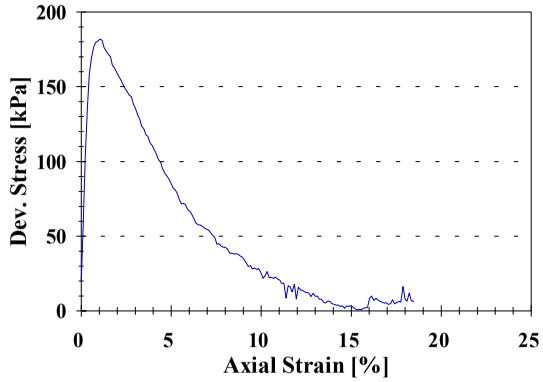

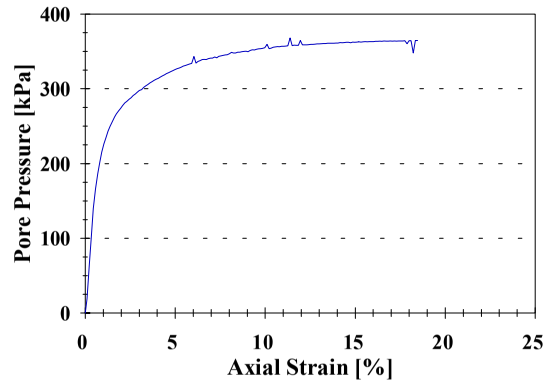

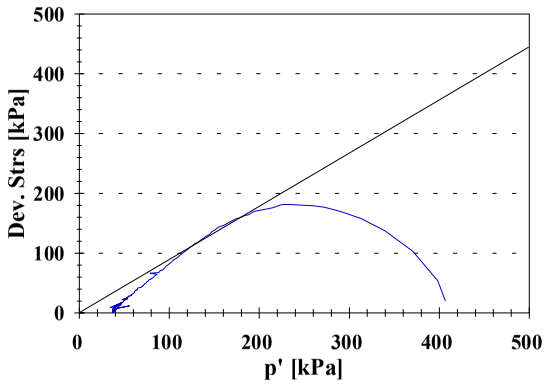

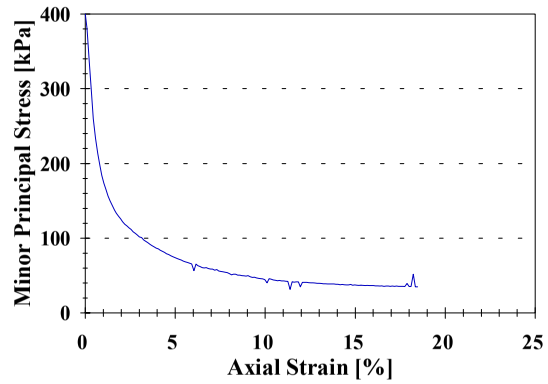

$\phi =$ 22.6 Confining stress = 400 kPa

GDS OS#55 GS#40

Date: 01/18/99 Fines= 40 e= 0.394 ec= n.a. ef= 0.984 (ef)eq= 0.753 (ec)eq= n.a.

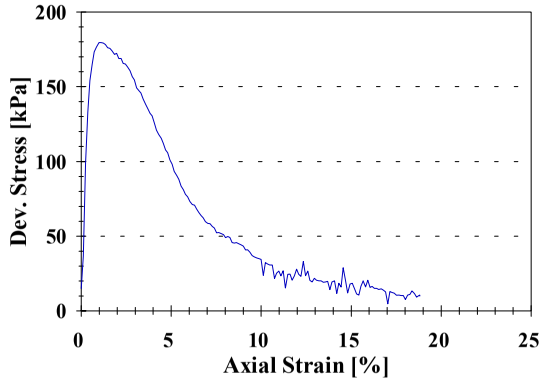

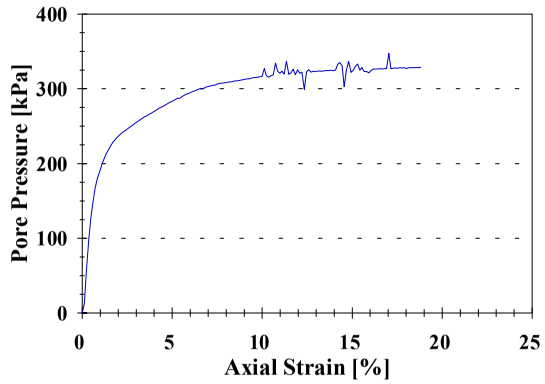

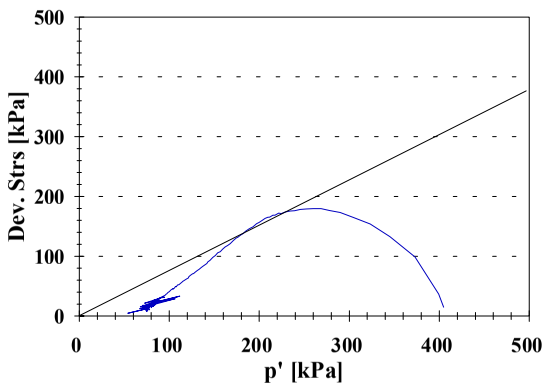

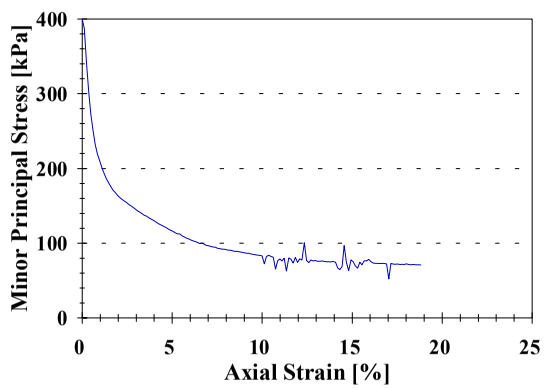

ϕ = 19.7 Confining stress = 400 kPa

Test Information Summary Table

Test Date: 8/19/99

Test Mode:	Geocomp		
File Name:	r081999	Fine Content (%):	60
Soil Type:	OSF55-40	Preparation Method:	MT
Dry Soil Weight (g):	1068.6	Initial Water in Sample (g) (preparation):	215.4
Sample Height (cm):	15.9	Final Water in Sample (g) (shear phase):	207.8
Final B Value:	0.95	Void Ratio:	0.515
Intergranular Void Ratio:	2.788	Interfine Void Ratio:	0.858
Final Consolidation Confining Stress (kPa):	100	Final Strain (%):	18
Final Cell Pressure (kPa):	640	Calculated Friction Angle:	32
Final Back Pressure (kPa):	545	Young's Modulus E (0.05%) (kPa):	39747
Final Shear Induced Pore Pressure (kPa):	5	Shear Modulus G (0.05%) (kPa):	13249
Final Effective Mean Stress p' (kPa):	158	Final Effective Sigma1 (kPa):	284
Final Effective Deviatoric Stress q' (kPa):	189	Final Effective Sigma3 (kPa):	95

sig3' vs strain

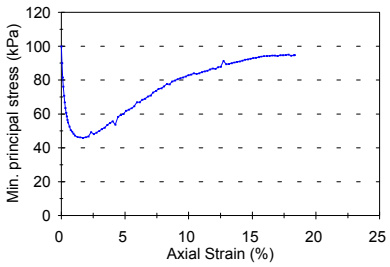

dev stress vs strain (overall)

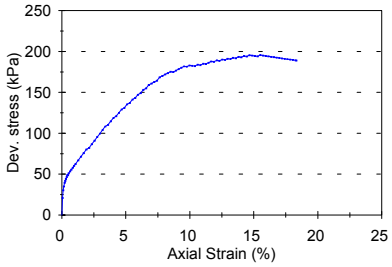

p(3)-q

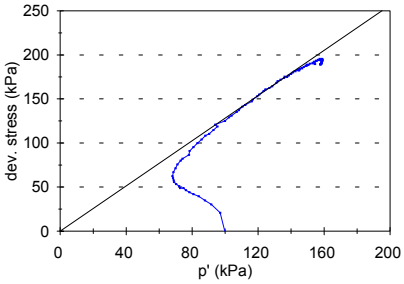

dev stress vs strain (2%)

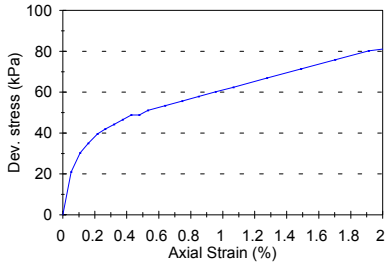

U (sh)

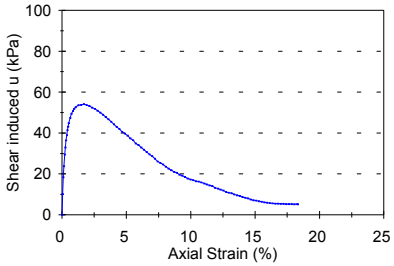

Test Information Summary Table

Test Date: 8/20/99

Test Mode:	Geocomp		
File Name:	r082099	Fine Content (%):	60
Soil Type:	OSF55-40	Preparation Method:	MT
Dry Soil Weight (g):	994.7	Initial Water in Sample (g) (preparation):	202.8
Sample Height (cm):	15.2	Final Water in Sample (g) (shear phase):	194.0
Final B Value:	0.96	Void Ratio:	0.517
Intergranular Void Ratio:	2.793	Interfine Void Ratio:	0.862
Final Consolidation Confining Stress (kPa):	100	Final Strain (%):	20
Final Cell Pressure (kPa):	600	Calculated Friction Angle:	33
Final Back Pressure (kPa):	520	Young's Modulus E (0.05%) (kPa):	38022
Final Shear Induced Pore Pressure (kPa):	20	Shear Modulus G (0.05%) (kPa):	12674
Final Effective Mean Stress p' (kPa):	137	Final Effective Sigma1 (kPa):	252
Final Effective Deviatoric Stress q' (kPa):	172	Final Effective Sigma3 (kPa):	80

sig3' vs strain

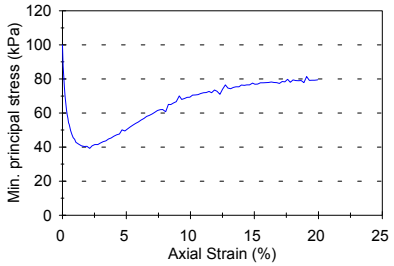

dev stress vs strain (overall)

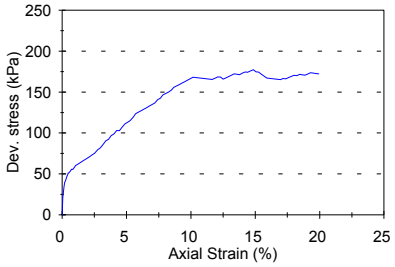

p(3)-q

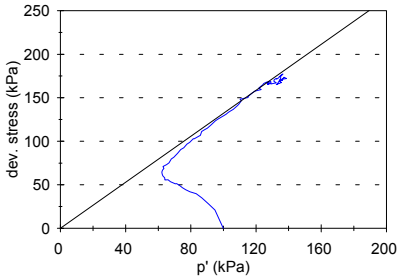

dev stress vs strain (2%)

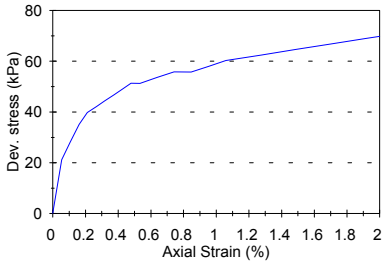

U (sh)

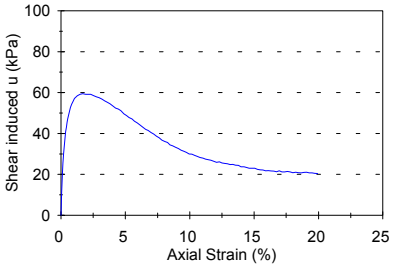

Test Information Summary Table

Test Date: 8/25/99

Test Mode:	Geocomp		
File Name:	r082599	Fine Content (%):	60
Soil Type:	OSF55-40	Preparation Method:	MT
Dry Soil Weight (g):	967.2	Initial Water in Sample (g) (preparation):	198.0
Sample Height (cm):	15.6	Final Water in Sample (g) (shear phase):	188.3
Final B Value:	0.95	Void Ratio:	0.516
Intergranular Void Ratio:	2.790	Interfine Void Ratio:	0.860
Final Consolidation Confining Stress (kPa):	100	Final Strain (%):	21
Final Cell Pressure (kPa):	650	Calculated Friction Angle:	31
Final Back Pressure (kPa):	581	Young's Modulus E (0.05%) (kPa):	38270
Final Shear Induced Pore Pressure (kPa):	30	Shear Modulus G (0.05%) (kPa):	12757
Final Effective Mean Stress p' (kPa):	112	Final Effective Sigma1 (kPa):	199
Final Effective Deviatoric Stress q' (kPa):	130	Final Effective Sigma3 (kPa):	69

sig3' vs strain

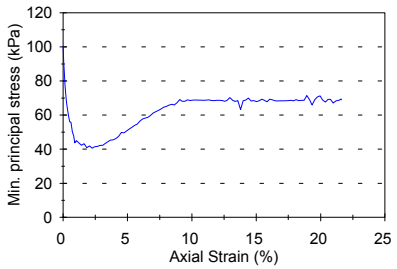

dev stress vs strain (overall)

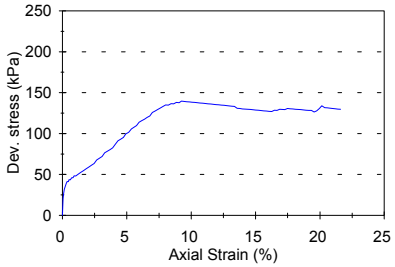

p(3)-q

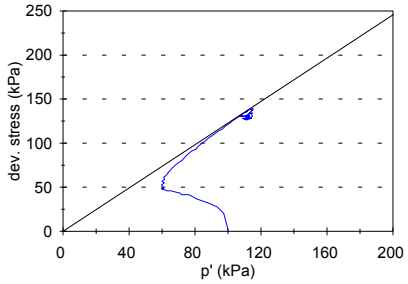

dev stress vs strain (2%)

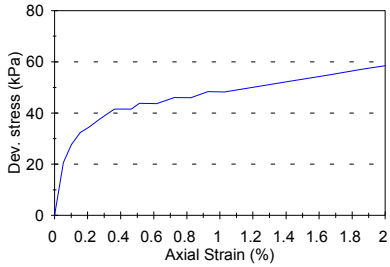

U (sh)

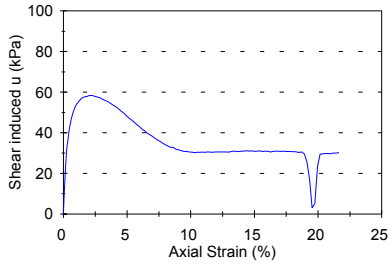

Test Information Summary Table

Test Date: 8/26/99

Test Mode:	Geocomp		
File Name:	r082699	Fine Content (%):	60
Soil Type:	OSF55-40	Preparation Method:	MT
Dry Soil Weight (g):	906.5	Initial Water in Sample (g) (preparation):	180.8
Sample Height (cm):	15.1	Final Water in Sample (g) (shear phase):	170.4
Final B Value:	0.90	Void Ratio:	0.498
Intergranular Void Ratio:	2.745	Interfine Void Ratio:	0.830
Final Consolidation Confining Stress (kPa):	100	Final Strain (%):	21
Final Cell Pressure (kPa):	730	Calculated Friction Angle:	32
Final Back Pressure (kPa):	622	Young's Modulus E (0.05%) (kPa):	33657
Final Shear Induced Pore Pressure (kPa):	-8	Shear Modulus G (0.05%) (kPa):	11219
Final Effective Mean Stress p' (kPa):	180	Final Effective Sigma1 (kPa):	324
Final Effective Deviatoric Stress q' (kPa):	216	Final Effective Sigma3 (kPa):	107

sig3' vs strain

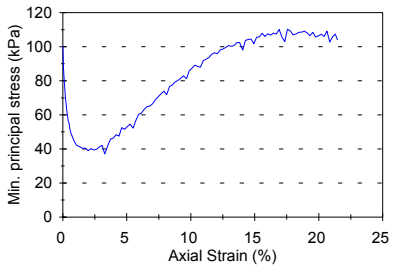

dev stress vs strain (overall)

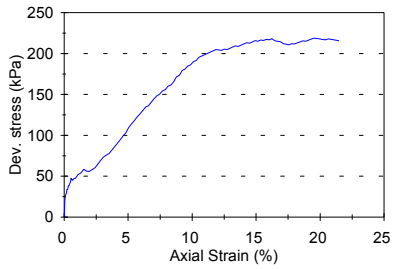

p(3)-q

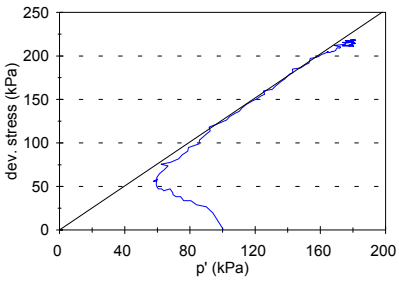

dev stress vs strain (2%)

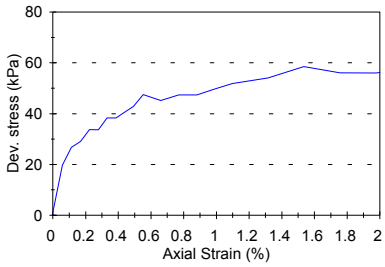

U (sh)

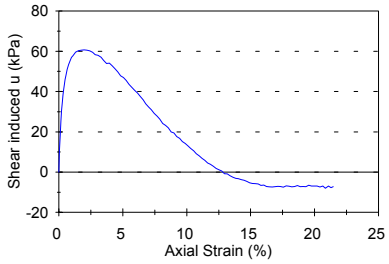

GDS OS#55 GS#40

Date: 08/18/99 Fines= 60 e= 0.552 ec= n.a. ef= 0.920 (ef)eq= 0.849

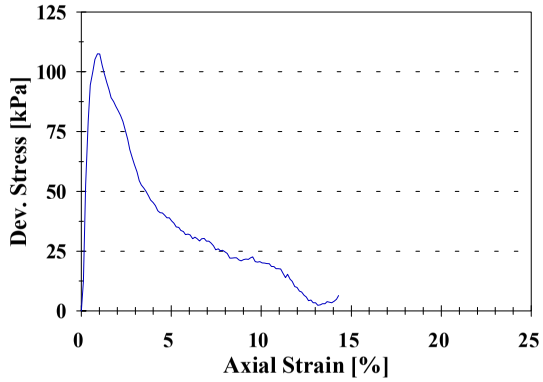

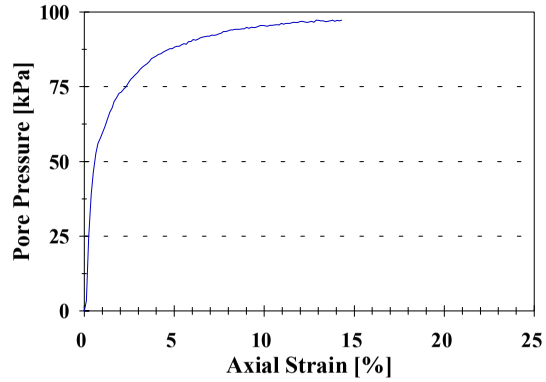

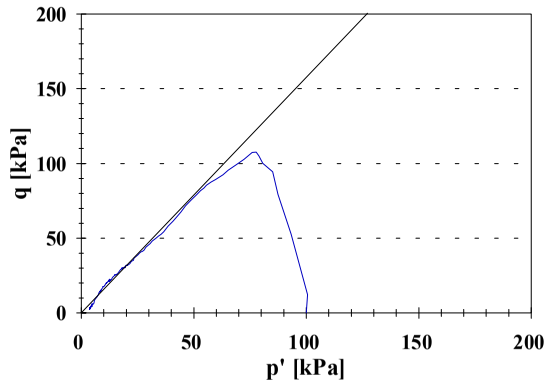

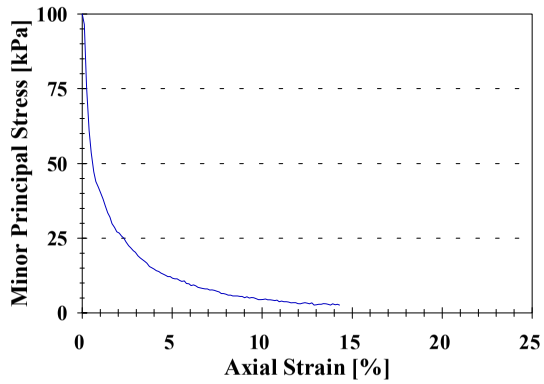

ϕ= 38.7 Confining stress = 100 kPa

GDS OS#55 GS#40

Date: 09/03/99 Fines= 60 e= 0.531 ec= n.a. ef= 0.885 (ef)eq= 0.818

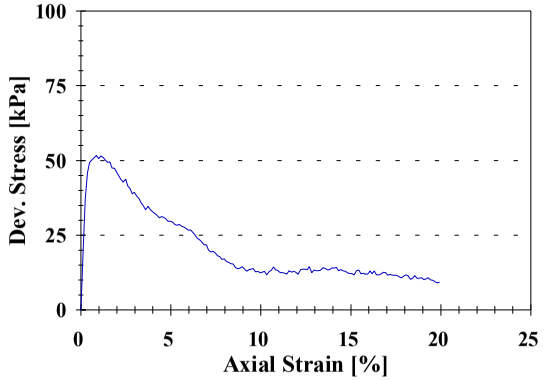

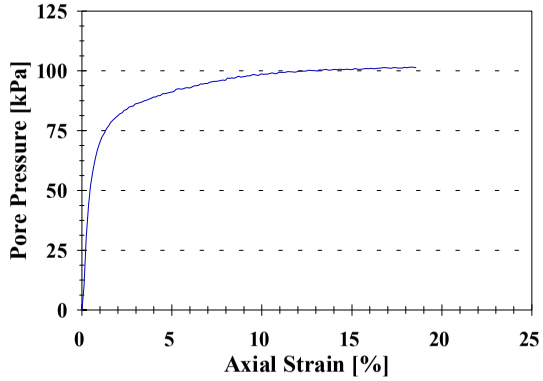

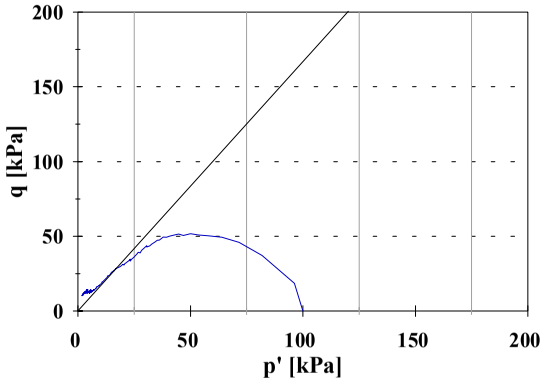

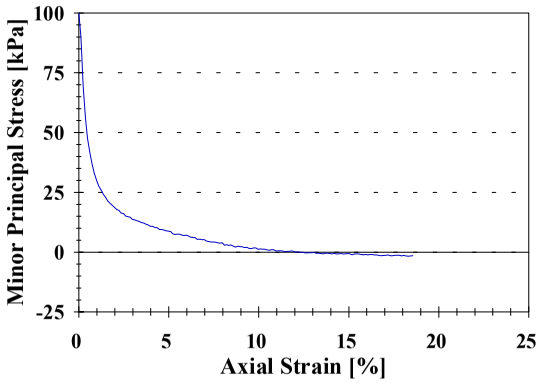

ϕ= 34.8 Confining stress = 100 kPa

GDS OS#55 GS#40

Date: 09/14/99 Fines= 60 e= 0.540 ec= n.a. ef= 0.900 (ef)eq= 0.792

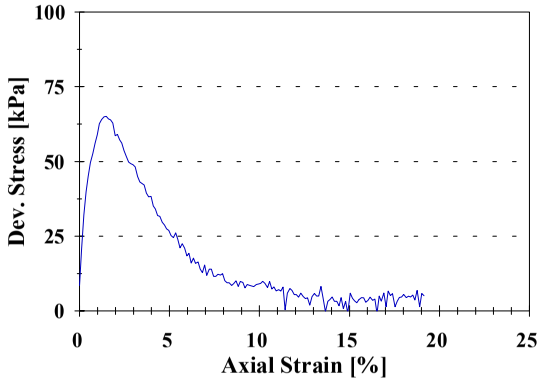

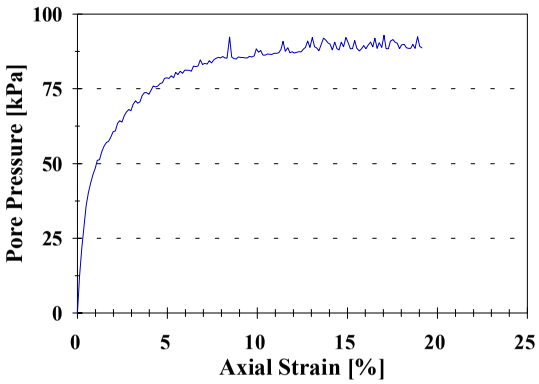

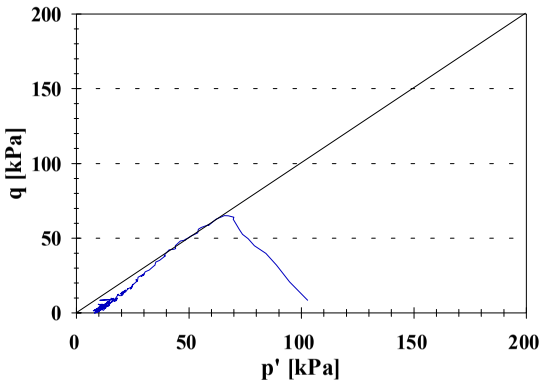

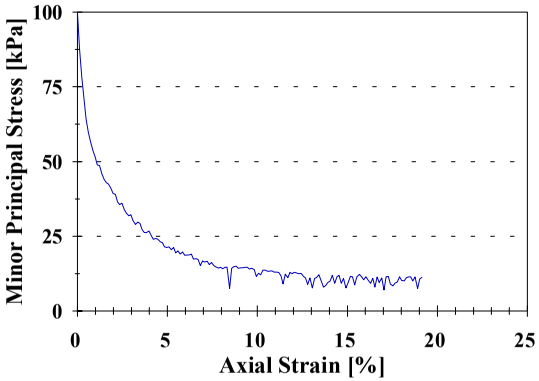

ϕ= 25.8 Confining stress = 100 kPa

GDS OS#55 GS#40

Date: 02/01/00 Fines= 60 e= 0.610 ec= n.a. ef= 1.017 (ef)eq= 0.895 (ec)eq= n.a.

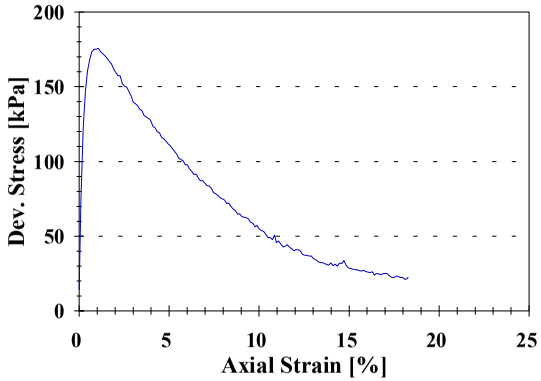

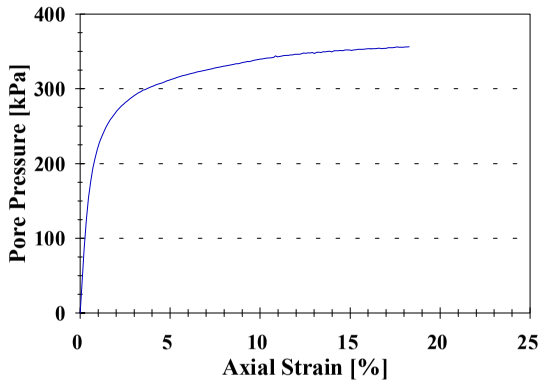

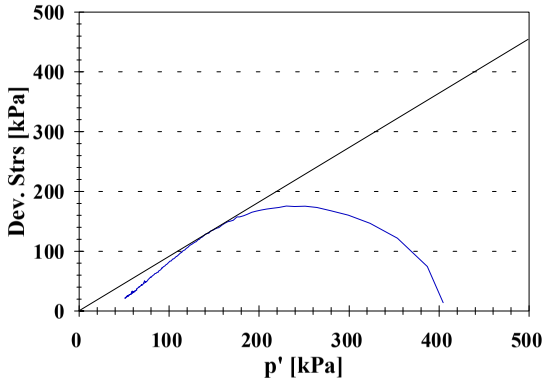

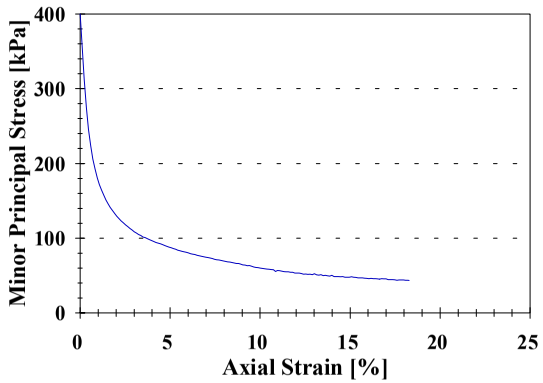

ϕ = 23.2 Confining stress = 400 kPa

GDS OS#55 GS#40

Date: 02/09/00 Fines= 60 e= 0.559 ec= n.a. ef= 0.932 (ef)eq= 0.820 (ec)eq= n.a.

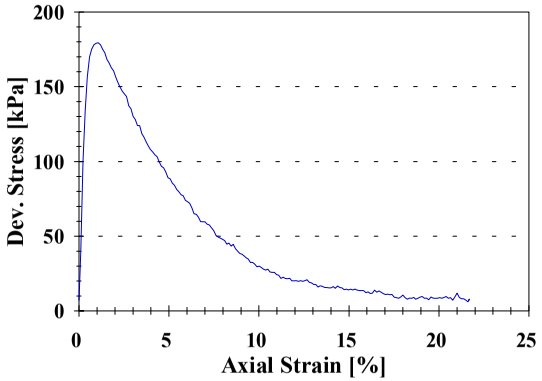

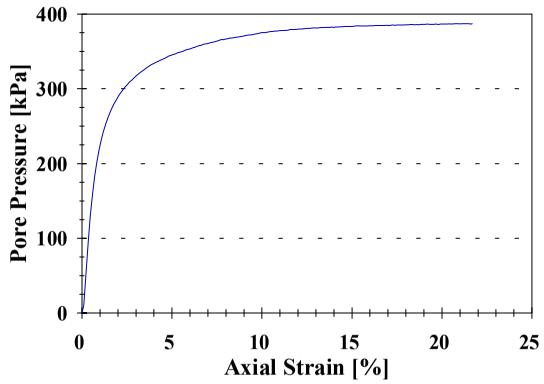

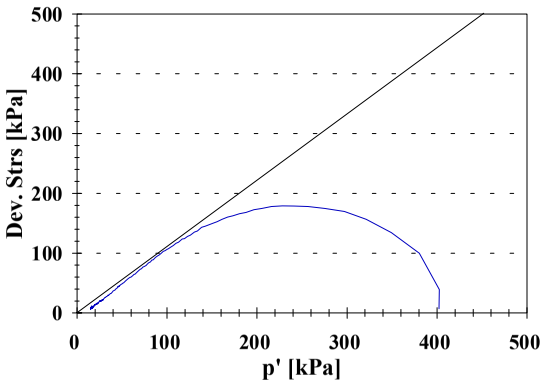

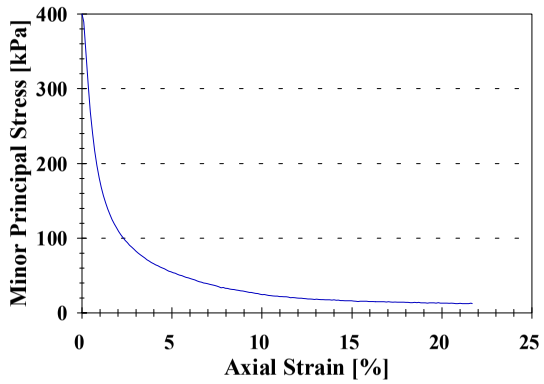

ϕ = 28.0 Confining stress = 400 kPa

GDS OS#55 GS#40

Date: 02/16/00 Fines= 60 e= 0.549 ec= n.a. ef= 0.915 (ef)eq= 0.805 (ec)eq= n.a.

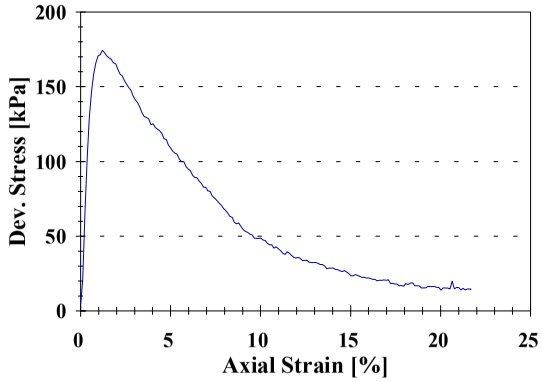

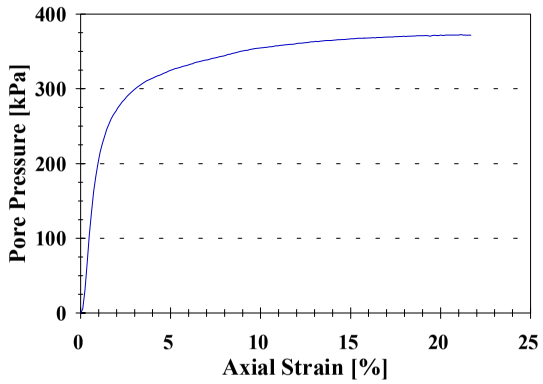

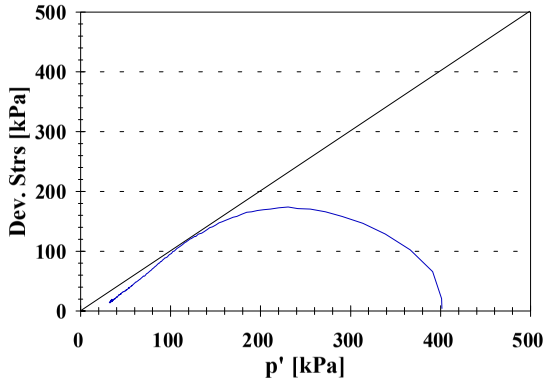

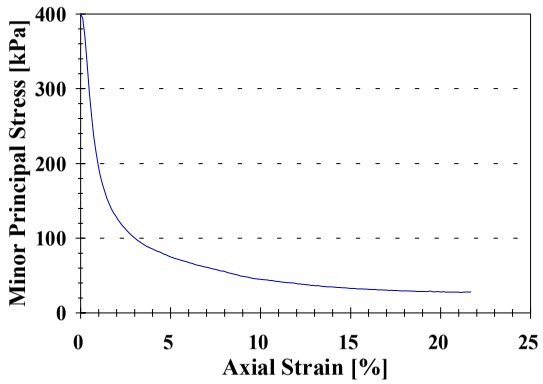

ϕ = 25.4 Confining stress = 400 kPa

GDS OS#55 GS#40

Date: 02/18/00 Fines= 60 e= 0.532 ec= n.a. ef= 0.887 (ef)eq= 0.781 (ec)eq= n.a.

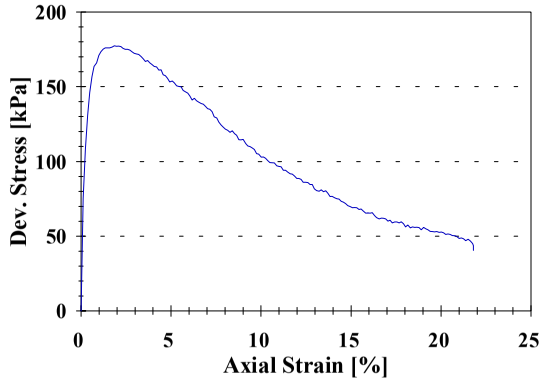

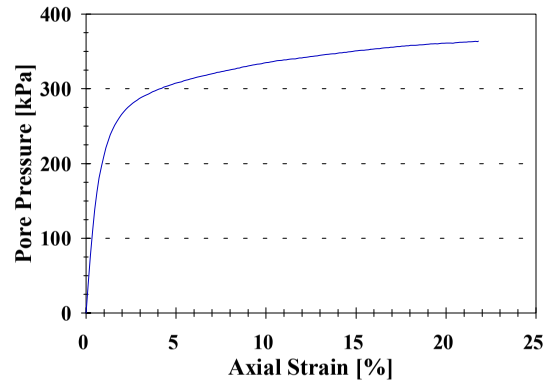

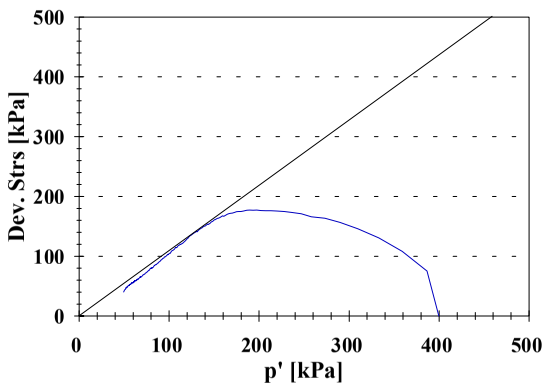

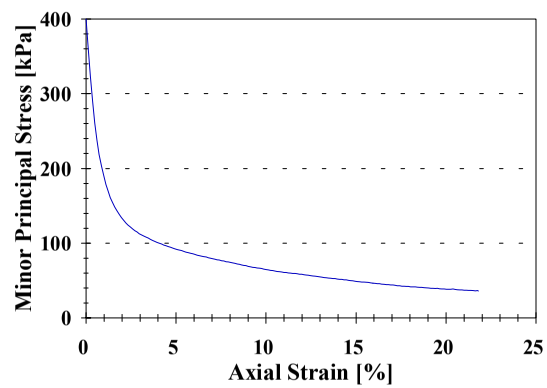

ϕ = 28.0 Confining stress = 400 kPa

GDS GS#40

Date: 09/09/99 Fines= 100 e= 0.879 ef= 0.879 (ef)eq= 0.879

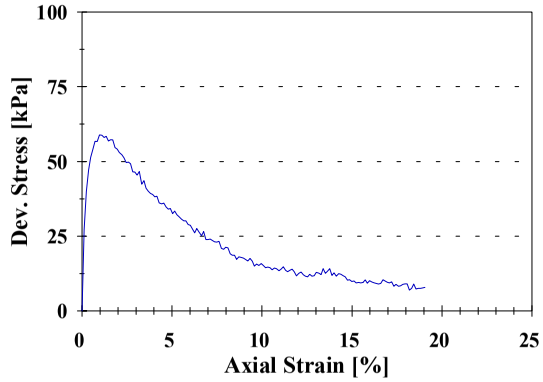

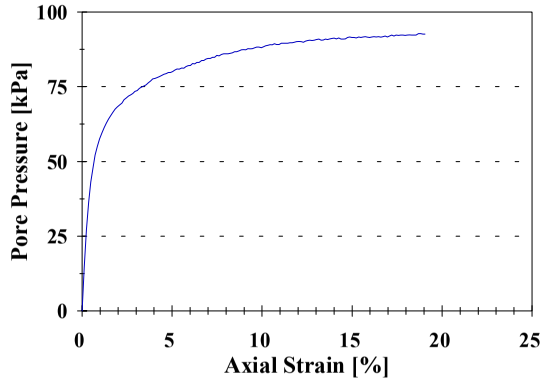

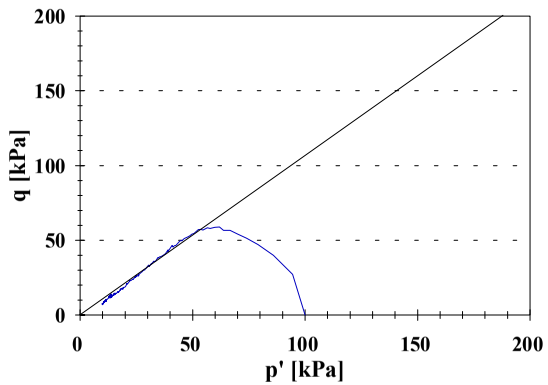

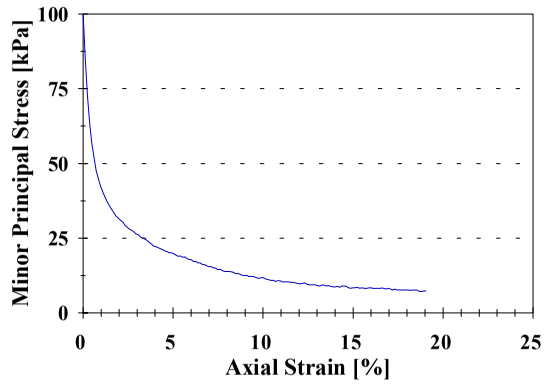

ϕ= 28.4 Confining stress = 100 kPa

GDS OS#55 GS#40

Date: 09/13/99 Fines= 100 e= 0.854 ef= 0.854 (ef)eq= 0.854

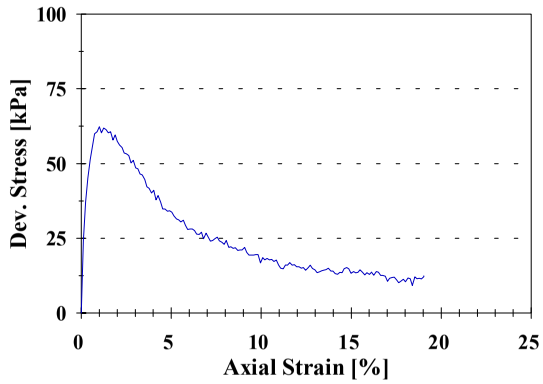

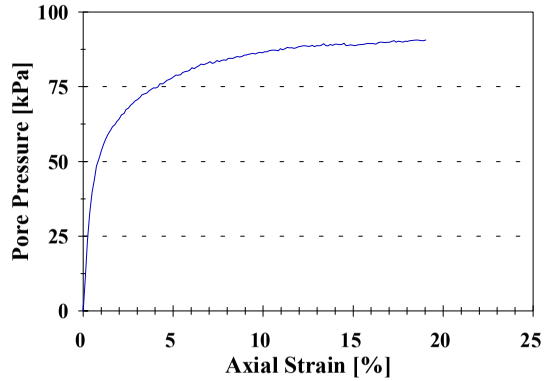

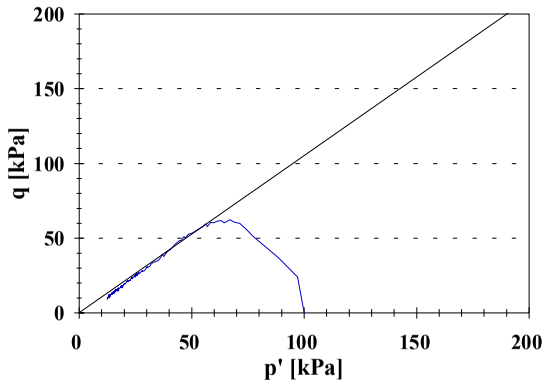

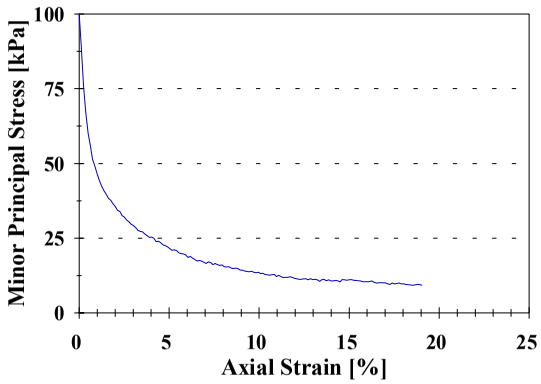

ϕ= 27.6 Confining stress= 100 kPa

GDS OS#55 GS#40

Date: 09/19/99 Fines= 100 e= 0.770 es= n.a. ef= 0.770 (ef)eq= 0.770

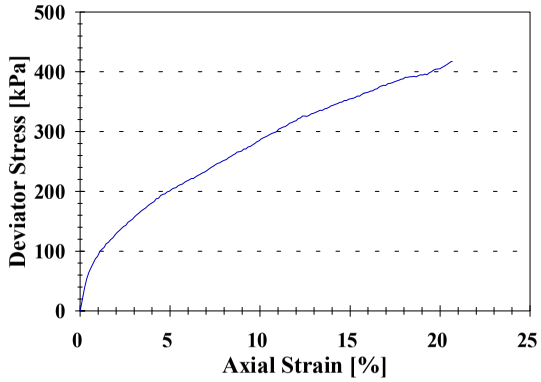

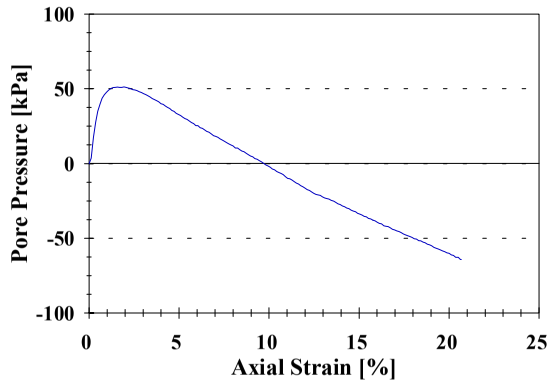

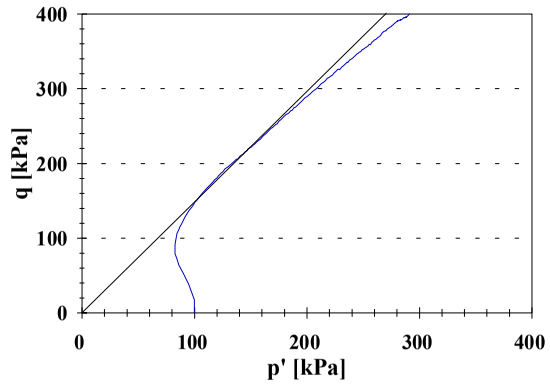

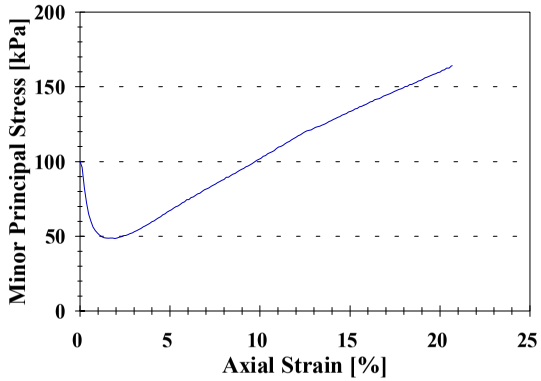

ϕ= 33.7 Confining stress= 100 kPa

GEOCOMP OS#55 GSF#40 Fines = 100%

Date: 9/27/99 e = 0.824 ef= 0.824 (ef)eq = 0.824

sig3' vs strain

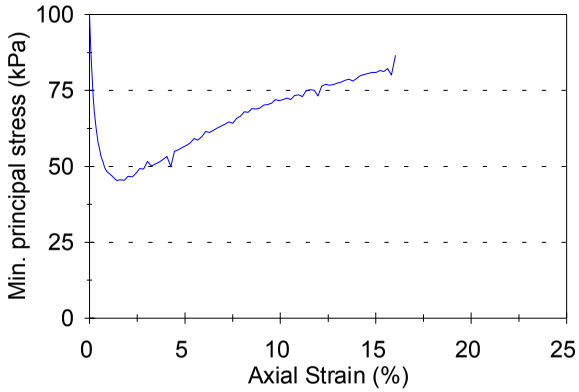

dev stress vs strain

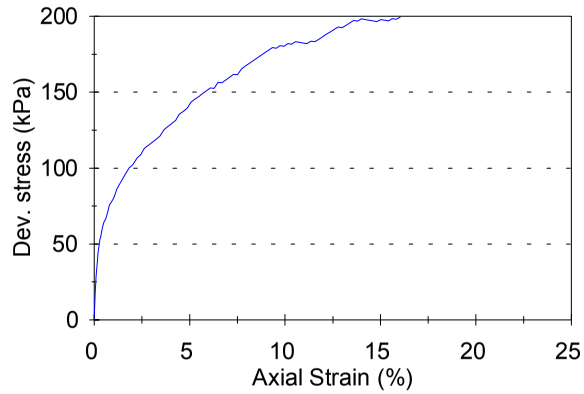

U(sh)

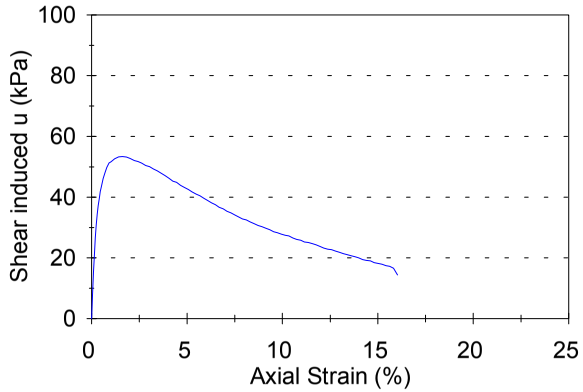

p'-q

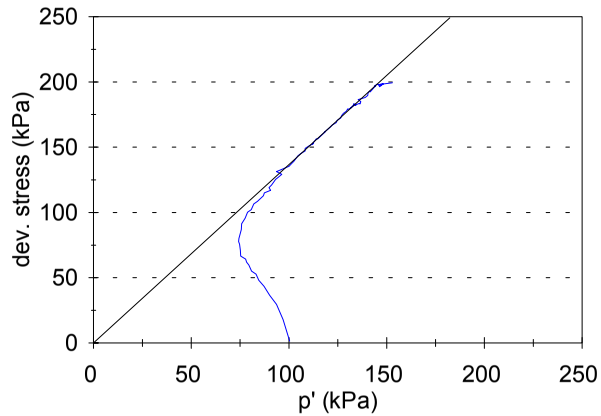

Confining stress = 100 kPa

ϕ = 34.3

GDS OS#55 GS#40

Date: 02/23/00 Fines= 100 e= 0.879 ec= n.a. ef= 0.879 (ef)eq= 0.879 (ec)eq= n.a.

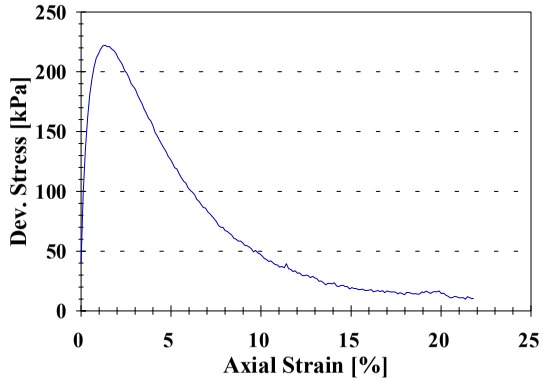

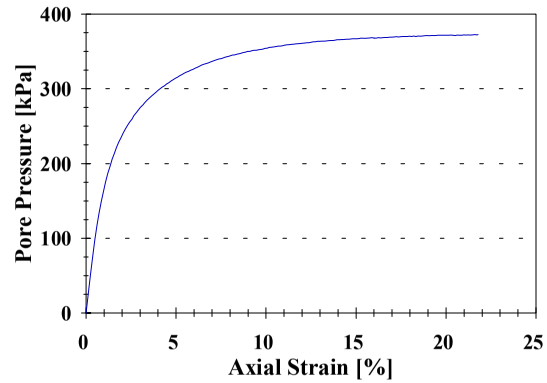

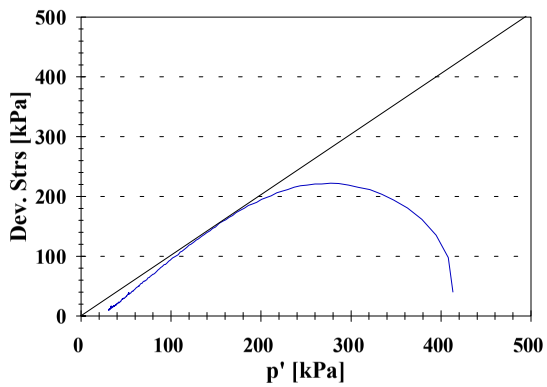

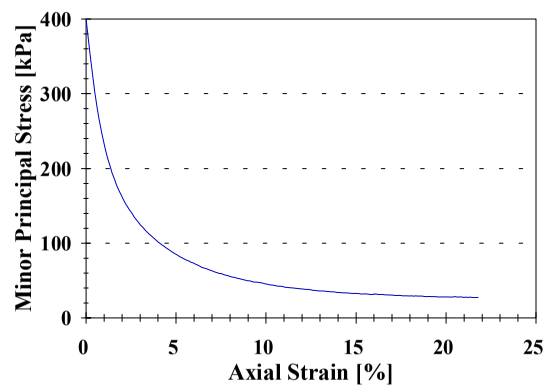

ϕ = 25.9 Confining stress = 400 kPa

GDS OS#55 GS#40

Date: 03/15/00 Fines= 100 e= 0.813 ec= n.a. ef= 0.813 (ef)eq= 0.813 (ec)eq= n.a.

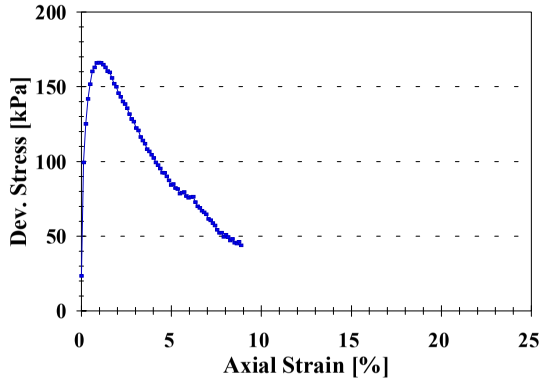

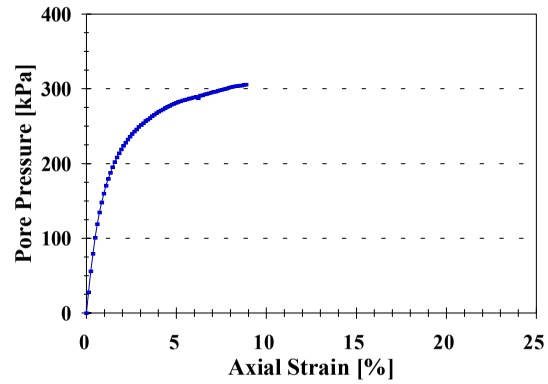

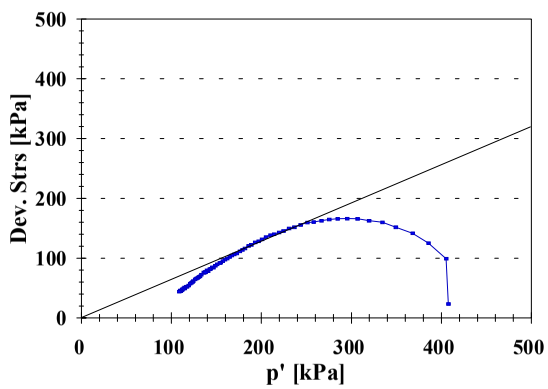

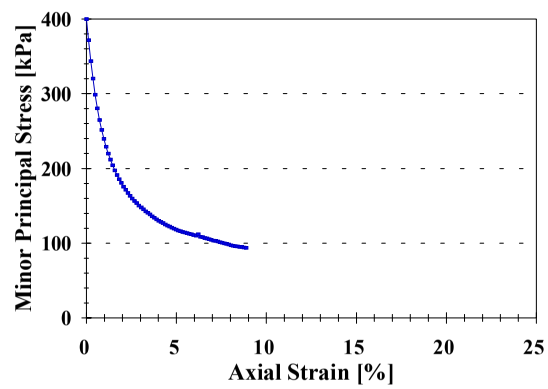

ϕ = 17.8 Confining stress = 400 kPa

GEOCOMP FJ#80

Date: 10/06/00	Fines= 0	e= 0.785	ec= 0.785	ef= n.a.	(ef)eq= n.a.	(ec)eq= 0.785

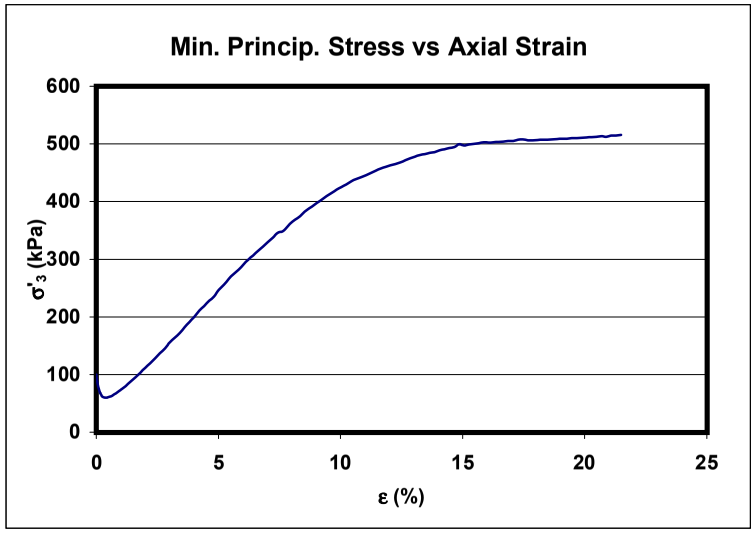

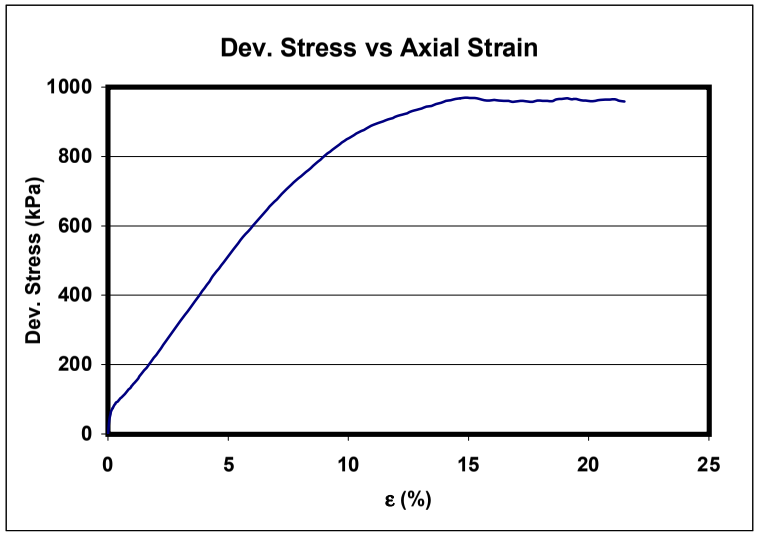

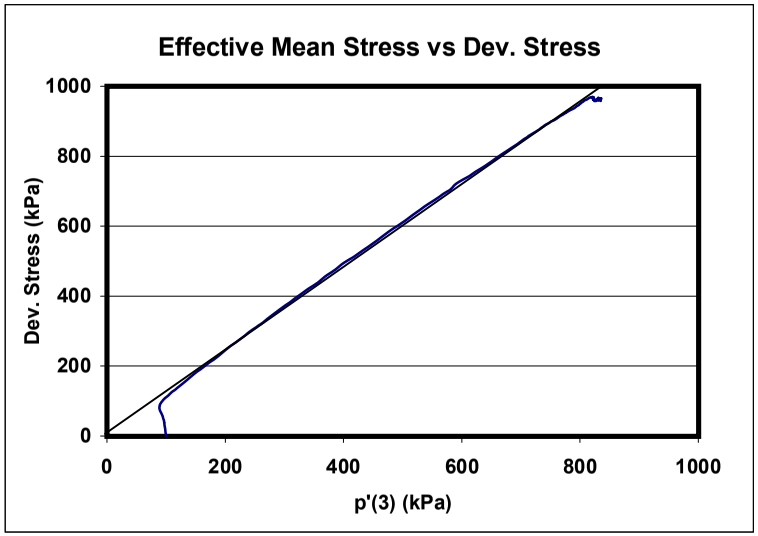

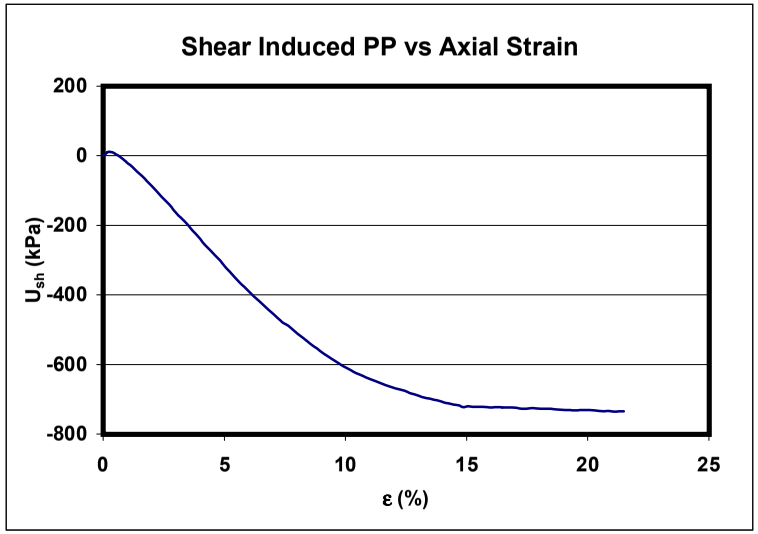

ϕ = 30.1 Confining stress = 100 kPa

GEOCOMP FJ#80

Date: 10/10/00	Fines= 0	e= 0.868	ec= 0.868	ef= n.a.	(ef)eq= n.a.	(ec)eq= 0.868

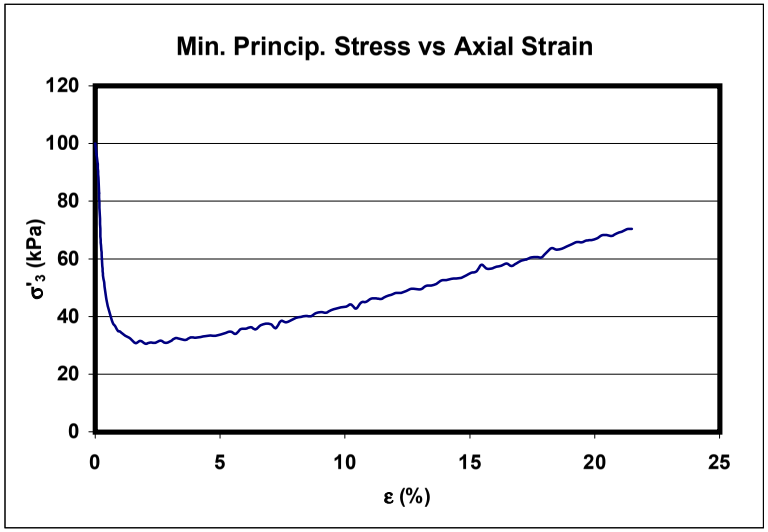

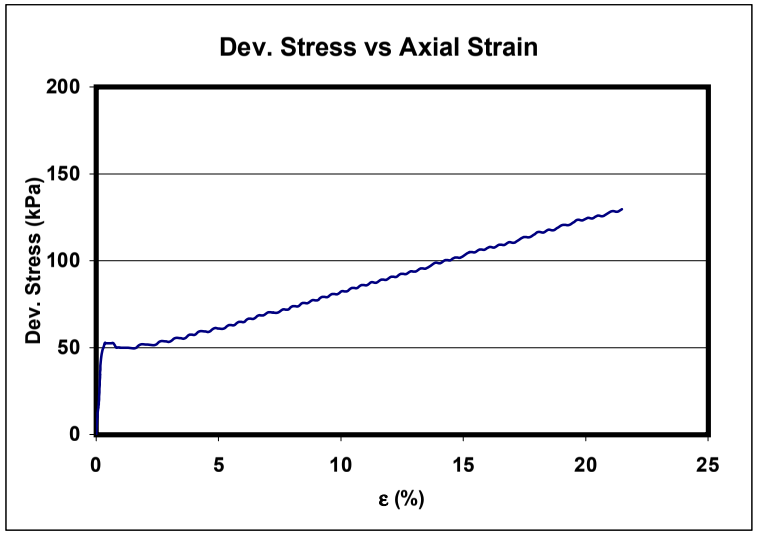

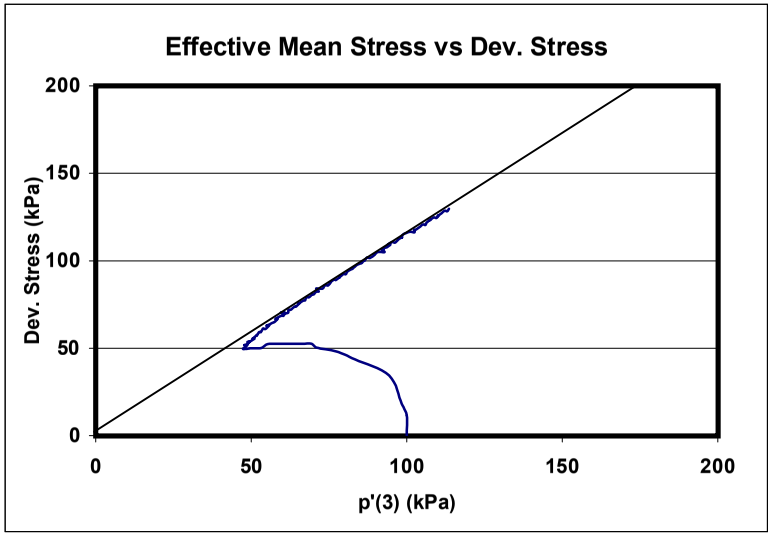

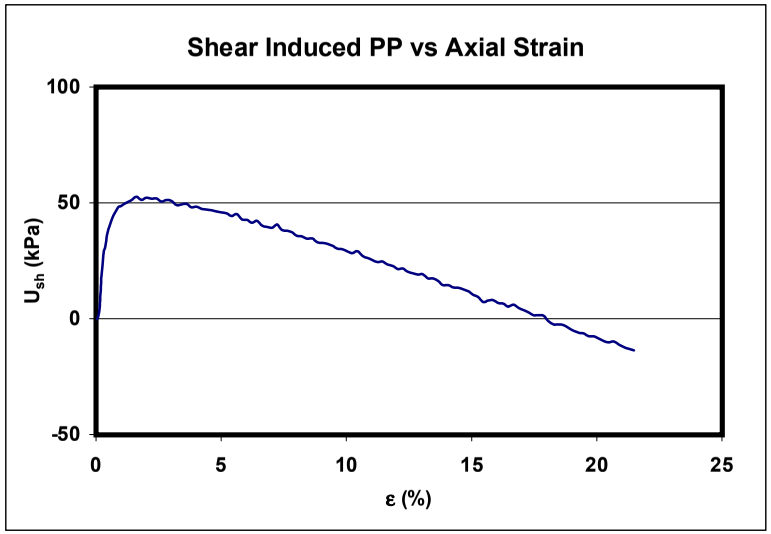

ϕ = 29.2 Confining stress = 100 kPa

GDS FJ#80

Date: 03.13.01	Fines= 0	e= 0.699	ec= 0.699	ef= n.a.	(ef)eq= n.a.	(ec)eq= 0.699

n

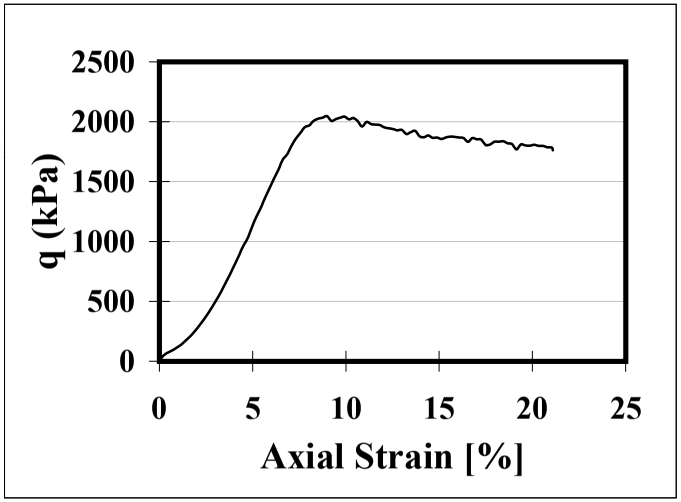

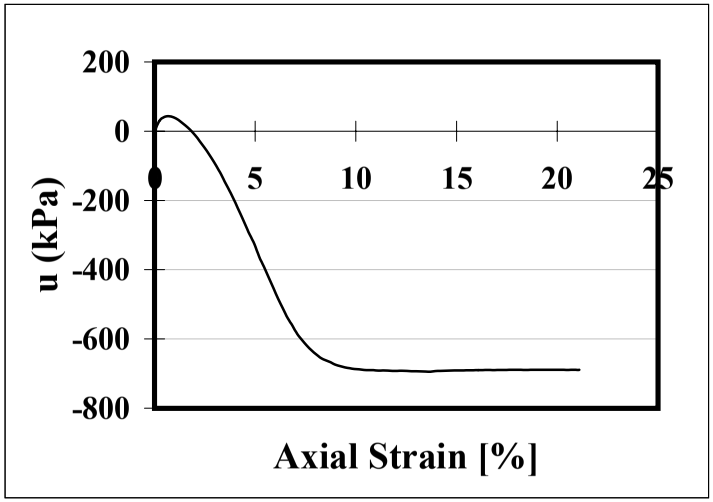

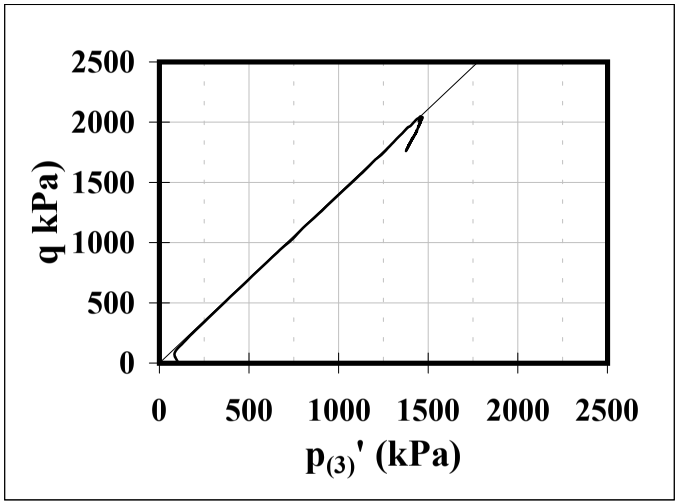

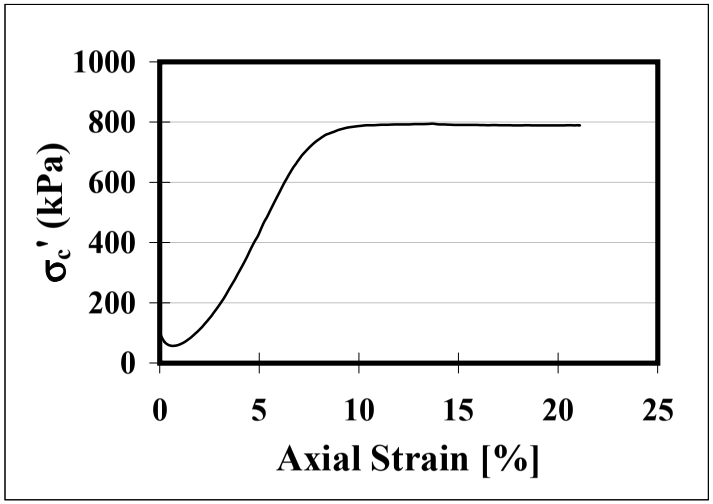

ϕ = 34.7 Confining stress = 100 kPa

GDS FJ#80

Date: 03/21/2001	Fines= 0	e= 0.784	ec= 0.784	ef= n.a.	(ef)eq= n.a.	(ec)eq= 0.784

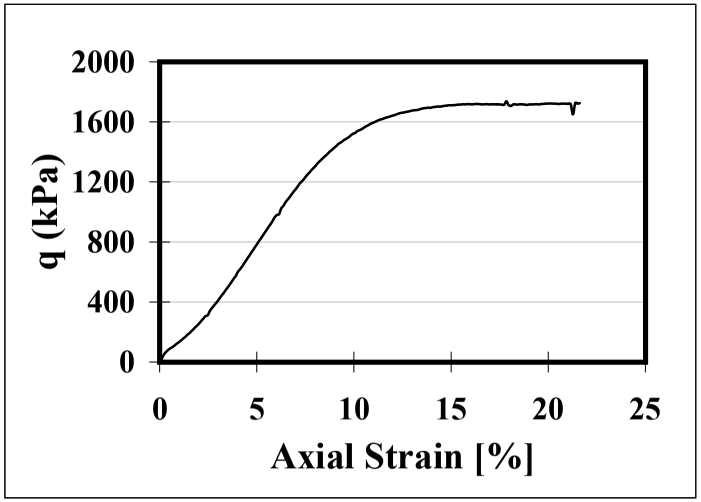

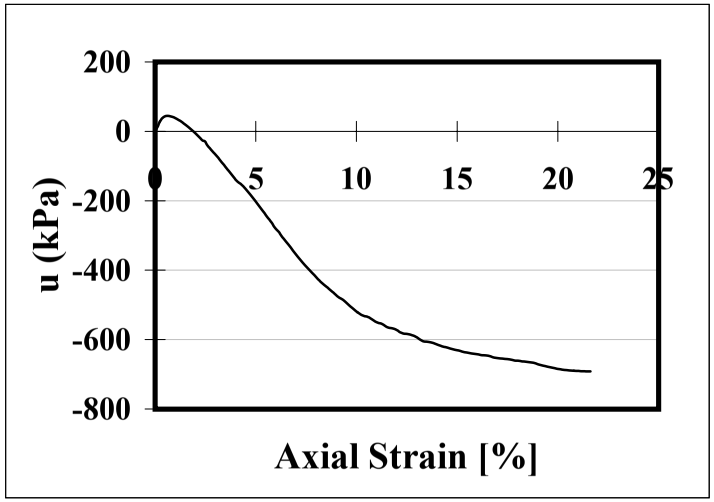

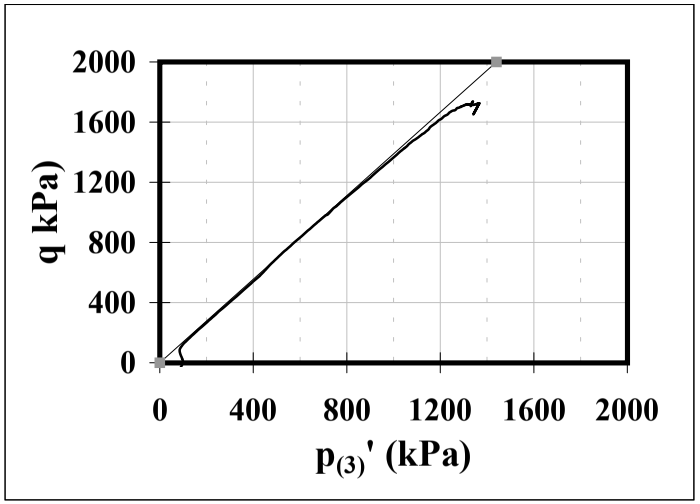

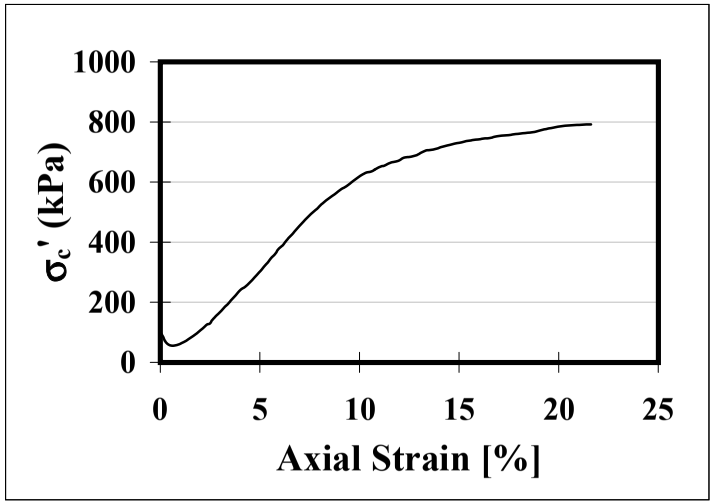

ϕ = 34.3 Confining stress = 100 kPa

GDS FJ#80

Date: 03/23/2001	Fines= 0	e= 0.800	ec= 0.800	ef= n.a.	(ef)eq= n.a.	(ec)eq= 0.800

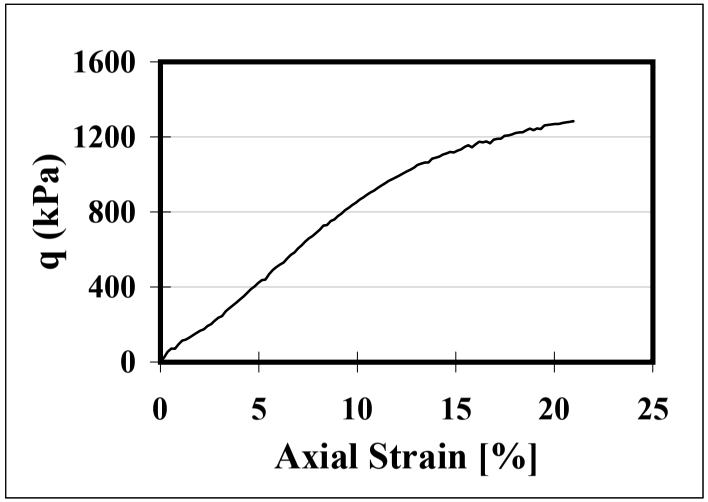

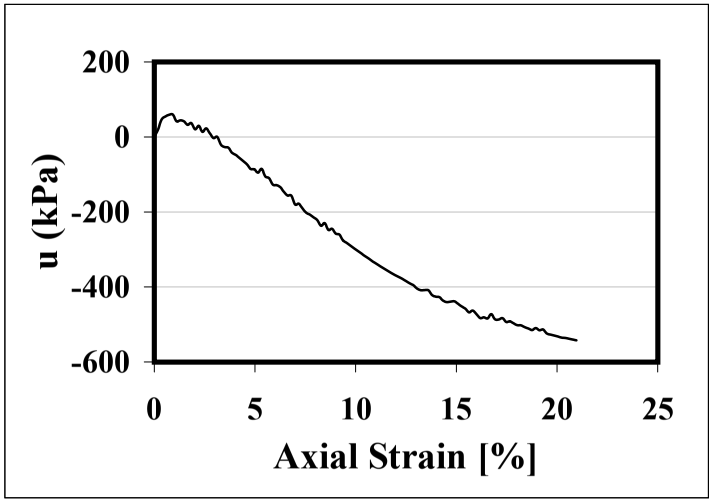

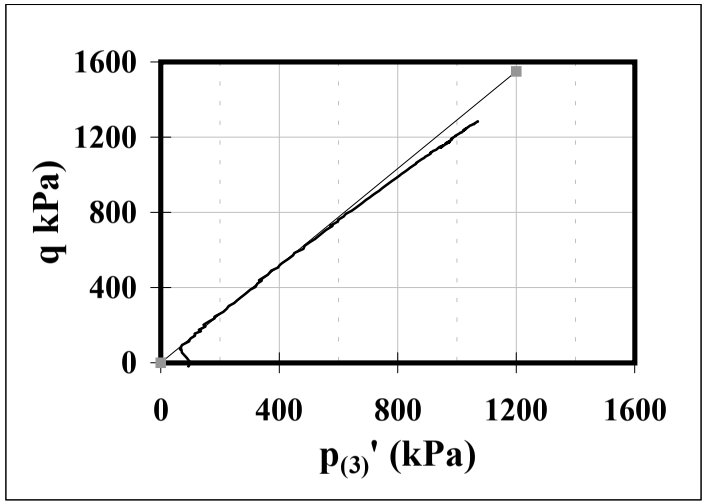

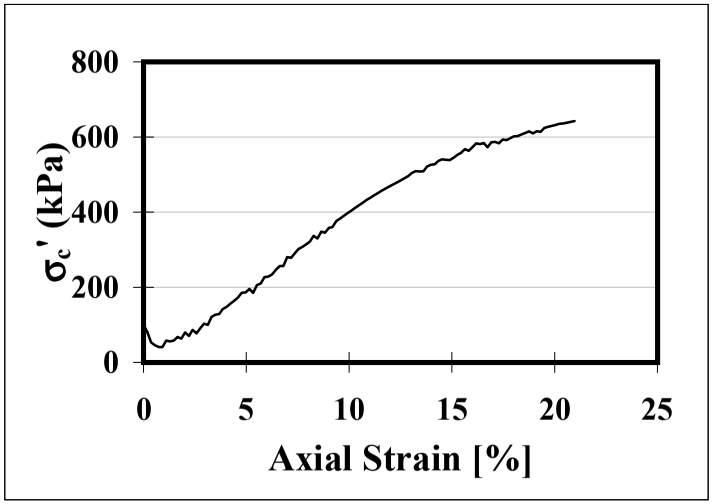

ϕ = 32.1 Confining stress = 100 kPa

GDS FJ#80

Date: 03/26/2001	Fines= 0	e= 0.794	ec= 0.794	ef= n.a.	(ef)eq= n.a.	(ec)eq= 0.794

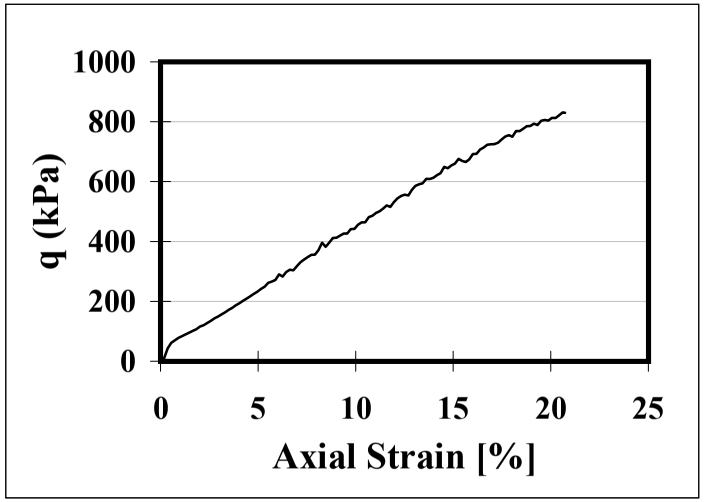

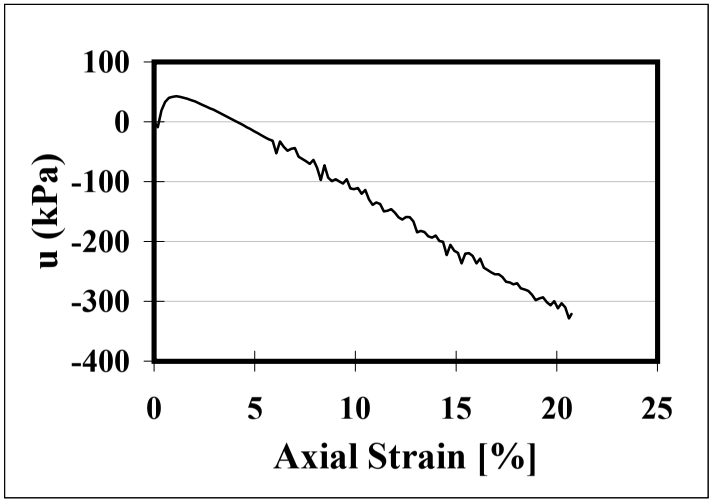

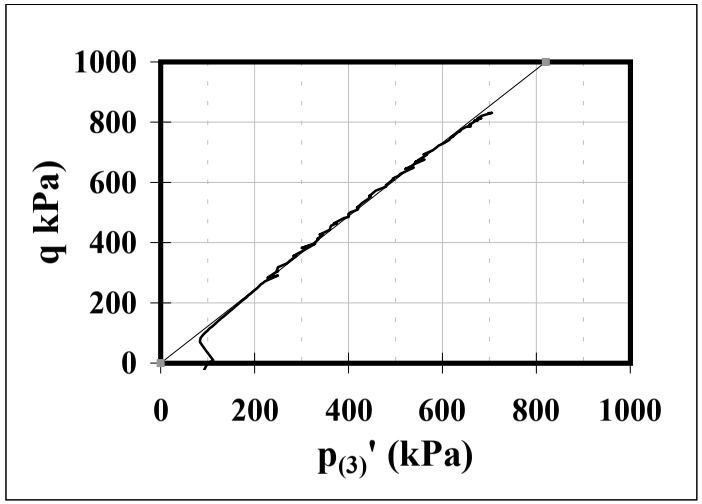

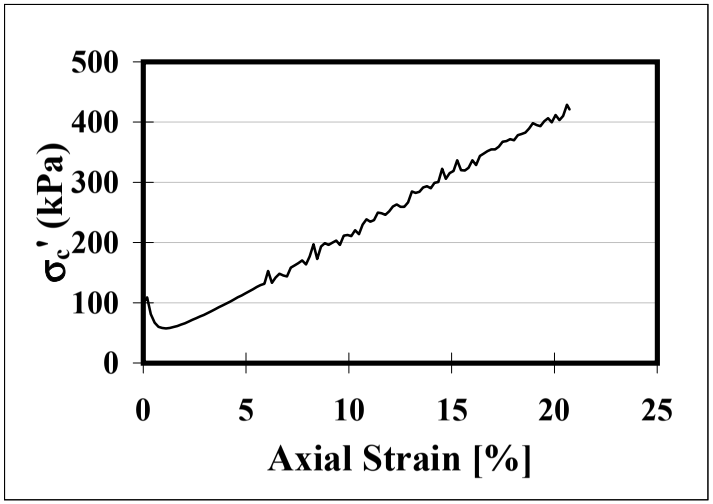

ϕ = 30.4 Confining stress = 100 kPa

GDS FJ#80

Date: 03/28/2001	Fines= 0	e= 0.851	ec= 0.851	ef= n.a.	(ef)eq= n.a.	(ec)eq= 0.851

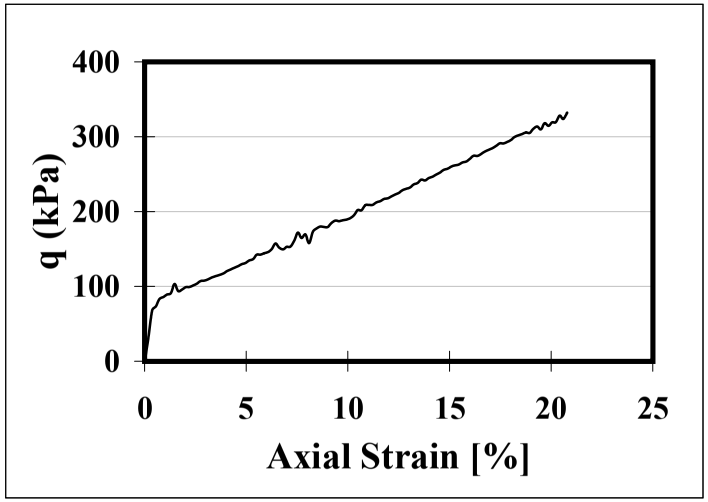

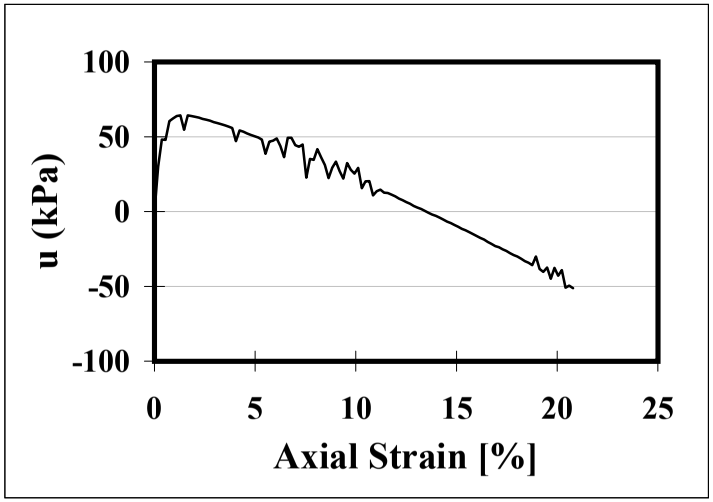

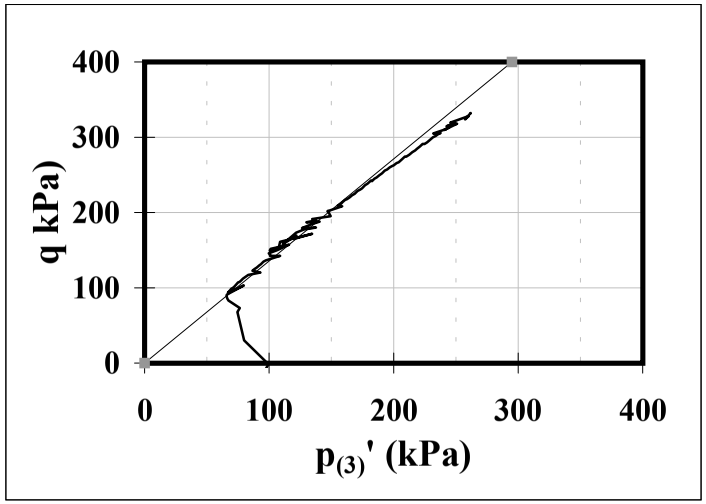

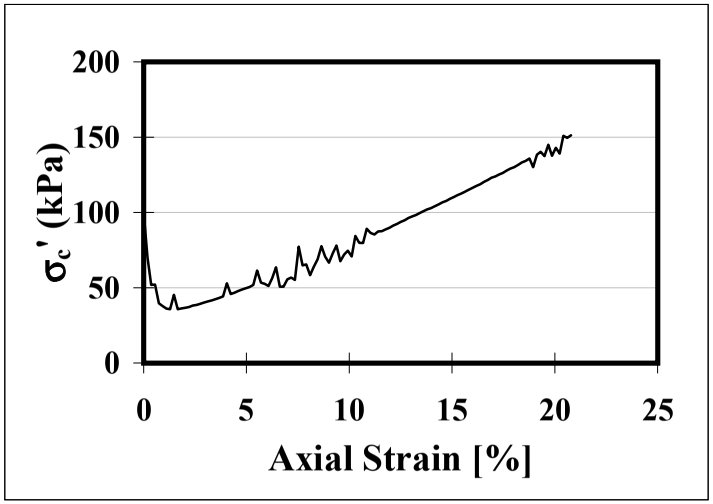

ϕ = 33.6 Confining stress = 100 kPa

GDS FJ#80

Date: 03/30/2001	Fines= 0	e= 0.869	ec= 0.869	ef= n.a.	(ef)eq= n.a.	(ec)eq= 0.869

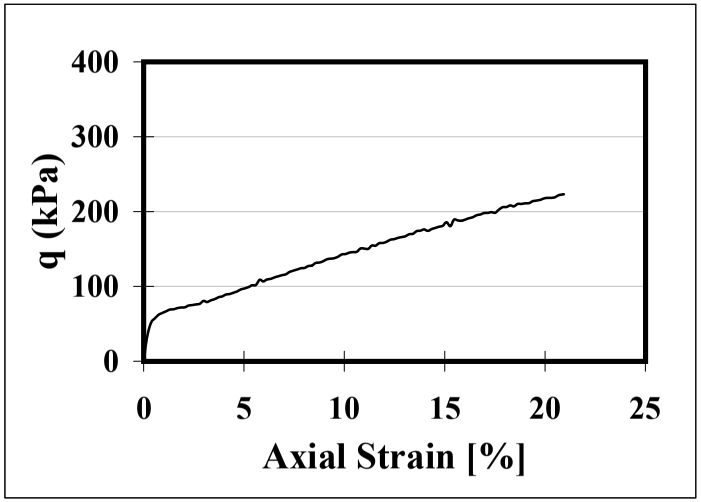

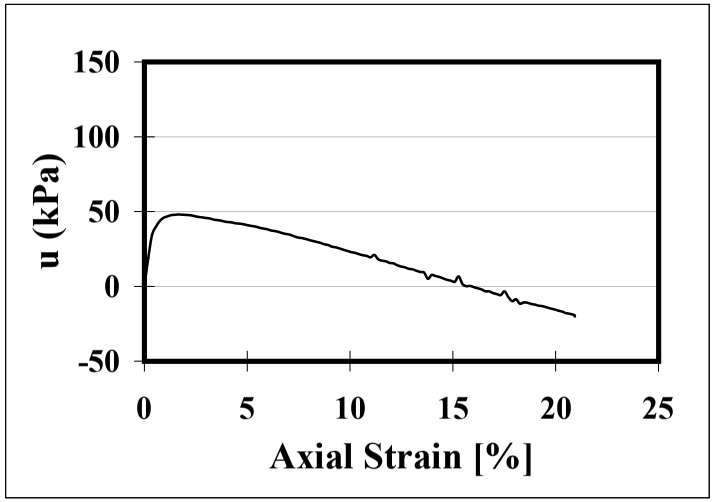

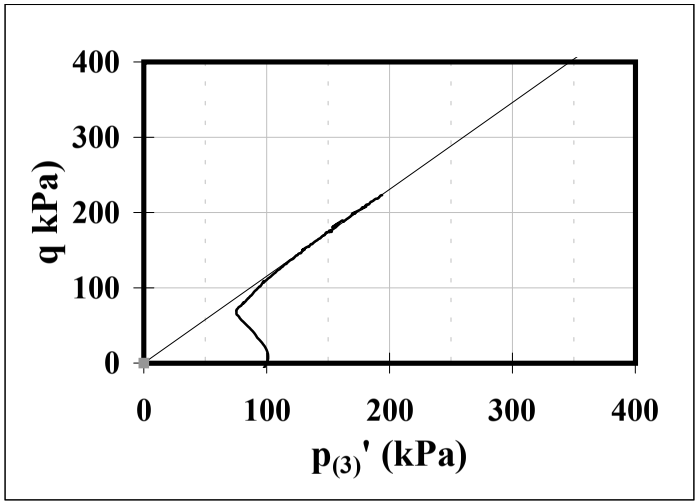

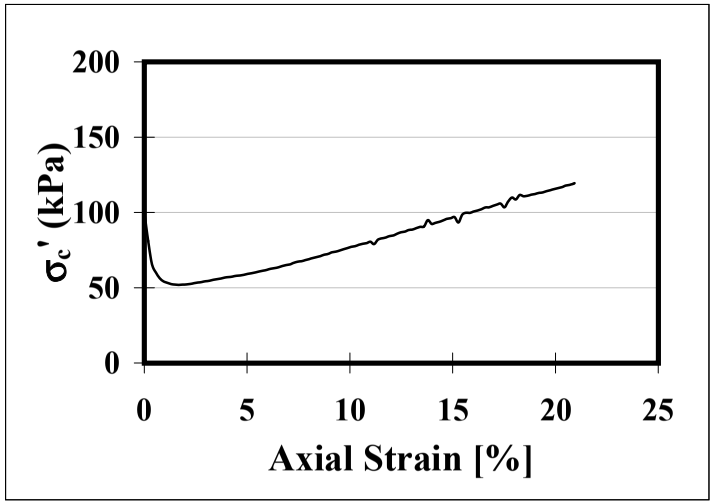

ϕ = 28.9 Confining stress = 100 kPa

GDS FJ#80 GS#40

Date: 05/24/01	Fines= 0	e= 0.854	ec= 0.854	ef= n.a.	(ef)eq= n.a.	(ec)eq= 0.854

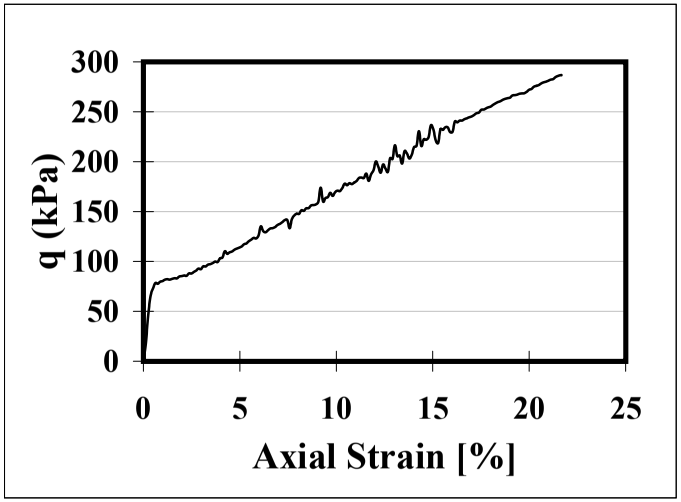

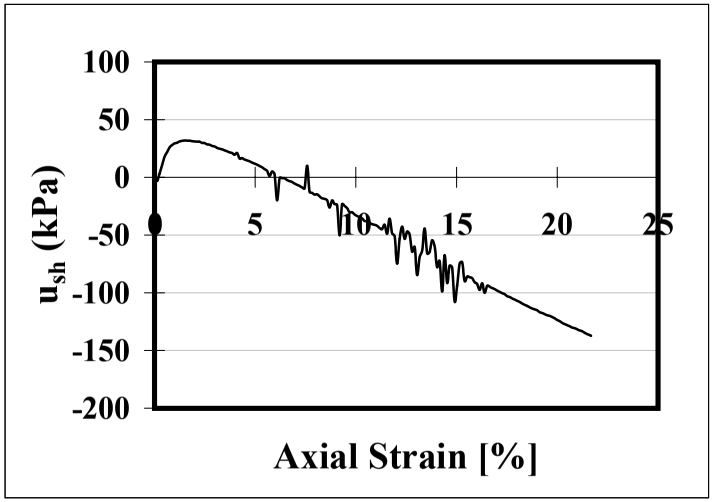

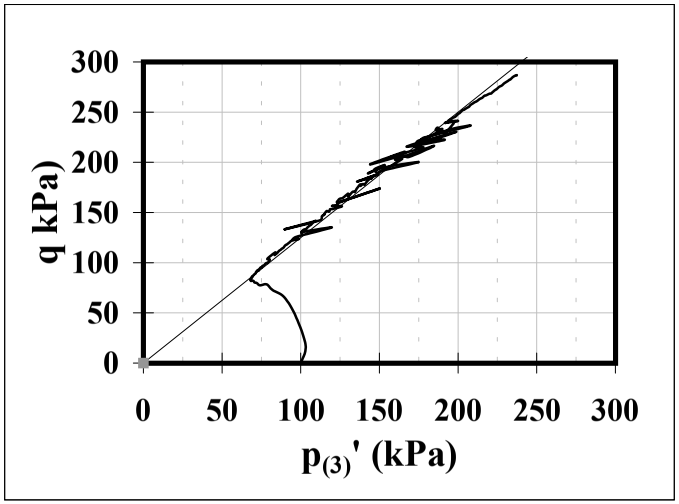

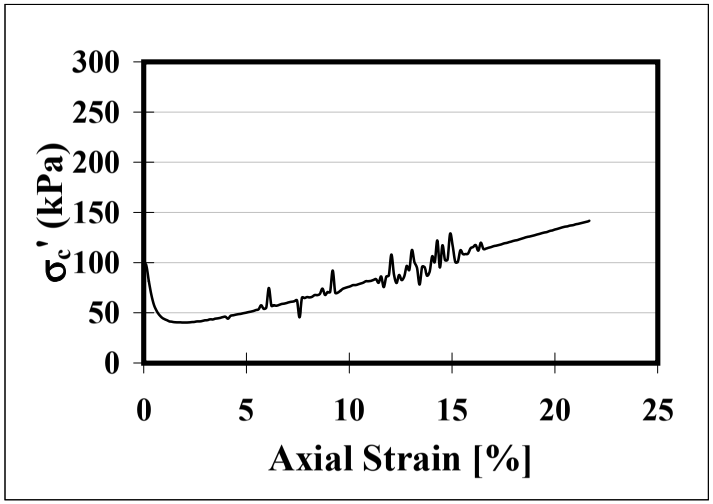

ϕ = 31.1 Confining stress = 100 kPa

GDS FJ#80 GS#40

Date: 05/25/01	Fines= 0	e= 0.938	ec= 0.938	ef= n.a.	(ef)eq= n.a.	(ec)eq= 0.938

n

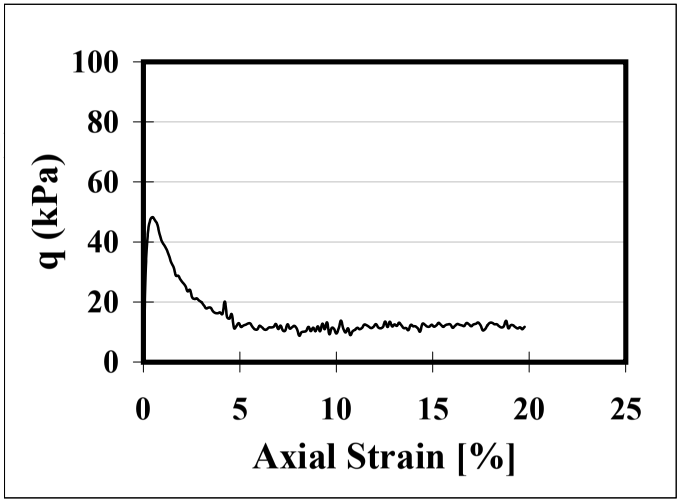

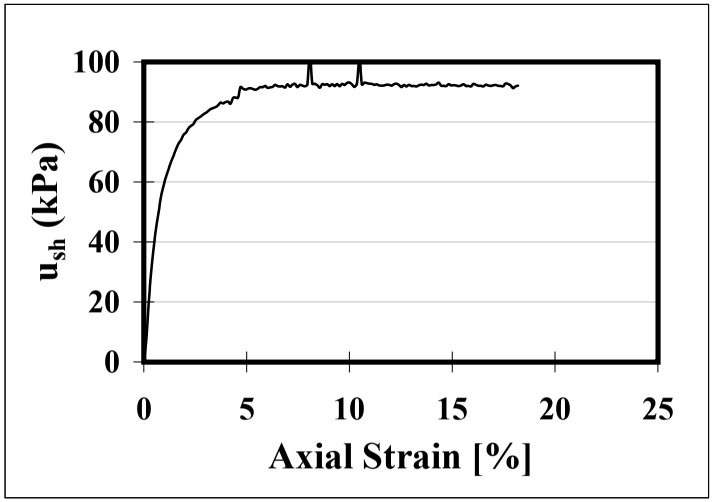

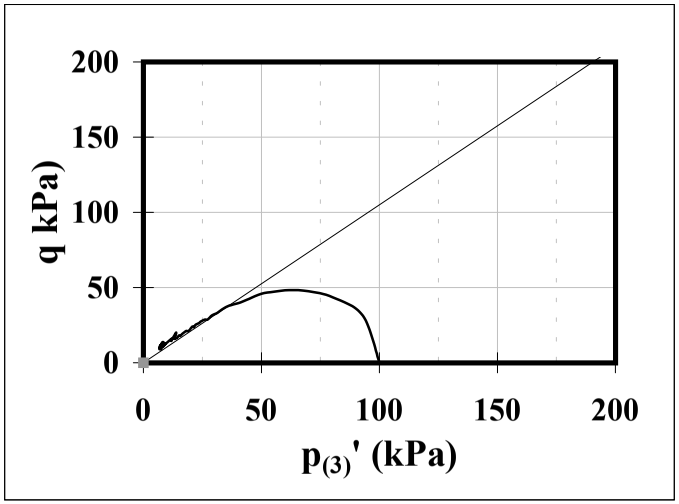

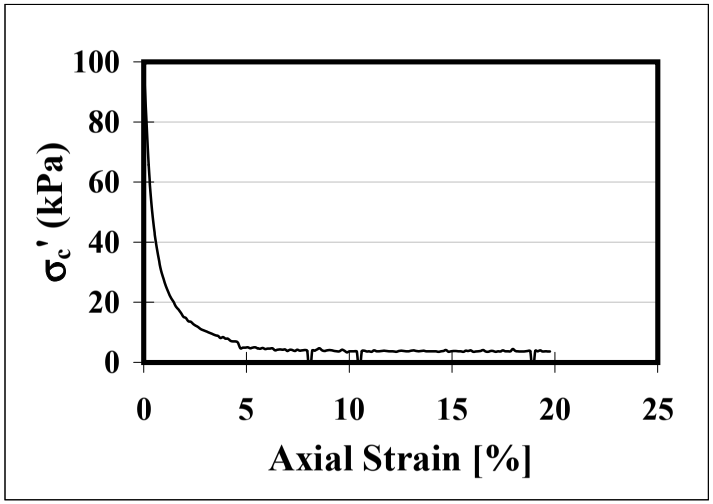

ϕ = 26.5 Confining stress = 100 kPa

GDS FJ#80 GS#40

Date: 07/19/01	Fines= 0	e= 0.878	ec= 0.878	ef= n.a.		

n

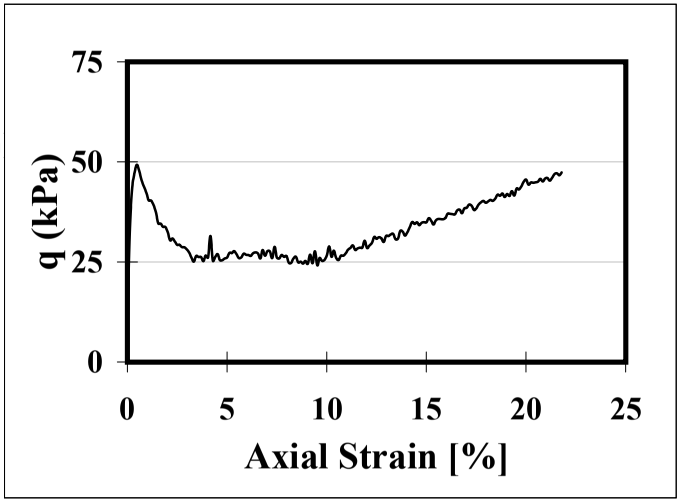

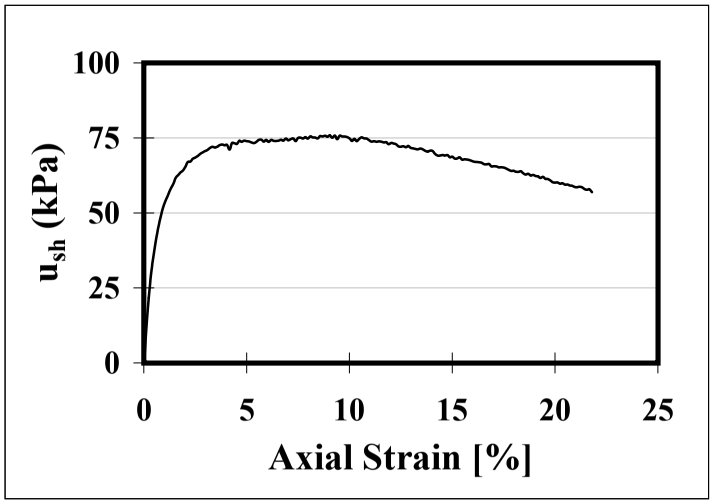

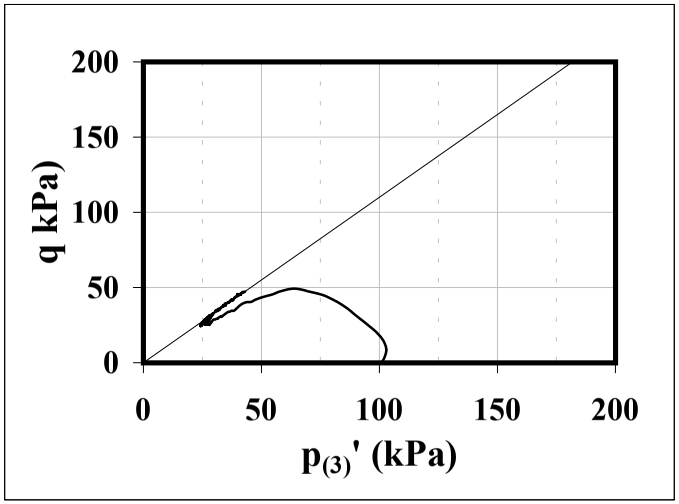

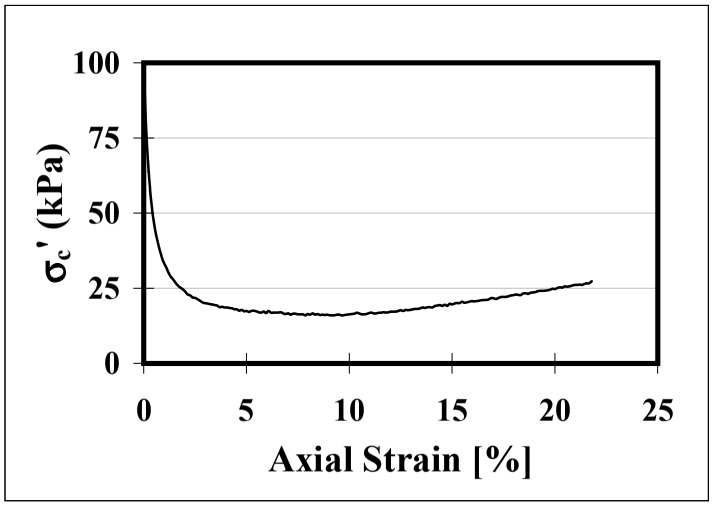

ϕ = 27.7 Confining stress = 100 kPa

GDS FJ#80 GS#40

Date: 07/19/00 Fines= 25 e= 0.590 ec= 1.120 ef= n.a. (ef)eq= n.a. (ec)eq= 0.957

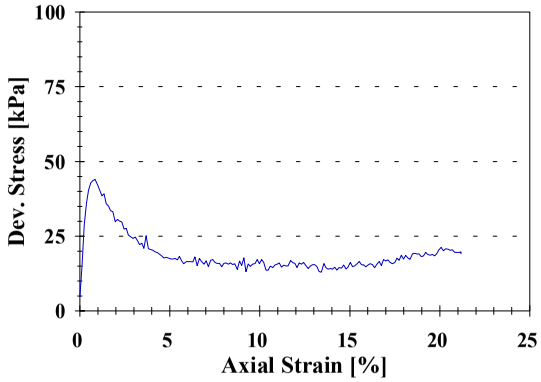

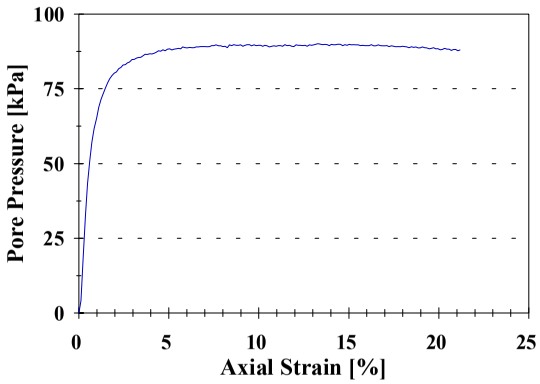

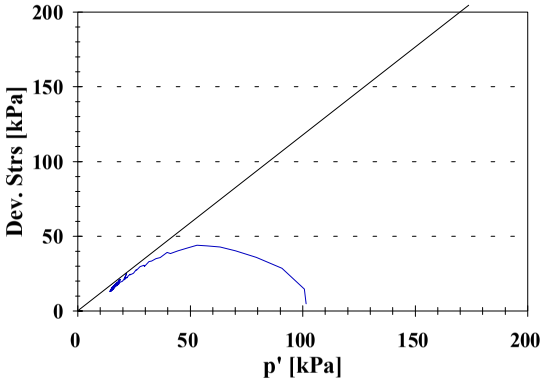

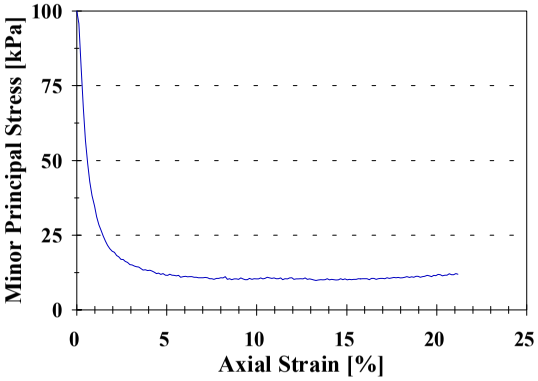

ϕ = 29.5 Confining stress = 100 kPa

GDS FJ#80 GS#40

Date: 07/24/00 Fines= 25 e= 0.618 ec= 1.158 ef= n.a. (ef)eq= n.a. (ec)eq= 0.992

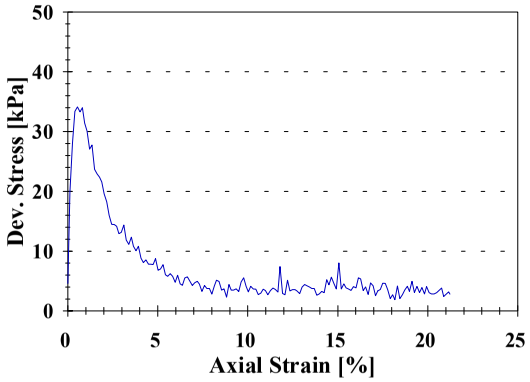

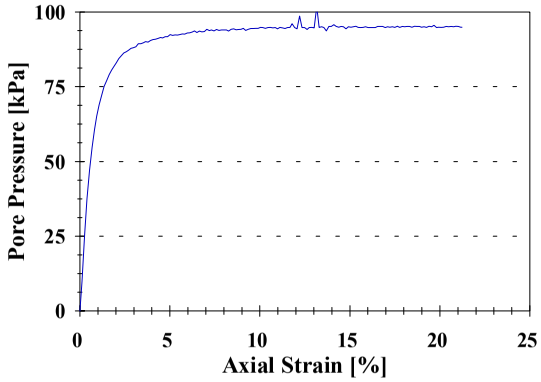

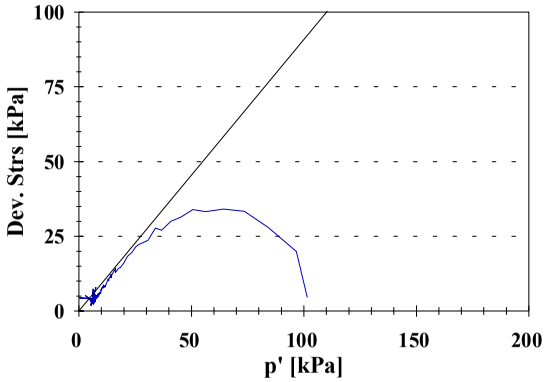

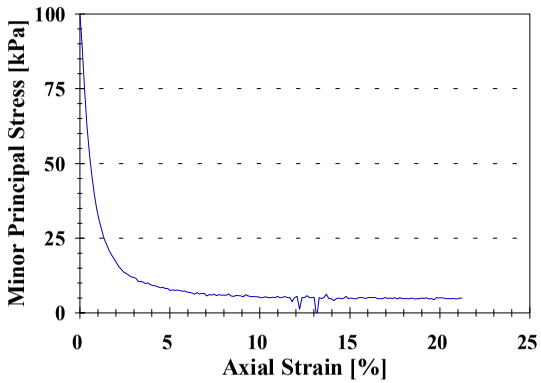

ϕ = 23.2 Confining stress = 100 kPa

GDS FJ#80 GS#40

Date: 08/01/00 Fines= 25 e= 0.610 ec= 1.147 ef= n.a. (ef)eq= n.a. (ec)eq= 0.982

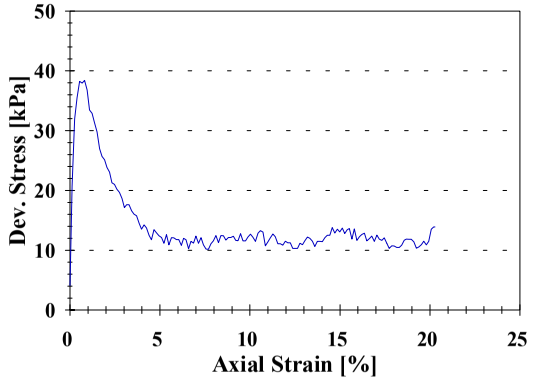

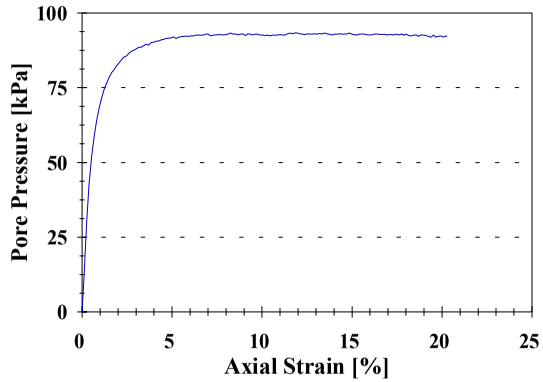

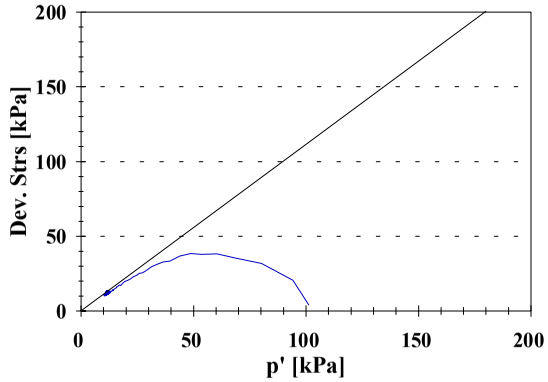

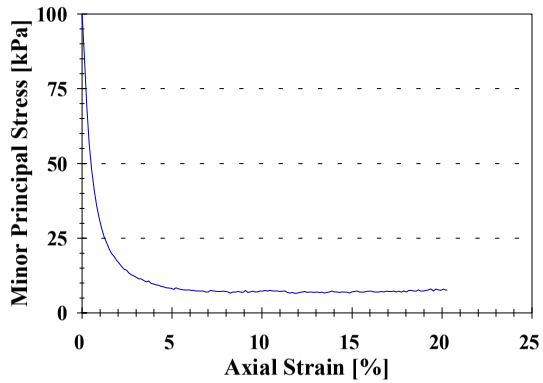

ϕ = 28.0 Confining stress = 100 kPa

GDS FJ#80 GS#40

Date: 08/11/00 Fines= 25 e= 0.584 ec= 1.112 ef= n.a. (ef)eq= n.a. (ec)eq= 0.950

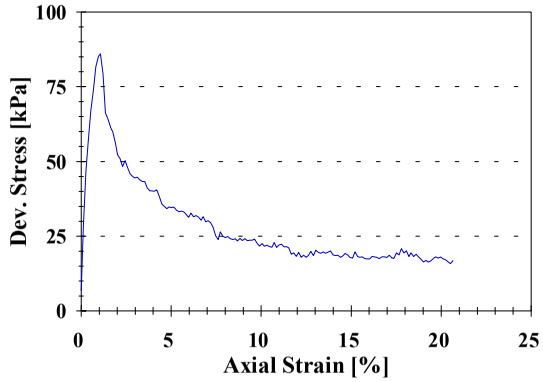

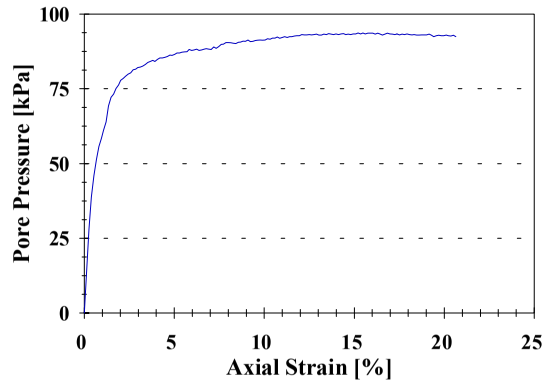

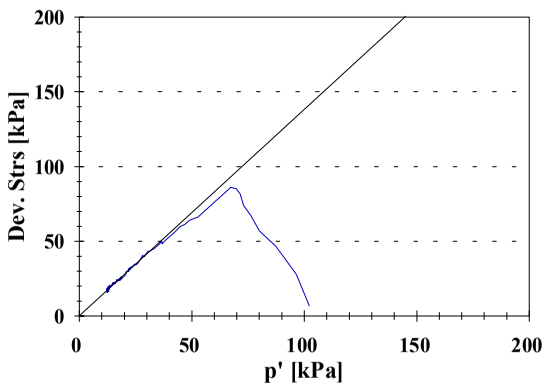

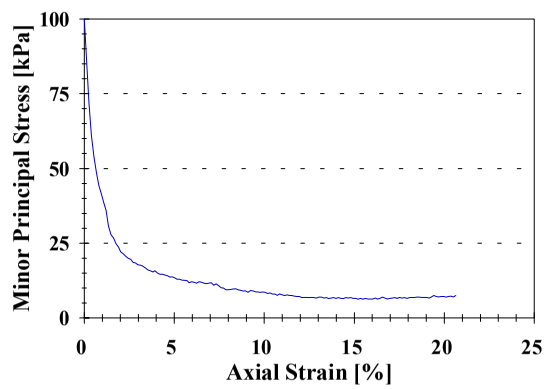

ϕ = 34.1 Confining stress = 100 kPa

GDS FJ#80 GS#40

Date: 10/11/00 Fines= 25 e= 0.442 ec= 0.922 ef= n.a. (ef)eq= n.a. (ec)eq= 0.774

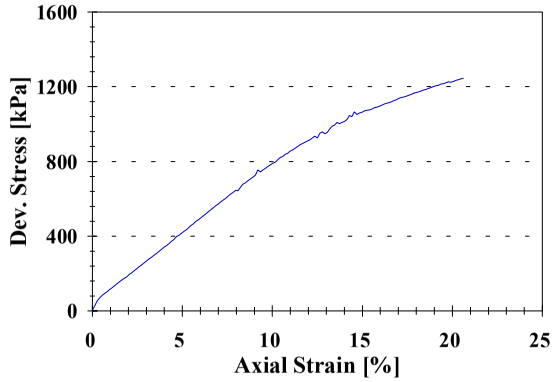

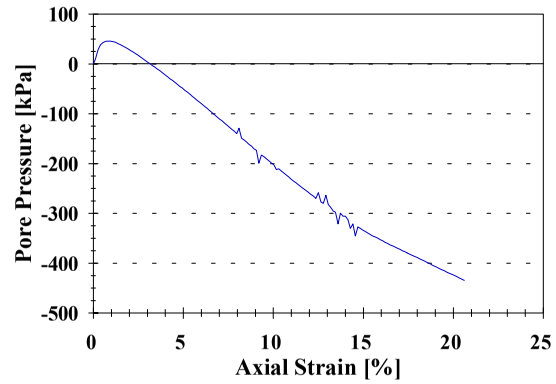

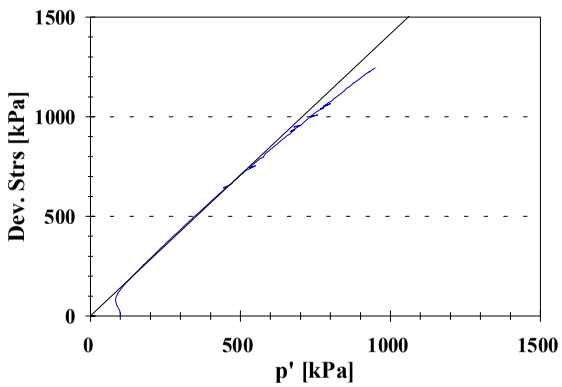

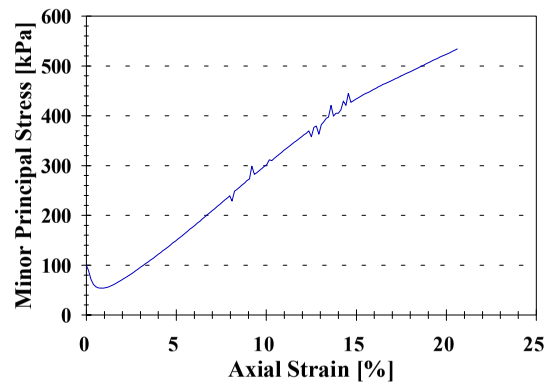

ϕ = 35.2 Confining stress = 100 kPa

GDS FJ#80 GS#40

Date: 10/19/00 Fines= 25 e= 0.587 ec= 1.116 ef= n.a. (ef)eq= n.a. (ec)eq= 0.953

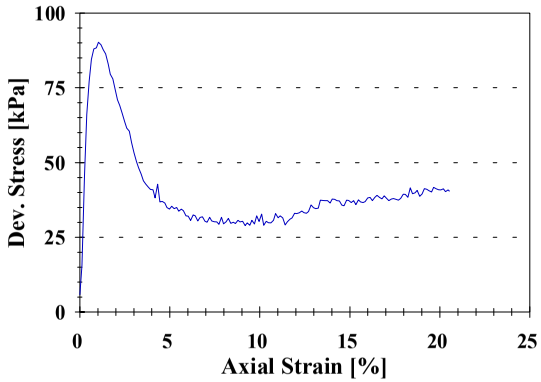

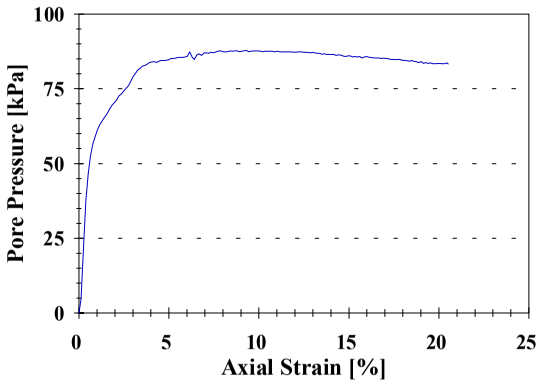

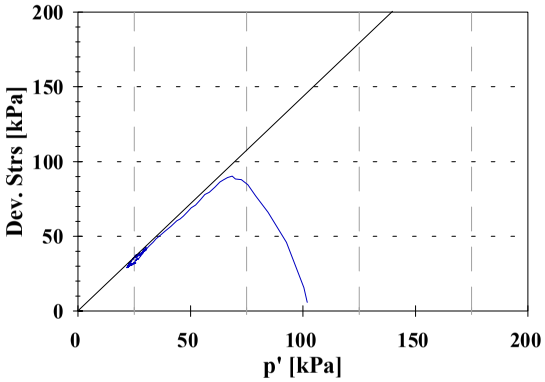

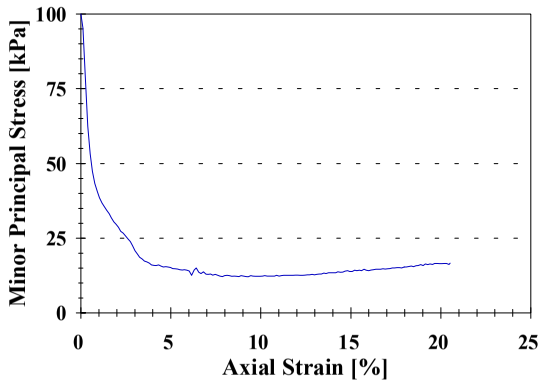

ϕ = 35.2 Confining stress = 100 kPa

GDS FJ#80 GS#40

Date: 12/22/00	Fines= 25	e= 0.548	ec= 1.064	ef= n.a.	(ef)eq= n.a.	(ec)eq= 0.905

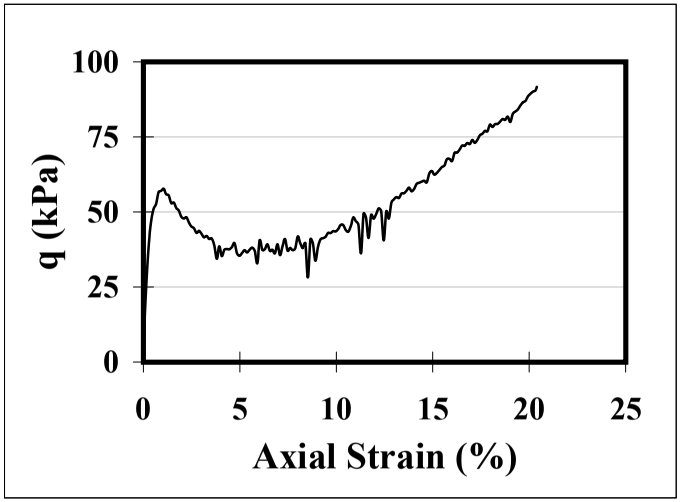

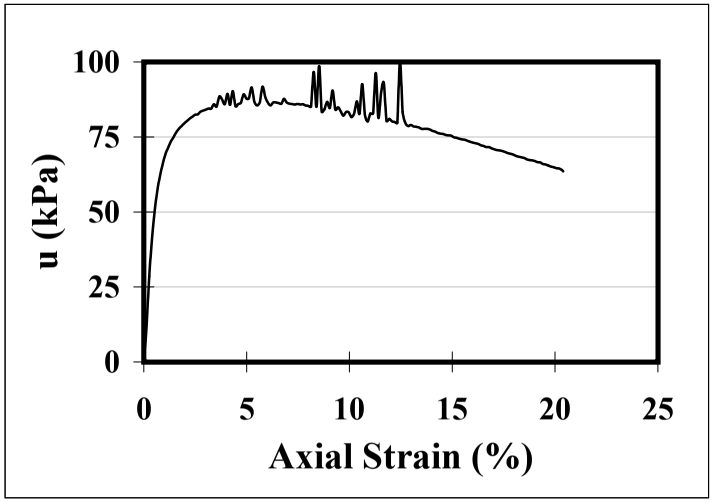

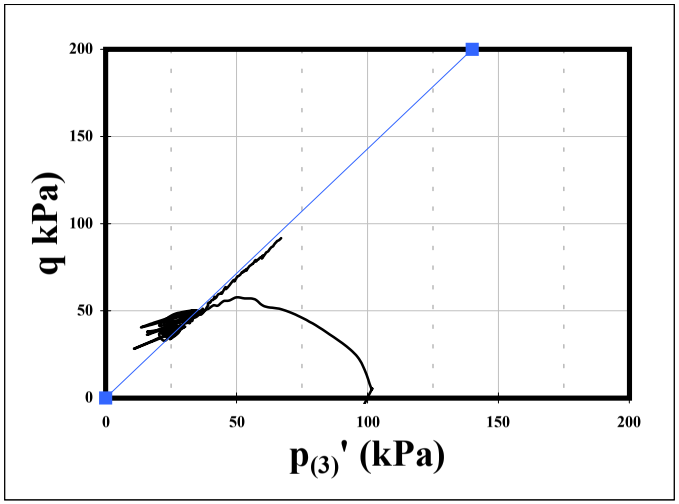

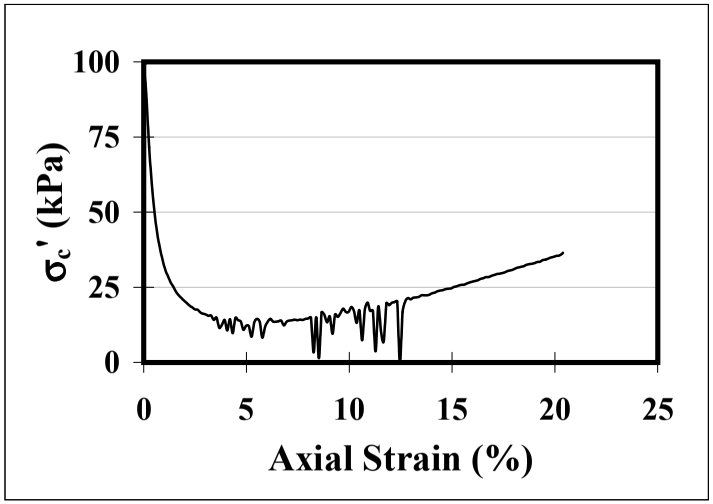

ϕ = 35.2 Confining stress = 100 kPa

GDS FJ#80 GS#40

Date: 12/27/00	Fines= 25	e= 0.459	ec= 0.945	ef= n.a.	(ef)eq= n.a.	(ec)eq= 0.796

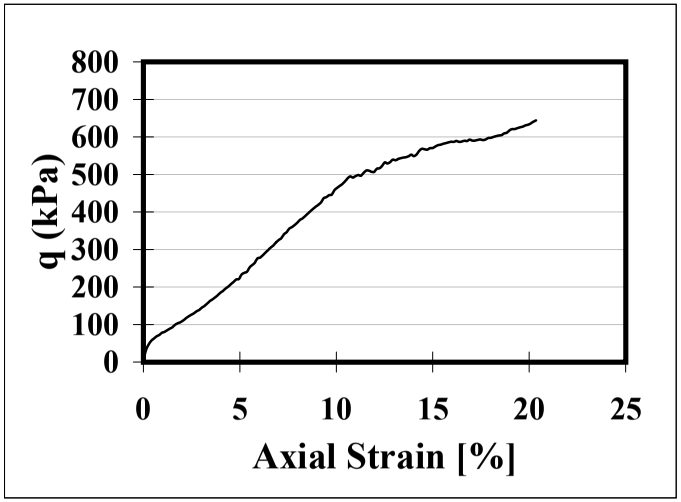

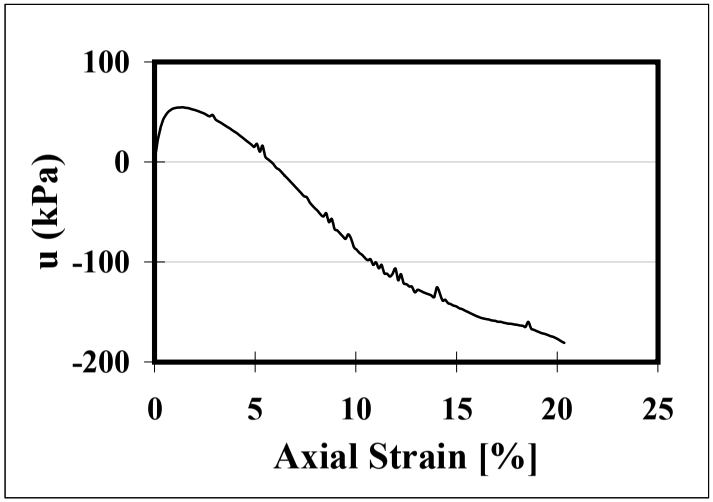

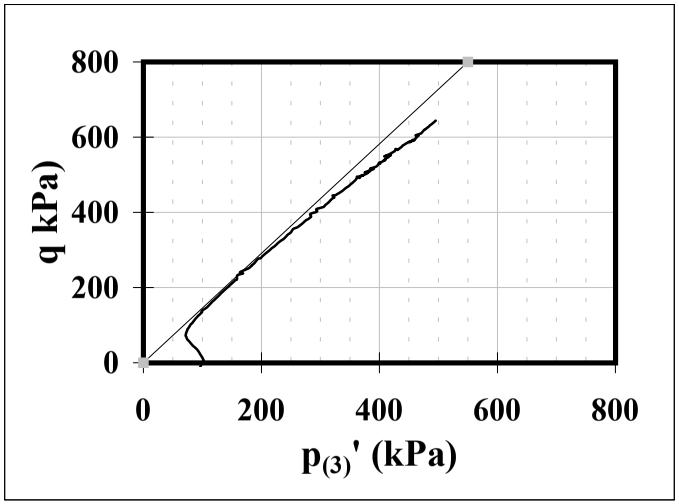

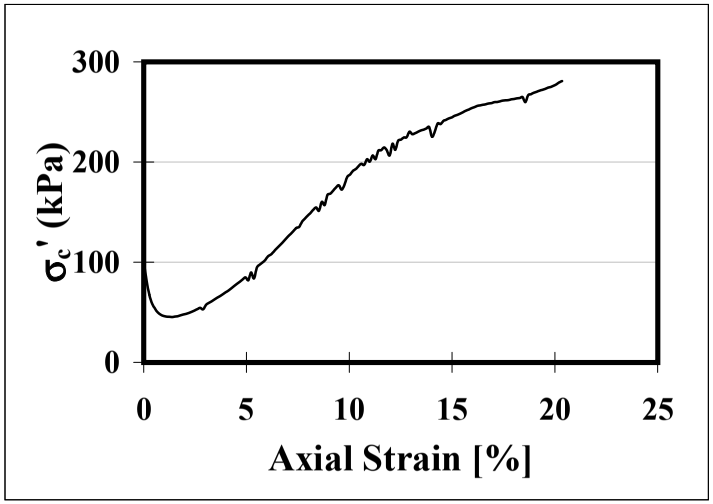

ϕ = 35.8 Confining stress = 100 kPa

GDS FJ#80 GS#40

Date: 01/05/01	Fines= 25	e= 0.522	ec= 1.029	ef= n.a.	(ef)eq= n.a.	(ec)eq= 0.873

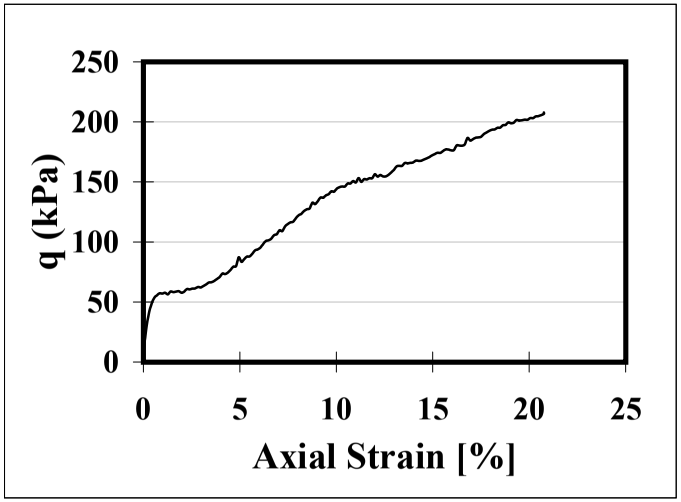

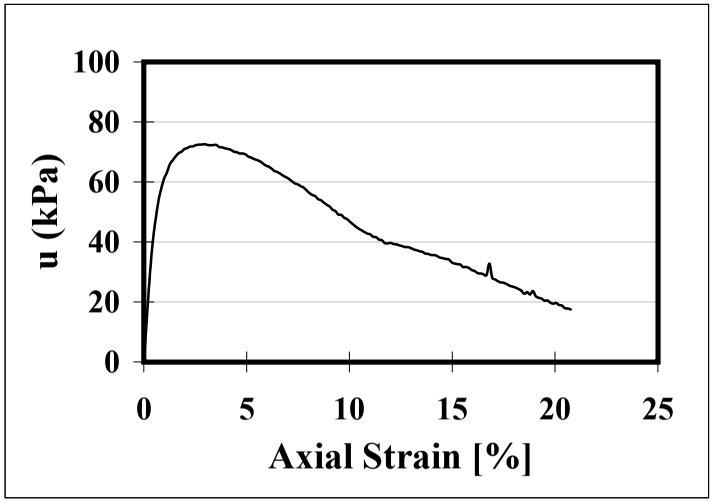

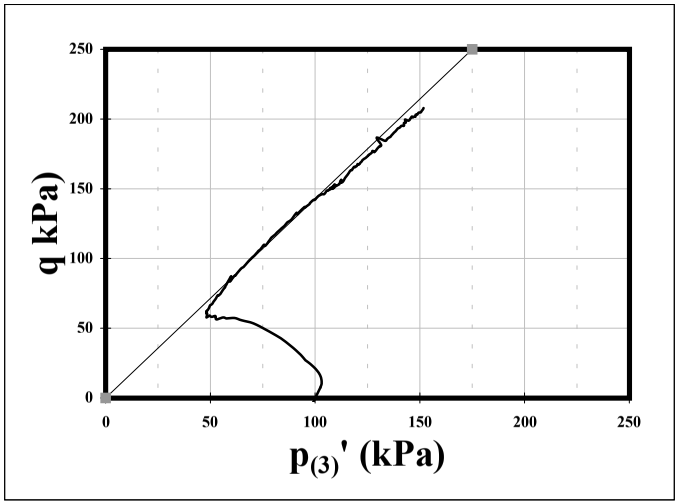

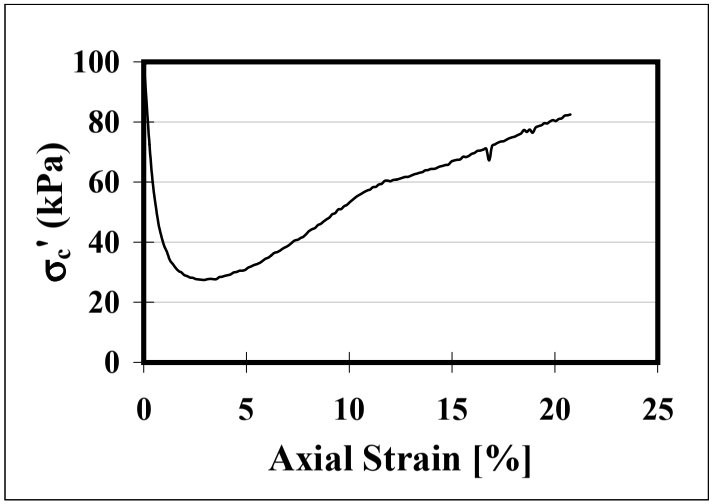

ϕ = 35.2 Confining stress = 100 kPa

GEOCOMP FJ#80 GSF#40

Date: 10/13/2000	Fines= 25	e= 0.554	ec=	1.073	ef= n.a.	(ef)eq= n.a.	(ec)eq= 0.913

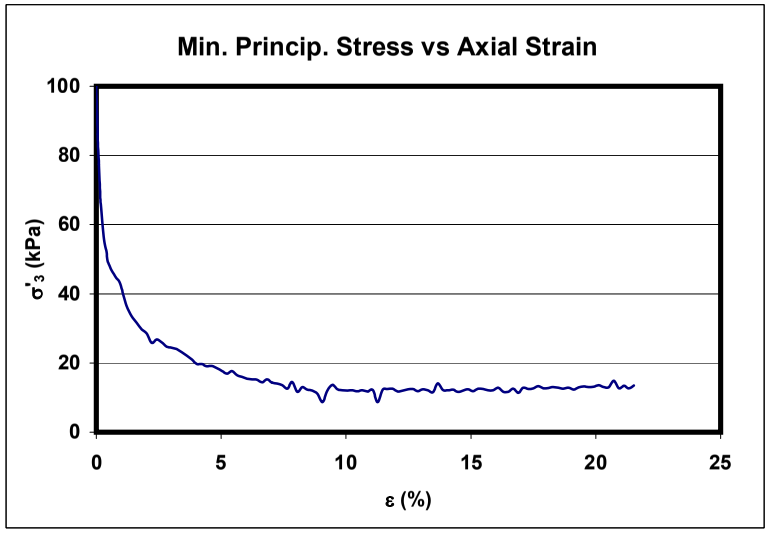

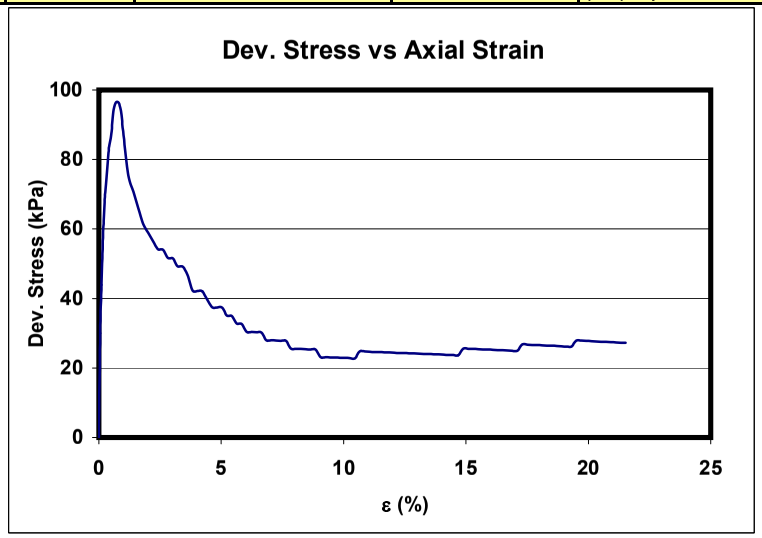

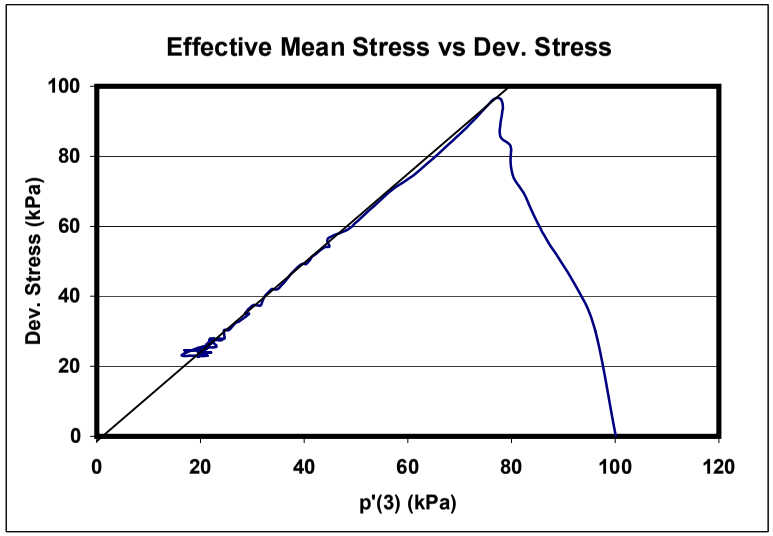

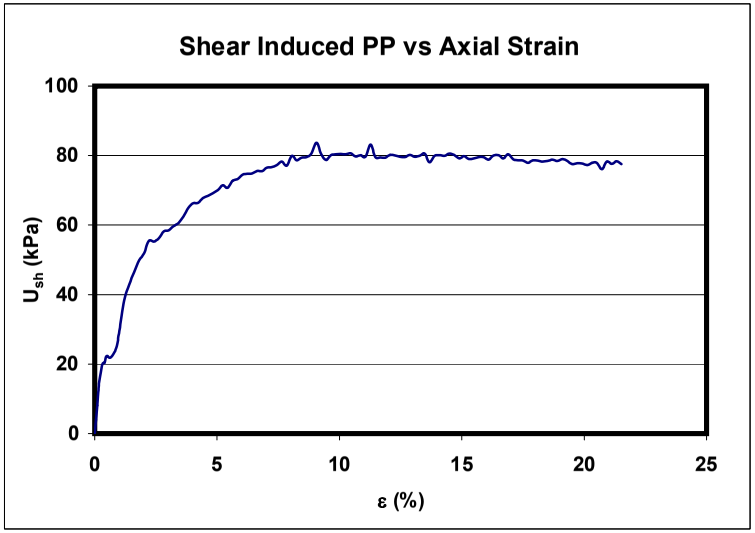

$\phi =$ 30.4 Confining stress = 100 kPa

GEOCOMP FJ#80 GSF#40

Date: 12/29/2000	Fines= 25	e= 0.532	ec=	1.043	ef= n.a.	(ef)eq= n.a.	(ec)eq= 0.886

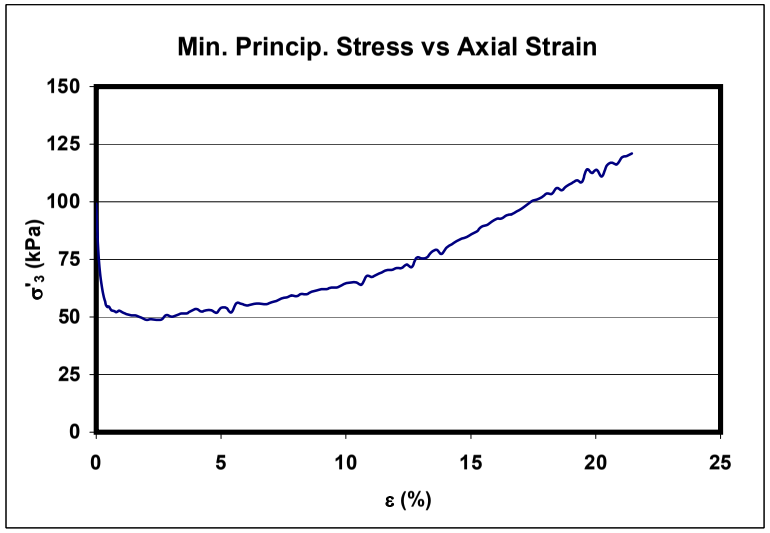

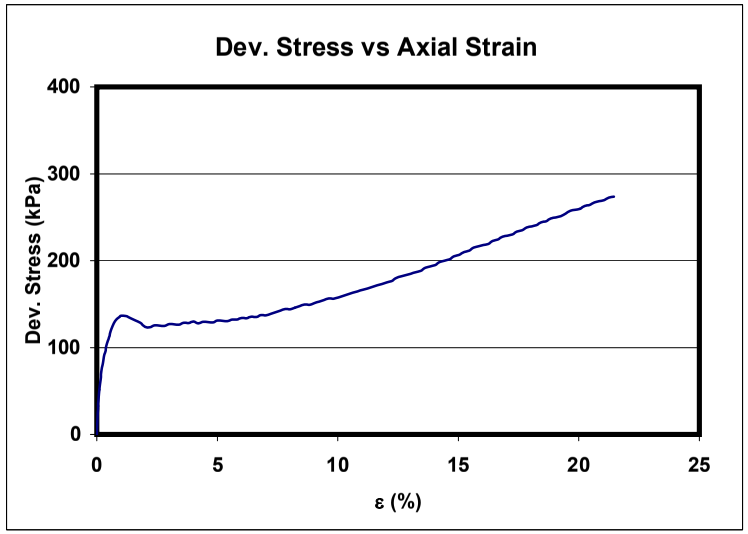

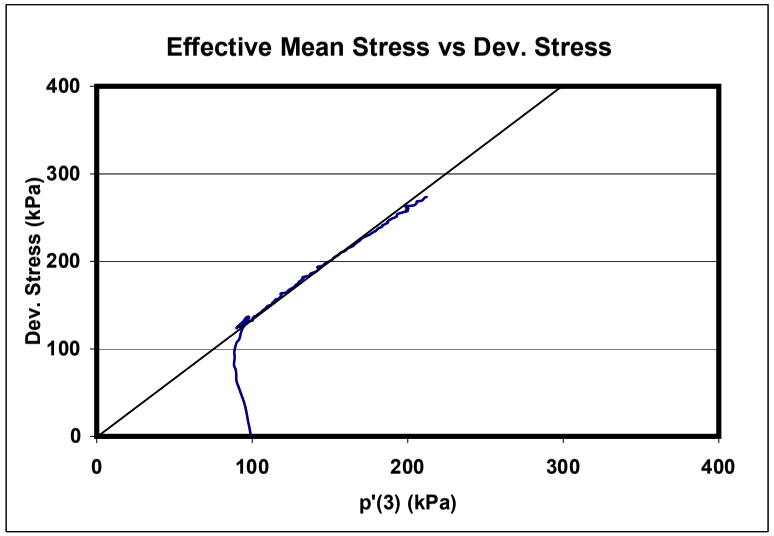

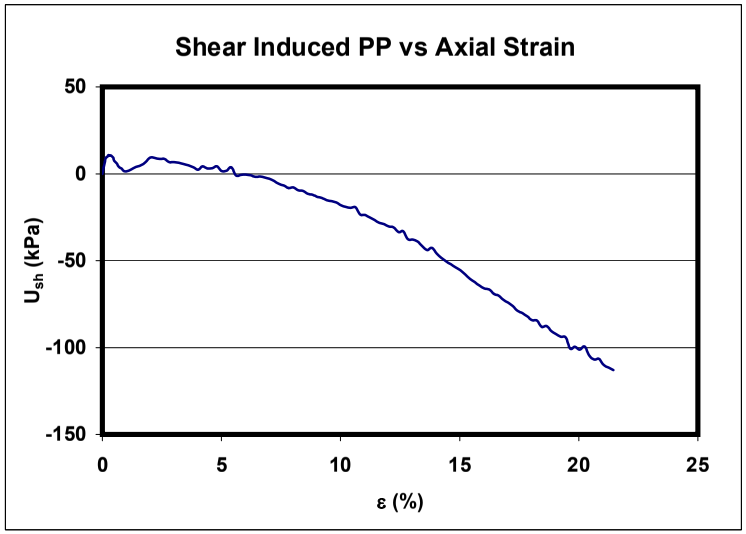

ϕ = 32.8 Confining stress = 100 kPa

GEOCOMP FJ#80 GSF#40

Date: 1/18/2001	Fines= 25	e= 0.548	ec=	1.065	ef= n.a.	(ef)eq= n.a.	(ec)eq= 0.906

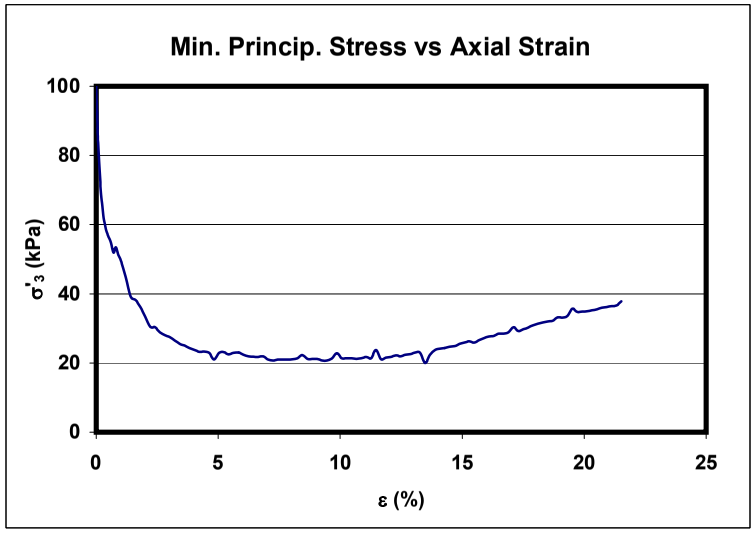

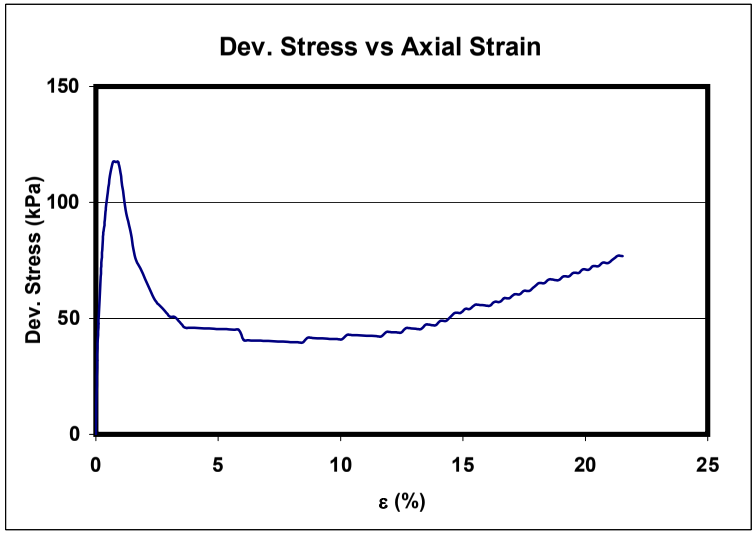

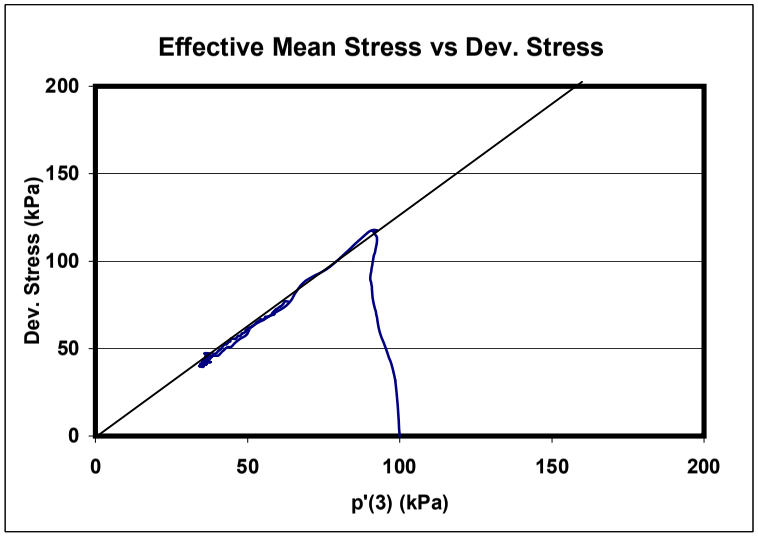

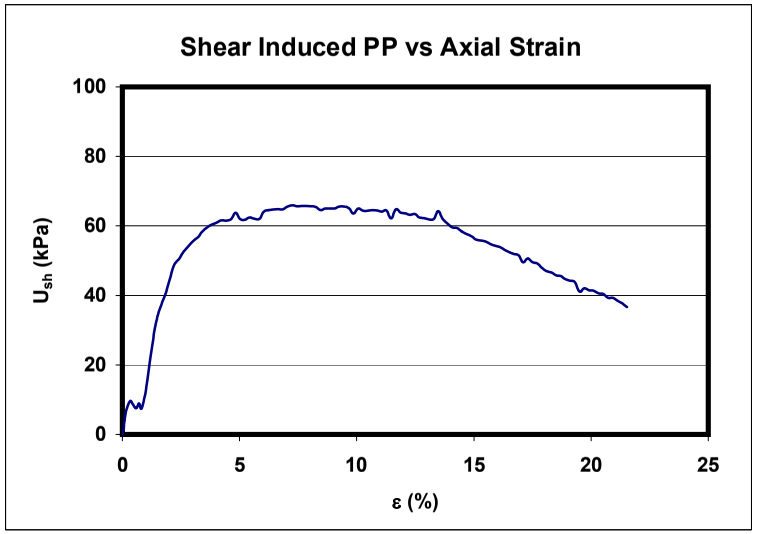

ϕ = 33.1 Confining stress = 400 kPa

GDS FJ#80 GS#40

Date: 07/25/00 Fines= 25 e= 0.576 ec= 1.101 ef= n.a. (ef)eq= n.a. (ec)eq= 0.939

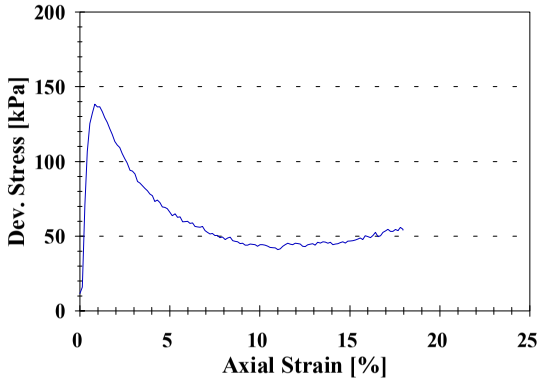

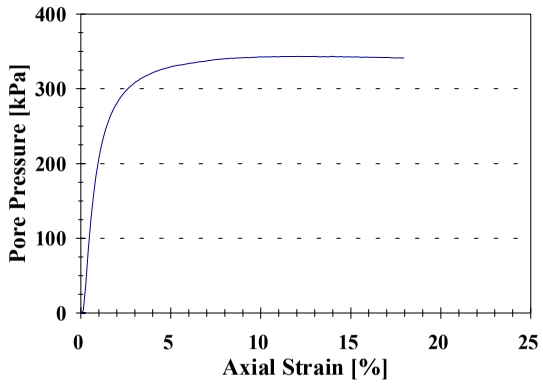

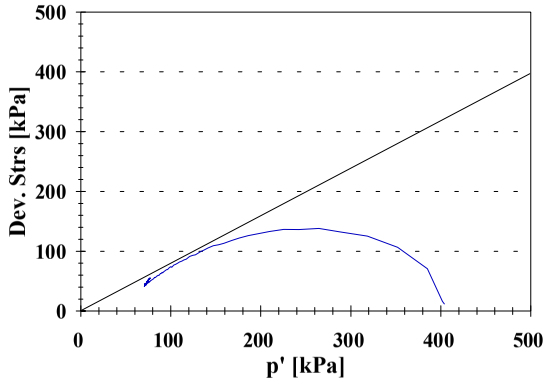

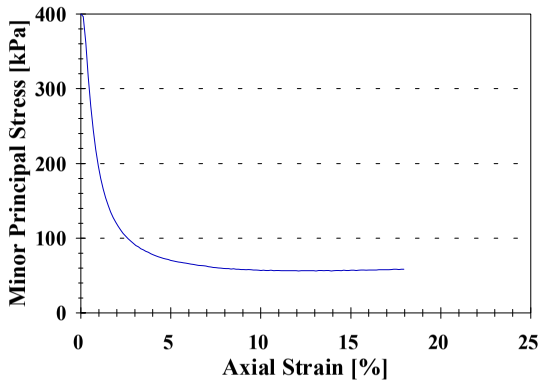

ϕ = 20.7 Confining stress = 400 kPa

GDS FJ#80 GS#40

Date: 08/15/00 Fines= 25 e= 0.551 ec= 1.068 ef= n.a. (ef)eq= n.a. (ec)eq= 0.909

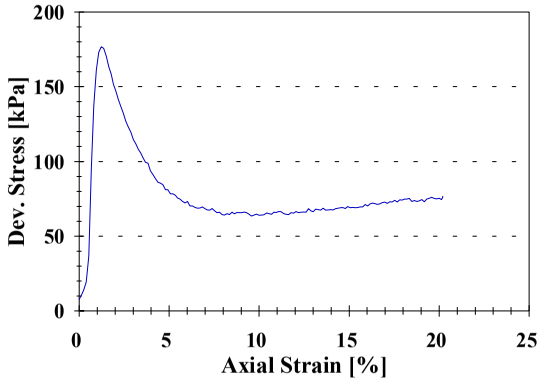

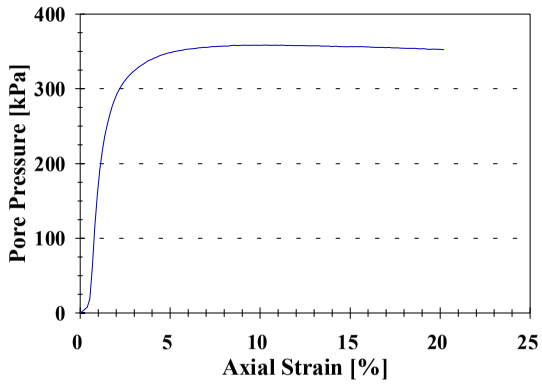

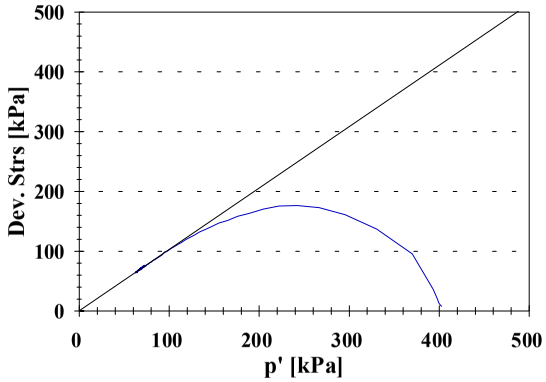

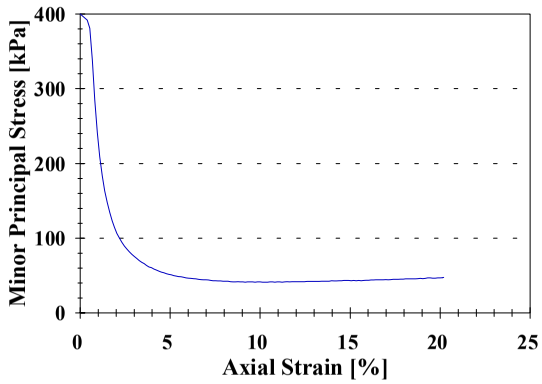

ϕ = 26.3 Confining stress = 400 kPa

GDS FJ#80 GS#40

Date: 10/09/00 Fines= 25 e= 0.559 ec= 1.078 ef= n.a. (ef)eq= n.a. (ec)eq= 0.918

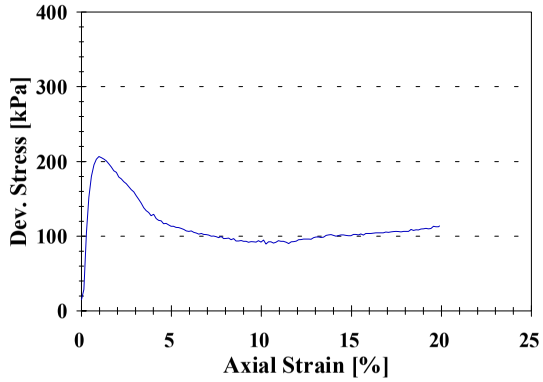

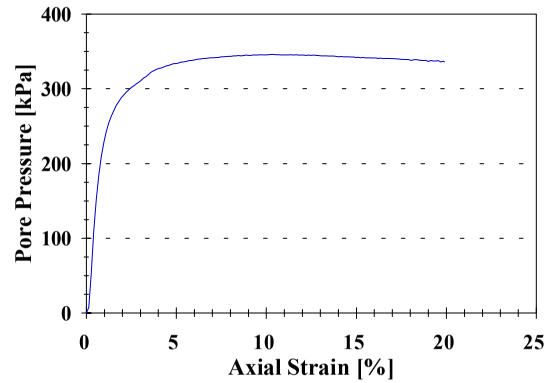

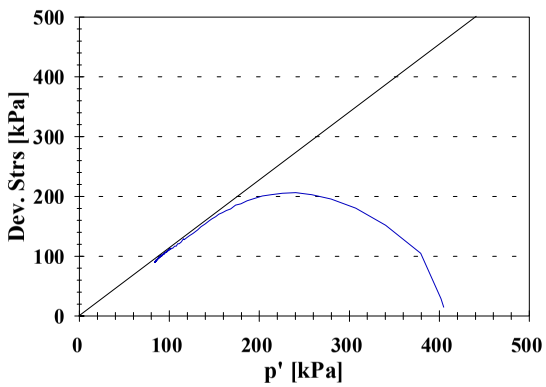

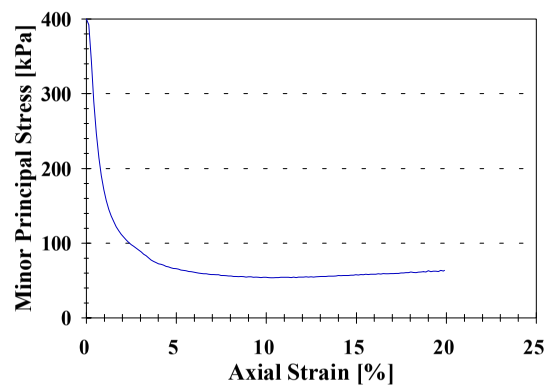

ϕ = 28.5 Confining stress = 400 kPa

GDS FJ#80 GS#40

Date: 10/20/00 Fines= 25 e= 0.491 ec= 0.988 ef= n.a. (ef)eq= n.a. (ec)eq= 0.835

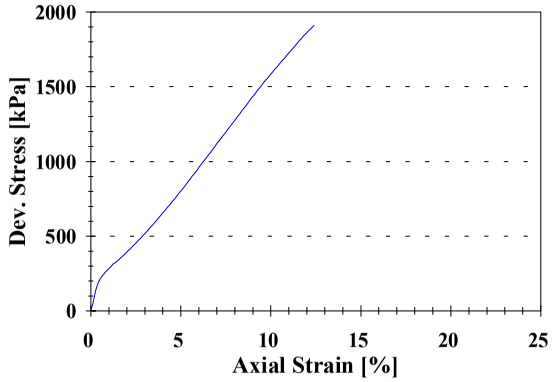

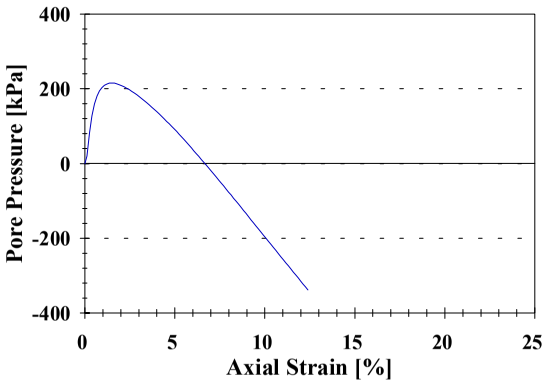

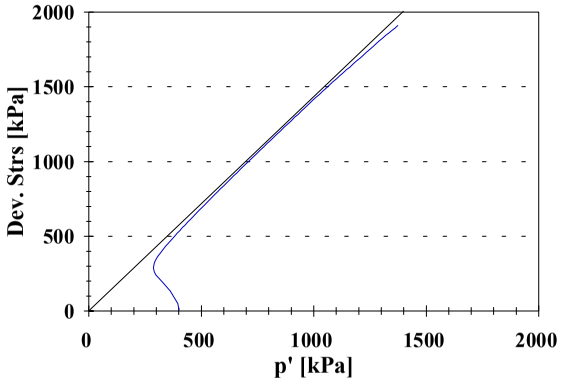

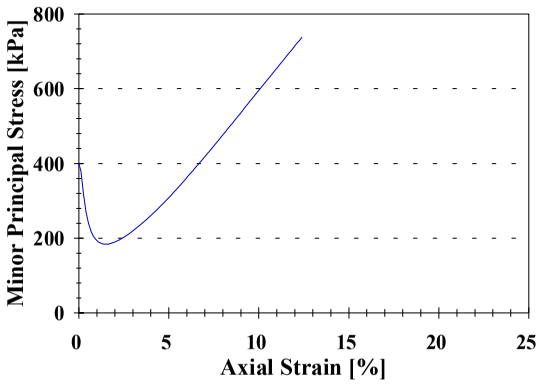

ϕ = 35.2 Confining stress = 400 kPa

GDS FJ#80 GS#40

Date: 10/27/00 Fines= 25 e= 0.444 ec= 0.925 ef= n.a. (ef)eq= n.a. (ec)eq= 0.777

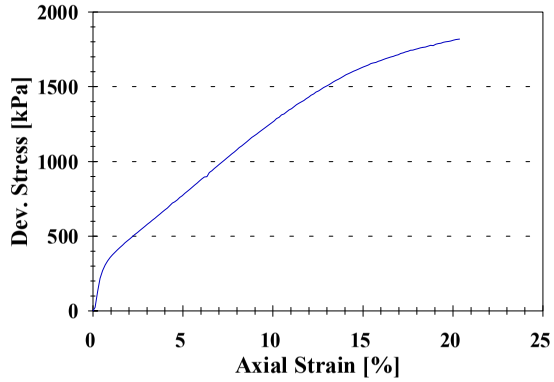

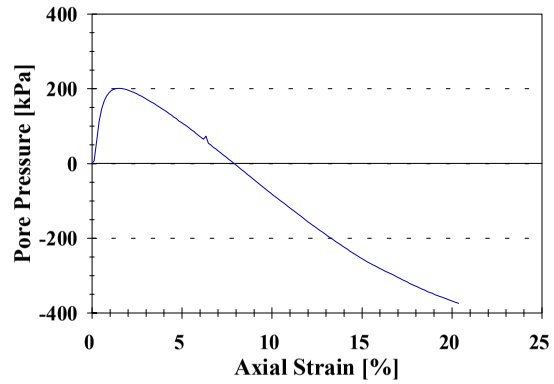

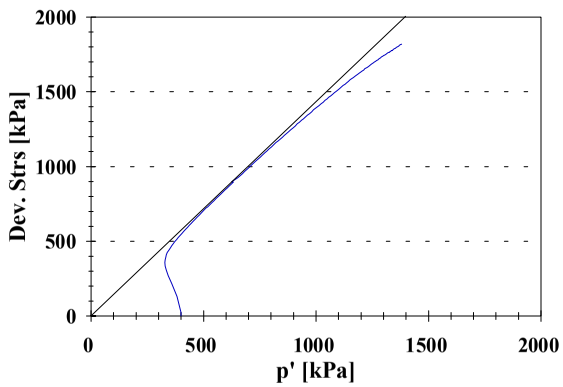

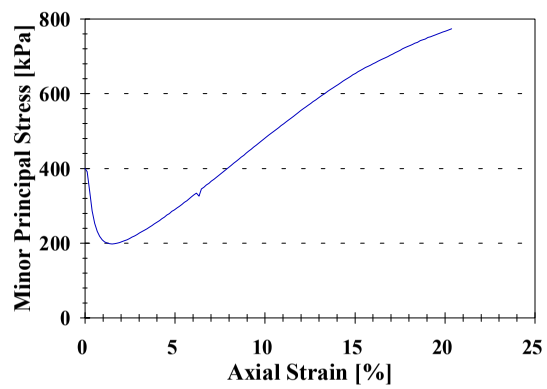

ϕ = 35.2 Confining stress = 400 kPa

GDS FJ#80 GS#40

Date: 01/02/01	Fines= 25	e= 0.500	ec= 1.000	ef= n.a.	(ef)eq= n.a.	(ec)eq= 0.846

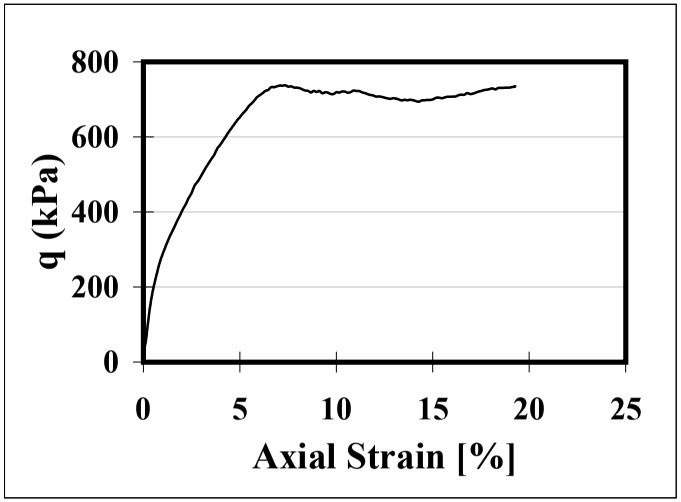

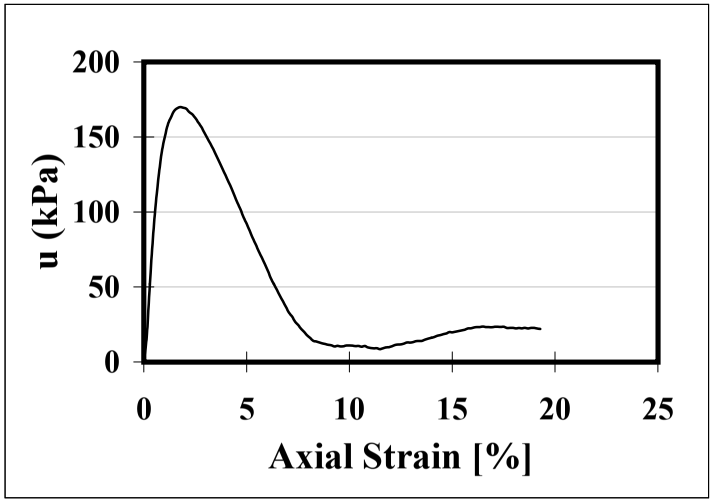

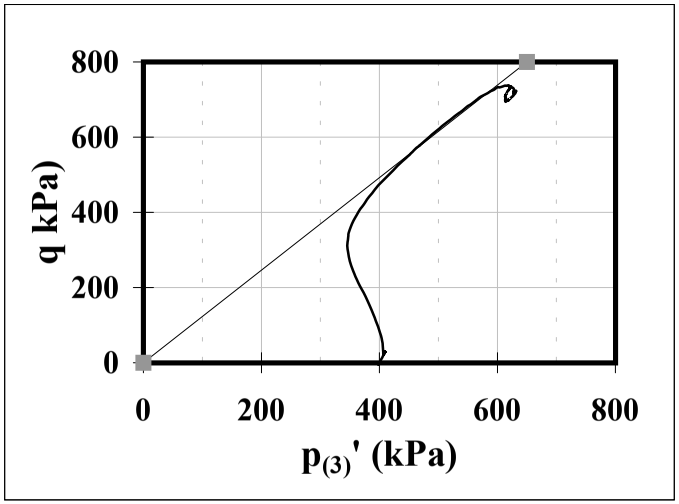

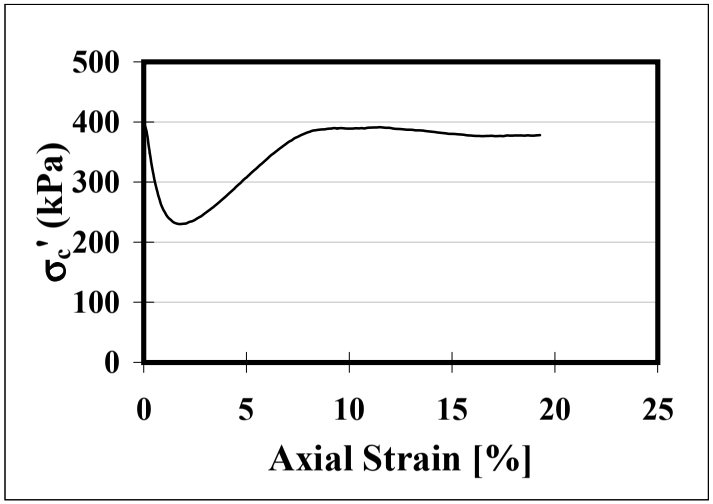

ϕ = 30.7 Confining stress = 400 kPa

GDS FJ#80 GS#40

Date: 01/12/01	Fines= 25	e= 0.562	ec= 1.083	ef= n.a.	(ef)eq= n.a.	(ec)eq= 0.923

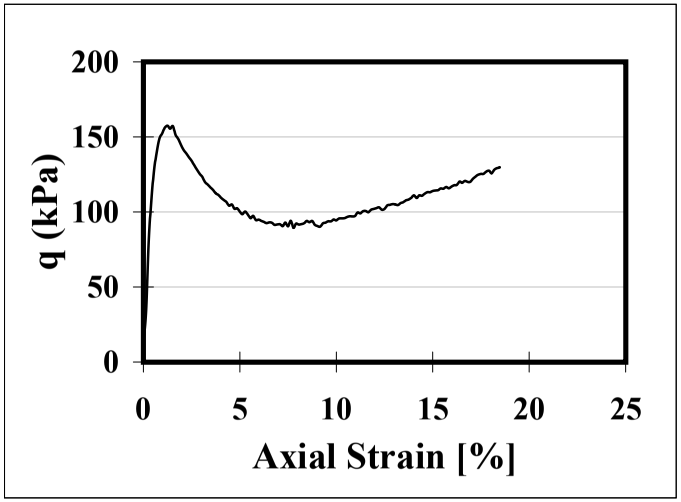

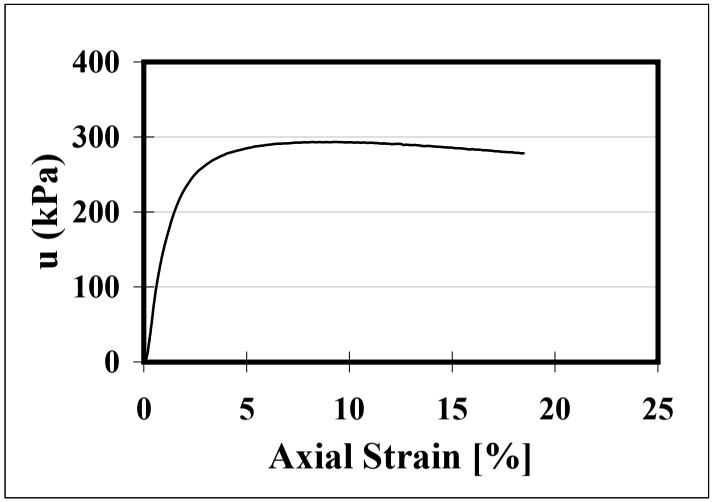

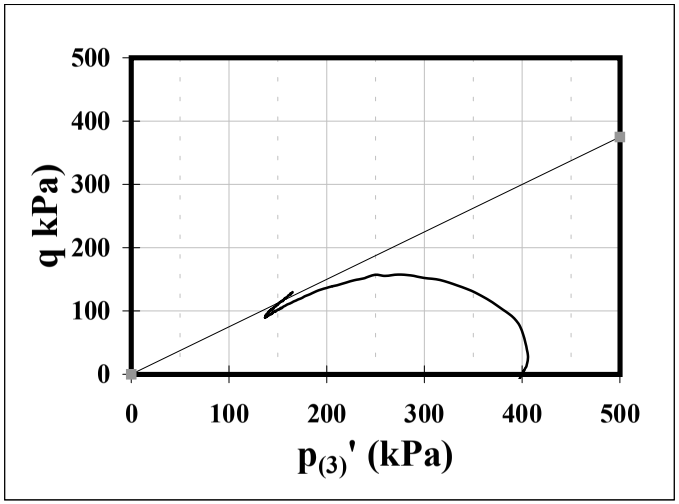

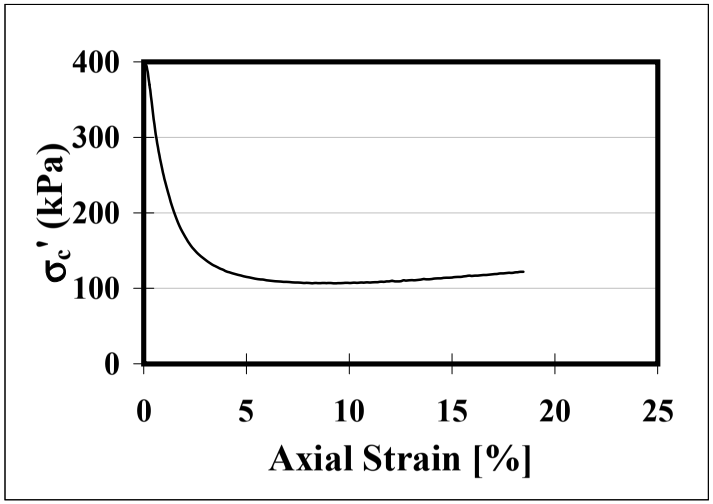

ϕ = 19.5 Confining stress = 400 kPa

GDS FJ#80 GS#40

Date: 01/16/01	Fines= 25	e= 0.613	ec= 1.151	ef= n.a.	(ef)eq= n.a.	(ec)eq= 0.986

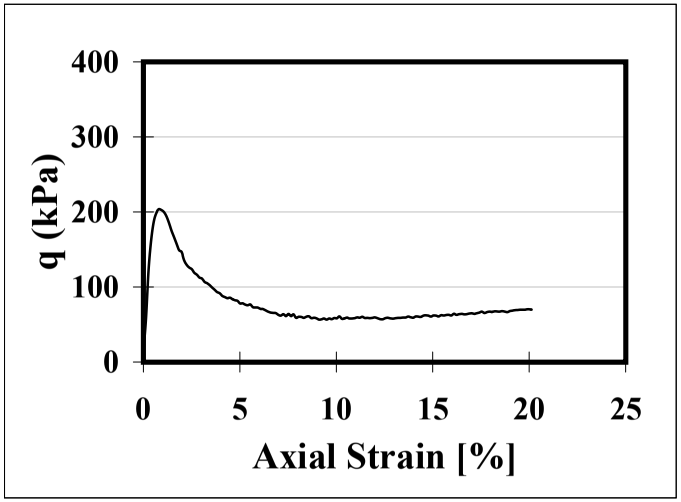

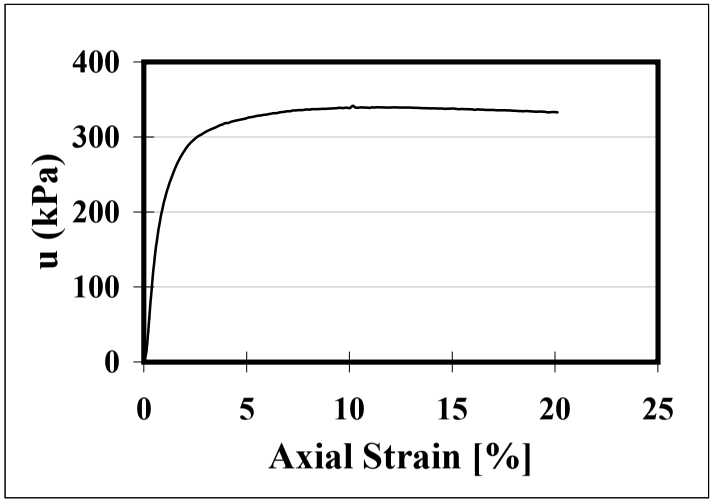

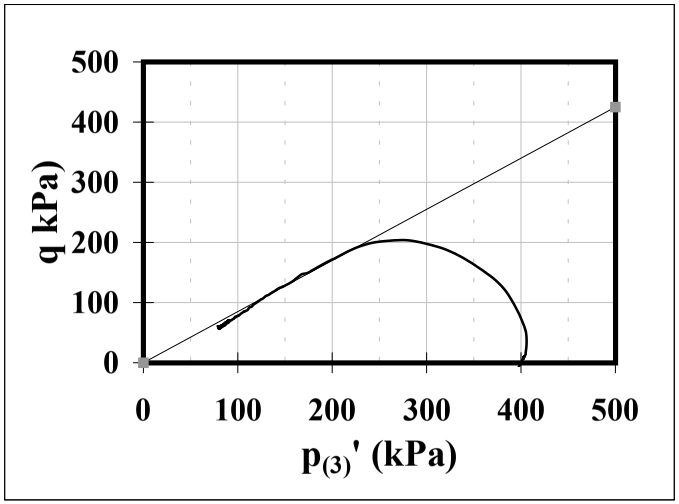

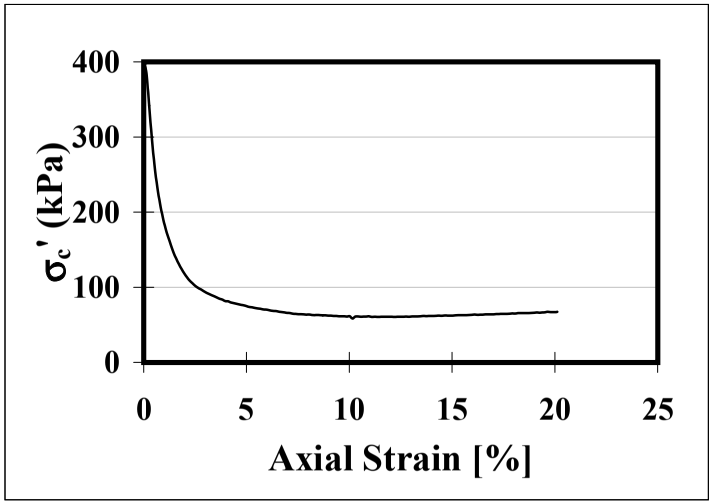

ϕ = 21.9 Confining stress = 400 kPa

GDS FJ#80 GS#40

Date: 01/18/01	Fines= 25	e= 0.550	ec= 1.066	ef= n.a.	(ef)eq= n.a.	(ec)eq= 0.907

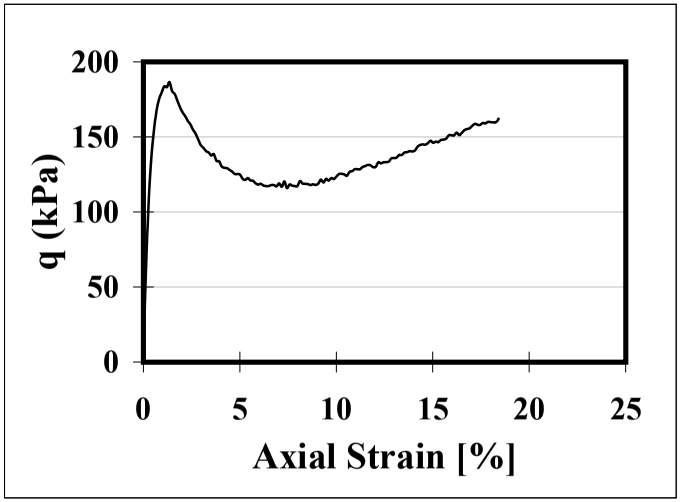

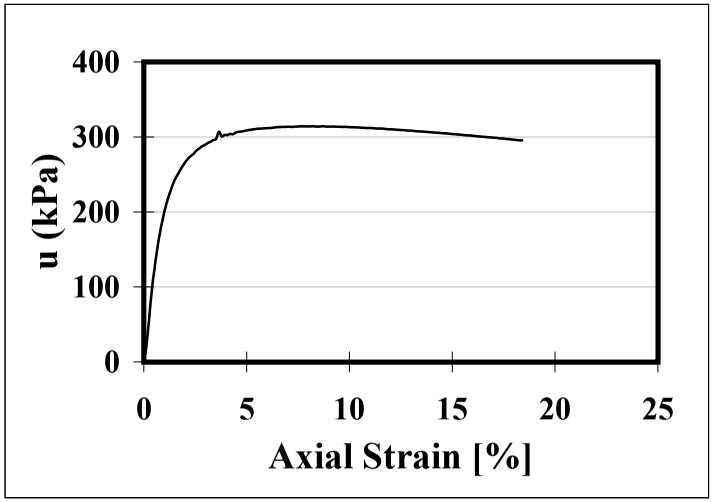

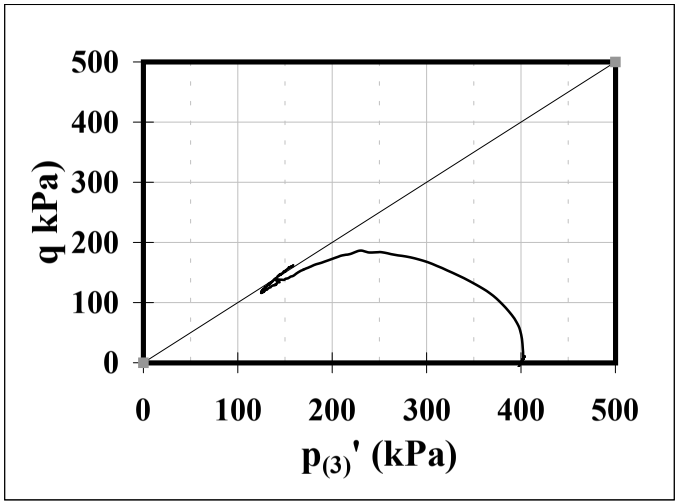

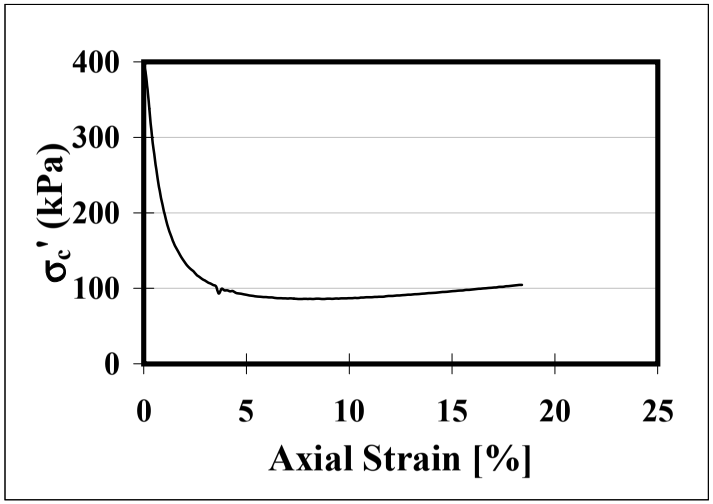

ϕ = 25.4 Confining stress = 400 kPa

GDS FJ#80 GS#40

Date: 01/30/01	Fines= 25	e= 0.576	ec= 1.102	ef= n.a.	(ef)eq= n.a.	(ec)eq= 0.940

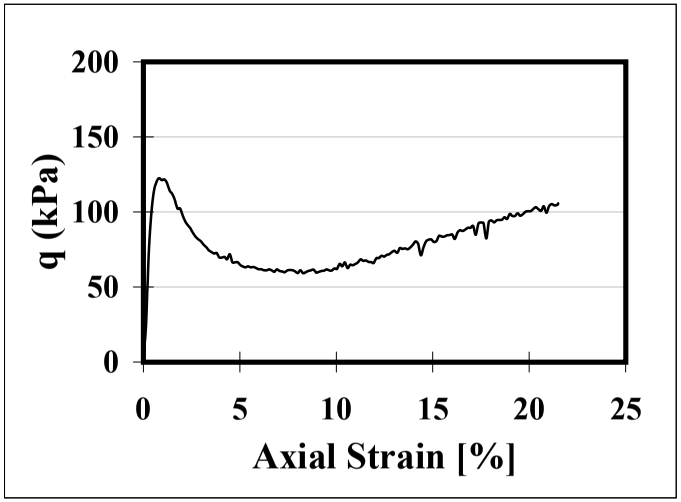

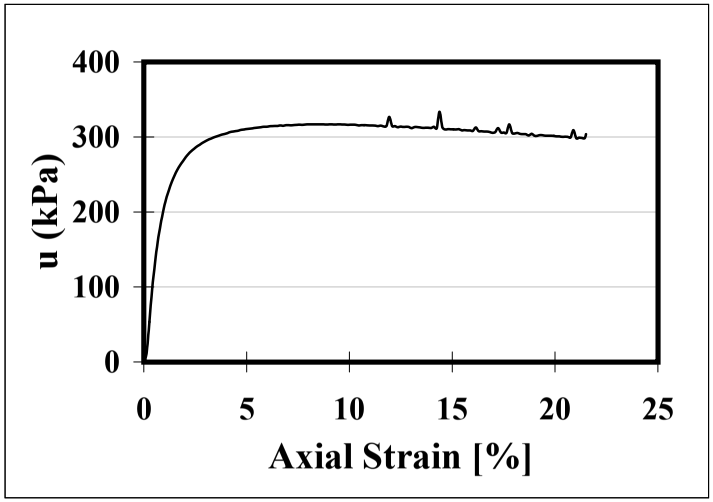

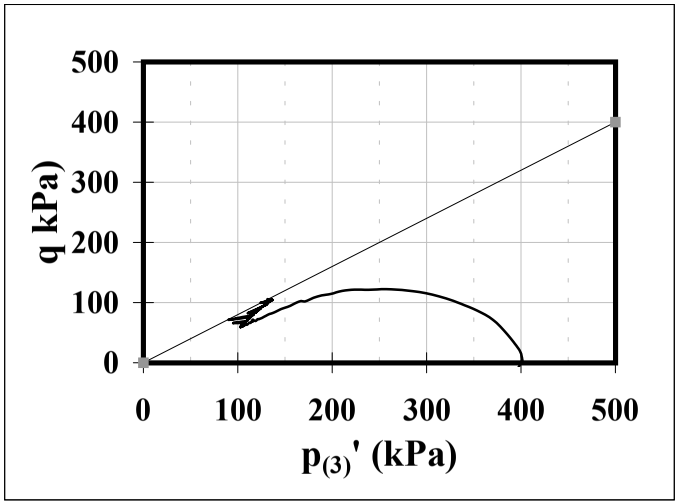

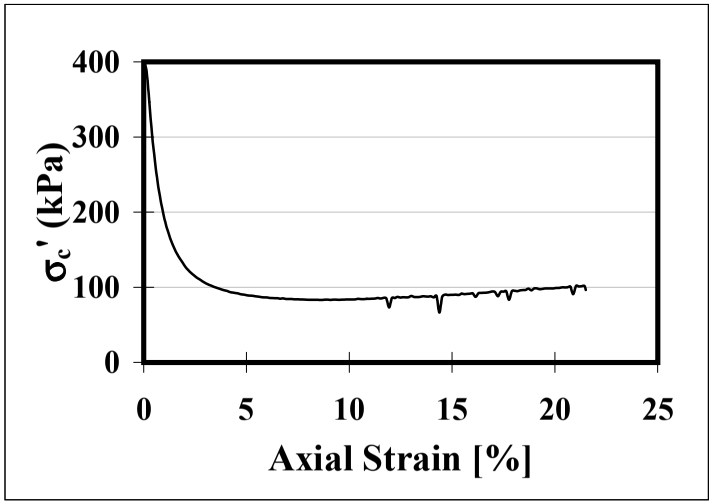

ϕ = 20.7 Confining stress = 400 kPa

GDS FJ#80 GS#40

Date: 02/01/01	Fines= 25	e= 0.548	ec= 1.065	ef= n.a.	(ef)eq= n.a.	(ec)eq= 0.906

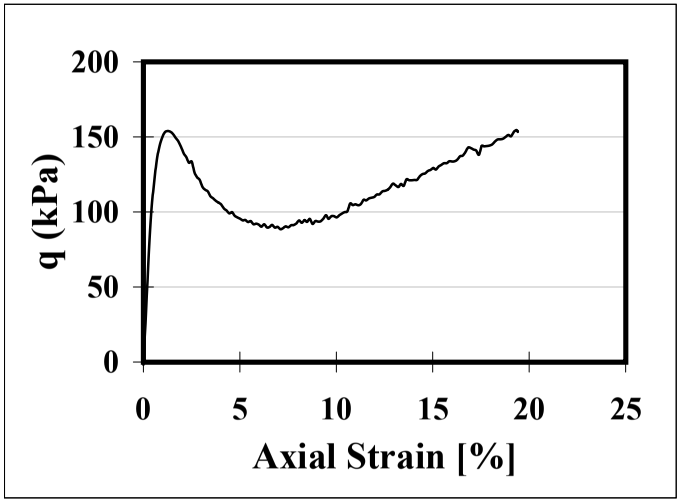

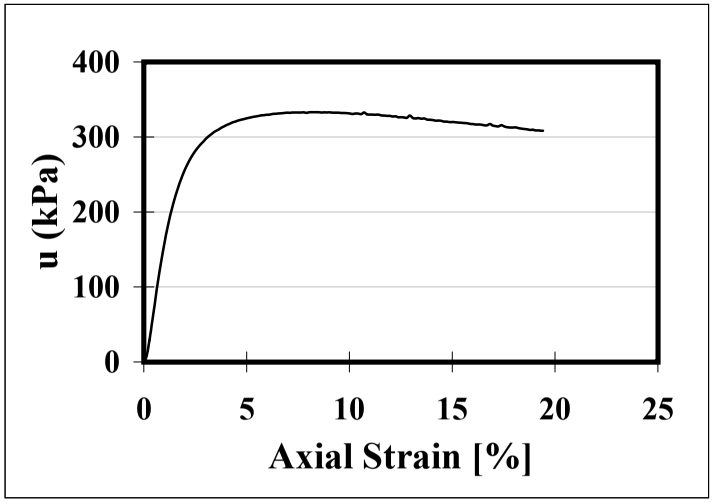

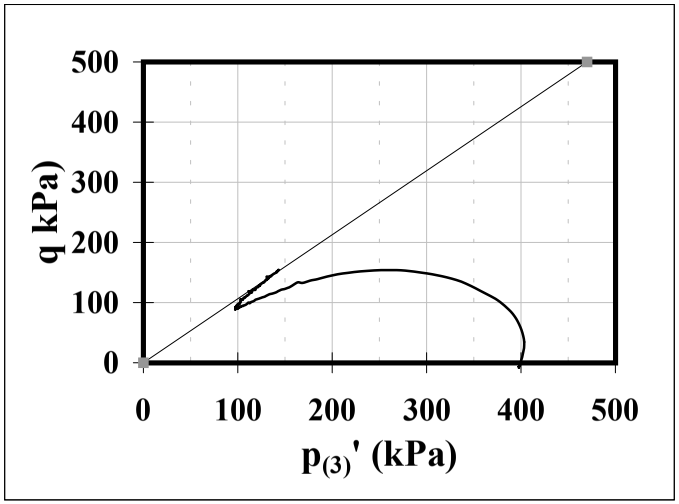

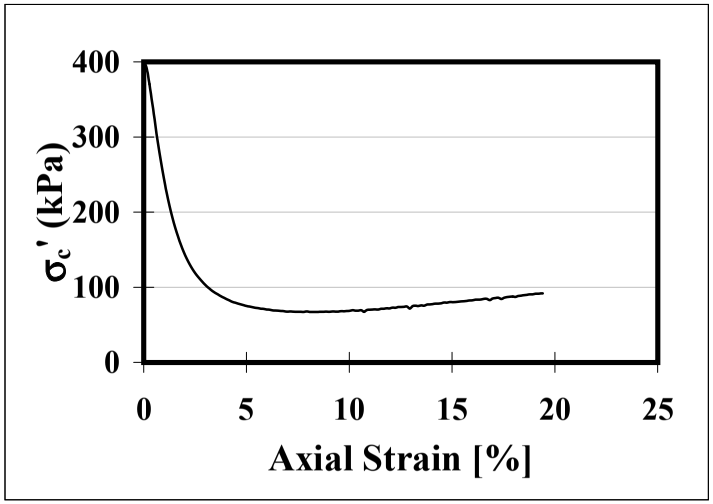

ϕ = 26.9 Confining stress = 400 kPa

GEOCOMP FJ#80 GSF#40

Date: 10/27/00	Fines= 25	e= 0.537	ec=	1.050	ef= n.a.	(ef)eq= n.a.	(ec)eq= 0.892

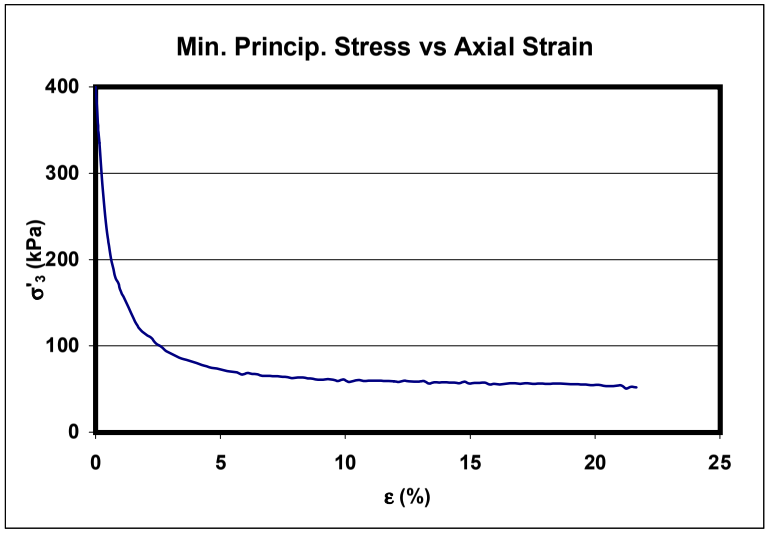

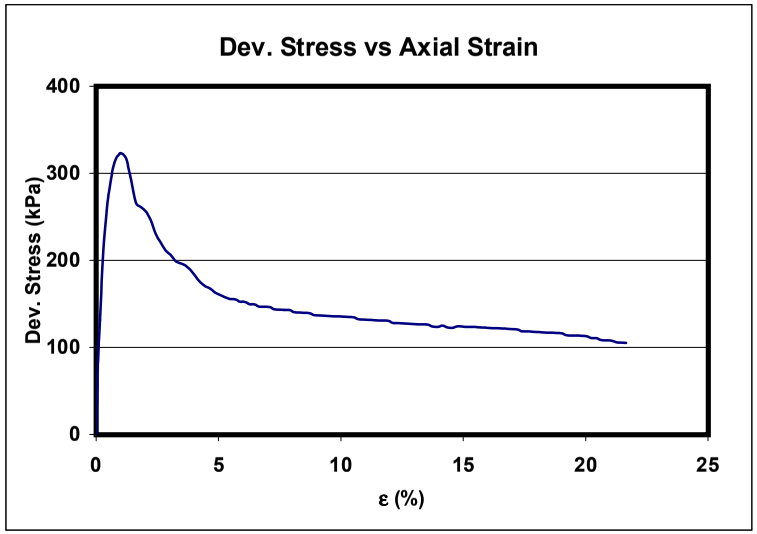

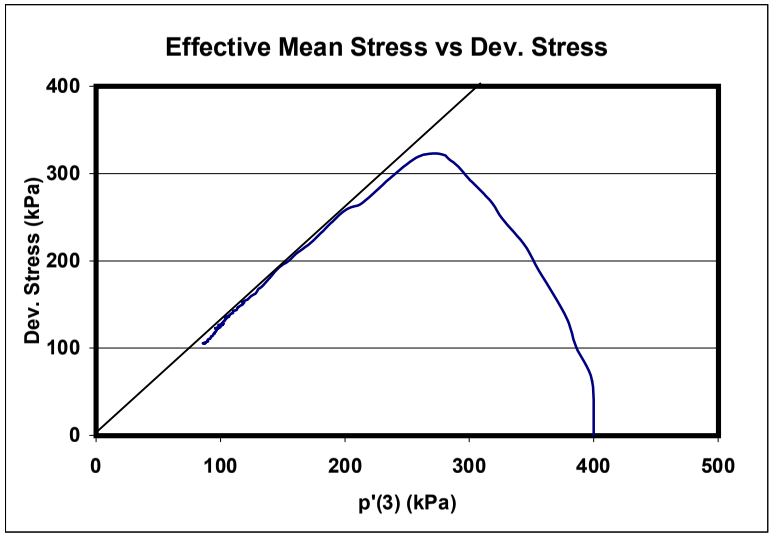

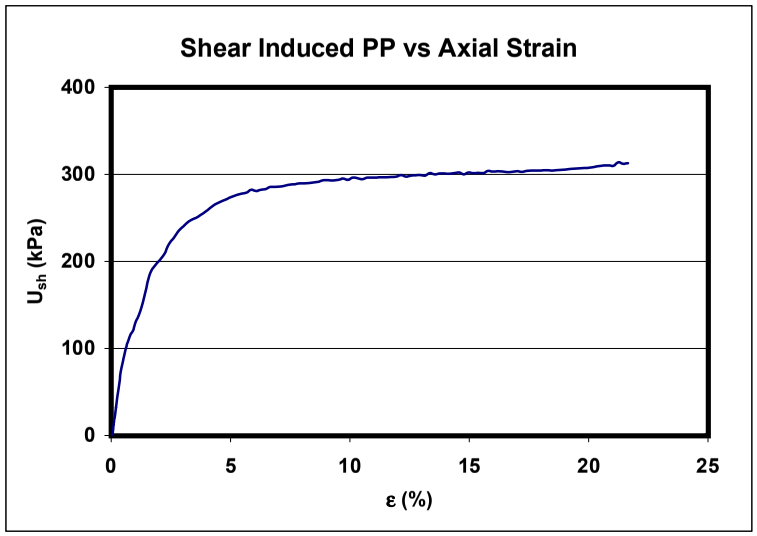

$\phi =$ 32.0 Confining stress = 400 kPa

GEOCOMP FJ#80 GSF#40

Date: 11/07/00	Fines= 25	e= 0.546	ec=	1.061	ef= n.a.	(ef)eq= n.a.	(ec)eq= 0.903

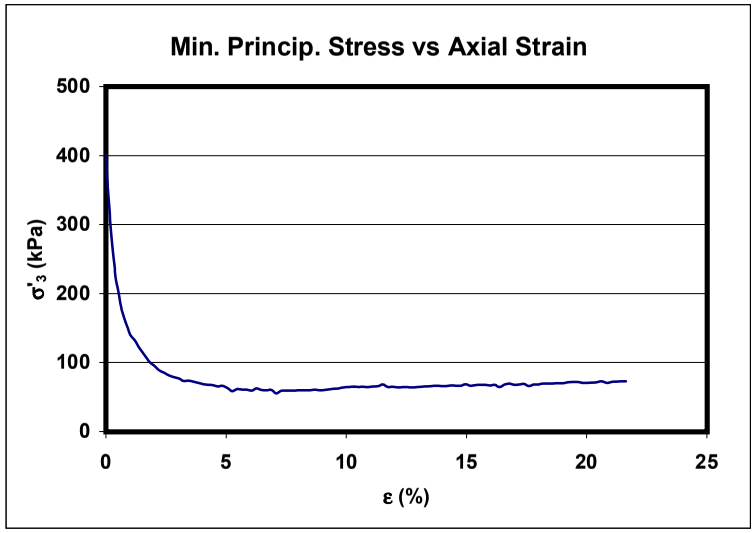

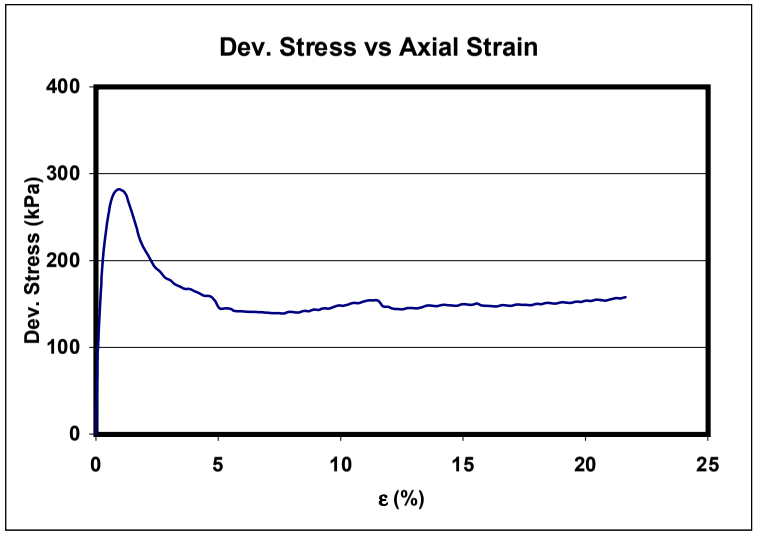

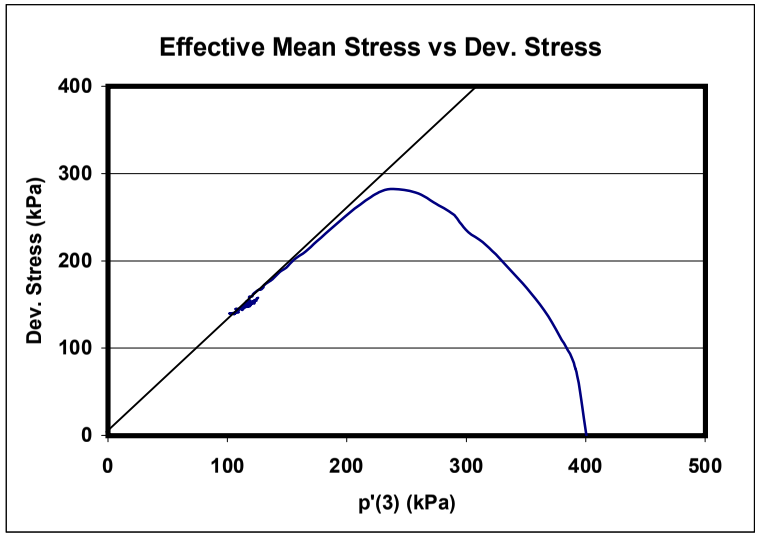

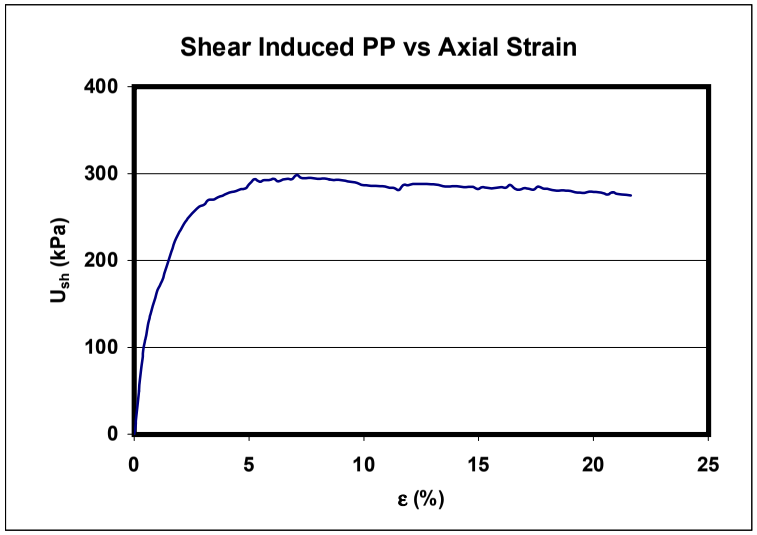

$\phi =$ 32.0 Confining stress = 400 kPa

GEOCOMP FJ#80 GSF#40

Date: 11/13/00	Fines= 25	e= 0.569	ec=	1.092	ef= n.a.	(ef)eq= n.a.	(ec)eq= 0.931

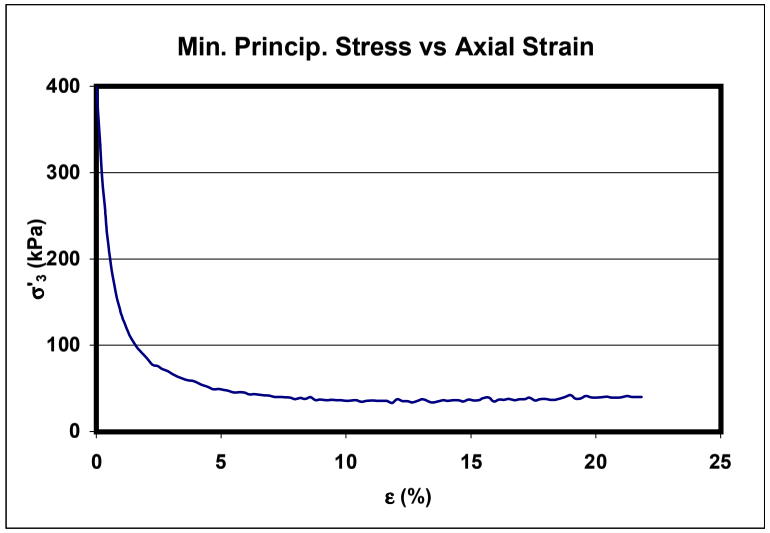

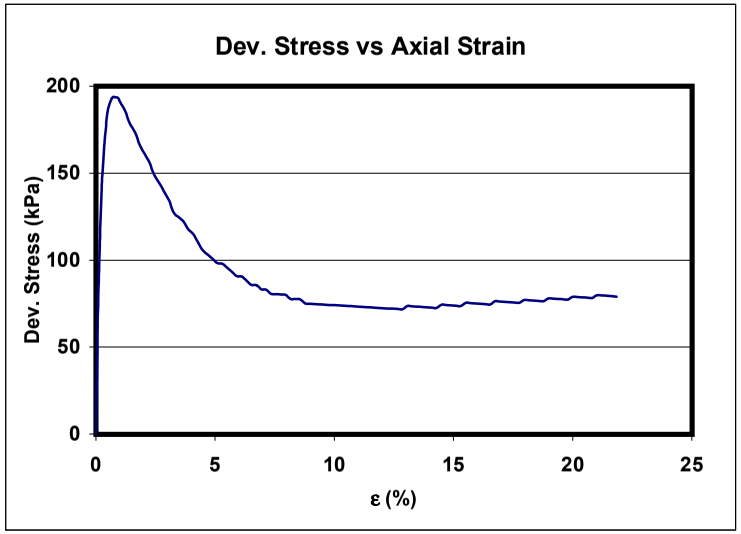

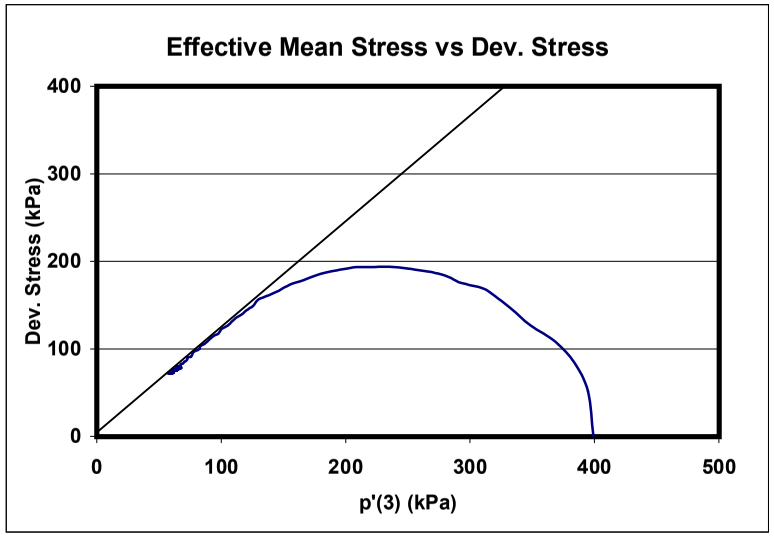

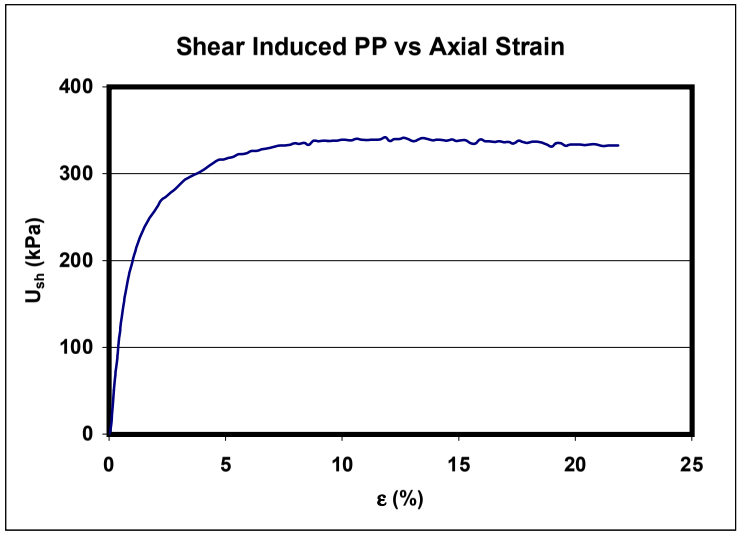

ϕ = 30.0 Confining stress = 400 kPa

GEOCOMP FJ#80 GSF#40

Date: 11/14/00	Fines= 25	e= 0.616	ec=	1.155	ef= n.a.	(ef)eq= n.a.	(ec)eq= 0.989

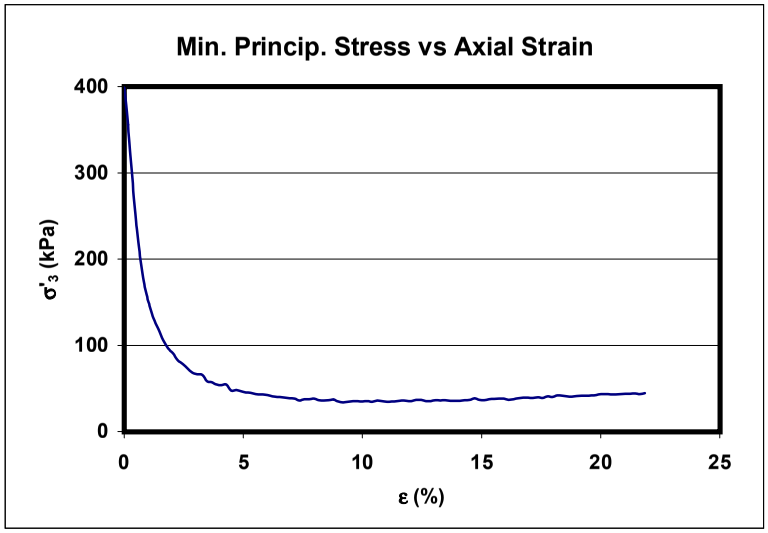

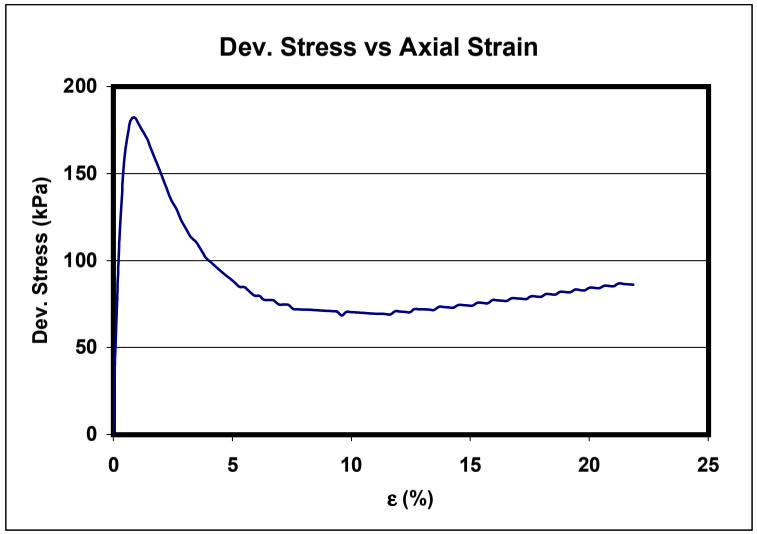

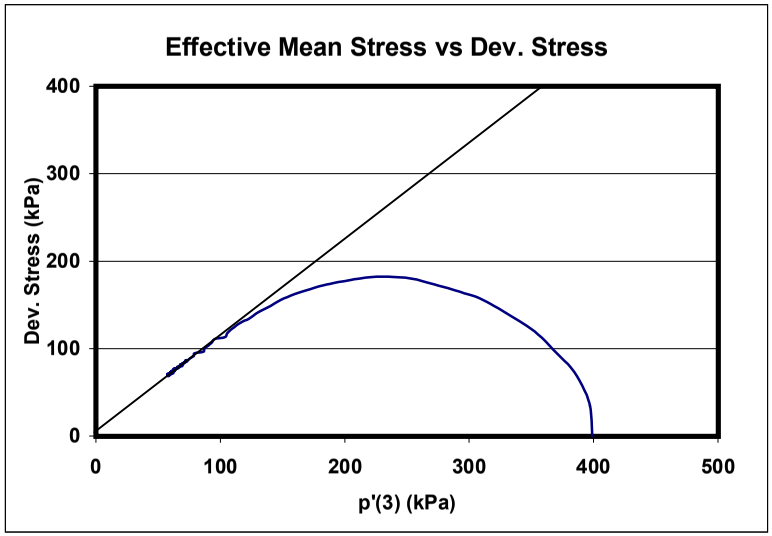

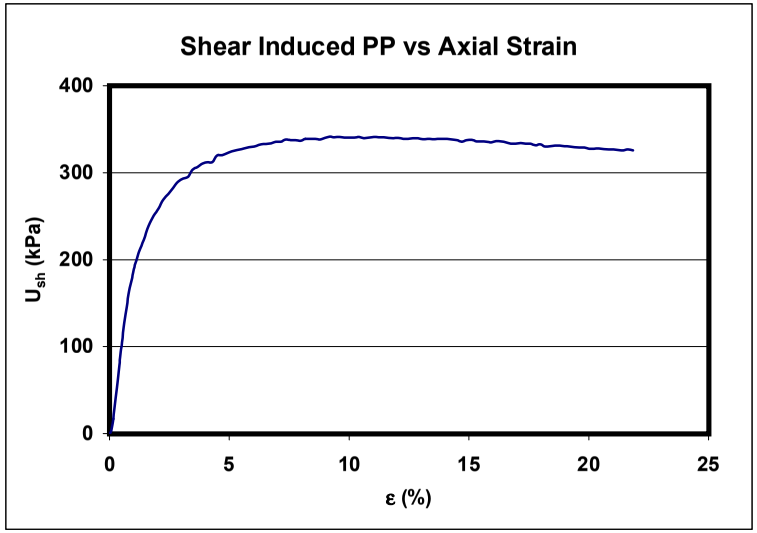

$\phi =$ 29.1 Confining stress = 400 kPa

GEOCOMP FJ#80 GSF#40

Date: 01/14/01	Fines= 25	e= 0.564	ec=	1.085	ef= n.a.	(ef)eq= n.a.	(ec)eq= 0.924

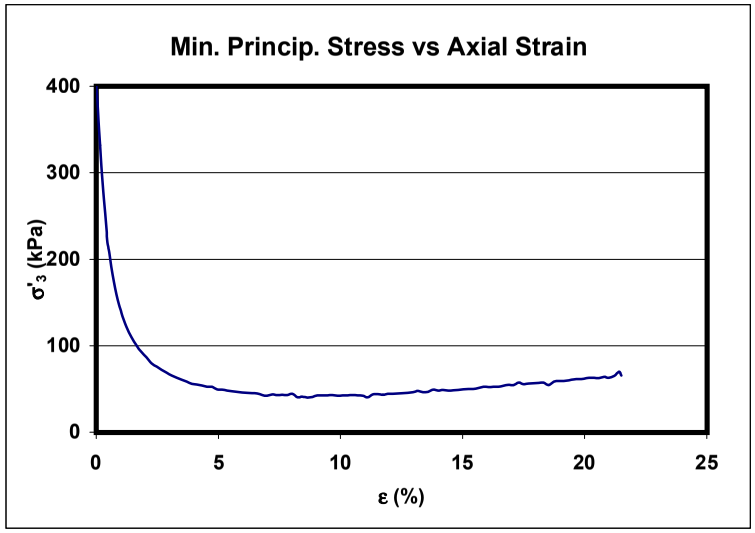

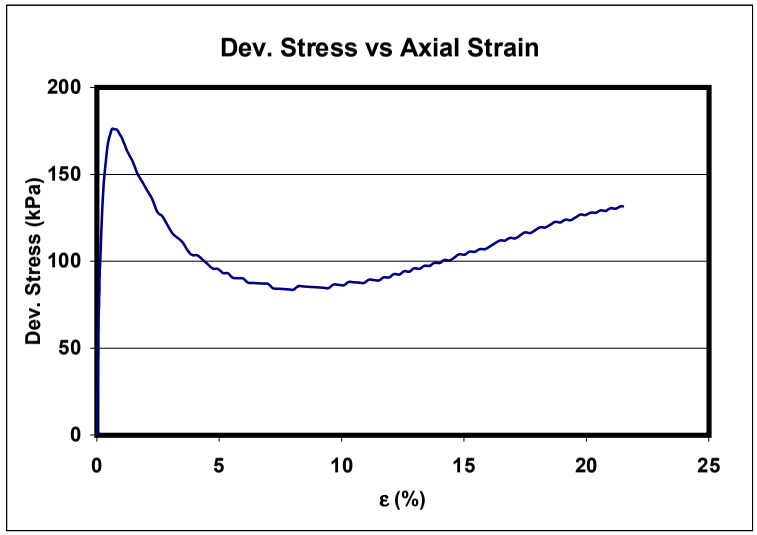

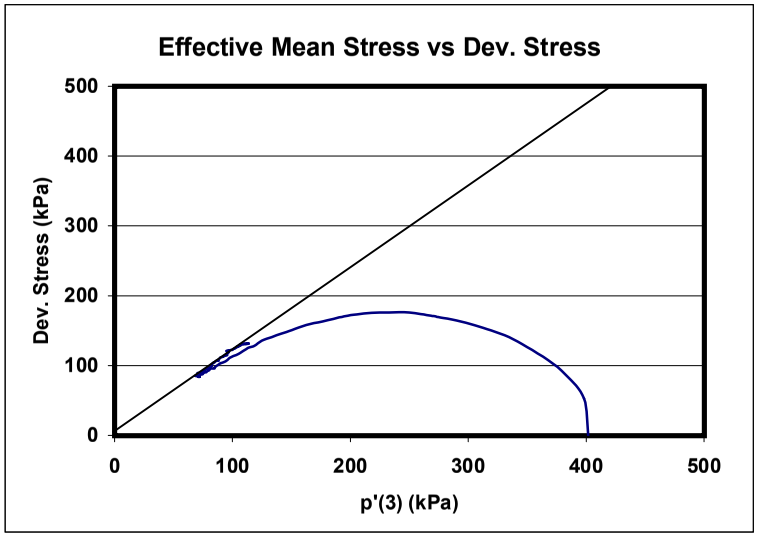

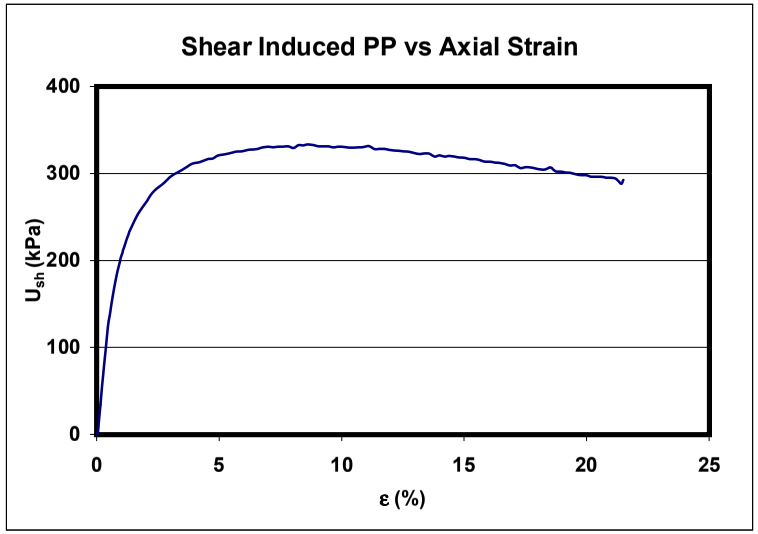

ϕ = 30.0 Confining stress = 400 kPa

GEOCOMP FJ#80 GSF#40

Date: 01/17/01	Fines= 25	e= 0.553	ec=	1.071	ef= n.a.	(ef)eq= n.a.	(ec)eq= 0.912

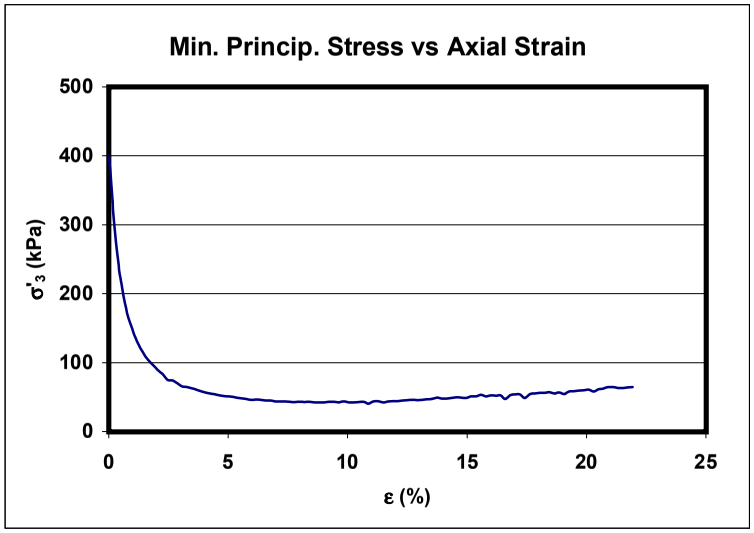

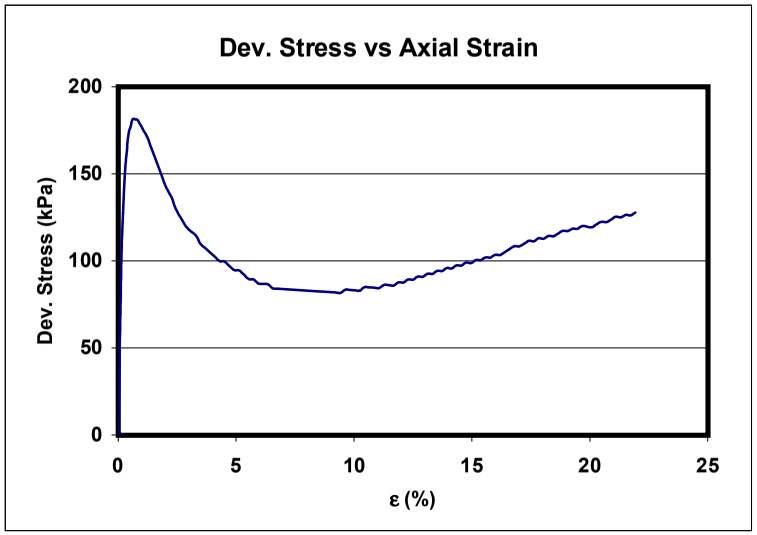

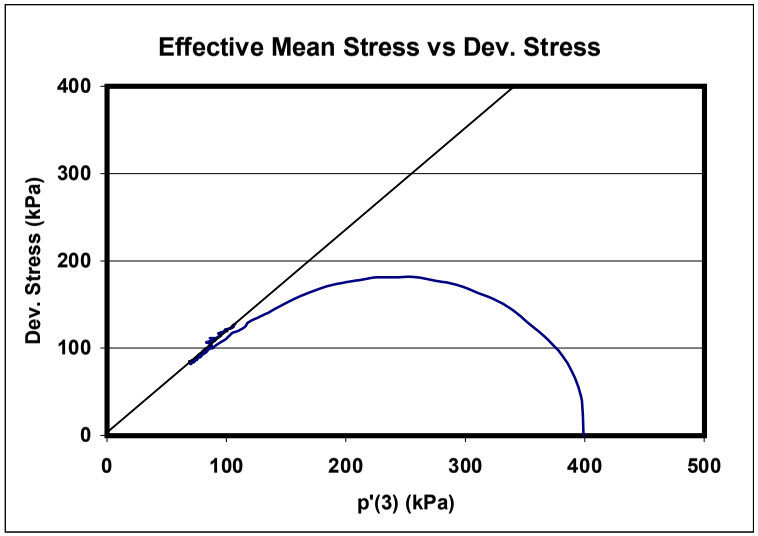

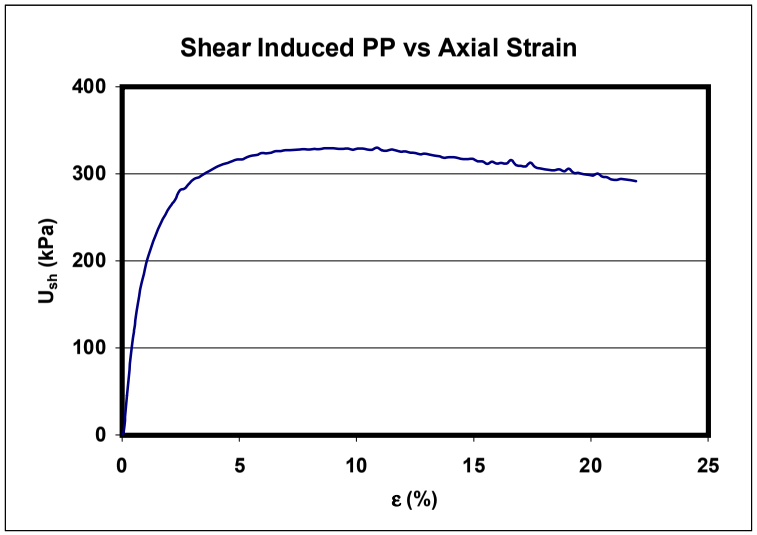

ϕ = 30.0 Confining stress = 400 kPa

GEOCOMP FJ#80 GSF#40

Date: 1/24/2001	Fines= 25	e= 0.569	ec=	1.092	ef= n.a.	(ef)eq= n.a.	(ec)eq= 0.931

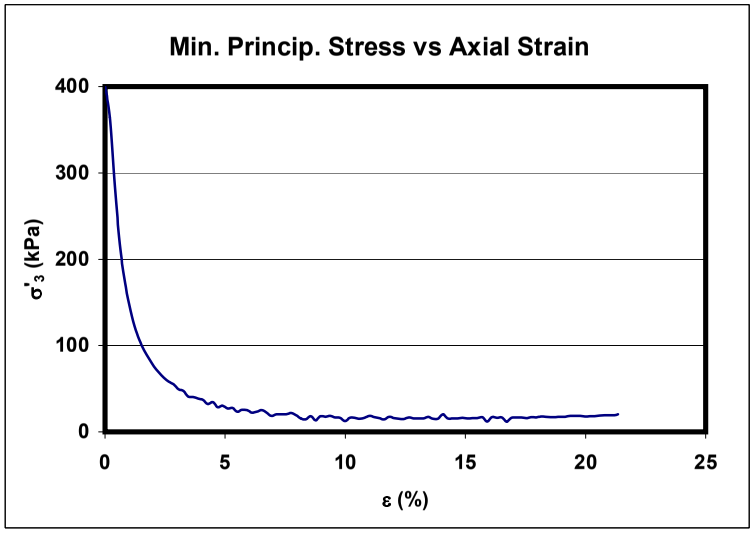

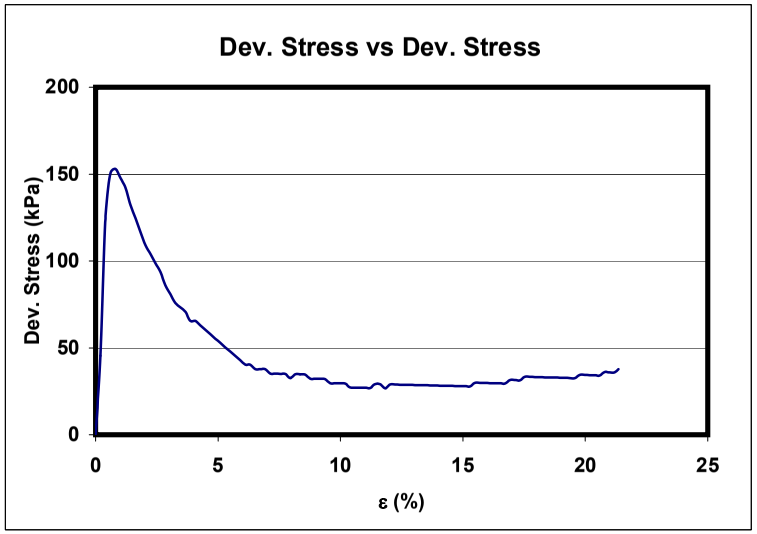

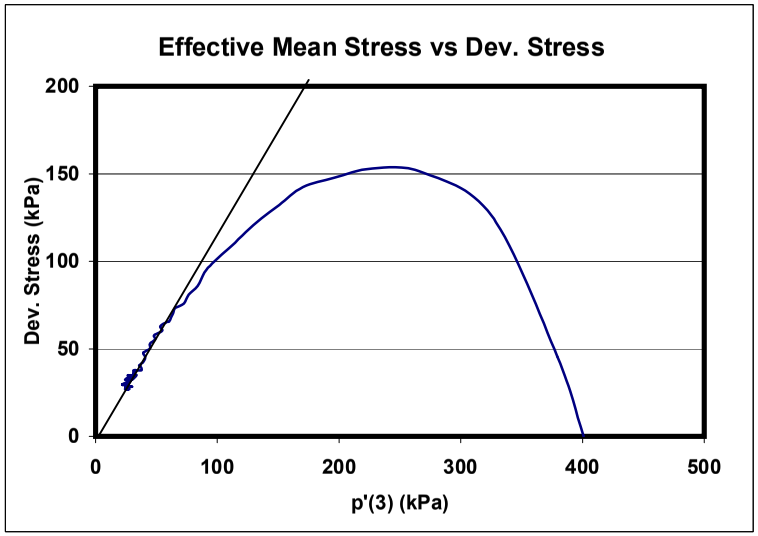

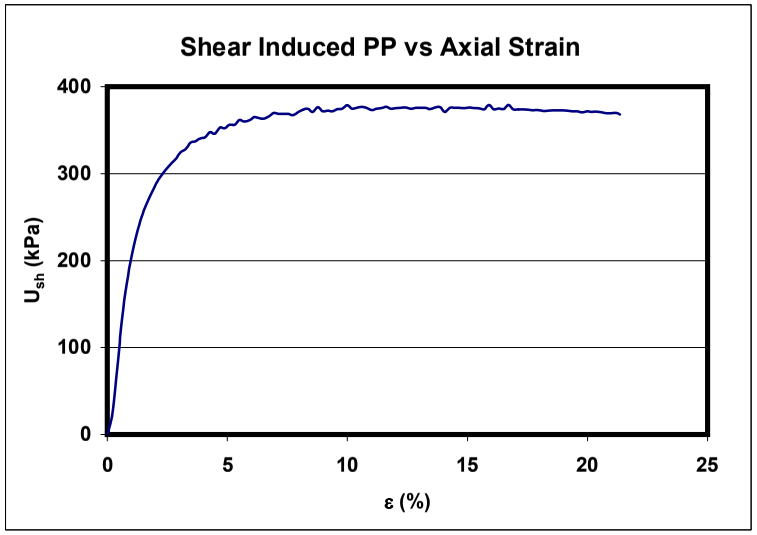

$\phi =$ 27.6 Confining stress = 400 kPa

GEOCOMP FJ#80 GSF#40

Date: 01/25/01	Fines= 25	e= 0.554	ec=	1.073	ef= n.a.	(ef)eq= n.a.	(ec)eq= 0.913

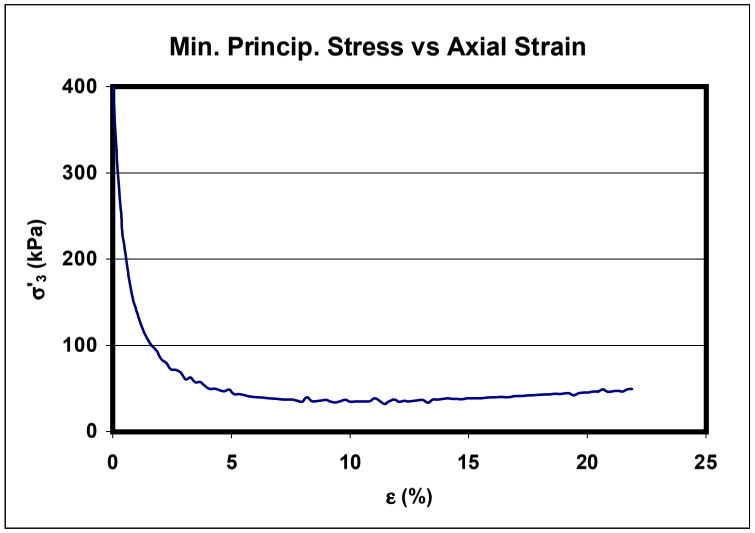

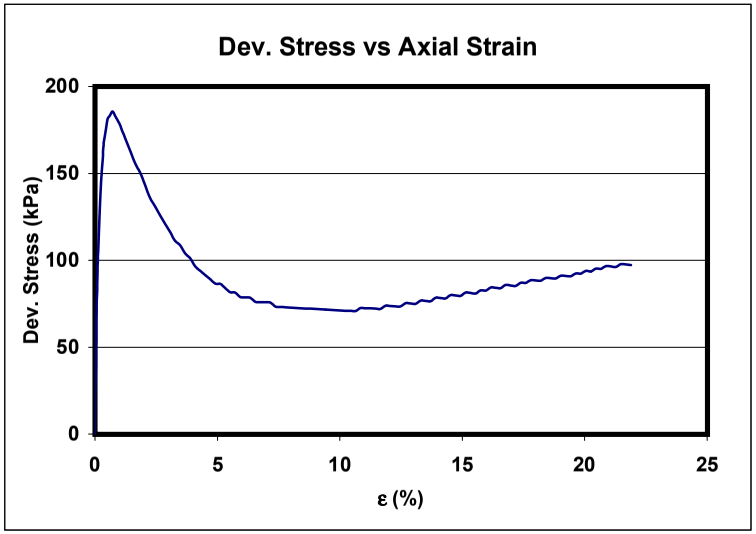

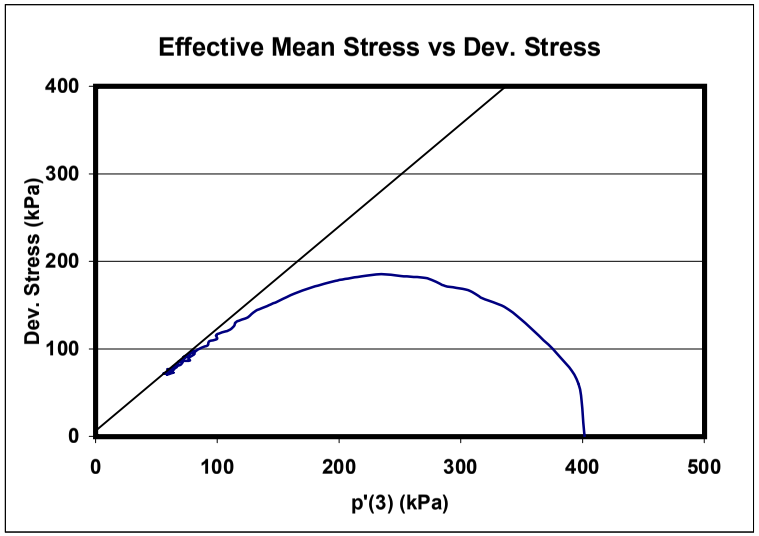

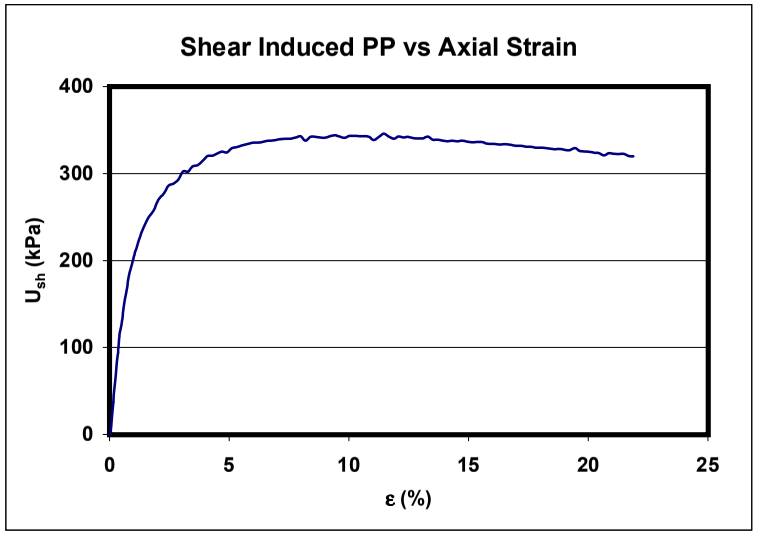

ϕ = 30.0 Confining stress = 400 kPa

GEOCOMP FJ#80 GSF#40

Date: 01/29/01	Fines= 25	e= 0.557	ec=	1.075	ef= n.a.	(ef)eq= n.a.	(ec)eq= 0.916

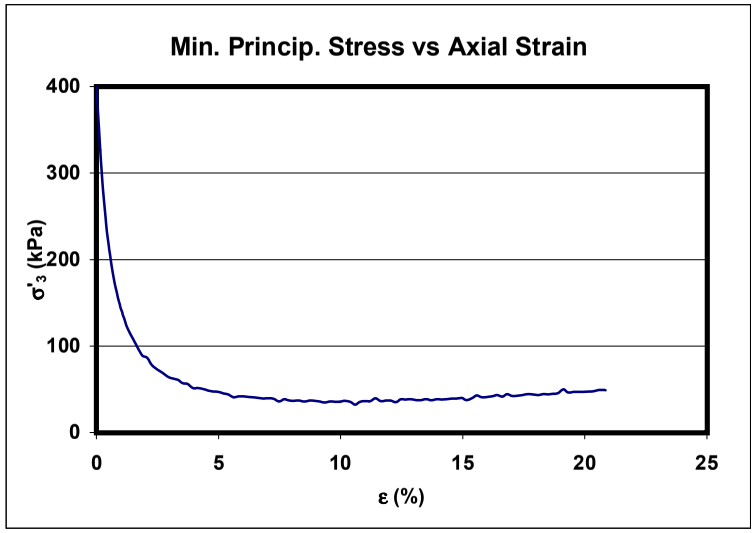

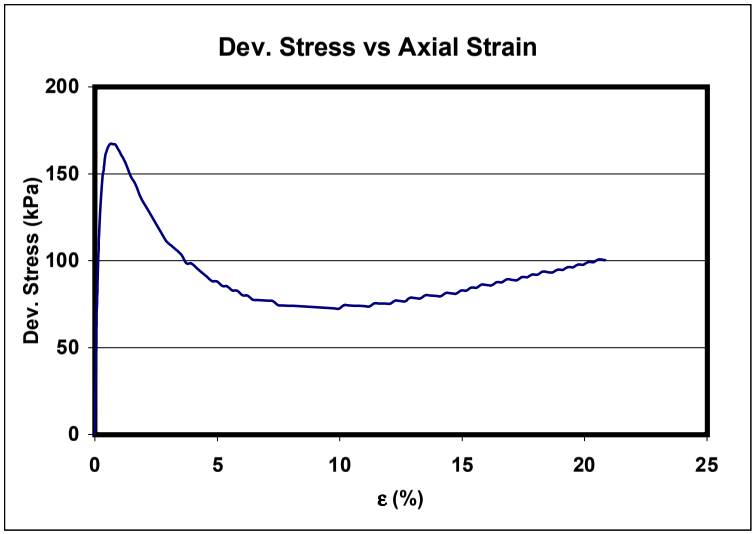

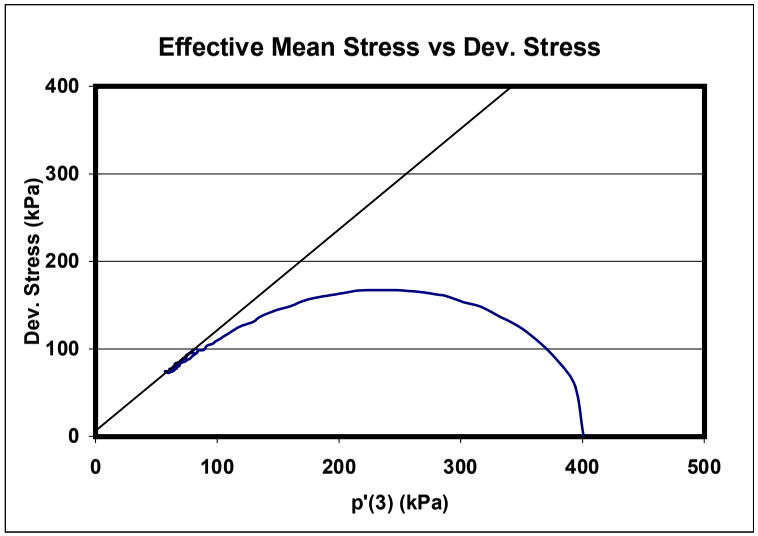

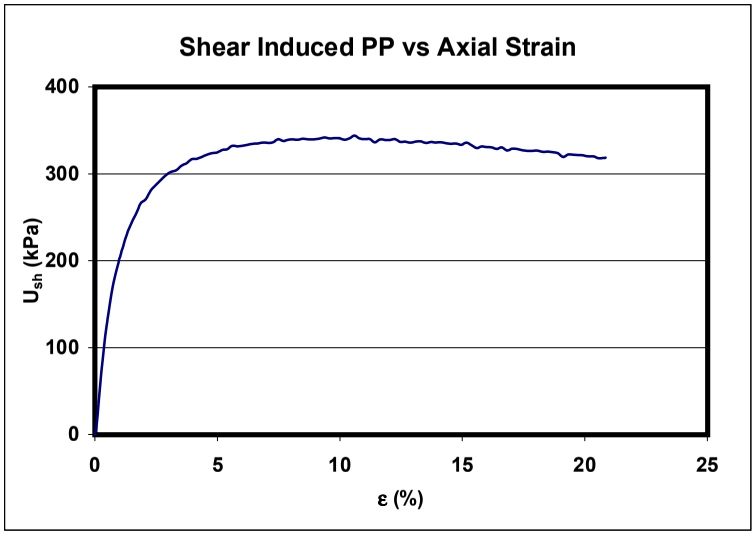

ϕ = 30.0 Confining stress = 400 kPa

GEOCOMP FJ#80 GSF#40

Date: 01/30/01	Fines= 25	e= 0.568	ec=	1.091	ef= n.a.	(ef)eq= n.a.	(ec)eq= 0.930

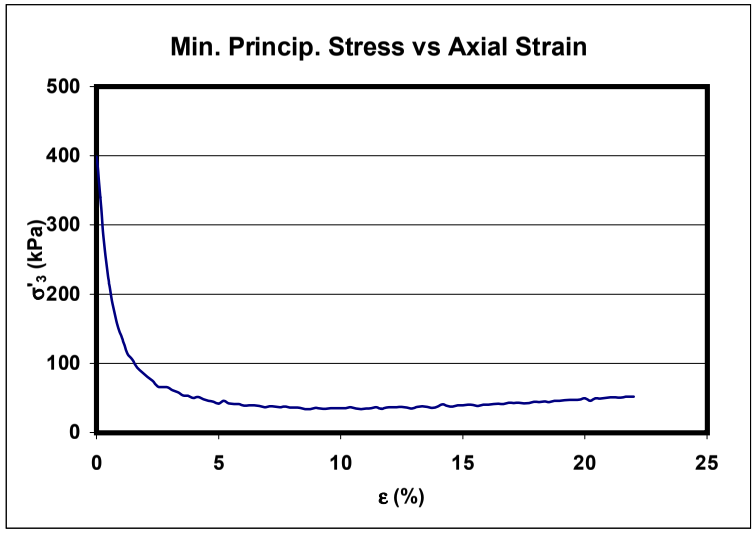

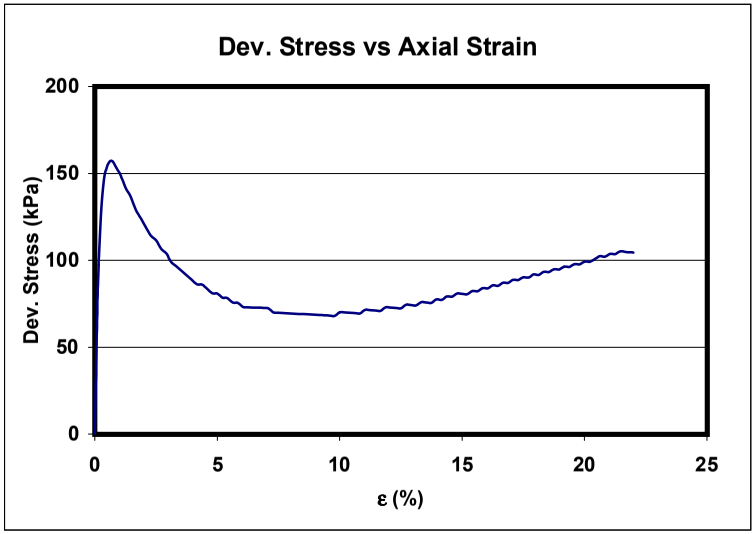

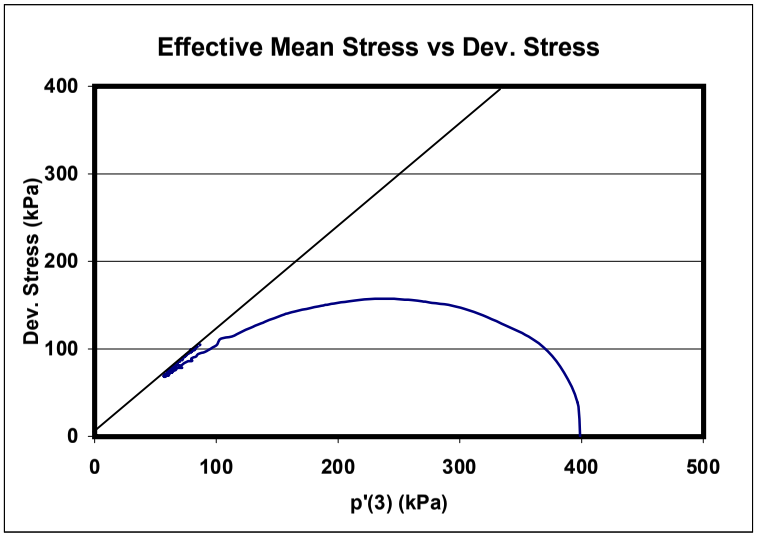

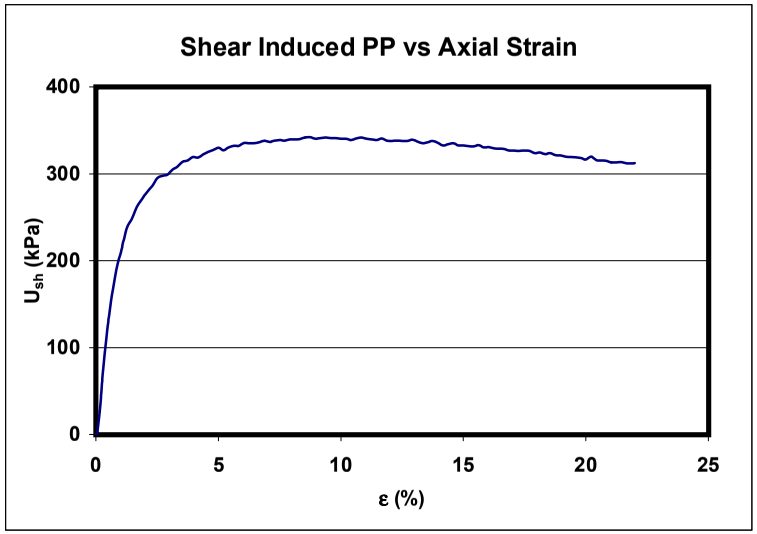

ϕ = 30.0 Confining stress = 400 kPa

GEOCOMP FJ#80 GSF#40

Date: 02/05/01	Fines= 25	e= 0.546	ec=	1.062	ef= n.a.	(ef)eq= n.a.	(ec)eq= 0.903

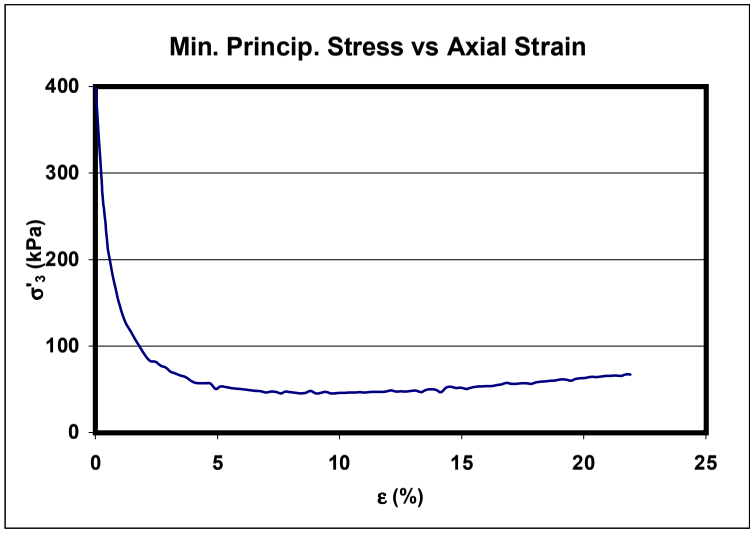

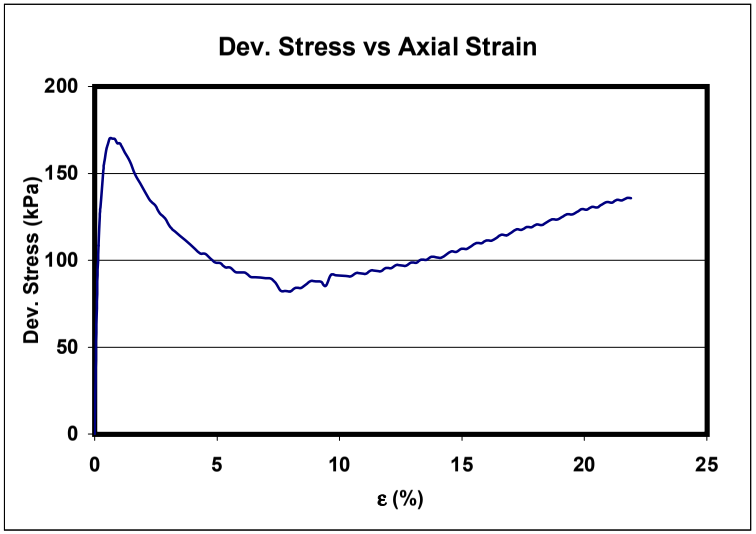

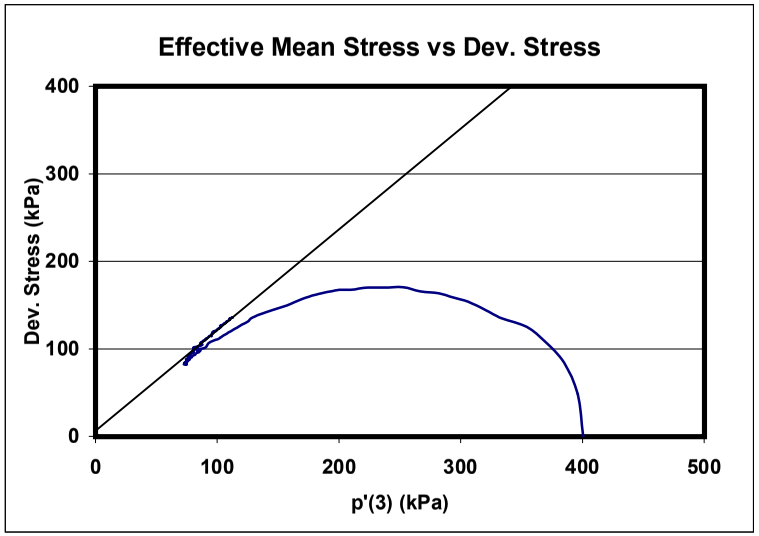

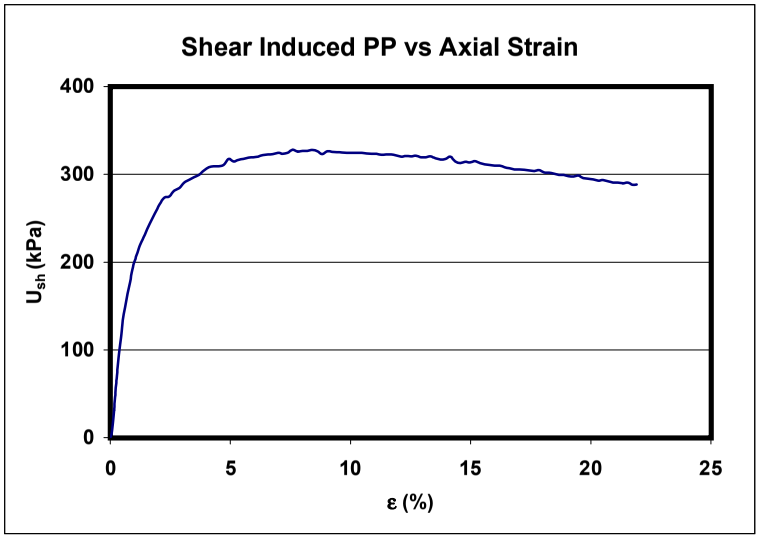

ϕ = 30.0 Confining stress = 400 kPa

GDS FJ#80 GS#40

Date: 07/28/00 Fines= 60 e= 0.640 ec= n.a. ef= 1.067 (ef)eq= 0.939 (ec)eq= n.a.

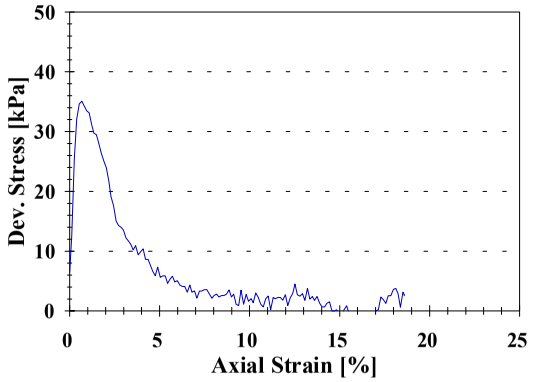

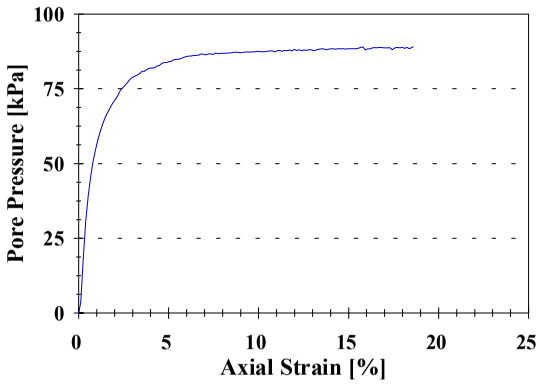

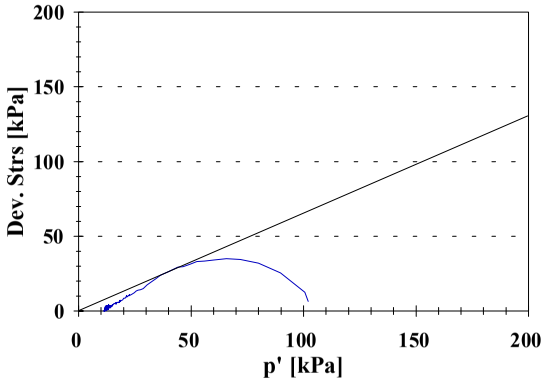

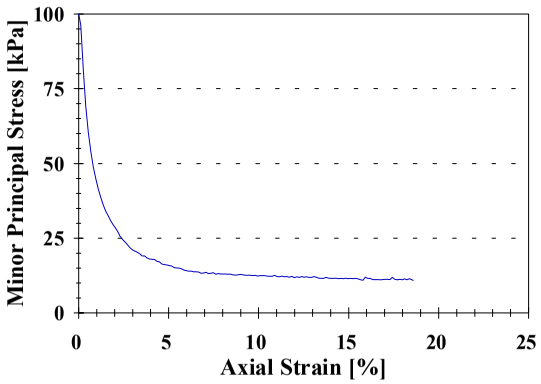

ϕ = 17.1 Confining stress = 100 kPa

GDS FJ#80 GS#40

Date: 05/17/01	Fines= 60	e= 0.641	ec= n.a.	ef= 1.069	(ef)eq= 0.884	(ec)eq= n.a.

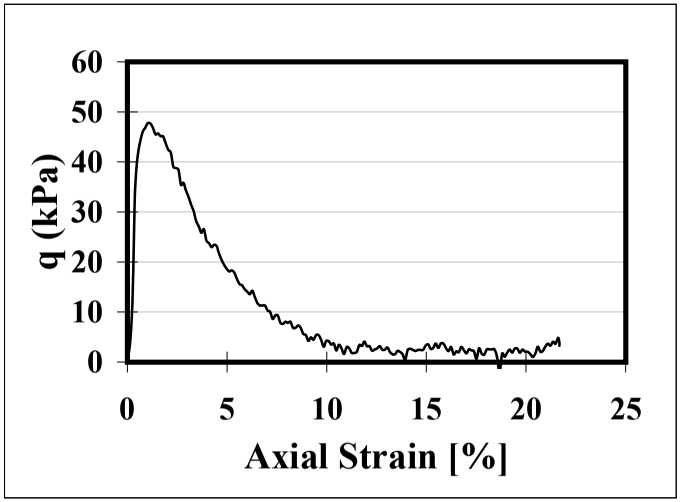

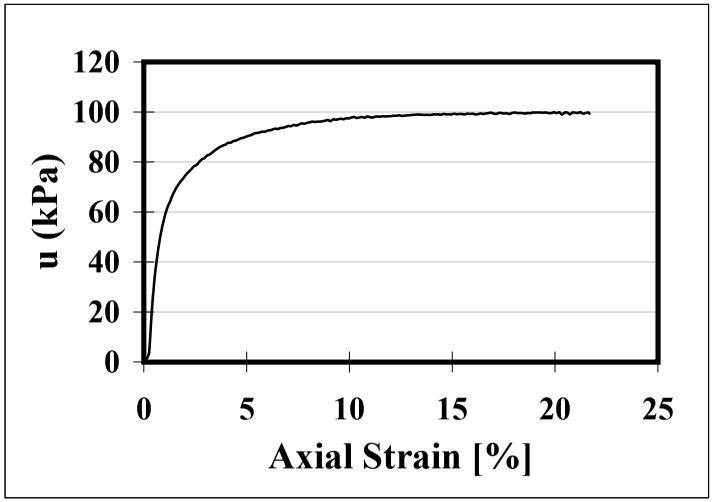

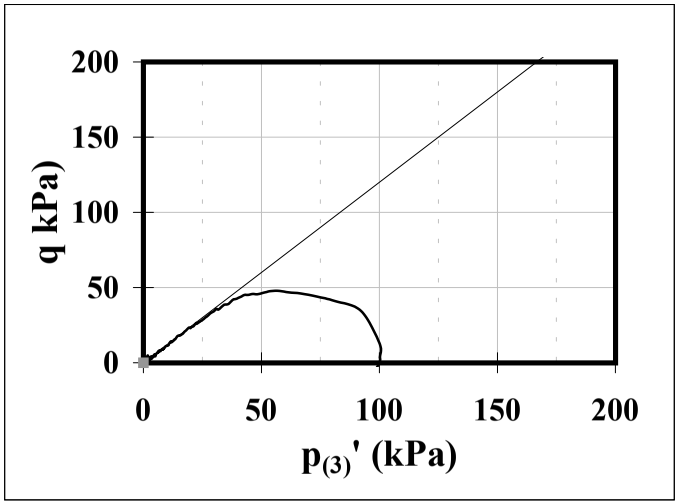

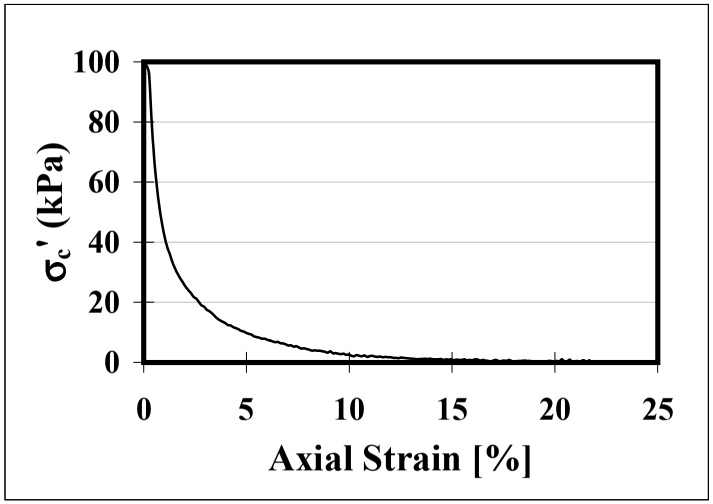

ϕ = 30.0 Confining stress = 100 kPa

GDS FJ#80 GS#40

Date: 05/18/01	Fines= 60	e= 0.623	ec= n.a.	ef= 1.038	(ef)eq= 0.858	(ec)eq= n.a.

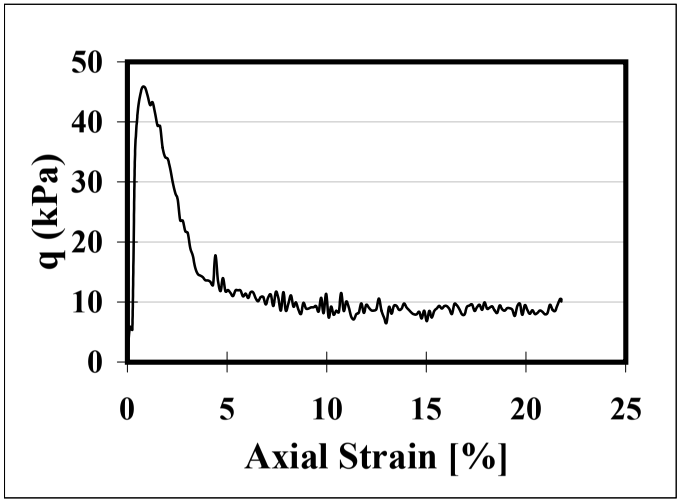

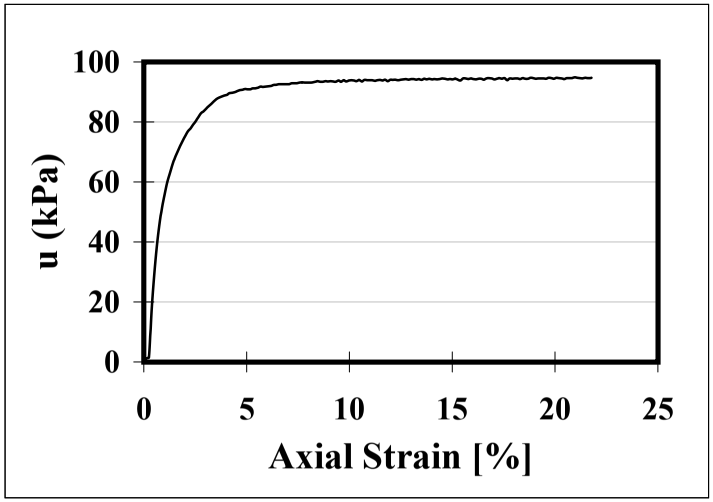

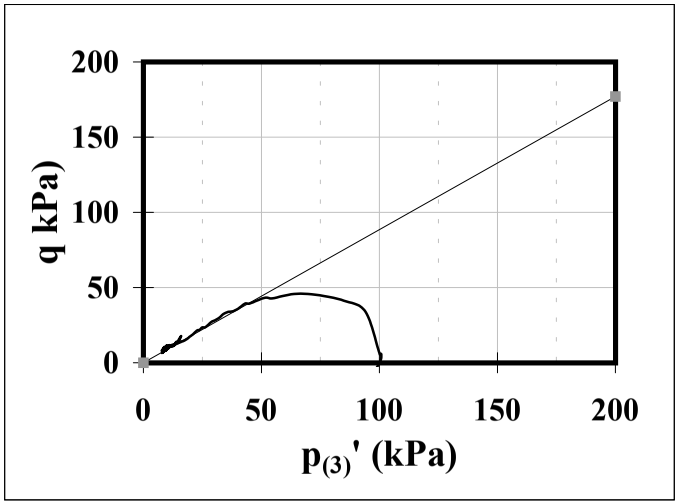

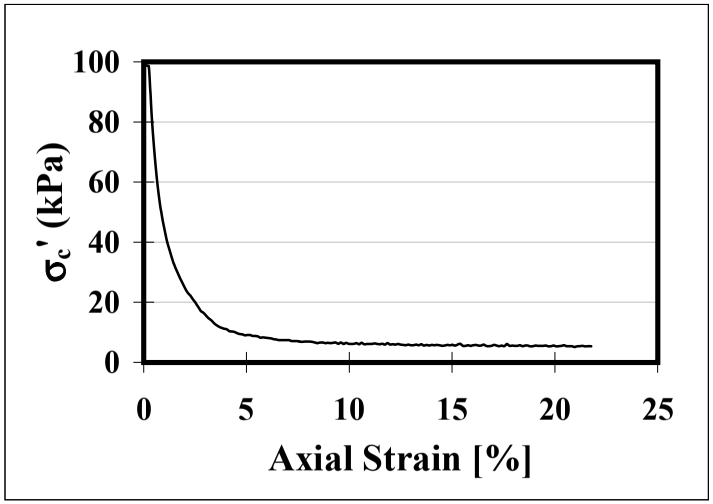

ϕ = 22.7 Confining stress = 100 kPa

GDS FJ#80 GS#40

Date: 05/20/01	Fines= 60	e= 0.615	ec= n.a.	ef= 1.024	(ef)eq= 0.847	(ec)eq= n.a.

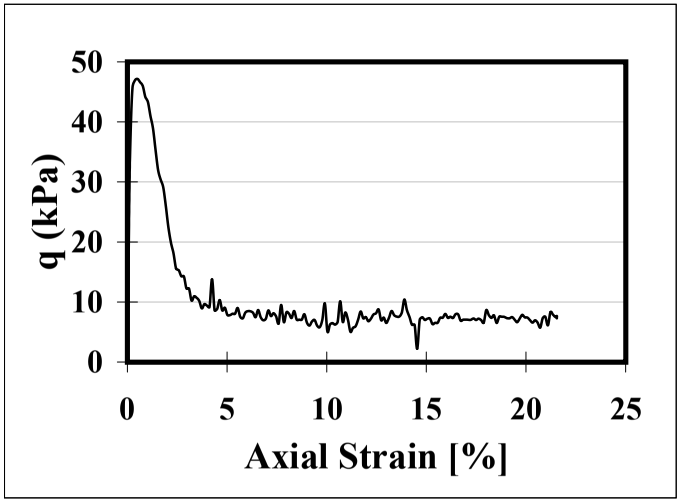

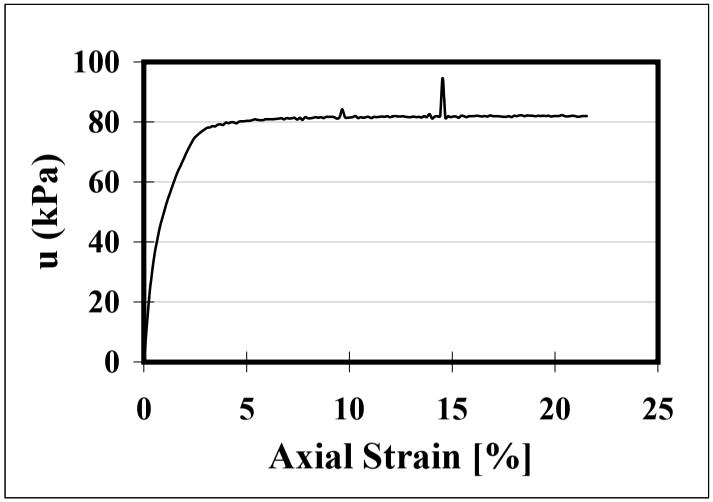

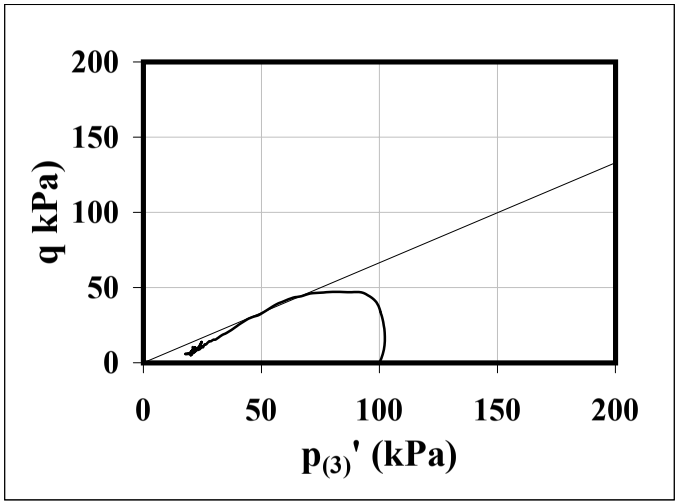

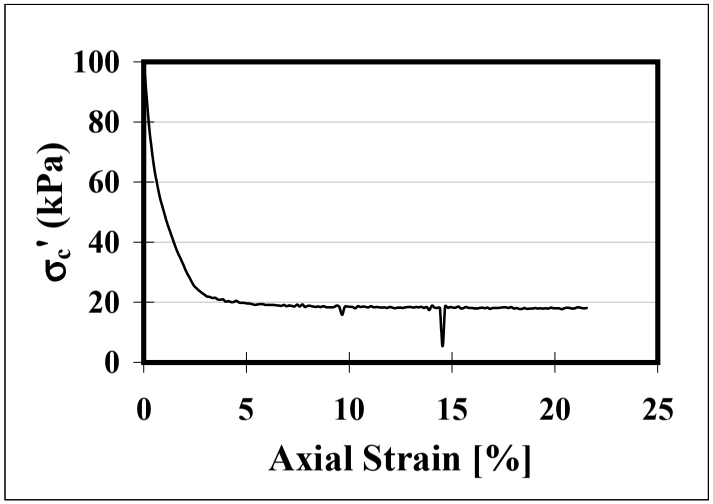

ϕ = 17.4 Confining stress = 100 kPa

GDS FJ#80 GS#40

Date: 05/26/01	Fines= 60	e= 0.613	ec= n.a.	ef= 1.021	(ef)eq= 0.844	(ec)eq= n.a.

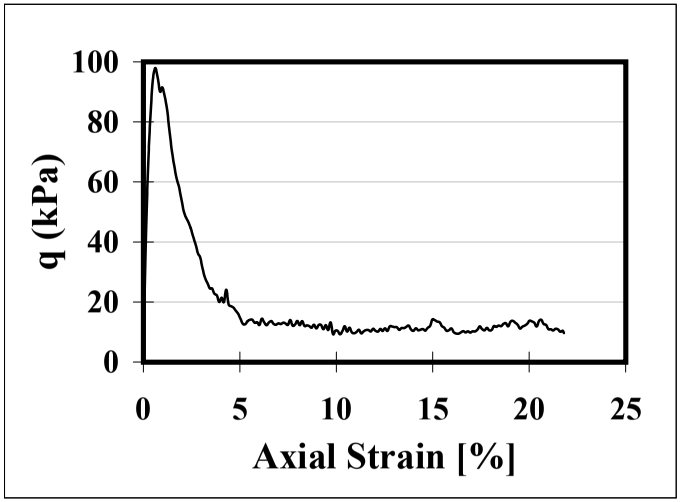

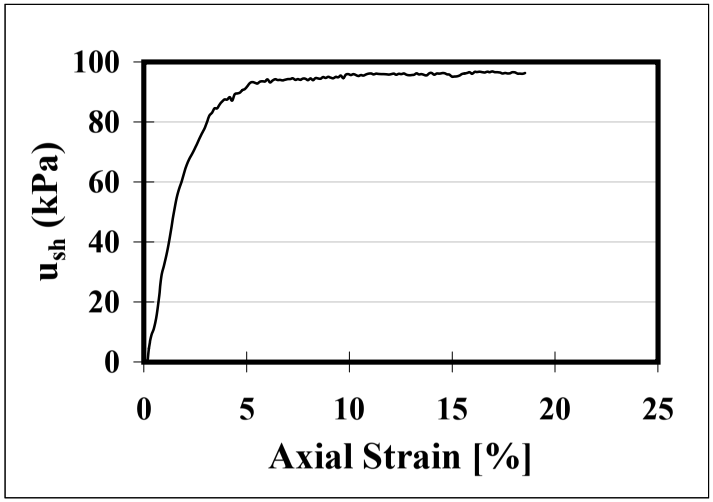

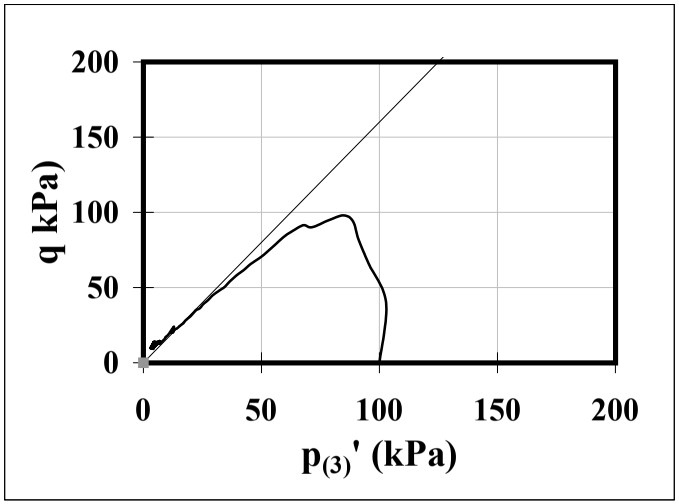

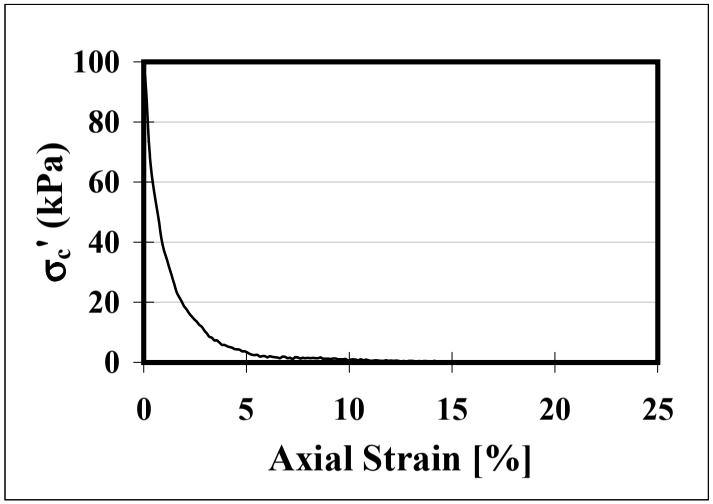

ϕ = 39.2 Confining stress = 100 kPa

GDS FJ#80 GS#40

Date: 10/04/00 Fines= 60 e= 0.616 ec= n.a. ef= 1.027 (ef)eq= 0.903 (ec)eq= n.a.

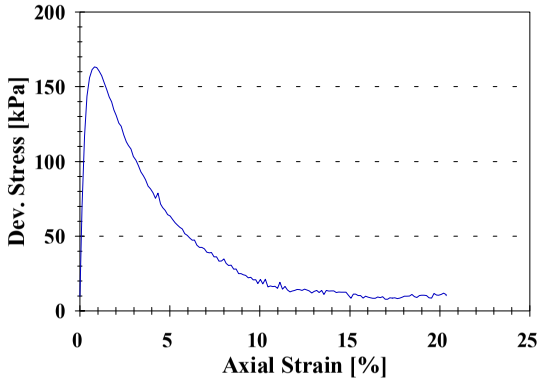

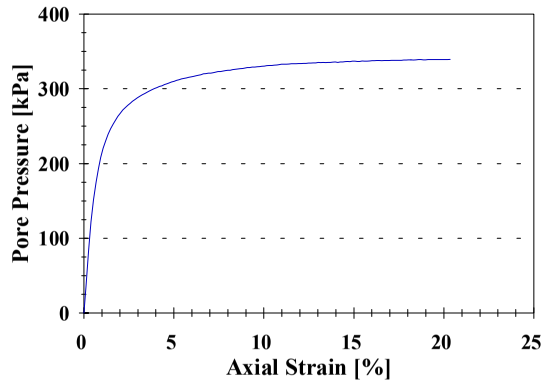

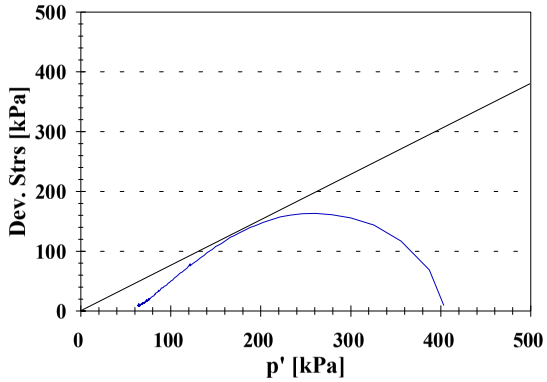

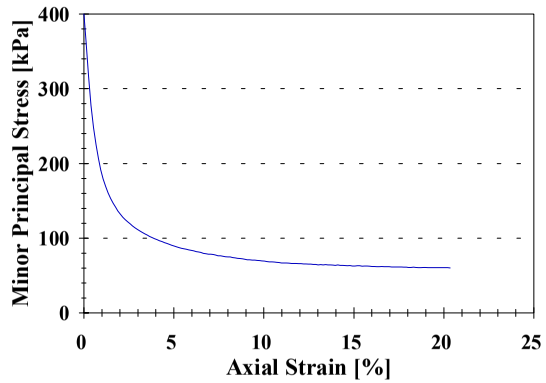

ϕ = 19.9 Confining stress = 400 kPa

GDS NSM GS#40

Date: 06/14/01	Fines= 0	e= 0.586	ec= 0.586	ef= n.a.	(ef)eq= n.a.	(ec)eq= 0.586

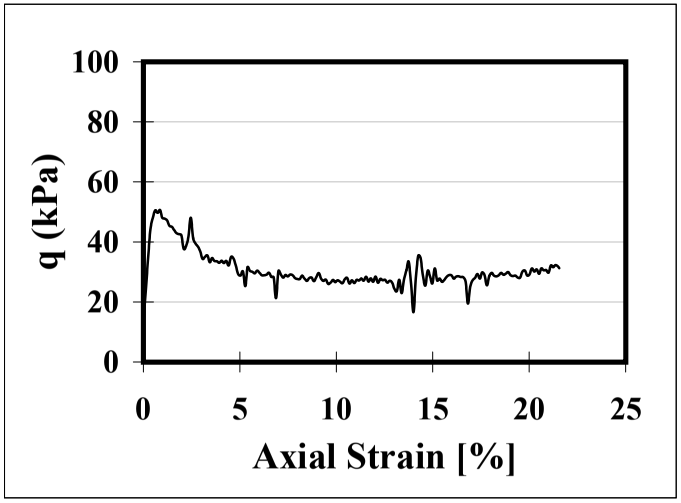

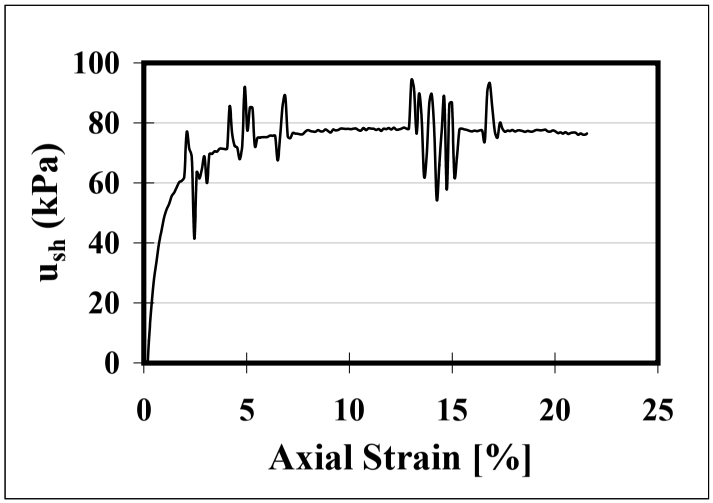

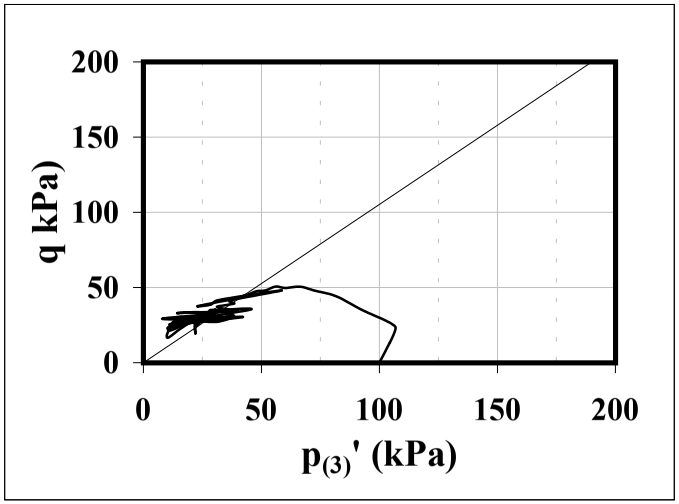

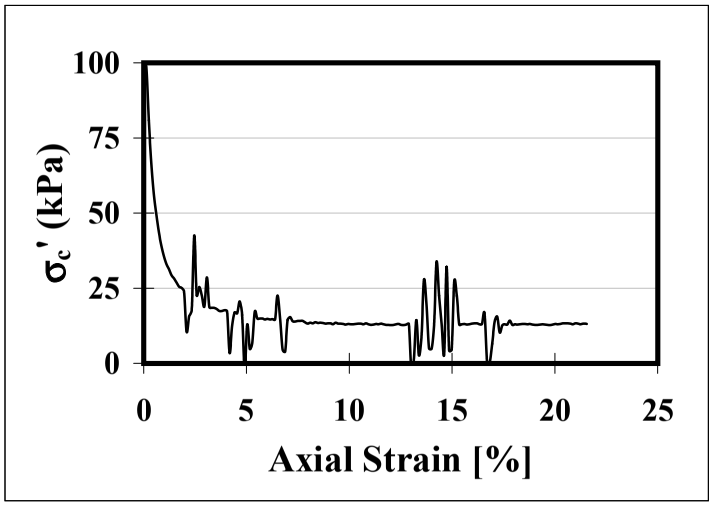

ϕ = 26.6 Confining stress = 100 kPa

GDS WG GS#40

Date: 06/15/01	Fines= 0	e= 0.633	ec= 0.633	ef= n.a.	(ef)eq= n.a.	(ec)eq= 0.633

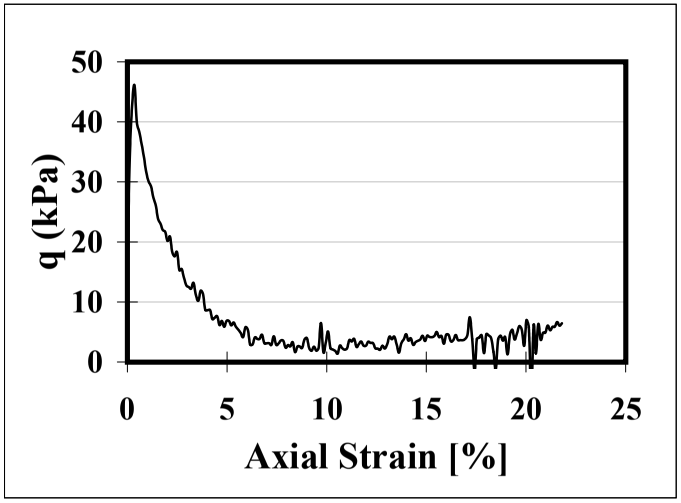

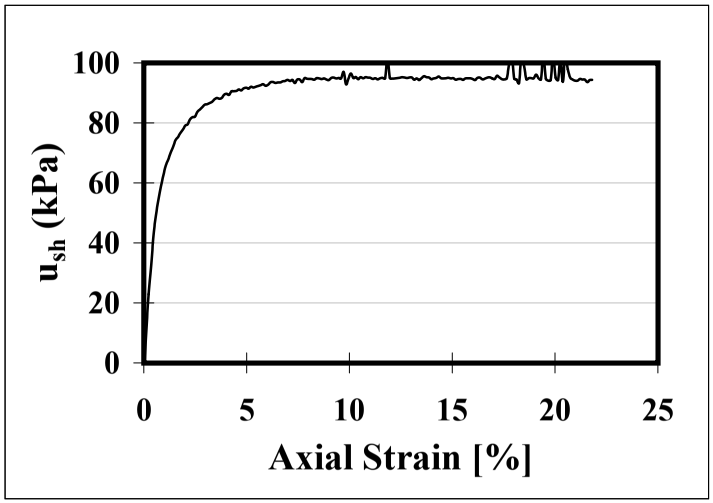

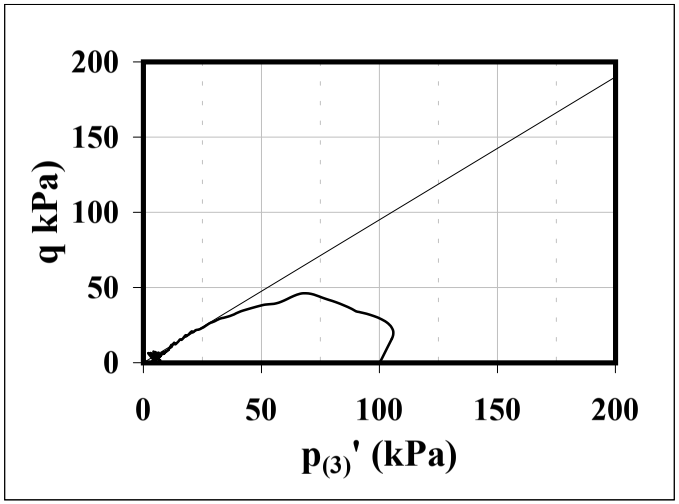

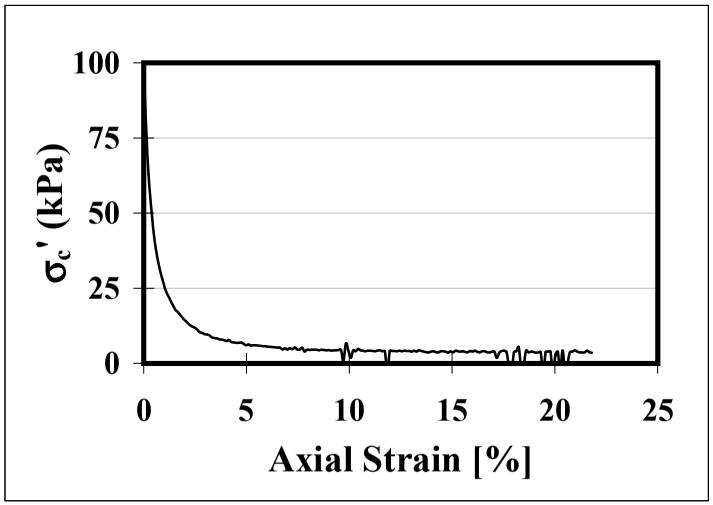

ϕ = 24.2 Confining stress = 100 kPa

GDS WG GS#40

Date: 06/16/01	Fines= 0	e= 0.569	ec= 0.569	ef= n.a.	(ef)eq= n.a.	(ec)eq= 0.569

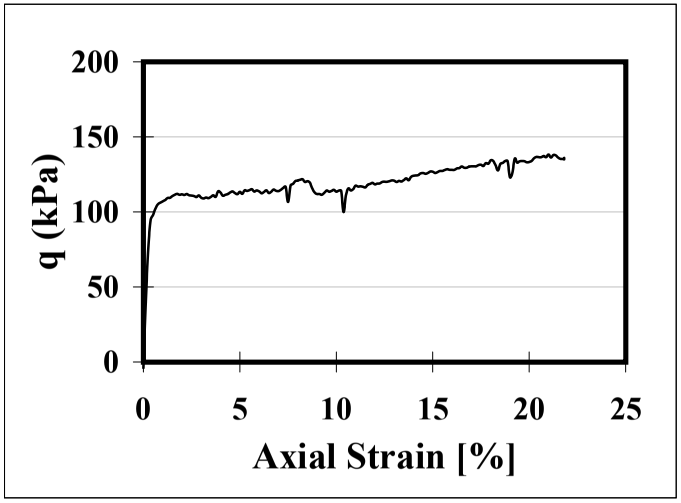

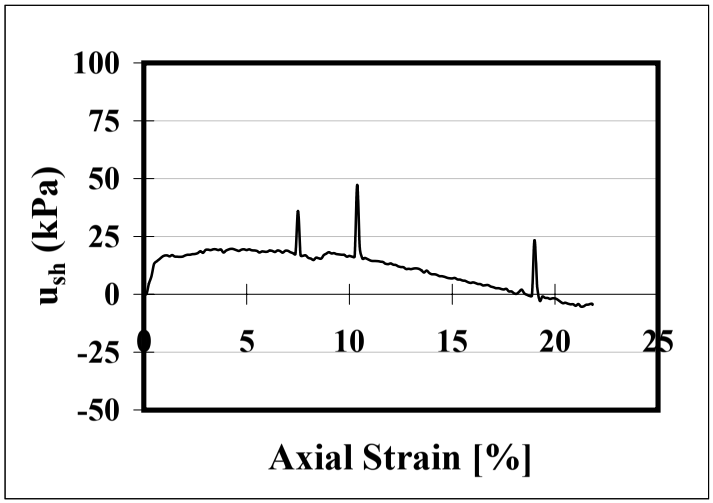

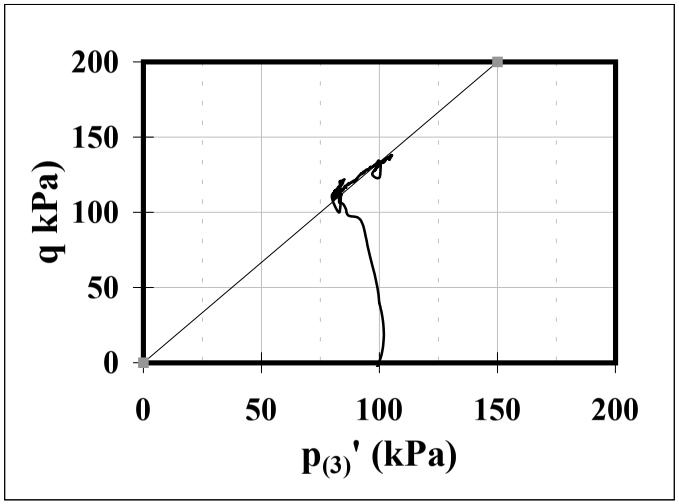

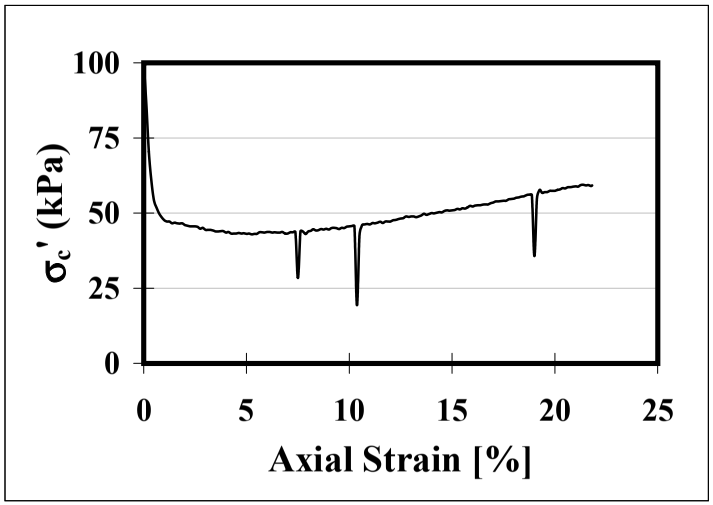

ϕ = 33.1 Confining stress = 100 kPa

GDS WG GS#40

Date: 06/17/01	Fines= 0	e= 0.556	ec= 0.556	ef= n.a.	(ef)eq= n.a.	(ec)eq= 0.556

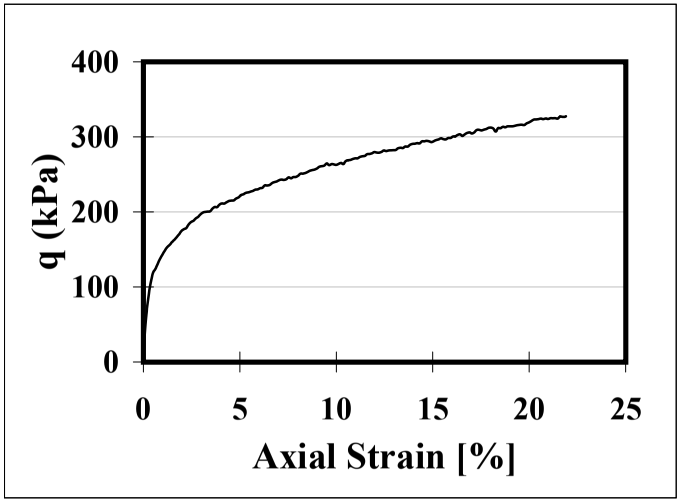

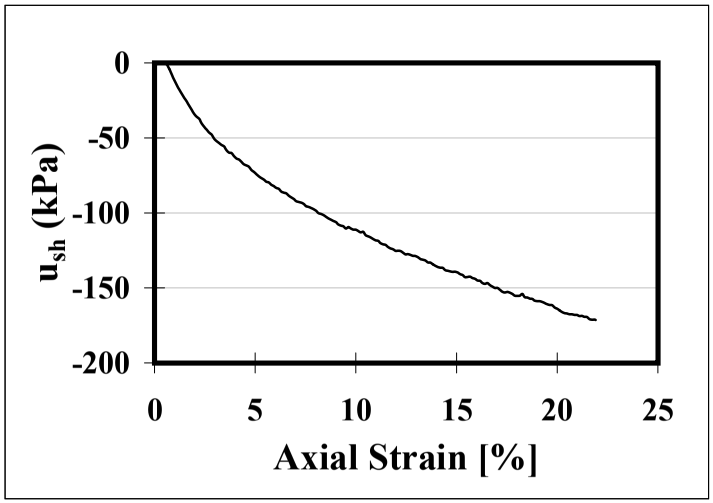

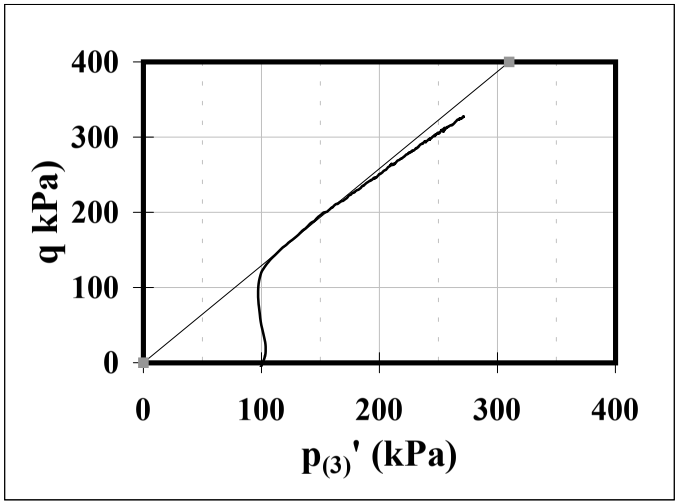

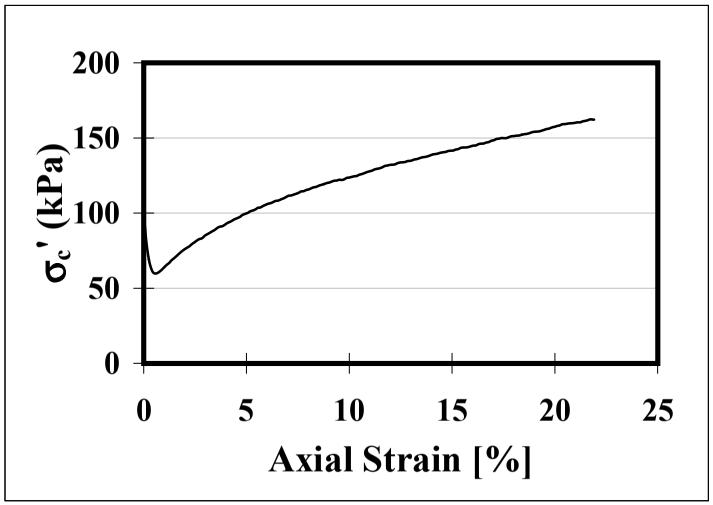

ϕ = 35.6 Confining stress = 100 kPa

GDS WG GS#40

Date: 06/18/01	Fines= 0	e= 0.646	ec= 0.646	ef= n.a.	(ef)eq= n.a.	(ec)eq= 0.646

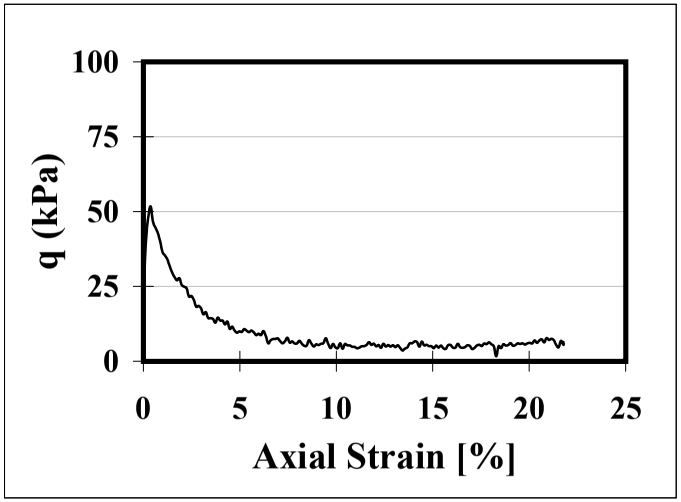

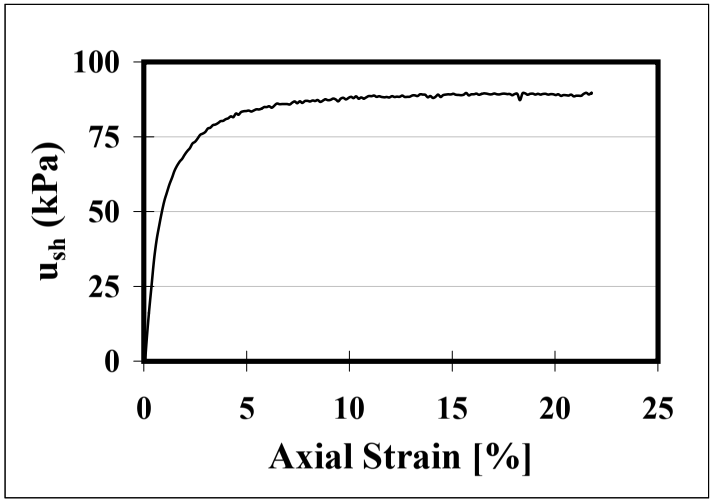

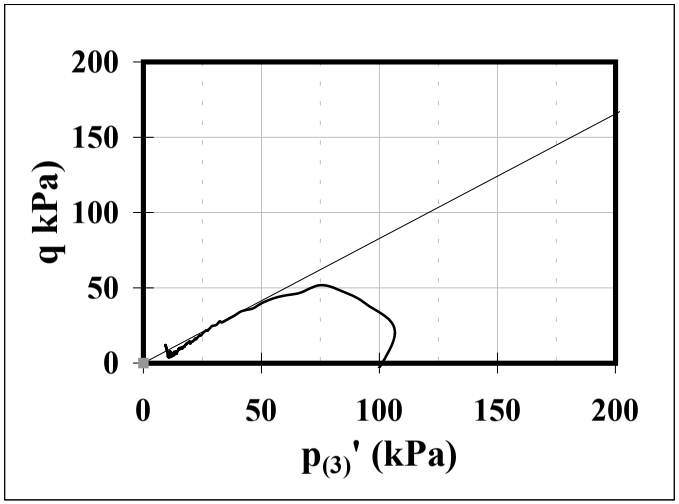

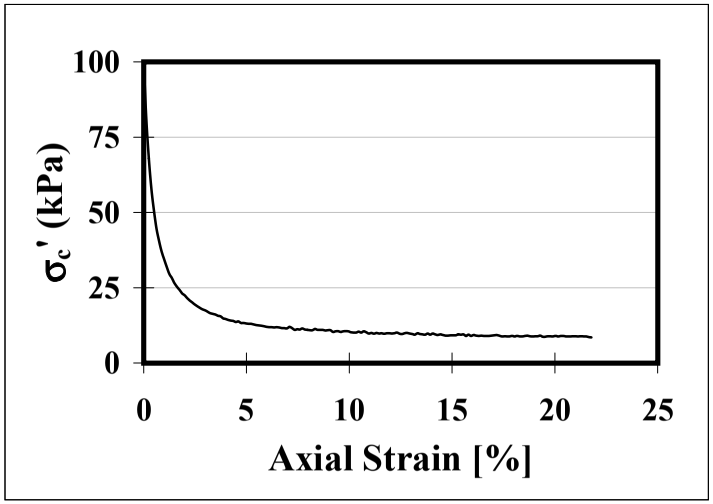

ϕ = 21.3 Confining stress = 100 kPa

GDS WG GS#40

Date: 06/27/01	Fines= 0	e= 0.644	ec= 0.644	ef= n.a.	(ef)eq= n.a.	(ec)eq= 0.644

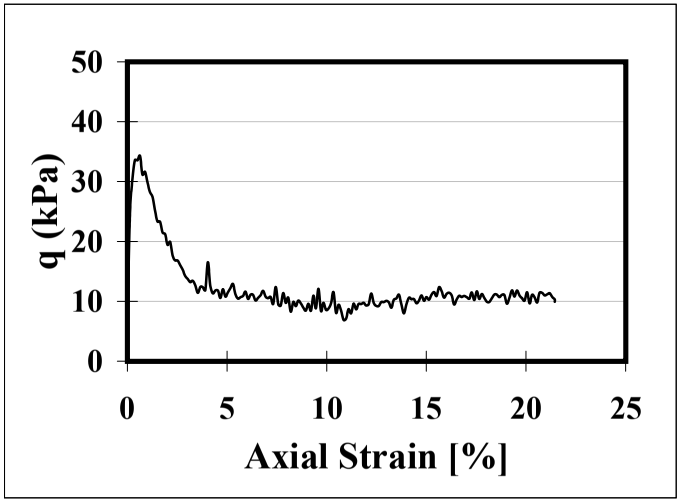

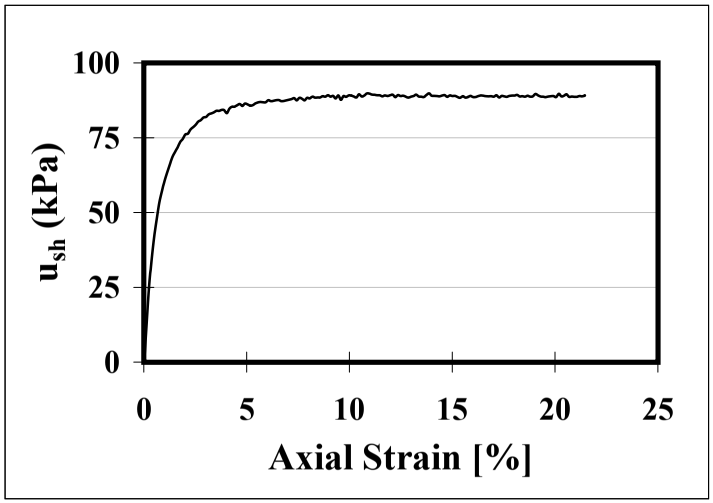

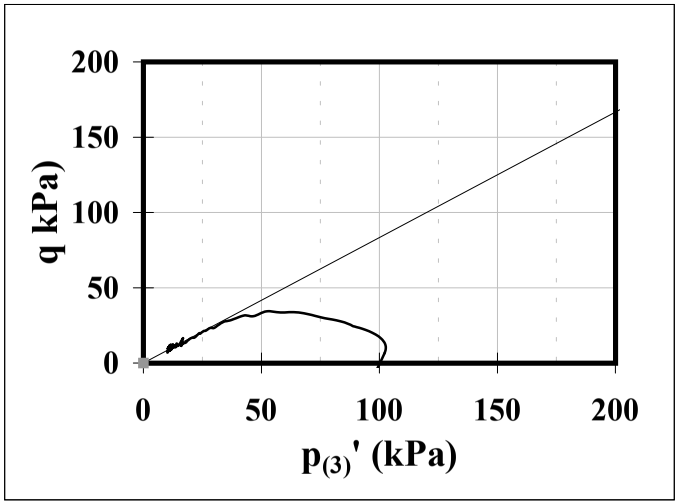

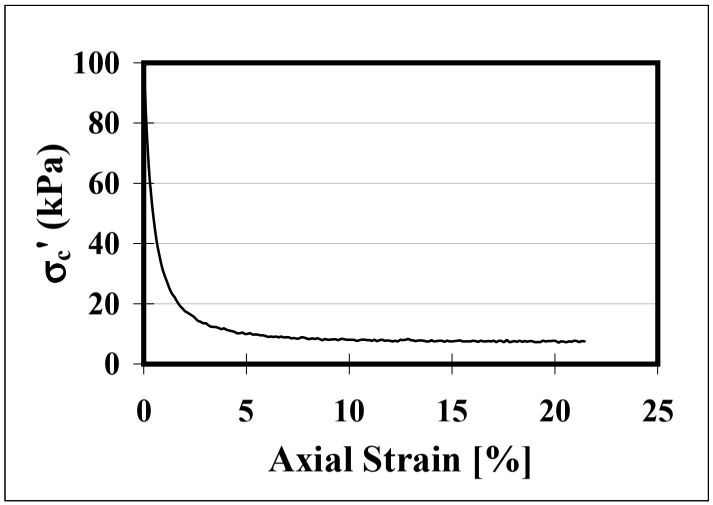

ϕ = 21.5 Confining stress = 100 kPa

GDS WG GS#40

Date: 06/27/01	Fines= 0	e= 0.604	ec= 0.604	ef= n.a.	(ef)eq= n.a.	(ec)eq= 0.604

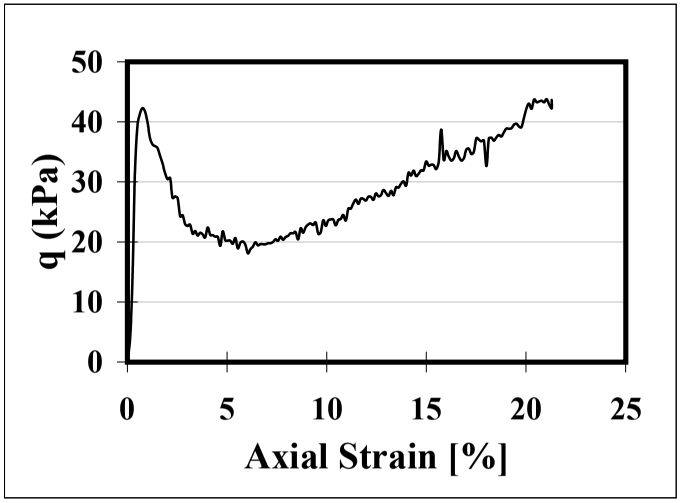

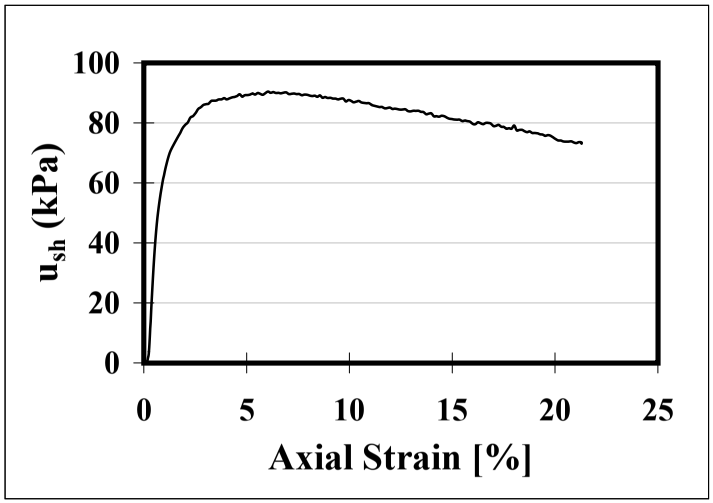

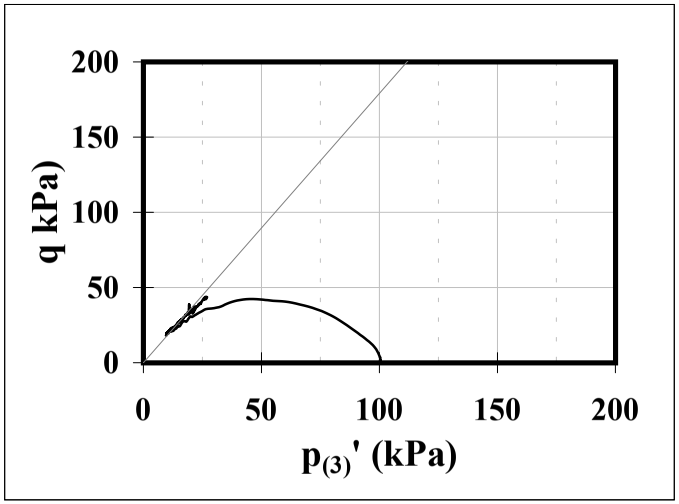

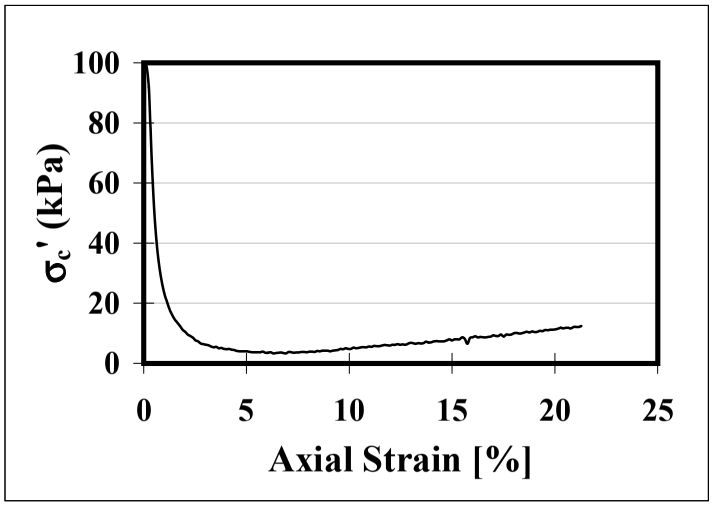

ϕ = 43.6 Confining stress = 100 kPa

GDS WG GS#40

Date: 06/28/01	Fines= 0	e= 0.501	ec= 0.501	ef= n.a.	(ef)eq= n.a.	(ec)eq= 0.501

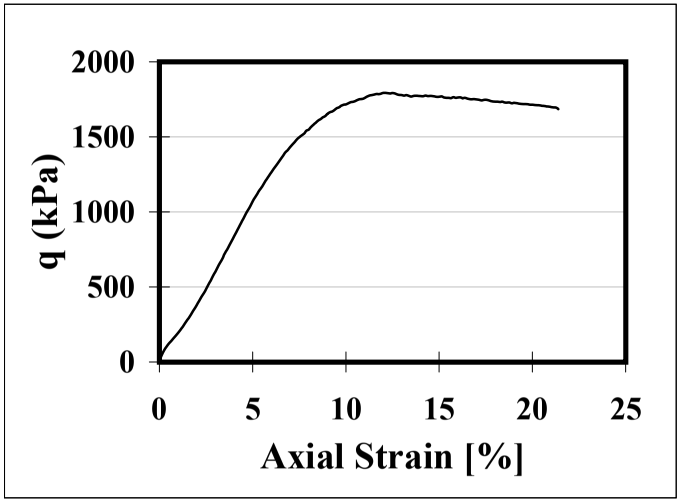

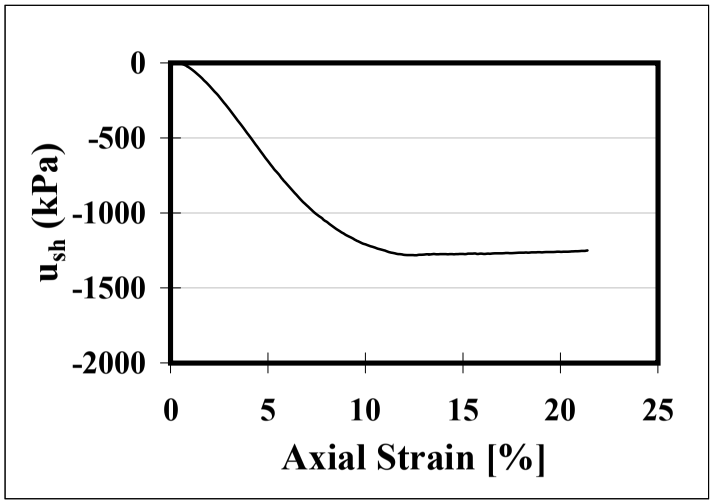

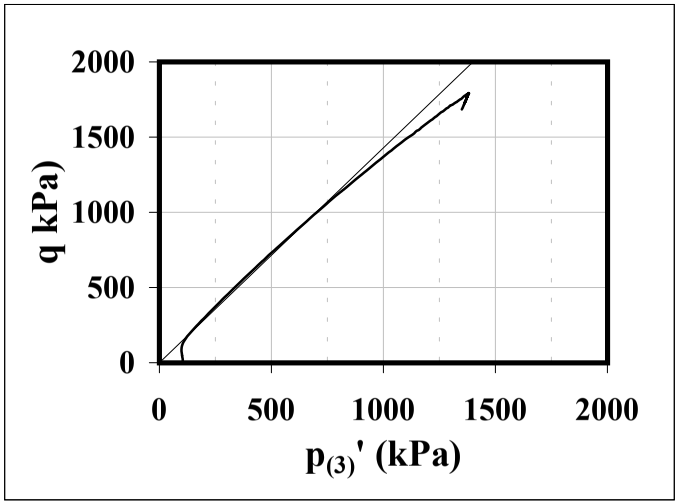

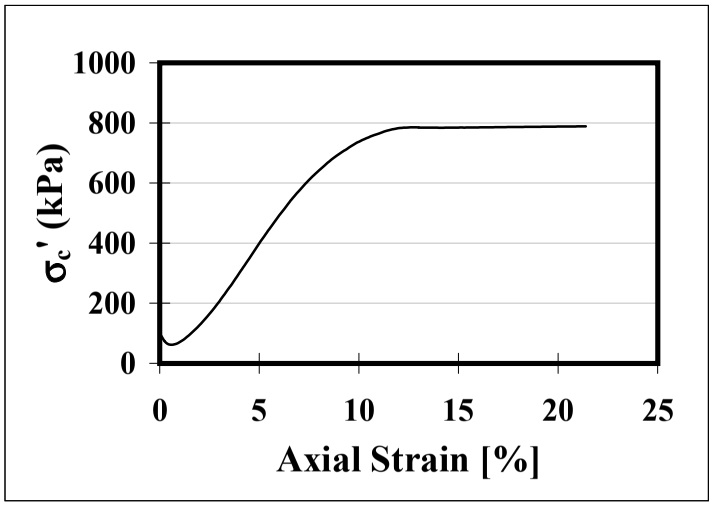

ϕ = 35.2 Confining stress = 100 kPa

GDS WG GS#40

Date: 07/01/01	Fines= 0	e= 0.481	ec= 0.481	ef= n.a.	(ef)eq= n.a.	(ec)eq= 0.481

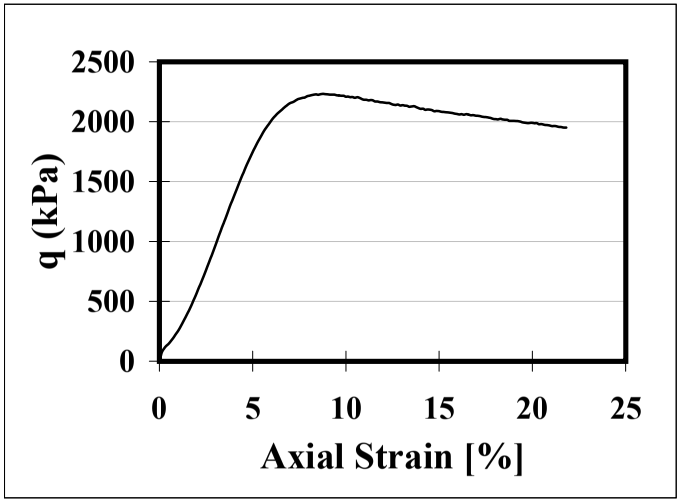

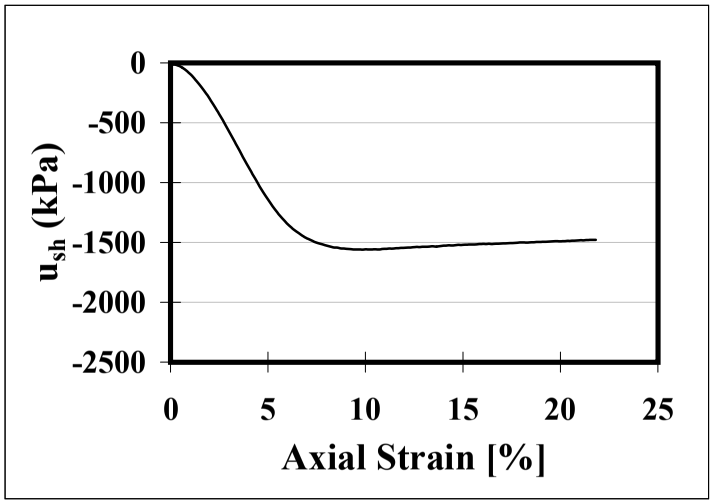

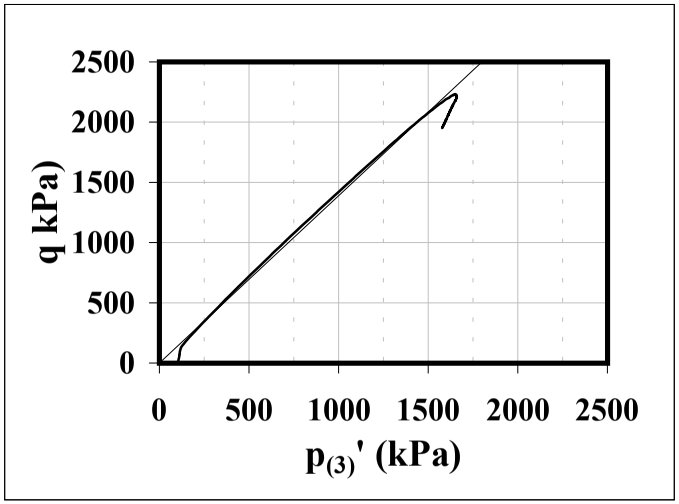

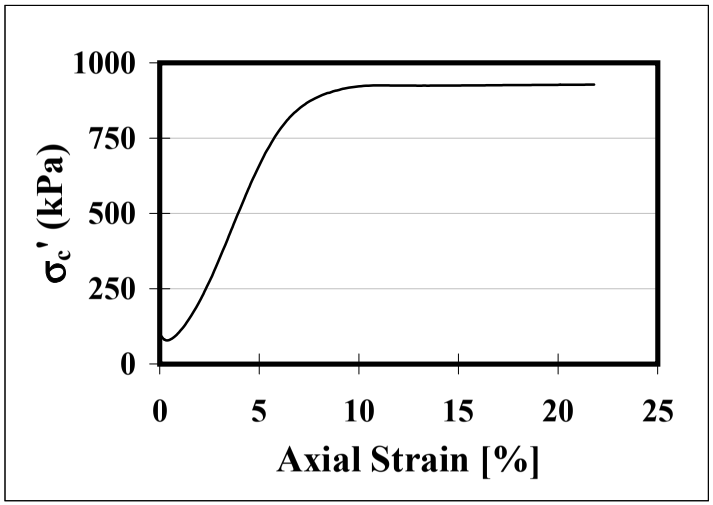

ϕ = 34.3 Confining stress = 100 kPa

GDS WG GS#40

Date: 07/02/01	Fines= 0	e= 0.642	ec= 0.642	ef= n.a.	(ef)eq= n.a.	(ec)eq= 0.642

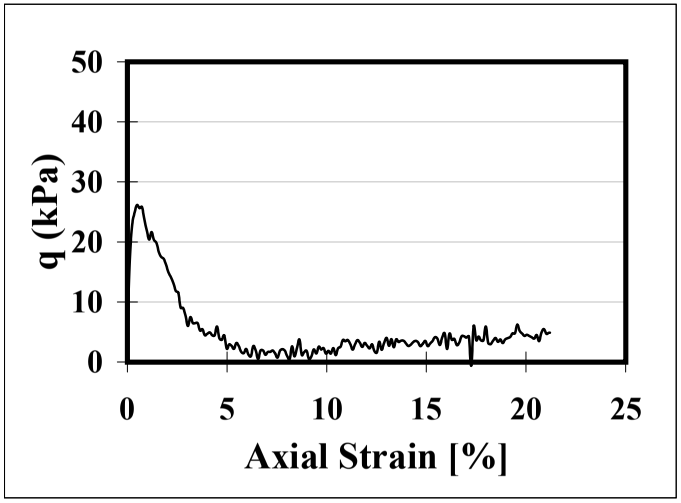

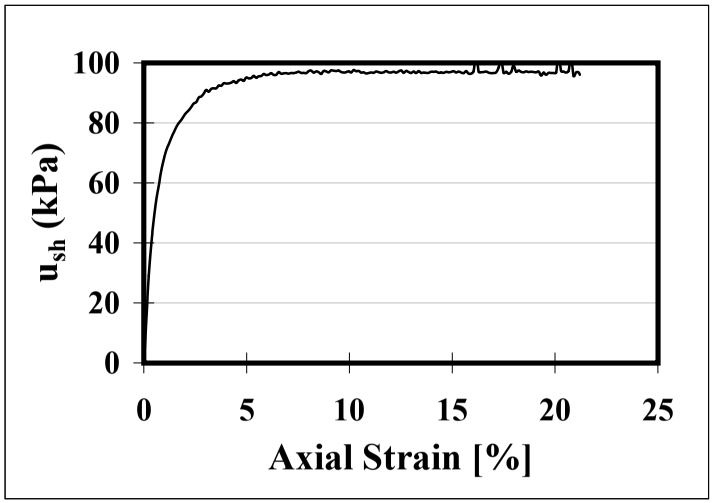

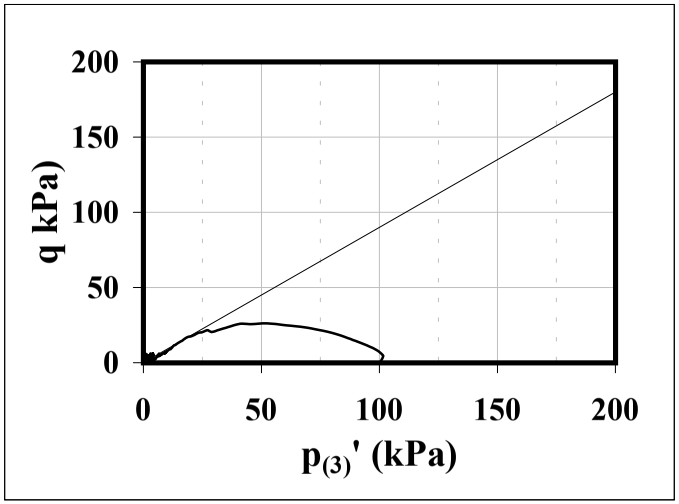

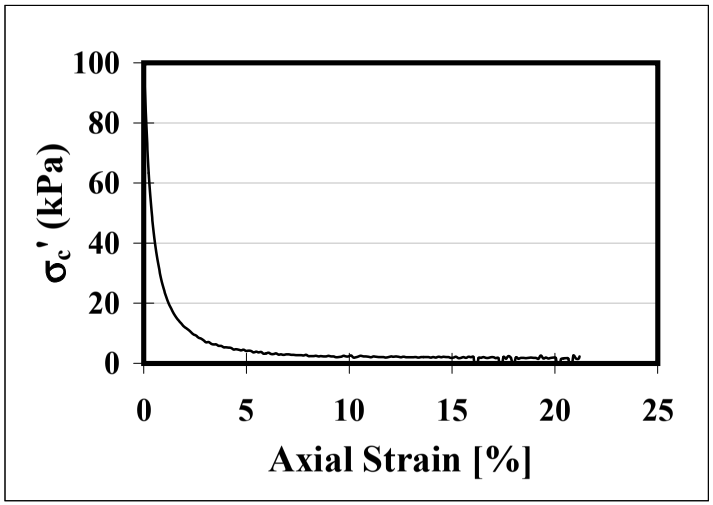

ϕ = 23.0 Confining stress = 100 kPa

GDS WG GS#40

Date: 07/05/01	Fines= 0	e= 0.631	ec= 0.631	ef= n.a.	(ef)eq= n.a.	(ec)eq= 0.631

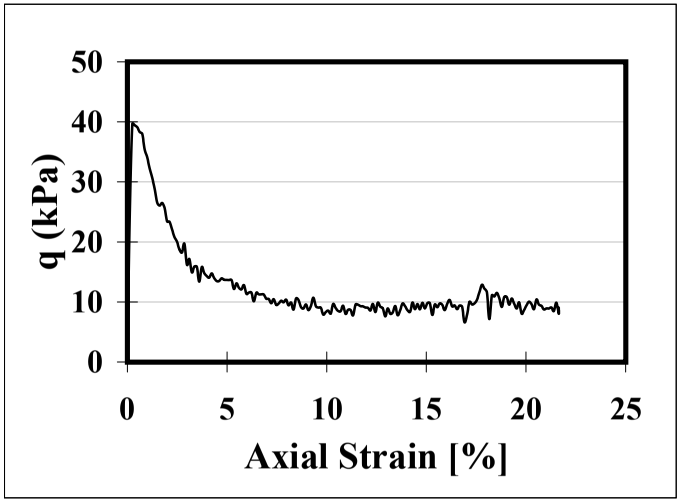

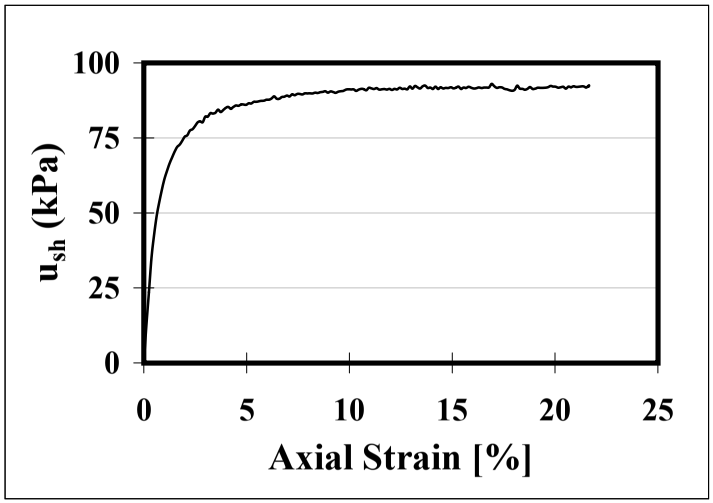

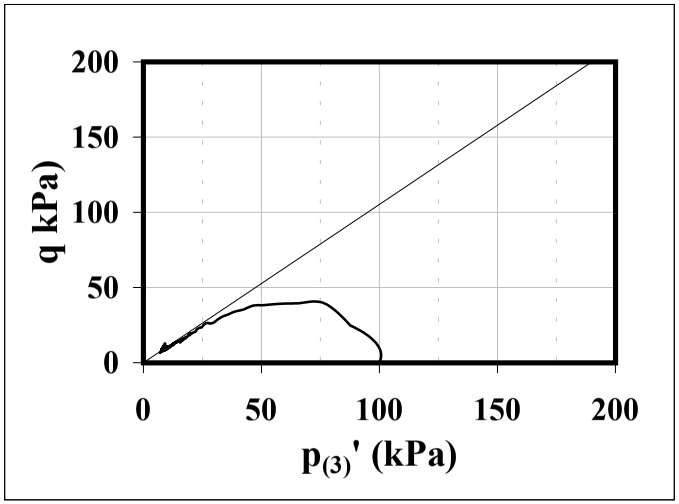

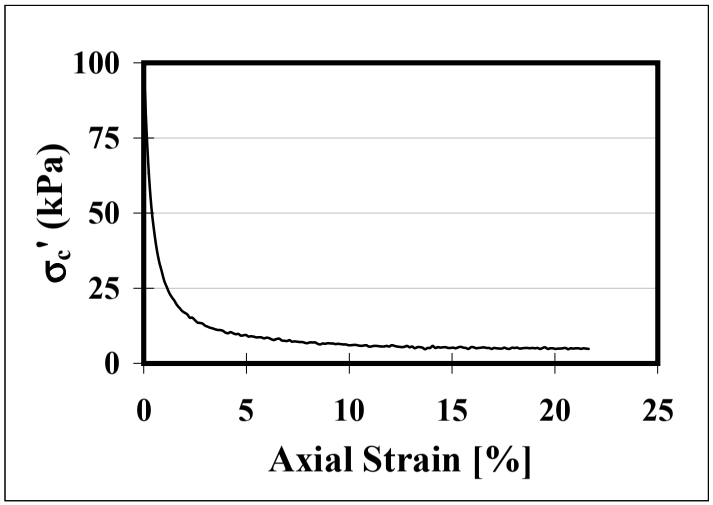

ϕ = 26.6 Confining stress = 100 kPa

GDS WG GS#40

Date: 07/05/01	Fines= 0	e= 0.629	ec= 0.629	ef= n.a.	(ef)eq= n.a.	(ec)eq= 0.629

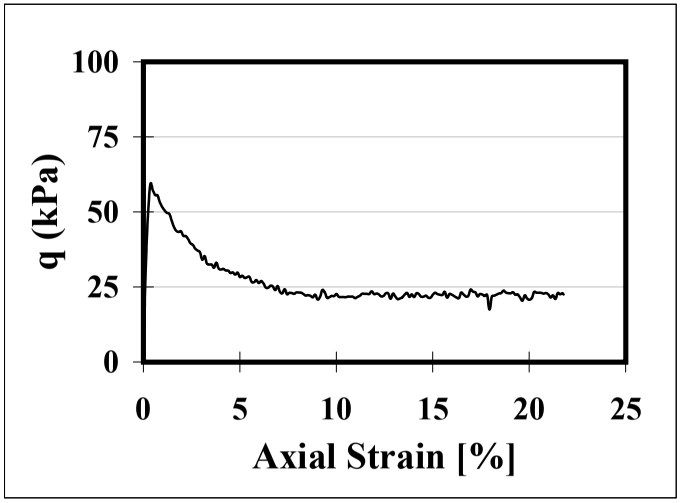

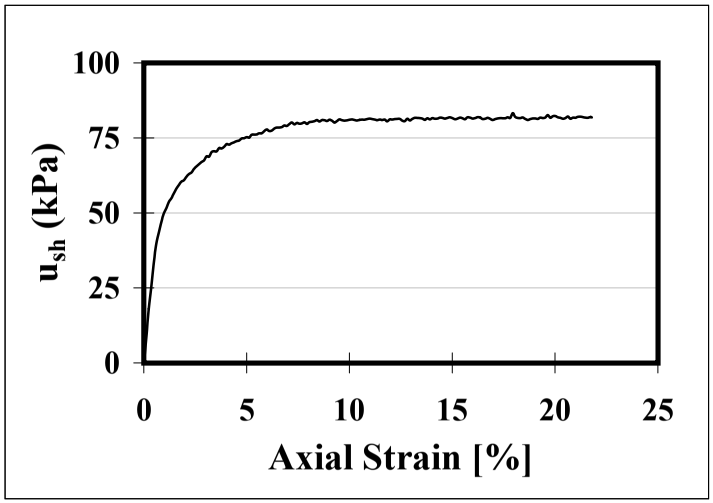

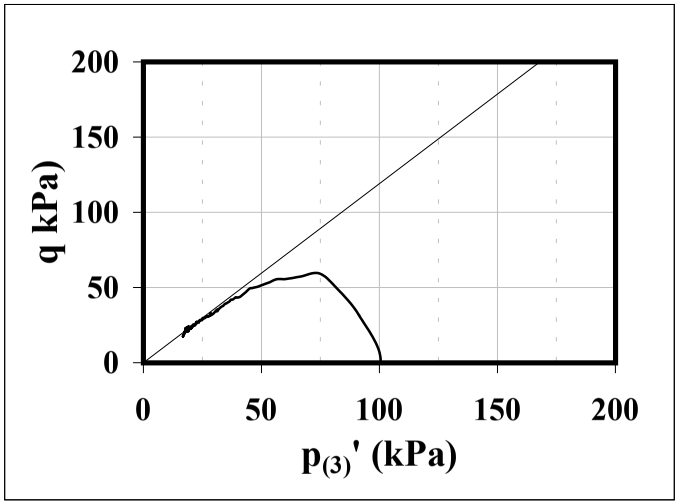

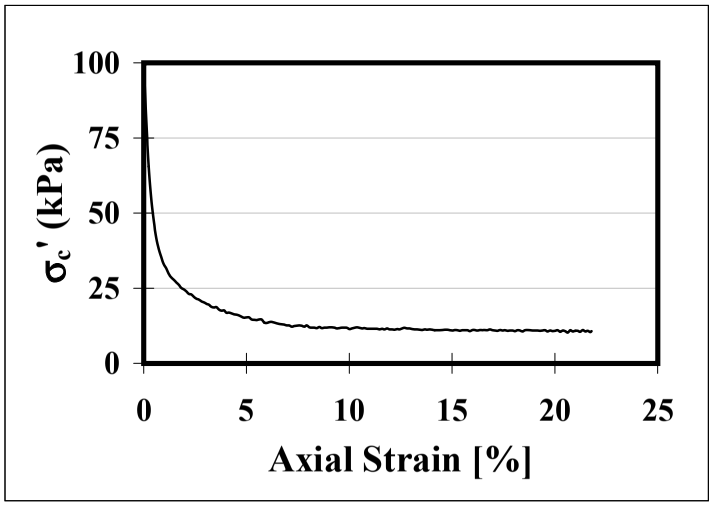

ϕ = 29.8 Confining stress = 100 kPa

GDS WG GS#40

Date: 07/06/01	Fines= 25	e= 0.427	ec= 0.903	ef= n.a.	(ef)eq= n.a.	(ec)eq= 0.617

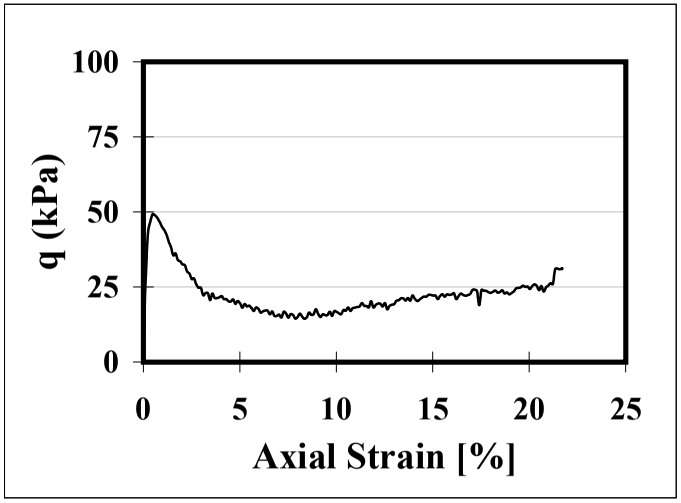

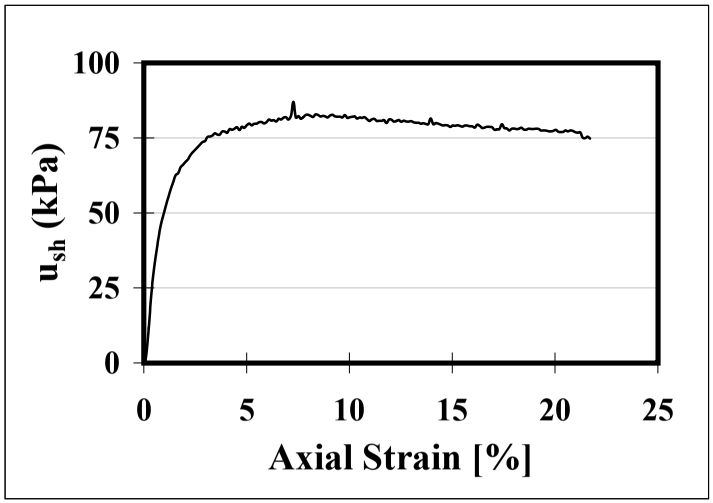

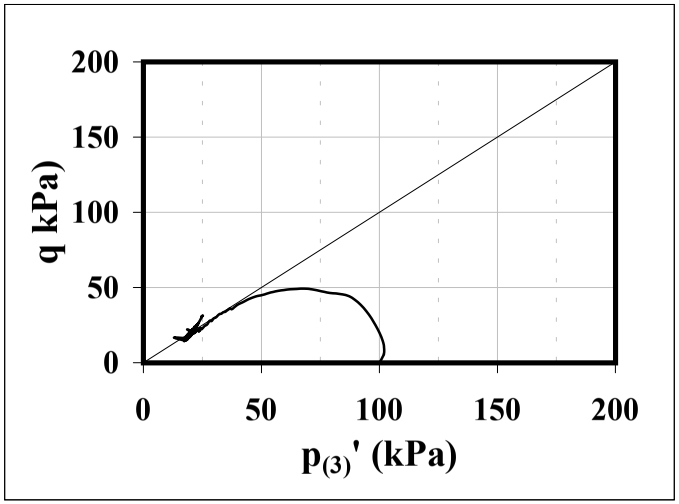

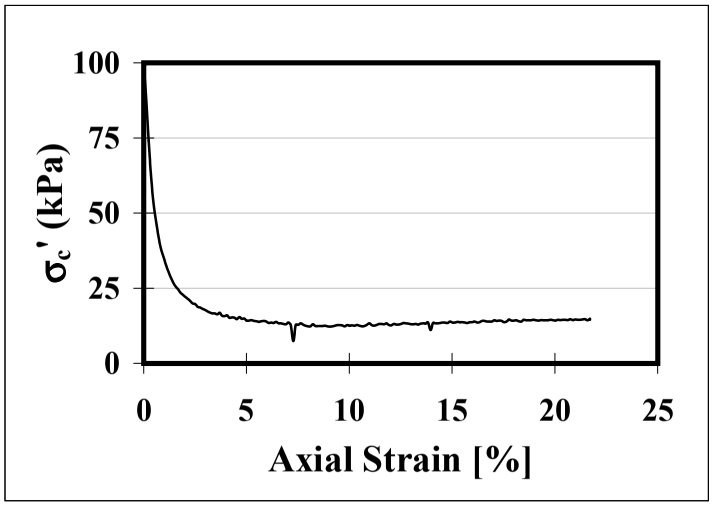

ϕ = 25.4 Confining stress = 100 kPa

GDS WG GS#40

Date: 07/10/01	Fines= 25	e= 0.423	ec= 0.897	ef= n.a.	(ef)eq= n.a.	(ec)eq= 0.612

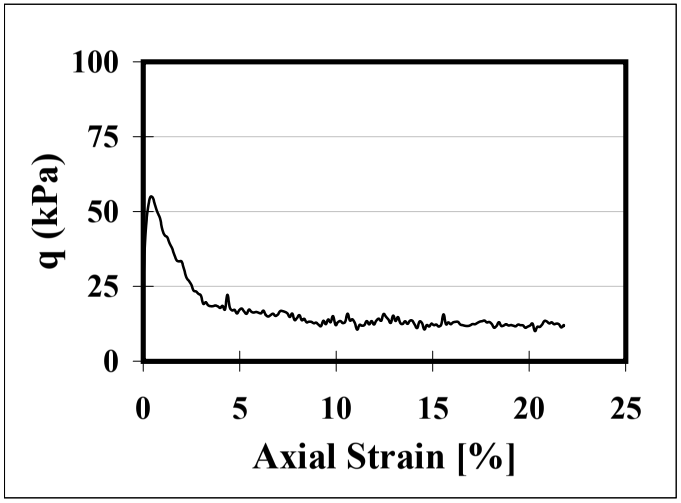

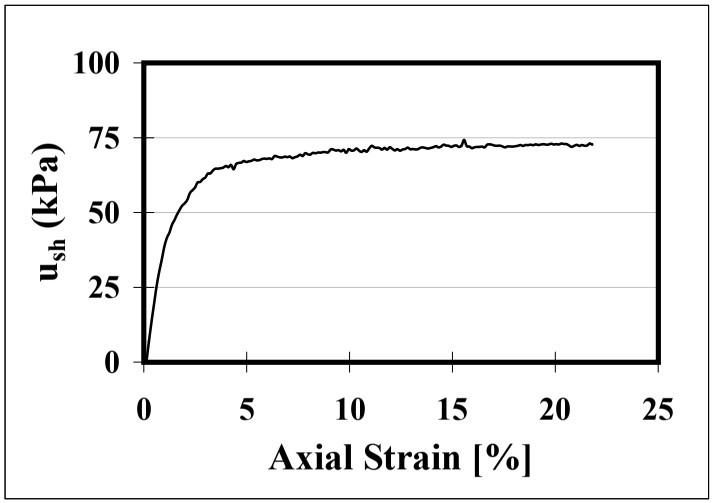

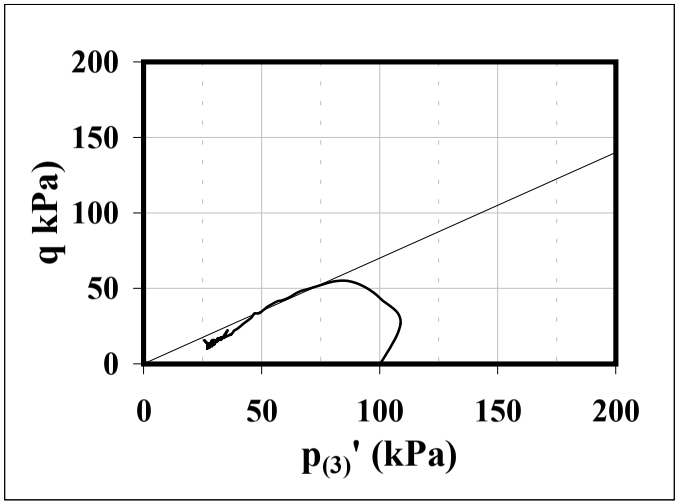

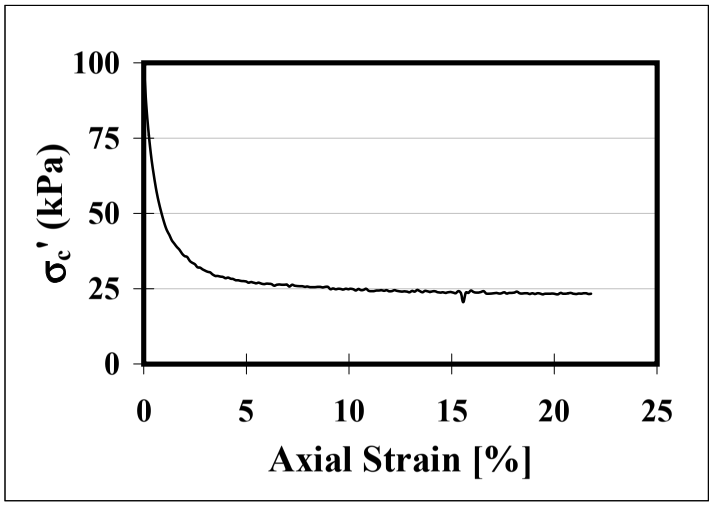

ϕ = 18.3 Confining stress = 100 kPa

GDS WG GS#40

Date: 07/11/01	Fines= 25	e= 0.440	ec= 0.920	ef= n.a.	(ef)eq= n.a.	(ec)eq= 0.632

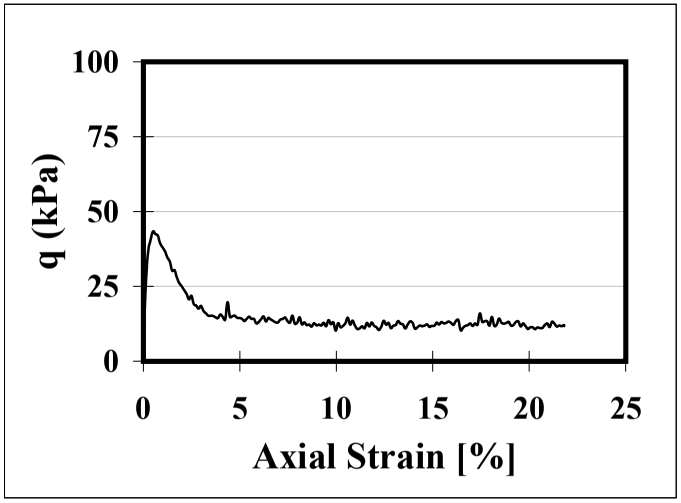

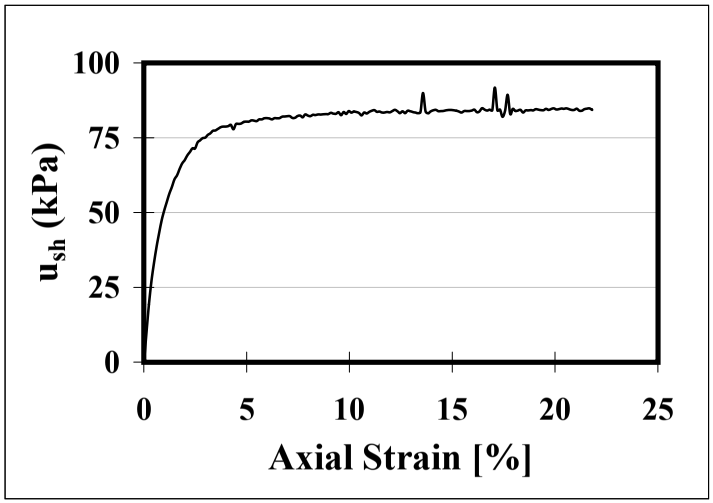

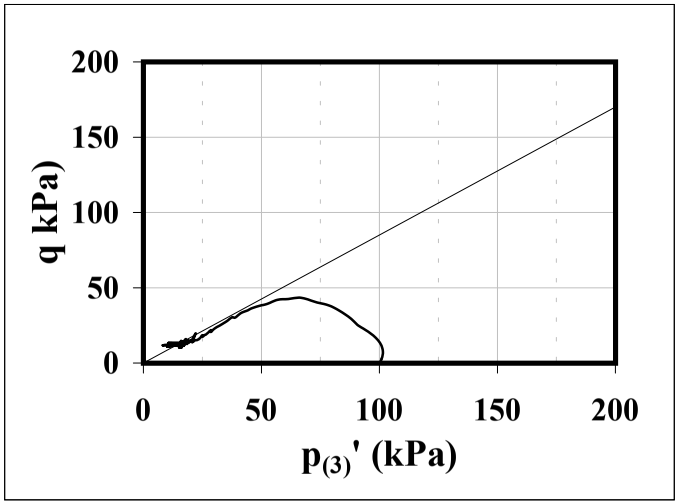

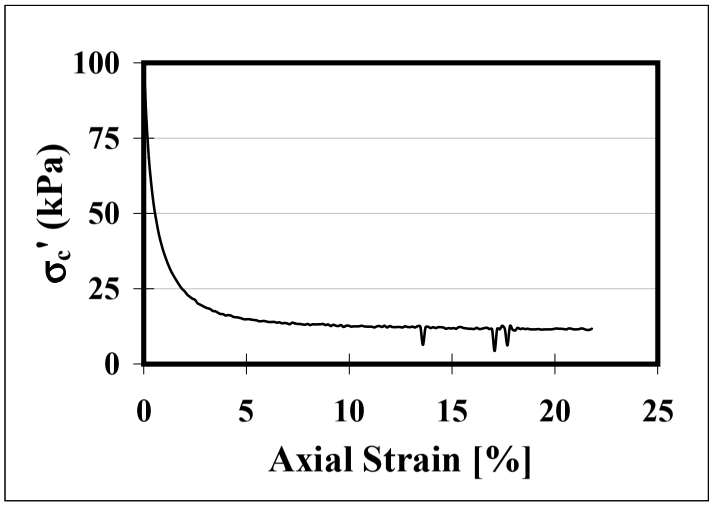

ϕ = 21.9 Confining stress = 100 kPa

GDS WG GS#40

Date: 07/12/01	Fines= 25	e= 0.415	ec= 0.887	ef= n.a.	(ef)eq= n.a.	(ec)eq= 0.604

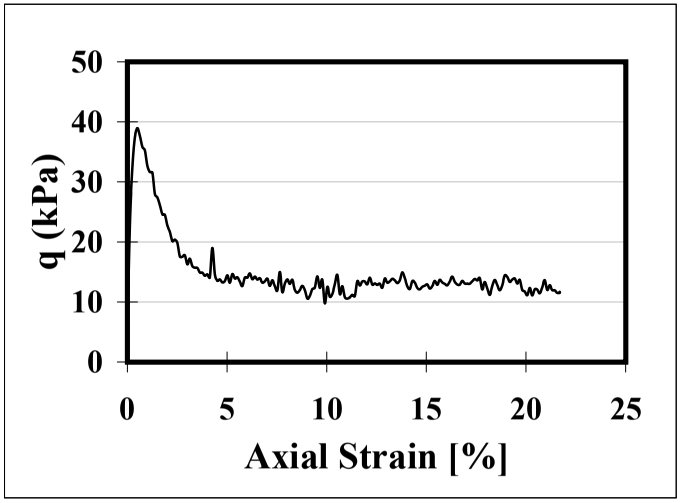

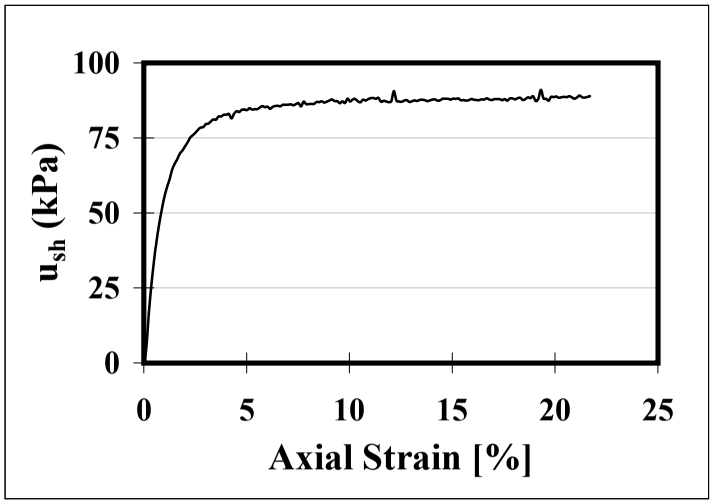

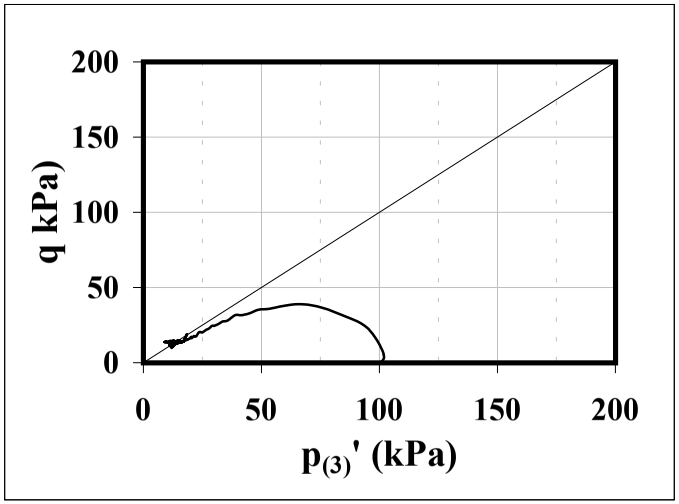

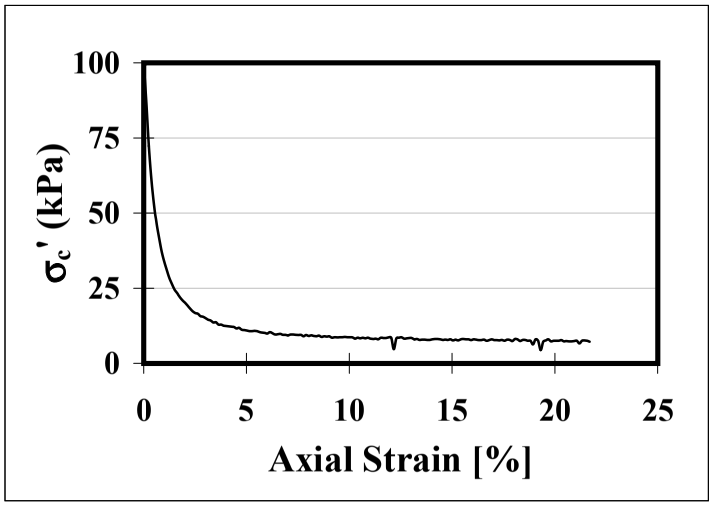

ϕ = 25.4 Confining stress = 100 kPa

GDS WG GS#40

Date: 07/16/01	Fines= 25	e= 0.441	ec= 0.921	ef= n.a.	(ec)eq =	0.632	

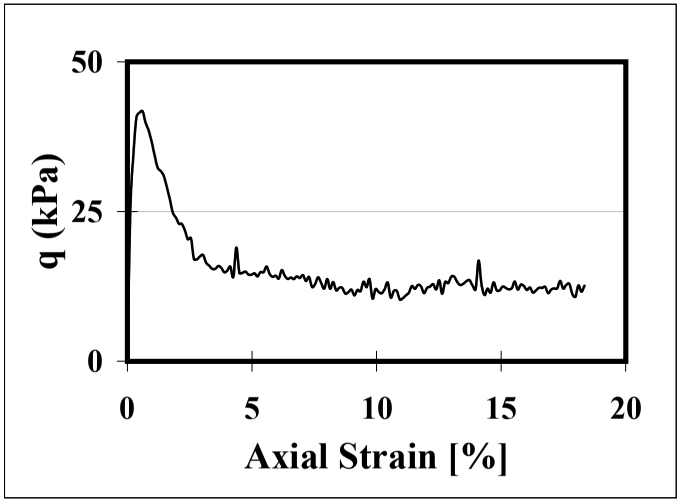

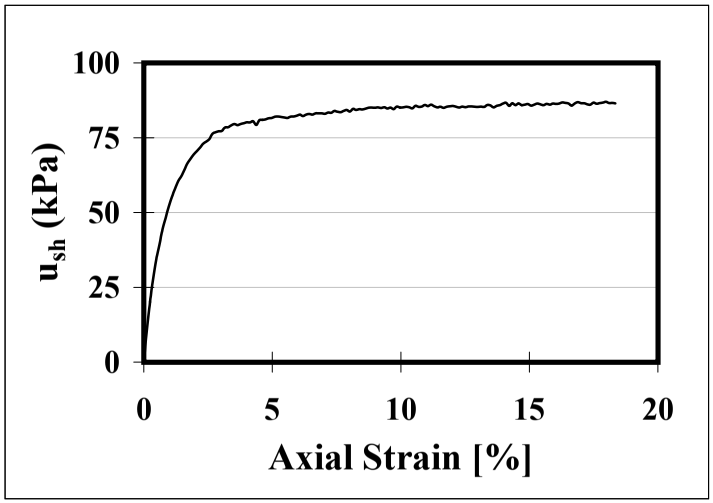

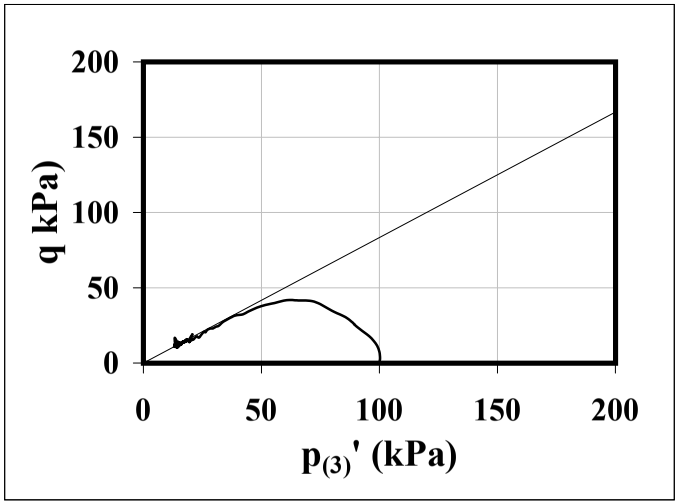

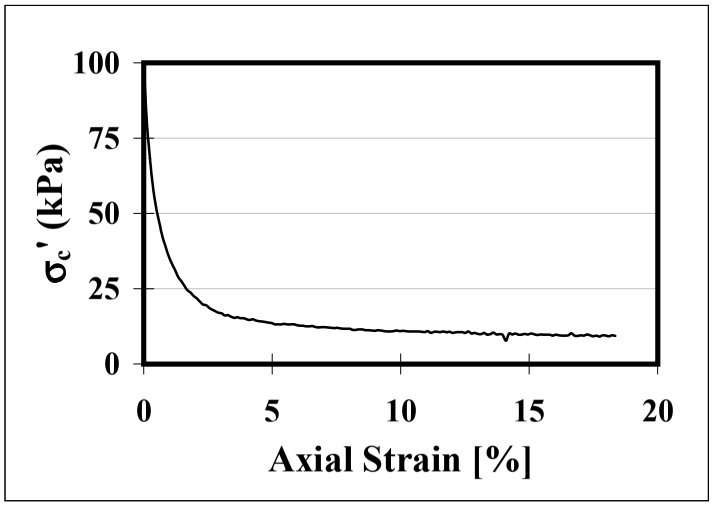

ϕ = 21.5 Confining stress = 100 kPa

GDS WG GS#40

Date: 07/17/01	Fines= 25	e= 0.426	ec= 0.902	ef= n.a.	(ec)eq=	0.616	

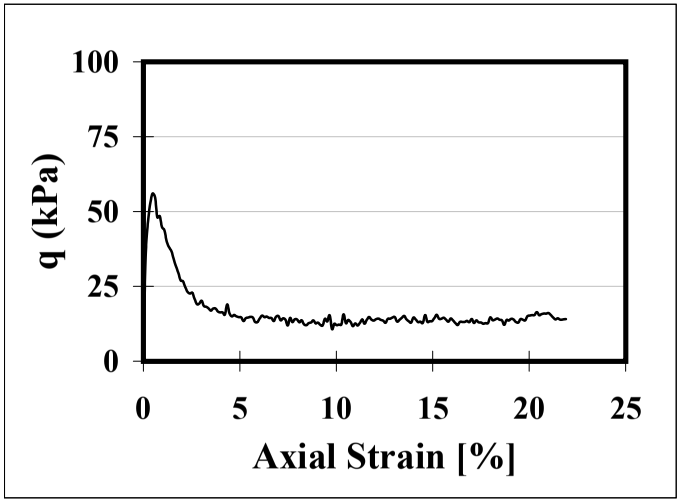

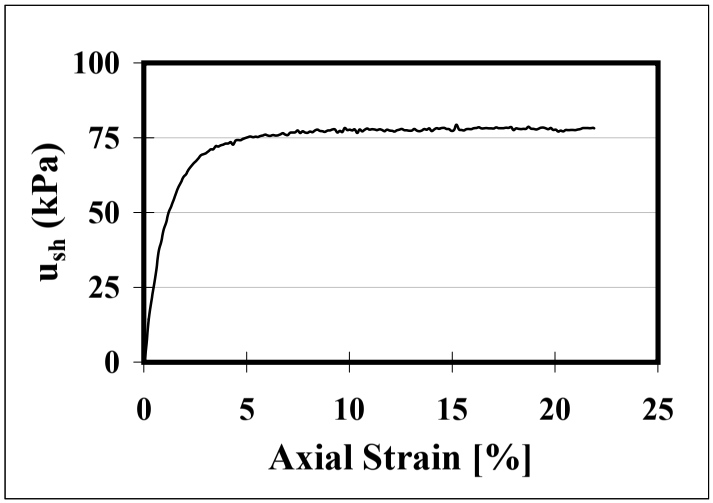

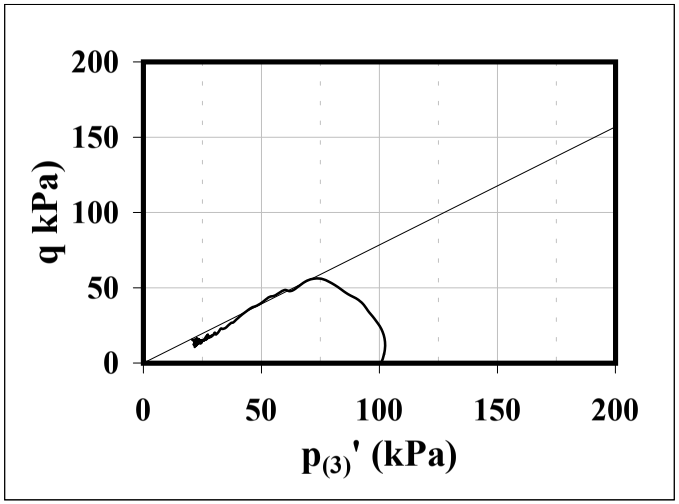

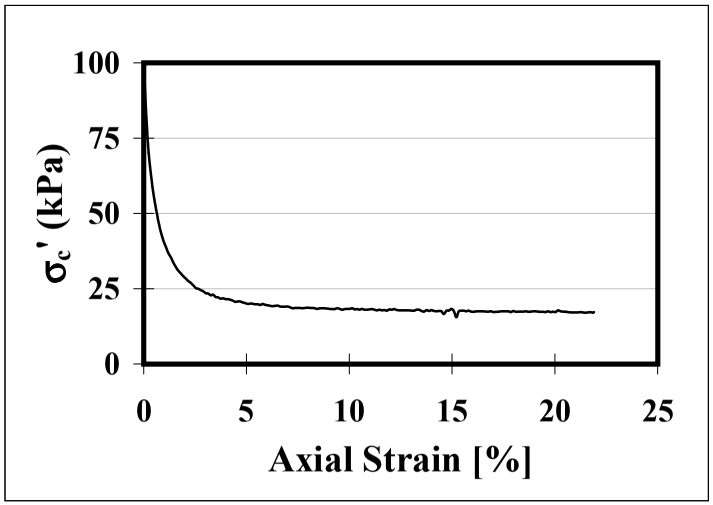

ϕ = 20.3 Confining stress = 100 kPa

GDS WG GS#40

Date: 07/20/01	Fines= 25	e= 0.448	ec= 0.931	ef= n.a.	(ec)eq=	0.641	

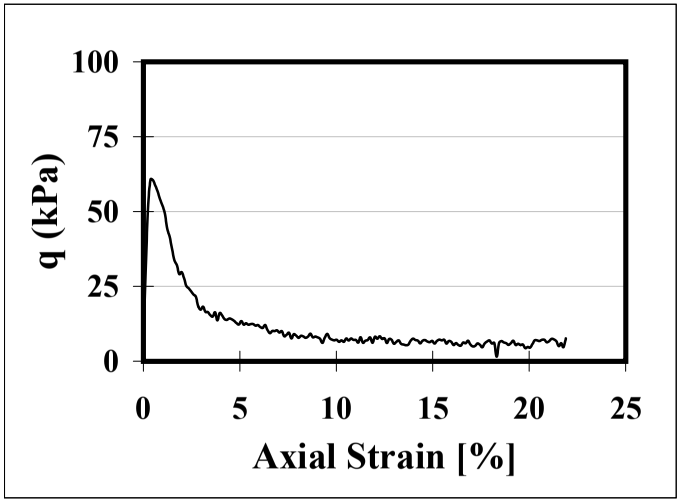

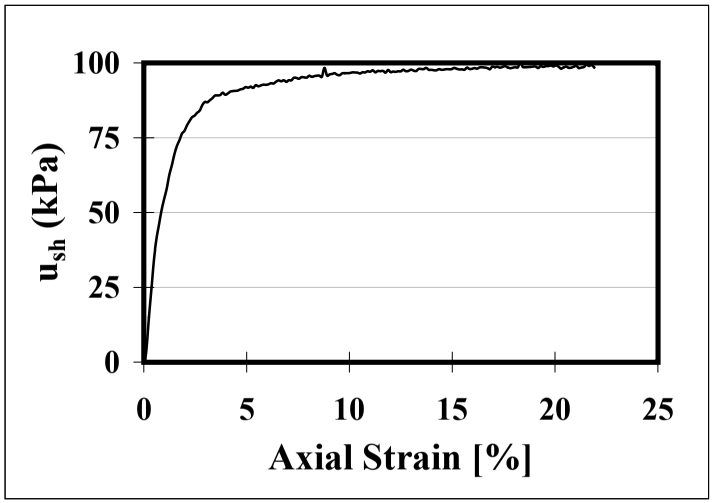

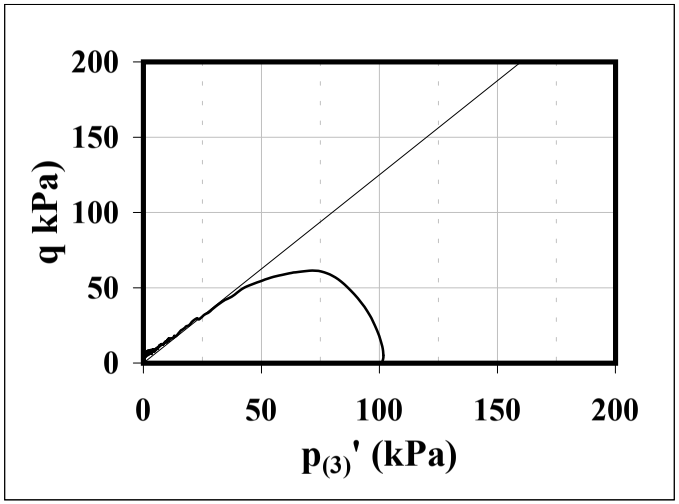

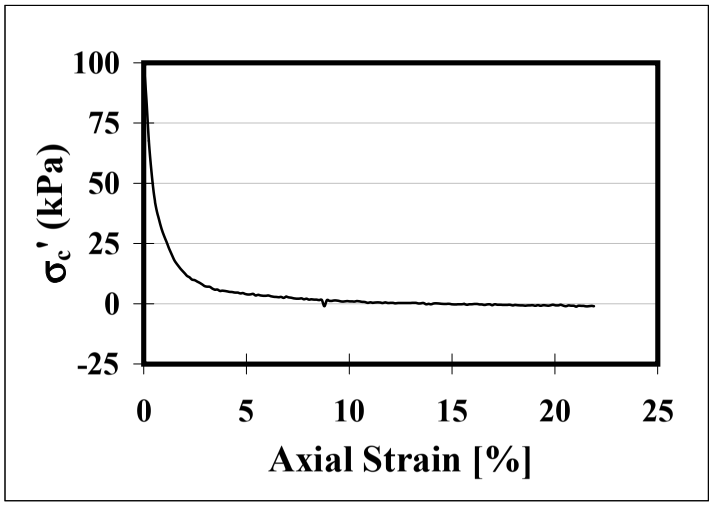

ϕ = 31.1 Confining stress = 100 kPa

GDS WG GS#40

Date: 07/23/01	Fines= 25	e= 0.415	ec= 0.886	ef= n.a.	(ec)eq= 0.603	

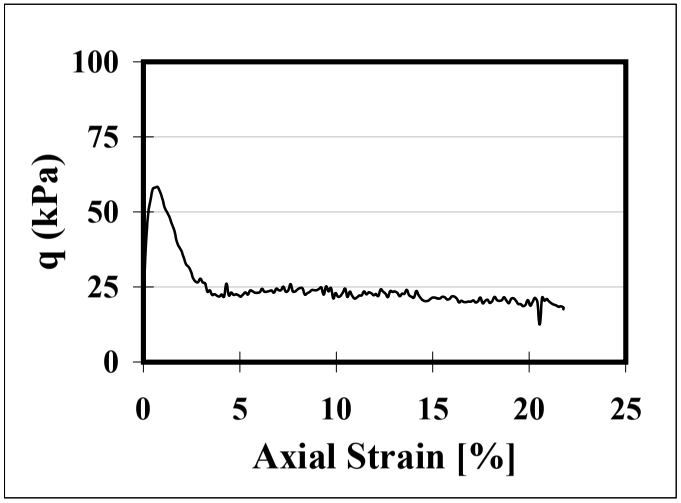

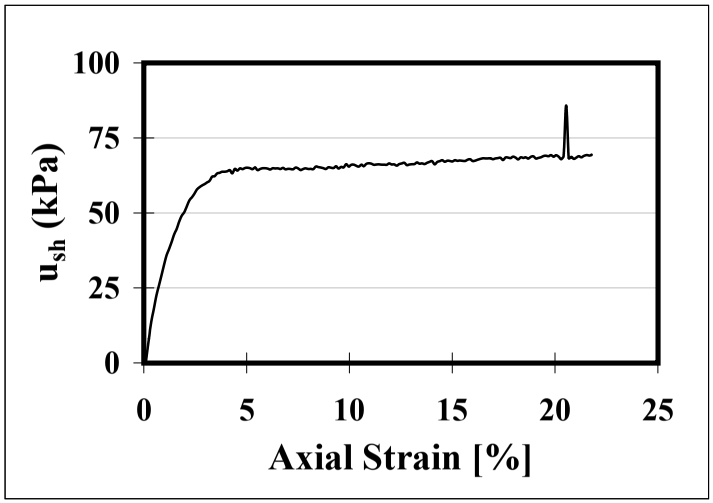

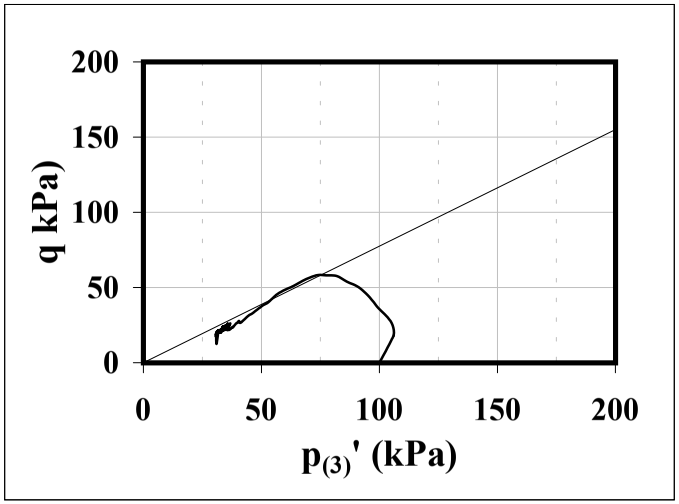

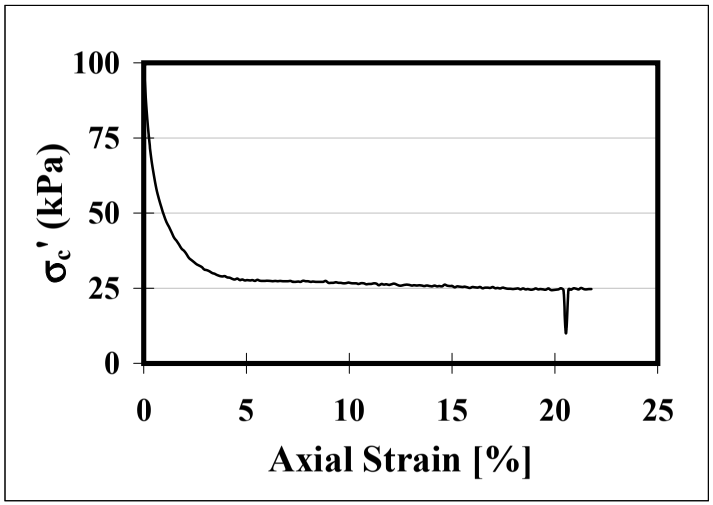

ϕ = 20.1 Confining stress = 100 kPa

GDS WG GS#40

Date: 07/25/01	Fines= 25	e= 0.442	ec= 0.923	ef= n.a.	(ec)eq= 0.635	

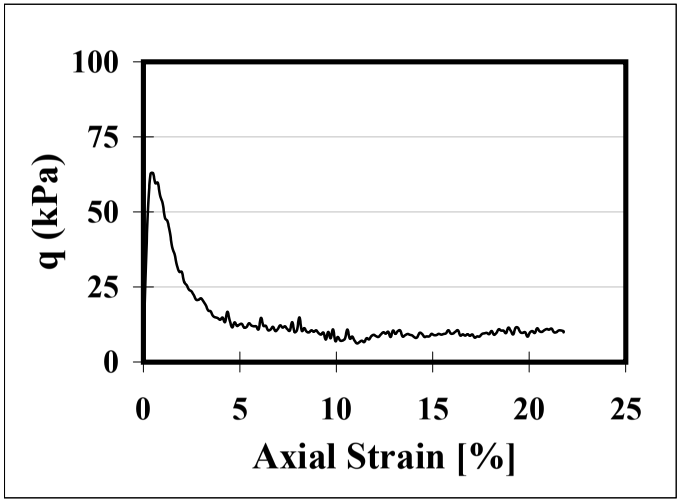

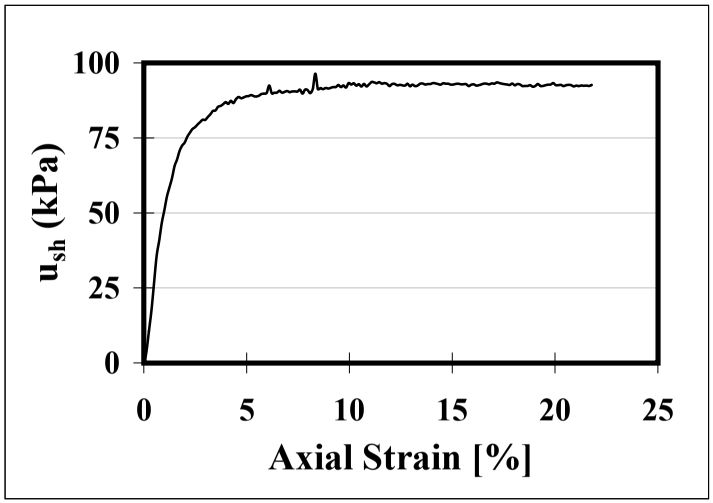

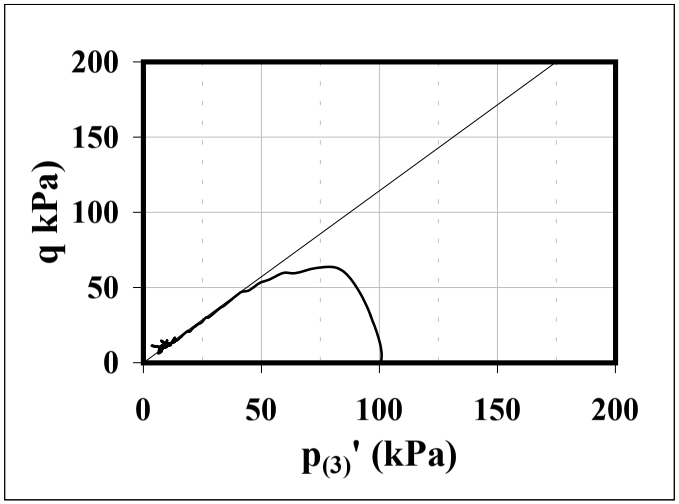

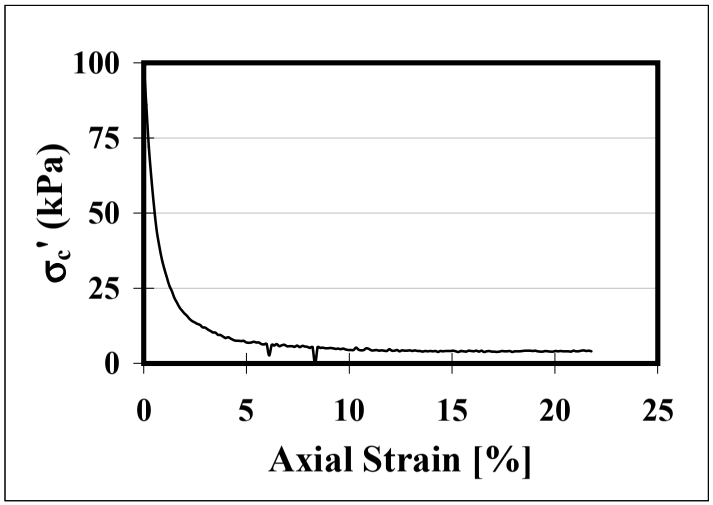

ϕ = 28.7 Confining stress = 100 kPa

GDS WG GS#40

Date: 07/26/01	Fines= 25	e= 0.364	ec= 0.818	ef= n.a.	(ec)eq= 0.545	

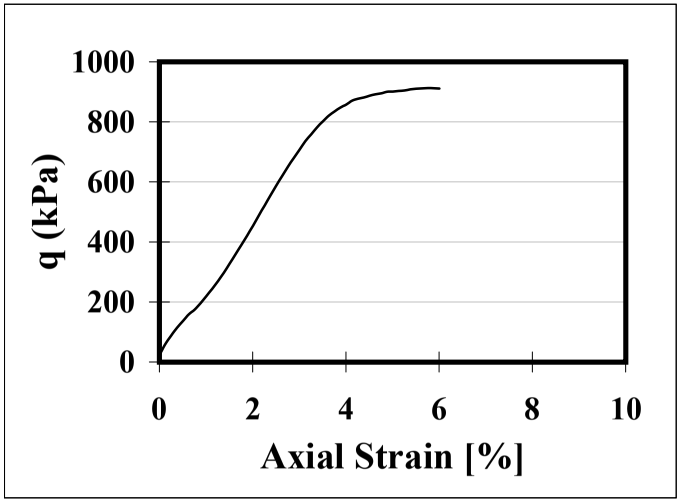

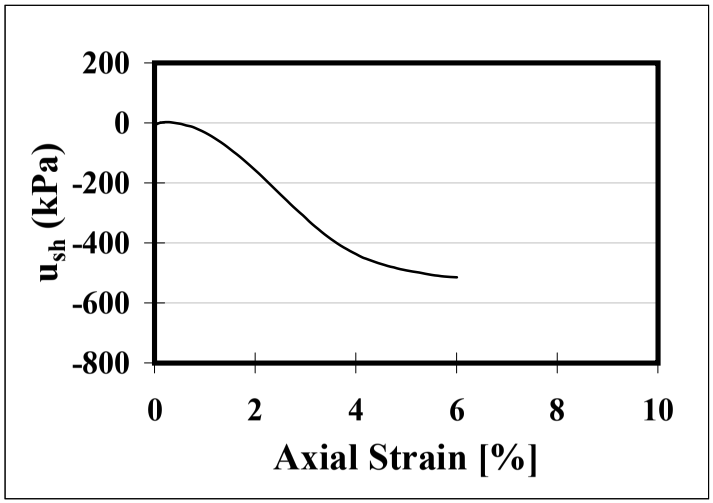

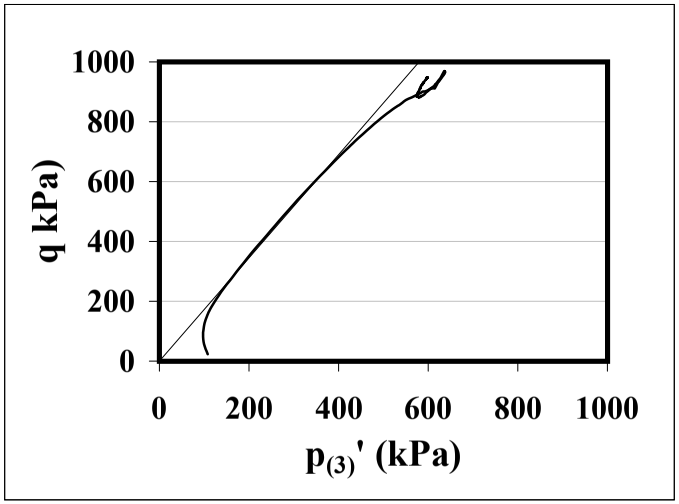

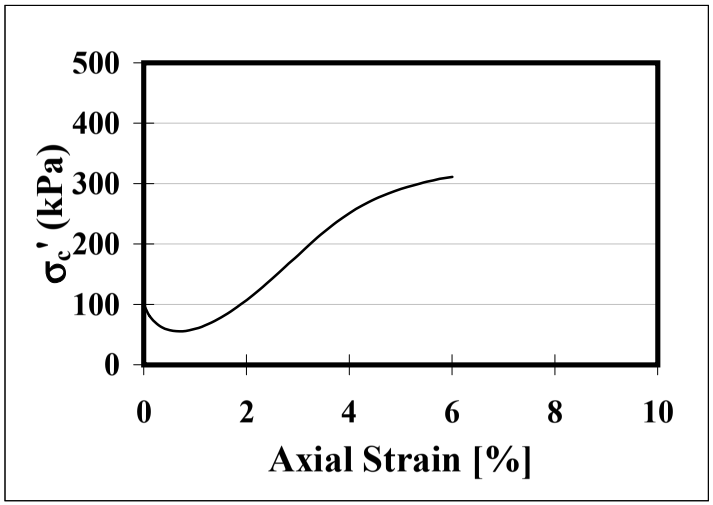

ϕ = 42.1 Confining stress = 100 kPa

The following table summarizes the soil parameters used to calculate the equivalent contact density indices in monotonic triaxial tests.

Table A.2 Contact Density Index Parameters - Monotonic

Soil Type	b ($FC \leq FC_{th}$)	m ($FC > FC_{th}$)	R_d
OS#55 sand – GSF#40 silt mix	0.25	0.65	25
FJ#80 sand – GSF#40 silt mix	0.25	0.65	18
WG sand – GSF#40 silt mix	0.53	-	32

R_d = size disparity ratio (= D_{50}/d_{50}, D_{50} = 50% passing dia. of coarser soil, and d_{50} = 50% passing dia. of finer soil).

Appendix B

Cyclic Triaxial Tests Data

Appendix B: Cyclic Triaxial Tests Data

Table B.1 Summary of Cyclic Triaxial Tests

Test No.	File Name	Soil Type	FC	Prep. Mtd	σ_c' (kPa)	CSR	B value	e	N_L	E_L (J/m^3)
C1	osc0-4RN	OS-00	0	DP	100	0.2	0.93	0.689	7	3010
C2	osc0-5R	OS-00	0	DP	100	0.2	0.96	0.631	15	6470
C3	c091099	OS-00	0	MT	100	0.2	0.97	0.753	7	1030
C4	c091699	OS-00	0	MT	100	0.2	0.94	0.719	8	1010
C5	c112299	OS-00	0	MT	100	0.2	0.96	0.782	1	670
C6	c112599	OS-00	0	MT	100	0.2	0.97	0.752	1	810
C7	c112699	OS-00	0	MT	100	0.2	0.92	0.731	3	1570
C8	c120199	OS-00	0	MT	100	0.2	0.92	0.699	6	1520
C9	c021100a	OS-00	0	MT	100	0.2	0.95	0.676	19	2140
C10	c022500	OS-00	0	MT	100	0.2	0.96	0.675	15	2120
C11	c022800	OS-00	0	MT	100	0.2	0.96	0.686	25	3750
C12	c031700	OS-00	0	MT	100	0.2	0.94	0.645	53	5030
C13	c032400	OS-00	0	MT	100	0.2	0.94	0.643	21	5260
C14	c090700	OS-00	0	MT	400	0.2	0.92	0.707	1	4750
C15	c092700	OS-00	0	MT	400	0.2	0.91	0.658	23	15000
C16	c100200	OS-00	0	MT	400	0.2	0.96	0.722	1	4220
C17	c100300	OS-00	0	MT	400	0.2	0.95	0.684	6	8110
C18	c120600	OS-00	0	MT	100	0.1	0.96	0.751	21	730
C19	c121500	OS-00	0	MT	100	0.1	0.98	0.755	16	780
C20	c042701	OS-00	0	MT	100	0.1	0.98	0.658	60	2660
C21	c121800	OS-00	0	MT	100	0.3	0.98	0.707	4	2830
C22	c030901	OS-00	0	MT	100	0.3	0.99	0.669	5	3510
C23	c052501	OS-00	0	MT	100	0.3	0.99	0.686	3	2980
C24	osc15-4R	OS-15	15	DP	100	0.2	0.91	0.580	7	2030
C25	osc15-5R	OS-15	15	DP	100	0.2	0.93	0.561	6	1130
C26	osc15-5N	OS-15	15	DP	100	0.2	0.92	0.577	7	1350
C27	c111599	OS-15	15	MT	100	0.2	0.93	0.567	13	1110
C28	c052600	OS-15	15	MT	100	0.2	0.95	0.555	15	1930
C29	c052900	OS-15	15	MT	100	0.2	0.96	0.617	3	960
C30	c053100	OS-15	15	MT	100	0.2	0.96	0.640	2	660

Table B.1 Summary of Cyclic Triaxial Tests (Cont.)

Test No.	File	Soil Type	FC	Prep. Mtd	σ_c' (kPa)	CSR	B value	e	N_L	E_L (J/m^3)
C31	c060100	OS-15	15	MT	100	0.2	0.94	0.658	2	590
C32	osc25-1R	OS-25	25	DP	100	0.2	0.95	0.466	6	1670
C33	osc25-2R	OS-25	25	DP	100	0.2	0.92	0.487	7	2410
C34	c110399	OS-25	25	MT	100	0.2	0.96	0.463	5	970
C35	c110599	OS-25	25	MT	100	0.2	1.00	0.457	5	1420
C36	c111299	OS-25	25	MT	100	0.2	1.00	0.470	5	780
C37	c111799	OS-25	25	MT	100	0.2	0.97	0.468	12	1880
C38	c060200	OS-25	25	MT	100	0.2	0.99	0.462	2	1160
C39	c060500	OS-25	25	MT	100	0.2	0.97	0.408	13	3010
C40	c061200	OS-25	25	MT	100	0.2	0.94	0.505	2	590
C41	c061500	OS-25	25	MT	100	0.2	0.94	0.402	17	3130
C42	c110801	OS-25	25	MT	100	0.1	0.97	0.504	35	890
C43	c110901	OS-25	25	MT	100	0.1	0.98	0.518	13	740
C44	c111001	OS-25	25	MT	100	0.3	0.98	0.473	5	1920
C45	c090501	OS-25	25	MT	400	0.2	0.99	0.487	1	4090
C46	c091001	OS-25	25	MT	400	0.2	0.99	0.464	5	5350
C47	c111101	OS-25	25	MT	400	0.2	0.98	0.492	3	6770
C48	c111301	OS-25	25	MT	400	0.2	0.96	0.444	6	12230
C49	c020200	OS-60	60	MT	100	0.2	1.00	0.540	5	3160
C50	c020300	OS-60	60	MT	100	0.2	1.00	0.545	4	4300
C51	c020700	OS-60	60	MT	100	0.2	0.99	0.539	4	3500
C52	c081800	OS-60	60	MT	100	0.2	1.00	0.528	5	2680
C53	c082500	OS-60	60	MT	100	0.2	0.95	0.505	17	3710
C54	c082800	OS-60	60	MT	100	0.2	0.98	0.490	31	5740
C55	c030300	OS-100	100	MT	100	0.2	1.00	0.858	3	1590
C56	c041700	OS-100	100	MT	100	0.2	1.00	0.862	4	1650
C57	c062100	OS-100	100	MT	100	0.2	0.95	0.866	5	1810
C58	c062600	OS-100	100	MT	100	0.2	0.99	0.838	9	3200
C59	c071000	OS-100	100	MT	100	0.2	1.00	0.875	5	1860
C60	c072100	OS-100	100	MT	100	0.2	0.95	0.812	6	2190
C61	c072600	OS-100	100	MT	100	0.2	0.97	0.848	5	2110
C62	c081100	OS-100	100	MT	100	0.2	0.93	0.811	22	3600
C63	c052901	FJ-00	0	MT	100	0.2	0.98	0.788	4	1170
C64	c053101	FJ-00	0	MT	100	0.2	0.97	0.746	13	2500
C65	c060801	FJ-00	0	MT	100	0.2	0.97	0.715	69	7750
C66	c061401	FJ-25	25	MT	100	0.2	0.97	0.552	32	3460

Table B.1 Summary of Cyclic Triaxial Tests (Cont.)

Test No.	File	Soil Type	FC	Prep. Mtd	σ_c' (kPa)	CSR	B value	e	N_L	E_L (J/m^3)
C67	c061501	FJ-25	25	MT	100	0.2	0.98	0.619	9	1330
C68	c061701	FJ-25	25	MT	100	0.2	0.98	0.643	3	720
C69	c080601	FJ-60	60	MT	100	0.2	1.00	0.563	2	1240
C70	c081001	FJ-60	60	MT	100	0.2	1.00	0.564	3	1470
C71	c092901	WG-00	0	MT	100	0.2	0.96	0.601	2	720
C72	c100401	WG-00	0	MT	100	0.2	0.97	0.549	9	1710
C73	c101801	WG-00	0	MT	100	0.2	0.97	0.528	12	2010
C74	c102501	WG-25	25	MT	100	0.2	0.98	0.412	5	1350
C75	c102601	WG-25	25	MT	100	0.2	0.99	0.382	6	1350

Notes: CSR = cyclic stress ratio; N_L = number of cycles to reach ±5% axial strain; E_L = energy to to reach ±5% axial strain.

Test No.: C01 **File Name: osc0-4RN** **Soil Type: OS-00** **e=0.689**

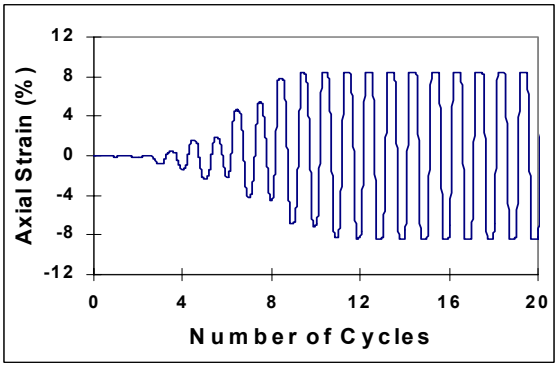

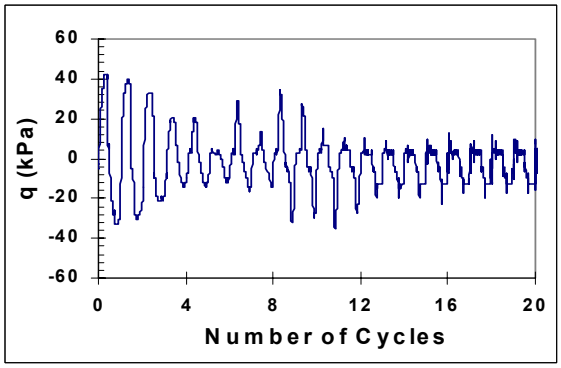

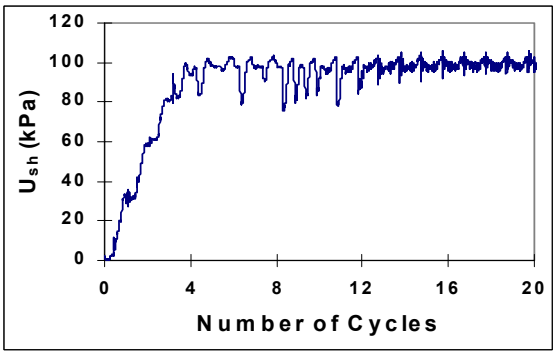

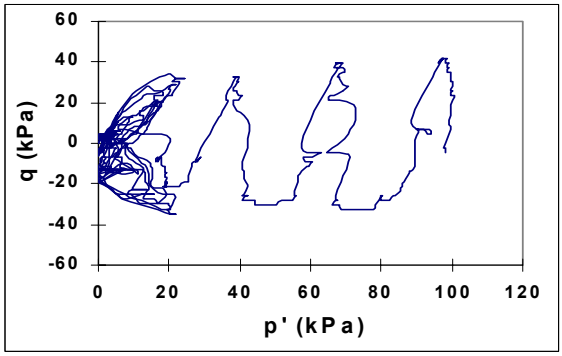

Test No.: C02 **File Name: osc0-5R** **Soil Type: OS-00** **e=0.631**

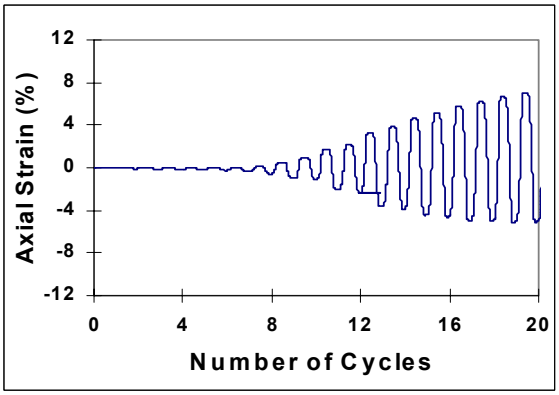

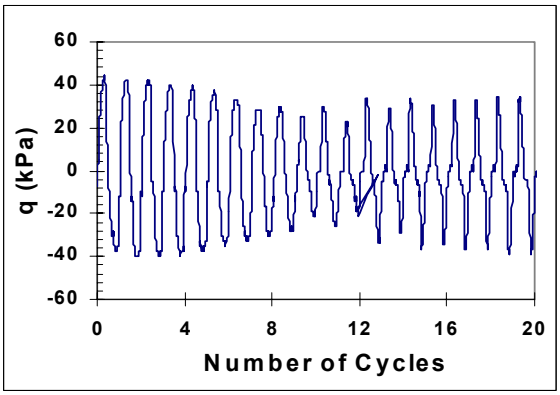

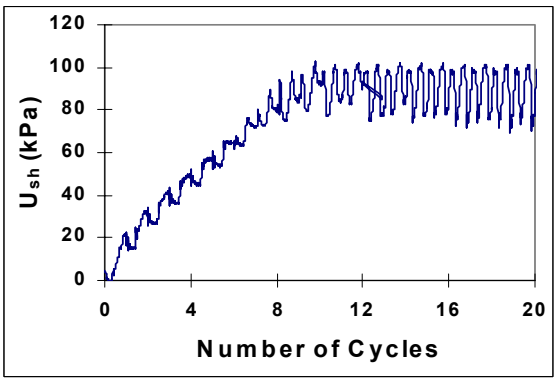

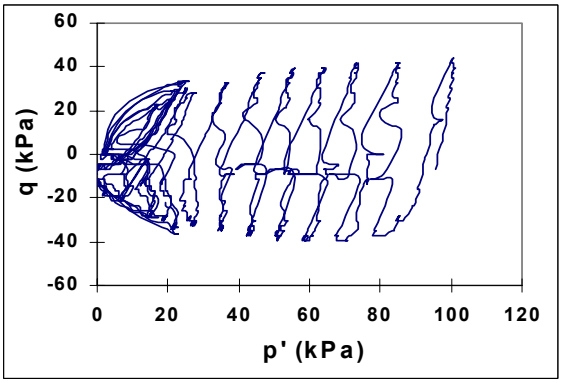

Test No.: C03 **File Name: c091099** **Soil Type: OS-00** **e=0.753**

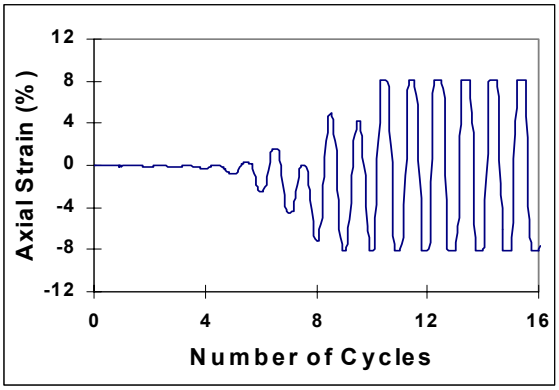

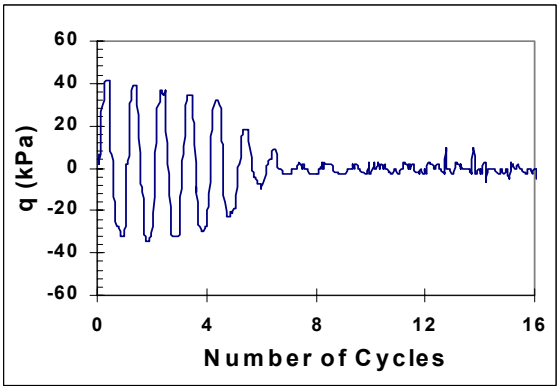

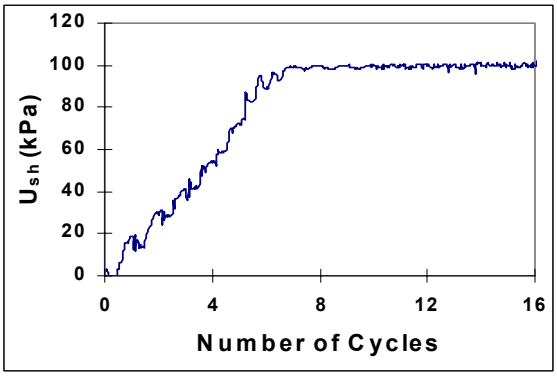

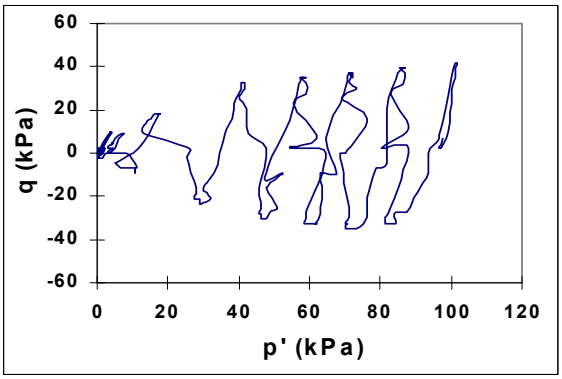

Test No.: C04 **File Name: c091699** **Soil Type: OS-00** **e=0.719**

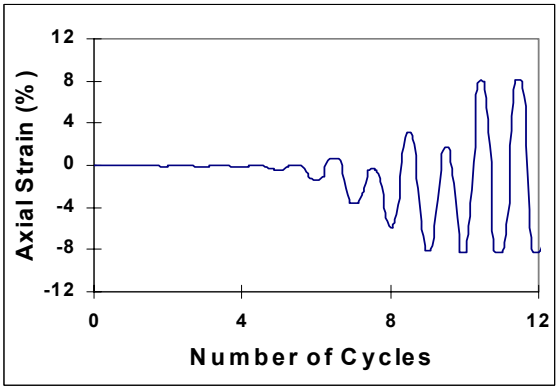

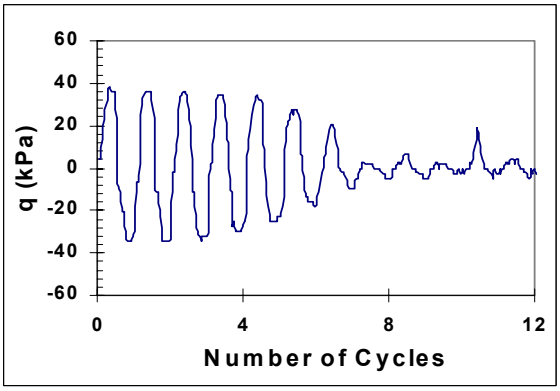

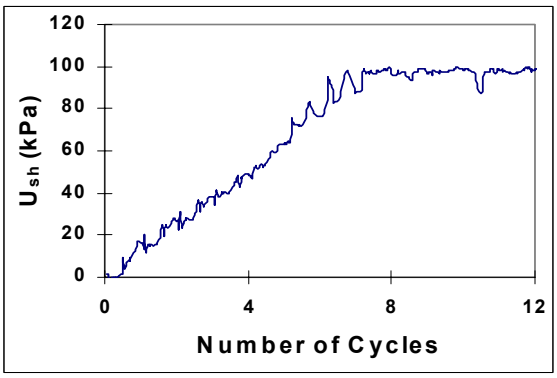

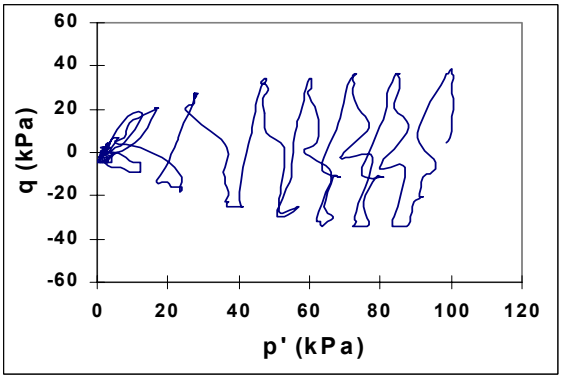

Test No.: C05 **File Name: c112299** **Soil Type: OS-00** **e=0.782**

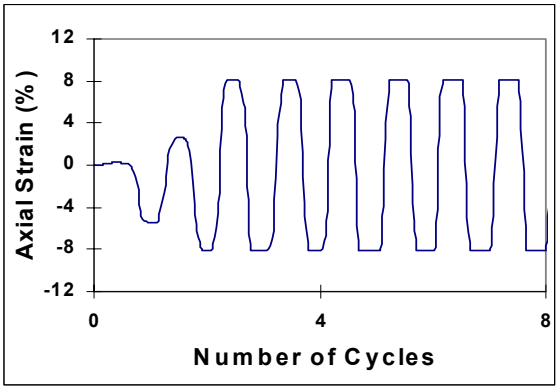

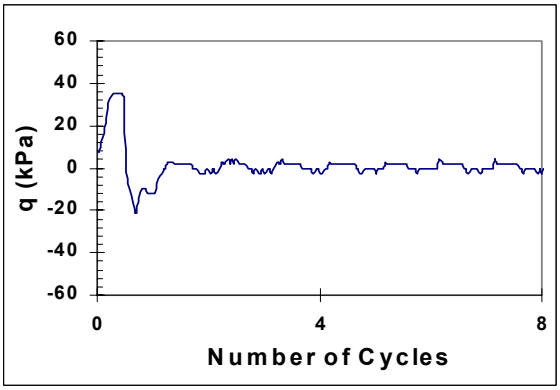

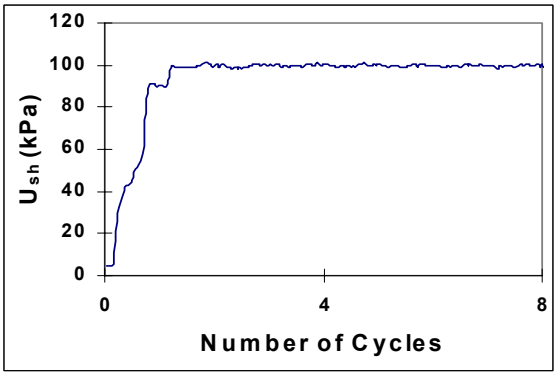

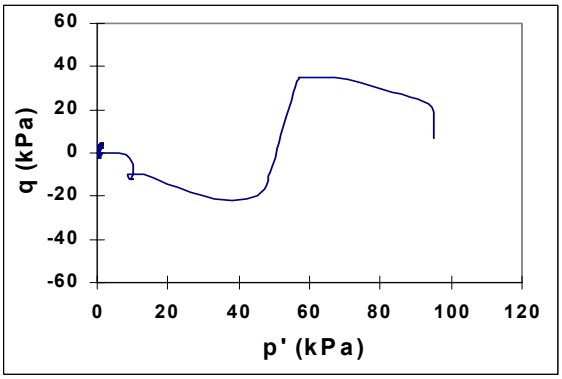

Test No.: C06 **File Name: c112599** **Soil Type: OS-00** **e=0.752**

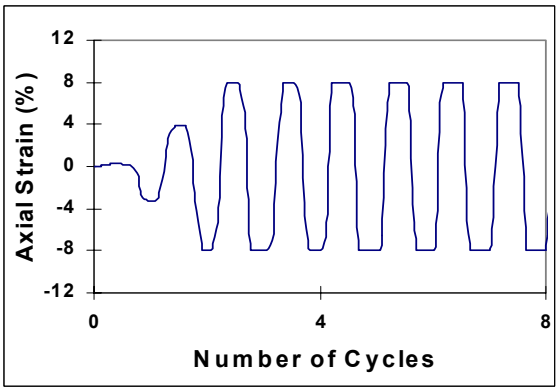

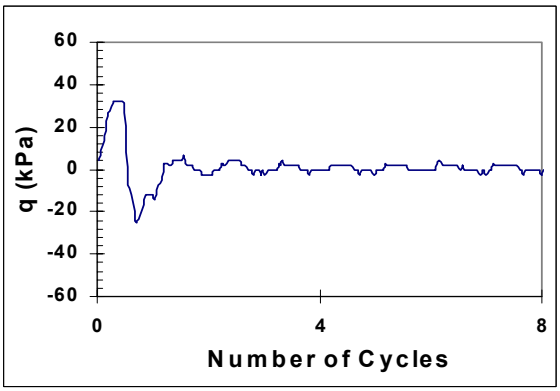

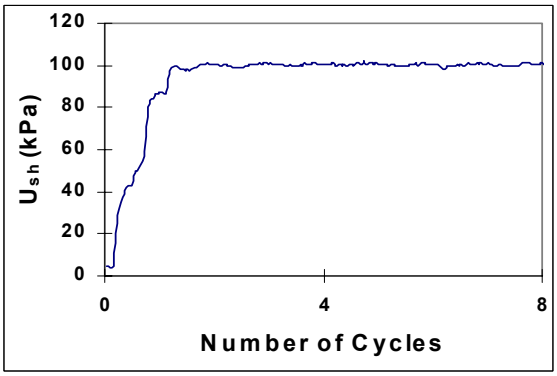

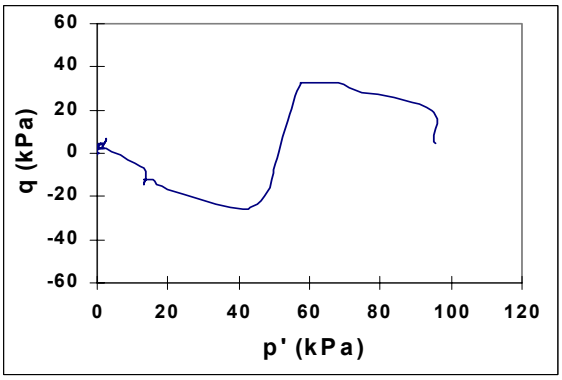

Test No.: C07 **File Name: c112699** **Soil Type: OS-00** **e=0.731**

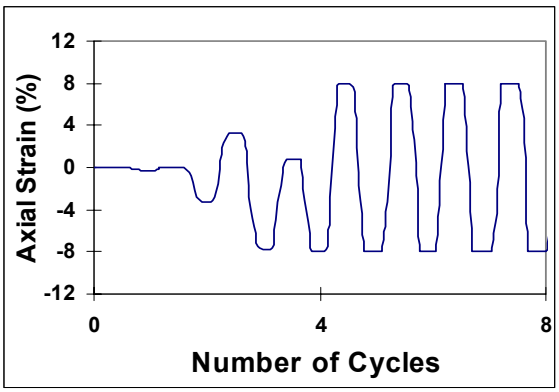

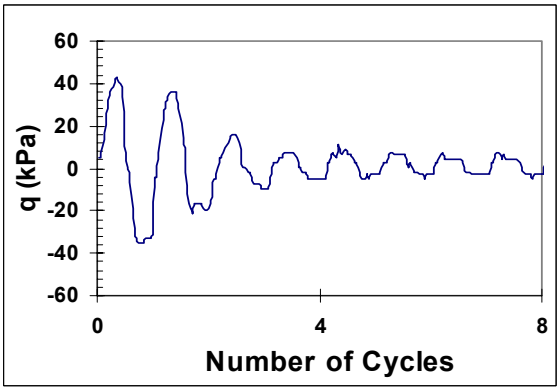

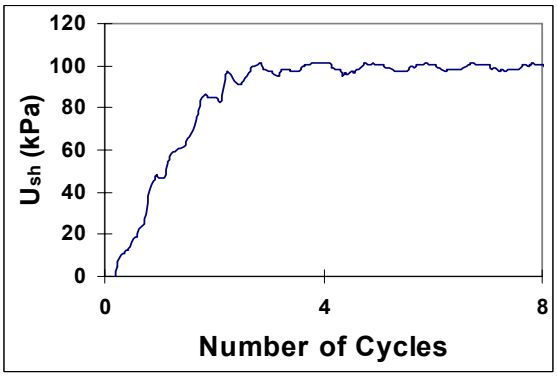

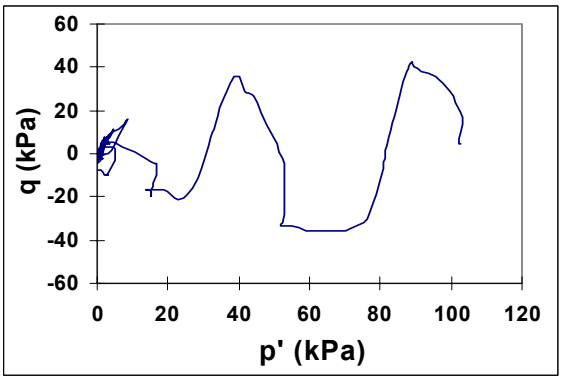

Test No.: C08 **File Name: c120199** **Soil Type: OS-00** **e=0.699**

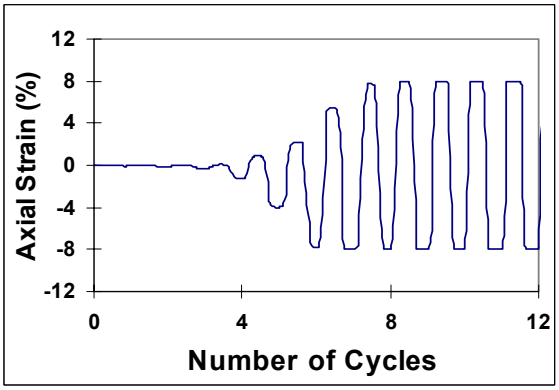

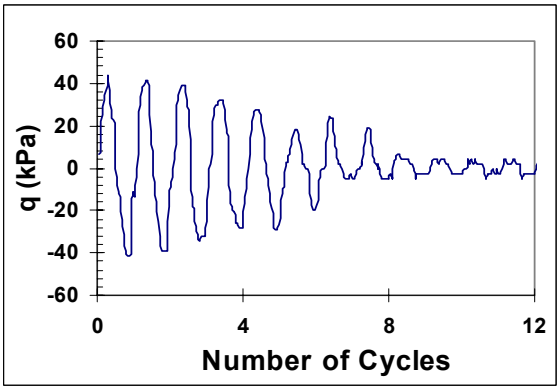

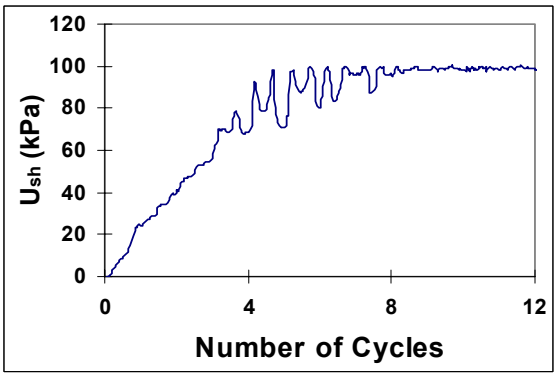

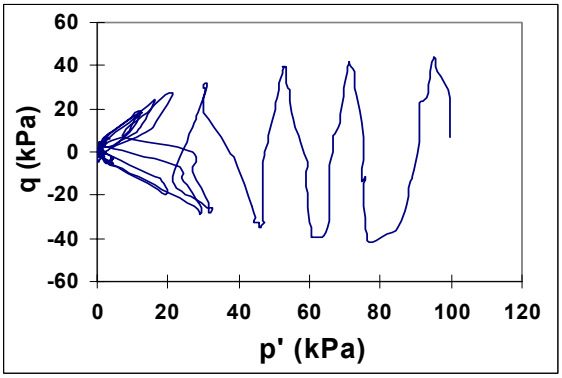

Test No.: C09 **File Name: c021100a** **Soil Type: OS-00** **e=0.676**

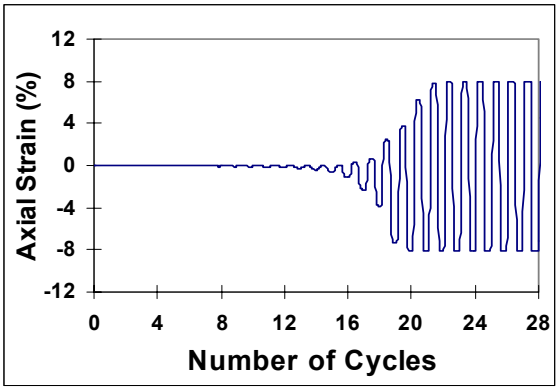

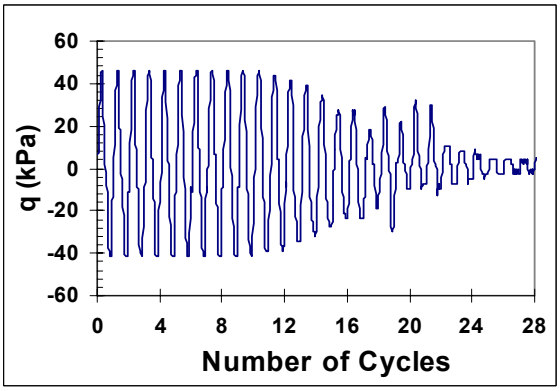

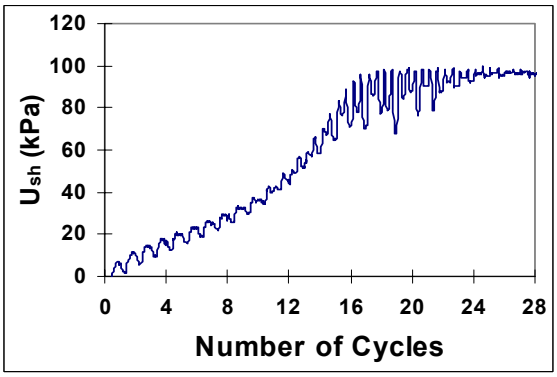

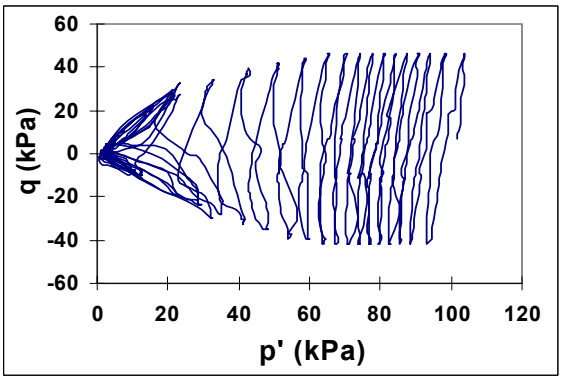

Test No.: C10 **File Name: c022500** **Soil Type: OS-00** **e=0.675**

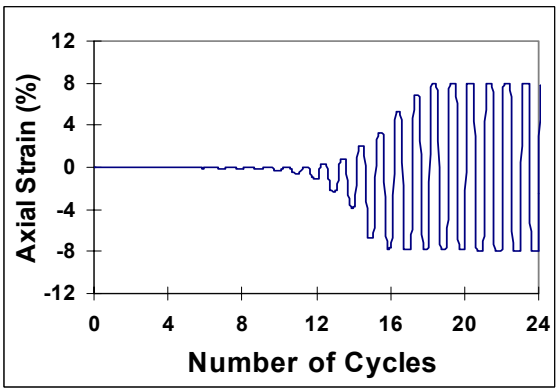

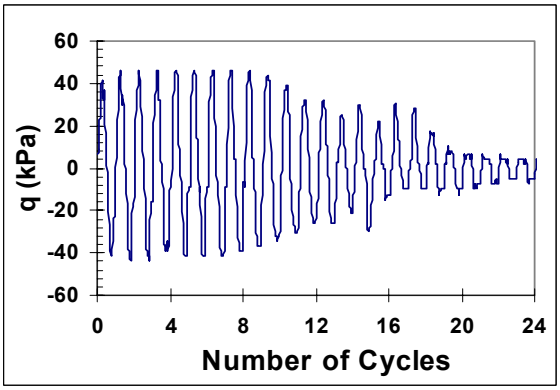

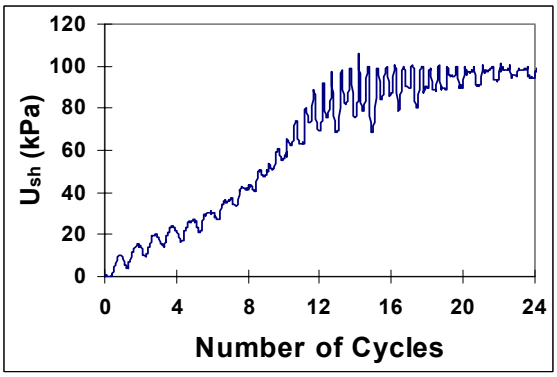

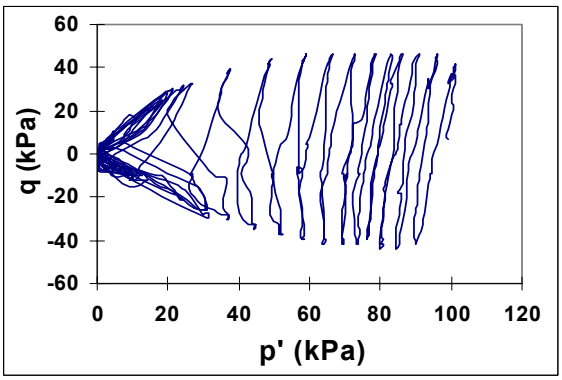

Test No.: C11 **File Name: c022800** **Soil Type: OS-00** **e=0.686**

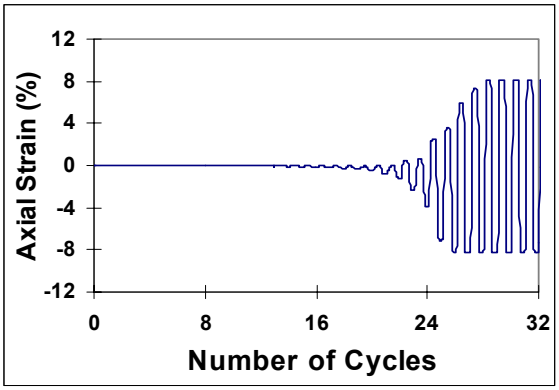

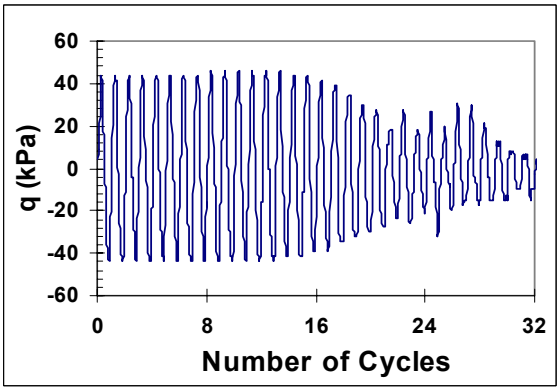

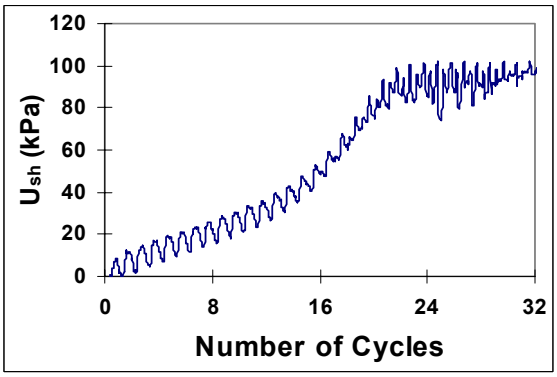

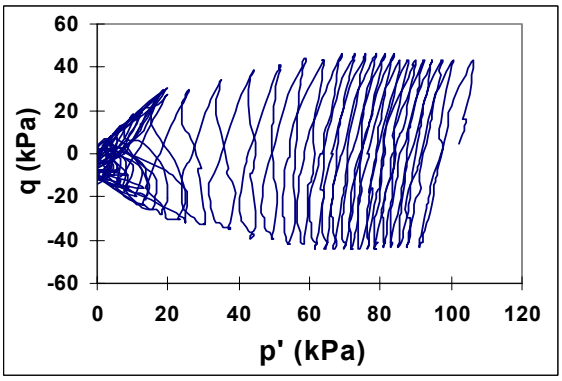

Test No.: C12 **File Name: c031700** **Soil Type: OS-00** **e=0.645**

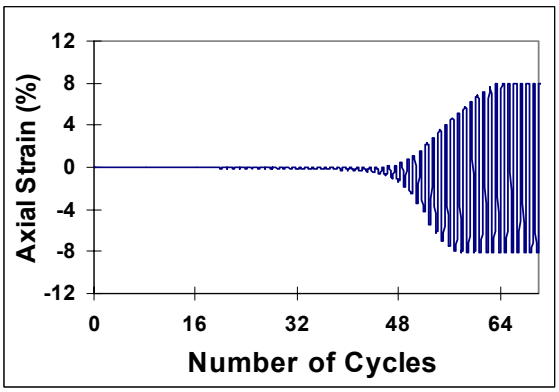

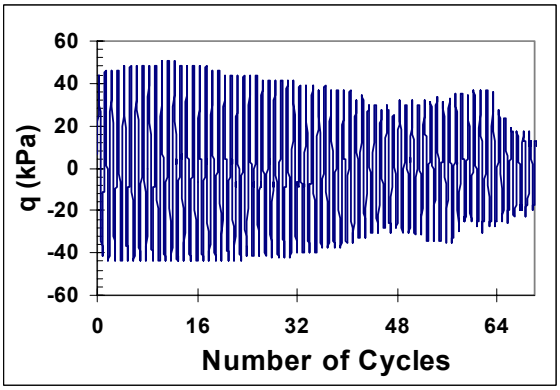

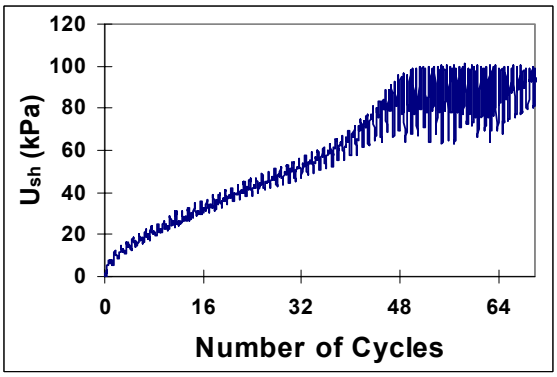

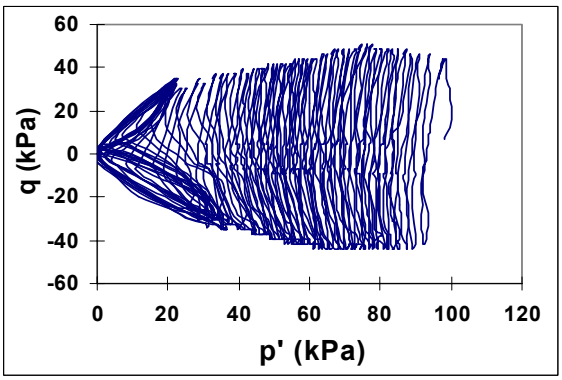

Test No.: C13 **File Name: c032400** **Soil Type: OS-00** **e=0.643**

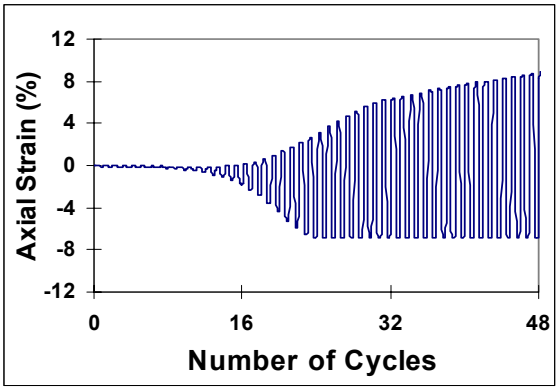

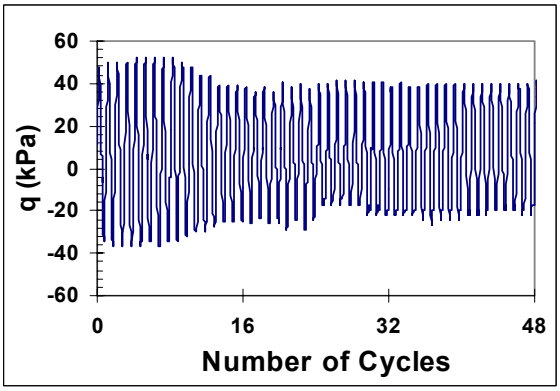

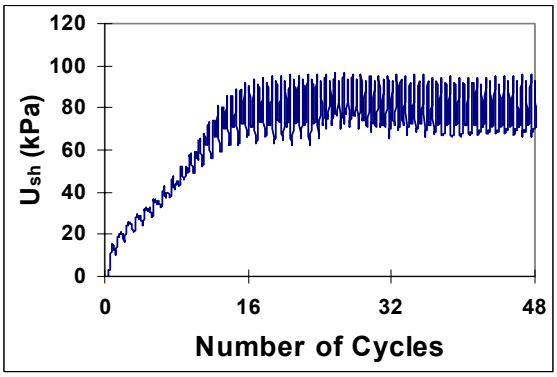

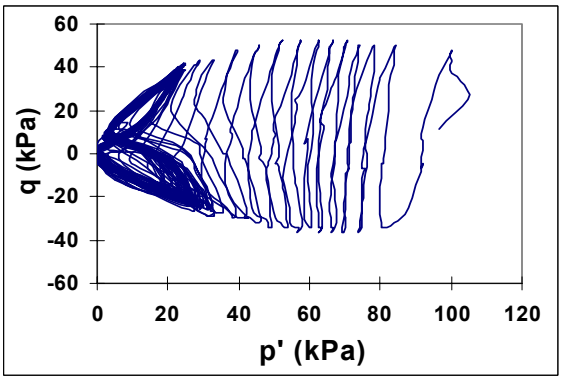

Test No.: C14 **File Name: c090700** **Soil Type: OS-00** **e=0.707**

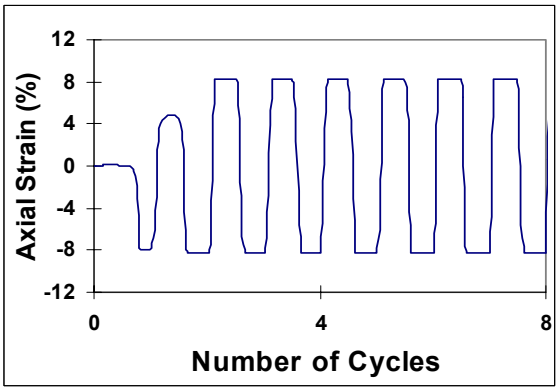

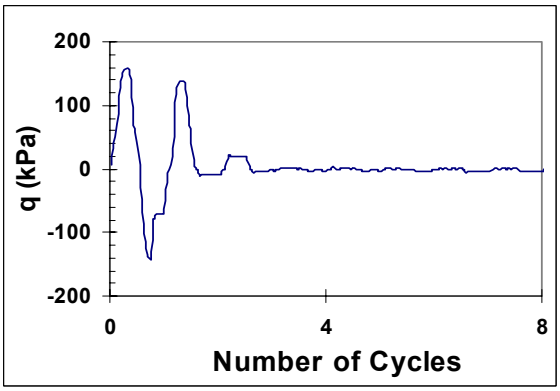

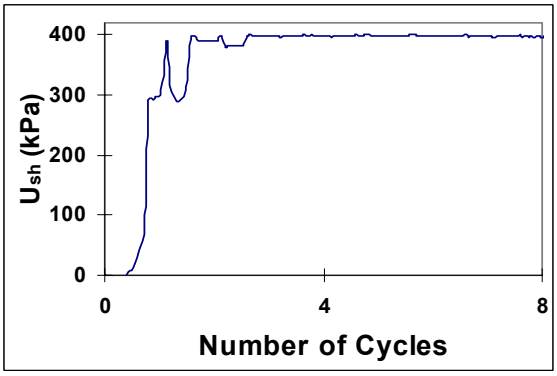

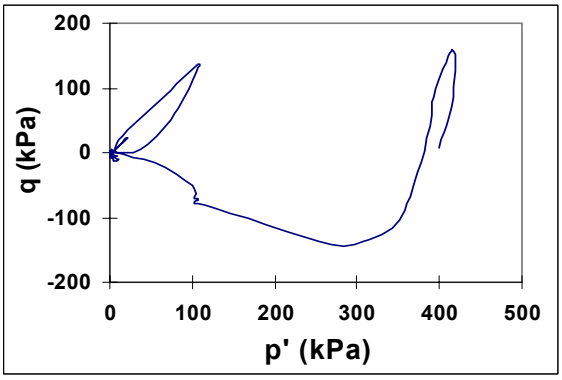

Test No.: C15 **File Name: c092700** **Soil Type: OS-00** **e=0.658**

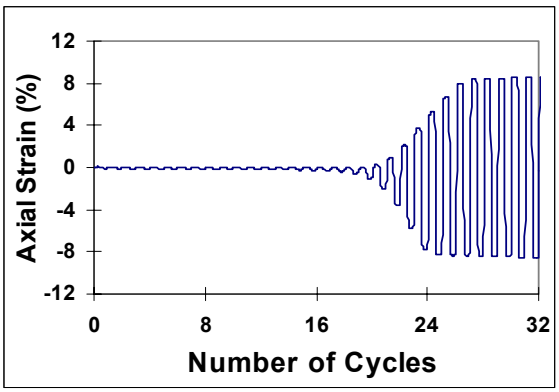

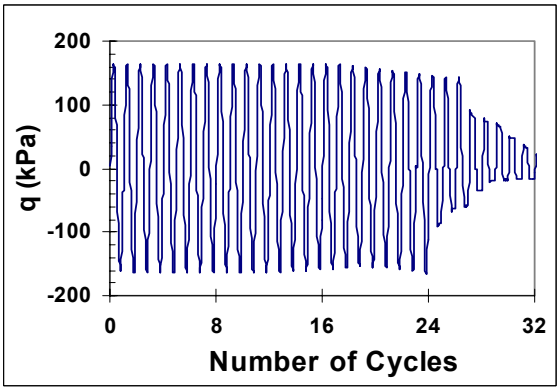

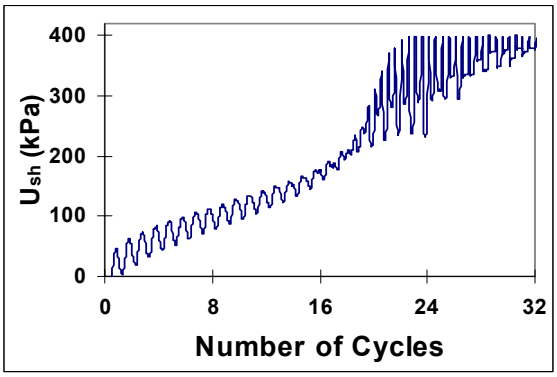

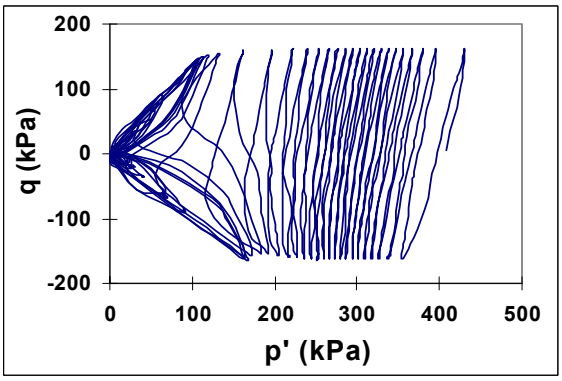

Test No.: C16 **File Name: c100200** **Soil Type: OS-00** **e=0.722**

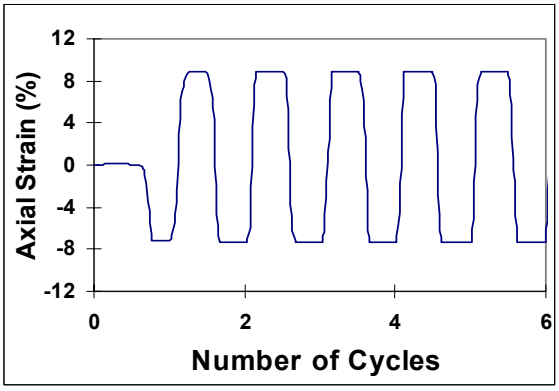

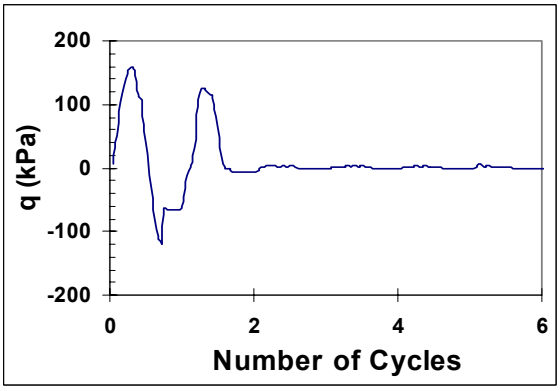

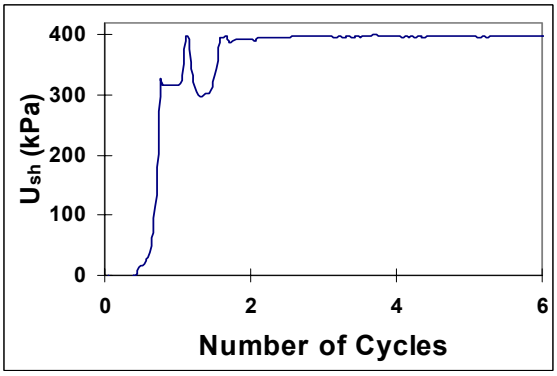

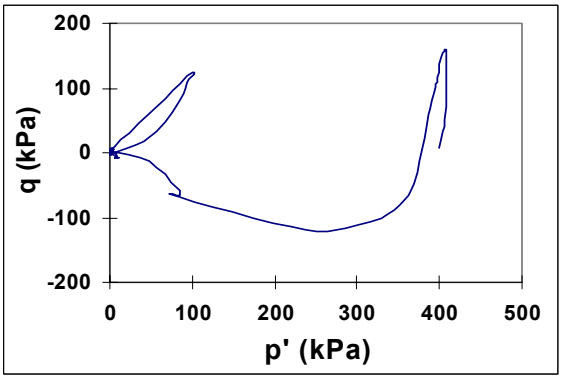

Test No.: C17 **File Name: c100300** **Soil Type: OS-00** **e=0.684**

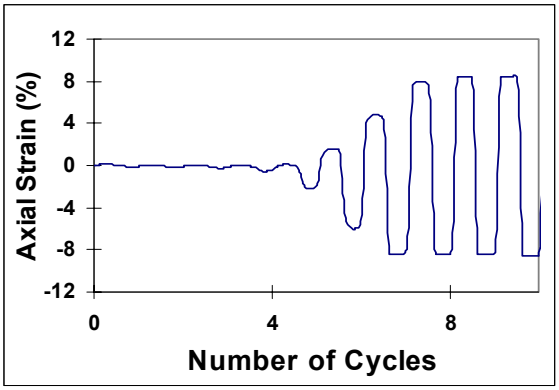

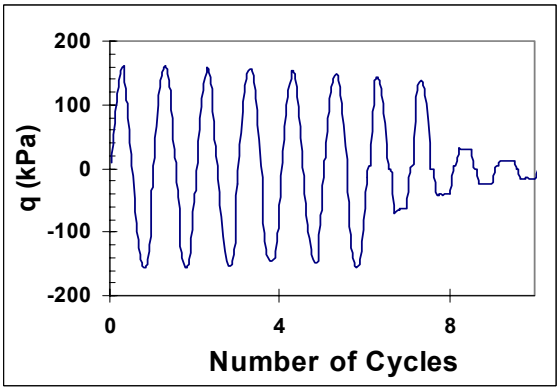

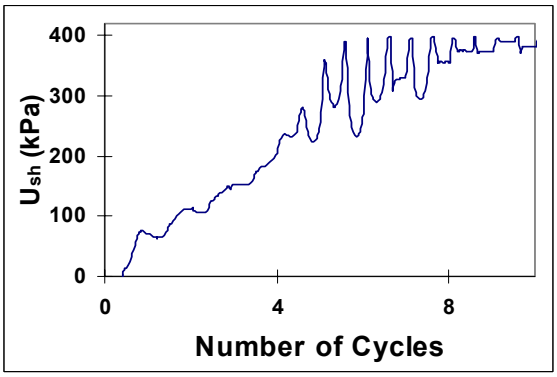

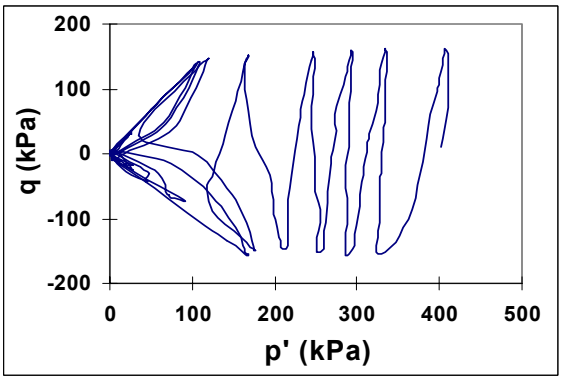

Test No.: C18 **File Name: c120600** **Soil Type: OS-00** **e=0.751**

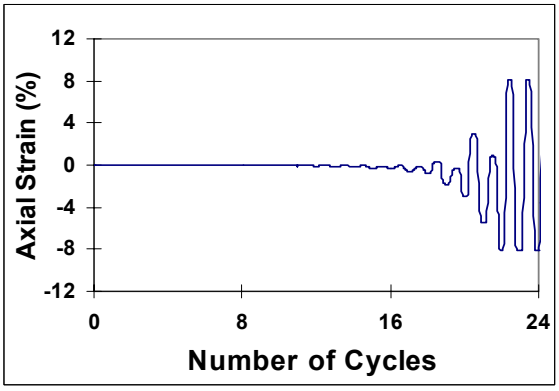

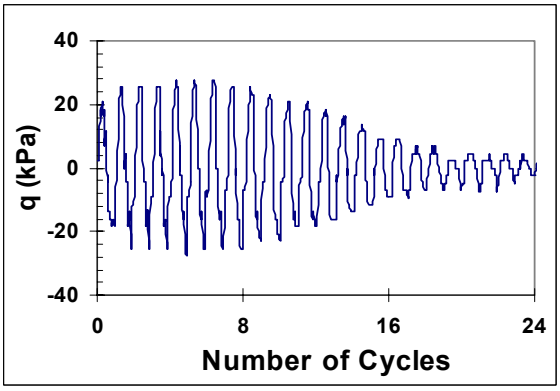

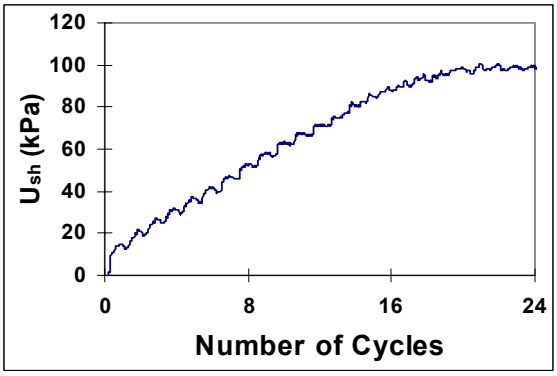

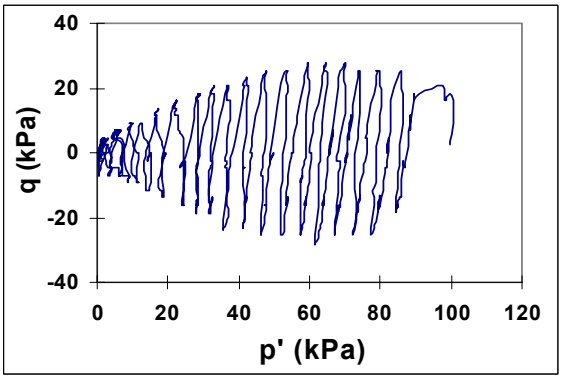

Test No.: C19 File Name: c121500 Soil Type: OS-00 e=0.755

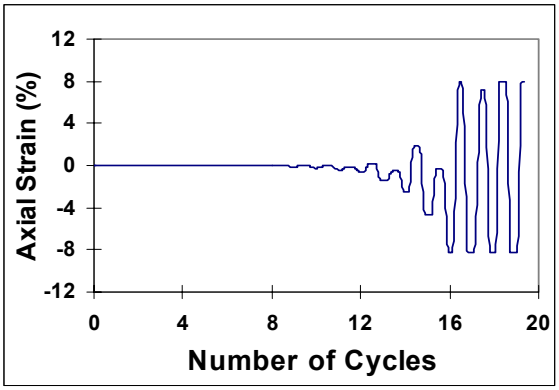

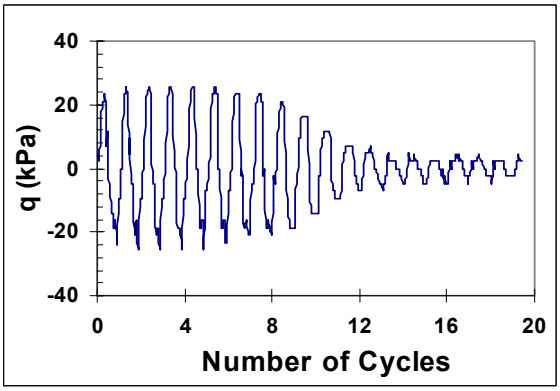

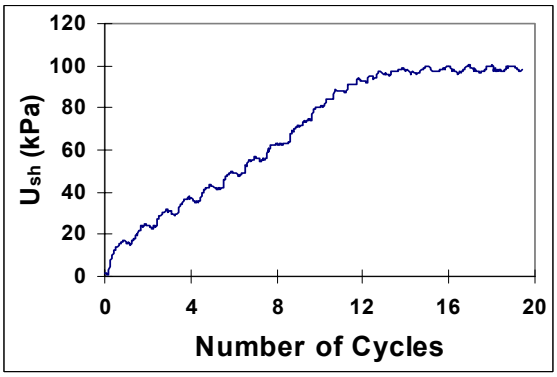

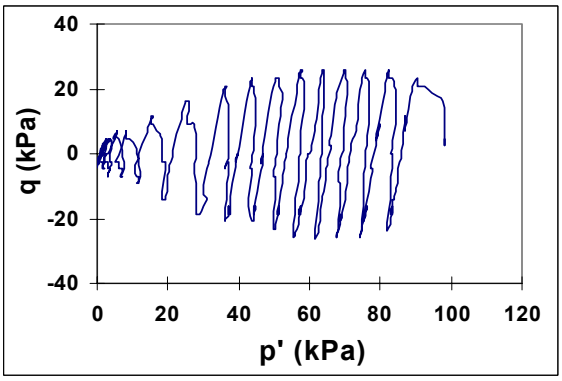

Test No.: C20 File Name: c042701 Soil Type: OS-00 e=0.658

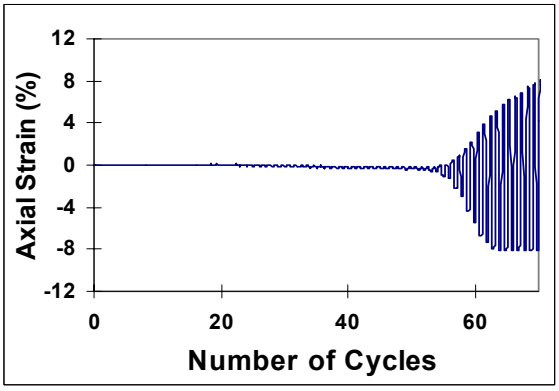

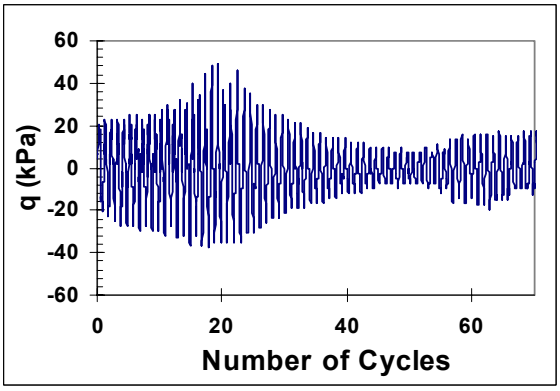

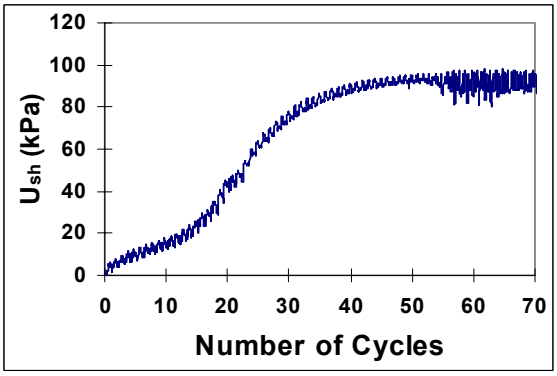

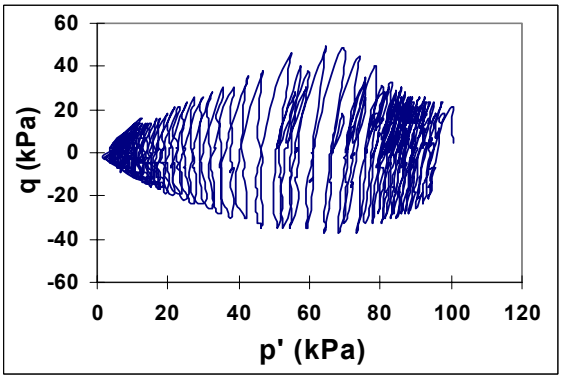

Test No.: C21 **File Name: c121800** **Soil Type: OS-00** **e=0.707**

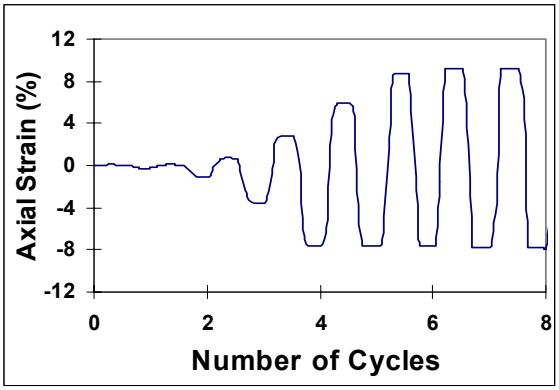

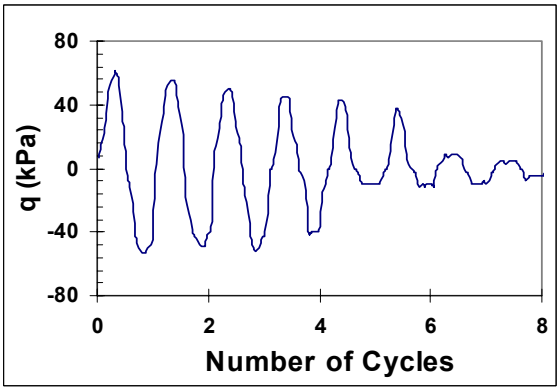

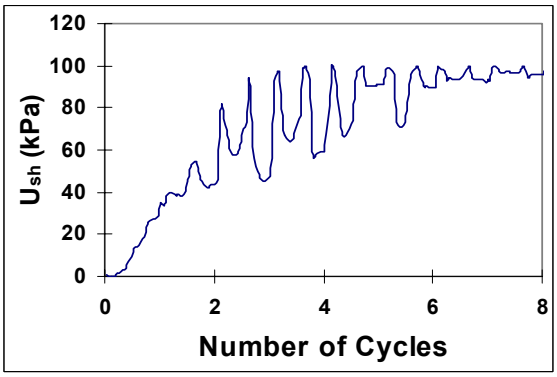

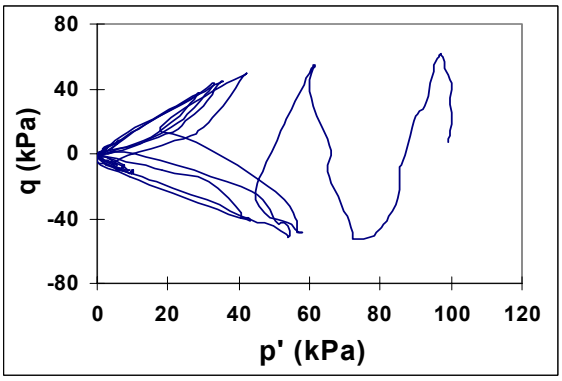

Test No.: C22 **File Name: c030901** **Soil Type: OS-00** **e=0.669**

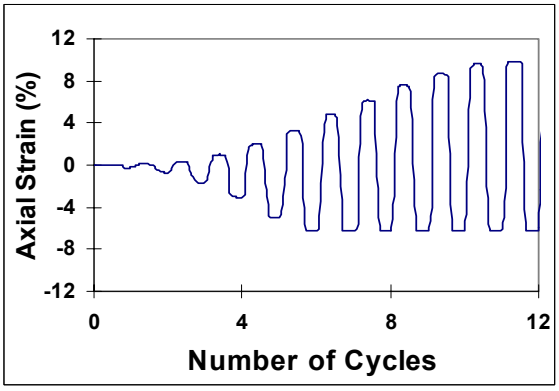

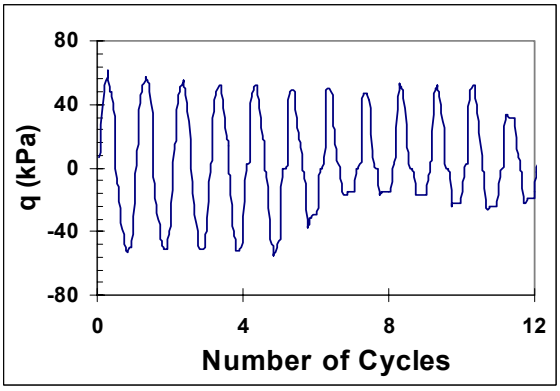

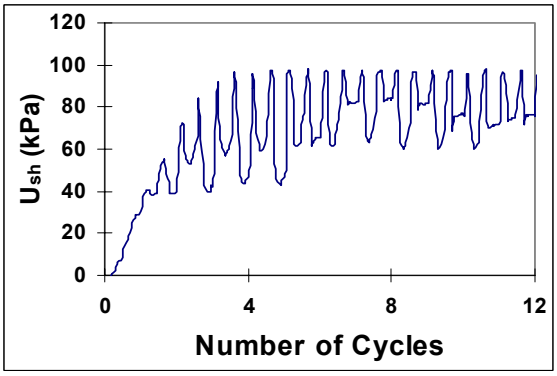

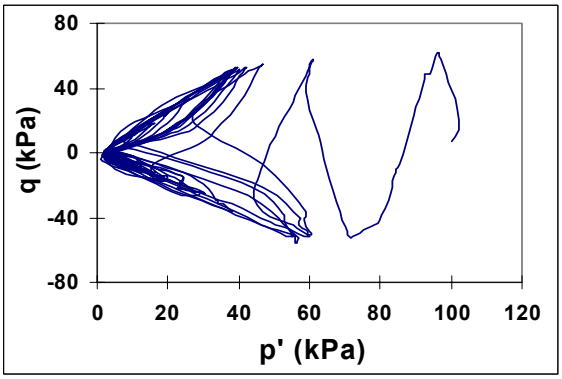

Test No.: C23 **File Name: c052501** **Soil Type: OS-00** **e=0.686**

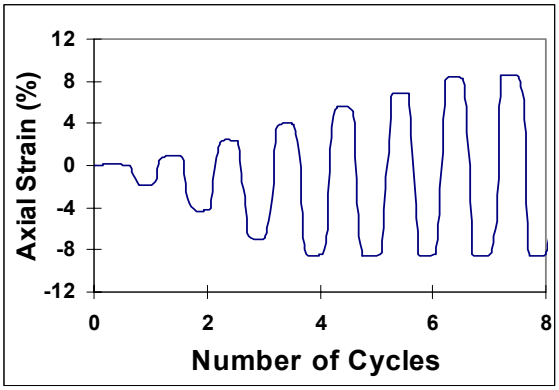

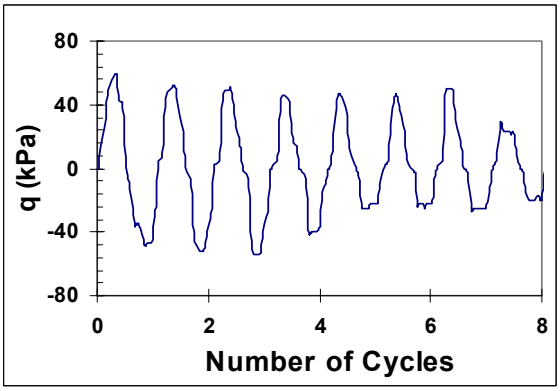

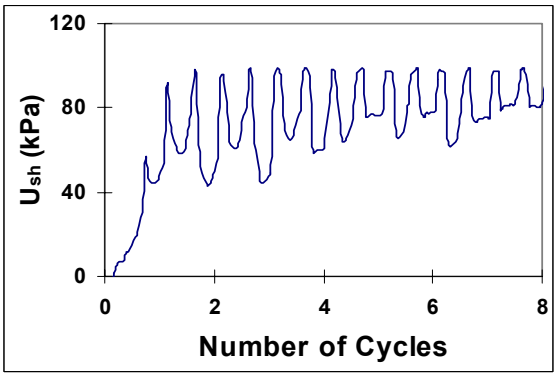

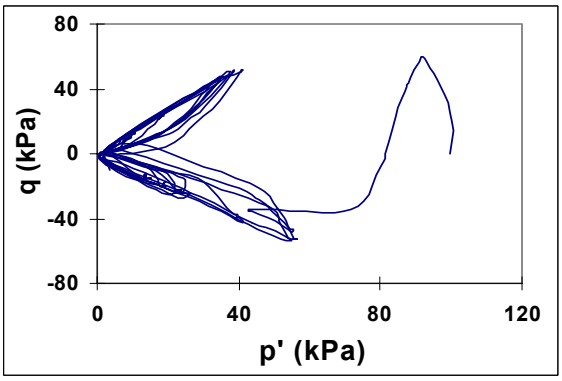

Test No.: C24 **File Name: osc15-4R** **Soil Type: OS-15** **e=0.580**

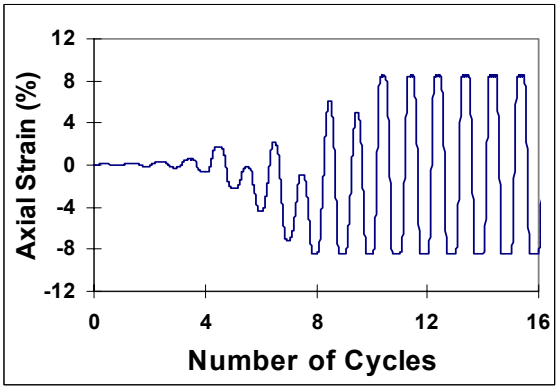

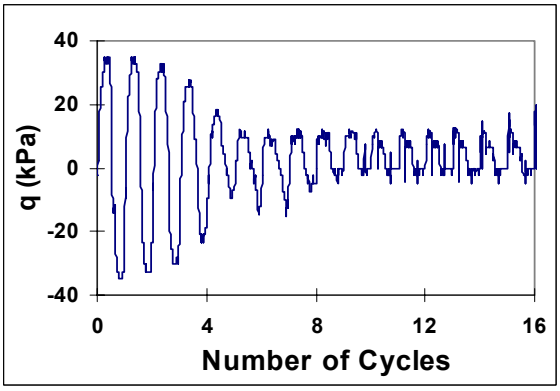

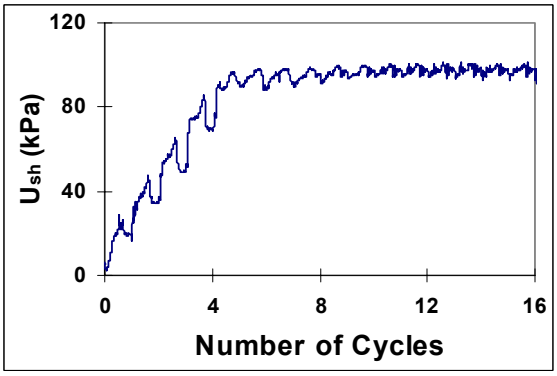

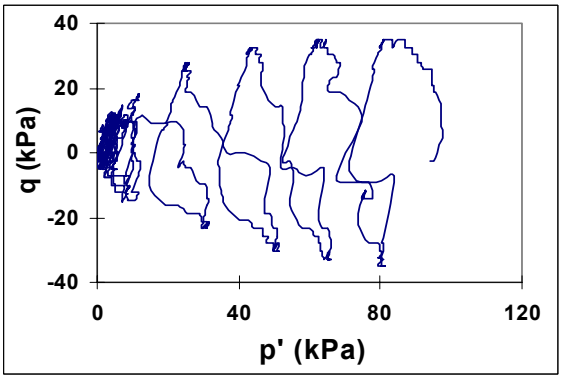

Test No.: C25 **File Name: osc15-5R** **Soil Type: OS-15** **e=0.561**

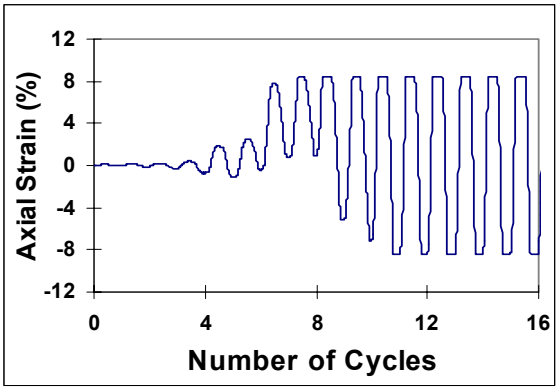

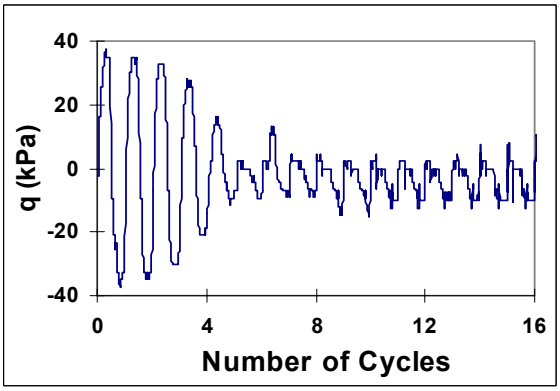

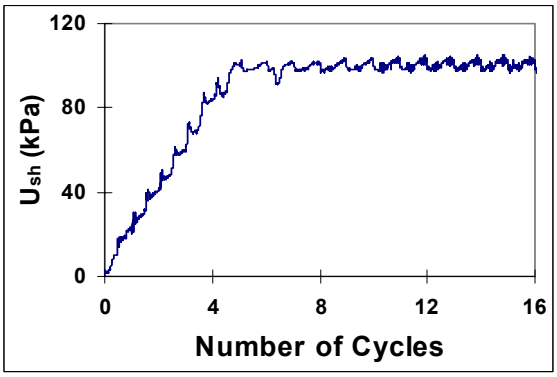

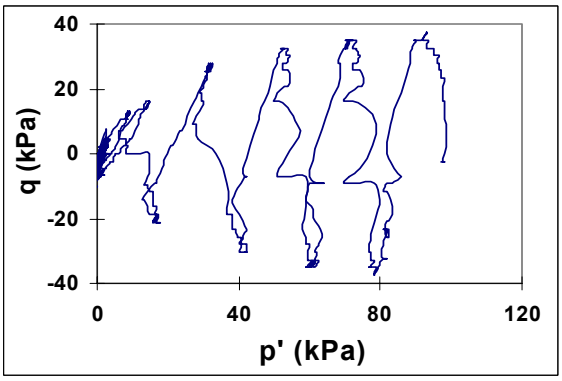

Test No.: C26 **File Name: osc15-5N** **Soil Type: OS-15** **e=0.577**

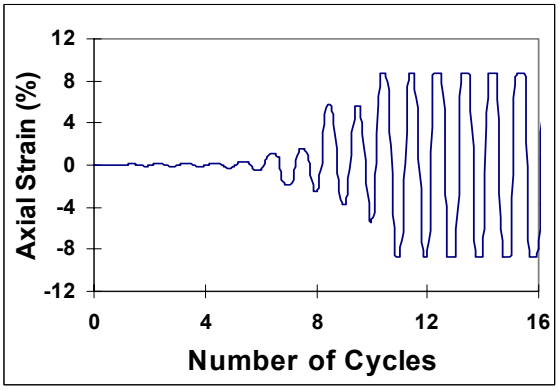

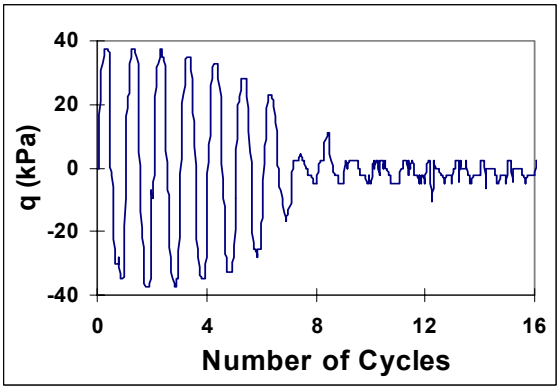

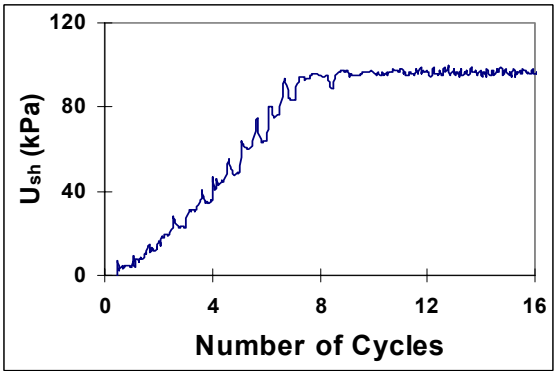

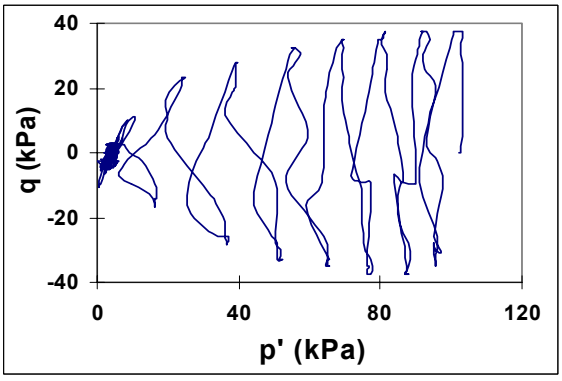

Test No.: C27 **File Name: c111599** **Soil Type: OS-15** **e=0.567**

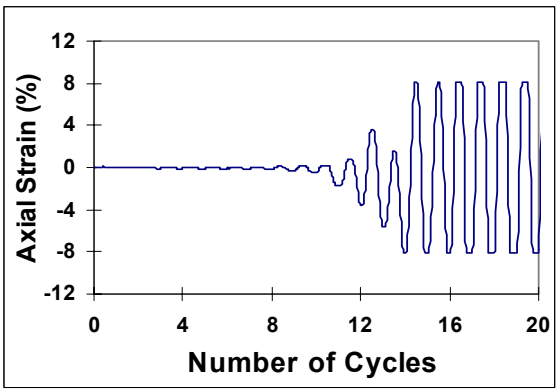

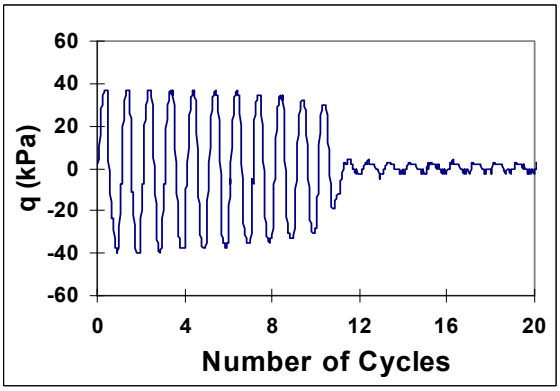

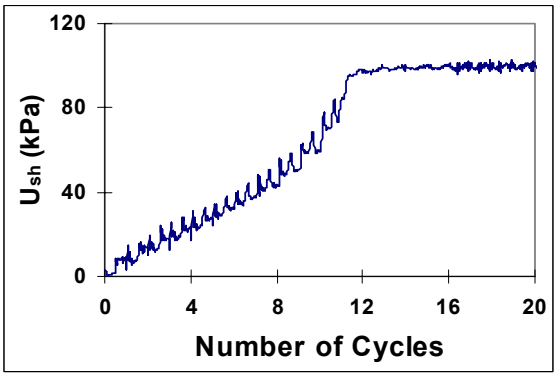

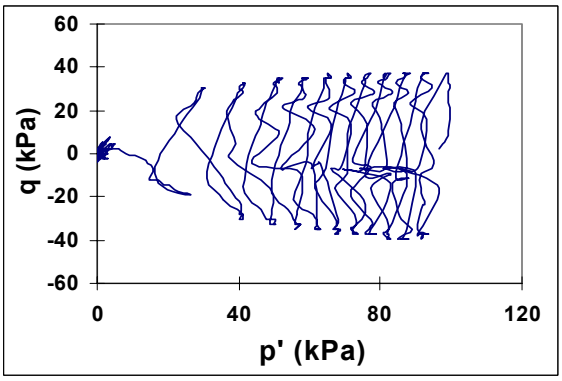

Test No.: C28 **File Name: c052600** **Soil Type: OS-15** **e=0.555**

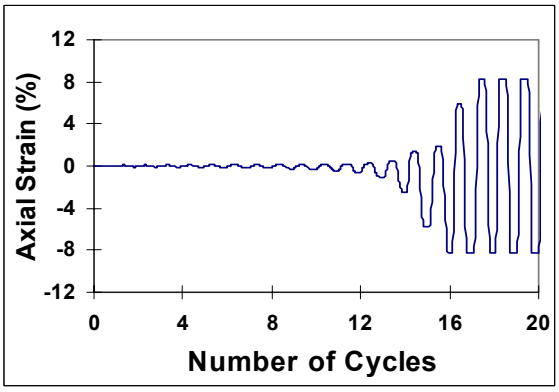

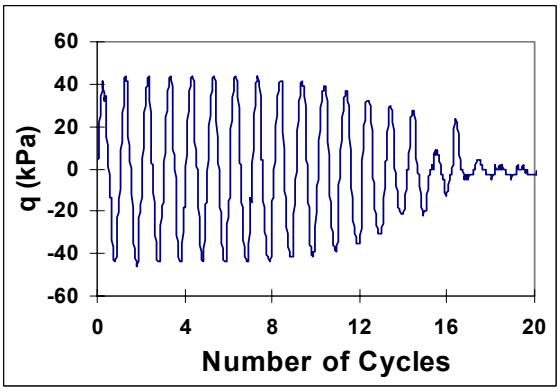

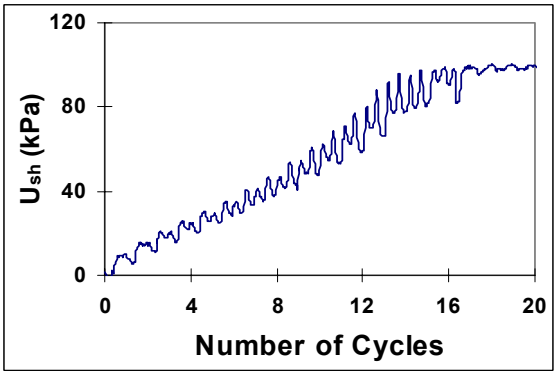

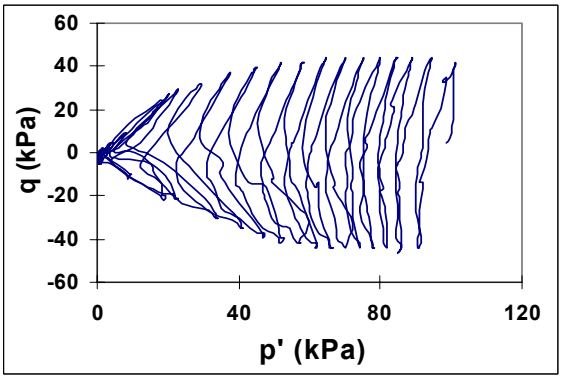

Test No.: C29 **File Name: c052900** **Soil Type: OS-15** **e=0.617**

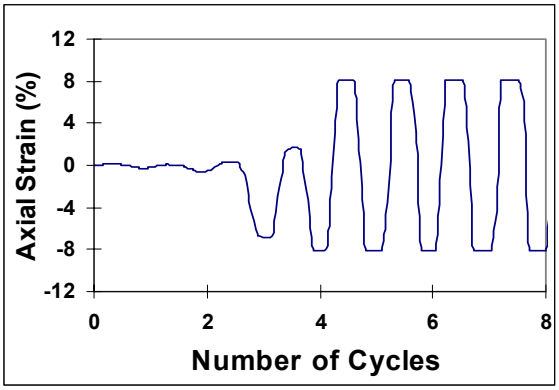

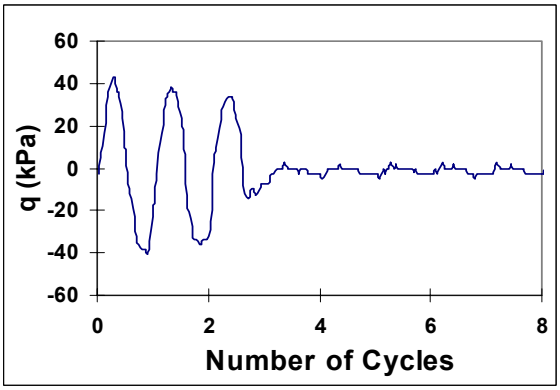

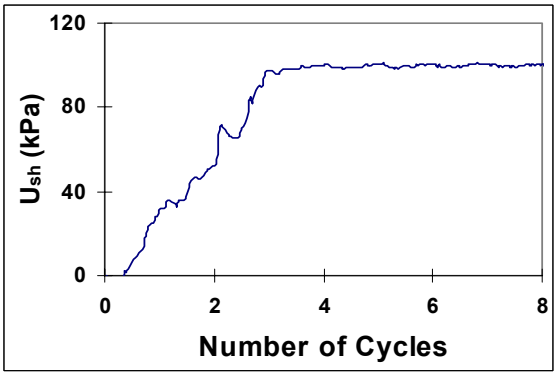

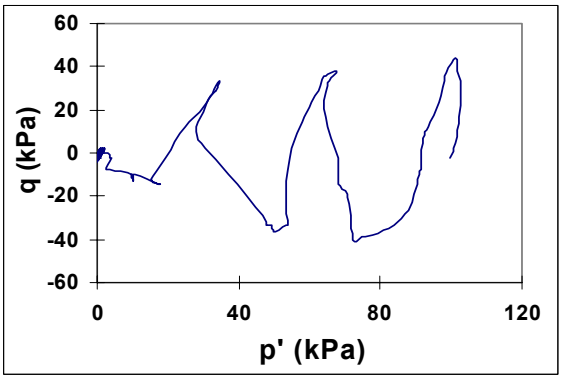

Test No.: C30 **File Name: c053100** **Soil Type: OS-15** **e=0.640**

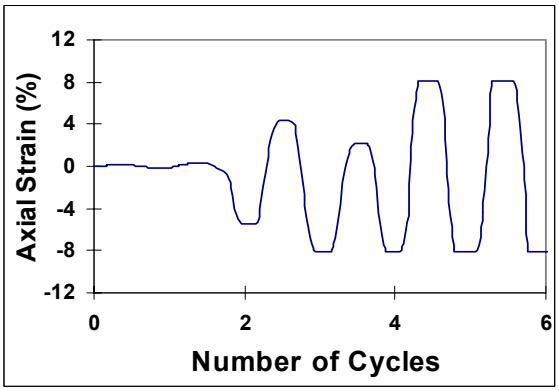

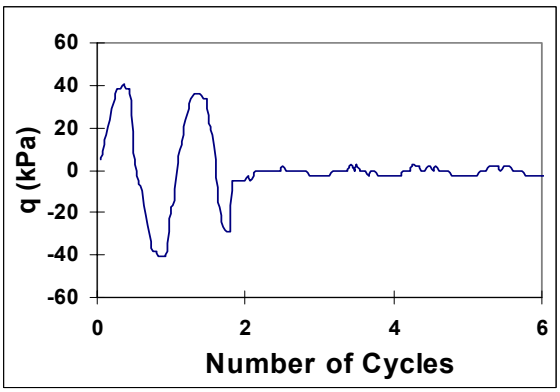

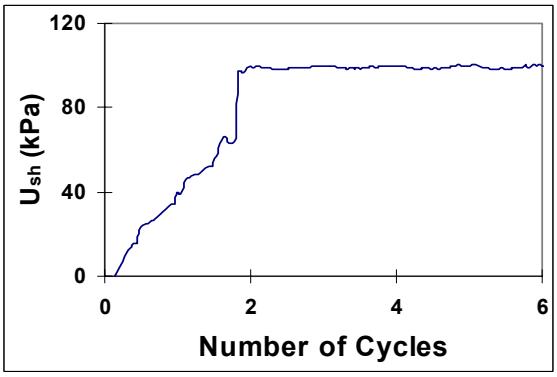

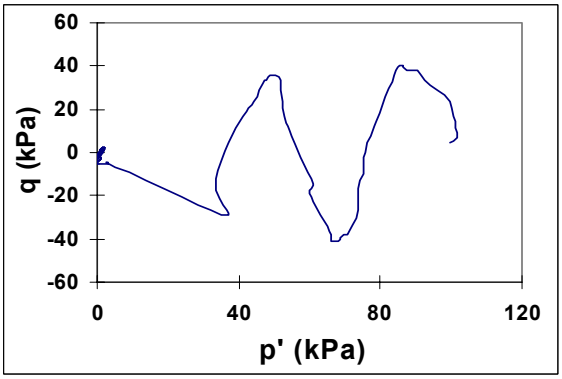

Test No.: C31 **File Name: c060100** **Soil Type: OS-15** **e=0.658**

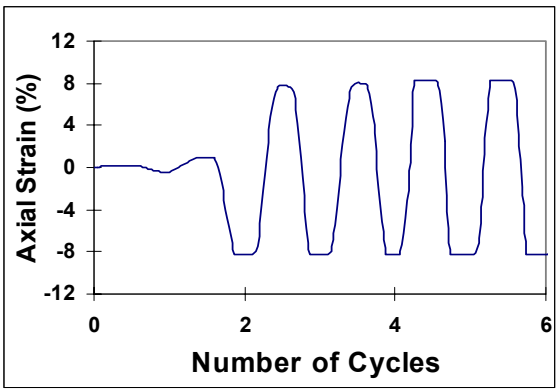

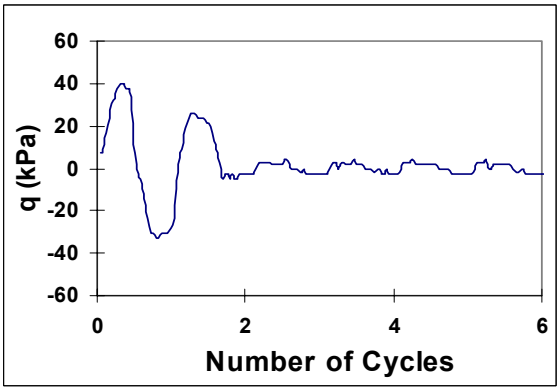

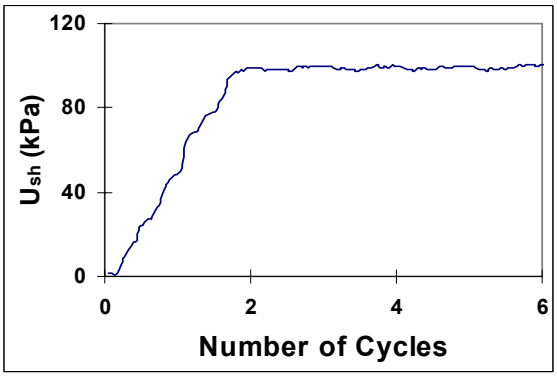

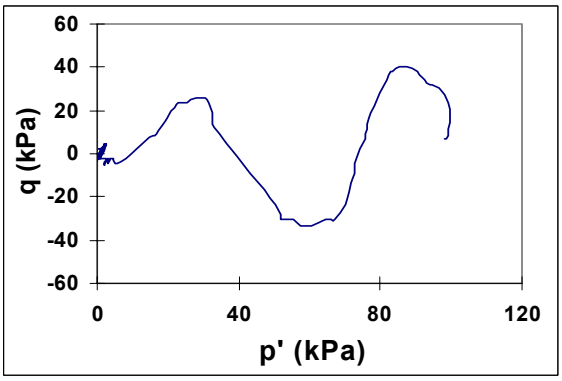

Test No.: C32 **File Name: osc25-1R** **Soil Type: OS-25** **e=0.466**

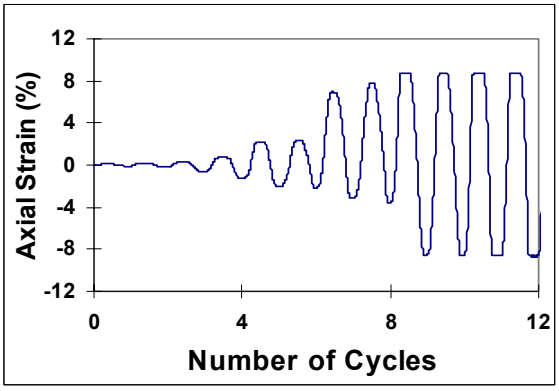

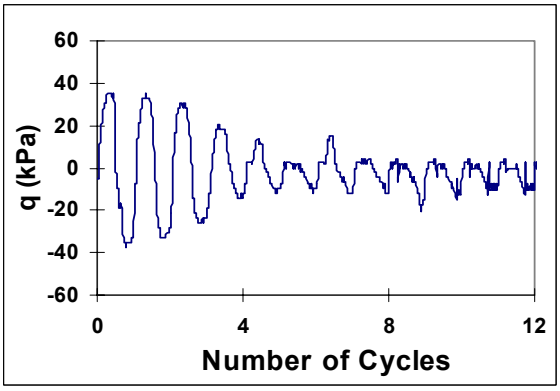

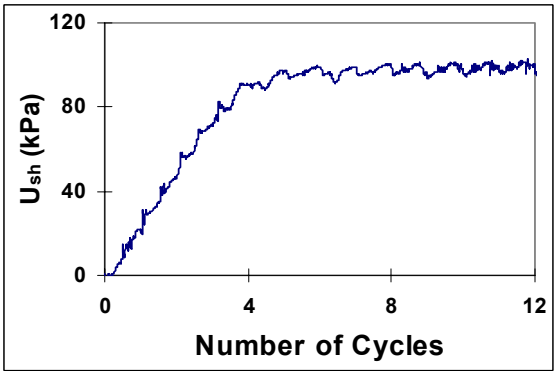

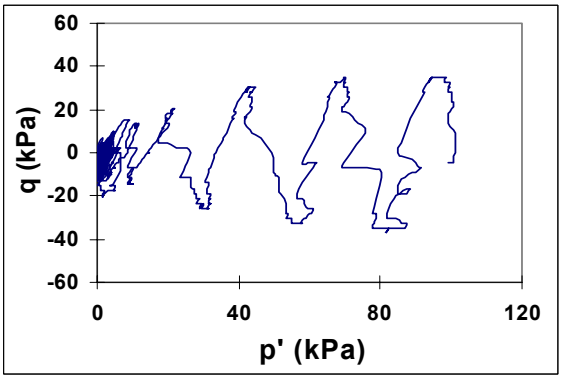

Test No.: C33 **File Name: osc25-2R** **Soil Type: OS-25** **e=0.487**

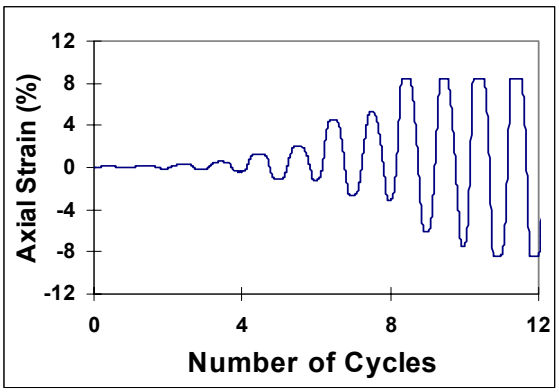

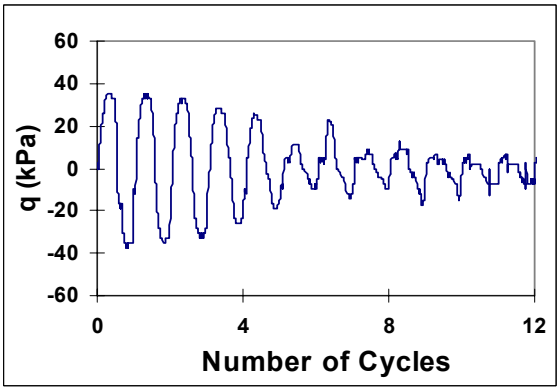

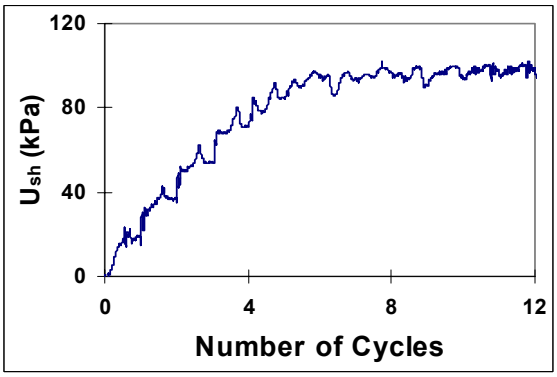

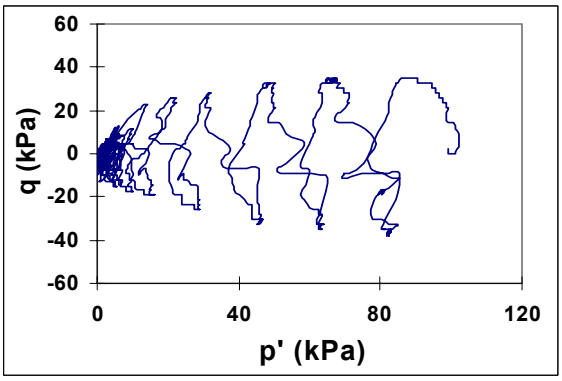

Test No.: C34 **File Name: c110399** **Soil Type: OS-25** **e=0.463**

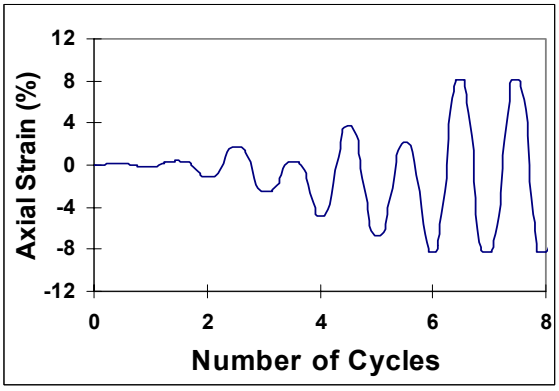

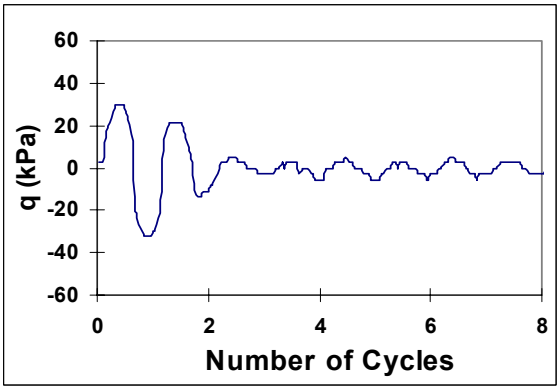

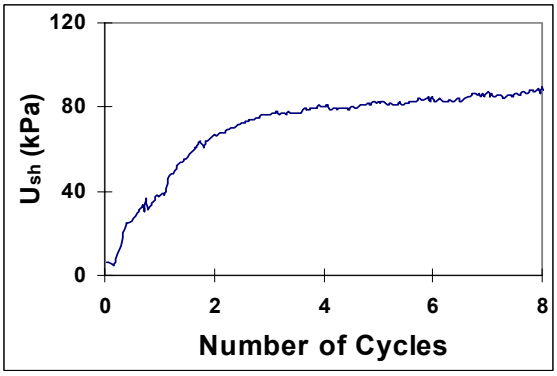

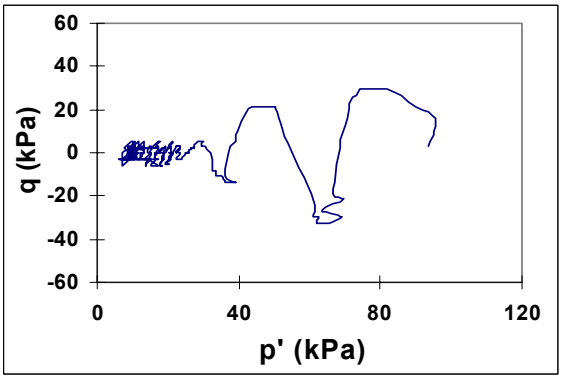

Test No.: C35 **File Name: c110599** **Soil Type: OS-25** **e=0.457**

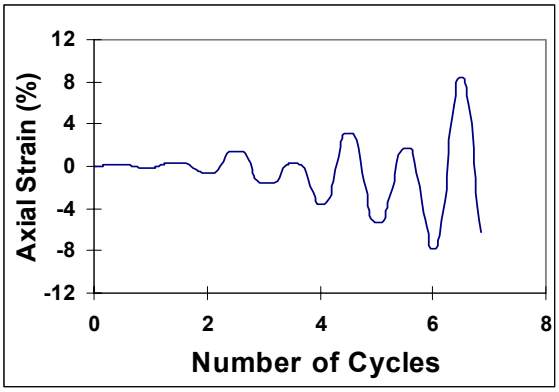

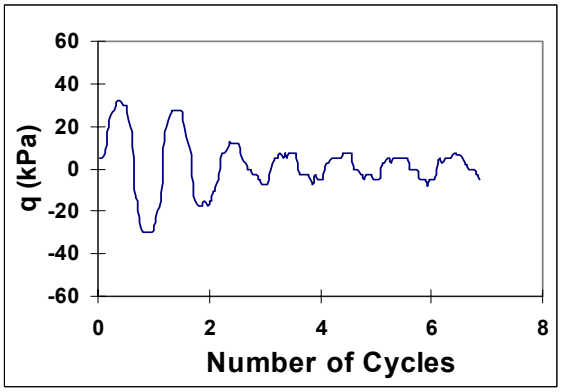

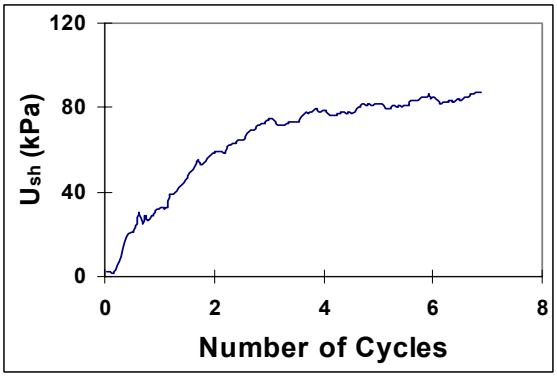

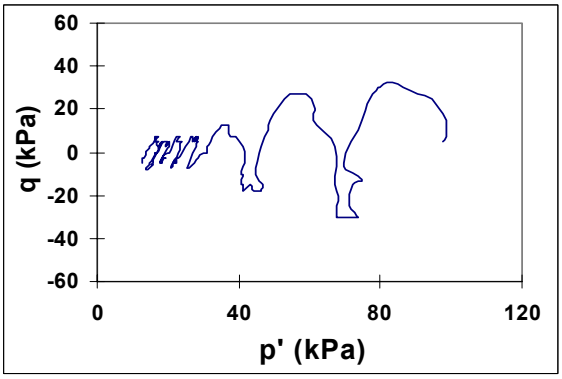

Test No.: C36 **File Name: c111299** **Soil Type: OS-25** **e=0.470**

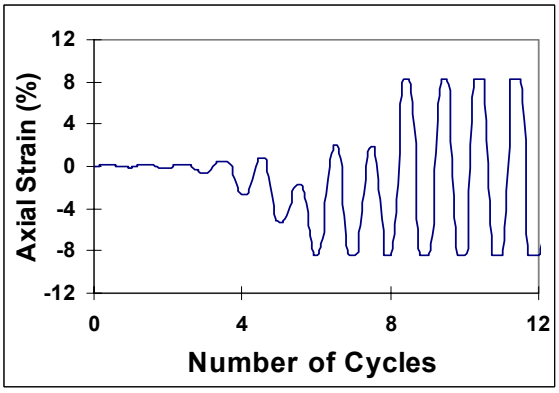

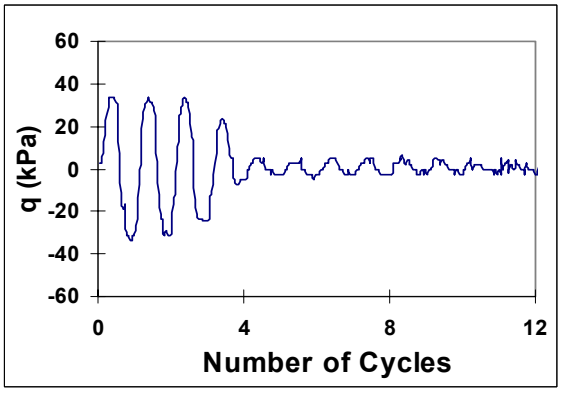

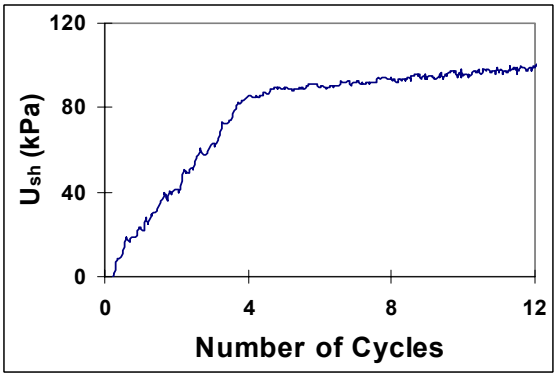

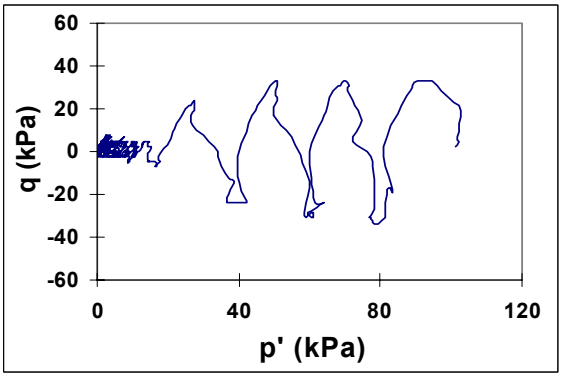

Test No.: C37 **File Name: c111799** **Soil Type: OS-25** **e=0.468**

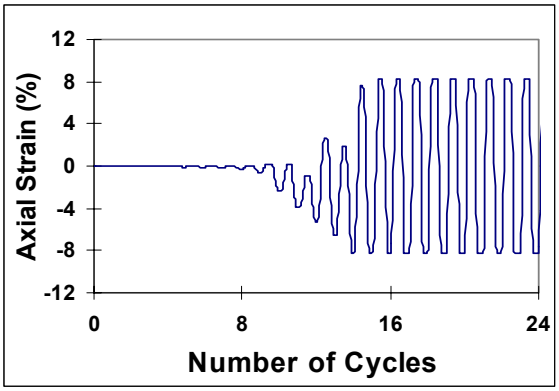

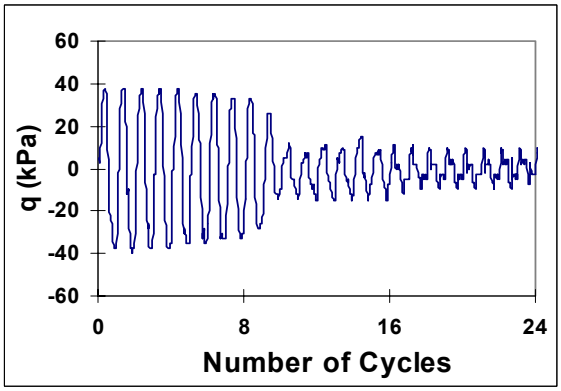

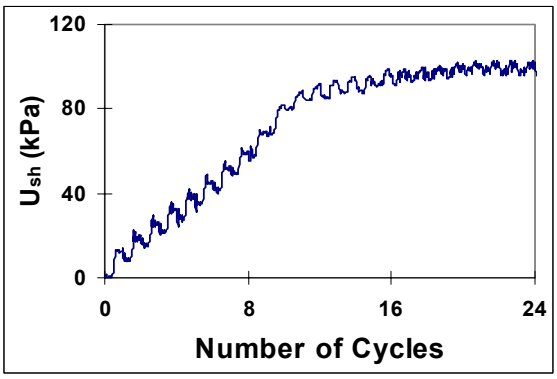

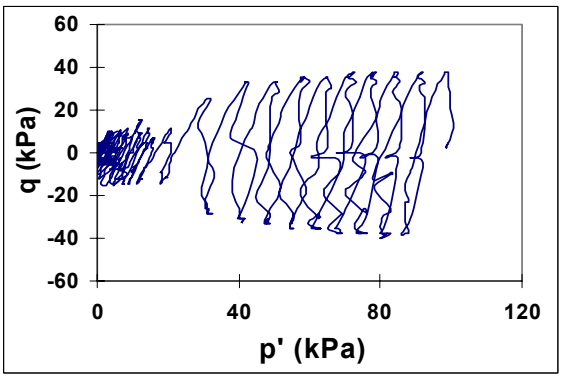

Test No.: C38 **File Name: c060200** **Soil Type: OS-25** **e=0.462**

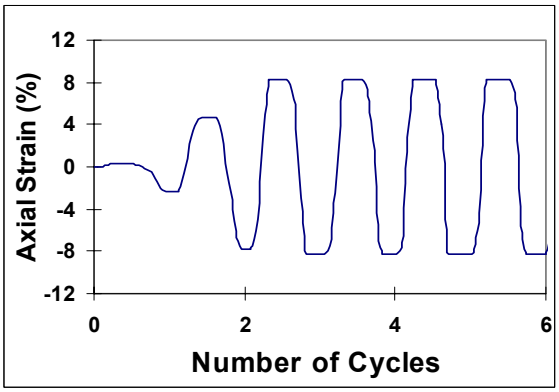

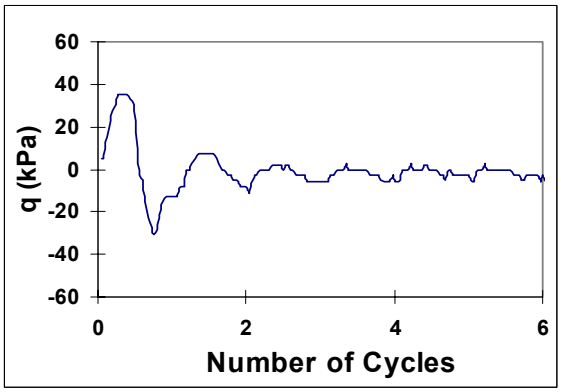

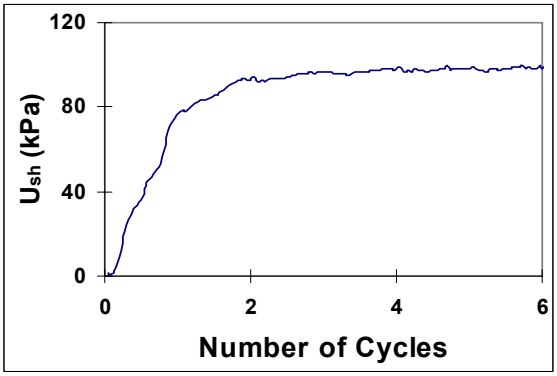

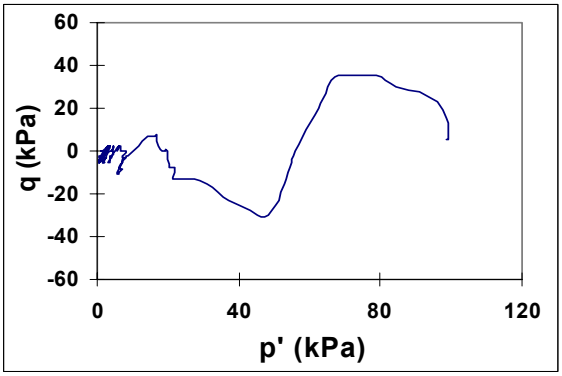

Test No.: C39 **File Name: c060500** **Soil Type: OS-25** **e=0.408**

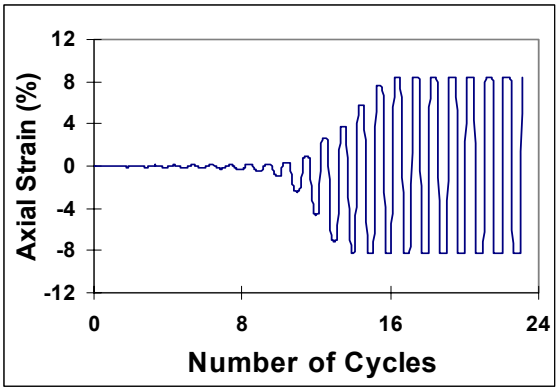

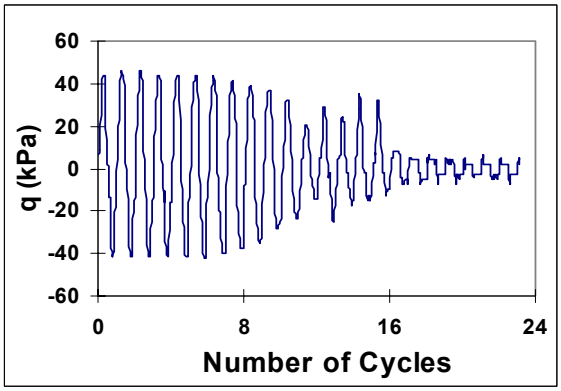

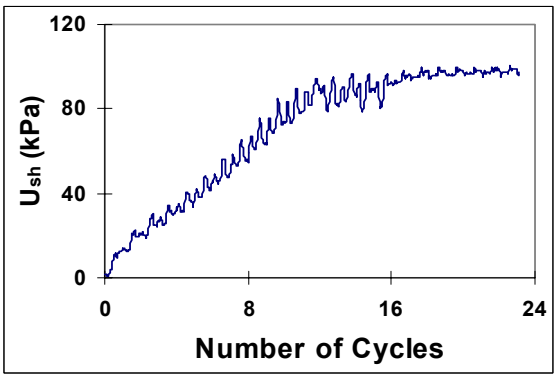

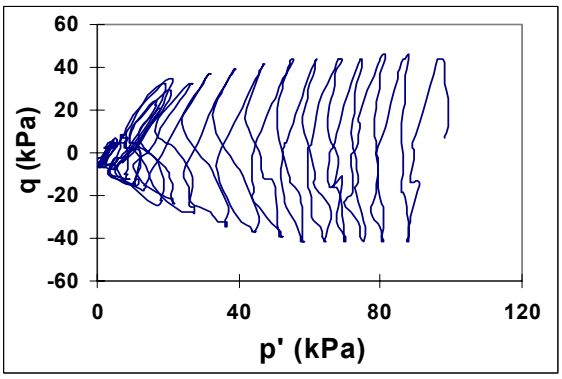

Test No.: C40 **File Name: c061200** **Soil Type: OS-25** **e=0.505**

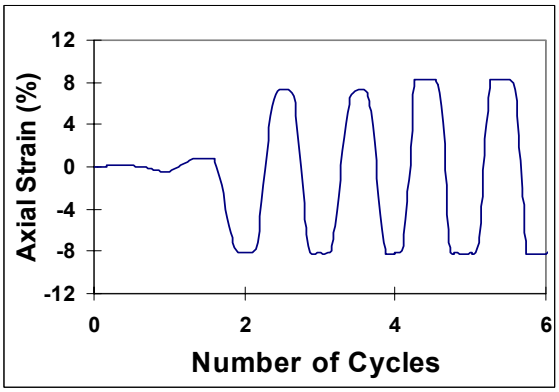

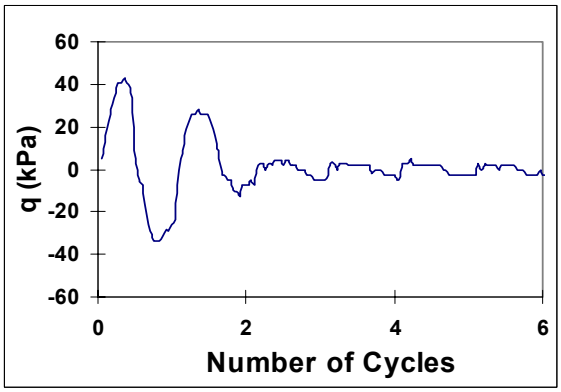

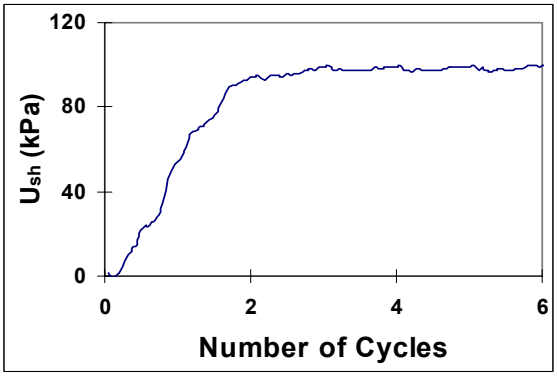

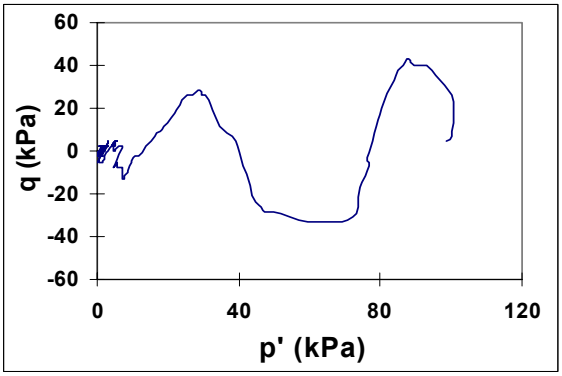

Test No.: C41 **File Name: c061500** **Soil Type: OS-25** **e=0.402**

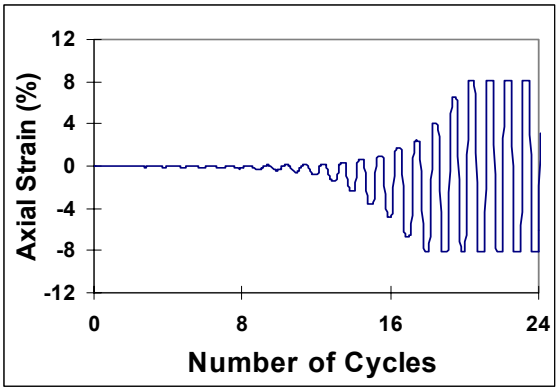

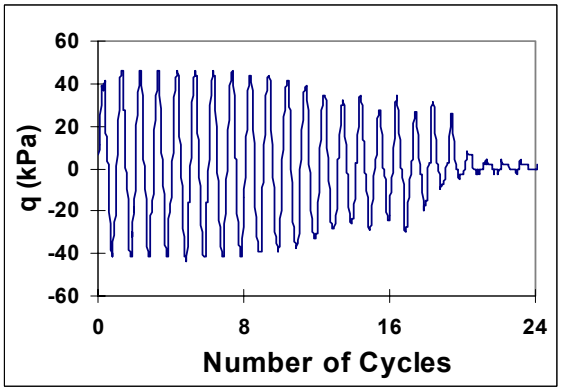

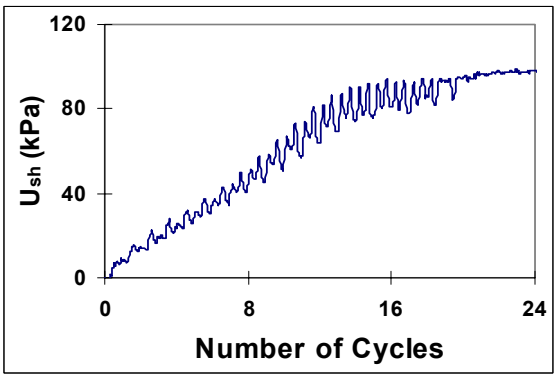

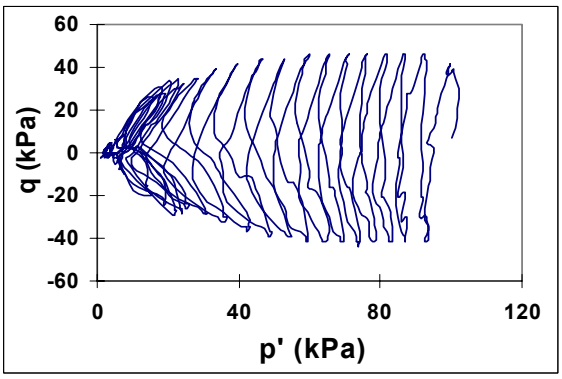

Test No.: C42 **File Name: c110801** **Soil Type: OS-25** **e=0.504**

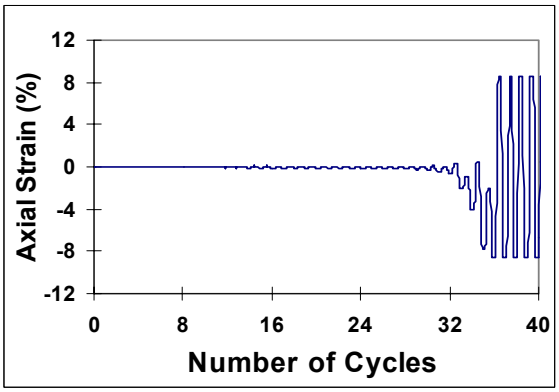

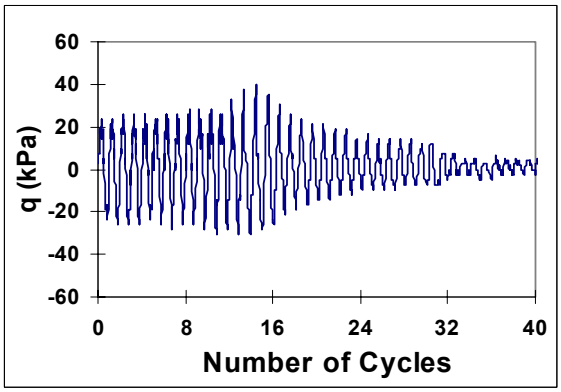

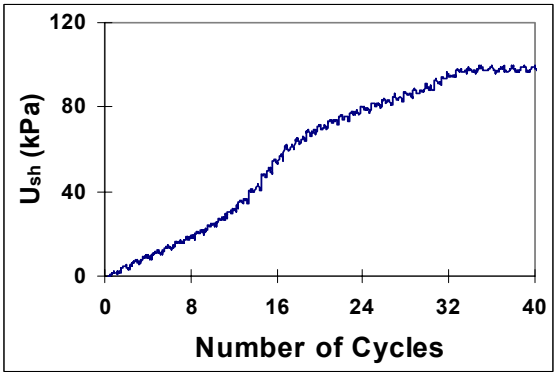

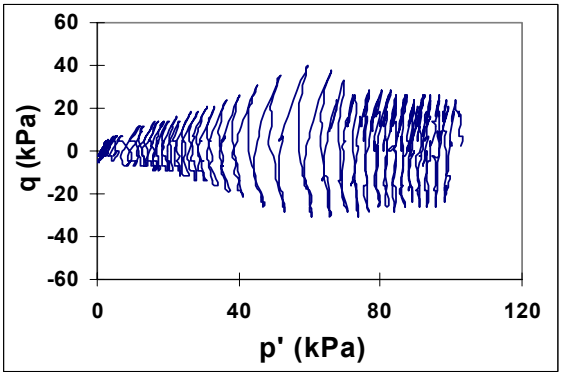

Test No.: C43 **File Name: c110901** **Soil Type: OS-25** **e=0.518**

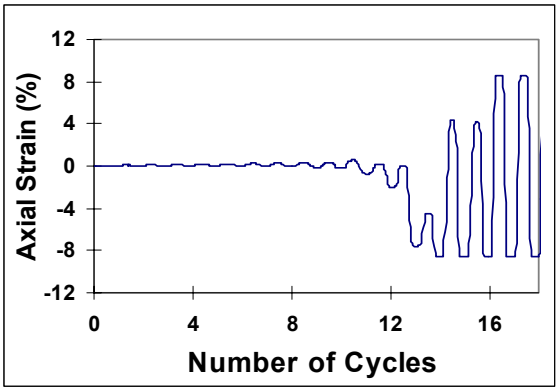

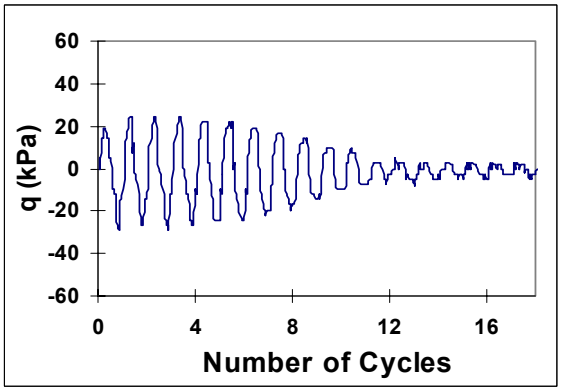

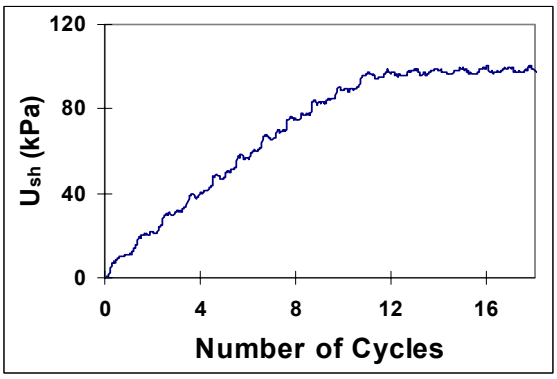

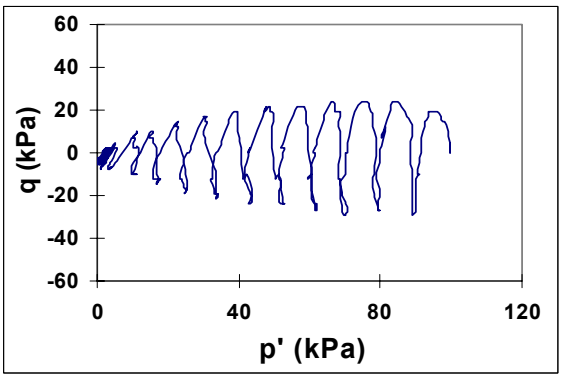

Test No.: C44 **File Name: c111001** **Soil Type: OS-25** **e=0.473**

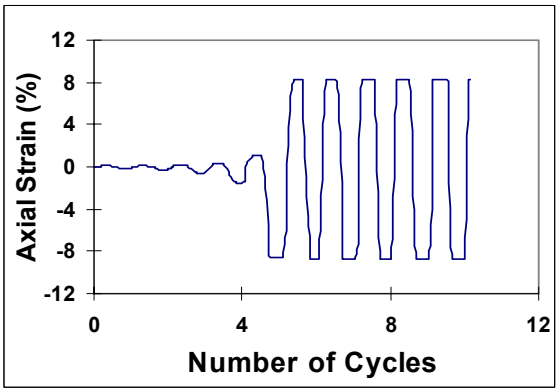

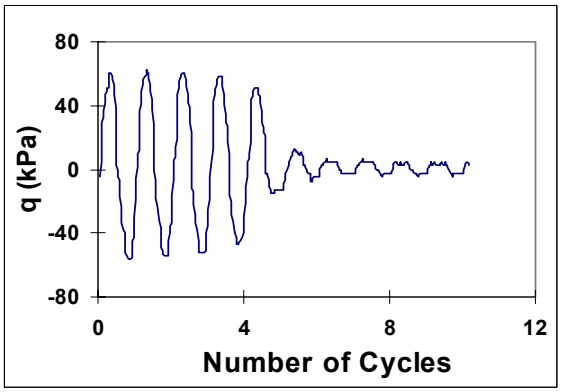

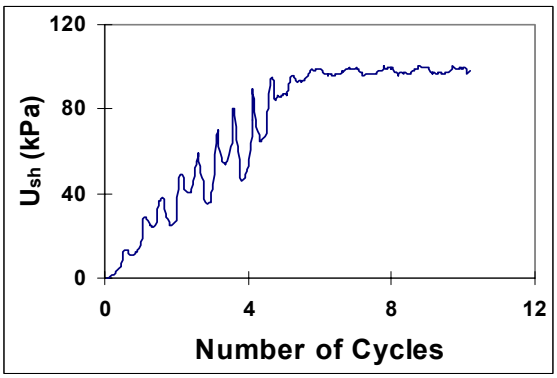

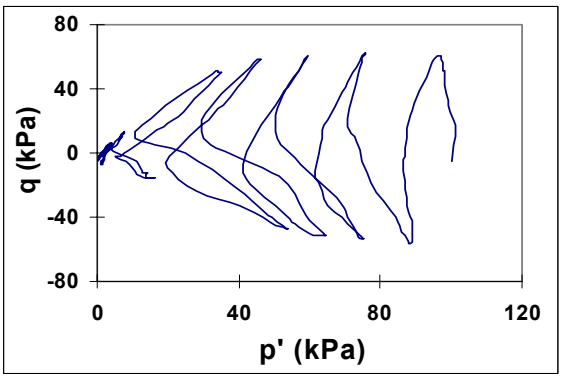

Test No.: C45 **File Name: c090501** **Soil Type: OS-25** **e=0.487**

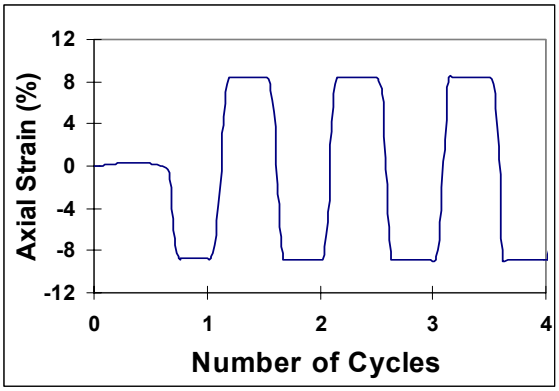

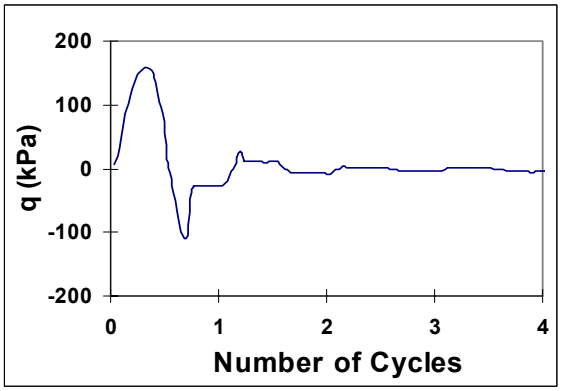

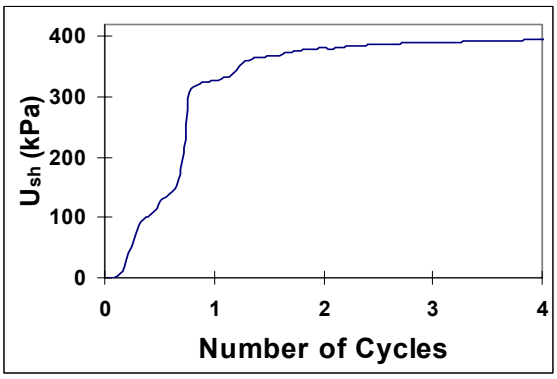

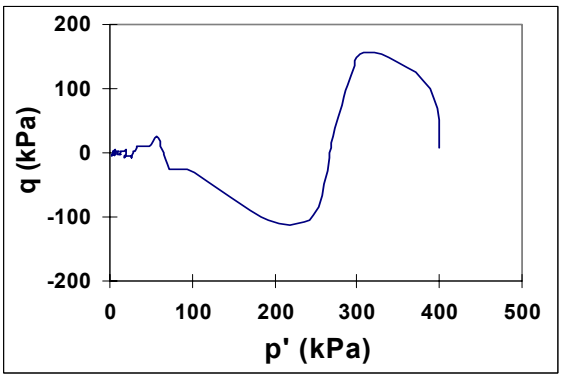

Test No.: C46 **File Name: c091001** **Soil Type: OS-25** **e=0.464**

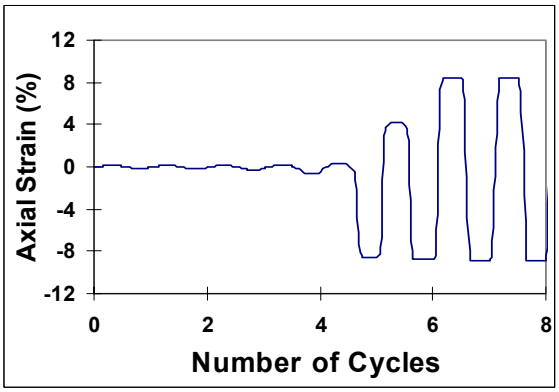

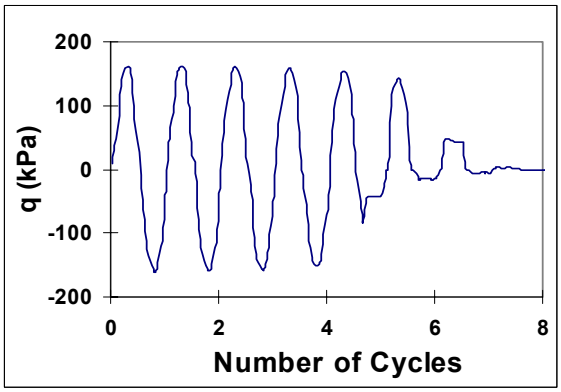

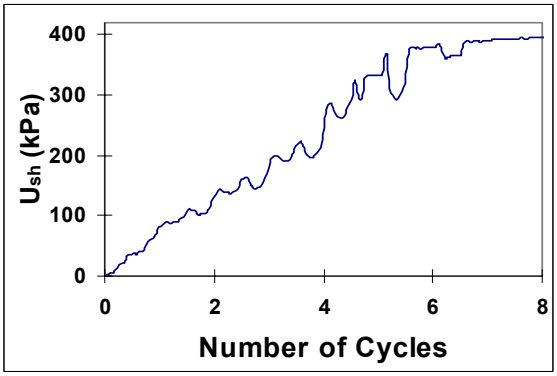

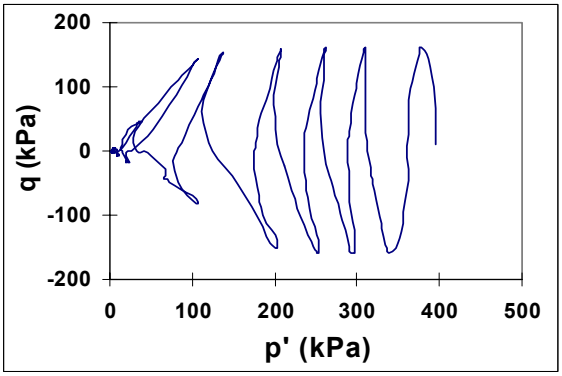

Test No.: C47 **File Name: c111101** **Soil Type: OS-25** **e=0.492**

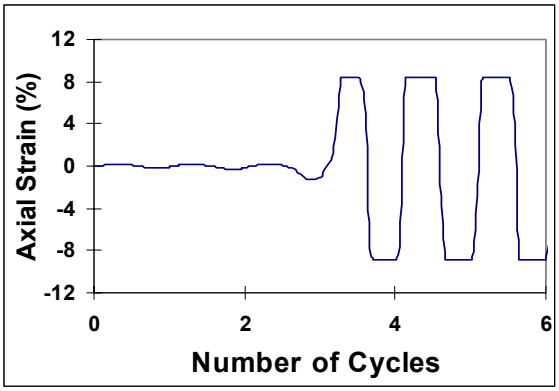

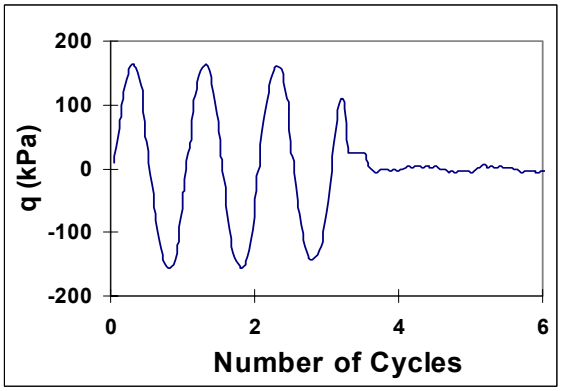

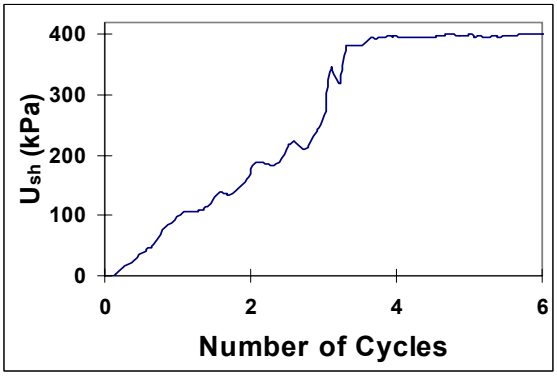

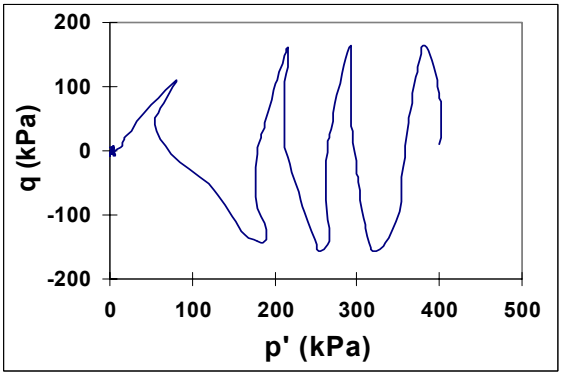

Test No.: C48 **File Name: c111301** **Soil Type: OS-25** **e=0.444**

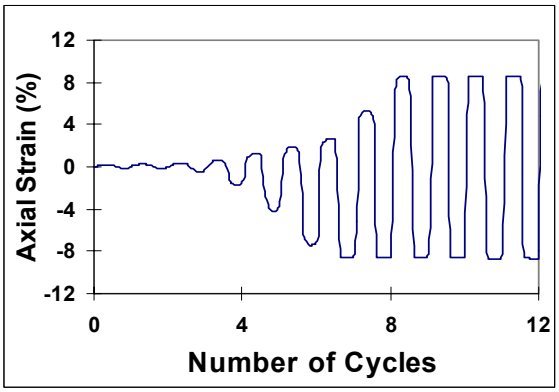

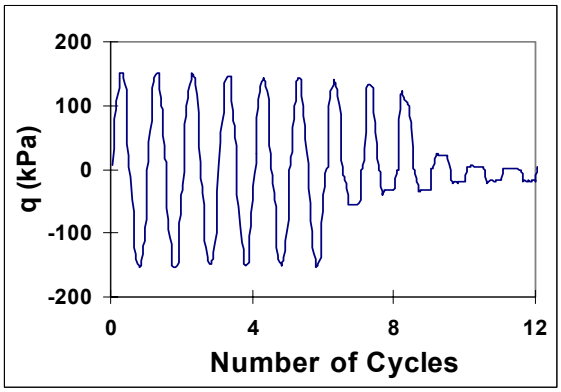

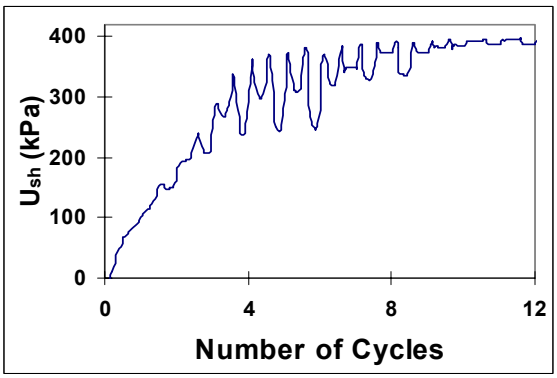

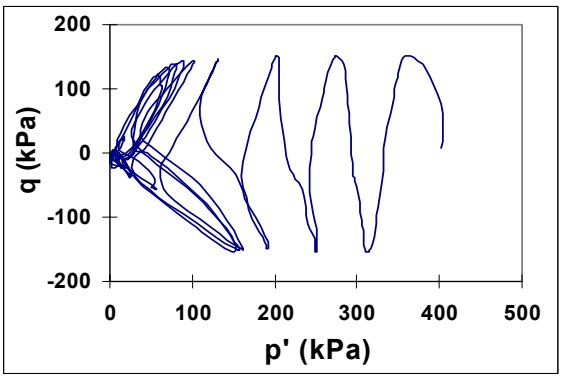

Test No.: C49 **File Name: c020200** **Soil Type: OS-60** **e=0.540**

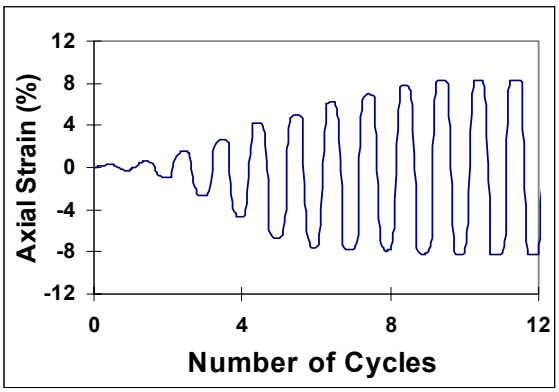

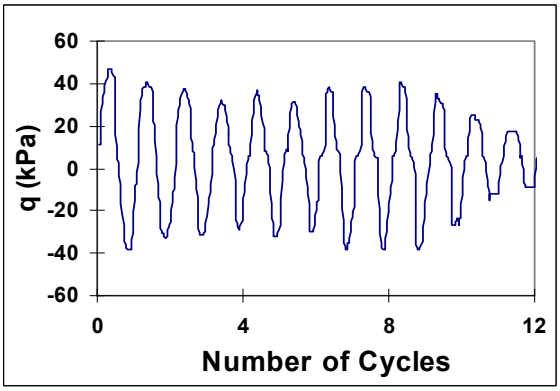

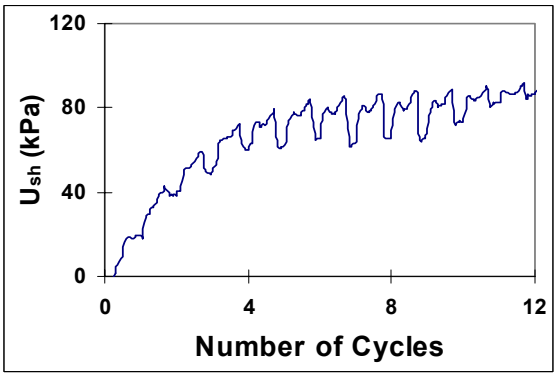

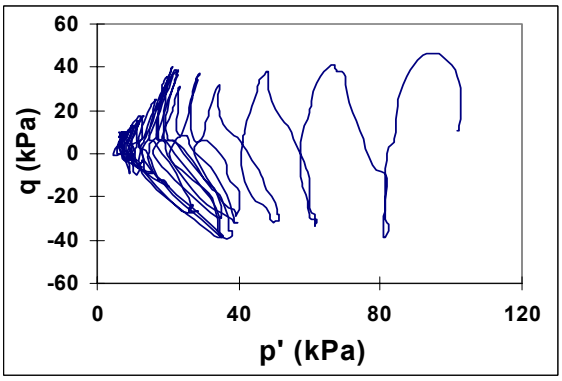

Test No.: C50 **File Name: c020300** **Soil Type: OS-60** **e=0.545**

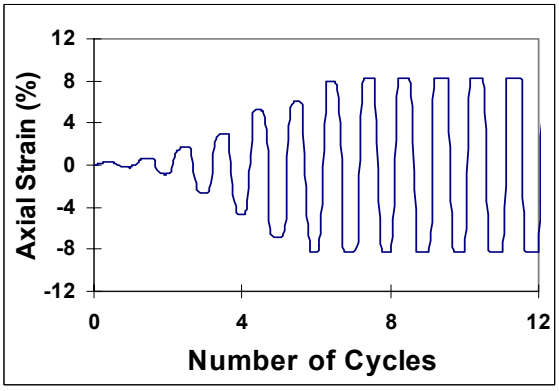

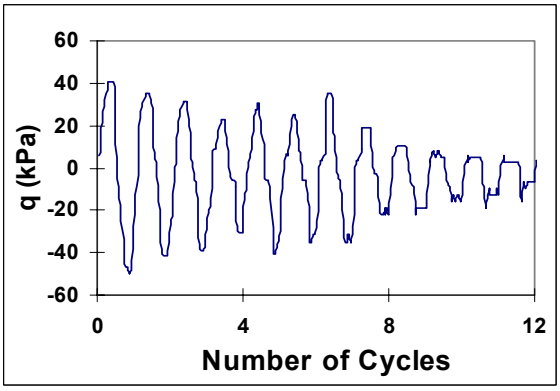

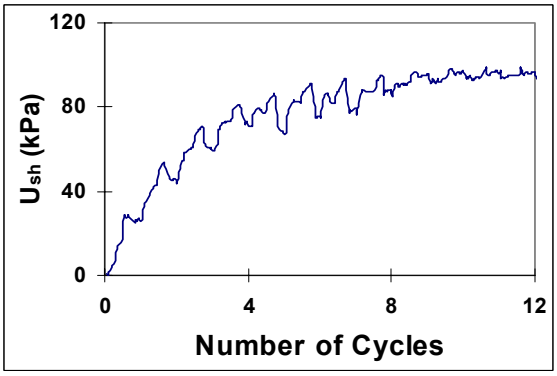

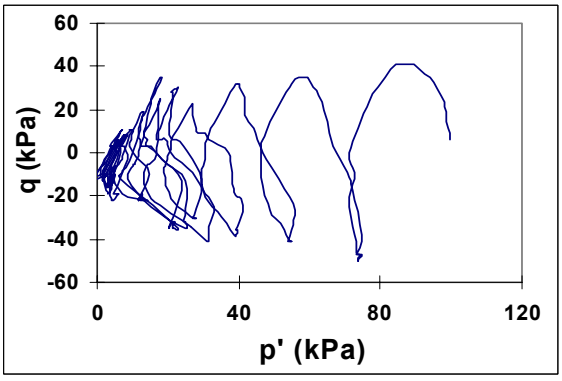

Test No.: C51 **File Name: c020700** **Soil Type: OS-60** **e=0.539**

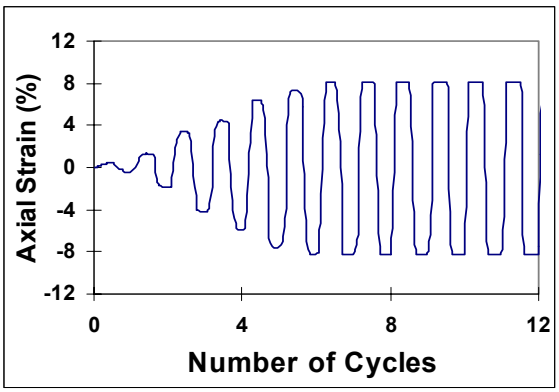

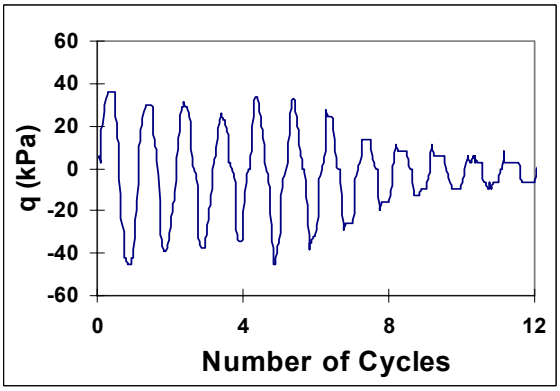

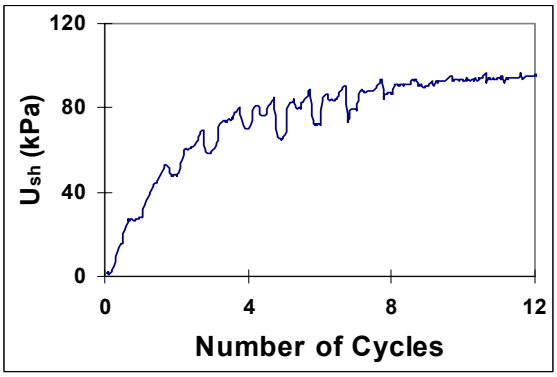

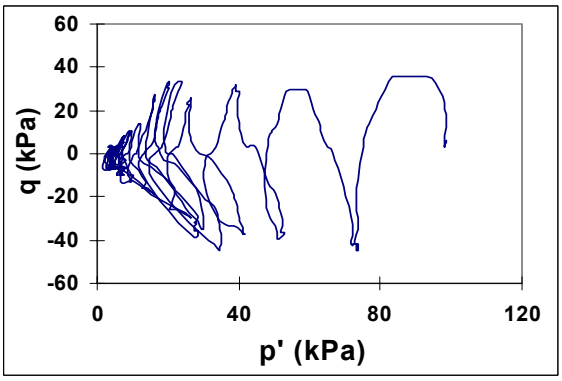

Test No.: C52 **File Name: c081800** **Soil Type: OS-60** **e=0.528**

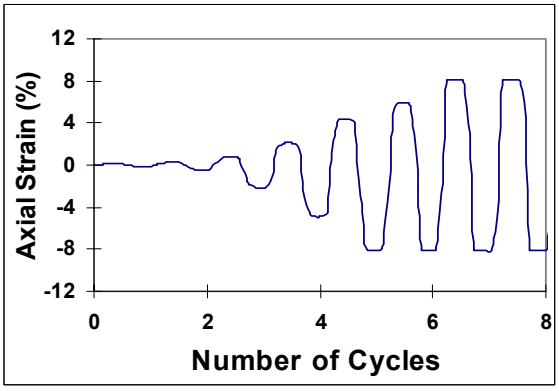

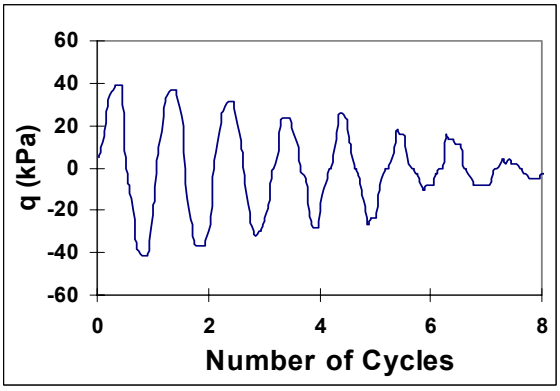

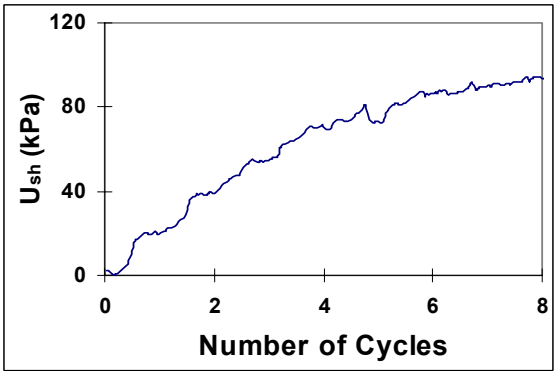

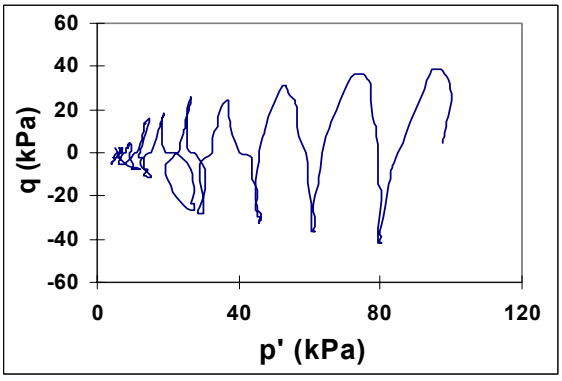

Test No.: C53 **File Name: c082500** **Soil Type: OS-60** **e=0.505**

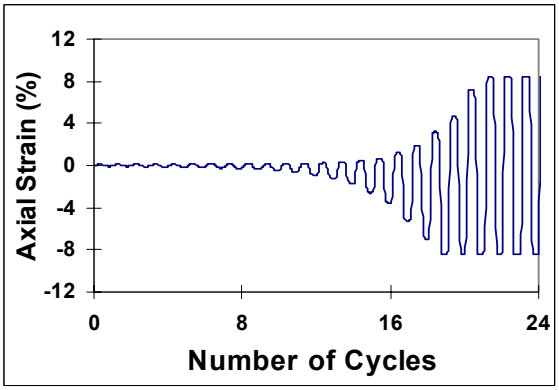

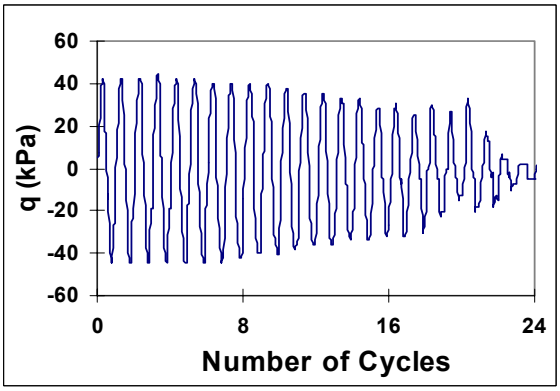

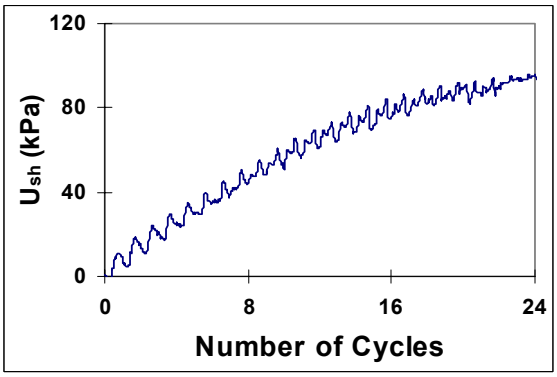

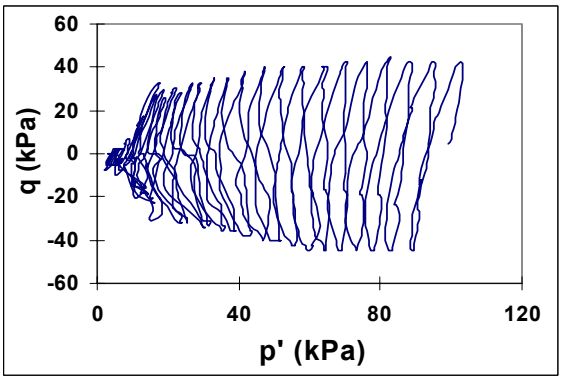

Test No.: C54 **File Name: c082800** **Soil Type: OS-60** **e=0.490**

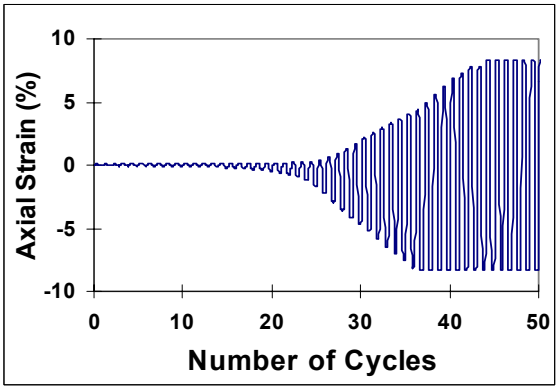

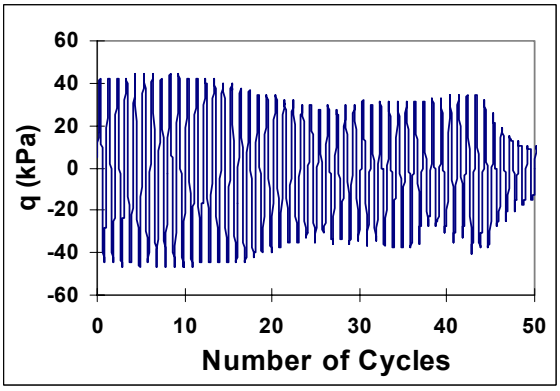

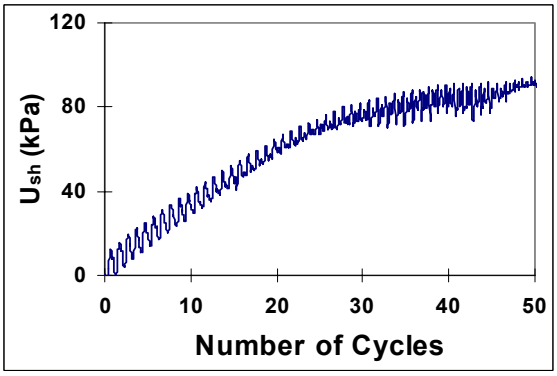

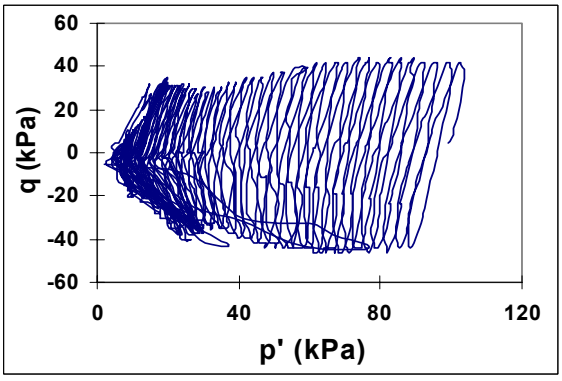

Test No.: C55 **File Name: c030300** **Soil Type: GSF#40** **e=0.858**

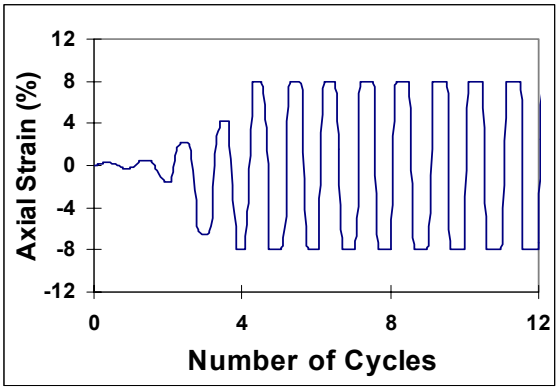

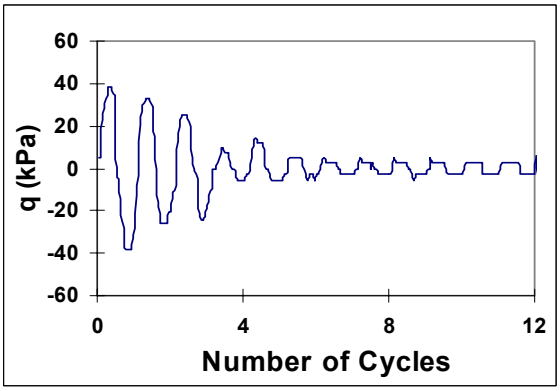

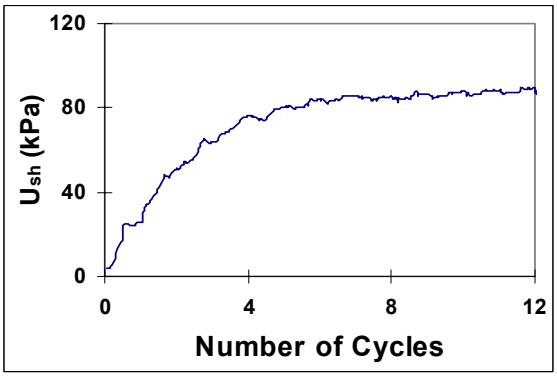

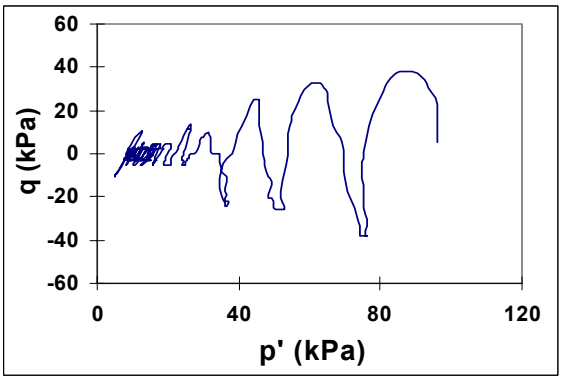

Test No.: C56 **File Name: c041700** **Soil Type: GSF#40** **e=0.862**

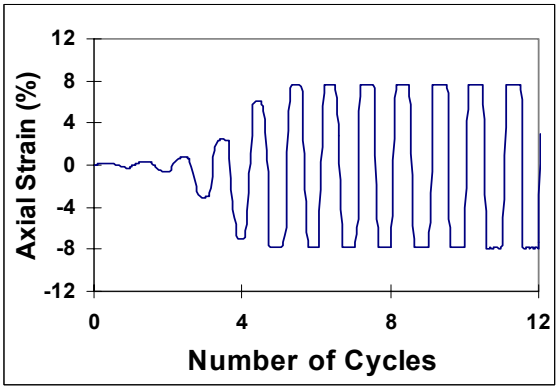

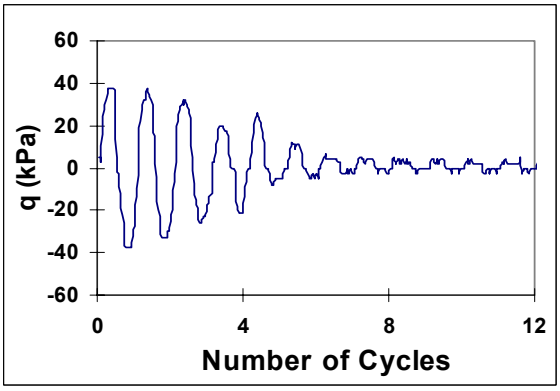

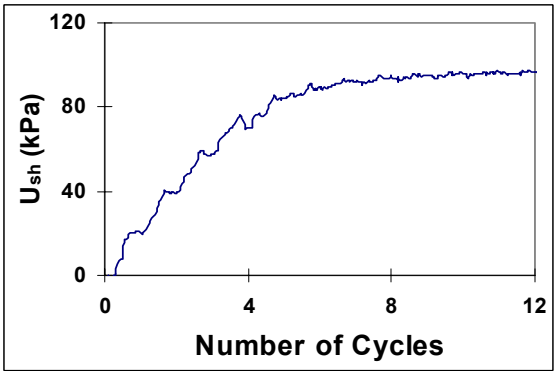

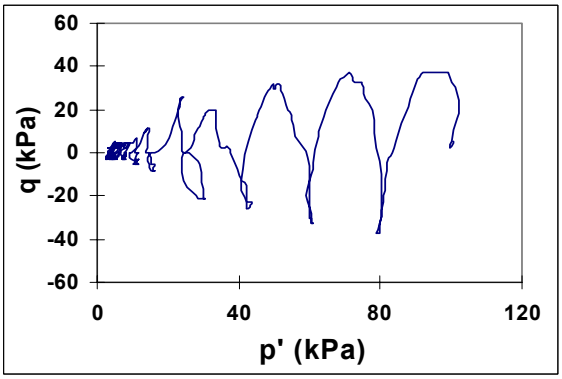

Test No.: C57 **File Name: c062100** **Soil Type: GSF#40** **e=0.866**

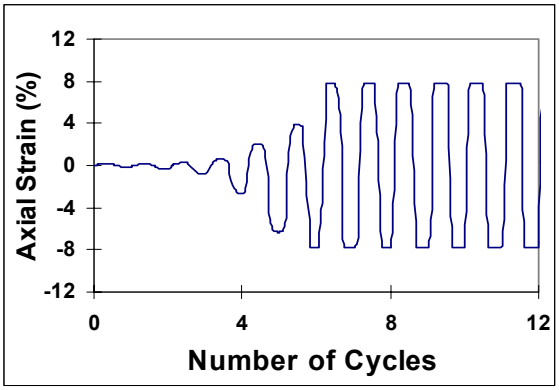

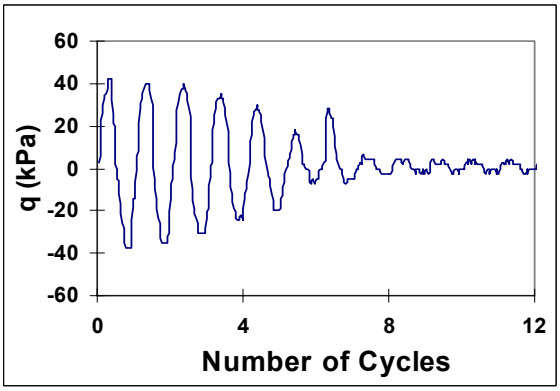

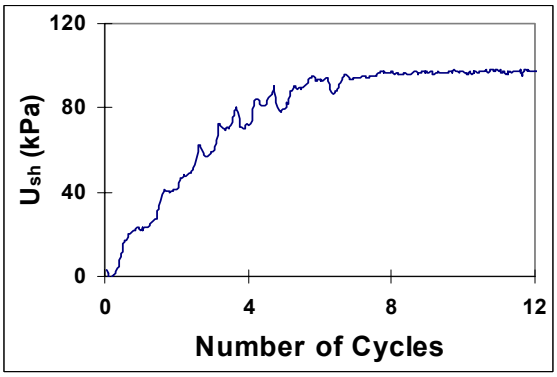

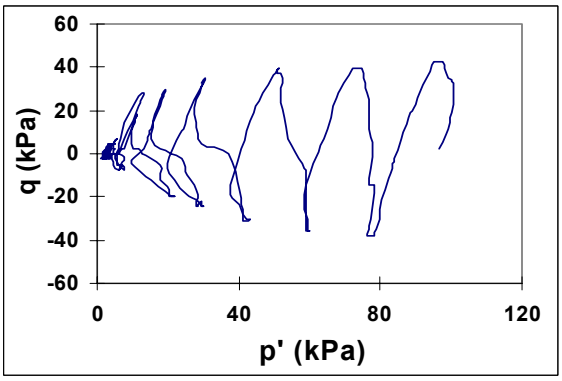

Test No.: C58 **File Name: c062600** **Soil Type: GSF#40** **e=0.838**

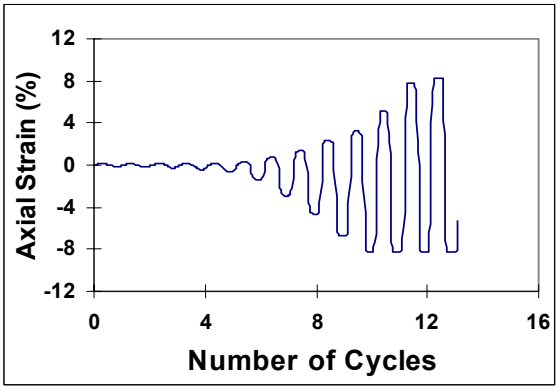

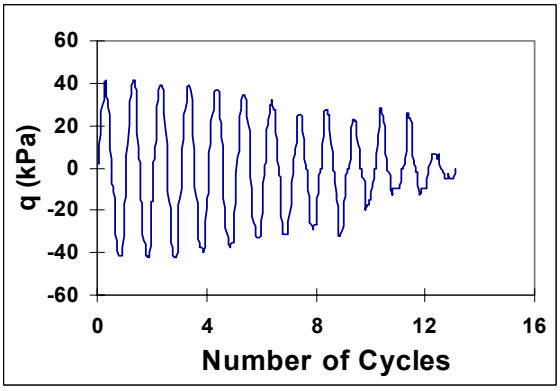

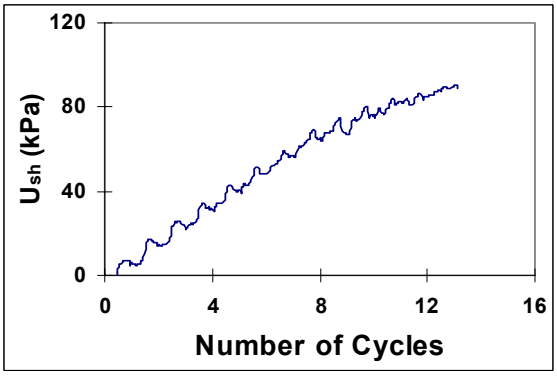

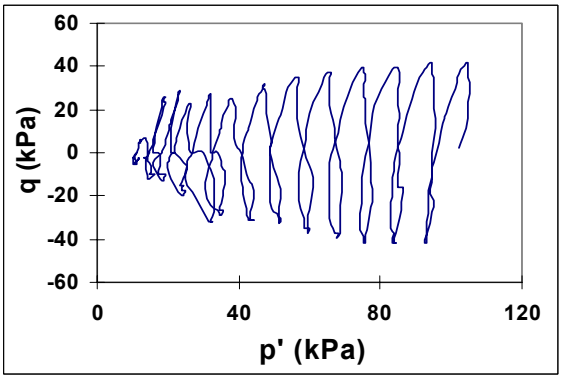

Test No.: C59 **File Name: c071000** **Soil Type: GSF#40** **e=0.875**

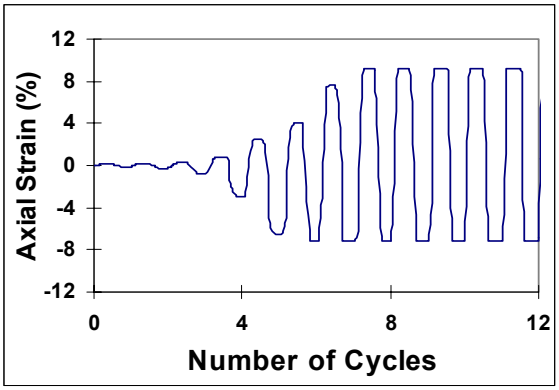

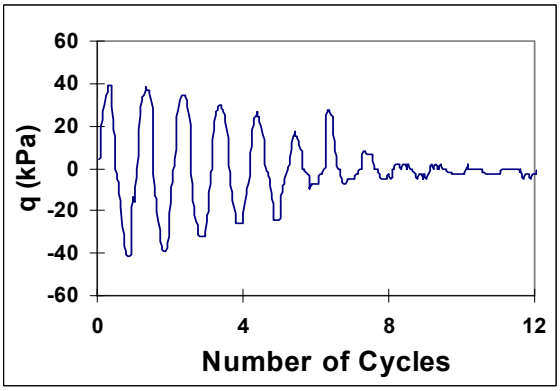

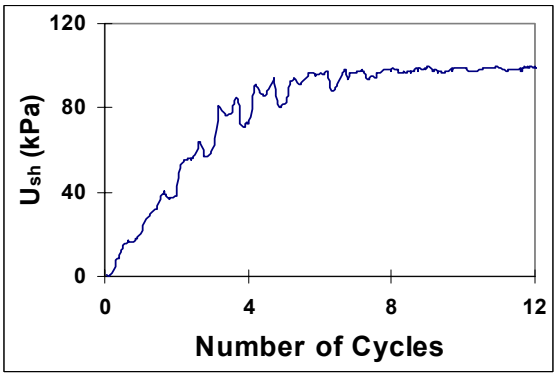

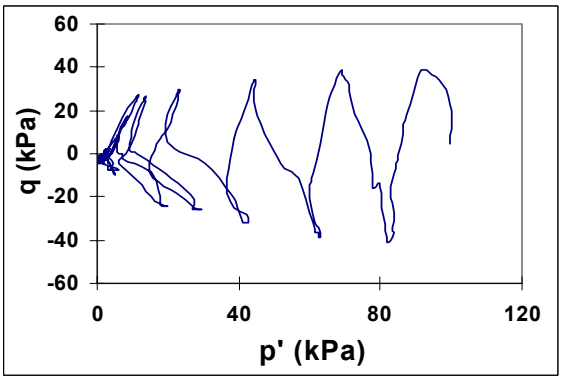

Test No.: C60 **File Name: c072100** **Soil Type: GSF#40** **e=0.812**

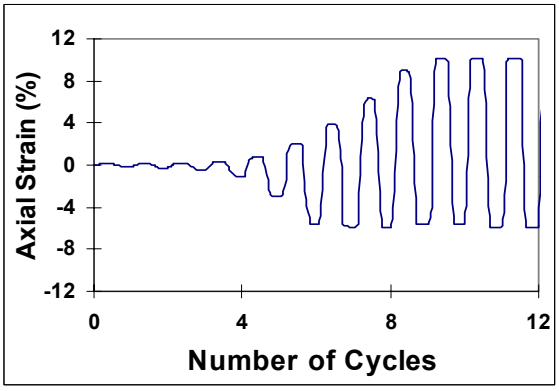

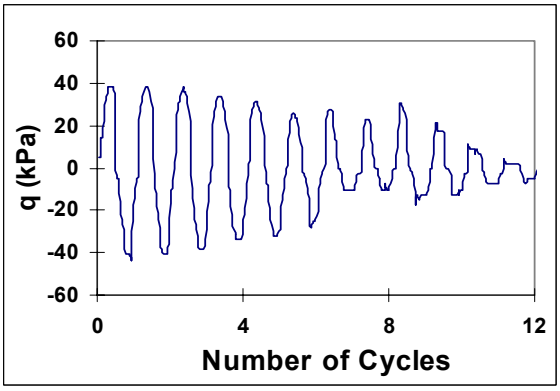

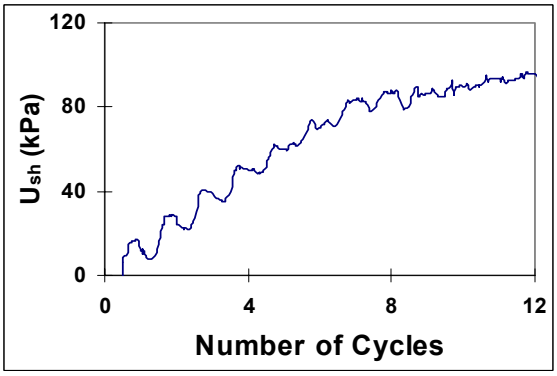

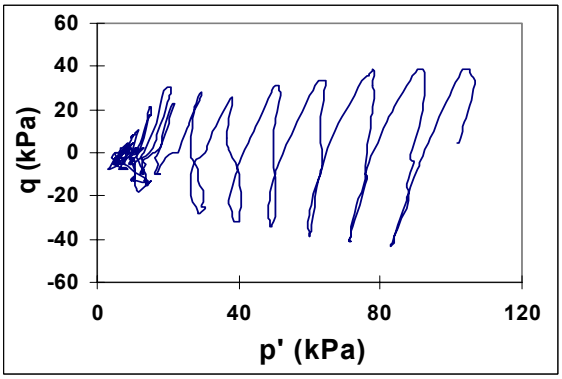

Test No.: C61 **File Name: c072600** **Soil Type: GSF#40** **e=0.848**

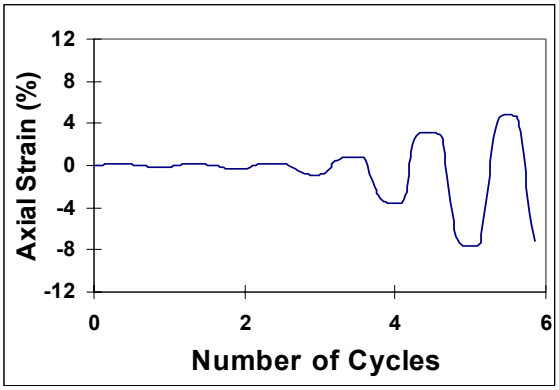

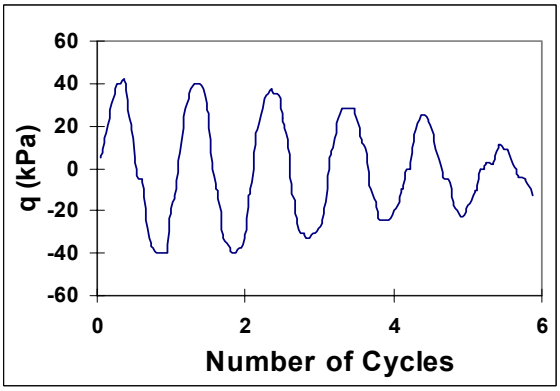

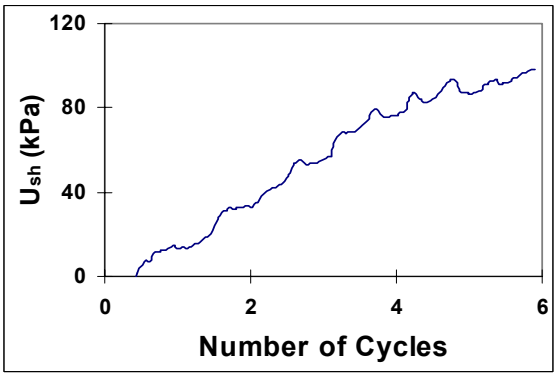

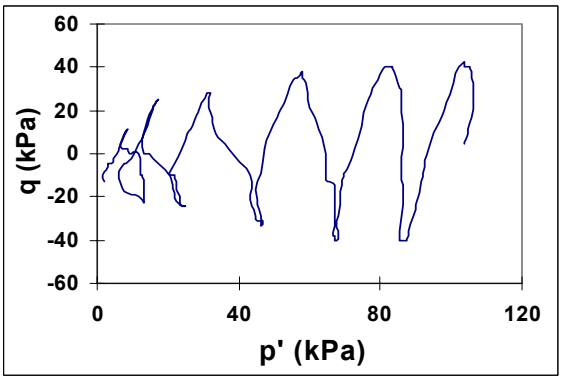

Test No.: C62 **File Name: c081100** **Soil Type: GSF#40** **e=0.811**

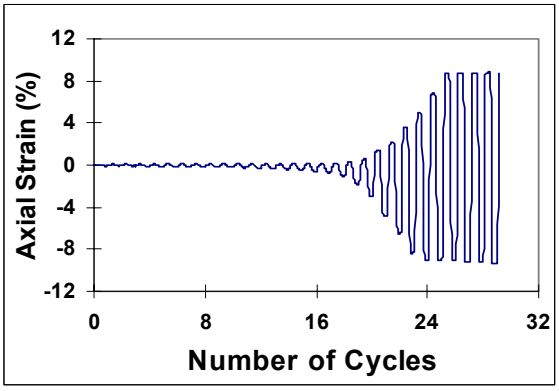

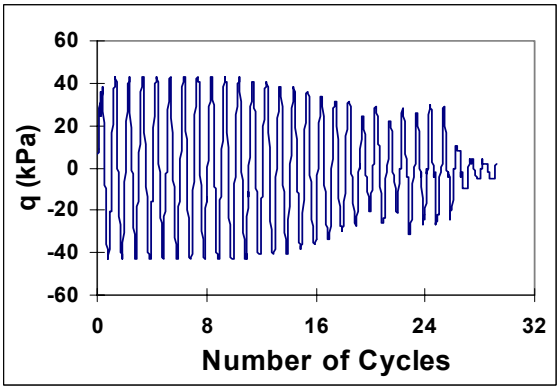

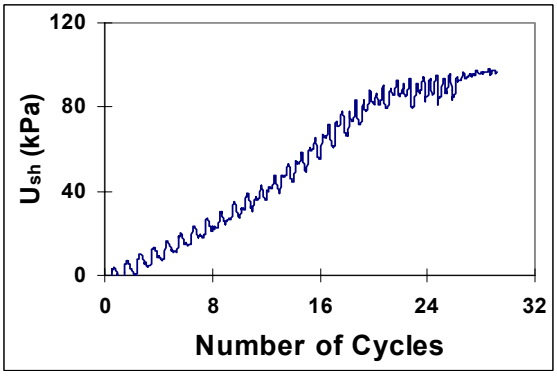

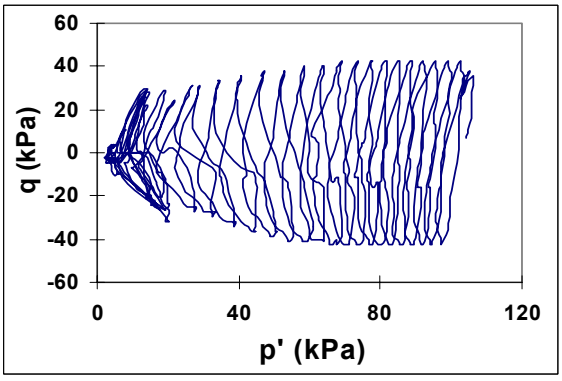

Test No.: C63 **File Name: c052901** **Soil Type: FJ-00** **e=0.788**

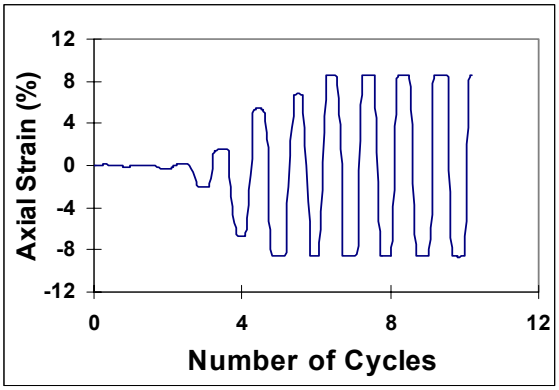

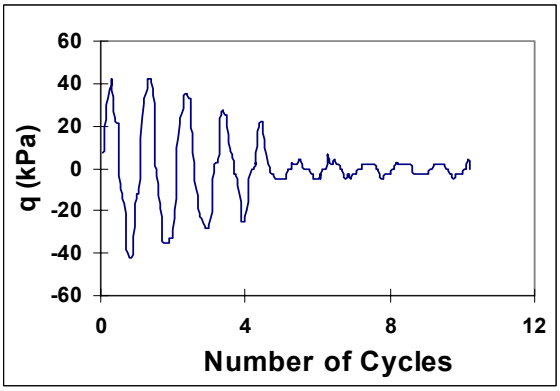

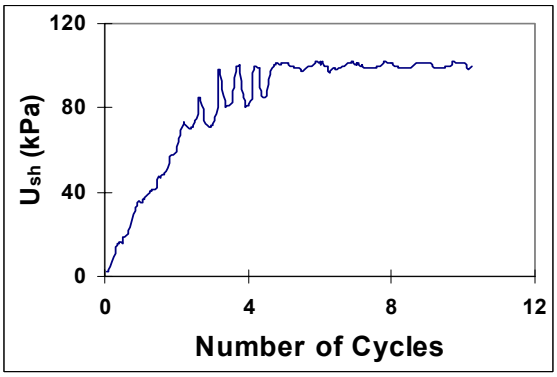

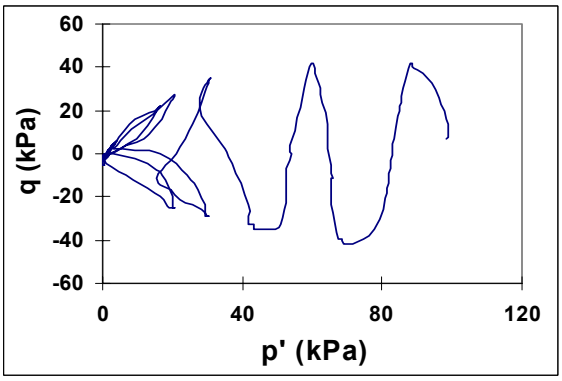

Test No.: C64 **File Name: c053101** **Soil Type: FJ-00** **e=0.746**

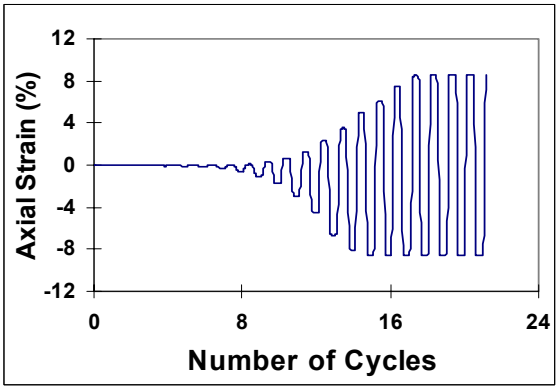

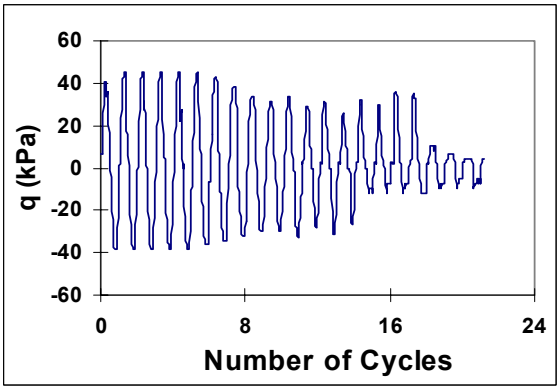

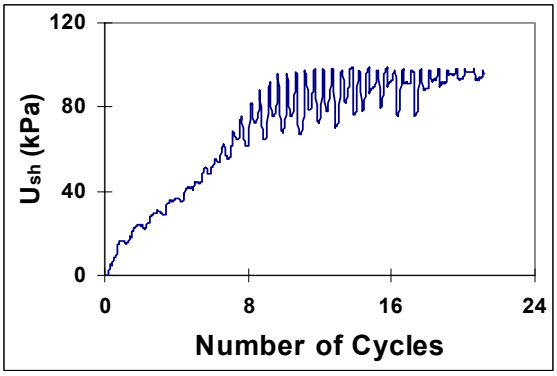

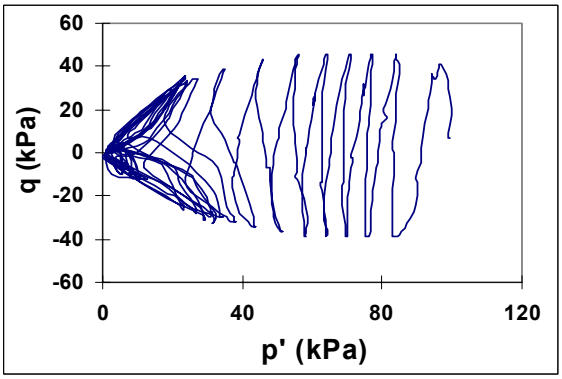

Test No.: C65 **File Name: c060801** **Soil Type: FJ-00** **e=0.715**

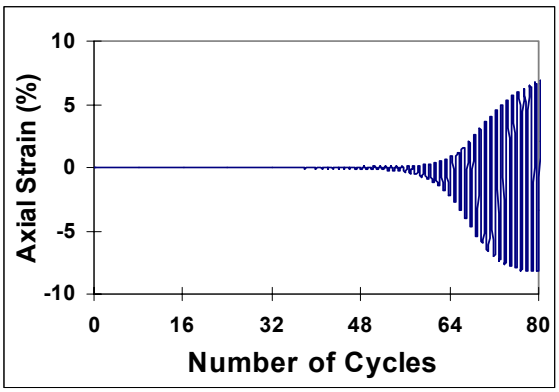

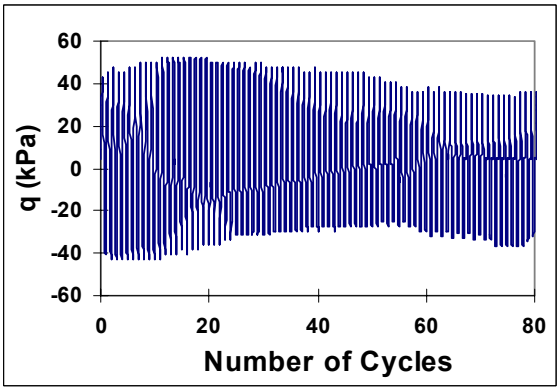

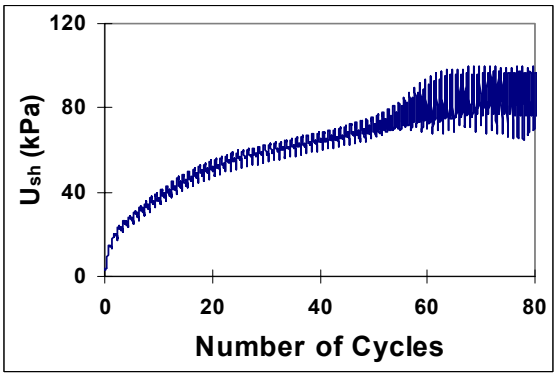

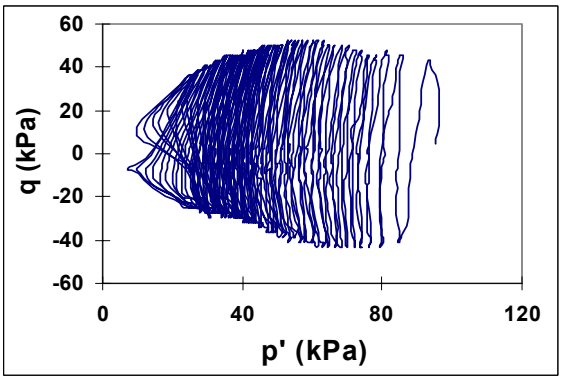

Test No.: C66 **File Name: c061401** **Soil Type: FJ-25** **e=0.552**

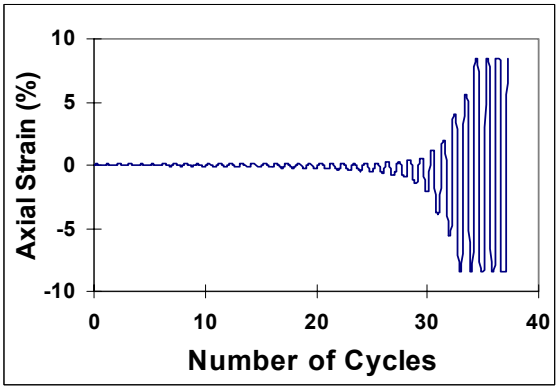

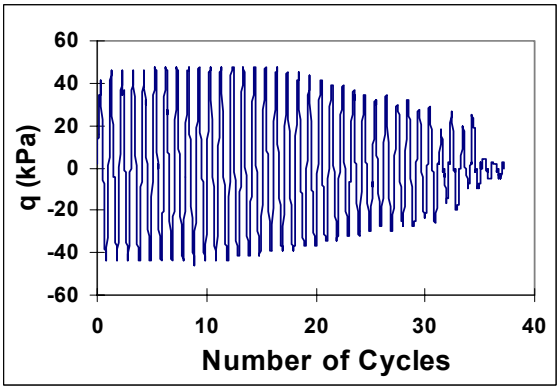

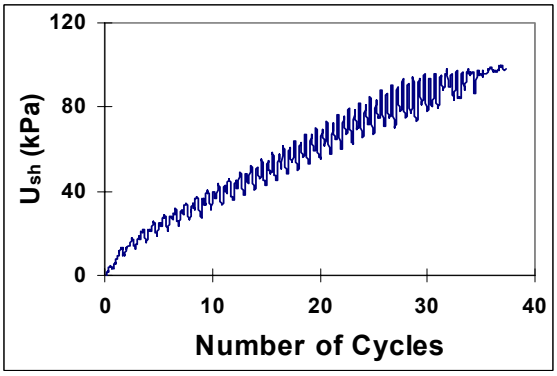

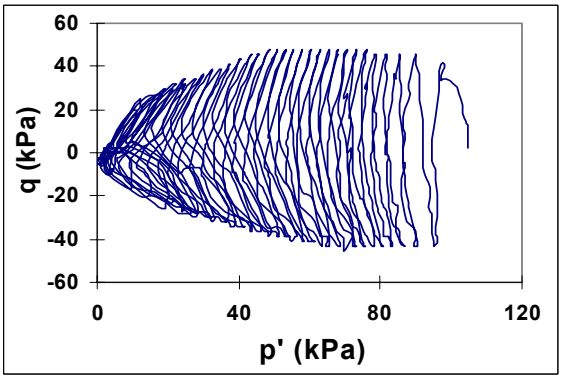

Test No.: C67 **File Name: c061501** **Soil Type: FJ-25** **e=0.619**

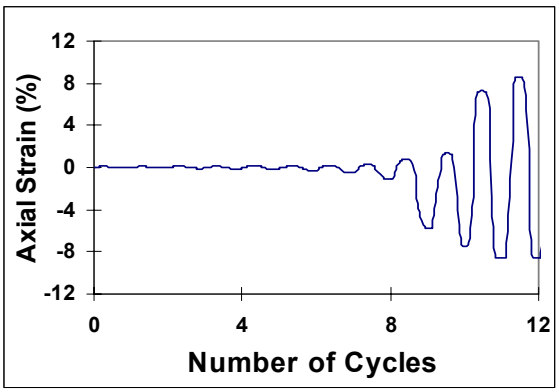

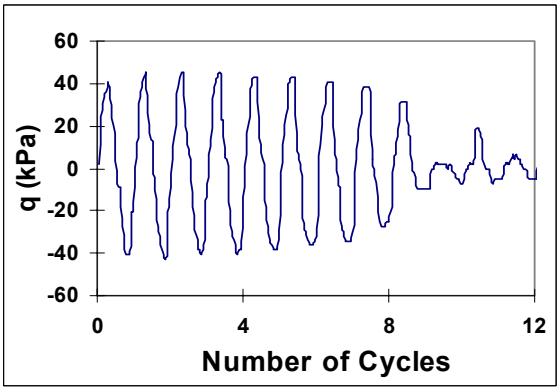

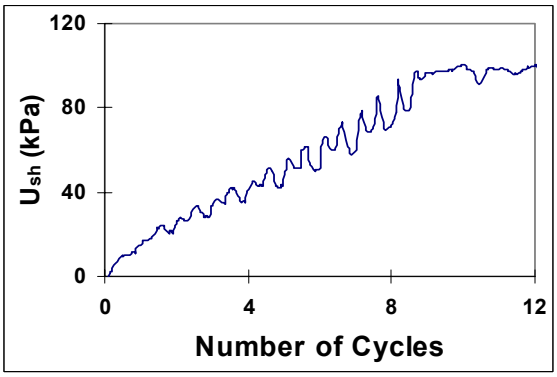

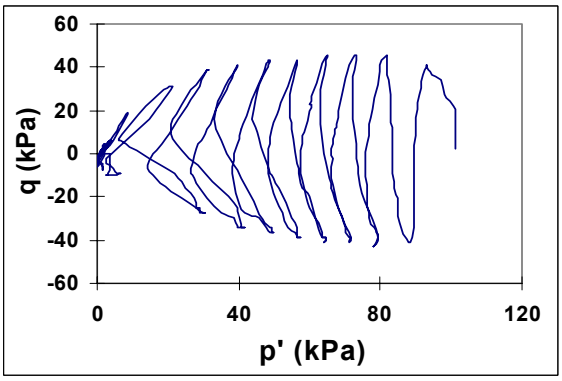

Test No.: C68 **File Name: c061701** **Soil Type: FJ-25** **e=0.643**

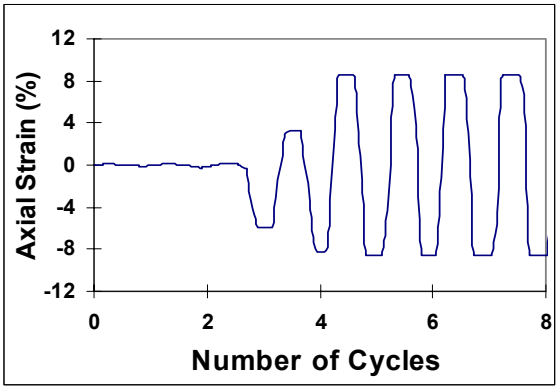

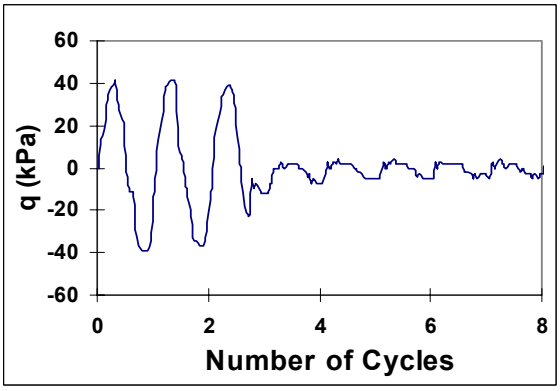

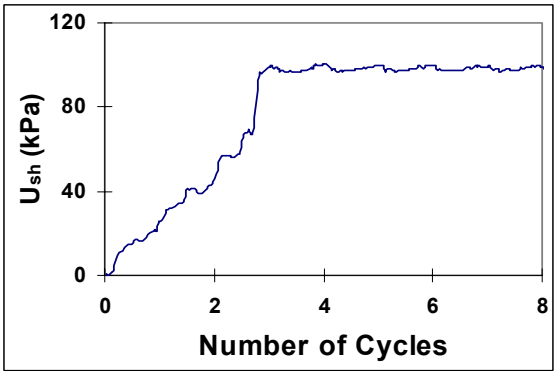

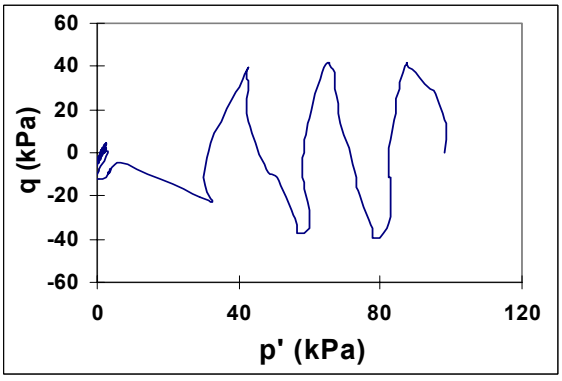

Test No.: C69 **File Name: c080601** **Soil Type: FJ-60** **e=0.563**

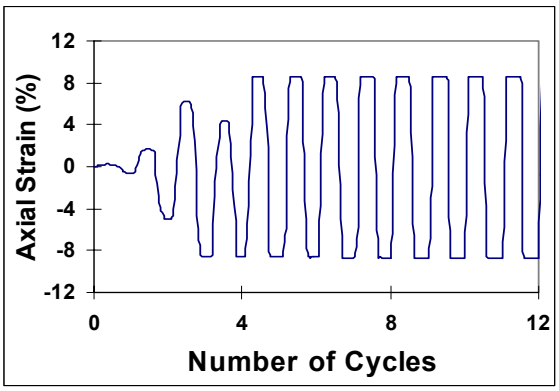

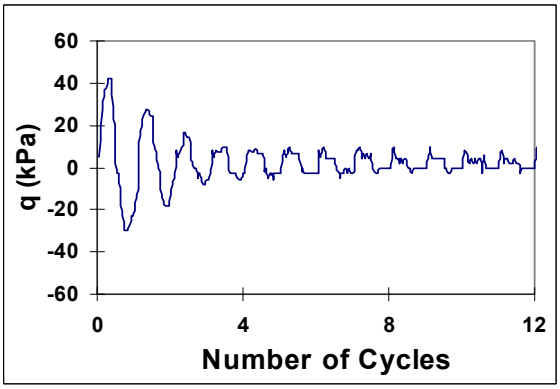

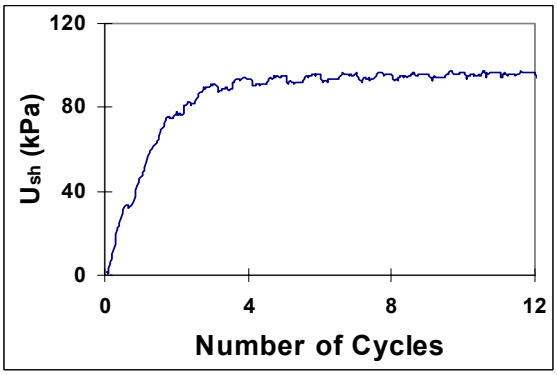

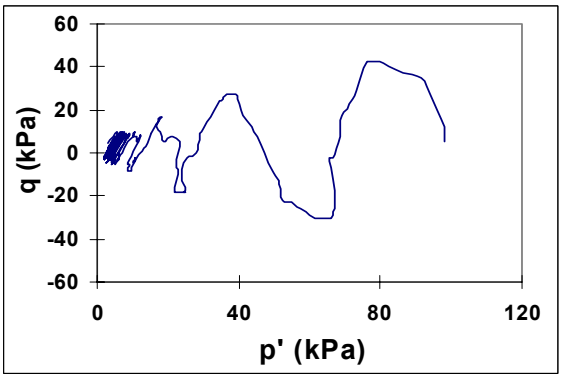

Test No.: C70 **File Name: c081001** **Soil Type: FJ-60** **e=0.564**

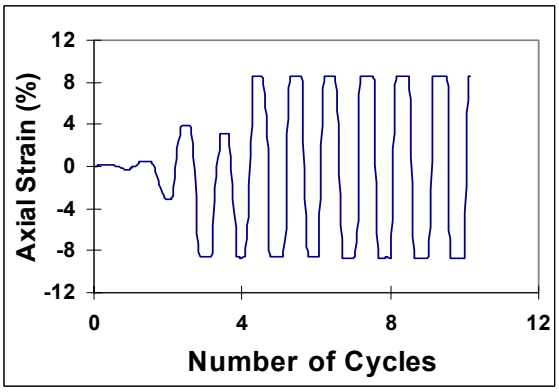

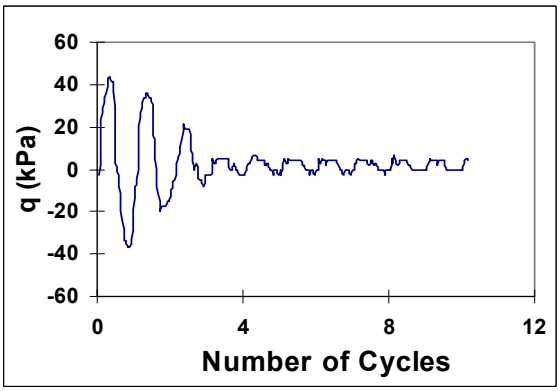

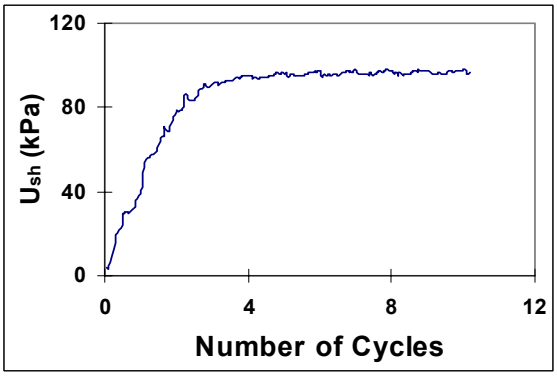

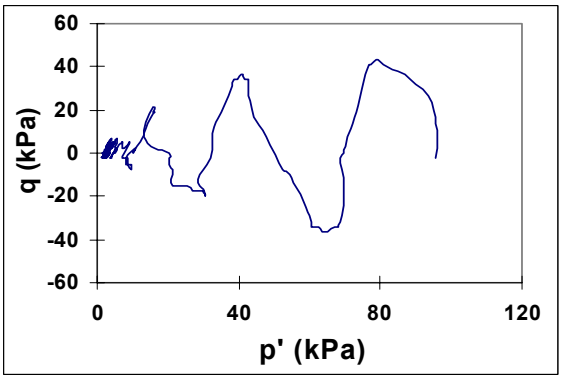

Test No.: C71 **File Name: c092901** **Soil Type: WG-00** **e=0.601**

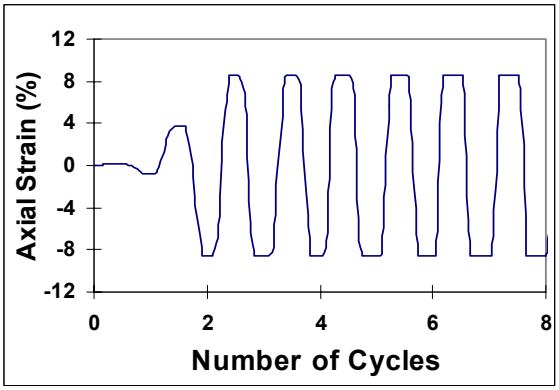

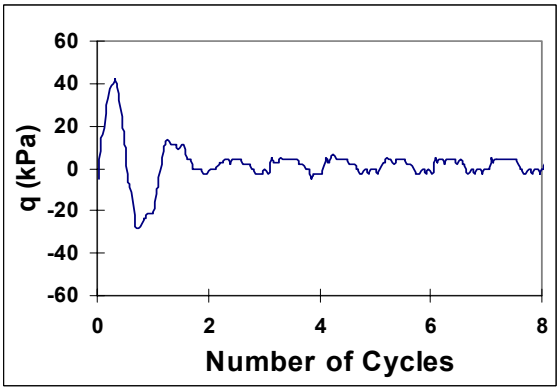

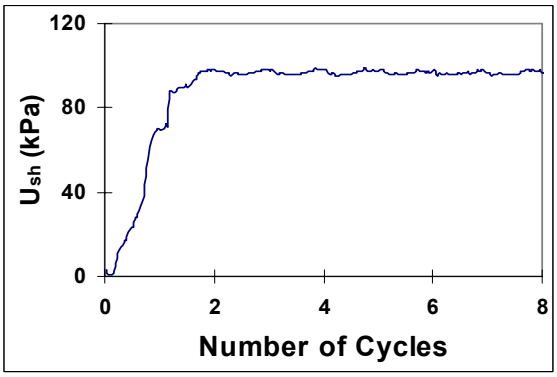

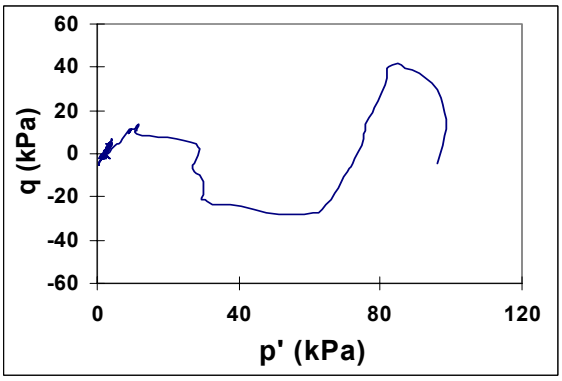

Test No.: C72 **File Name: c100401** **Soil Type: WG-00** **e=0.549**

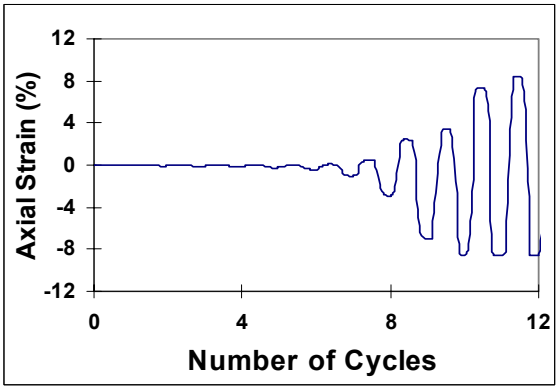

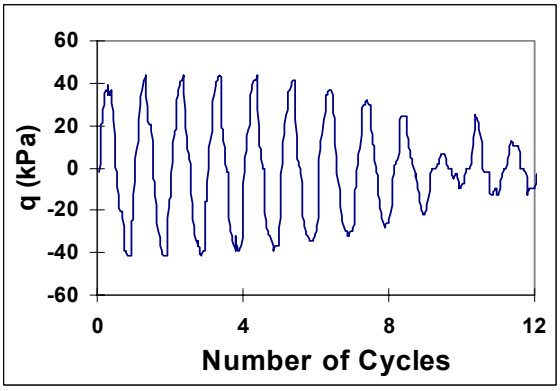

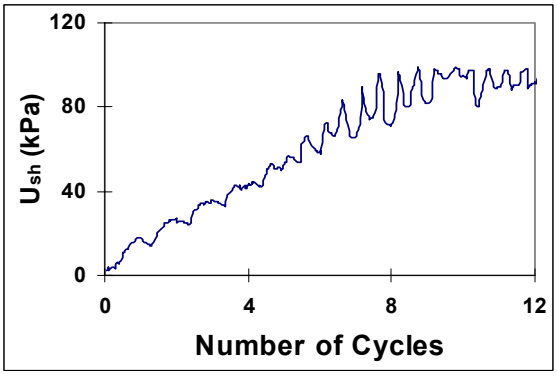

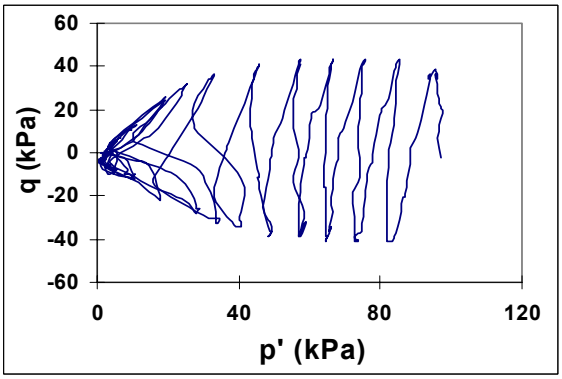

Test No.: C73 **File Name: c101801** **Soil Type: WG-00** **e=0.528**

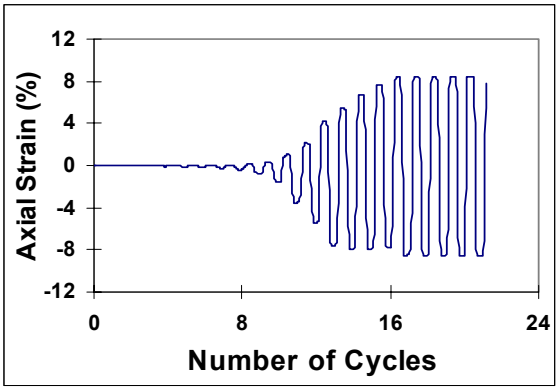

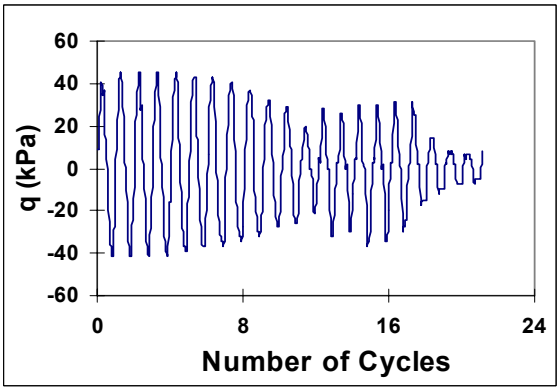

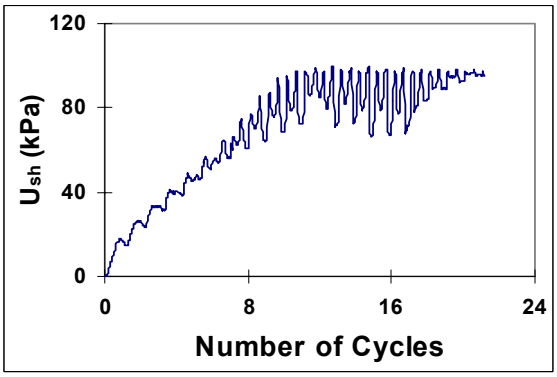

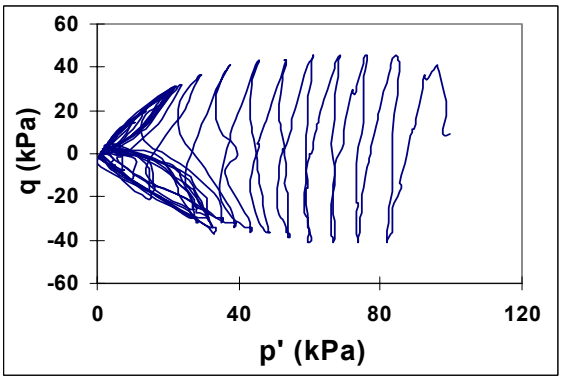

Test No.: C74 **File Name: c102501** **Soil Type: WG-25** **e=0.412**

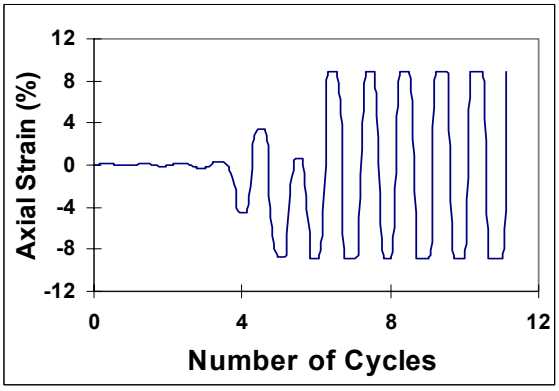

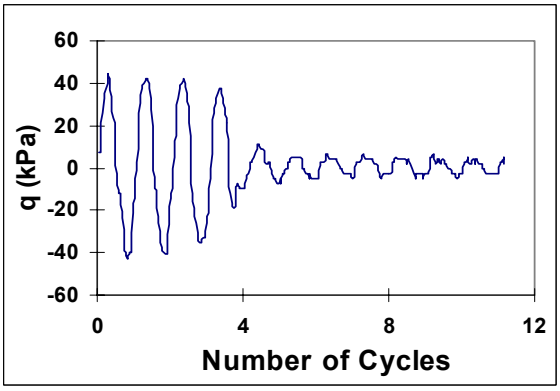

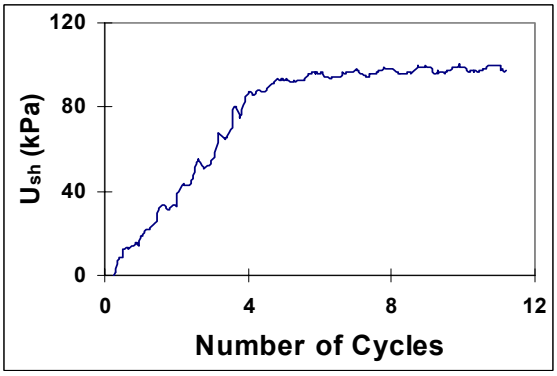

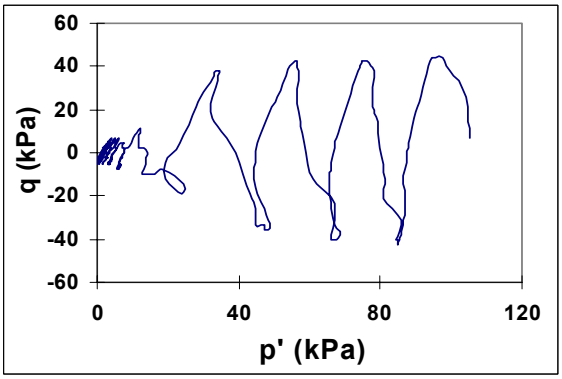

Test No.: C75 **File Name: c102601** **Soil Type: WG-25** **e=0.382**

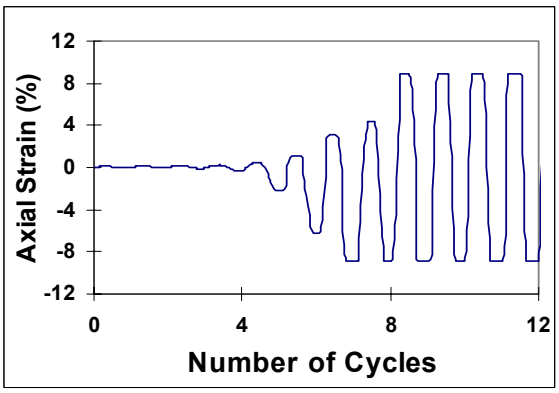

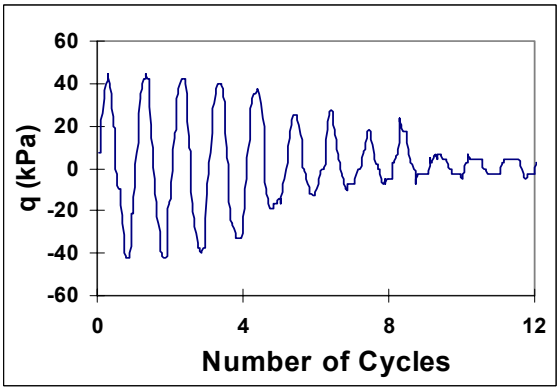

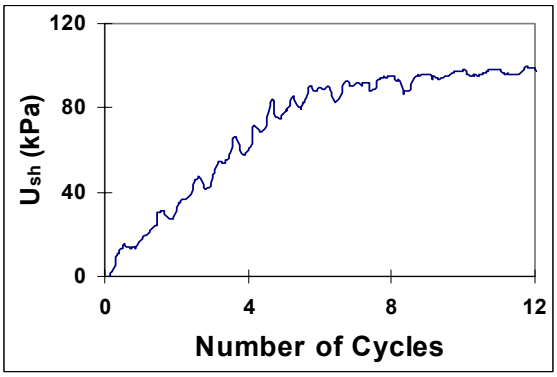

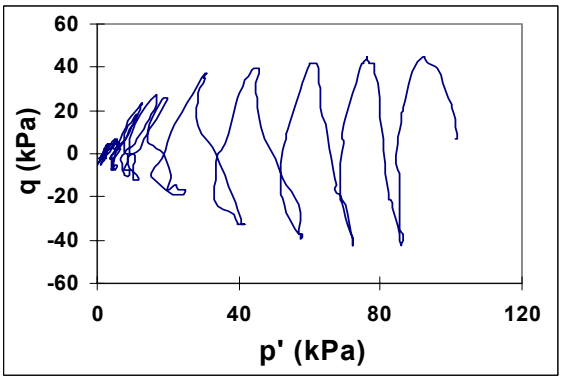

The following table summarizes the soil parameters used to calculate the equivalent contact density indices in cyclic triaxial tests.

Table B.2 Contact Density Index Parameters - Cyclic

Soil Type	b ($FC \leq FC_{th}$)	m ($FC > FC_{th}$)	R_d
OS#55 sand – GSF#40 silt mix	0.40	0.65	25
FJ#80 sand – GSF#40 silt mix	0.65	0.80	18
WG sand – GSF#40 silt mix	0.60	-	32

Appendix C

Notations

Appendix C: Notations

b = Contribution factor for fine grains
BCC = Body centered cubic arrangement
C_c = Coefficient of concavity
CSR = Cyclic stress ratio
CT = Cubical-tetrahedral arrangement
C_u = Coefficient of uniformity
D = Particle diameter of coarser grain
d = Particle diameter of fine grain
$d\varepsilon_{ij}$ = Differential increase in strain level
E = Cumulative energy dissipated per unit volume of material up to n^{th} load increment
e = Global void ratio
e_c = Intergranular void ratio
$(e_c)_{eq}$ = Equivalent intergranular void ratio
e_f = Interfine void ratio
$(e_f)_{eq}$ = Equivalent interfine void ratio
E_L = Cumulative dissipated energy to reach ±5% axial strain
e_{max} = Maximum void ratio
$e_{max,HF}$ = the maximum void ratio of the pure silt
e_{min} = Minimum void ratio
f_c =FC/100
FC =Fines content
FCC = Face centered cubic arrangement
FC_L = Limiting fines content
FC_{th} = Threshold fines content
G = Shear modulus of solid
I = Energy released from internal force chains
m = A coefficient that depends on grain characteristics and packing
m_g = Number of grains per unit volume
n = Number of load increments
N = Intergrain contact normal force
n_g = Number of slipping contacts per grain
N_L = Number of equal stress cycles required to reach ±5% axial strain
p' = Mean effective stress
P = Energy stored due to pore pressure increase
q = Deviatoric stress
R_d = Size disparity ratio
SC = Simple cubic arrangement
T = Tangential force acting along the contact
U_{sh} = Shear induced pore pressure
W = Cumulative internal frictional energy loss
ε = Axial strain
ΔW = Frictional energy loss per grain per contact
ΔE = Increment in the energy dissipated per unit volume
$\Delta\delta$ = Magnitude of slip between contacts
$\Delta\gamma$ = Incremental shear strain amplitude

$\varepsilon_{a,i}$ = Axial strain in i^{th} load increment
γ_i = Shear strain in the ith load increment
μ = contact friction coefficient
μ^* = Effective friction coefficient
ν = Poisson's ratio of solid
σ_c' = Initial effective confining stress